

PRELIMINARY

**CENTER FOR VOLCANIC AND TECTONIC STUDIES¹
DEPARTMENT OF GEOSCIENCE**

**University of Nevada, Las Vegas
Las Vegas, Nevada 89154**

Report No. 56

**ANNUAL REPORT for the Period 10/1/90 to 9/30/91 Submitted to
the Nuclear Waste Project Office
State of Nevada**

December 14, 1991

**¹Eugene I. Smith-Principal Investigator
Daniel Feuerbach-Research Associate
Terry Naumann-Research Associate**

300004

**9210020232 911231
PDR WASTE
WM-11 PDR**

*Submit
Please enter info
sup to
Shark
Bill/Bence
9/29/91*

*102.8
WM-11
NH03*

INTRODUCTION

The annual report of the Center for Volcanic and Tectonic Studies (CVTS) contains a series of papers, maps, reprints and theses that review the progress made by the CVTS between October 1, 1990 and September 30, 1991. During this period CVTS staff focused on several topics that had direct relevance to volcanic hazards related to the proposed high-level nuclear waste repository at Yucca Mountain, Nevada. These topics included:

- (1) The role of the mantle in controlling the location and composition of Pliocene-Holocene volcanism.
- (2) The nature of boundaries between compositionally different mantle domains. These domain boundaries may control the location of surface faults and volcanism.
- (3) The detailed geology of the Pliocene volcanic cones in Crater Flat.
- (4) The detailed geology of bedrock to the east of Crater Flat on Yucca Mountain.
- (5) The structural controls and emplacement mechanisms of Pliocene/Quaternary basaltic volcanic centers and dikes.
- (6) The study of young felsic volcanism in the southern Basin and Range.
- (7) Estimating the probability of disruption of the proposed repository by volcanic eruption (this topic is being studied by Dr. C. Ho-UNLV).

Activities

CVTS presented papers at several professional meetings including:

- (a) The Geological Society of America Cordilleran Section Meeting in San Francisco- March 25-27, 1991.
- (b) The Napoli '91 International Conference on Active Volcanoes and Risk Mitigation, in Naples, Italy - August, 1991.
- (c) The Geological Society of America National Meeting in San Diego, October, 1991.

In addition CVTS staff participated in several technical exchanges and field trips with NRC, ANCW and NWTRB panels, and presented numerous invited talks, seminars and field trips to the public about volcanism and the proposed nuclear waste repository.

The CVTS staff feel that part of their responsibility is to provide the public with unbiased and alternative views of the issues related to the proposed Yucca Mountain high-level nuclear waste repository. Invited talk and lectures to public meetings and civic groups as well as large enrollment classes at UNLV provide the community with a source of information regarding the geology and geologic hazards related to the project.

CVTS Staff

During the period October 1, 1990 to September 30, 1991, CVTS staff included Eugene I. Smith (PI), Dan Feuerbach and Terry Naumann (Research Associates), and Tracey Tuma (Student Assistant). Jim Faulds (University of Iowa) received partial support to complete his field studies in the Malpais Mesa area of Arizona and in Crater Flat. In addition, two graduate students (Tracey Cascadden and Hayden Bridwell) were partially funded to complete Master's Thesis projects.

Organization of the Annual Report

This report includes the following contributions:

- (1) "Evolution of a mantle domain boundary during regional extension: constraints from isotopic geochemistry of volcanic rocks in the Lake Mead area, Nevada and Arizona" by D.L. Feuerbach, E.I. Smith (CVTS-UNLV) and J.D. Walker (University of Kansas).
- (2) A summary of a paper entitled "Isotope geochemistry of the mafic lavas of the Reveille Range, Nevada: A window into the mantle of the central Great Basin." by T.R. Naumann, E.I. Smith (CVTS-UNLV) and J.D. Walker (University of Kansas).
- (3) The geologic map of Crater Flat, Nevada. The authors of the map are J. Faulds (University of Iowa), D. Feuerbach (CVTS-UNLV), A. Ramelli (UNR) and John Bell (UNR). This map and explanation will be published by the Nevada Bureau of Mines and Geology.
- (4) A summary of a paper regarding the structural control and emplacement mechanism of mafic dikes by J. Faulds (University of Iowa).
- (5) Copies of abstracts submitted by CVTS staff during the year of funding.

These include:

- (a) "Structural control of Pliocene volcanism in the vicinity of the Nevada Test Site, Nevada: an example from Buckboard Mesa" by Naumann, Feuerbach and Smith. Presented at the Geological Society of America Cordilleran Section

meeting in San Francisco.

(b) "The transition from subalkalic to alkalic volcanism in the Lake Mead area of Nevada and Arizona: geochemical and isotopic constraints" by Feuerbach, Smith, Walker and Tangeman (Kansas). Presented at the Geological Society of America Cordilleran Section meeting in San Francisco.

(c) "The eastern boundary of the extensional allochthon in the eastern Basin and Range: volcanic and structural geology of the northern White Hills, Arizona" by Cascadden and Smith. Presented at the Geological Society of America Cordilleran Section meeting in San Francisco.

(d) "New insights on structural controls and emplacement mechanisms of Pliocene/Quaternary basaltic dikes, southern Nevada and northwestern Arizona" by Faults, Feuerbach and Smith. Presented at the Geological Society of America National Meeting in San Diego.

(e) "Intermediate and mafic volcanic rocks of the northern White Hills, Arizona: implications for the production of intermediate composition volcanic rocks during regional extension" by Cascadden and Smith. Presented at the Geological Society of America National Meeting in San Diego.

(f) "Hornblende geobarometry from mid-Miocene plutons: implications regarding uplift and block rotation during Basin and Range extension" by Metcalf (UNLV) and Smith. Presented at the Geological Society of America National Meeting in San Diego.

(g) Volcanic risk assessment studies for the proposed high-level radioactive waste repository at Yucca Mountain, Nevada, USA" by Smith, Feuerbach, Naumann and Ho (UNLV). Presented at the Napoli '91 International Conference on Active Volcanoes and Risk Mitigation in Naples, Italy.

(6) Two papers describing new K-Ar dates from the Reville Range and Fortification Hill field published in Isochron/West.

Naumann, T.R., Smith, E.I., Shafiqullah, M., and Damon, P.E., New K-Ar ages for mafic to intermediate volcanic rocks in the Reville Range, Nevada: Isochron West.

Feuerbach, D.L., Smith, E.I., Shafiquallah, M., and Damon, P.E., New K-Ar dates for mafic late-Miocene to Pliocene volcanic rocks in the Lake Mead area, Arizona and Nevada: Isochron West.

(7) A thesis entitled "The Sloan Sag: A Mid-Miocene volcanotectonic depression, north-

central McCullough Mountains, southern Nevada" by Hayden Bridwell. This thesis deals with a section of young (< 12 Ma) felsic volcanic rocks in the McCullough Range, 16 kilometers south of Las Vegas.

(8) A thesis entitled "Style of volcanism and extensional tectonics in the eastern Basin and Range Province: northern Mohave County, Arizona" by Tracey Cascadden. The thesis deals with the formation of mafic volcanic rocks in an extensional environment.

If these theses are not included in your copy of the annual report and you wish more information, contact the CVTS (702) 739-3971.

**EVOLUTION OF A MANTLE DOMAIN BOUNDARY DURING REGIONAL
EXTENSION: CONSTRAINTS FROM ISOTOPIC GEOCHEMISTRY OF
VOLCANIC ROCKS IN THE
LAKE MEAD AREA, NEVADA AND ARIZONA**

by

D.L. Feuerbach, E.I. Smith

Center for Volcanic and Tectonic Studies

Department of Geoscience

University of Nevada, Las Vegas

Las Vegas, Nevada 89154

J.D. Walker

Department of Geology

University of Kansas

Lawrence, Kansas 66045

INTRODUCTION

In the southwestern U.S.A., three mantle isotopic provinces were defined by the use of Sr and Nd isotopic systems (Fitton et al., 1986; Menzies et al., 1983; Farmer et al., 1989) (Figure 1). These are: (1) Basin and Range characterized by ϵ Nd between +5 and +8 and initial $^{87}\text{Sr}/^{86}\text{Sr} = 0.703$ (Perry et al., 1987; Menzies et al., 1983; Farmer et al., 1989); (2) Transition zone between the Colorado Plateau and Basin and Range with $^{87}\text{Sr}/^{86}\text{Sr}$ between 0.7038 and 0.707 and ϵ Nd between -4 and +5 (Cooper and Hart, 1990; Fitton et al., 1986); and (3) Sierra Nevada or Western Great Basin province distinguished by $^{87}\text{Sr}/^{86}\text{Sr} > 0.706$ and ϵ Nd between 0 and -11 (Menzies et al., 1983; Fitton et al., 1986; Fitton et al., 1991). Basalts with similar $^{87}\text{Sr}/^{86}\text{Sr}$ and ϵ Nd in southern Nevada (Farmer et al., 1989) also lie within this province.

The boundary between the Western Great Basin and Basin and Range provinces (Menzies et al., 1983; Fitton et al., 1991) and the contact between the OIB and EM2 mantle domains of Menzies (1989) pass through the Lake Mead area of southern Nevada (Figure 1). The Lake Mead area also contains an important crustal boundary. The Lake Mead fault zone (LMFZ) (Anderson, 1973; Bohannon, 1984; Duebendorfer and Wallin, 1991), a northeast trending set of left-lateral strike-slip faults separates the "amagmatic zone" from the Northern Colorado River extensional corridor (NCREC). The amagmatic zone is a region of minor igneous activity and little to moderate Tertiary extension that separates the Great Basin from the Sonoran Desert sections of the Basin-and-Range province in the western U.S.A. This region between 36° and 37° north, corresponds to a regional topographic slope and a gravity gradient with an amplitude of about 100 mgals (Eaton, 1982; Eaton et al., 1978). The zone also represents a boundary between contrasting migration directions of magmatism and extension (Bartley et al., 1988; Bartley, 1989; Glazner and Supplee, 1982; Reynolds et al., 1987). In contrast, the NCREC (Howard and John, 1987) experienced over 100% extension and abundant magmatism during Tertiary time. The LMFZ also separates thick sections of Paleozoic and Mesozoic sedimentary sections (to the north) from the NCREC, an area nearly devoid of these sections (Longwell et al., 1965; Anderson, 1971).

This paper focuses on the boundary between the amagmatic zone and the NCREC. We use Miocene and Pliocene mafic volcanic rocks ($\text{SiO}_2 < 55\%$) that span this mantle-crustal boundary as "a probe" into the mantle to determine (1) the nature of isotopic differences across the boundary, (2) the timing of formation of the boundary, and (3) any link between crustal and mantle processes. Our goal is to develop a three-dimensional model for the evolution of a mantle isotopic domain boundary.

In continental settings, the boundary between lithospheric mantle and asthenosphere is marked by differences in isotopic and trace-element signatures. Lithospheric mantle is enriched in incompatible elements and has high Rb/Sr and low Sm/Nd compared to asthenospheric mantle. As a result, lithospheric mantle has higher $^{87}\text{Sr}/^{86}\text{Sr}$ and lower ϵ Nd values than asthenospheric mantle. The difference in isotopic values between lithospheric and asthenospheric mantle is probably due to the long-term isolation of the lithospheric mantle from mixing caused by mantle convection.

Mafic volcanism is useful in the mapping of mantle domains (Menzies, 1989). The

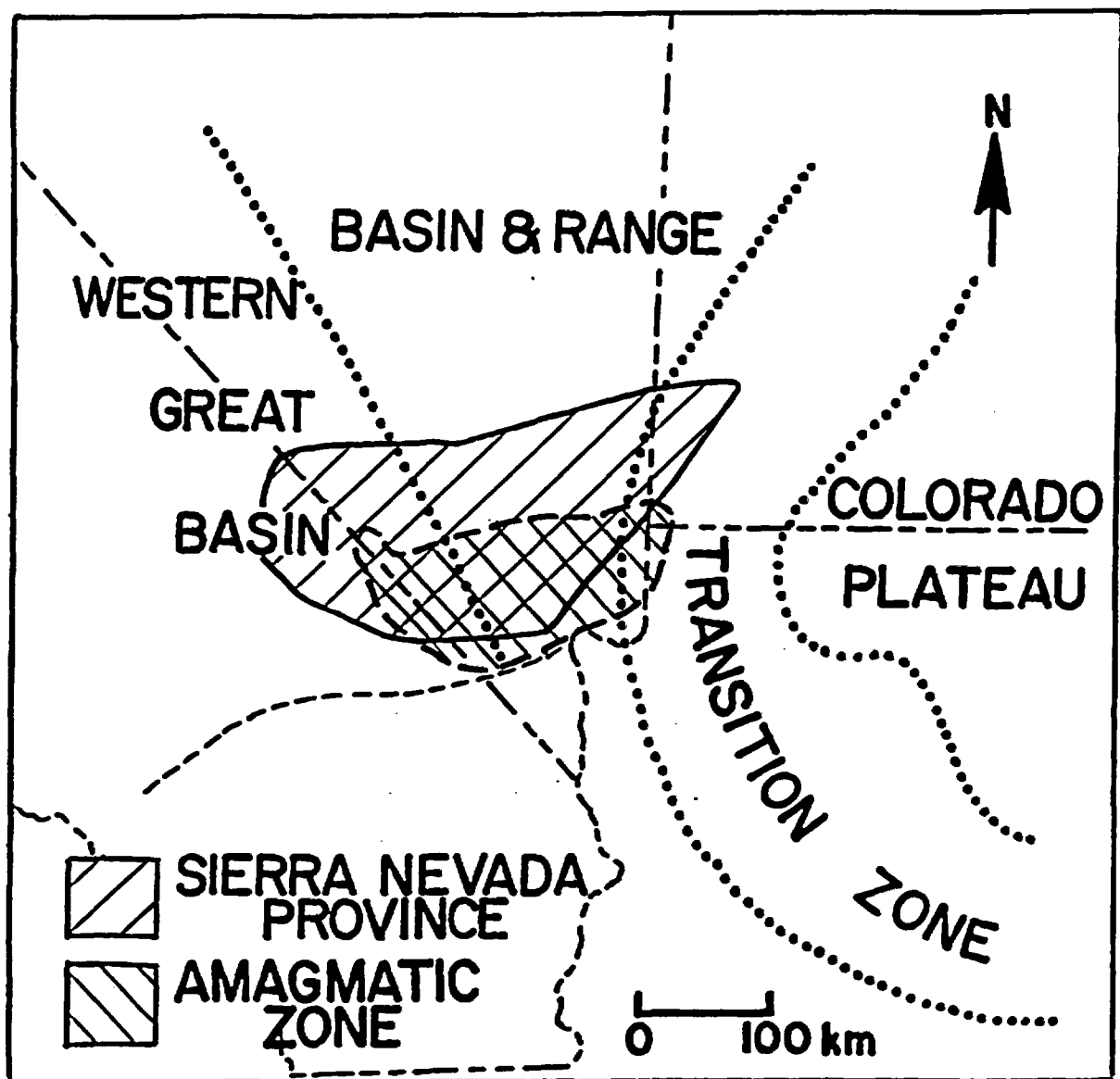


Figure 1. Map showing the major mantle domain boundaries proposed for the southern Basin and Range.

lithospheric mantle is isotopically enriched and heterogeneous (Zindler and Hart, 1986; Hart, 1985; Weaver, 1991a; Leat et al., 1990; Cooper and Hart, 1990; Walker and Coleman, 1991). Chemical and isotopic heterogeneity may be due to the incorporation of oceanic crust and terrigenous or pelagic sediments (Weaver, 1986, 1991a) or be a result of mantle metasomatism (Hart, 1988). Mantle components such as EM1, EM2 and HIMU probably reside in the lithospheric mantle because their isotopic signature requires isolation from the convecting asthenosphere for 1.0 to 2.0 Ga (Zindler and Hart, 1986). Recently, however, Weaver (1991b) suggested that these components may reside in detached slabs of oceanic crust that have accumulated deep within the mantle (mesosphere) and have not appreciably mixed with asthenosphere.

INSTRUMENTAL TECHNIQUES

Whole rock major element concentrations were determined by Inductively Coupled Plasma techniques (ICP) at Chemex Labs, Inc. (Sparks, NV). Rare-earth elements and Cr, V, Sc, Co, Ta, Hf, Th were analyzed by Instrumental Neutron Activation Analysis (INAA) at the Phoenix Memorial Laboratory, University of Michigan. The multi-element standards G-2, GSP-1, BHVO-1, and RGM-1 were used as internal standards. Ba, Rb, Ni and Sr were determined by atomic absorption and Nb and Sr were determined by X-ray Fluorescence at Chemex Labs, Inc. Rb and Sr were determined by isotope dilution for samples which were analyzed for Nd, Sr and Pb isotope concentrations. Ni, Nb, Rb, Sr, Zr, Y, Ba for the samples from Fortification Hill were analyzed by XRF at the U.S. Geological Survey in Menlo Park. This study includes 45 new isotopic analyses from 11 volcanic sections which represent all major volcanic centers and a fairly complete sample of mafic volcanic rocks in the Lake Mead area. Geochemical data is summarized in Table 1.

VOLCANOLOGY

Distribution and Description of Volcanic Sections

Volcanism is rare to the north of the LMFZ in the "amagmatic" zone and is limited to low-volume Pliocene basalt centers at Black Point and in the Las Vegas Range (Figure 2a). In the eastern part of the Lake Mead area in the Gold Butte and Grand Wash trough there are numerous late-Cenozoic alkali basalt centers (Cole, 1989). Adjacent to the LMFZ is the middle- to late-Miocene Hamblin-Cleopatra volcano (Thompson, 1985; Barker and Thompson, 1989); Boulder Wash volcanic section (Naumann, 1987); Callville Mesa volcano (Feuerbach et al., 1991); and flows of late-Miocene basalt interbedded with Tertiary sediments in Government Wash north of Lake Mead (Figure 2b). The area to the south of the LMFZ contains numerous Miocene and Pliocene volcanic centers (Figure 2b). The most notable of the Miocene centers are in the River Mountains (Smith, 1982); McCullough Range (Smith et al., 1988); Eldorado Mountains (Anderson, 1971); Hoover Dam (Mills, 1985); at Malpais Flattop and in the White Hills (Cascadden, 1991). Pliocene centers comprise the Fortification Hill volcanic

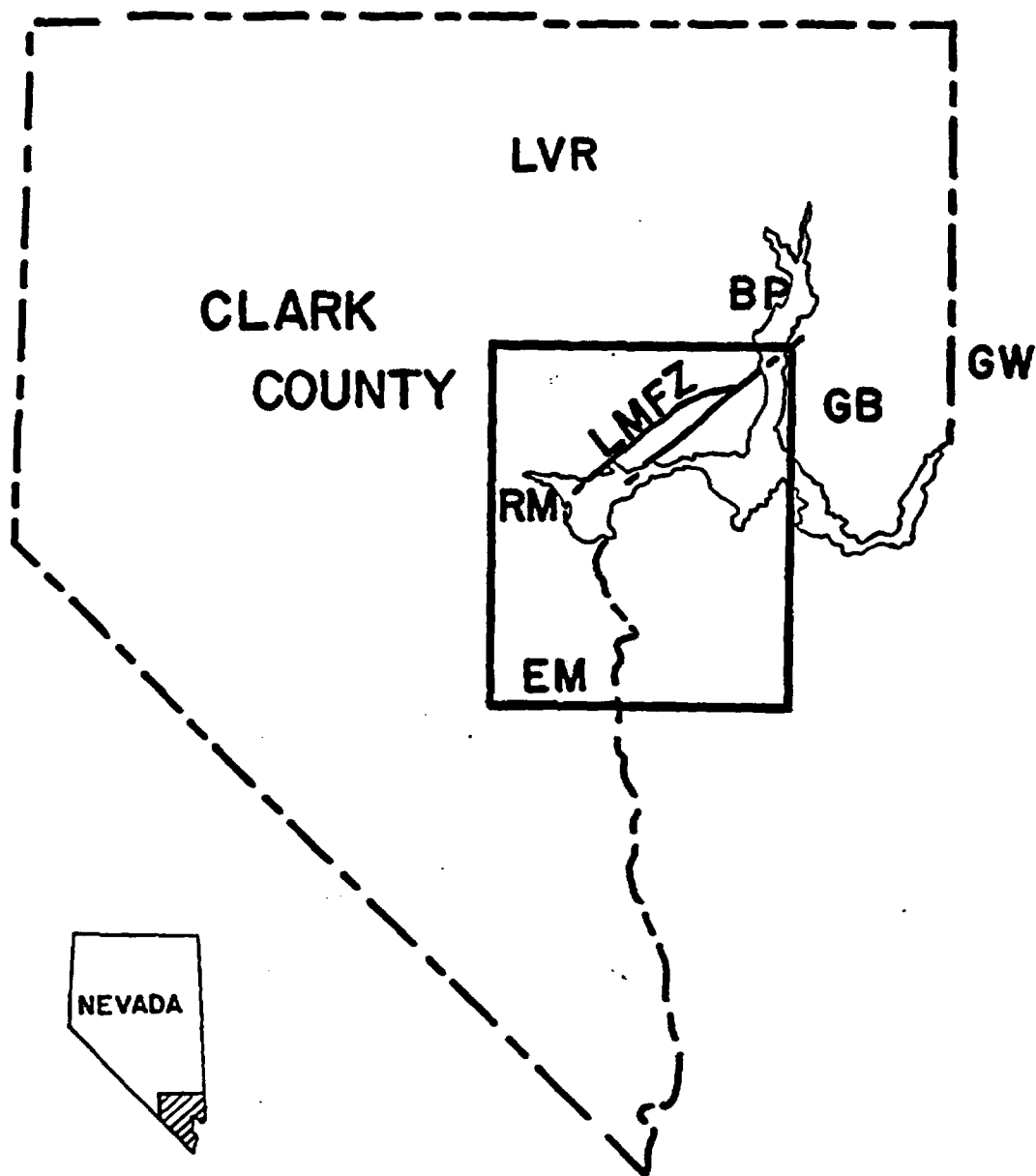


Figure 2a. Index map of the southern Great Basin and adjacent Basin and Range and Colorado Plateau showing location of mafic volcanoes. Box indicates area shown in Figure 2b. LVR = Las Vegas Range, BP = Black Point, GB = Gold Butte, GW = Grand Wash, RM = River Mountains, EM = Eldorado Mountains, LMFZ = Lake Mead Fault Zone.

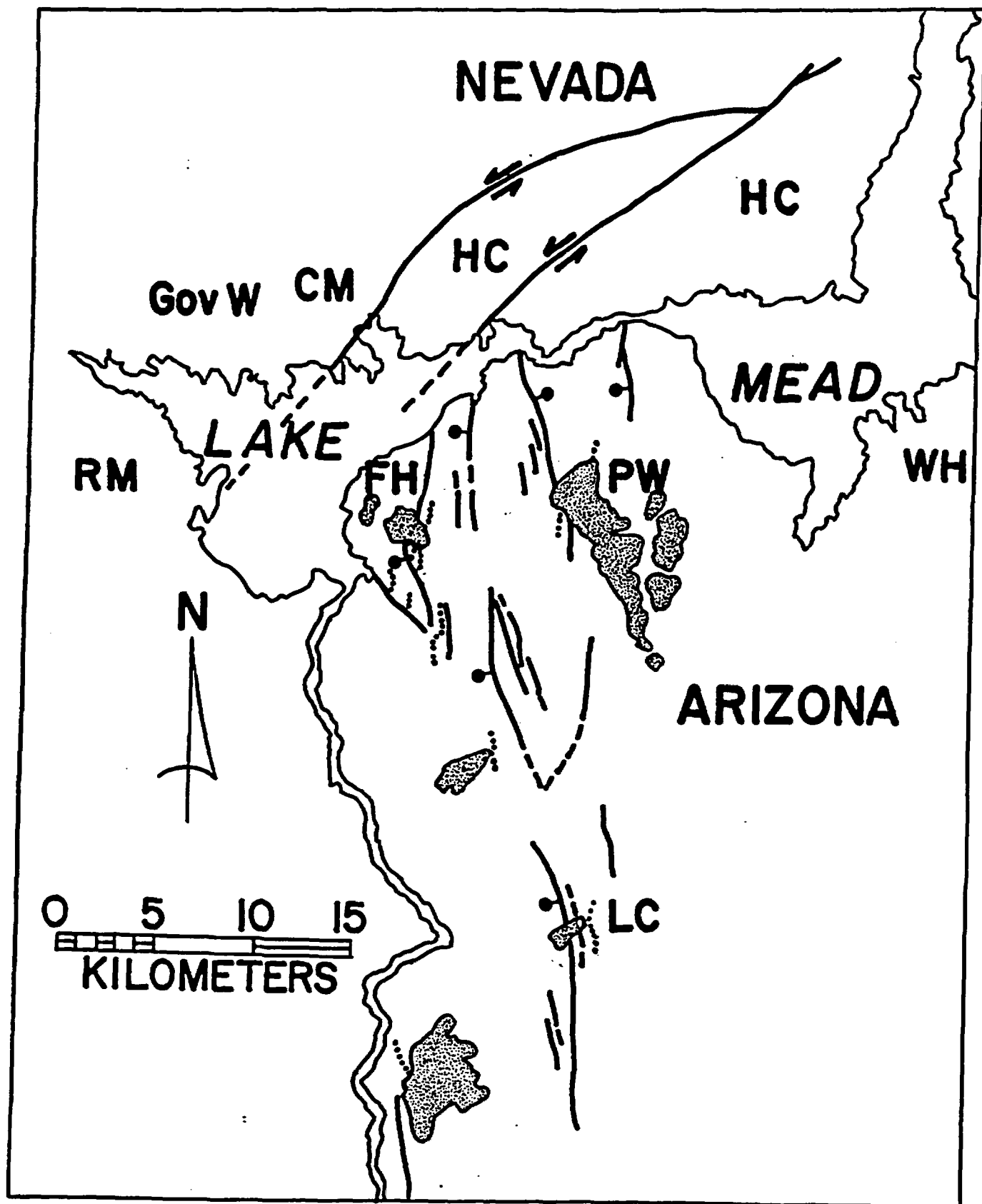


Figure 2b. Index map of the Lake Mead area showing localities described in text and major structures. HC= Hamblin-Cleopatra volcano, WH = White Hills, LC = Lava Cascade, PW = Petroglyph Wash, CM = Callville Mesa, FH = Fortification Hill, GovW= Government Wash.

Table 1

Isotopic and Geochemical Data from the Volcanic Rocks in the Lake Mead Area

Sample	YAB 25-2	YAB 42-76	OAB 57-107	OAB 57-113	SAB 42-82	SAB 38-13	SAB 38-143	TH 10-120
SiO ₂	44.9	45	45.35	44.15	47.52	45.79	47.97	46.32
Al ₂ O ₃	16.5	16.79	16.71	15.22	16.61	14.5	16.05	15.3
FeO	11.1	10.88	13.81	13.38	10.56	12.8	11.87	13.39
MgO	5.7	6.21	5.54	8.06	5.35	8.78	5.32	8.92
CaO	7.7	8.78	11.13	10.69	9.79	8.38	10.16	7.93
Na ₂ O	4.7	4.94	3.15	2.88	3.57	2.86	3.26	2.97
TiO ₂	1	3.7	1.2	1.1	2.11	0.84	1.4	0.9
K ₂ O	2.4	2.54	2.07	1.76	1.76	1.41	1.46	1.16
P ₂ O ₅	0.7	0.88	0.53	0.52	0.57	0.28	0.49	0.34
MnO	0.2	0.18	0.19	0.18	0.16	0.16	0.17	0.19
LOI	2.93	0.6	0.06	0.52	1.42	1.48	0.49	4.11
Total	97.83	100.5	99.74	98.46	99.42	97.28	98.64	101.53
Trace and Rare Earth Elements (PPM) (XRF, ID, AA or INAA) noted								
Cr(INAA)	139	113	80	268	50	361	70	326
Co(INAA)	29.1	29.6	34.69	43.12	31.8	52.58	32.79	53.7
Sc(INAA)	18	18.6	28.63	30.22	25	26.5	26.32	24.68
V (INAA)		216	245	229	281	213	236	177
Hf(INAA)	6.5	7.22	4.51	3.26	4	3.38	4.18	2.83
Th(INAA)	8.5	12.4	3.66	3.15	5.28	2.87	3.23	1.16
Ta(INAA)	4	6.01	2.07	1.66	1.87	1.69	1.31	
La(INAA)	59.9	75.1	37.21	32.11	37.7	24.58	32.69	11.79
Ce(INAA)	116.3	151	69.7	59.18	72.3	52.42	57.45	24.73
Eu(INAA)	2.4	2.3	1.61	1.46	1.61	1.59	1.53	1.05
Yb(INAA)	2.8	2.43	2.59	2.79	2.49	2.2	2.52	2.3
Lu(INAA)	0.3	0.22	0.35	0.26	0.37		0.37	0.17
U (INAA)					1.83			
Sm(INAA)	8.8	8.61	5.95	5.27	6.16	4.83	5.53	3.07
Tb(INAA)		1.33						
Sr(ID)	999.69	873.59	463.93	451.23	597.57	434.24	491.11	306.35
Rb(ID)	20.24	43.4	11.09	9.68	22.13	14.31	14.86	14.45
Nd(ID)	46.29	49.48	27.26	24.77	32.26		25.45	190
Ba(AA)	744	1320	536	480	800	475	690	
Ni(AA)	70	68	42	126	30	166	24	
Nb(XRF)	60	85	36	30	34	28	28	10
Zr(XRF)	250	300	160	140	155	138	138	90
Isotopic analysis by Mass Spectrometry								
¹⁴³ Nd/ ¹⁴⁴ Nd	0.5126	0.5128	0.5127	0.5128	0.5126	0.5126	0.5126	0.5125
Epsilon Nd	3.18	3.63	1.42	1.42	-0.68	-0.84	-0.9	-2.3
(⁸⁷ Sr/ ⁸⁶ Sr) _i	0.7043	0.7035	0.7048	0.7051	0.7055	0.7057	0.7057	0.7075
²⁰⁶ Pb/ ²⁰⁴ Pb	18.737	18.741	18.591	18.67	18.263	18.194	18.123	18.033
²⁰⁷ Pb/ ²⁰⁴ Pb	15.564	15.523	15.555	15.57	15.548	15.523	15.541	15.581
²⁰⁸ Pb/ ²⁰⁴ Pb	38.639	38.476	38.535	38.612	38.397	38.309	38.156	38.9

Table 1

Sample	TH 10-121	LV Range LV-104	G. Butte 3-6	G. Wash 4-13	G. Wash 5-14	G. Wash 6-39	G. Wash 7-33	G. Wash 8-62
SiO ₂	44.58	42.49	46.3	47.58	48.81	48.44	47.85	47.31
Al ₂ O ₃	14.35	10.76	14.64	14.4	14.95	14.57	14.53	15.99
FeO	13.82	12.79	12.59	14.53	11.73	12.75	13.83	11.37
MgO	8.76	13.45	9.16	8.55	7.14	8.42	7.86	4.73
CaO	6.55	9.78	7.98	8.74	8.64	9.88	7.41	10.43
Na ₂ O	4.17	2.39	3.16	3	3.22	3.1	4.32	3.49
TiO ₂	0.7	1	1.19	1.25	1.54	0.91	1.85	2.29
K ₂ O	1.1	1.69	1.59	1.55	1.57	1.92	2.42	1.72
P ₂ O ₅	0.3	0.67	0.27	0.26	0.43	0.29	0.59	0.18
MnO	0.19	0.16	0.18	0.19	0.16	0.17	0.17	0.16
LOI	3.14	1.79	1.06	0.19	1.09	0.01	0.01	1.63
Total	97.66	96.97	98.12	100.24	99.28	100.46	100.75	99.3
Cr(INAA)	271	816	253	326	256	459	189	223
Co(INAA)	56.33	57.55	46.68	50.49	39.52	47.2	47	34.3
Sc(INAA)	24.53	22.21	23.73	27	23.91	26.7	15.4	0.4
V (INAA)	194	234	216	242	215	208	182	255
Hf(INAA)	1.7	5.22	3.63	3.14	3.24	3.59	6.42	3.84
Th(INAA)		5.2	2.72		2.78	3.21	3.62	2.25
Ta(INAA)	0.95	0.71					3.16	1.35
La(INAA)	12.61	46.02	23.86	9.04	19.21	20.9	34.6	18.9
Ce(INAA)	24.27	91.97	46.11	21.87	44.26	44.8	71	39.1
Eu(INAA)	0.93	2.34	1.45	0.95	1.33	1.4	1.96	1.31
Yb(INAA)	1.75	1.74	2.47	1.96	2.28	0.16	1.55	2.11
Lu(INAA)	0.28	0.13	0.35	0.3	0.24	0.22	0.18	0.37
U (INAA)								
Sm(INAA)	3.07	10.23						
Tb(INAA)								
Sr(ID)	246.12	795.58	421.14	321.83	378.36	419.48	723.94	447.64
Rb(ID)	8.98	48.27	14.88	7.47	8.06	12.45	22.94	10.04
Nd(ID)		55.76	22.47	14.35	17.89	20.52	29.65	16.21
Ba(AA)	176							
Ni(AA)	206							
Nb(XRF)	13							
Zr(XRF)	77							
143Nd/144Nd	0.5125	0.5123	0.5126	0.5126	0.5127	0.5126	0.513	0.5128
Epsilon Nd	-3.55	-7.2	-0.9	-0.27	1.87	-0.04	6.75	3.49
(87Sr/86Sr) _i	0.7079	0.7068	0.705	0.7046	0.7046	0.704	0.7033	0.7042
206Pb/204Pb	17.947	18.963	18.13	17.821	18.13	18.119	18.075	17.999
207Pb/204Pb	15.499	15.642	15.527	15.55	15.51	15.518	15.473	15.5
208Pb/204Pb	38.291	38.845	38.068	38.05	37.83	38.034	37.704	37.758

Table 1

Sample	C.Mesa 24-49	C.Mesa 24-68	R.Mtns 78-218	R.Mtns 78-222	R.Mtns 78-223	R.Mtns 83-348	W.Ridge LL-88-41
SiO ₂	55.24	55.18	47.1	59	67.2	72.9	54.1
Al ₂ O ₃	15.98	15.84	14.5	16.6	14.2	12.6	16.9
FeO	8.97	8.49	10.9	6.9	3.5	2.7	8.9
MgO	4.1	4.33	6.3	2.6	0.9	0.2	4.5
CaO	6.9	6.64	11.2	5.5	2.3	0.5	7.4
Na ₂ O	3.55	3.52	2.8	3.9	3.6	2.2	4.2
TiO ₂	2.33	2.45	1.2	2.3	4.9	7.5	2.1
K ₂ O	1.13	1.07	1.8	0.9	0.4	0.2	1.5
P ₂ O ₅	0.25	0.3	1	0.6	0.1		0.7
MnO	0.14	0.1	0.1	0.1	0.1		0.1
LOI	0.4	2.17	2.3	1	3	0.1	0.5
Total	96.98	100.18	99.2	99.4	100.2	98.9	100.9
Cr(INAA)	145	134					
Co(INAA)	28.79	27.7					20
Sc(INAA)	19.62	18.2	29.6	11.2	3.8	1.5	
V (INAA)	171	153					198
Hf(INAA)	3.86	4.29	8.1	7.3	4.8	4.9	5.1
Th(INAA)	4.89	5.46	13.2	14.9	17.6	31.2	12.4
Ta(INAA)	0.97	0.96	1.5	1	1.2	15.3	2.1
La(INAA)	33.95	34.2	107.6	81.7	52.4	55.6	123
Ce(INAA)	67.61	72.1	242.4	167.9	90.7	124.5	213
Eu(INAA)	1.38	1.4	3.9	2	1.2	1	2.6
Yb(INAA)	2.18	2.6	2.1	2.3	1.3	2.2	2.3
Lu(INAA)	0.34	0.34	0.4	0.4	0.2	0.3	0.3
U (INAA)			6.4	4.6	9.1	3.9	
Sm(INAA)	5.32	5.22	15.5	8.7	4.2	3.7	10.9
Tb(INAA)			3	1.5	0.3	0.4	
Sr(ID)	970.19	423.51		959.65	467.99	79.76	1155.78
Rb(ID)	40.1	50.94		83.62	129.26	198.08	42.05
Nd(ID)	29.96	25.97	98.57	54.9	28.2	22.84	76.018
Ba(AA)	840	800					
Ni(AA)	36	60					
Nb(XRF)	23	17					
Zr(XRF)	185	145					
143Nd/144Nd	0.5122	0.5121	0.5122	0.512	0.512	0.512	0.5121
Epsilon Nd	-8.49	-10.69	-8.35	-11.28	-11.37	-12.29	-9.85
(87Sr/86Sr) _i	0.7089	0.7079		0.7089	0.7092	0.71	0.7082
206Pb/204Pb	17.332	17.173	18.299	17.922	17.885	18.156	17.887
207Pb/204Pb	15.496	15.453	15.605	15.537	15.553	15.578	15.537
208Pb/204Pb	38.01	37.814	38.699	38.791	38.982	38.906	38.725

Table 1

Sample	Gov. Wash EMD-209	H. Cleo KT82-15	H. Cleo KT82-183	M. Flattop 60-4
SiO ₂	51.9	56.43	55.89	47.3
Al ₂ O ₃	15.2	16.36	16.34	14.9
FeO	9.4	6.76	7.17	12.4
MgO	3.8	3.43	3.48	6.8
CaO	8.2	6.56	5.4	8.9
Na ₂ O	3.7	3.98	4.1	2.9
TiO ₂	3.2	2.47	2.72	1.1
K ₂ O	1.8	1.31	1.39	1.4
P ₂ O ₅	1.8	0.49	0.49	0.2
MnO	0.2	0.1	0.11	0.2
LOI	1.2	1.38	2.85	0.77
Total	100.4	99.27	99.94	96.87
Cr(INAA)		63	47	241
Co(INAA)		20.65	22.76	41.1
Sc(INAA)		14.06	14.11	30
V (INAA)		147	145	221
Hf(INAA)		6.76	8.15	3.6
Th(INAA)		10.46	13.53	
Ta(INAA)		2.75	2.84	
La(INAA)		65.23		14.8
Ce(INAA)		114.03	126.79	35.7
Eu(INAA)		1.89	1.99	1.1
Yb(INAA)		1.73	2.04	2.6
Lu(INAA)			0.26	0.3
U (INAA)				
Sm(INAA)		7.75	8.29	3.9
Tb(INAA)				1.4
Sr(ID)	1299.65	432.85	588.44	297.25
Rb(ID)	75.97	45.83	47.52	16.69
Nd(ID)	74.18	45.08	45.27	16.72
Ba(AA)				280
Ni(AA)				84
Nb(XRF)				13
Zr(XRF)				105
¹⁴³ Nd/ ¹⁴⁴ Nd	0.5121	0.5124	0.5124	0.5122
Epsilon Nd	-9.95	-4.84	-3.51	-8.33
(⁸⁷ Sr/ ⁸⁶ Sr) _i	0.7073	0.7044	0.7056	0.7075
²⁰⁶ Pb/ ²⁰⁴ Pb	18.16	17.971	18.096	17.742
²⁰⁷ Pb/ ²⁰⁴ Pb	15.56	15.515	15.538	15.531
²⁰⁸ Pb/ ²⁰⁴ Pb	38.939	38.344	38.549	38.83

field that extends discontinuously from near Willow Beach, Arizona to Lake Mead. In the Lake Mead area, for the most part, volcanism preceded block tilting related to regional extension (9 to 12 Ma; Duenbendorfer and Wallin, 1991). Calc-alkaline intermediate lavas were erupted between 18.5 and about 11 Ma. Low-volume basaltic andesite (10.3 to 8.5 Ma) and tholeiitic and alkalic basalt (4.7 to 6 Ma) mainly postdate extension (Smith et al., 1990).

Volcanic Rocks of the NCREC

Fortification Hill Field

Fortification Hill (FH) basalt crops out in a 75 km long by 30 km wide north-northeast elongate area that extends from Lava Cascade, Arizona to Black Point, Nevada (Figure 2b). Volcanic centers occur near north-northwest trending high-angle normal faults in the northern part of the NCREC. We divide the Fortification Hill basalts into three groups based on $\text{Na}_2\text{O} + \text{K}_2\text{O}$, light rare-earth element (REE) enrichment (Figure 3 and 4) and modal mineralogy. The groups are: (1) Sub-alkalic basalt (SAB) (5.88–4.73 Ma; Feuerbach et al., 1991)– sub-alkalic hypersthene-normative lavas with Ce/Yb_n (4–6). SAB lavas form a cinder cone-flow sequence on the north side of Fortification Hill. (2) Older alkali-basalt (OAB) (5.88 to 4.73 Ma; Feuerbach et al., 1991)– mildly alkalic hypersthene or nepheline-normative olivine-basalt with high Ce/Yb_n (4–8). OAB lavas erupted from north-northwest aligned coalesced cinder cones on Fortification Hill and from cinder cones at Lava Cascade and in Petroglyph Wash (Figure 2b). SAB and OAB lavas contain porphyritic iddingsitized olivine phenocrysts in a trachytic to pilotaxitic groundmass of olivine, andesine, labradorite, diopsidic-augite and iron oxide. Coarse-grained plugs of OAB and SAB in volcanic centers consist of olivine phenocrysts in a coarse-grained interstitial groundmass of andesine, labradorite, diopsidic-augite and olivine. (3) Young alkalic-basalt (YAB) (4.64–4.3 Ma; Feuerbach et al., 1991; Anderson et al., 1972)– highly alkalic nepheline-normative olivine basalt with elevated Ce/Yb_n (8–16). YAB lava occurs in three locations: (1) a diatreme at Petroglyph Wash, (2) en-echelon dikes and a vent, along U.S. highway 93, 10 km south of Hoover Dam, and (3) south of Saddle Island between the North Shore road and Lake Mead (Smith, 1984). The matrix of YAB ranges from glassy to interstitial or pilotaxitic and contains microlites of plagioclase, altered olivine, altered diopsidic-augite and magnetite. Olivine is the primary phenocryst phase. Rare xenoliths of plagioclase-hornblende diorite occur in YAB. Ubiquitous to these young lavas are ultramafic inclusions and megacrysts of augite and kaersutite (Nielson, manuscript in preparation; Campbell and Schenk, 1950). Besides the presence of diorite inclusions in YAB, there is no petrographic evidence of crustal contamination in Fortification Hill lavas.

River Mountains

In the River Mountains (Smith, 1982; Smith et al., 1990) (Figure 2a and 2b) an andesite-dacite stratovolcano is surrounded by a field of dacite domes. Volcanism

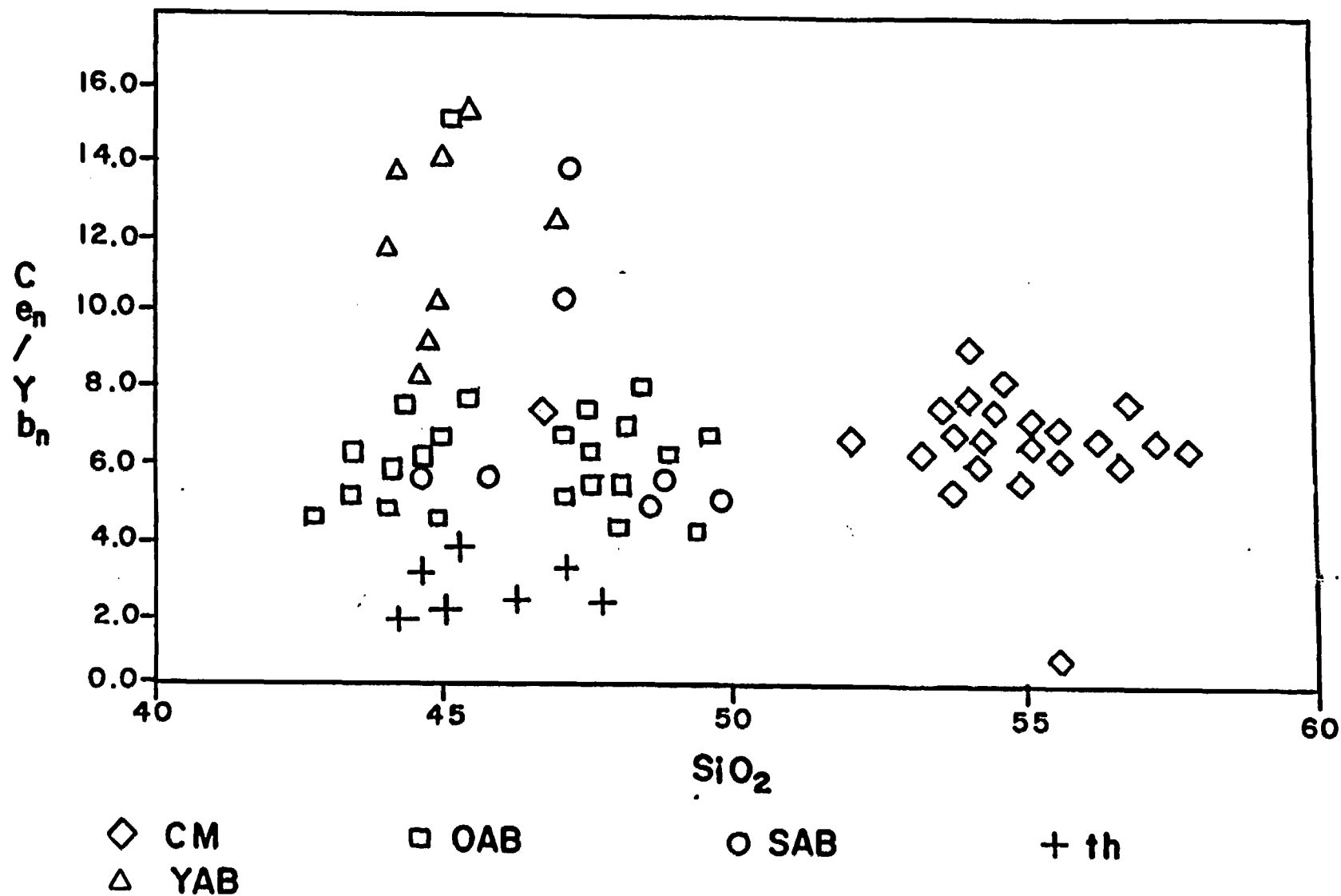


Figure 3. Plot of Ce/Yb normalized to chondrite vs. SiO_2 for volcanic rocks in the Lake Mead area. This plot divides mafic lavas into CM=Callville Mesa (open diamonds), OAB= old alkali basalts (open squares), SAB= subalkalic basalts (open circles), th=tholeiitic basalts (+), YAB= alkali basalts (open triangles).

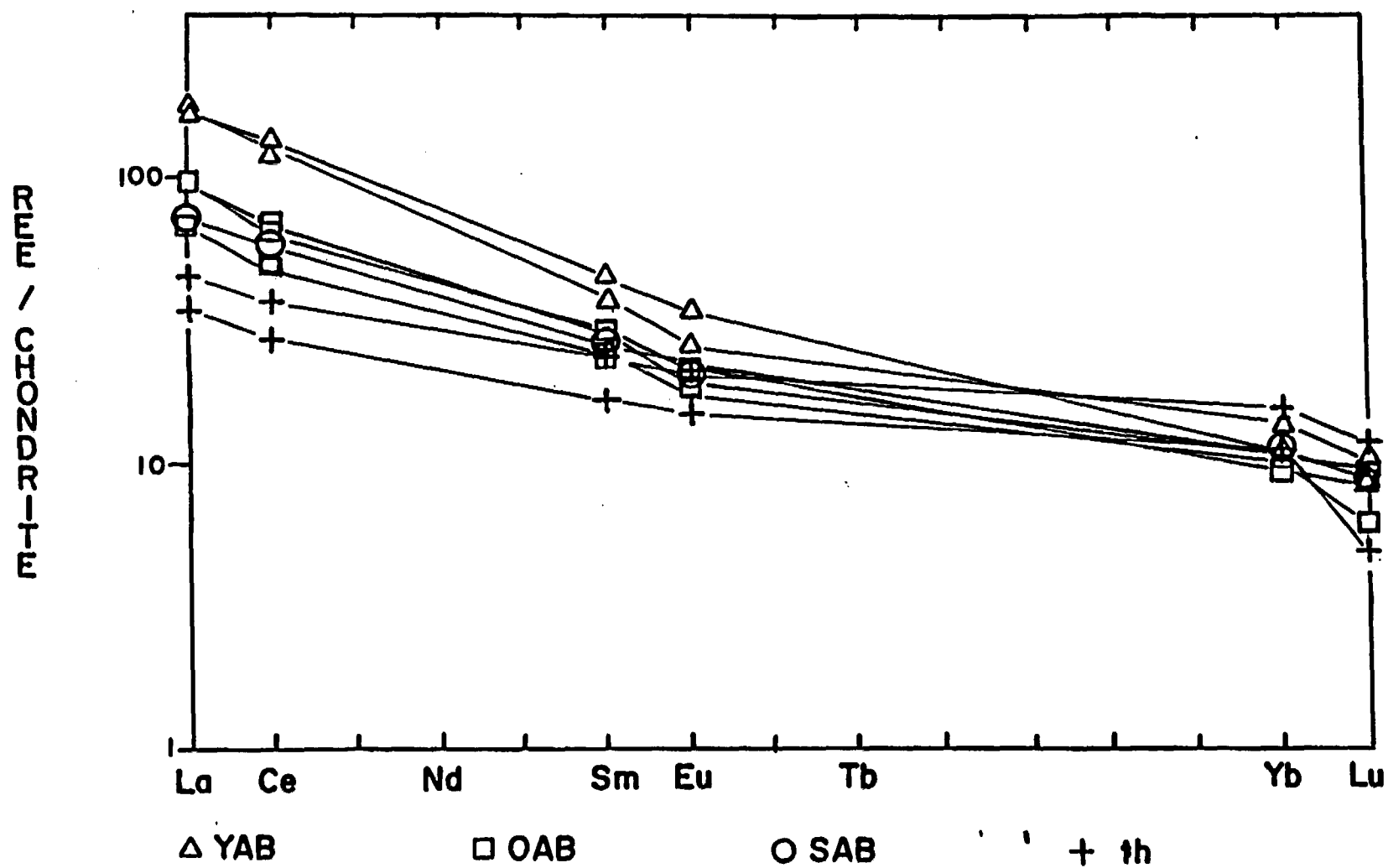


Figure 4. Chondrite normalized rare-earth element plot of volcanic rocks in the Lake Mead area. Explanation of symbols is in the caption of Figure 3.

occurred in four pulses, the first three are characterized by the eruption of calc-alkaline andesite and dacite flows and the last by rhyolite and alkali basalt. Based on available K-Ar whole rock dates (Anderson et al., 1972) volcanism began in the River Mountains at about 13.5 Ma and terminated at 12 Ma.

Boulder Wash

The Boulder Wash in the northern Black Mountains (Figure 2b) contain a 700-m-thick section of calc-alkaline dacite flows and flow breccias interbedded with flows of pyroxene-olivine andesite containing abundant xenocrysts of quartz and orthoclase (Smith et al., 1990; Naumann and Smith, 1987; Naumann, 1987). Petrographic and textural evidence of magma commingling is well developed in the volcanic section and associated plutonic rocks. Smith et al. (1990) and Naumann (1987) concluded that various mixing ratios of alkali olivine basalt and rhyolite end members are responsible for the textural variations. A dacite flow in the eastern part of the volcanic field was dated at 14.2 Ma (Thompson, 1985).

Malpais Flattop

Malpais Flattop near Willow Beach, Arizona (Figure 2b) contains a 100 m thick stack of tholeiitic basalt flows that erupted from at least two centers now expressed as wide (40 m) dikes and plugs on the west side of the Malpais Flattop mesa. A K-Ar whole rock date of 15.4 Ma was obtained from one of the dikes, however an $^{40}\text{Ar}/^{39}\text{Ar}$ date of 10.24 Ma was acquired from the same rock. These dates contrast with a 6 Ma age determined by Anderson et al. (1972). Even though the date of the Malpais Flattop is not well constrained, we conclude that eruptions at Malpais mesa occurred prior to 10 Ma; 4 m.y. earlier than the production of Fortification Hill basalts.

Eldorado Mountains

A sequence of mafic to felsic volcanic rocks erupted between 18.5 and about 12 Ma in the Eldorado Mountains (Anderson, 1971; Darvall et al., 1991) (Figure 2a). The sequence is divided into a lower section of basaltic-andesite (predominant) and rhyolite lavas (Patsy Mine volcanics; Anderson, 1971); and an upper section of basaltic andesite, dacite and rhyolite (Mt. Davis volcanics; Anderson, 1971). Mafic lavas lack petrographic and field textures characteristic of crustal contamination or magma commingling. A similar section of mafic lavas in the White Hills, Arizona (Figure 2b) formed by partial melting of mantle peridotite without significant crustal interaction (Cascadden and Smith, 1991; Cascadden, 1991). In the Eldorado Range, lavas and associated plutonic rocks span the period of most rapid extension. Patsy Mine and the lower parts of the Mt. Davis section are tilted nearly 90 degrees. Younger units are rotated less in the same structural blocks (Anderson, 1971; Darvall et al., 1991).

Volcanic Rocks in the Amagmatic Zone

Black Point

At Black Point on the west shore of the Overton Arm of Lake Mead (Figure 2b), thin flows of tholeiitic basalt (6.02 Ma; Feuerbach et al., 1991) associated with north-striking en-echelon dikes overlie gypsiferous sediments of the Tertiary Horse Spring Formation. Total outcrop area is about 12 km². Basalts at Black Point are hypersthene-normative tholeiites (TH) and have low Ce/Yb_n (2-4). They contain iddingsitized olivine, labradorite and diopsidic-augite phenocrysts within either a trachytic or ophitic groundmass. Tholeiitic lavas also contain groundmass hypersthene and pigeonite.

Callville Mesa

Basaltic andesite erupted from compound cinder cones on Callville Mesa and in West End Wash between 10.46 and 8.49 Ma (Feuerbach et al., 1991) (Figure 2b). Basaltic-andesite contains phenocrysts of euhedral to subhedral iddingsitized olivine; subhedral andesine and labradorite; and subhedral, poikilitic diopsidic-augite. Subhedral hypersthene and pigeonite are also present. Quartz and alkali-feldspar (sanidine) occur as xenocrysts that are rimmed by glass and acicular clinopyroxene (diopsidic-augite).

The vent on Callville Mesa sits on the footwall of an east-west striking down-to-the-south normal fault (Figure 2b). Flows on Callville Mesa are offset from 5 to 20 m by south-dipping west-southwest striking high-angle normal faults. Since the presence of a Paleozoic and/or Mesozoic sedimentary section is characteristic of the amagmatic zone but not of the NCREC, the presence or absence of these rocks is our main field criterion for assigning a volcano to a specific province. The volcanic center at Callville Mesa sits on the boundary between the two provinces within the Las Vegas Valley-Lake Mead fault zone. The Bitter Spring Valley fault passes just to the north and the Hamblin Bay fault projects just to the south. It is unclear whether Mesozoic and Paleozoic sedimentary rocks lie beneath the volcanic centers on Callville Mesa since volcanoes sit on a thick section of Tertiary sediments. However just to the northeast of Callville Mesa, flows of basaltic andesite rest on Tertiary sediments which in turn sit unconformably on steeply tilted Triassic and Jurassic sedimentary section. This relationship prompts the assignment of the Callville Mesa volcano to the amagmatic zone.

Las Vegas Range

The Las Vegas Range locality is composed of thin flows of alkaline basalt in a fault bounded basin just to the west of U.S. highway 93 (Figure 2a). Flows (2 km²) are mostly covered by Quaternary fanglomerate and alluvium and as a result no source area was discovered. Las Vegas Range basalt has not been dated, but since the flows are neither tilted or faulted, they are assumed to be Pliocene in age.

Hamblin-Cleopatra Volcano

The Hamblin-Cleopatra volcano (14.2-11.5 Ma) (Anderson, 1973; Thompson, 1985) which lies along the north shore of Lake Mead (Figure 2b), is a 60 km³ stratovolcano comprised of shoshonite, latite, trachydacite and trachyte lava (Barker and Thompson, 1989). In addition, tephra, epiclastic sediments, intrusions and a well developed radial dike system form the volcano. The volcano was dissected into three segments by left-lateral strike-slip faulting associated with the LMFZ (Anderson, 1973; Thompson, 1985; Barker and Thompson, 1989).

Basalt of Government Wash

Olivine-phyric alkali basalt crops out in Government Wash just north of Lake Mead. An 80-m-thick section of flows and agglomerates are interbedded with the Lovell Wash member of the Tertiary Horse Spring Formation (Duebendorfer, personal communication, 1991). Basalt of Government Wash is dated at 12 Ma (Duebendorfer et al., 1991).

Volcanic Rocks at Gold Butte and in the Grand Wash Trough

The Grand Wash trough and the Gold Butte area (Figure 2a) contain flows of olivine-phyric alkali basalt (Cole, 1989). Basalt in the Grand Wash trough is dated at 3.99 to 6.9 Ma and is younger than basalt flows to the west in the Gold Butte area (9.1 to 9.4 Ma) (Cole, 1989). Cole (1989) suggested that the alkali basalt formed by partial melting of asthenospheric spinel peridotite. Melts were not appreciably fractionated during ascent or contaminated by crustal materials.

SOURCE OF MAFIC LAVAS AND CRUSTAL CONTAMINATION

Introduction

In this section we argue that the source of the mafic volcanic rocks in the Lake Mead area was either the lithospheric mantle or asthenosphere. Our assumption is that isotopic variation is due to differences in the mantle source. The possibility exists, however, that some or all of the variation could be due to crustal contamination. We demonstrate that crustal contamination was only significant in intermediate lavas of the River Mountains and mafic lavas at Callville Mesa and was not an important component in the source of mafic lavas in other areas.

Isotopic and trace element data divide the mafic lavas into two groups (Figure 5).
1. Low $^{87}\text{Sr}/^{86}\text{Sr}$, high ϵNd . This group is characterized by $^{87}\text{Sr}/^{86}\text{Sr} = 0.703\text{-}0.705$ and $\epsilon\text{Nd} = -1$ to $+4$ and includes the alkali basalts of the Fortification Hill field and Grand Wash trough. Trace-element distributions are similar to the OIB average of Fitton et al. (1991) (Figure 6). Basalts with this isotopic and trace element signature probably originated by partial melting of the asthenospheric mantle.

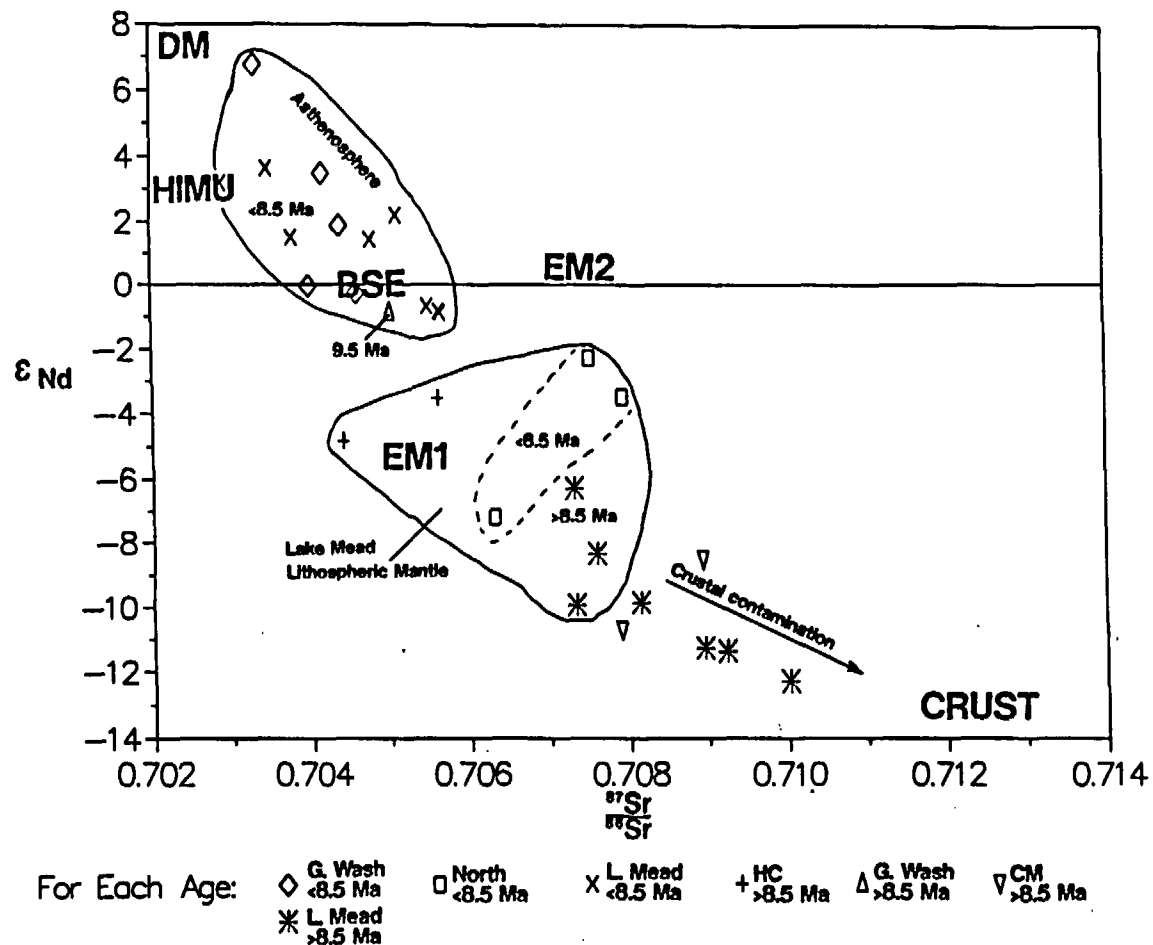
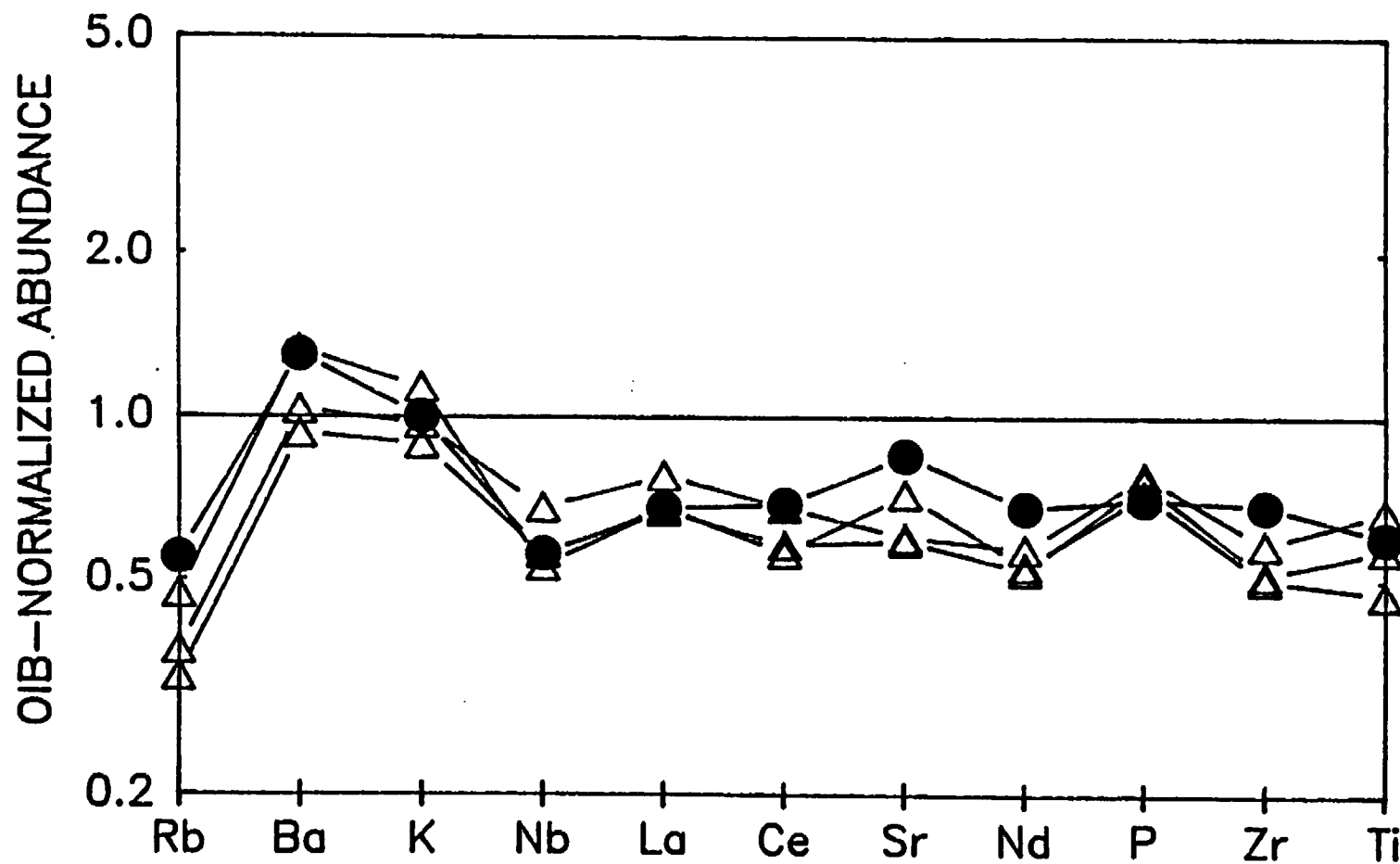


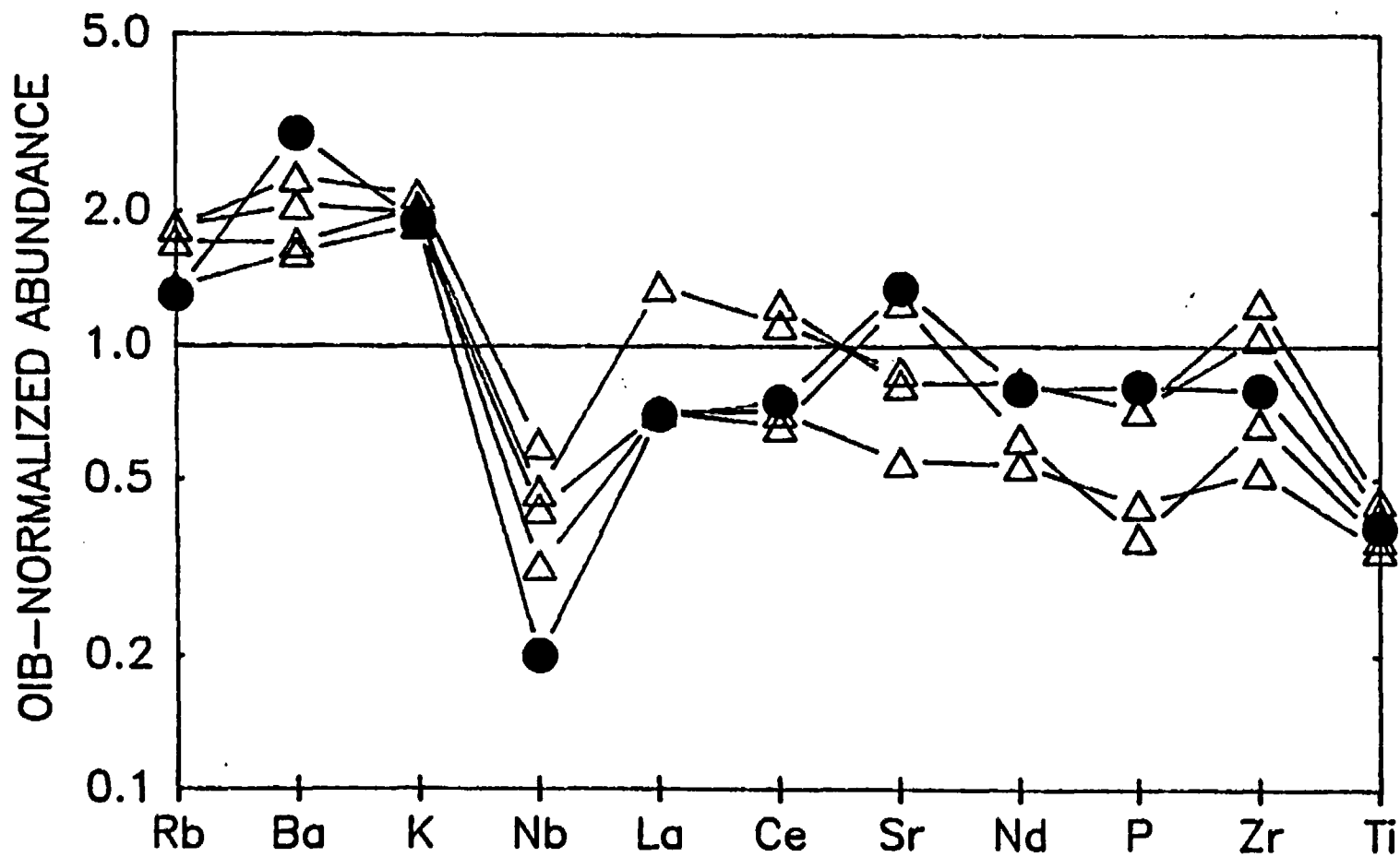
Figure 5. ϵ Nd vs. $^{87}\text{Sr}/^{86}\text{Sr}$ plot for volcanic rocks in the Lake Mead area. Isotopic data divides the volcanic rocks into two groups. One with high $^{87}\text{Sr}/^{86}\text{Sr}$ and low ϵ Nd and the other characterized by lower $^{87}\text{Sr}/^{86}\text{Sr}$ and higher ϵ Nd. Prior to extension (pre-9 Ma) mafic volcanic rocks both to the north and south of the Lake Mead fault zone had isotopic compositions characteristic of a lithospheric mantle source (group 2 with higher $^{87}\text{Sr}/^{86}\text{Sr}$ and lower ϵ Nd). After extension, the isotopic composition of volcanic rocks to the south of the LMFZ shifts to lower $^{87}\text{Sr}/^{86}\text{Sr}$ and higher ϵ Nd, while the signature of mafic volcanic rocks to the north of the LMFZ remains unchanged. These changing patterns of isotopic compositions demonstrate that a mantle domain boundary formed in late-Miocene time during an episode of upper crustal extension. Crustal contamination affected rocks of the River Mountains, but resulted in only a minor shift in isotopic ratios (refer to Figure 7). Mantle components are provided for reference.

Figure 6. Spiderplots of incompatible elements vs. abundance normalized to OIB average of Fitton et al. (1991).

a. Mafic volcanic rocks in the NCREC erupted after about 9 Ma (open triangles) compared with average Transition Zone lavas (solid circles) of Fitton et al. (1991).



b. Mafic volcanic rocks in the Lake Mead area erupted prior to 9 Ma (open triangles) compared with average Western Great Basin lavas (solid circles) of Fitton et al. (1991).



2. High $^{87}\text{Sr}/^{86}\text{Sr}$, low $\epsilon \text{ Nd}$. This group has $^{87}\text{Sr}/^{86}\text{Sr} = 0.705\text{--}0.710$ and $\epsilon \text{ Nd} = -4$ to -12 and includes mafic lavas in the River Mountains, Eldorado range, Boulder Wash area, Hamblin-Cleopatra volcano, Malpais Flattop, Government Wash exposure and in the Las Vegas Range. This group is similar in isotopic and trace element composition to mafic lavas of the Western Great Basin mantle province (Fitton et al., 1991; equivalent to the Southern Nevada basalts of Farmer et al., 1989) (Figure 6) and probably formed by partial melting of the lithospheric mantle.

Mantle Components and Crustal Contamination

Andesite and dacite in the River Mountains show abundant field and petrographic evidence of assimilation and magma commingling (Smith et al., 1990). Alkali basalt lacks evidence of contamination and was considered by Smith et al. (1990) to have been generated by partial melting of mantle peridotite. Intermediate lavas in the River Mountains may represent hybrid compositions formed by the commingling of mafic and felsic end-members. This is confirmed by a positive correlation between $^{87}\text{Sr}/^{86}\text{Sr}$ and SiO_2 (Figure 7). A mixing line between basalt and rhyolite end members of the mixing sequence provides a quantitative estimate of the magnitude of isotopic shift due to magma commingling (Figure 5). This shift is no more than 4 units in $\epsilon \text{ Nd}$ and 0.002 in $^{87}\text{Sr}/^{86}\text{Sr}$.

OAB, SAB and YAB in the Fortification Hill field have $\epsilon \text{ Nd} = -1$ to 3 , $^{87}\text{Sr}/^{86}\text{Sr} = 0.703\text{--}0.705$, $^{206}\text{Pb}/^{204}\text{Pb} = 17.8\text{--}18.7$ and $^{208}\text{Pb}/^{204}\text{Pb} = 38\text{--}38.5$ and lie within the field of OIB-lavas (Figures 8 and 9) (Zindler and Hart, 1986). We infer that these magmas represent the melting of a source composed of a mixture of enriched mantle with a bulk earth signature with variable amounts of depleted asthenosphere (PREMA) and HIMU-mantle. YAB, SAB and OAB plot between bulk earth composition and higher values of $\epsilon \text{ Nd}$ and $^{206}\text{Pb}/^{204}\text{Pb}$ (Figure 10). If PREMA were the other end-member, trends toward lower $^{206}\text{Pb}/^{204}\text{Pb}$ and higher $\epsilon \text{ Nd}$ would be expected. This is the case for alkali basalts in the Grand Wash trough, Arizona plotted for comparison on Figure 10 (Cole, 1989). We suggest that the trend toward higher rather than lower Pb is due to the addition of HIMU-mantle ($\epsilon \text{ Nd} = 3.5$, $^{207}\text{Pb}/^{204}\text{Pb} = 15.85$). The residence of HIMU, however, is enigmatic. It may reside in the lithospheric mantle or upper asthenosphere (Zindler and Hart, 1985; Hart, 1988) or as detached oceanic slabs deep within the mantle (Weaver, 1991b). High Sr and Ba and low Nb on spiderplots normalized to the OIB average island composition of Fitton et al. (1991) suggest that OAB and SAB also contain a lithospheric component and are more similar to Transition Zone than Basin and Range suites (Figure 6). EM1, a potential candidate for the lithospheric component is ruled out, since addition of this component will result in negative values of $\epsilon \text{ Nd}$.

The isotopic characteristics of the Fortification Hill field are similar to those of the Springerville volcanic field in the Transition Zone of southeastern Arizona (Cooper and Hart, 1990). These authors attribute isotopic variation throughout the suite of Springerville lavas to mixing of PREMA, EM1 and HIMU. The other group contains high $^{87}\text{Sr}/^{86}\text{Sr}$, low $\epsilon \text{ Nd}$ and displays enriched an enriched trace element pattern compared to OIB. These mafic lavas originated by partial melting of mantle lithosphere.

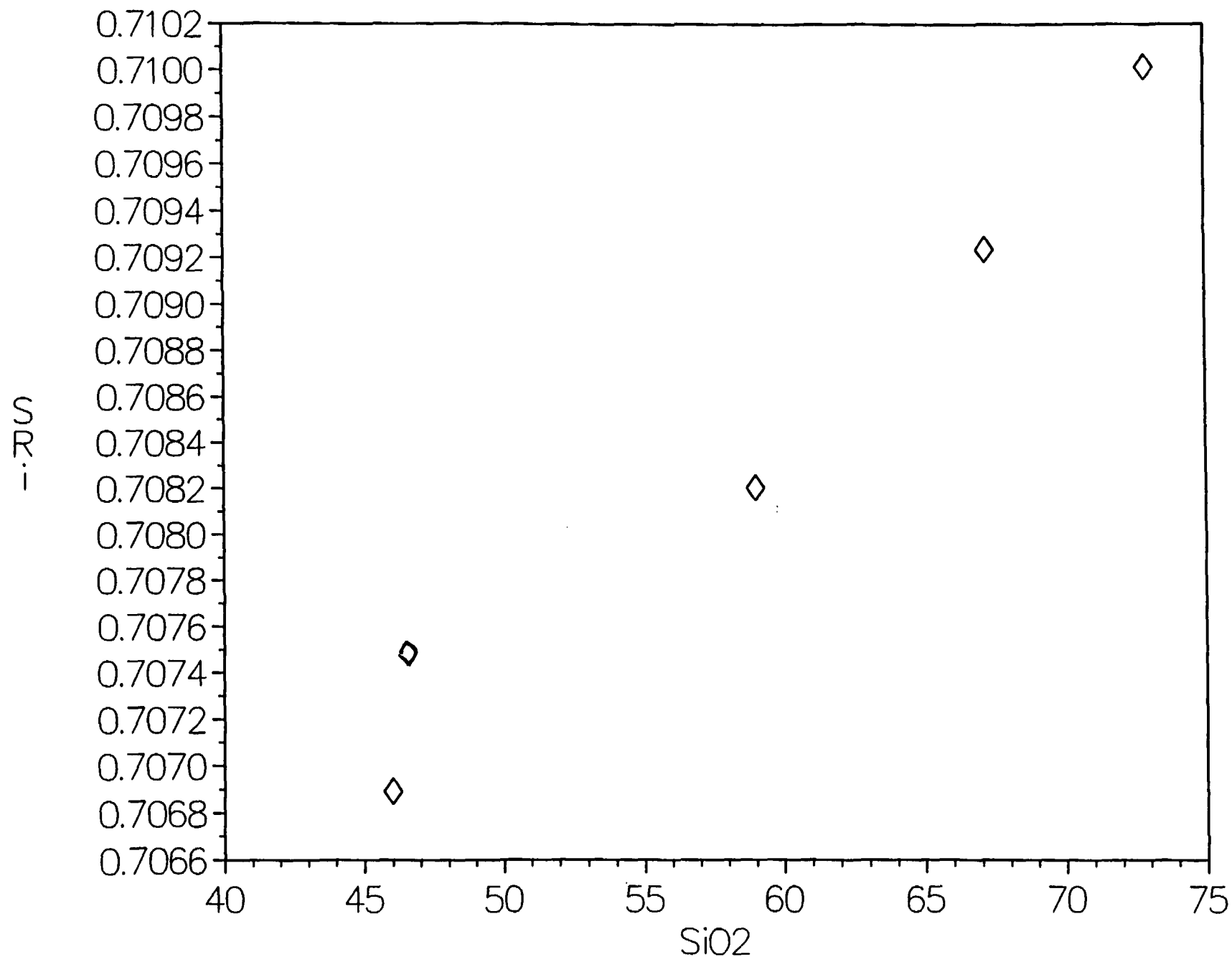


Figure 7. Plot of $^{87}\text{Sr}/^{86}\text{Sr}$ vs. SiO_2 for volcanic rocks of the River Mountains. The positive correlation suggests that contamination with a crustal component played a part in their evolution.

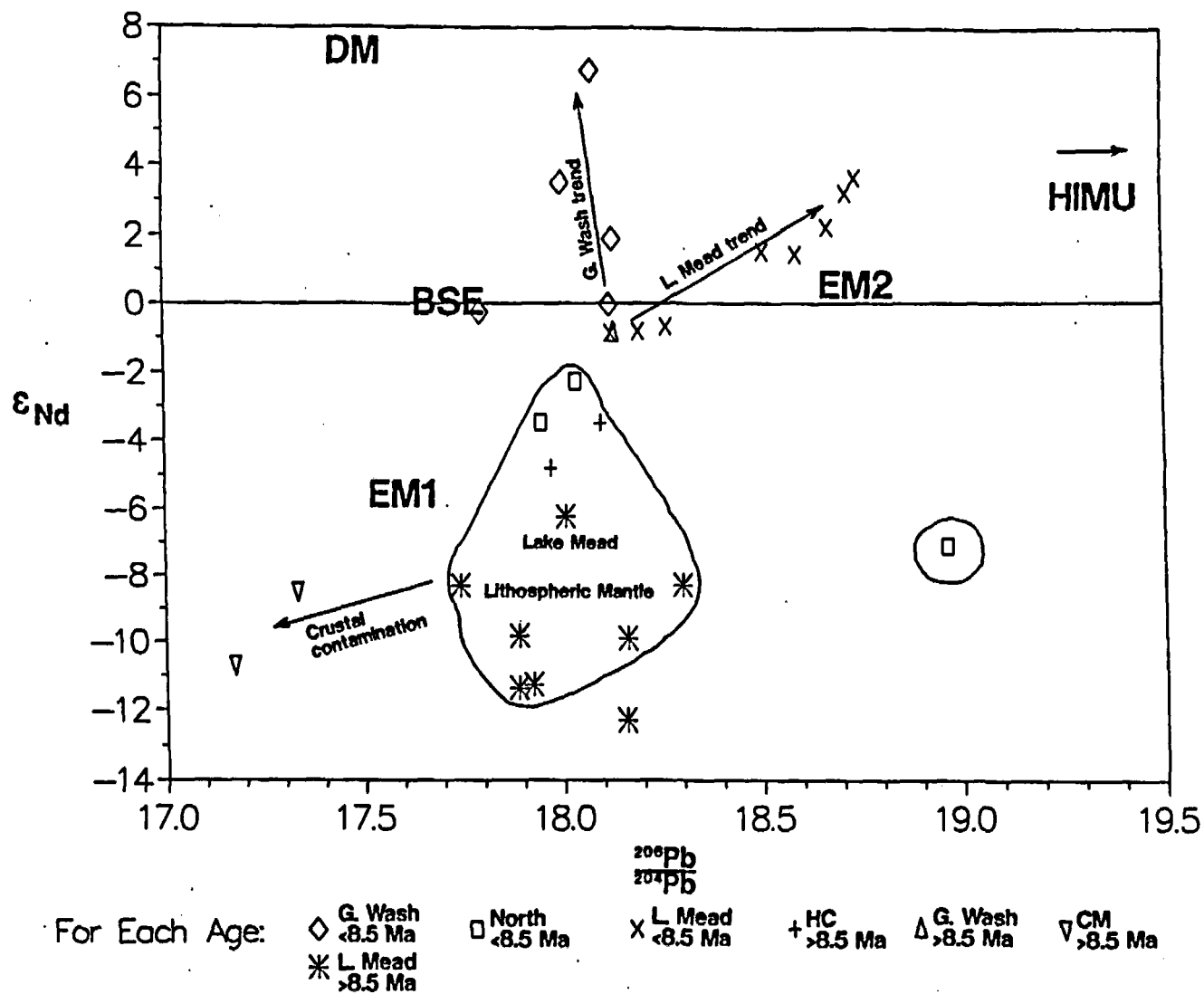


Figure 8. Plot of ϵ_{Nd} vs. $^{206}Pb/^{204}Pb$ for volcanic rocks of the Lake Mead area. Rocks of the Lake Mead trend (Fortification Hill basalt) plot on a line that projects toward HIMU-mantle, whereas the field of Grand Wash basalts points toward PREMA. Crustal contamination of Callville Mesa lavas with a low $^{206}Pb/^{204}Pb$, and lower ϵ_{Nd} crustal is also displayed.

Tholeiitic magmas at Black Point, Nevada plot on a line between enriched mantle and EM1 lithospheric mantle (Hart, 1985) on $\epsilon \text{ Nd}$ - $^{206}\text{Pb}/^{204}\text{Pb}$ and $^{208}\text{Pb}/^{204}\text{Pb}$ - $^{206}\text{Pb}/^{204}\text{Pb}$ plots and probably represent a mixture of these components (Figure 8 and 9). Also, trends toward increasing Rb/Sr, Th/Nb and La/Nb (Figure 10) and elevated (0.708) suggest that these lavas may have been contaminated as they passed through the crust, however this contamination was not sufficient to appreciably change either the $^{87}\text{Sr}/^{86}\text{Sr}$ or $\epsilon \text{ Nd}$ values.

Callville Mesa lavas have $^{87}\text{Sr}/^{86}\text{Sr} = 0.708\text{-}0.709$ and $\epsilon \text{ Nd} = -8$ to -10 and are similar in isotopic compositions to mafic lavas of the Western Great Basin mantle province (Fitton et al., 1991; equivalent to the Southern Nevada basalts of Farmer et al., 1989) (Figure 6), however, Callville Mesa lavas differ by having lower Pb ratios ($^{207}\text{Pb}/^{204}\text{Pb} = 15.45\text{-}15.5$; $^{208}\text{Pb}/^{204}\text{Pb} = 37.7\text{-}38$; $^{206}\text{Pb}/^{204}\text{Pb} = 17.2\text{-}17.4$) than basalts of the Western Great Basin province ($^{207}\text{Pb}/^{204}\text{Pb} = 15.6$; $^{208}\text{Pb}/^{204}\text{Pb} = 38.7$; $^{206}\text{Pb}/^{204}\text{Pb} = 18.3$) (Figure 6) and by displaying ample evidence of crustal contamination. The low $\epsilon \text{ Nd}$ and high $^{87}\text{Sr}/^{86}\text{Sr}$ of Callville Mesa lavas suggests the addition of a lithospheric component like EM1. When incompatible trace element abundances (Figure 6) (Fitton et al., 1991) are compared to average distributions of magmatic provinces in the western U.S.A., Callville Mesa lavas are enriched in Ba, K, and Sr and depleted in Nb and Ti. This signature is typical of lithospheric mantle and especially of mafic lavas of the Western Great Basin and Transition zone provinces (Fitton et al., 1991). Whether Callville Mesa-magma represents a direct partial melt of lithospheric mantle or a mixture of enriched mantle and lithosphere is a matter of conjecture. The most primitive Callville Mesa lava has chemical similarities to Fortification Hill basalt which has a strong enriched mantle contribution. This flow may represent Callville Mesa magma uncontaminated by lithosphere. Other Callville Mesa lavas may be mixtures of enriched mantle and a lithospheric component. Petrography, trace element chemistry and low Pb isotopic compositions suggest that Callville Mesa lavas were subsequently contaminated by crust. The crustal component has ($^{87}\text{Sr}/^{86}\text{Sr}$) > 0.710 , low Pb isotope ratios, and $\epsilon \text{ Nd} < -10$ (Figure 5, 9 and 10). We suggest that the crustal contaminant is similar in chemistry to Proterozoic rocks of the Mojave crustal province which extends into the Lake Mead area (Wooden and Miller, 1990). Although, rocks of the Mojave province display a wide range of Pb isotope values, low ratios ($^{207}\text{Pb}/^{204}\text{Pb} < 15.5$; $^{208}\text{Pb}/^{204}\text{Pb} < 38$; $^{206}\text{Pb}/^{204}\text{Pb} < 17.4$) are common (Figure 8 and 9). Because of the common occurrence of Quartz and sanidine xenocrysts in Callville Mesa lavas, however, the contaminant is assumed to be a felsic rock. AFC models suggest that no more than 20% of the crustal component is required to model the generation of the basaltic andesites from their basaltic parent. This amount of assimilation would result in a maximum shift of 5 units of $\epsilon \text{ Nd}$ and 0.002 in $^{87}\text{Sr}/^{86}\text{Sr}$.

Summary and Discussion

Summary

There are two isotopically and chemically distinct groups of mafic volcanic rocks

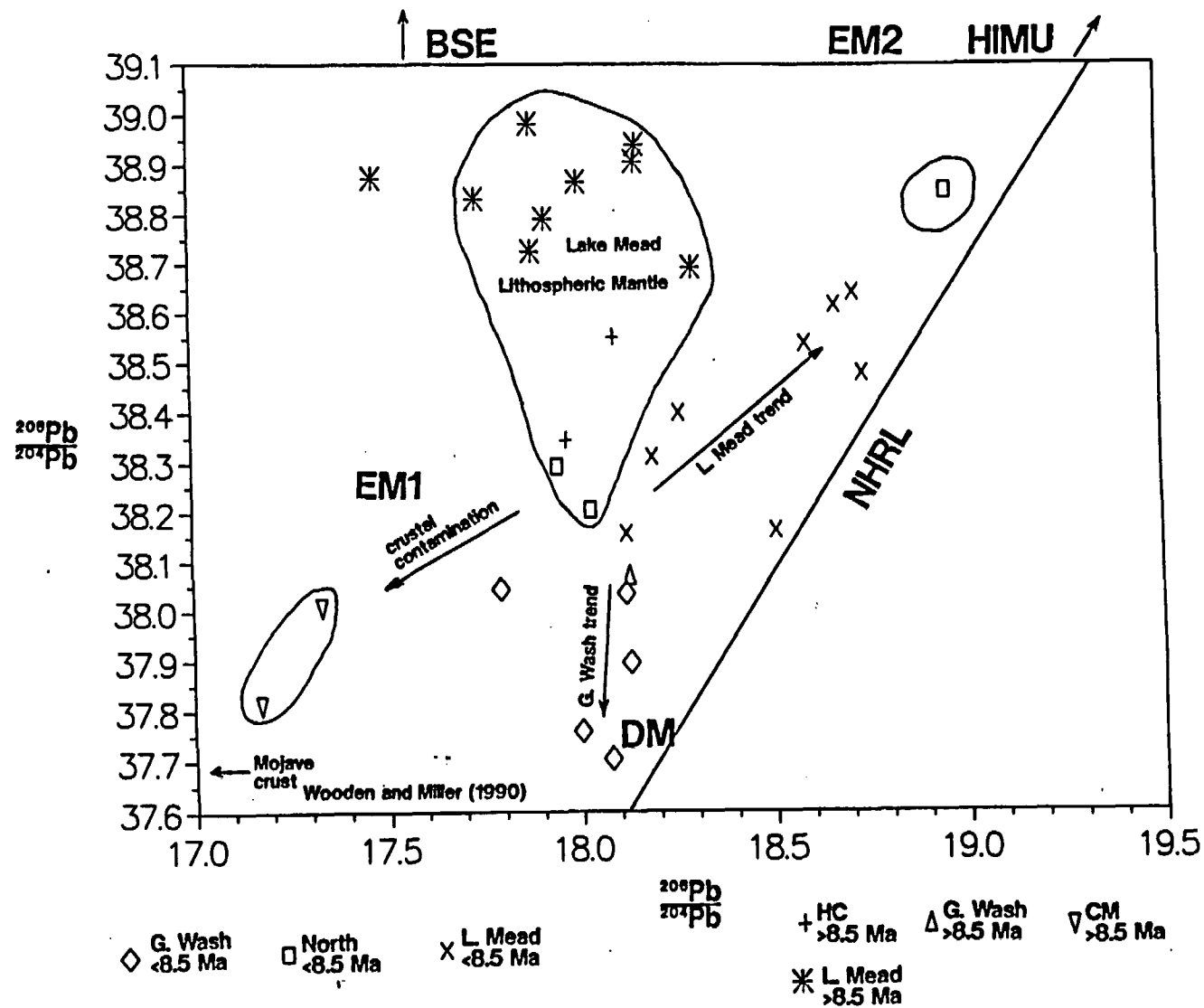


Figure 9. Plot of $^{208}\text{Pb}/^{204}\text{Pb}$ vs. $^{206}\text{Pb}/^{204}\text{Pb}$ for volcanic rocks of the Lake Mead area. Fortification Hill lavas project toward HIMU-mantle whereas Grand Wash basalts trend toward PREMA. Crustal contamination of Callville lavas with a Mojave-type crust is also shown.

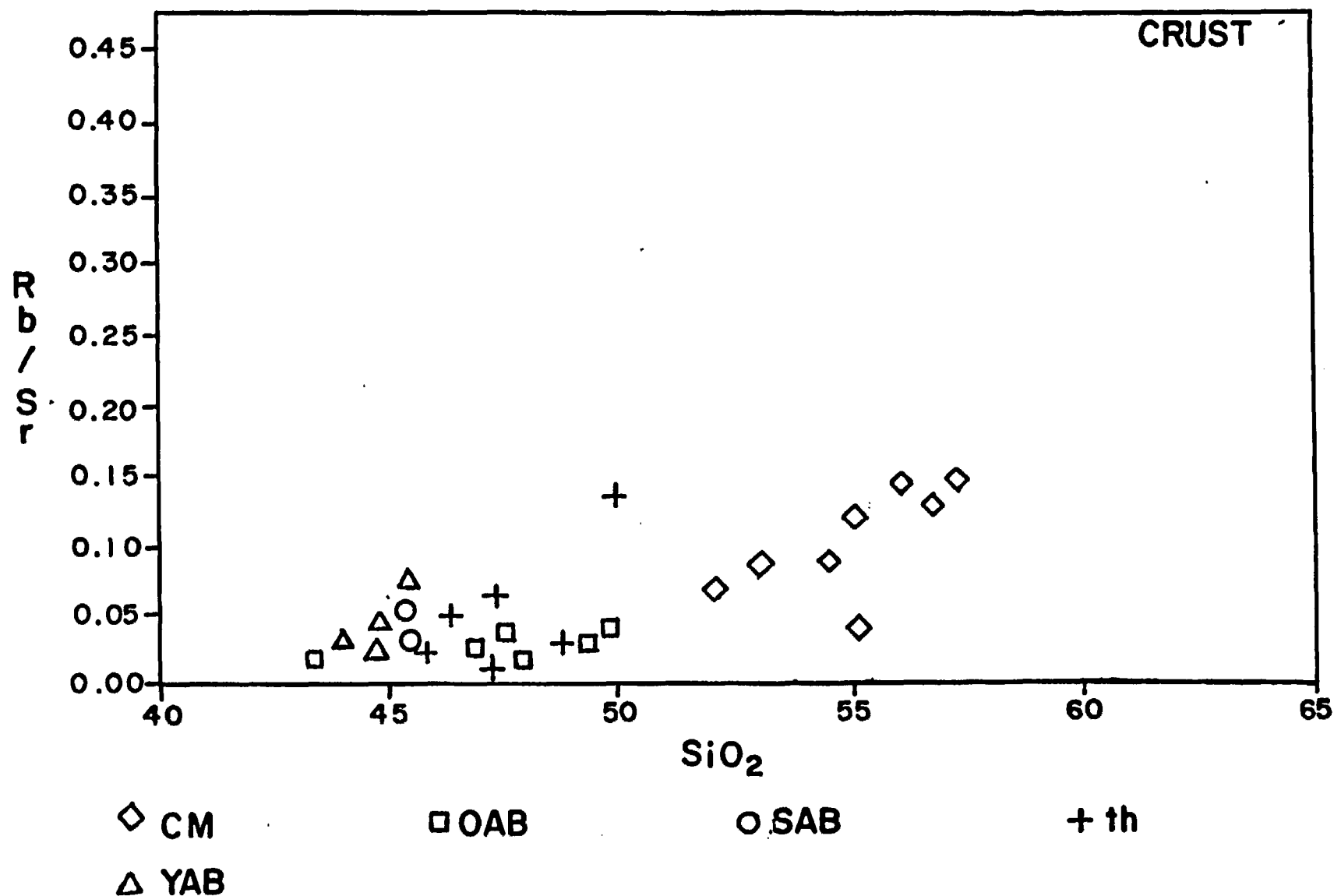
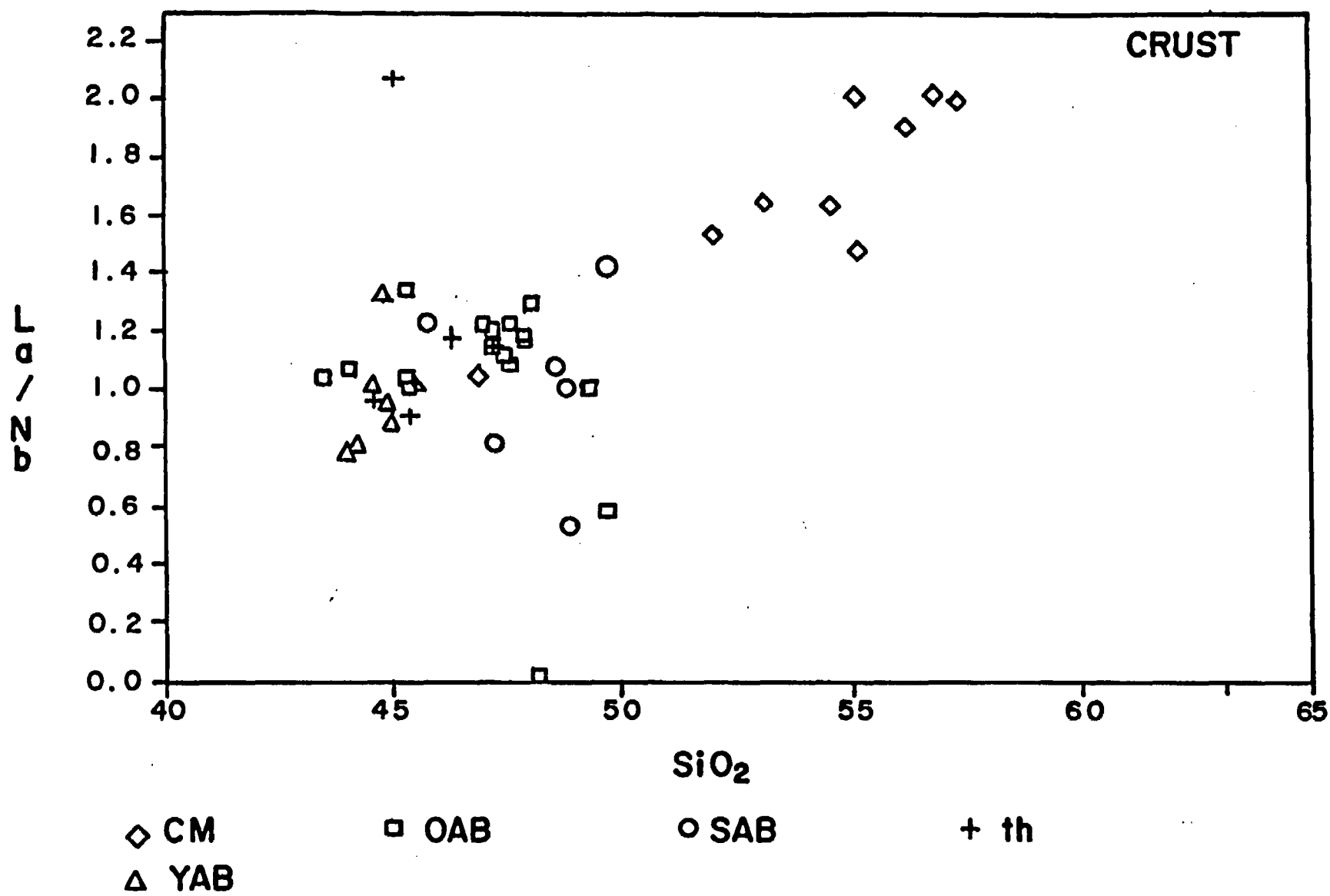
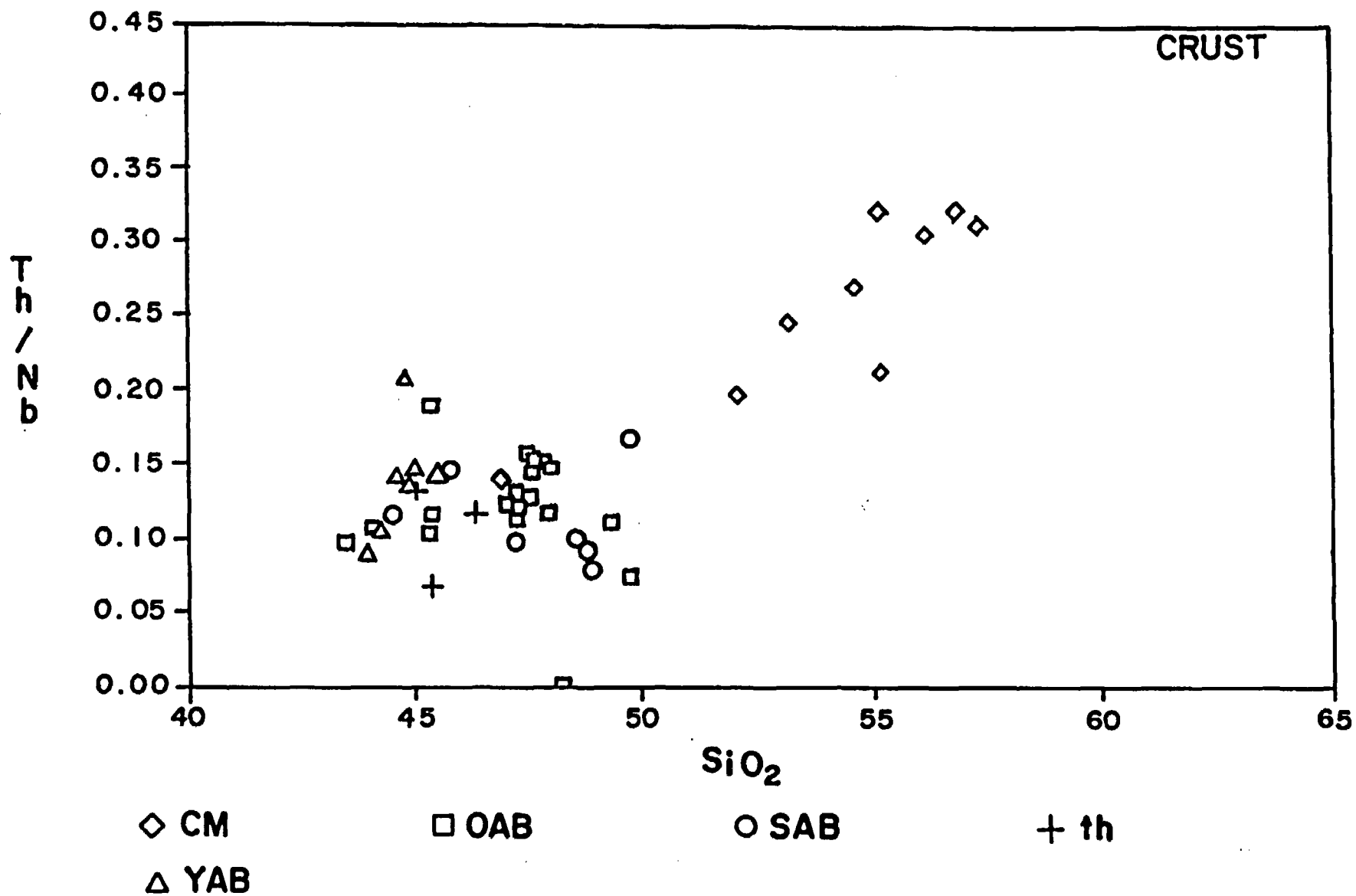


Figure 10. Plots of incompatible element ratios vs. SiO₂ for mafic lavas of Callville Mesa and Fortification Hill volcanic field. (a) Rb/Sr vs. SiO₂, (b) La/Nb vs. SiO₂ and (c) Th/Nb vs. SiO₂. Explanation of symbols is in the caption to Figure 3. Fortification Hill lavas show no evidence of crustal contamination, but Callville Mesa and to a lesser extent the tholeiitic lavas trend toward crustal values and may have been contaminated.



10C



in the Lake Mead area. One characterized by low $^{87}\text{Sr}/^{86}\text{Sr}$, high ϵ Nd and OIB trace element patterns. Lavas of this group mainly occur in the NCREC. They are similar to OIB and are the result of mixing of asthenospheric and lithospheric components. OAB and SAB are mixtures of enriched mantle of bulk earth composition with depleted mantle (PREMA) and HIMU-mantle. YAB have a greater contribution of depleted mantle than either OAB or SAB, and also contain a component of HIMU-mantle. The other group contains higher $^{87}\text{Sr}/^{86}\text{Sr}$ and lower ϵ Nd values and formed by melting of lithospheric mantle.

Crustal Contamination

Crustal contamination is a significant component only in the River Mountains and at Callville Mesa. It would require the addition of about 75% of a crustal component with ϵ Nd of -18 to change the ϵ Nd of basaltic magma from +4 to -12. This amount of contamination would greatly affect the major and trace-element composition of the mafic rocks and would significantly raise their SiO_2 content to values above 65%. Contamination is less of a factor for alkaline rocks since they are low in volume and less likely to reside in upper crustal chambers where open system processes occur. Also, high Sr and light rare-earth element concentrations of alkaline magmas tend to mask crustal contamination. Furthermore, alkaline magmas commonly contain mantle xenoliths and apparently rose quickly through the crust without contamination.

Glazner (1991) documents a time progressive trend of Sr and Nd isotopes for the Pleistocene Pisgah and Amboy volcanoes in the Mojave Desert. He attributes this trend to hybridization of an asthenospherically derived partial melt by commingling with partial melts of Late Jurassic gabbro and Proterozoic diabase. Pisgah and Amboy lavas evolved toward higher $^{87}\text{Sr}/^{86}\text{Sr}$ and lower ϵ Nd with time (Glazner, 1991). The opposite is true for FH lavas. A possible crustal contaminant for FH lavas is Precambrian (1.7 Ga) amphibolite in the footwall of the Saddle Island detachment. The amphibolite is chemically similar to FH basalts and probably is a sample of the middle to lower crust in the Lake Mead area (Duebendorfer et al., 1991). The amphibolite has $^{87}\text{Sr}/^{86}\text{Sr}=0.703$ and may represent melting of PREMA or MORB. Mixing of this crustal component with asthenospherically derived enriched mantle will result in the observed linear trend in the $^{87}\text{Sr}/^{86}\text{Sr}$ - ϵ Nd system. We do not favor this interpretation, since the amphibolite is a rare rock type in Proterozoic exposures and therefore may not be a representative sample of the middle-lower crust in the Lake Mead area.

Depth of Melting

Our models assume that the depth of melting remains relatively constant with time. This assumption can be tested by applying what is known regarding the geochemistry of the volcanic rocks and petrologic studies of depth of magma generation (Takahashi and Kushiro, 1983). Tholeiitic basalts are generated by partial melting of mantle peridotite with the mineral assemblage clinopyroxene, olivine, orthopyroxene at pressures of 8 to 15 Kb corresponding to depths of 24 to 45 km. Alkali basalts are

produced from a similar source at pressures between 15 and 20 Kb corresponding to a depth of about 45 to 60 km. Crustal extension is accompanied by the rise of the geotherm to higher levels of the lithosphere. Therefore the expected relationship between extension and volcanism is the production of tholeiitic (subalkalic) basalts during extension when isotherms are elevated and alkali basalts late when isotherms relax. In the Lake Mead area, however, the most primitive basalts are generally alkalic regardless of age and relationship to extension. Exceptions are tholeiitic basalts at Black Point and Malpais Flattop. Depth of melting appears to remain relatively constant with time. Therefore, we assume that variations in chemical and isotopic compositions are due to the rise of the lithospheric mantle-asthenosphere boundary rather than changes in the depth of melting.

DISCUSSION

In this section, we argue that the boundary between two crustal provinces, the NCREC and the amagmatic zone, corresponds to a boundary between asthenospheric mantle beneath the NCREC and lithospheric mantle beneath the amagmatic zone. We also suggest that the mantle boundary formed contemporaneously with the crustal boundary; both formed during Tertiary extension (9 to 16 Ma). Our data also show that lithospheric delamination occurred progressively to the west beneath the NCREC and reflects westward migration of crustal extension in the Lake Mead area as suggested by Axen and Wernicke (1988); Smith et al. (1990); Fitzgerald et al. (1991). We also suggest that the LMFZ represents the surface expression of the mantle boundary.

Nature of the Boundary

The boundary between the amagmatic zone and the Colorado River Extensional corridor corresponds to a contact between two mantle domains (Figures 11 and 12). The domain to the north is characterized by lithospheric mantle (EM1) ($\epsilon \text{ Nd} = -3$ to -9 ; $^{87}\text{Sr}/^{86}\text{Sr} = 0.706\text{--}0.707$). To the south mafic lavas have a OIB-mantle signature and appear to have only a minor lithospheric mantle component in their source ($\epsilon \text{ Nd} = 0$ to $+4$; $^{87}\text{Sr}/^{86}\text{Sr} = 0.703\text{--}0.705$). The contact appears to be sharp. Callville Mesa with a lithospheric mantle source is separated from Fortification Hill (OIB-lavas) by only 10 km. The contact trends to the northeast and passes between basalts exposed at Gold Butte (OIB-lavas) and the Hamblin-Cleopatra volcano (lithospheric mantle).

Mafic lavas in the terrane directly to the north of the boundary appear to be transitional in Pb isotopic signature between the NCREC and the Western Great Basin province (Figure 12). Grand Wash, Gold Butte, Black Point, Hamblin-Cleopatra and Callville Mesa have $^{206}\text{Pb}/^{204}\text{Pb}$ from 17.2 to 18. This compares to values of $^{206}\text{Pb}/^{204}\text{Pb}$ to the north between 18.2 and 18.9 and values to the south between 18.2 to 18.7. The origin of this northeast trending lower $^{206}\text{Pb}/^{204}\text{Pb}$ zone is unknown. It may represent a slice of low-Pb lithospheric mantle preserved along the domain boundary.

Age of the boundary

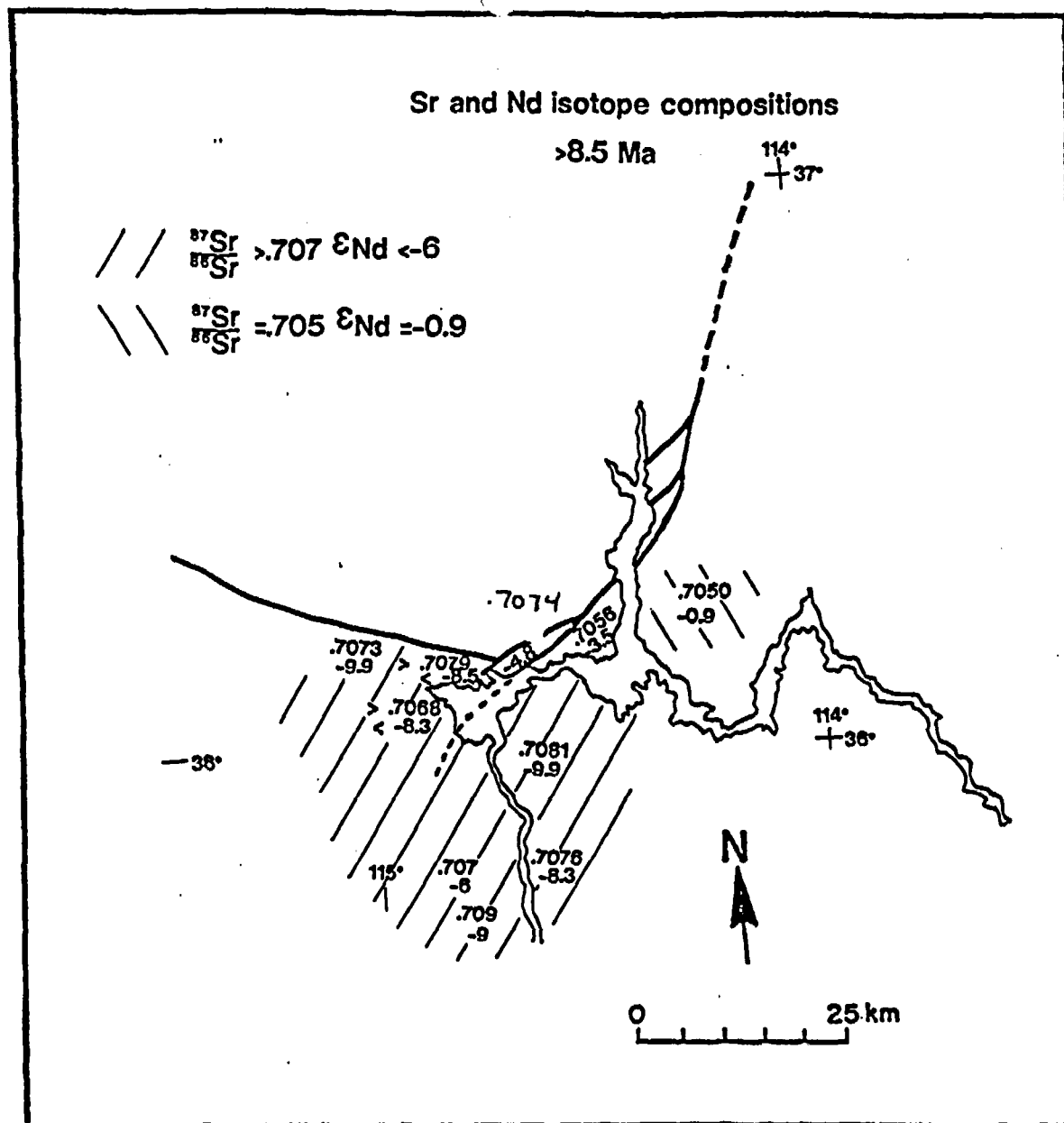
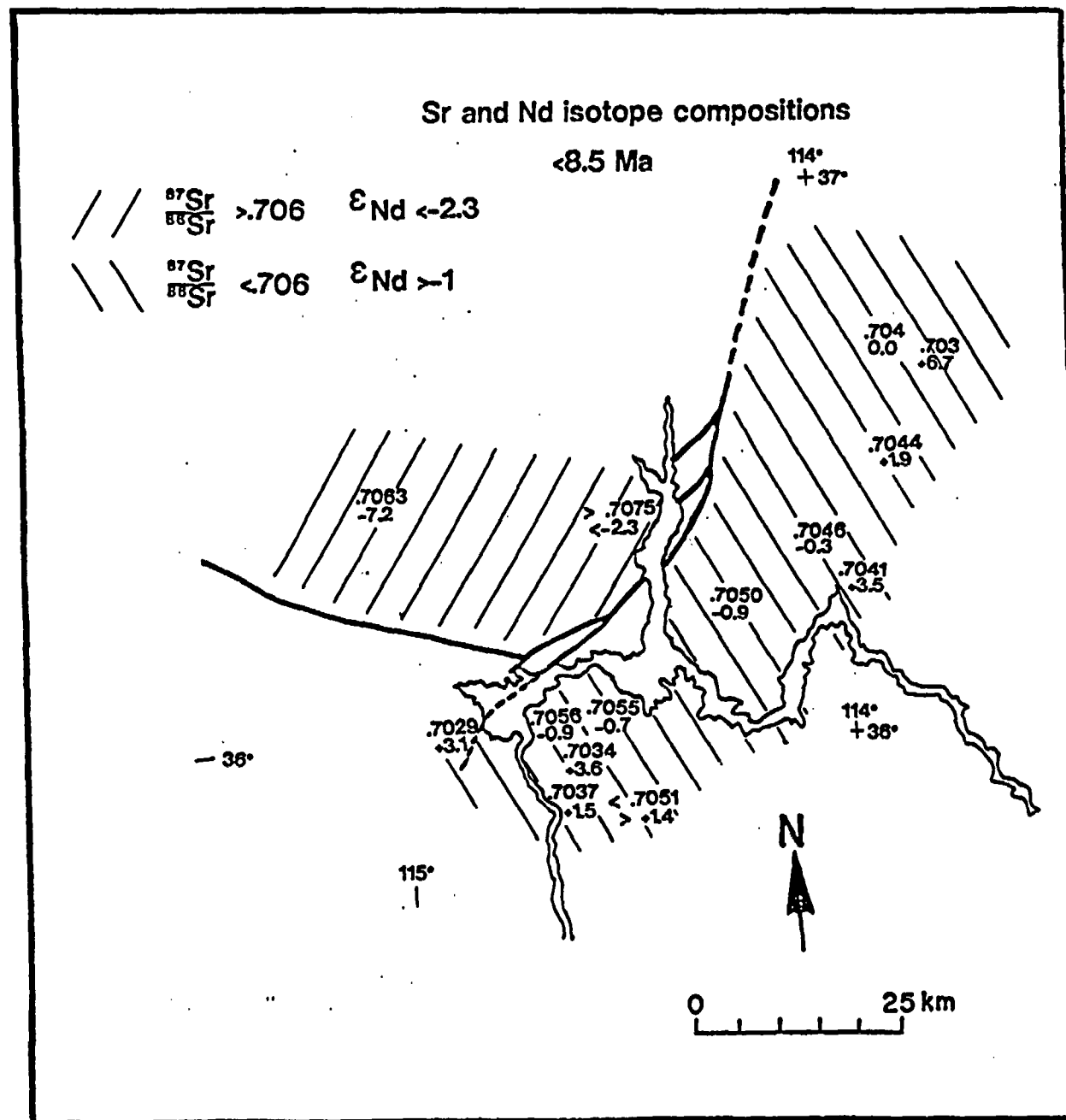


Figure 11. Map of the Lake Mead area showing distribution of Sr and Nd isotopic compositions pre- and post-8.5 Ma. Pre-8.5 Ma values are similar to the north and south of the Lake Mead fault zone and suggest the presence of a lithospheric mantle component in their source. After 8.5 Ma, values of Sr and ϵ Nd shift to lower and higher values respectively suggesting that magma formed by partial melting of asthenosphere.

Fig. 11



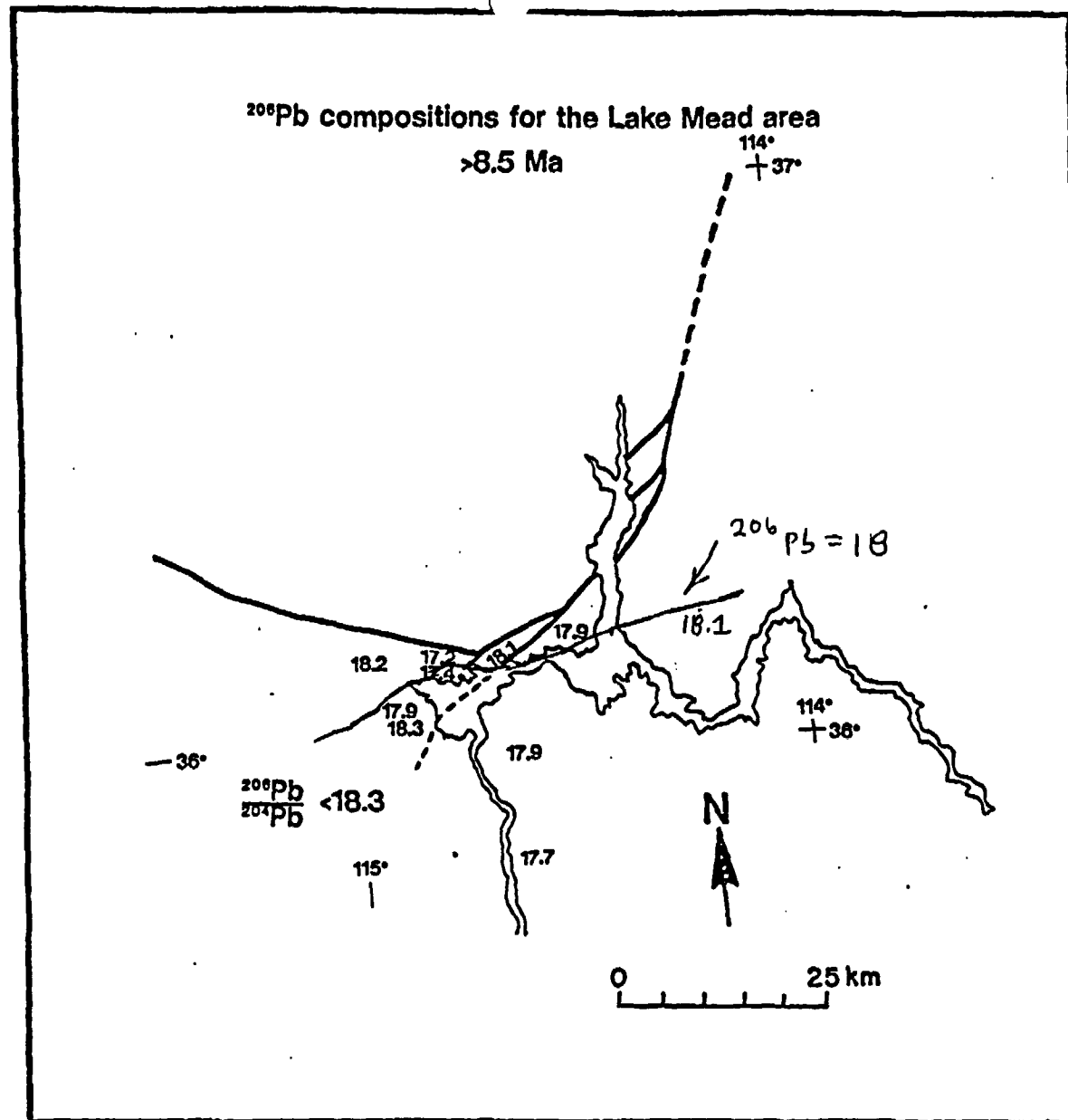
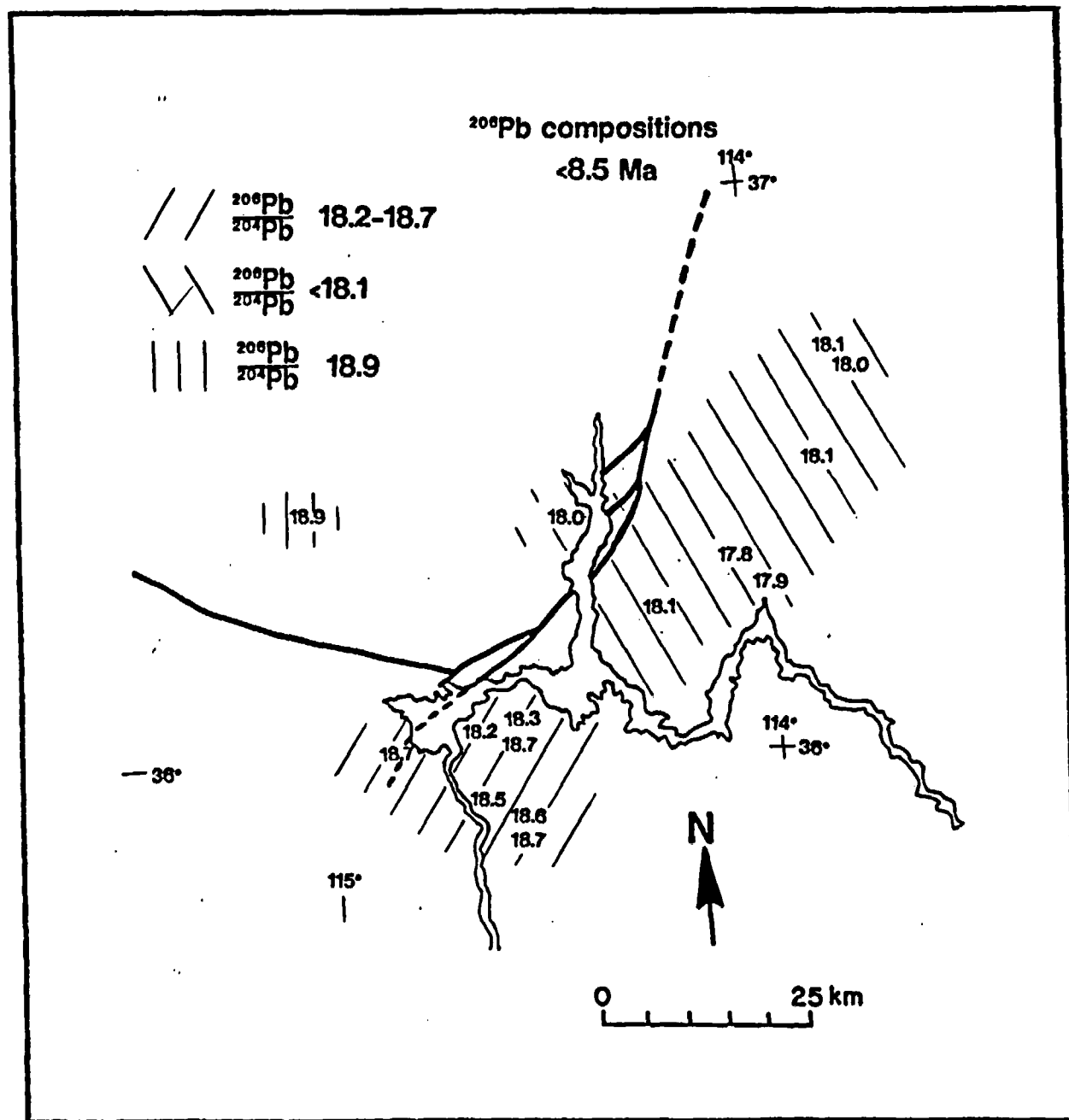


Figure 12. Map of the Lake Mead area showing the distribution of Pb isotopic compositions pre- and post-8.5 Ma. Pre-8.5 Ma values are uniform across the area. However the $^{206}\text{Pb} = 18$ contour separates lower values to the south from higher Pb values to the north and is subparallel to the Lake Mead fault zone. After 8.5 Ma Pb compositions change. Higher values are found to the south of the LMFZ and higher values to the north.

Fig. 12



Pre-extension (pre-10 Ma) ϵ Nd and $^{87}\text{Sr}/^{86}\text{Sr}$ is uniform across the boundary at about -9 and 0.707-0.708 respectively. Higher values of ϵ Nd and lower $^{87}\text{Sr}/^{86}\text{Sr}$ occur only at the Hamblin Cleopatra volcano (-4 to -6; 0.704-0.705) and in the Mount Davis lavas in the Eldorado Range (-5 to -7; 0.7067). After extension $^{87}\text{Sr}/^{86}\text{Sr}$ and ϵ Nd values shift dramatically to higher and lower values, respectively, to the south of the boundary, but remain similar to pre-extension values north of the boundary. These relationships demonstrate that the mantle boundary formed in late-Miocene time during a period of upper crustal extension.

Prior to extension, $^{206}\text{Pb}/^{204}\text{Pb}$ values are slightly but significantly higher to the north of the boundary (18-18.16) than to the south (17.7-17.9)(Figure 12). The $^{206}\text{Pb}/^{204}\text{Pb} = 18$ contour corresponds to the post-9 Ma boundary suggesting that there was a compositional difference in the lithospheric mantle at the boundary between the NCREC and amagmatic zone prior to the extensional event (Figure 12). This compositional variation may be controlled by mechanical properties of the mantle and facilitated extension south of the boundary rather than to the north. Post-extension $^{206}\text{Pb}/^{204}\text{Pb}$ values flip across the boundary; higher values are present to the south rather than to the north. Higher post-extension Pb values argue for a enriched mantle or plume component in the source of basalts erupted in the NCREC. Speculatively, this plume component may be HIMU-mantle.

Three-dimensional Model for Mantle Evolution.

Spatial and Temporal Variation in Isotopic Composition

Basalt at Gold Butte in the eastern part of the Lake Mead area erupted at 9.4 Ma and has an asthenospheric mantle component in its source. To the west of Gold Butte, contemporaneous eruptions at Callville Mesa (9.7-10.5 Ma) and Malpais Flattop (about 10 Ma) produced mafic lavas with a lithospheric mantle signature. This pattern suggests that at about 9.5 Ma lithospheric mantle was absent or thin in the east but present in the west. By 6 Ma, mafic lavas in the west display an asthenospheric source. These patterns infer that lithospheric mantle was thinned to the west during extension (Figure 13).

Daley and DePaolo (1991) report isotopic compositions of basalts and basaltic-andesites from the Eldorado Range. Samples plot in two groups. Those collected from the younger Mount Davis section (15-12 Ma) have ϵ Nd = -6 to -7 and $^{87}\text{Sr}/^{86}\text{Sr} = 0.707$ and from the older Patsy Mine section (15-18.5 Ma) have ϵ Nd = -10 and $^{87}\text{Sr}/^{86}\text{Sr} = 0.708-0.709$. Daley and DePaolo (1991) suggested that these lavas formed by melting of lithospheric mantle without recognizable crustal contamination. These changes may reflect increased asthenospheric contribution to the source of the Mt. Davis section due to the thinning of the lithospheric mantle during extension.

The Three-Dimensional Model for Mantle Evolution

During extension in the NCREC, lithospheric mantle was thinned and replaced by asthenosphere progressively to the west. The replacement front moved to the west at a

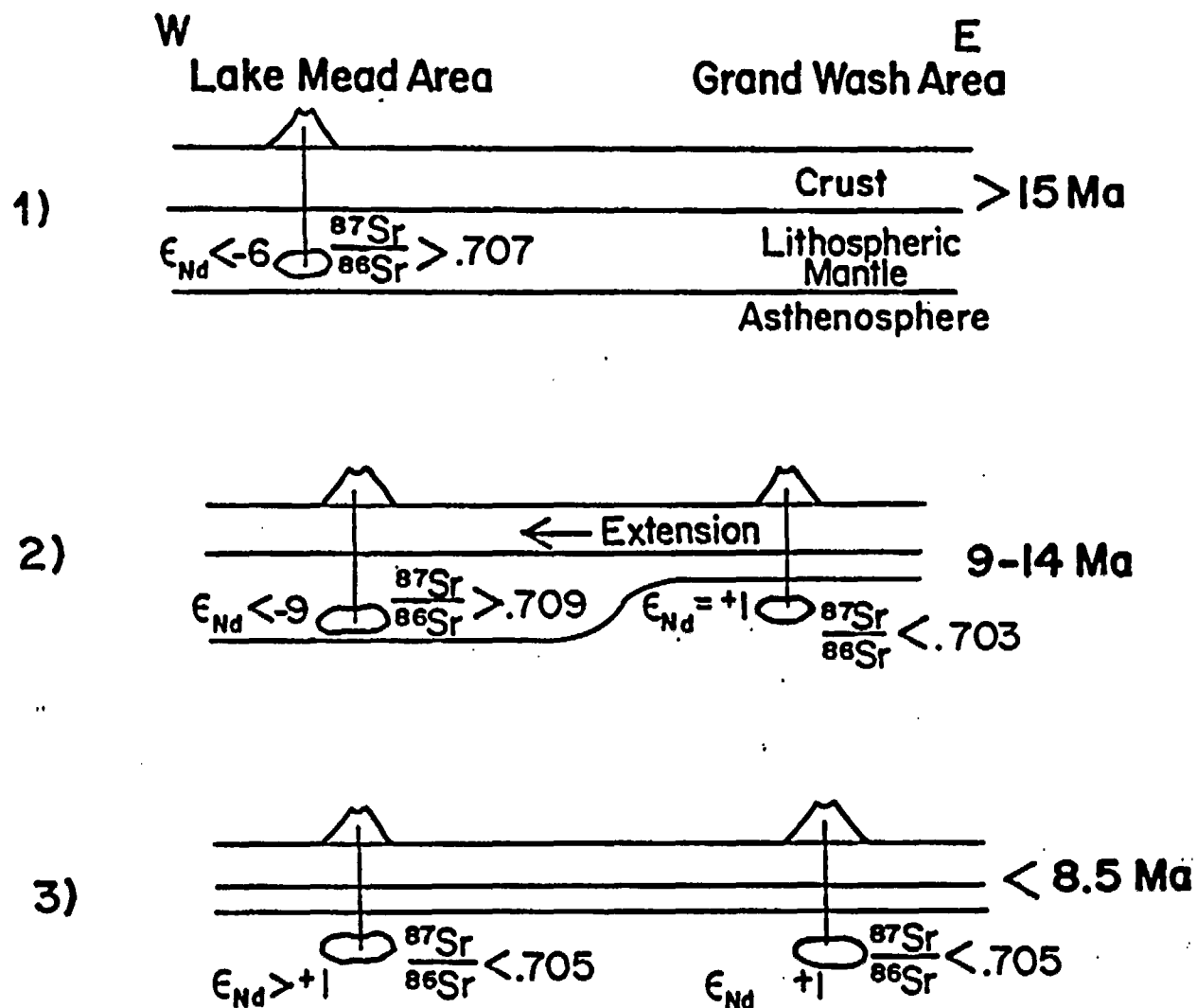


Figure 13. Model showing the evolution of mantle in the Lake Mead area during Tertiary extension.

- (1) East-West cross section prior to the major phase of extension.
- (2) Extension in the east is accompanied by the thinning of the lithospheric mantle. Thinning occurs progressively to the west in concert with upper crustal extension.
- (3) Section after the main phase of extension.

rate comparable to the westward sweep of upper crustal extension (Figure 13). To the west of the asthenosphere replacement front, lithospheric mantle apparently thins before being overrun by this front (i.e., Eldorado Mountains). During thinning and replacement of the lithospheric mantle in the NCREC, the lithospheric mantle in the amagmatic zone remained intact. Contrasting behavior to the north and south of this boundary requires that the lithospheric mantle beneath the NCREC be ripped from mantle to the north. This tear produced the mantle domain boundary over a period of nearly 6 Ma during the westward migration of extension across the Lake Mead area. The reason for the localization of the tear is somewhat speculative. However, the difference in pre-extension $^{206}\text{Pb}/^{204}\text{Pb}$ values across the boundary suggest that the domain boundary formed subparallel to an older mantle compositional contact or gradient.

Links Between Mantle and Crustal Processes

There are two competing models for upper crustal extension. The simple shear model (Wernicke, 1981) predicts that the crust will fail along a single lithospheric penetrating detachment fault. According to this model, rocks in the allochthon will deform at about the same time. The alternate model proposed by Buck (1988), Axen and Wernicke (1988), and Hamilton (1988) suggests that the allochthon deforms progressively, so that the age of extension migrates toward the active high-angle segment of the detachment ("rolling hinge model"). In the Lake Mead area, Wernicke and Axen (1988), Fitzgerald et al. (1991), and Smith et al. (1990) have suggested that upper crustal extension migrated from east to west between 16 Ma and about 9 Ma. Our geochemical data indicate that lithospheric mantle was thinned progressively to the west. At Gold Butte area in the eastern part of the Lake Mead, lithospheric mantle was thinned prior to 9.4 Ma. At Callville Mesa and Malpais Flattop, thinning occurred between about 9 and 6 Ma. Therefore, there is a spatial and temporal relationship between thinning of the lithospheric mantle and crustal extension. These data support the "rolling hinge" extensional model as applied to the Lake Mead area.

Crustal Structures and Mantle Boundaries

The Lake Mead Fault zone (LMFZ), a major late-Miocene left-lateral strike-slip fault system, closely parallels the boundary described above. The LMFZ accommodated nearly 60 km of slip between about 18 and 11 Ma. The LMFZ closely corresponds to the mantle boundary over most of its length (Figure 1 and 2b). This correspondence argues for a genetic relationship between the two features (Figure 14). The LMFZ may reflect the rejuvenation of an older lithospheric structure (evidenced by the change in pre-extension Pb values across the boundary) or it may represent the surface expression of contrasting mantle behavior across the boundary during extension. Whatever the connection, it appears that the LMFZ reflects mantle processes. It is unlikely that the fault represents a transfer structure in the upper plate of shallow detachment or that the correspondence of the crustal and mantle features is a coincidence.

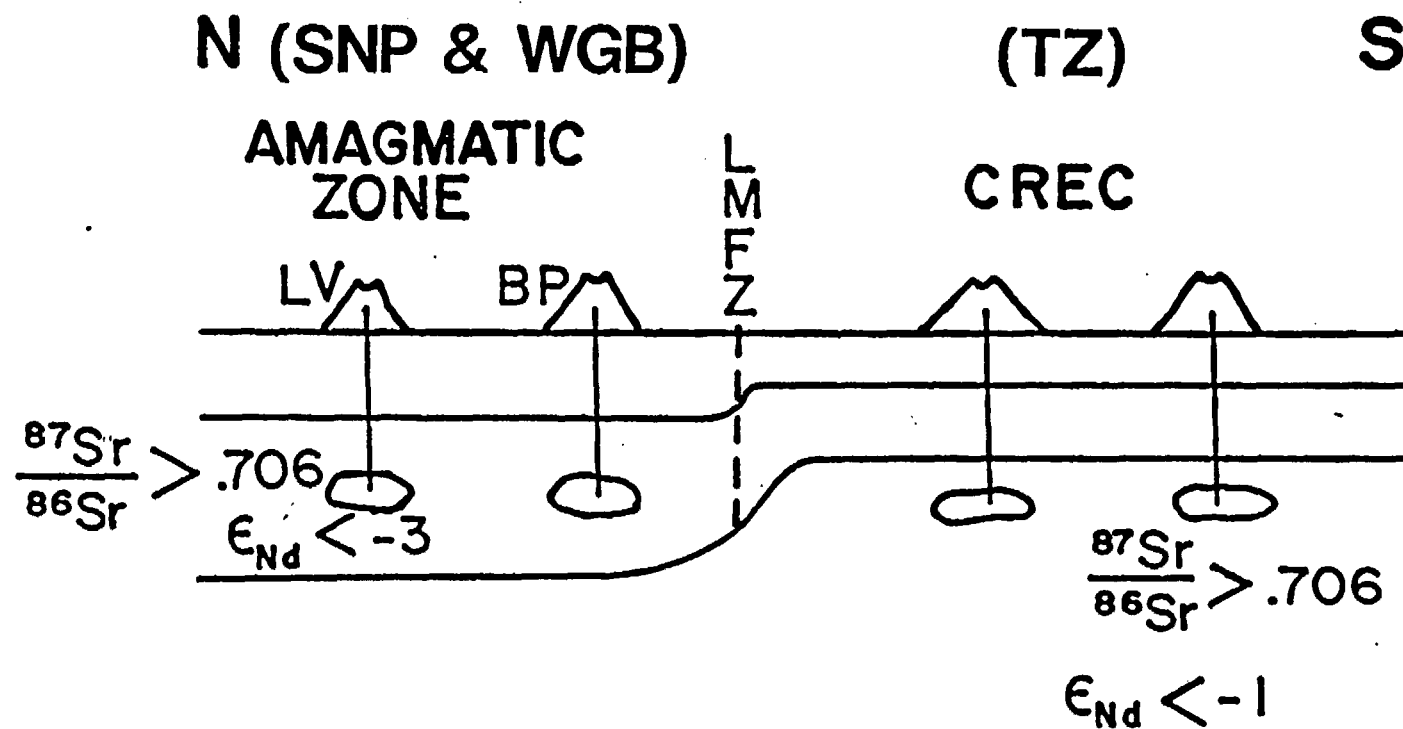


Figure 14. North-south cross section showing the change in the thickness of the lithospheric mantle at the boundary between the "amagmatic zone" and the NCREC.

CONCLUSIONS

1. There are two isotopically and chemically distinct groups of mafic volcanic rocks in the Lake Mead area. One characterized by low $^{87}\text{Sr}/^{86}\text{Sr}$, high ϵ Nd and OIB trace element patterns. They are similar to OIB and are the result of mixing of asthenospheric and lithospheric components. OAB and SAB are mixtures of enriched mantle of bulk earth composition with depleted mantle (PREMA) and HIMU-mantle. YAB have a greater contribution of depleted mantle than either OAB or SAB, and also contain a component of HIMU-mantle. The other group is characterized by higher $^{87}\text{Sr}/^{86}\text{Sr}$ and lower ϵ Nd values. These lavas formed by melting of lithospheric mantle.
2. The boundary between the amagmatic zone and the Colorado River Extensional corridor corresponds to a contact between two mantle domains. The domain to the north is characterized by lithospheric mantle (EM1) (ϵ Nd = -3 to -9; $^{87}\text{Sr}/^{86}\text{Sr}$ = 0.706-0.707). To the south mafic lavas have a OIB-mantle signature and appear to have only a minor lithospheric mantle component in their source (ϵ Nd = 0 to +4; $^{87}\text{Sr}/^{86}\text{Sr}$ = 0.703-0.705).
3. There is a spatial and temporal relationship between upper crustal extension and the thinning of the lithospheric mantle. During extension in the NCREC, Lithospheric mantle was thinned and replaced by asthenosphere progressively to the west. The replacement front moved to the west at a rate comparable to the westward sweep of upper crustal extension. To the west of the asthenosphere replacement front, lithospheric mantle apparently thins before being overrun by this front. During thinning and replacement of the lithospheric mantle in the NCREC, the lithospheric mantle in the amagmatic zone remained intact. Contrasting behavior to the north and south of this boundary requires that the lithospheric mantle beneath the NCREC be ripped from mantle to the north. This tear produced the mantle domain boundary over a period of nearly 6 Ma during the westward migration of extension across the Lake Mead area.
4. The $^{206}\text{Pb}/^{204}\text{Pb} = 18$ contour corresponds to the post-9 Ma boundary suggesting that there was a compositional difference in the lithospheric mantle at the boundary between the NCREC and amagmatic zone prior to the extensional event. This compositional variation may be controlled by mechanical properties of the mantle and facilitated extension south of the boundary rather than to the north.
5. The Lake Mead fault zone, a major crustal shear zone, parallels the mantle domain boundary and its location is probably directly or indirectly controlled by mantle processes.

REFERENCES

- Anderson, R.E., 1971, Thin skin distension in Tertiary rocks of southeastern Nevada: Geological Society of America Bulletin, v. 82, p. 42-58.
- Anderson, R.E., 1973, Large-magnitude late Tertiary strike-slip faulting north of Lake Mead, Nevada: U.S. Geological Survey Professional Paper 794, 18p.

- Anderson, R.E., Longwell, C.R., Armstrong, R.L., and Marvin, R.F., 1972, Significance of K-Ar ages of Tertiary rocks from the Lake Mead region, Nevada-Arizona: Geological Society of America Bulletin, v. 83, p. 273-288.
- Barker, D.S., and Thompson, K.G., 1989, Hamblin-Cleopatra volcano, Nevada: genesis of a shoshonite-latitude-trachydacite-trachyte suite: in Continental Magmatism abstracts, IAVCEI, New Mexico Institute of Mining and Geology Bulletin 131, p. 17.
- Bartley J.M., Axen, G.J., Taylor, W.J., and Fryxell, J.E., 1988, Cenozoic tectonics of a transect through eastern Nevada near 38 degrees N. latitude: in This Extended Land Geological Journeys in the Southern Basin and Range, Field Trip Guidebook, Geological Society of America Cordilleran Section Meeting, Las Vegas Nevada, eds. Weide, D.L. and Faber, M.L., p. 1-20.
- Bohannon, R.G., 1984, Nonmarine sedimentary rocks of Tertiary age in the Lake Mead region: U.S. Geological Survey Professional Paper 1259, 72p.
- Buck, W.R., 1988, Flexural rotation of normal faults: Tectonics, v. 7, p. 959-973.
- Campbell, I. and Schenk, E.T., 1950, Camptonite dikes near Boulder Dam, Arizona: American Mineralogist, v. 35, no. 9-10, p. 671-692.
- Cascadden, T.E. and Smith, E.I., 1991, Intermediate and mafic volcanic rocks of the northern White Hills, Arizona: Implications for the production of intermediate composition volcanic rocks during regional extension: Geological Society of America, Abstracts with Programs, v. 23, no. 5, p. 390.
- Cascadden, T.E., 1991, Style of volcanism and extensional tectonics in the eastern Basin and Range province: northern Mohave County, Arizona: M.S. thesis, University of Nevada, Las Vegas, 156 pp.
- Cole, E.D., 1989, Petrogenesis of late Cenozoic alkalic basalt near the eastern boundary of the Basin and Range: upper Grand Wash trough, Arizona and Gold Butte, Nevada: M.S. thesis, University of Nevada, Las Vegas, 68 pp.
- Cooper, J.L., and Hart, W.K., 1990, Mantle sources in the Arizona transition zone and global mantle heterogeneity: Geology, v. 18, p. 1146-1149.
- Daley, E.E., and DePaolo, D.J., 1991, Isotopic evidence for lithospheric thinning during extension: southeastern Great Basin: submitted to Geology.
- Darvall, P., Gans, P.B., and Lister, G.S., 1991, Normal faulting in the Eldorado Mountains, southeastern Nevada: Geological Society of America, Abstracts with

Programs, v. 23, no. 2, p. 17.

Duebendorfer, E.M., Sewall, A.J., and Smith, E.I., 1991, The Saddle Island Detachment fault, an evolving shear zone in the Lake Mead area of southern Nevada: in Wernicke, B., Mid-Tertiary extension at the latitude of Las Vegas: Geological Society of America Memoir 176, p. 77-97.

Duebendorfer, E.M., and Wallin, E.T., 1991, Basin development and syntectonic sedimentation associated with kinematically coupled strike-slip and detachment faulting, southeastern Nevada: *Geology*, v. 19, p. 87-90.

Eaton, G.P., 1982, The Basin and Range province: Origin and tectonic significance: *Annual Review of Earth and Planetary Sciences*: v. 10, p. 409-440.

Eaton, G.P., Wahl, R.R., Prostka, H.J., Mabey, D.R., and Kleinkopf, M.D., 1978, Regional gravity and tectonic patterns: Their relation to late Cenozoic epeirogeny and lateral spreading in the western Cordillera: in R.B. Smith and Eaton, G.P., eds., *Cenozoic Tectonics and Regional Geophysics of the Western Cordillera*, Geological Society of America Memoir 152, p. 51-93.

Farmer, G.L., Perry, F.V., Semken, S., Crowe, B., Curtis, D., and DePaolo, D.J., 1989, Isotopic evidence of the structure and origin of subcontinental lithospheric mantle in southern Nevada: *Journal of Geophysical Research*, v. 94, p. 7885-7898.

Feuerbach, D.L., Smith, E.I., Walker, J.D., and Tangeman, J.A., 1991, The transition from subalkalic to alkalic volcanism in the Lake Mead area of Nevada and Arizona: Geochemical and isotopic constraints: *Geological Society of America Abstracts with Programs*, v. 23, p. 24.

Fitton, J.G., James, D., Kempton, P.D., Ormerod, D.S., and Leeman, W.P., 1988, The role of lithospheric mantle in the generation of Late Cenozoic basic magmas in the western United States: *Journal of Petrology*, Special Lithosphere Issue, p. 331-349.

Fitton, J.G., James, D., and Leeman, W.P., 1991, Basic magmatism associated with Late Cenozoic extension in the western United States: compositional variations in space and time, *Journal of Geophysical Research*, v. 96, no. B8, p. 13,693-13,711.

Fitzgerald, P.G., Fryxell, J.E., and Wernicke, B.P., 1991, Miocene crustal extension and uplift in southeastern Nevada: constraints from fission track analysis: *Geology*, v. 19, p. 1013-1016.

Glazner, A.F. and Farmer, G.L., 1991, Production of isotopic variability in basalts by cryptic mafic contamination: *Transactions of the American Geophysical Union*, v.

72, p. 267.

- Glazner, A.F. and Supplee, J.A., 1982, Migration of Tertiary volcanism in the southwestern United States and subduction of the Mendocino fracture zone: *Earth and Planetary Science Letters*, v. 60, p. 429-436.
- Hart, W.K., 1985, Chemical and isotopic evidence for mixing between depleted and enriched mantle, northwestern U.S.A.: *Geochemica and Cosmochemica Acta*, v. 49, p. 131-144.
- Hart, S.R., 1988, Heterogeneous mantle domains: signatures, genesis and mixing chronologies: *Earth and Planetary Science Letters*, v. 90, p. 273-296.
- Howard, K.A. and John, B.E., 1987, Crustal extension along a rooted system of low-angle normal faults; Colorado River extensional corridor, California and arizona, in Coward, M.D., and others, eds., *Continental extensional tectonics: geological Society of London Special Publication*, p. 299-311.
- Leat, P.T., Thompson, R.N., Dicken, A.P., Morrison, M.A., and Hendry, G.L., 1989, Quaternary volcanism in northwestern Colorado: implications for the roles of asthenosphere and lithosphere in the genesis of continental basalts: *Journal of Volcanology and Geothermal Research*, v. 37, p. 291-310.
- Leat, P.T., Thompson, R.N., Morrison, M.A., Hendry, G.L., and Dicken, A.P., 1991, Alkaline hybrid mafic magmas of the Yampa area, NW Colorado, and their relationship to the Yellowstone mantle plume and lithospheric mantle domains: *Contributions to Mineralogy and Petrology*, v. 107, p. 310-327.
- Longwell, C.R., Pampeyan, E.H., Bower, B., and Roberts, R.J., 1965, *Geology and mineral deposits of Clark County, Nevada: Nevada Bureau of Mines and Geology Bulletin 62*, 218 pp.
- Menzies, M.A., 1989, Cratonic, circumcratonic and oceanic mantle domains beneath the western United States: *Journal of Geophysical Research*, v. 94, p. 7899-7915.
- Menzies, M.A., Leeman, W.P., and Hawkesworth, C.J., 1983, Isotope geochemistry of Cenozoic volcanic rocks reveals mantle heterogeneity below western U.S.A.: *Nature*, v. 303, 9. 205-209.
- Mills, J.G., 1985, The geology and geochemistry of volcanic and plutonic rocks in the Hoover Dam 7.5 minute quadrangle, Clark County, Nevada and Mojave County, Arizona: M.S. thesis, University of Nevada, Las Vegas, 119 pp.
- Naumann, T.R., 1987, *Geology of the central Boulder Canyon quadrangle, Clark County,*

- Nevada: M.S. thesis, University of Nevada, Las Vegas, 68 pp.
- Naumann, T.R. and Smith, E.I., 1987, Evidence for magma mixing in Mid-Tertiary rocks, Lake Mead region, southern Nevada: Geological Society of America Abstracts with Programs, v. 19, p. 435-436.
- Nielson, manuscript in preparation
- Hamilton, W.B., 1988, Detachment faulting in the Death Valley region, California and Nevada, in Carr, M.D., and Yount, J.C., eds., Geologic and hydrologic investigations of a potential nuclear waste disposal site at Yucca Mountain, southern Nevada: U.S. Geological Survey Bulletin 1790, p. 50-85.
- Perry, F.V., Baldrige, W.S., and DePaolo, D.J., 1987, Role of asthenosphere and lithosphere in the genesis of late Cenozoic basaltic rocks from the Rio Grande Rift and adjacent areas of the southwestern United States: Journal of Geophysical Research, v. 92, p. 9193-9213.
- Reynolds, S.J., 1988, Geologic map of Arizona: Arizona Geological Survey map 26, scale 1:1,000,000.
- Smith, E.I., Feuerbach, D.L., Naumann, T.R., and Mills, J.G., 1990, Geochemistry and evolution of mid-Miocene igneous rocks in the Lake Mead area of Nevada and Arizona, in Anderson, J.L. ed, Cordilleran Magmatism: Geological Society of America Memoir 176, p. 169-194.
- Smith, E.I., 1982, Geology and geochemistry of the volcanic rocks in the River Mountains, Clark County, Nevada and comparisons with volcanic rocks in nearby areas: in Mesozoic-Cenozoic Tectonic Evolution of the Colorado River Region, California, Arizona, and Nevada, edited by E.G. Frost, and D.L. Martin, Cordilleran Publishers, San Diego, California, p. 41-54.
- Smith, E.I., Schmidt, C.S., and Mills, J.G., 1988, Mid-Tertiary volcanoes of the Lake Mead area of southern Nevada and Northwestern Arizona: in Weide, D.L., and Faber, M.L., This Extended Land, Geological Journeys in the southern Basin and Range, Geological Society of America, Cordilleran Section Field Trip Guidebook; UNLV Department of Geoscience, Special Publication No. 2, p. 107-122.
- Takahashi, E., and Kushiro, I., 1983, Melting of dry peridotite at high pressures and basalt magma genesis: American Mineralogist, v. 68, p. 859-879.
- Thompson, K.G., 1985, Stratigraphy and petrology of the Hamblin-Cleopatra volcano, Clark County, Nevada: M.S. Thesis, University of Texas, Austin, 306 pp.

- Walker, J.D. and Coleman, D.S., 1991, Geochemical constraints on mode of extension in the Death Valley region: *Geology*, v. 19, no. 10, p. 971-974.
- Weaver, B.L., 1991a, The origin of ocean island basalt end-member compositions: trace element and isotopic constraints: *Earth and Planetary Science Letters*, v. 104, p. 381-397.
- Weaver, B.L., 1991b, Trace element evidence for the origin of ocean-island basalts: *Geology*, v. 19, p. 123-126.
- Weaver, B.L., Wood, D.A., Tarney, J., and Joron, J.L., 1986, Role of subducted sediment in the genesis of ocean island basalts: Geochemical evidence from South Atlantic Ocean Islands: *Geology*, v. 14, p. 275-278.
- Wernicke, B., 1980, Low-angle normal faults in the Basin and Range province: Nappe tectonics in an extending orogen: *Nature*, v. 291, p. 645-648.
- Wernicke, B., and Axen, G.J., 1988, On the role of isostasy in the evolution of normal fault systems: *Geology*, v. 16, p. 848-861.
- Wooden, J.L. and Miller, D.M., 1990, Chronologic and Isotopic framework for early Proterozoic crustal evolution in the eastern Mohave Desert region, SE California: *Journal of Geophysical Research*, v. 95, B12, p. 20,133-20,146.
- Zindler, A., and Hart, S.R., 1986, Chemical geodynamics: *Annual Review of Earth and Planetary Science Letters*, v. 14, p. 493-571.

**ISOTOPIC GEOCHEMISTRY AND EVOLUTION OF MAFIC LAVAS IN THE
REVEILLE RANGE, NEVADA: A WINDOW INTO THE MANTLE OF THE CENTRAL
GREAT BASIN**

**(Summary of a paper without Figures or Tables, A complete version of the paper will be
available about April 1, 1992)**

T.R. Naumann and E.I. Smith

Center for Volcanic and Tectonic Studies

University of Nevada, Las Vegas

Las Vegas, Nevada 89154

and

J.D. Walker

Department of Geology

University of Kansas

Lawrence, Kansas

INTRODUCTION

The study of rift-related basaltic magmatism is an important tool in investigations of the structure and composition of the subcontinental mantle and the tectonic modification of the continental lithosphere. Geochemical and isotopic studies of late Cenozoic basalts in the Basin and Range province have revealed the provinciality of their mantle source domains as well as their derivation from both asthenospheric mantle and lithospheric mantle reservoirs (Semkin, 1984; Hart, 1985; Fitton et al., 1988, 1991; Ormerod et al., 1988; Lum et al., 1989; Farmer et al., 1989; Walker and Coleman, 1991). The asthenospheric mantle includes depleted MORB-mantle from the upper asthenosphere and the less depleted, OIB-source mantle from the deeper asthenosphere. The OIB source mantle may in part be plume-derived. The lithospheric mantle represents a highly heterogeneous reservoir enriched in incompatible elements. Melts derived from the lithospheric mantle have distinctive trace element ratios and higher $^{87}\text{Sr}/^{86}\text{Sr}$ and lower $^{143}\text{Nd}/^{144}\text{Nd}$ than asthenospheric mantle.

Through the study of rift-related basalts it is also possible to constrain the processes involved with thinning of the continental lithosphere. Extension by pure or simple shear may eventually lead to the physical displacement of the lithospheric mantle from beneath the rift resulting in basaltic magmas derived exclusively from the asthenospheric mantle. If thermal conversion and/or erosion of the lithospheric mantle is the dominant process by which thinning occurs then the basaltic magmas could initially be derived from a lithospheric mantle reservoir or a mixture of both lithospheric mantle and asthenospheric mantle (Bosworth, 1987; Perry et al., 1987, 1988; Fitton et al., 1988; Farmer et al., 1989; Leat et al., 1989, 1991; Altherr et al., 1990; Walker and Coleman, 1991). With continued extension and/or heating, the lithospheric mantle will eventually be replaced by the asthenospheric mantle and the isotopic compositions of both alkali and tholeiitic basalts will first show signatures of the lithospheric mantle and then change to asthenospheric mantle with time.

Basaltic volcanism has predominated throughout the Great Basin following the termination of subduction-related calc-alkalic intermediate to silicic volcanism approximately 17 Ma (Christiansen and Lipman, 1972; Best and Brimhall, 1974). In the southern Great Basin, the onset of lithospheric extension and transition to fundamentally basaltic volcanism began approximately at 10 Ma and has continued into the Holocene (Luedke and Smith, 1974; Stewart and Carlson, 1978). In the Great Basin, lithospheric extension has effected an area up to 800 km wide (Stewart, 1978) but late Cenozoic basaltic activity is not evenly distributed across the province. Rift-related basaltic volcanism has migrated through time to the margins of the Great Basin and most Late Miocene to Holocene volcanic fields are concentrated in semi-continuous zones along the boundary of the Colorado Plateau (Transition Zone) to the east and the Sierra Province to the west (Christiansen and Lipman, 1972; Best and Brimhall, 1974; Luedke and Smith, 1974). Basaltic activity in the central part of the Great Basin is restricted to the Reveille Range and Lunar Crater volcanic fields (RR-LCVF). The RR-LCVF

combine to form a 20 km wide, 100 km long N to N30°E trending belt of alkali basalts that extends from 37° 45' to 38° 45' in the central Great Basin. The RR-LCVF contain approximately 100 eruptive centers and lavas occur as shallow intrusions, maars, domes, flows, and cinder cones. Basaltic eruptions began approximately 6 m.y. ago in the Reville Range and 4 m.y. ago in the Lunar Crater field (Bergman et al., 1981; Foland et al., 1987; Kargel, 1987; Naumann et al., 1991). The location of the RR-LCVF in the central Great Basin represents an exception to the late Cenozoic migration pattern of basaltic volcanism. Because of the isolated location of the RR-LCVF relative to other basaltic fields, this belt represents an important "window" into the mantle (Kargel, 1987) of the vast central Great Basin where little other data on mantle compositions and structure is available.

Previous studies of the RR-LCVF have focused primarily on the geology, geochemistry and petrogenesis of the alkali basalts and mantle inclusions in the Lunar Crater volcanic field (Scott, 1969; Trask, 1969; Scott and Trask, 1971; Bergman et al., 1981; Bergman, 1982; Lum, 1986; Kargel, 1987; Foland et al., 1987). A small number of samples from the Reville Range have been included in geochemical studies that concentrated primarily on the basalts of the Lunar Crater field (Bergman, 1982; Lum, 1986; Kargel, 1987; Foland et al., 1987; Fitton et al., 1991) and a limited number of Reville basalts have been incorporated in provincial isotopic studies (Semkin, 1984; Lum et al., 1989; Farmer et al., 1989). Previous geochemical and isotopic studies by Foland et al., (1988); Lum et al., (1989) and Fitton et al., (1991) concluded that the earliest basaltic lavas of the RR-LCVF may have resulted from a combination of lithospheric mantle and asthenospheric mantle components. However, isotopic studies by Farmer et al., (1989), Kempton et al., (1991) and Foland et al., (1991) concluded that basalts of the RR-LCVF were derived solely from asthenospheric mantle. The identification of a lithospheric mantle component in the central Great Basin remains a pertinent question and has an important bearing on models that involve the structure and composition of the subcrustal mantle as well as geodynamic models involving the generation of rift-related magmas. No previous work has presented geologic mapping or documentation of the volcanic stratigraphy of the RR-LCVF as part of geochemical or isotopic investigations.

In this paper, we describe the Reville Range volcanic field, a suite of predominantly basaltic lavas ranging from mildly alkalic (transitional to tholeiites) to alkalic and having trace and isotopic compositions similar to many ocean island basalts (OIB). The purpose of this study is twofold. First, through the use of major and trace element geochemistry and Nd, Sr, and Pb isotopic data we investigate whether lithospheric mantle resides beneath this portion of the Great Basin by identifying its involvement in the generation of the basaltic magmas. Second, this paper addresses the anomalous location of the RR-LCVF itself. We explore the possibility that the origin of the belt is the result of voluminous partial melting by decompression of hot asthenosphere as it convectively upwells with divergent lateral flow beneath the central Great Basin.

GEOLOGY OF THE REVILLE RANGE VOLCANIC FIELD

Introduction

The Reville Range is an excellent locality for determining the temporal evolution of chemical and isotopic compositions as well as the control of different mantle components on the petrogenesis of rift-related continental basalts. The western margin of the Reville Range is the only location along the RR-LCVF where significant amounts of tectonic uplift and erosion have exposed thick volcanic sequences. Geologic mapping of this area has resulted in the discovery of multiple eruptive episodes and the establishment of a well defined volcanic stratigraphy that spans over 3 Ma of time. Detailed sampling of this stratigraphy documents the temporal evolution of chemical and isotopic trends beginning with the onset of RR-LCVF basaltic volcanism at 6 Ma (Naumann et al., 1991). In addition, the presence of ultramafic xenoliths, megacrysts and nodules in the alkalic lavas provide evidence that they ascended rapidly from their mantle source precluding significant contamination by continental crust.

Basement rocks of the Reville Range consist primarily of intermediate to silicic ash-flow sheets of Oligocene to Miocene age that unconformably overlie Paleozoic sedimentary rocks in the northern half of the range (Ekren et al., 1973). The range is bounded by en-echelon north to northeast striking high-angle normal faults. On the western range margin, 5.7 Ma basalt flows are offset up to 300 m by three segments of the fault system but a basalt flow of similar age to the south covers a range front fault (Diggles et al., 1986). On the eastern range margin the fault system cuts Holocene valley fill deposits (Ekren et al., 1973; Dohrenwend, 1987) indicating that the range has been tilted to the west in Holocene time (Kleinhampl and Ziony, 1985).

Basaltic lavas cover approximately 180 km² and occur as shallow intrusions, domes, flows and over 60 effusive vents and dissected cinder cones. The vents are composed of massively bedded red to brown scoria, cinder, spatter, agglutinated scoria and ash. Dikes are exposed in the dissected cones and in bedrock. Dikes in bedrock pinch and swell and cut obliquely across pervasive bedrock joints. Where dikes leave bedrock and intrude scoria cones they commonly swell from a initial width of between 1.0 m - 2.0 m below the vent to become plug-like intrusions up to 20 m wide within the central vent areas. This pattern is likely the result of initial volatile-rich fissure eruptions that fountained along the length of the dike that progressively became focused at one or more nodes along the strike of the intrusion as the magma supply rate decreased. Most vents are distributed on the east and west flanks of the range and show a preferred north-northeast alignment that crudely parallels the location of extensional structures. However, even though there is a close spatial association between vents and extensional structures, no dikes or vents are located within or above mappable structures indicating that at least in the upper crust, magmas did not use joints or faults as primary conduits to the surface.

Stratigraphy, Age and Volume of Volcanism

Geologic mapping of the volcanic field was completed at a scale of 1:24,000. Map

units were distinguished on a flow-by-flow basis, based primarily on lithologic (type, size and abundance of phenocrysts and megacrysts) and morphologic criteria. Some map units represent composite assemblages of overlapping flows that originated from multiple vents while other units are spatially isolated and are composed of multiple flows from a single vent. Naumann et al., (1991) divided the lavas into three separate groups based on lithology, field relationships and K-Ar geochronology. All data and sample locations for the K-Ar ages used in this paper are found in Naumann et al., (1991). Volume estimates for each episode were calculated by determining the areal extent of each map unit with a planimeter and then combining this value with an average outcrop thickness based on field measurements and topographic data. Volume estimates represent a minimum due to the extensive dissection of most eastern and northwestern map units and the coverage of southwestern map units that lie below modern grade level.

Episode 1 consists of basalt that crops out over approximately 150 km² on both the east and west flanks and crest of the range. Lavas range in age from 5.9 to 5.0 Ma and erupted from fifty two vents. An estimated volume of Episode 1 basalts is 8 km³. Episode 1 basalts are distinguished from Episode 2 in outcrop by a greater abundance of plagioclase megacrysts and lack of augite megacrysts. Episode 1 basalts are coarse grained with intergranular and rare trachytic texture. Lavas are porphyritic with total phenocryst content up to 20 percent. Basalts of Episode 1 contain megacrysts of andesine and labradorite (up to 40%). Plagioclase megacrysts commonly occur in glomeroporphyritic clots that range in size from 5 to 15 cm. Some feldspar megacrysts are partially resorbed and commonly contain abundant poikilolites of olivine. Olivine and plagioclase are the major phenocryst phase in all samples. Diopsidic augite phenocrysts are subhedral with strong dispersion. Groundmass phases within Episode 1 basalts include olivine (mostly altered to iddingsite), diopsidic augite, feldspar and opaque Fe-Ti oxides.

Episode 2 consists of basalts that crop out over approximately 15 km². Basalts range in age from 4.6 to 3.0 Ma and erupted from fourteen vents on the northeast flank and range crest. An estimated volume of Episode 2 lavas is 1 km³. Basalt of Episode 2 contains abundant megacrysts of diopsidic-augite (up to 40%), amphibole (up to 35%) and plagioclase (<5%) and coarse grained xenoliths of gabbro and dunite (up to 20 cm in length). Episode 2 basalts is coarse grained with intergranular to subophitic and rare trachytic texture and all samples are porphyritic with total phenocryst content up to 20 percent. Olivine, clinopyroxene and plagioclase are the major phenocryst phases. Oxyhornblende was identified in two samples. Groundmass phases are olivine, pyroxene, opaque Fe-Ti oxides with a trace of biotite and apatite. Episode 2 basalts contain mantle xenoliths while most Episode 1 lavas do not.

Trachytic domes erupted just prior to the onset of Episode 2 volcanism at 4.4 and 4.2 Ma in the northwestern Reveille Range. Trachyte and tristanite magmas containing ferrosillite and hedenburgite, anorthoclase, sanidine and andesine produced two constructional domes <0.01 km³ and 0.3 km³ in volume. Initial eruptions at both domes were explosive and generated a pyroclastic apron between 2 and 10 m thick that extends up to 5 km from the larger dome. The flanks of the larger dome are composed of stubby flows which originated at or near the summit. The dome is compositionally zoned from

flows which originated at or near the summit. The dome is compositionally zoned from 60 % SiO_2 at the base to 58 % SiO_2 at the top (Naumann et al., 1990). Trachyte lavas are vesicular and porphyritic with approximately 10 percent total phenocrysts. Subhedral to anhedral grains of clinopyroxene (salite to ferrosilite) are the only phenocryst phase. Sanidine is present as microlites and microphenocrysts that are sub-parallel and are set in a matrix of colorless to pale green glass.

RESULTS (SUMMARY)

Major Elements

Reveille basalts are alkalic and are similar to alkalic basalts from extensional environments worldwide. Episode 1 (which is more voluminous) is more highly evolved than Episode 2. Smaller volume Episode 2 lavas contain xenoliths and represent more primitive magma as indicated by higher Mg #, lower SiO_2 , and higher normative Ne content.

Trace Elements

Trace-element data indicates that Episode 1 lavas are produced by partial melting of lithospheric mantle and Episode 2 by melting of asthenospheric mantle. Evidence includes:

- (1) lower Zr/Ba in Episode 1 compared to higher values in Episode 2 lavas. Elevated Zr/Ba is characteristic of magma generated in the asthenosphere. Lower values are indicative of a lithospheric mantle source (Ormerod, 1988).
- (2) Enriched light rare-earth element (REE) abundances in Episode 1 lavas suggest a source in the lithospheric mantle.
- (3) Linear trends between Episode 1 and 2 lavas on La vs. Nb and La vs. Ba plots suggest that the Reveille Range lavas in detail formed from sources that are a mixture (to varying degrees) of asthenospheric and lithospheric mantle reservoirs.

Isotopes

Older Episode 1 lavas are higher $^{87}\text{Sr}/^{86}\text{Sr}$ and lower in $\epsilon \text{ Nd}$ than younger Episode 1 and Episode 2 basalts. This time progressive shift in isotopic composition represents a fundamental change in the locus of melting from asthenosphere to lithospheric mantle with time (see discussion of trace elements). Pb values are consistent throughout the range of basalt compositions indicating that crustal contamination probably played a minor role in their evolution.

DISCUSSION

Source of Reveille Magmas

We document that lithospheric mantle was involved in the generation of the Reveille

lavas and that there was a temporal shift in the mantle source from lithospheric mantle to asthenospheric mantle.

The chemical and isotopic variations in the basalts from the Reville Range require that more than one isotopically distinct mantle component was involved in their petrogenesis. Previous geochemical and isotopic studies by Foland et al., (1988); Lum et al., (1989) and Fitton et al., (1991) concluded that the earliest basaltic lavas of the RR-LCVF may have resulted from a combination of lithospheric mantle and asthenospheric mantle components. However, isotopic studies by Farmer et al., (1989), Kempton et al., (1991) and Foland et al., (1991) concluded that basalts of the RR-LCVF were derived solely from asthenospheric mantle. A fundamental observation from our study is that Nd and Sr isotopic compositions of the alkali basalts vary systematically with time but Pb isotopic compositions remain constant. The geochemical and isotopic signature of basalts from the Reville Range are compatible with an origin involving mixing of lithospheric mantle and asthenospheric mantle components. The small range in incompatible element ratios regardless of the relative lithospheric mantle or asthenospheric mantle contribution indicates that both lithospheric mantle and asthenospheric mantle from the region have similar ratios. This is compatible with the nearly straight-line mixing in the isotopic values. The isotopic and trace element concentrations fall within the range of known oceanic island basalt concentrations. Early Episode 1 basalts were derived from a mantle reservoir with low ϵ Nd, high $^{87}\text{Sr}/^{86}\text{Sr}$, interpreted by Menzies, Perry, Farmer and Fitton to represent lithospheric mantle. Ormerod et al., (1988) discriminated lithospheric mantle from asthenospheric mantle based on trace element concentrations with lithospheric mantle being depleted in HFSE relative to asthenospheric mantle. Late Episode 1 and Episode 2 were derived from a mantle reservoir with high ϵ Nd and low $^{87}\text{Sr}/^{86}\text{Sr}$. Menzies et al., 1983, Perry et al., 1987, Farmer et al., 1989, Lum et al., 1989, Fitton et al., 1991 interpreted similar compositions from the Basin and Range and Rio Grande Rift to have been derived from upwelling asthenospheric mantle.

What are the implications of this two component system for the structure of the mantle? We prefer the two-layer mantle of Perry et al., (1987) where lithospheric and asthenospheric mantle constitute different layers rather than a single source that is isotopically heterogeneous (plum pudding). Why? because the shift in isotopic and trace-element concentrations is temporal not geographical. Early Episode 1 lavas derived from lithospheric mantle occur from varying geographic positions prior to 5 Ma. The temporal shift in the geochemical and isotopic concentrations are consistent with a model involving upwelling asthenosphere/ mantle plume where initial melts are produced in the lithospheric mantle and with time as the isotherms relax successive melt fractions are produced from the underlying asthenospheric mantle. After 5 Ma, all melts are produced from asthenospheric mantle.

Crustal Contamination?

Foland et al. (1991) have suggested that Episode 1 lavas and their isotopic signatures are the result of contamination of mantle derived magmas by continental lithosphere rather than partial melting of lithospheric mantle (enriched source) as suggested in this paper.

Magma passing through continental crust will almost certainly be contaminated by crust. To the extent that this contamination is recognizable will depend upon the quantity of continental crust consumed which will in turn depend on residence time in the crust. Isotopes of lead and oxygen are sensitive indicators of crustal contamination. Other indicators of contamination include petrographic criteria. We argue against the model of Foland et al., (1991) for the following reasons:

- (1) lead values for all sample have narrow distribution (e.g., $^{206}\text{Pb}/^{204}\text{Pb} = 19.1$ to 19.4). Pb is a very sensitive indicator of crustal contamination and should show a wider variation if contamination was a significant factor.
- (2) Incompatible trace element ratios do not vary significantly.
- (3) There is a very narrow range of silica contents for mafic lavas (42 to 48%). The contaminant would have to be mafic (gabbro).
- (4) Variations in Sr and Nd do not correlate with SiO_2

Origin of the Lunar Crater - Reveille Range Volcanic Belt

Why does basaltic volcanism occur in the Death Valley-Pancake Range belt and nowhere else in the central Great Basin during Pliocene time?

Lithospheric extension has effected an area up to 800 km wide in the Great Basin (Stewart, 1978), but late Cenozoic basaltic activity is not evenly distributed across the province. Most Late Miocene to Holocene volcanic fields are concentrated in semi-continuous zones along the boundary of the Colorado Plateau (Transition Zone) on the east and the Sierra Province on the west (Christiansen and Lipman, 1972; Best and Brimhall, 1974; Luedke and Smith, 1974). Basaltic activity in the central part of the Great Basin is restricted to the Reveille Range and Lunar Crater volcanic fields (RR-LCVF). There are several important questions about the RR-LCVF. Including:

- (1) What is the significance of the RR-LCVF volcanic field?
- (2) What information do these lavas provide about mantle and crustal processes.
- (3) Why is there no Pliocene basaltic activity in other highly extended areas of the central Great Basin?

If the crust throughout the Great Basin has been thinned equally then the controlling mechanism may be the presence of abnormally high heat flow associated with a rising convective plume.

Several lines of evidence support the hypothesis that a thermal plume is responsible for the location of the RR-LVCF lavas rather than any structural property of the crust:

- (1) Asthenospheric mantle is an important component in the generation of both Episode 1 and 2 lavas in the Reveille Range.
- (2) There are no major crustal structures in the Reveille Range that might focus volcanism in this area. Also, Taylor et al., (1989) demonstrated a lack of correlation between extensional periods and volcanism indicating no direct relationship between extension and volcanism in this area.
- (3) The lack of dikes in the Reveille Range indicates that there was little dilational stress at the time of the emplacement of the lavas. This observation suggests that crustal extension is not the cause of volcanism.

an intrusion rate of 570 km³/m.y. vs. an extrusion rate of 5.4 to 2.4 km³/m.y. for the Coso Field, California. He also estimated a 10:1 ratio (intrusion/extrusion) for Kilauea volcano, Hawaii. Bergman (1982) calculated an eruption rate of 10-20 km³/m.y. for the RR-LCVF. If 10 times as much basalt intruded the upper mantle/lower crust and stagnated (=1000 km³), then the crust below RR-LCVF (40 Km long x 10 km wide x 50 km thick = an approximate volume of 20,000 km³) increased in volume by 5% over the last 5 m.y. This very high production rate of mafic magma is consistent with high heat flow associated with a thermal plume.

We propose that the RR-LVCF Volcanic Field resulted from voluminous partial melting related to a plume/hot spot in the asthenosphere. The upwelling may be in response to mantle convection that provided the driving force for much of the extension in the Great Basin.

The RR-LCVF is located slightly west of the north-south axis of bilateral symmetry of the Great Basin (Eaton et al., 1978). This symmetry is expressed in regional topography, gravity, heat flow, seismic activity, crustal thickness, and the chemistry of late Cenozoic volcanism (Eaton et al., 1978; Fitton et al., 1988). The symmetry and high heat flow in the Great Basin is evidence that asthenospheric mantle was upwelling to shallow depths in the region.

IMPLICATIONS FOR VOLCANIC MODELS OF THE GREAT BASIN

The RR-LCVF represents a thermal anomaly where volcanic activity has been concentrated for 6 Ma. Since the RR-LCVF represents the northern limit of a 300 km long semicontinuous belt of Pliocene to Holocene basalts defined by Crowe and Vaniman, (1980) and Vaniman et al., (1982) as the Death Valley-Pancake Range (DVPR) volcanic belt. The DVPR belt extends from the RR-LCVF in central Nevada south-southwestward through the southern Nevada volcanic field to southern Death Valley in California. The distribution of cinder cones and the geometry of basaltic vent systems within volcanic fields or individual volcanic centers along the DVPR belt show a preferred north-northeast alignment that parallels the location of late Cenozoic extensional structures (Crowe and Vaniman, 1980; Smith et al., 1989; Naumann et al., 1991). The DVPR Belt/Zone is well documented and we suggest that it is an important component of the Great Basin, since it represents the thermal anomaly that may be responsible for the geophysical and topographic characteristics of the Great Basin.

Pliocene-Holocene volcanoes in Crater Flat and at Lathrop Wells near the proposed high-level nuclear waste repository also lie within this belt.

REFERENCES

- Altherr, R., Henjes-Kunst, F., and Baumann, A., 1990, Asthenosphere versus lithosphere as possible sources for basaltic magmas erupted during formation of the Red Sea: constraints from Sr, Pb and Nd isotopes: *Earth and Planetary Science Letters*, v. 96,

- constraints from Sr, Pb and Nd isotopes: *Earth and Planetary Science Letters*, v. 96, p. 269-286.
- Anderson, R.E., 1988, Hazard implications of joint-controlled basaltic volcanism in southwestern Utah: *Geological Society of America Abstracts with Programs*, v. 20, no. 7, p. 115.
- Bacon C.R., Macdonald, R., Smith, R.L., and Baedeker, P.A., 1981, Pleistocene high-silica rhyolites of the Coso Volcanic Field, Inyo County, California: *Journal of Geophysical Research*, v. 86, no. B11, p. 10223-10241.
- Bergman, S.C., 1982, Petrogenetic aspects of the alkali basaltic lavas and included megacrysts and nodules from the Lunar Crater Volcanic Field, Nevada, U.S.A.: Ph.D dissertation, Princeton University, Princeton, New Jersey. 432 pp.
- Bergman, S.C., Foland, K.A., and Spera, F.J., 1981, On the origin of an amphibole-rich vein in a peridotite inclusion from the Lunar Crater Volcanic Field, Nevada, U.S.A.: *Earth and planetary Science Letters*, v. 56, p. 343-361.
- Best, M.G., and Brimhall, W.H., 1974, Late Cenozoic alkalic basaltic magmas in the western Colorado Plateaus and Basin and Range transition zone, U.S.A., and their bearing on mantle dynamics: *Geological Society of America Bulletin*, v. 85, p.1677-1690.
- Bosworth, W., 1987, Off-axis volcanism in the Gregory rift, east Africa: Implications for models of continental rifting: *Geology*, v. 15, no. 5, p. 397-400.
- Christiansen, R. L., and Lipman, P.W., 1972, Cenozoic volcanism and plate tectonic evolution of the western United States, II, Late Cenozoic: *Philosophical Transactions of the Royal Society of London*, v. 271, p. 249-284.
- Crowe, B.M., Vaniman, D., Carr, W.J., and Fleck, R.J., 1980, Geology and tectonic setting of a Neogene volcanic belt within the south central Great Basin, Nevada and California: *Geological Society of America Abstracts with Programs*, v. 93, p. 409.
- Diggles, M.F., Saunders, J.A., Ponce, P.A., Rochette, E.A., and Neubert, J.T., 1986: Mineral Resources of the south Reville Range wilderness study area, Nye County, Nevada: *U.S. Geological Survey Bulletin 1731-C*, 11 pp.
- Dohrenwend, J.C., Turrin, B.D., and Diggles, M.F., 1985, Topographic distribution of dated basaltic lava flows in the Reville Range, Nye County, Nevada: implications for Late Cenozoic erosion of upland areas in the Great Basin: *Geological Society of America Abstracts with Programs*, v. 17, no. 6, p. 352.
- Eaton, G.P., Wahl, R.R., Prostka, H.J., Mabey, D.R., and Kleinkopf, M.D., 1978, Regional

- gravity and tectonic patterns: Their relation to late Cenozoic epeirogeny and lateral spreading in the western Cordillera: in R.B Smith and Eaton, G.P., eds., *Cenozoic Tectonics and Regional Geophysics of the Western Cordillera*, Geological Society of America Memoir 152, p. 51-93.
- Ekren, E.B., Quinlivan, W.D., and Marvin, R.F., 1974, Pre-Basin and Range strike-slip faulting in the Reville and Hot Creek ranges, central Nevada: *Geological Society of America Abstracts with Programs*, v. 6, no. 3, p. 172.
- Ekren, E.B., Rogers, C.L., and Dixon, G.L., 1973, Geologic and Bouguer gravity map of the Reville Quadrangle, Nye County, Nevada: U.S. Geological Survey Miscellaneous Geologic Investigations Map I-806.
- Farmer, G.L., Perry, F. V., Semken, S., Crowe, B., Curtis, D., and DePaolo, D.J., 1989, Isotopic evidence on the structure and origin of subcontinental lithospheric mantle in southern Nevada: *Journal of Geophysical Research*, v. 94, no. B6, P. 7885-7898.
- Fitton, J.G., James, D., Kempton, P.D., Ormerod, D.S., and Leeman, W.P., 1988, The role of lithospheric mantle in the generation of Late Cenozoic basic magmas in the western United States: *Journal of Petrology*, Special Lithosphere Issue, p. 331-349.
- Fitton, J.G., James, D., and Leeman, W.P., 1991, Basic magmatism associated with Late Cenozoic extension in the western United States: compositional variations in space and time, *Journal of Geophysical Research*, v. 96, no. B8, p. 13,693-13,711.
- Foland, K.A., Kargel, J.S., Lum, C.L., and Bergman, S.C., 1987, Time-spatial-composition relationships among alkali basalts in the vicinity of the Lunar Crater, south-central Nevada: *Geological Society of America Abstracts with Programs*, v. 19, no. 7, p. 666.
- Foland, K.A., Kargel, J.S., Schucker, D.E., Hubacker, F.A., and Bergman, S.C., 1988, Sources for Cenozoic alkalic basalts in the vicinity of the Lunar Crater volcanic field, south-central Nevada: *Transactions of the American Geophysical Union*, v. 69, no. 16, p. 519.
- Foland, K.A., Schucker, D.E., Smith, B.M., Todt, W., and Bergman, S.C., 1991, Isotope geochemistry of Cenozoic alkali basalts in the vicinity of the Lunar Crater volcanic field, south-central Nevada: O and Pb evidence for crustal components: *Geological Society of America Abstracts with Programs*, v. 23, no. 5, p. 45.
- Hart, W.K., 1985, Chemical and isotopic evidence for mixing between depleted and enriched mantle, northwestern U.S.A.: *Geochemical and Cosmochemical Acta*, v. 49, p. 131-144.
- Kargel, J.S., 1986, The geochemistry of basalts and mantle inclusions from the Lunar Crater

Volcanic Field, Nevada: petrogenetic and geodynamic implications: M.S. thesis, Ohio State University, Columbus Ohio, 393 pp.

- Kempton, P.D., Fitton, J.G., Hawkesworth, C.J., and Ormerod, D.S., 1991, Isotopic and trace element constraints on the composition and evolution of the lithosphere beneath the southwestern United States: Journal of Geophysical Research, v. 96, no. B8, p. 13,713-13,735**
- Kleinhampl F.J., and Ziony, J.I., 1985, Geology of northern Nye County, Nevada: Nevada Bureau of Mines and Geology Bulletin 99A, 172 pp.**
- Le Bas, M.J., LeMaitre, R.W., Streckeisen, A., and Zanettin, B., 1986, A chemical classification of volcanic rocks based on the total alkali-silica diagram: Journal of Petrology, v. 27, part 3, p. 745-750.**
- Leat, P.T., Thompson, R.N., Dicken, A.P., Morrison, M.A., and Hendry, G.L., 1989, Quaternary volcanism in northwestern Colorado: implications for the roles of asthenosphere and lithosphere in the genesis of continental basalts: Journal of Volcanology and Geothermal Research, v. 37, p. 291-310.**
- Leat, P.T., Thompson, R.N., Morrison, M.A., Hendry, G.L., and Dicken, A.P., 1991, Alkaline hybrid mafic magmas of the Yampa area, NW Colorado, and their relationship to the Yellowstone mantle plume and lithospheric mantle domains: Contributions to Mineralogy and Petrology, v. 107, p. 310-327.**
- Luedke, R.G., and Smith, R.L., 1981, Map showing distribution, composition, and age of Late Cenozoic volcanic centers in California and Nevada: U.S. Geological Survey Miscellaneous Investigations Series Map, I-1091-C.**
- Lum, C.C., 1986, Aspects of the petrogenesis of alkali basalts from the Lunar Crater Volcanic Field, Nevada: M.S. thesis, Ohio State University, Columbus Ohio, 146 pp.**
- Lum, C.C., Leeman, W.P., Foland, K.A., Kargel, J.A., and Fitton, J.G., 1989, Isotopic variations in continental basaltic lavas as indicators of mantle heterogeneity: examples from the western U.S. Cordillera: Journal of Geophysical Research, v. 94, no. B6, p. 7871-7884.**
- Menzies, M.A., Leeman, W.P., and Hawkesworth, C.J., 1983, Isotope geochemistry of Cenozoic volcanic rocks reveals mantle heterogeneity below western U.S.A.: Nature, v. 303, 9. 205-209.**
- Mutter, J.C., Buck, W.R., and Zehnder, C.M., 1988, Convective partial melting, a model for the formation of thick basaltic sequences during the initiation of spreading: Journal of Geophysical Research, v. 93, no. B2, p. 1031-1048.**

- Naumann, T.R., and Smith, E.L., 1988, Compositional trends within Late-Cenozoic alkalic basalts of the central Great Basin, Nevada: Geological Society of America Abstracts with Programs, v. 20, no. 7, p. 114
- Naumann, T.R., Smith, E.L., and Shafiqullah, M., 1990, Post-6 Ma intermediate (trachytic) volcanism in the Reville Range, Central Great Basin, Nevada: Geological Society of America Abstracts with Programs, v. 22, no. 3, p. 72.
- Naumann, T.R., Smith, E.L., and Shafiqullah, M., 1991, New K-Ar ages for Pliocene mafic to intermediate volcanic rocks in the Reville Range, Nevada: Isochron/West, no. 57, p. 12-16.
- Ormerod, D.S., Hawkesworth, C.J., Rogers, N.W., Leeman, W.P., and Menzies, M.A., 1988, Tectonic and magmatic transitions in the western Great Basin, U.S.A.: *Nature*, v. 333, p. 349-353.
- Perry, F.V., Baldrige, W.S., and Depaolo, D.J., 1987, Role of asthenosphere and lithosphere in the genesis of late Cenozoic basaltic rocks from the Rio Grande Rift and adjacent regions of the southwestern United States: *Journal of Geophysical Research*, v. 92, no. B9, p. 9193-9213.
- Perry, F.V., Baldrige, W.S., and Depaolo, D.J., 1988, Chemical and isotopic evidence for lithospheric thinning beneath the Rio Grande rift, *Nature*, v. 332, p. 432-434.
- Scott, D.H., 1969, The geology of the southern Pancake Range and Lunar Crater volcanic field, Nye County, Nevada: Ph.D dissertation, University of California, Los Angeles, 128 pp.
- Scott, D.H., and Trask, N.J., 1971, Geology of the Lunar Crater volcanic field, Nye County, Nevada: U.S. Geological Survey Professional Paper 599-I, 22 pp.
- Semkin, S., 1984, A neodymium and strontium isotopic study of late Cenozoic basaltic volcanism in the southwestern Basin and Range province, M.S. thesis, University of California, Los Angeles, 68 pp.
- Smith, E.L., Feuerbach, D.L., Naumann, T.R., and Mills, J.G., 1990, Geochemistry and evolution of mid-Miocene igneous rocks in the Lake Mead area of Nevada and Arizona, in Anderson, J.L. ed, *Cordilleran Magmatism: Geological Society of America Memoir 176*, p. 169-194.
- Stewart, J.H., 1978, Basin and Range structure in western North America: in R.B Smith and Eaton, G.P., eds., *Cenozoic Tectonics and Regional Geophysics of the Western Cordillera*, Geological Society of America Memoir 152, p. 1-31.

- Stewart, J.H. and Carlson, J.E., 1978, Generalized maps showing distribution, lithology, and age of Cenozoic igneous rocks in the western United States: in R.B Smith and Eaton, G.P., eds., *Cenozoic Tectonics and Regional Geophysics of the Western Cordillera*, Geological Society of America Memoir 152, p. 263-265.
- Taylor, W.J., Bartley, J.M., Lux, D.R., and Axen, G.J., 1989, Timing of Tertiary extension in the Railroad Valley-Pioche transect, Nevada: Constraints from $^{40}\text{Ar}/^{39}\text{Ar}$ ages of volcanic rocks: *Journal of Geophysical Research*, v. 94, no. B6, p. 7757-7774.
- Trask, N.J., 1969, Ultramafic xenoliths in basalt, Nye County, Nevada: U.S. Geological Survey Professional Paper, 650-D, p. 43-48.
- Vaniman, D.T., Crowe, B.M., and Gladney, E.S., 1982, Petrology and geochemistry of hawaiite lavas from Crater Flat, Nevada: *Contributions to Mineralogy and Petrology*, v. 80, p. 341-353.
- Walker, J.D. and Coleman, D.S., 1991, Geochemical constraints on mode of extension in the Death Valley region: *Geology*, v. 19, no. 10, p. 971-974.
- White, R.S., 1987, The earths crust and lithosphere: *Journal of Petrology*, Special Lithosphere Issue, p. 1-10.
- White, R.S., Spence, G.D., Fowler, S.R., McKenzie, D.P., Westbrook, G.K., and Bowen, A.D., 1988, Magmatism at rifted continental margins: *Nature*, v. 330, p.439-444.
- White, R.S. and McKenzie, D., 1989, Magmatism at rift zones: The generation of volcanic continental margins and flood basalts: *Journal of Geophysical Research*, v. 94, no. B6, p. 7685-7729.

**AN EXPLANATION TO ACCOMPANY THE GEOLOGIC MAP OF CRATER
FLAT, NEVADA**

(First Draft)

**James E. Faulds
Department of Geology
University of Iowa
Iowa City, Iowa**

**Dan Feuerbach
Center for Volcanic and Tectonic Studies
Department of Geoscience
University of Nevada, Las Vegas
Las Vegas, Nevada 89154**

**A. Ramelli and J. Bell
Nevada Bureau of Mines and Geology
University of Nevada, Reno
Reno, Nevada**

MAP LEGEND

The map "Geological Map of Crater Flat, Nevada" is included in the pocket of this annual report.

- Qal** Alluvium-poorly sorted gravel, sand, and silt.
- Qc** Colluvium-unconsolidated angular blocks.
- QTs** Late Miocene to Quaternary, flat-lying pebble to cobble conglomerate, weakly indurated, primarily of fanglomerate origin.

Geology of the Pliocene Volcanoes

- Qab** Locally derived alluvium; Non-consolidated, poorly sorted angular fragments ranging from gravel to boulders. Clasts consist of basalt with subordinant pyroclastic material shed from the local basalt flows and scoria mounds and cones.
- Qts** Scoria colluvium; Non-consolidated fragments of pyroclastic material shed from cinder cones and scoria mounds.
- Qb** Undifferentiated Quaternary basalt flows and pyroclastic material.
- Qs** Primary pyroclastic deposits; Poorly-to-moderately welded scoria, ash, bombs, and agglutiated scoria deposited by Strombolian to Hawaiian type eruptions. Deposits range from bedded to non-bedded and form the major cinder cones. Scoria mounds at Black Cone and Red Cone are comprised primarily of non-bedded poorly-to-moderately welded scoria and volcanic bombs.
- Qbn** Northern basalt flows at Black Cone; Aa and block flows of alkali-basalt that erupted from scoria mounds north of Black Cone. Basalt is porphyritic with euhedral to subhedral phenocrysts of olivine in a matrix of plagioclase, diopsidic augite and olivine.
- Qbsm** Scoria mound basalt flows; Aa and block flows of alkali-basalt that erupted from scoria mounds south and southeast of Black Cone. The basalt is porphyritic with euhedral to subhedral phenocrysts of olivine in a matrix of plagioclase, diopsidic augite and olivine.
- Qbl** Lava lake on Black Cone; Alkali-basalt flows that probably erupted by lava fountaining at the summit of Black Cone. Basalt locally grades into

agglutinate. Sparce inclusions of Timber Mountain tuff are present.

- Qbsw** Southwestern basalt flows; Aa and block flows of alkali-basalt southwest of Black Cone. The basalt is porphyritic with euhedral to subhedral phenocrysts of olivine in a matrix of plagioclase, diopsidic augite and olivine.
- Qb3** Basalt erupted from the base of Red Cone; Aa and block flows of alkali-basalt east and west of Red Cone. The basalt is porphyritic with euhedral to subhedral phenocrysts of olivine in a matrix of plagioclase, diopsidic augite and olivine.
- Qb2** Basalt flows erupted from scoria mounds southeast of Red Cone. Aa and block flows of alkali-basalt. Basalt is porphyritic with euhedral to subhedral phenocrysts of olivine in a matrix of plagioclase, diopsidic augite and olivine.
- Qb1** Basalt flows erupted from scoria mounds south and southwest of Red Cone. Aa and block flows of alkali-basalt. Basalt is porphyritic with euhedral to subhedral phenocrysts of olivine in a matrix of plagioclase, diopsidic augite and olivine.

Pliocene Units

- Tb** Pliocene alkali-basalt flows erupted from a north-south fissure in southeastern Crater Flat. Olivine is the dominant phenocryst. Olivine, plagioclase and clinopyroxene phenocrysts are set in a matrix of plagioclase, olivine, and clinopyroxene. Glomeroporphyritic clots of olivine, clinopyroxene, and plagioclase are common.
- Tbs** Pliocene-aged pyroclastic deposits; Poorly-to-moderately welded scoria, ash, bombs, and agglutiated scoria deposited by Strombolian to Hawaiian eruptions.

Quaternary and Pliocene Alkali-basalt dikes; Dikes intrude scoria and range in thickness from 0.5 to 3 m wide.

- Tbc** Alkali basalt flows of Crater Flat; K/Ar ages cluster at 3.7 Ma.

Miocene Volcanic Units

Tmr Timber Mountain Tuff, Rainier Mesa Member
undifferentiated.

Tmrw Timber Mountain Tuff, Rainier Mesa Member: Light gray welded ash-flow tuff containing 20-25% phenocrysts of sanidine, quartz, lesser plagioclase and biotite, and rare clinopyroxene.

Tmrn Timber Mountain Tuff, Rainier Mesa Member: White to light gray, thinly bedded to massive nonwelded tuff, air-fall, and surge deposits. Thickness increases across some faults. Contains 10% phenocrysts of sanidine, quartz, lesser plagioclase and biotite, and accessory clinopyroxene.

Tpc Paintbrush Tuff, Tiva Canyon Member: Light purplish-gray to brown generally densely welded ash-flow tuff, with thin (< 5 m) basal nonwelded unit. Contains 5 to 15% phenocrysts of sanidine, lesser plagioclase and biotite, and rare clinopyroxene and quartz. Abundance of phenocrysts increases upward in section. Lenticular fiamme common.

Tr Rhyolite flows: Light gray, coarse-grained, crystal-rich rhyolite containing phenocrysts of plagioclase, quartz, alkali feldspar, and biotite.

Tpy Paintbrush Tuff, Yucca Mountain Member: Light gray to brownish-gray ash-flow tuff containing sparse (2%) phenocrysts of sanidine and plagioclase.

Tpt Paintbrush Tuff, Topopah Spring Member: Light purplish gray to light brownish-gray welded ash-flow tuff containing 10% phenocrysts of sanidine, biotite, and minor plagioclase.

Tptn Paintbrush Tuff, Topopah Spring Member: Pale orange to light brown nonwelded basal part of Tpt. Contains sparse phenocrysts of sanidine, plagioclase, and biotite.

Tcp Crater Flat Tuff, Prow Pass Member: Light gray to brownish-gray ash-flow tuff containing approximately 8% phenocrysts of plagioclase, sanidine, quartz, orthopyroxene, biotite, and magnetite.

Tcb Crater Flat Tuff, Bullfrog Member: Light gray to light brownish-gray, moderate to densely welded ash-flow tuff containing phenocrysts of quartz, plagioclase, sanidine, biotite, hornblende, and magnetite.

**NEW INSIGHTS ON STRUCTURAL CONTROLS AND EMPLACEMENT
MECHANISMS OF PLIOCENE/QUATERNARY BASALTIC DIKES,
SOUTHERN NEVADA AND NORTHWESTERN ARIZONA**

**James E. Faulds
Department of Geology
University of Iowa
Iowa City, Iowa**

INTRODUCTION

Yucca Mountain in southern Nevada has been proposed as the sole repository for the nation's high-level nuclear waste. Five Quaternary basaltic volcanic centers lie within 20 km of the proposed repository block. Four Quaternary centers in Crater Flat have yielded isotopic ages ranging from 1.1 to 0.7 Ma. The Lathrop Wells Cone, 20 km south of the proposed repository block, may be as young as 15 Ka (Wells et al., 1990). In addition, Pliocene (3.7 Ma) basalts were erupted from a separate 4-km-long chain of volcanic centers in Crater Flat. The youthfulness of these basaltic volcanic centers has prompted assessment of the potential volcanic hazard on the proposed repository block.

Assessment of the volcanic hazard must incorporate (1) the composition of the magmas, (2) structural controls (i.e., nature of pathways and geometry of dike systems), (3) emplacement mechanisms of dikes, and (4) probability of future eruptions. This paper focuses on the structural controls and emplacement mechanisms of basaltic dikes in the southern Nevada region. These data are then used to constrain probability estimates of future eruptions in the Yucca Mountain area.

COMPOSITION OF BASALTS

Alkali basalts characterize Quaternary and Pliocene volcanism in southern Nevada and northwestern Arizona. Geochemical and isotopic characteristics indicate derivation of most of the basalts from mantle lithosphere with little, if any, contamination or fractionation within the crust (Vaniman and Crowe, 1981; Vaniman et al., 1982). This, in turn, implies fast rates of ascent for the basaltic magmas. However, alkali basalts in the Reville Range, central Nevada, also contain an asthenospheric component. In addition, tholeiitic basalts occur in a few areas, such as Malpais Mesa in the Fortification Hill field, northwestern Arizona.

STRUCTURAL CONTROLS

Pliocene volcanism in Crater Flat occurred along a 4-km-long north- to north-northeast-trending fissure system. Dikes within this system dip steeply (75 to 90°) and strike north-south to north-northeast. Late Tertiary/Quaternary basin-fill sedimentary rocks obscure relations between Pliocene basaltic dikes and bedrock structures.

North-south to north-northeast-trending alignments dominate the Quaternary volcanic centers near Yucca Mountain. The four Quaternary basaltic volcanic centers in Crater Flat are aligned along a north-northeast to northeast-trending, 12-km-long arcuate chain (Fig 1). The two largest centers, Black Cone and Red Cone, consist of one large cinder cone and many smaller mounds composed of scoria, cinder, ash, and bombs. Dikes commonly project into the mounds, which suggests that the mounds correspond to

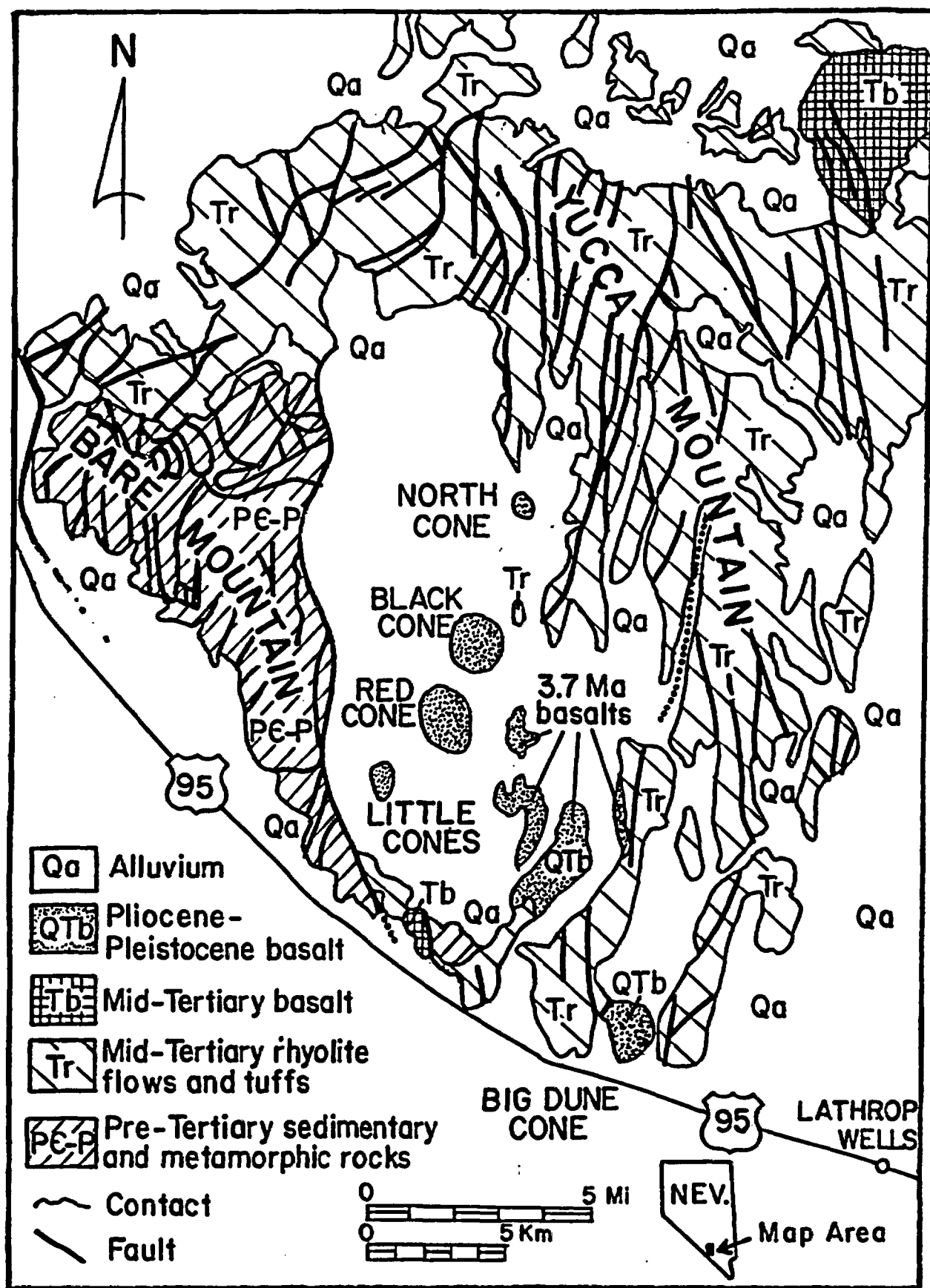


Figure 1. Geologic index map of the Crater Flat-Yucca Mountain area.

volcanic vents. The dikes have near-vertical dips and range up to 3 m in width. Both the dikes and scoria mounds generally trend north-northeast (see geologic map of Crater Flat in pocket). However, at Red Cone a subordinate set of vents strikes N50°W. The Lathrop Wells cone contains both a northwest- and east-west-trending fissure system (Crowe et al., 1988).

Detailed geologic mapping of nearby bedrock geology (Faulds et al., in press; Scott and Bonk, 1984) indicates several potential near-surface north-northeast-trending channelways for the basalts. These include: (1) north-northeast-trending fault segments (see geologic map of Crater Flat in pocket); (2) layering in highly deformed Proterozoic and Paleozoic rocks (Carr and Monsen, 1988); and (3) joints. Closely-spaced north- to north-northeast-trending, generally west-dipping normal faults fragment Yucca Mountain into several gently east-tilted fault blocks. The irregular, en echelon boundary between Yucca Mountain and Crater Flat and the continuation of several bedrock faults into Quaternary faults within Crater Flat indicate that the bedrock geology beneath Crater Flat resembles that at Yucca Mountain.

North-northeast-trending normal faults may be the best candidate for near-surface north-northeast-trending channelways for the basalts. Geologic relations and drill hole data indicate that major normal faults lie in the direct vicinity of some of the volcanic centers (Fig. 2). Furthermore, we suspect that north-northeast-striking normal faults penetrate more deeply than either joints or layering in Proterozoic and Paleozoic strata and thus were more likely to influence the flow paths of the magmas. However, lack of dissection of the young volcanic centers near Yucca Mountain precludes direct observation of feeder dikes and controlling structures. To elucidate the geometry of plumbing systems beneath Quaternary volcanoes near Yucca Mountain, highly dissected Pliocene basaltic centers were studied in several fields within southern Nevada and northwestern Arizona (Fig 3.).

ANALOGUE STUDIES: FORTIFICATION HILL FIELD, NORTHWESTERN ARIZONA

The Fortification Hill field, northwestern Arizona, is best suited for investigating structural controls on basaltic volcanism because the Colorado River drainage has significantly dissected several volcanic centers. The basalts in the Fortification Hill field range from 6.0 to 4.5 Ma. Most are alkali basalts, but tholeiites dominate at Malpais Mesa. Preliminary geochronologic, geochemical, and structural data suggest that the Malpais Mesa basalts may be approximately 10 Ma. Variable levels of erosion of volcanic centers within the Fortification Hill field may ultimately permit construction of a composite cross section of a Pliocene volcano.

At Fortification Hill, the Colorado River has exhumed the periphery of several volcanic centers. Dikes have near vertical dips and are generally less than 2 m in width. A few dikes range up to 10 m in width near some of the volcanic centers at Fortification

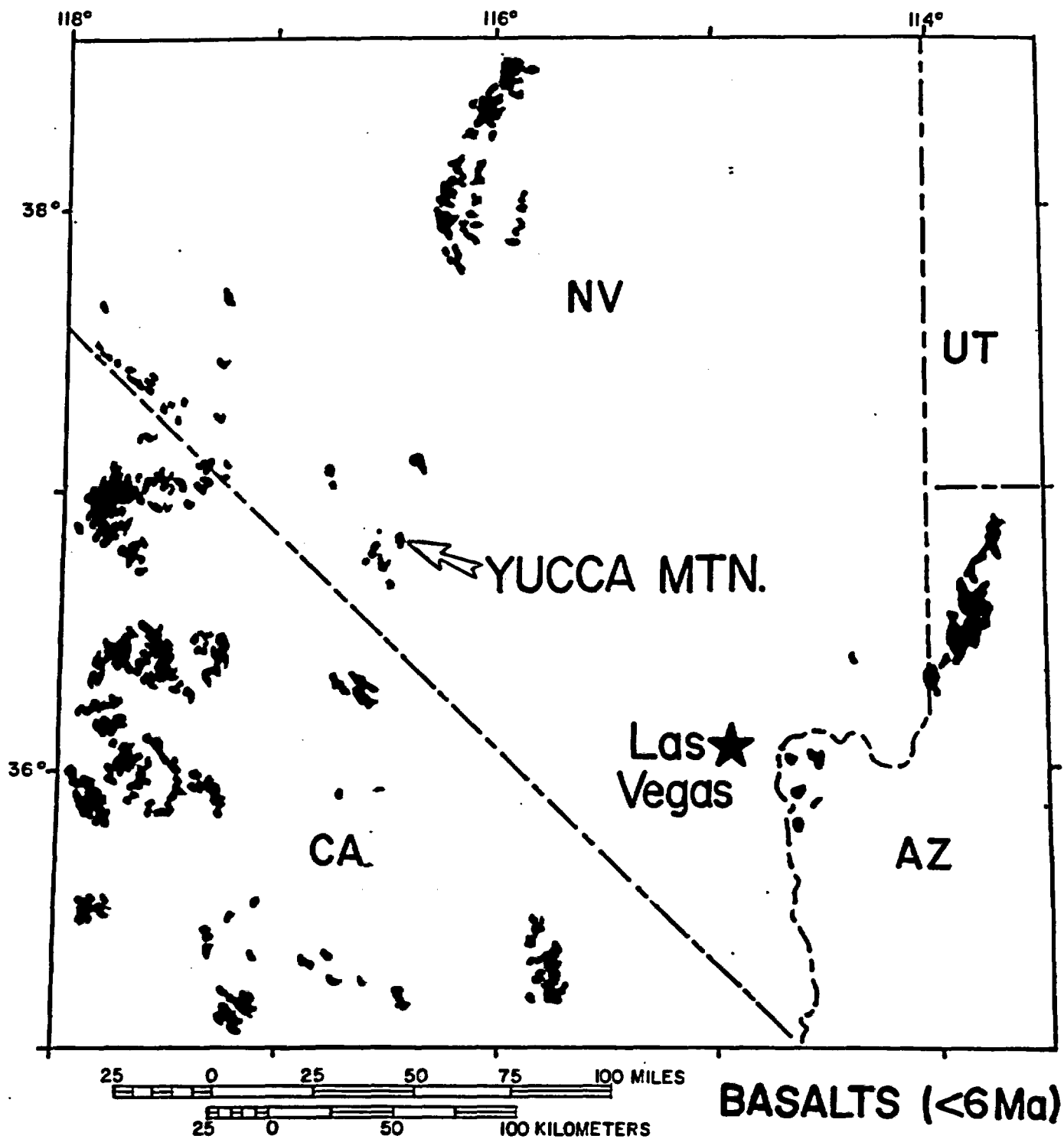


Figure 2. Distribution of pre-6 Ma mafic volcanic rocks in the southern Basin and Range.

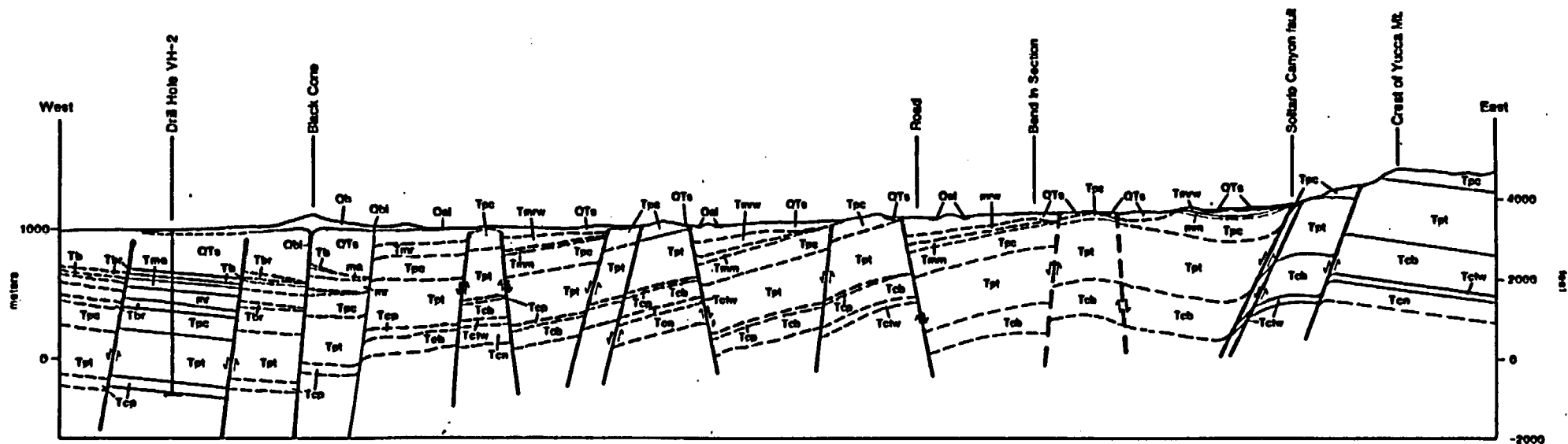


Figure 3. Geologic cross section from the summit of Yucca Mountain to the center of Crater Flat near Black Cone.

Hill. Although they parallel major normal faults, dikes are rarely intruded directly along faults. Unfortunately, dikes cannot be observed directly beneath major volcanic centers at Fortification Hill.

Major volcanic centers are highly dissected, however, at both Lava Cascade and Malpais Mesa. A north-northwest-trending, 3 m wide, steeply dipping dike near the apex of Wilson Ridge fed the flows at Lava Cascade. Although parallel to nearby faults, this dike is not intruded along a fault and clearly cross cuts foliation in Proterozoic metamorphic rocks. Thus, the structural control on the dike remains obscure. However, the distribution of the lava flows suggests that only the uppermost structural level (< 100 m beneath original surface) of this dike is exposed.

The most highly dissected centers in the Fortification Hill field occur on the west flank of Malpais Mesa. The dissected parts of individual centers lie 75 to 365 m beneath the basal flows on Malpais Mesa. Dikes within and directly beneath three centers range from 10-30 m in width, 100-225 m in length, and have near vertical dips. The dikes pinch and swell, widening beneath individual centers. Two centers are linked by a 1-2 m wide dike. At one center, a dike widens upward from 2 to 26 m approximately 170 m beneath the basal basalt flows. At another center, a dike widens laterally from 2 to 10 m more than 300 m beneath the basal basalt flows.

The southernmost center is the largest and least dissected. Two plug-like bodies at this center have widths ranging from 10 to 26 m. One of the plugs clearly feeds flows at the base of Malpais Mesa. This 10 m wide plug thins to less than 1 m directly beneath the flows. Abundant scoria and volcanic bombs flank this volcanic center on the north. Although once again parallel to Miocene normal faults, the north-northwest to northwest-striking dikes at Malpais Mesa are rarely intruded along faults and some cut Miocene faults.

In summary, the dikes in the Fortification Hill field (1) have near vertical dips; (2) commonly parallel Miocene normal faults, but are rarely intruded directly along them; (3) locally cut Miocene normal faults; (4) strike north-northwest to northwest perpendicular to the inferred least principal stress during Pliocene time; (5) widen significantly 170 to 300+ m directly beneath the original topographic surface. These data strongly suggest that At exposed structural levels, dikes within the Fortification Hill field were not intruded along preexisting structures. The only apparent structural control was the orientation of least principal stress.

By analogy, we propose that dikes beneath the Quaternary basaltic volcanoes near Yucca Mountain: (1) have near vertical dips; (2) probably do not follow preexisting structures; (3) may widen significantly upward 300 m beneath the surface; (4) may widen laterally, perhaps by an order of magnitude, directly beneath some centers; and (5) may branch out into smaller feeder dikes within several meters of the surface. Some of the volcanic centers may be underlain by large plug-like bodies. Dike widths in the Yucca

Mountain region are probably narrower than those in the Fortification Hill field, as evidenced by smaller volumes of basalt flows. However, the analogue studies suggest that dike widths directly beneath Quaternary volcanoes near Yucca Mountain may be larger than previously thought.

Although these data constrain the geometry of the basaltic dike systems, they do not directly resolve the structural controls on the centers. Anderson and Christenson (1989) concluded that joints commonly controlled alignments of Quaternary basaltic volcanoes in southwestern Utah. We cannot preclude joint control on some of the volcanic centers in the Yucca Mountain region. We suspect, however, that any control by joints is confined to discrete lithologies (e.g., Pollard and Aydin, 1988) and that such joints do not penetrate deeply. The nature of crustal-penetrating channelways that afford quick transport of magmas remains elusive.

DISCUSSION

The near vertical dips and lack of definitive structural controls may imply that the basaltic dikes propagated upward through "self-generated" fractures produced by tensile stresses near the dike tip, magmatic overpressure and buoyancy, and regional tension. The dikes were probably initiated in the mantle lithosphere perpendicular to the least principal stress. The first increments of melt presumably formed on planes normal to the least principal stress (Savage, 1969; Shaw, 1980). The melting reaction was the first in a sequence of rock failures. It was the most important, however, because it governed the eventual location of surficial volcanism. Tensile stresses near the dike tip, induced by magmatic pressure, and buoyancy (Delaney et al., 1986) allowed the dike to propagate upward to at least the level of neutral buoyancy (i.e., the level at which density of melt equals that of the surrounding rock) (Lister and Kerr, 1991). Dike propagation far beyond the level of neutral buoyancy is problematic. Lateral propagation (i.e., in a horizontal direction) could continue at the level of neutral buoyancy, but vertical propagation would be stymied.

Glazner and Ussler (1989) concluded, however, that crustal thinning and emplacement of mafic plutons during crustal extension will increase mean crustal density and consequently induce a rise in the level of neutral buoyancy. Basaltic volcanism in both the Yucca Mountain and Fortification Hill regions followed prolonged episodes of voluminous Tertiary magmatism and moderate to severe extension (e.g., Anderson, 1971; Maldonado, 1990; Schweickert and Caskey, 1990) during which the level of neutral buoyancy probably rose significantly. In addition, the Yucca Mountain region is currently under high extensional stress (Stock and Healey, 1984).

We therefore propose that magmatic overpressure and the resultant tensile stresses near the dike tip, exsolution of volatiles, a relatively shallow level of neutral buoyancy resulting from prior episodes of magmatism and extension, and concurrent

regional tension allowed the basaltic dikes in the Yucca Mountain region to propagate to the surface through "self-generated" fractures oriented perpendicular to the N60°W trend of least principal stress (Fig. 4). Regional tension and magmatic overpressure were probably the most critical components to this process. Regional tension favored both the vertical and lateral propagation of cracks perpendicular to the least principal stress and magmatic overpressure allowed melt to quickly fill the cracks. If situated directly above a rising batch of magma, preexisting north-northeast-striking structures may have locally facilitated melt transport. Theoretical data suggest that basaltic magmas may rise through the entire crust in a matter of hours or days (e.g., Spence and Turcotte, 1985).

These conclusions have significant implications for hazard assessments of the proposed repository at Yucca Mountain. The potential for dike intrusion along self-generated fractures not associated with preexisting faults must be considered. Probability estimates of future eruptions must therefore involve delineation of an area of most recent volcanism (AMRV) (Smith et al., 1990) that is comparable in size to other Pliocene/Quaternary basaltic volcanic fields in the Basin and Range and whose long axis is perpendicular to the least principal stress. Probabilities of future eruptions can be estimated from the temporal and spatial distribution of eruptions within (a) the AMRV near Yucca Mountain, (b) analogous Pliocene volcanic fields where volcanism has ceased, or (c) larger regional volcanic belts such as the Pliocene/Quaternary Death Valley/Pancake Range belt. The available data may not permit, however, accurate determination of weighted probabilities or risk zones within an individual AMRV.

The location of at least some of the Pliocene/Quaternary basaltic volcanic fields in the Basin and Range may be related to small pull-aparts on crustal penetrating strike-slip fault zones. The Fortification Hill field occurs near the southeastern terminus of the right-lateral Las Vegas Valley shear zone (Duebendorfer and Wallin, 1991). The Yucca Mountain region may occupy a large right-step between the Las Vegas Valley shear zone and Walker Lane belt (Carr, 1984; Stewart, 1986). The continuation of the Las Vegas Valley shear zone across several extensional domains implies that the shear zone is not confined to the upper-plate of a detachment system but instead may penetrate much of the crust. Extension within small pull-aparts along this strike-slip fault zone may have served to localize melts within the mantle lithosphere and ultimately controlled the location of basaltic volcanic fields.

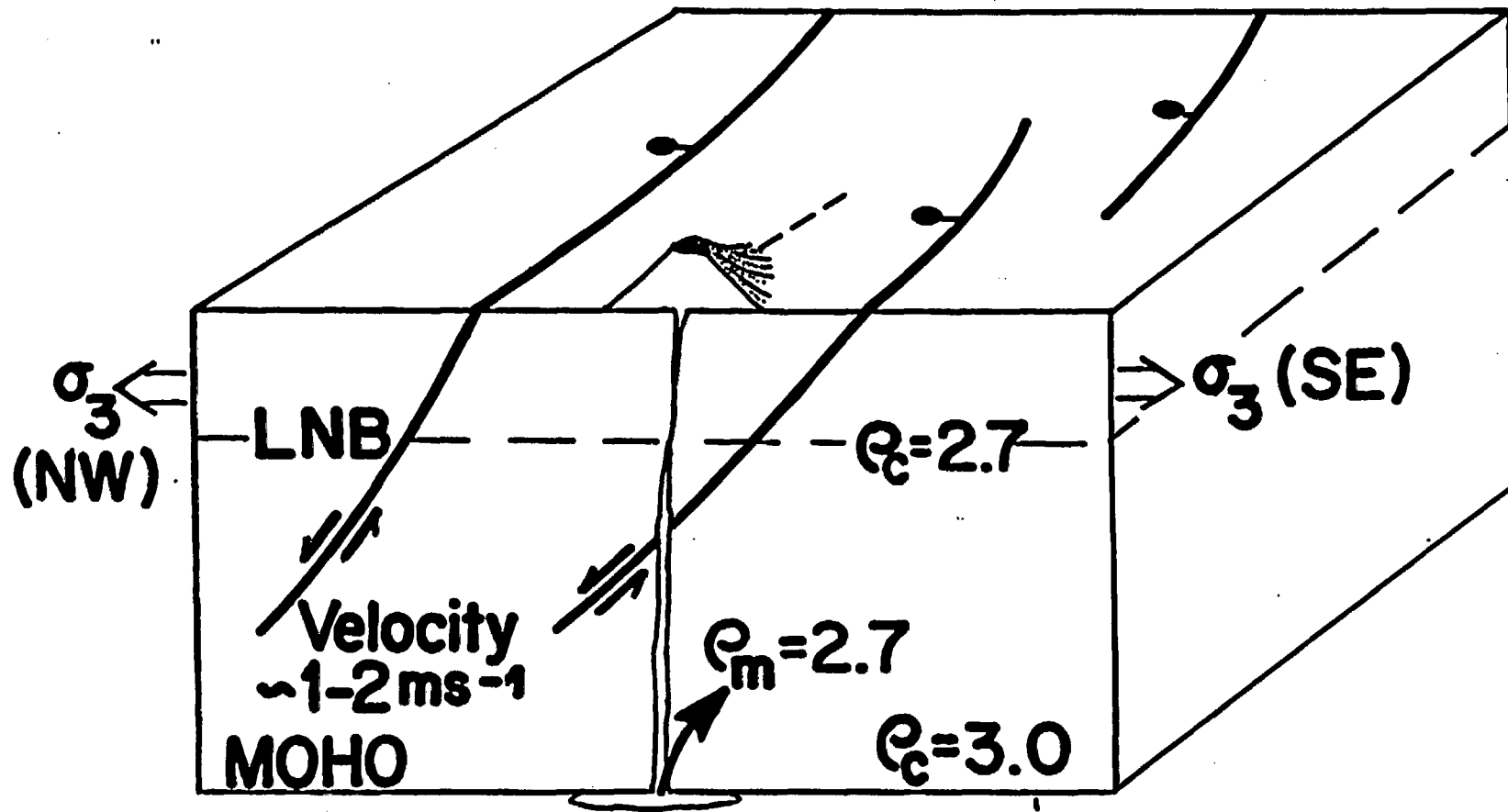


Figure 4. Model for the emplacement of mafic dikes during regional extension. See text for explanation.

REFERENCES

- Anderson, R. E., and Christenson, G. E., 1989, Quaternary faults, folds, and selected volcanic features in the Cedar City 1° X 2° quadrangle, Utah: Utah Geological and Mineral Survey Miscellaneous Publication 89-6, 29 p.
- Burchfiel, B. C., and 6 others, 1989, Intracrustal detachment within zones of continental deformation: *Geology*, v. 17, p. 748-752.
- Carr, M. D., and Monsen, S. A., 1988, Field trip guide to the geology of Bare Mountain, in Weide, D. L., and Faber, M. L., eds., *This extended land—Geological journeys in the southern Basin and Range: Geological Society of America, Cordilleran Section, Field Trip Guidebook*, p. 50-57.
- Carr, W. J., 1984, Regional structural setting of Yucca Mountain, southwestern Nevada, and late Cenozoic rates of tectonic activity in part of the southwestern Great Basin, Nevada and California: U.S. Geological Survey Open-File Report 84-854, 109 p.
- Crowe, B. M., Harrington, C., McFadden, L., Perry, F., Wells, S. Turrin, B., and Champion, D., 1988, Preliminary geologic map of the Lathrop Wells volcanic center: Los Alamos National Laboratory Report LA-UR-88-4155.
- Delaney, P. T., Pollard, D. D., Ziony, J. I., and McKee, E. H., 1986, Field relations between dikes and joints: Emplacement processes and paleostress analysis: *Journal of Geophysical Research*, v. 91, p. 4920-4938.
- Duebendorfer, E. M., and Wallin, E. T., 1991, Basin development and syntectonic sedimentation associated with kinematically coupled strike-slip and detachment faulting, southern Nevada: *Geology*, v. 18, p. 87-90.
- Glazner, A. F., and Ussler, W., 1989, Crustal extension, crustal density, and the evolution of Cenozoic magmatism in the Basin and Range of the western United States: *Journal of Geophysical Research*, v. 94, p. 7952-7960.
- Lister, J. R., and Kerr, R. C., 1991, Fluid-mechanical models of crack propagation and their application to magma transport in dykes: *Journal of Geophysical Research*, v. 96, p. 10,049-10,077.
- Maldonado, F., 1990, Structural geology of the upper plate of the Bullfrog Hills detachment fault system, southern Nevada: *Geological Society of America Bulletin*, v. 102, p. 992-1006.
- Pollard, D. D., and Aydin, A., 1988, Progress in understanding jointing over the past

century: Geological Society of America Bulletin, v. 100, p. 1181-1204.

Schweickert, R. A., and Caskey, S. J., 1990, Pre-middle Miocene extensional history of the Nevada Test Site (NTS) region, southern Nevada: Geological Society of America Abstracts with Programs, v. 22, no. 3, p. 81.

Scott, R. B., and Bonk, J., 1984, Preliminary geologic map of Yucca Mountain, Nye County, Nevada, with geologic sections: U.S. Geological Survey Open-File Report 84-494, scale 1:12,000.

Shaw, H. R., 1980, The fracture mechanisms of magma transport from the mantle to the surface, in Hargraves, R. B., ed., Physics of magmatic processes: Princeton University Press, p. 201-259.

Smith, E. L., Feuerbach, D. L., Naumann, T. R., and Faulds, J. E., 1990, The area of most recent volcanism near Yucca Mountain, Nevada: Implications for volcanic risk assessment: American Nuclear Society, High level radioactive waste management, v. 1, p. 81-90.

Spence, D. A., and Turcotte, D. L., 1985, Magma-driven propagation of cracks: Journal Geophysical Research, v. 90, p. 575-580.

Stewart, J. H., 1986, Tectonics of the Walker Lane belt, western Great Basin--Mesozoic and Cenozoic deformation in a zone of shear: Metamorphism and crustal evolution of the western United States, v. 7, Prentice-Hall, Inc., Englewood Cliffs, New Jersey.

Stock, J. M., and Healy, J. H., 1988, Stress field at Yucca Mountain, Nevada: U.S. Geological Survey Bulletin 1790, p. 87-94.

Vaniman, D. T., and Crowe, B. M., 1981, Geology and petrology of the basalt of Crater Flat: Applications to volcanic risk assessment for the Nevada Nuclear Waste Storage Investigations: Los Alamos National Laboratory Report LA-8845-MS.

Vaniman, D., Crowe, B., and Gladley, E. S., 1982, Petrology and geochemistry of hawaiite lavas from Crater Flat, Nevada: Contributions to Mineralogy and Petrology, v. 80, p. 341-357.

Wells, S. G., McFadden, L. D., Renault, C. E., and Crowe, B. M., 1990, Geomorphic assessment of late Quaternary volcanism in the Yucca Mountain area, southern Nevada: Implications for the proposed high-level Society of America Bulletin, v. 100, p. 1738-1757.

ABSTRACTS

LANDSLIDING AND GROUND-CRACKING IN THE EPICENTRAL REGION OF THE 1989 LOMA PRIETA EARTHQUAKE

MOUTOUX, T.E.; VICK, G.S.; NOLAN, J.M.; WEBER, G.E.; BOL, A.J.; MILLER, S.L. Weber and Associates, 120 Westgate Dr., Watsonville, CA 95076

The epicenter of the 1989 Loma Prieta earthquake lies in a large, rugged tract of uninhabited land included within the Forest of Wicente Marks State Park in Santa Cruz County, California. We mapped surface deformation within the epicentral region of the earthquake (ground-cracks and landslides) on 1:4800 scale topographic maps. Because the earthquake related ground deformation showed an intimate association with older deformation, we also mapped of pre-existing features, including old landsliding and an older series of ground-cracks.

Landslides were categorized into three failure-type groups: rotational, translational, or debris flow; and three age groups: earthquake related (1989), recent (about 50 years or less in age), and older. We recorded displacement magnitudes for cracks related to the Loma Prieta earthquake.

Earthquake related landslides were sparse, and were predominantly small to medium sized translational type landslides, indicating failure of weathered surficial material. We did not see wholesale reactivation of the many large, older landslide complexes, nor did we observe the formation of new large landslides. These observations suggest that formation of the larger, more deep seated landslides is not being driven by Loma Prieta type events, at least, not under present climatic conditions. The earthquake deformation concentrates in a broad band trending parallel to the regional bedding and faulting, and lying just north of the Sayante fault along the axis of the Glenwood Syncline.

FLUVIAL GEOMORPHIC INDICATORS OF NEOTECTONISM IN THE SOUTHWESTERN SACRAMENTO VALLEY, CALIFORNIA

MUNK, L.P. (Dept. of Land, Air and Water Resources); UNRUH, J.R. (Dept. of Geology); MOORES, E.M. (Dept. of Geology); and SOUTHWARD, R.J. (Dept. of Land, Air and Water Resources); all at: University of California, Davis 95616

The Dunnigan Hills and Plainfield Ridge are anomalous areas of subtle positive relief in the otherwise nearly level southwestern Sacramento Valley. Seismic reflection data suggest that these geomorphic features are underlain by east-vergent blind thrust faults at depths of 4-7 km. We propose that Quaternary movement on these thrusts has produced surface uplift and subsequent alteration of the local fluvial system. Longitudinal stream profiles, determined from topographic maps that predate major agricultural modifications of the drainage system, indicate that east-draining streams have convex profiles along reaches that cross the Plainfield Ridge and southern Dunnigan Hills. Best-fit exponential curves developed for similar-sized streams south of the study area were used as a standard of comparison in order to analyze deviations from a graded condition. The local departures from a concave-up profile for reaches crossing the Plainfield Ridge and Dunnigan Hills are interpreted as evidence of recent tectonism. Additional evidence for recent uplift includes underfit and abandoned stream valleys, locally developed flights of fluvial terraces, and poorly integrated drainage networks developed on the uplifted terrain. Soil-stratigraphic studies are being conducted to constrain the rate and timing of deformation. These data, combined with subsurface analysis and studies of microseismicity (Eaton, 1986; Wong et al. 1988) suggest that the Dunnigan Hills and Plainfield Ridge may be the easternmost surface expression of an actively growing fold-thrust belt in the southwestern Sacramento Valley.

DEVELOPMENTS IN JURASSIC STRATIGRAPHY OF THE FRANCISCAN COMPLEX, CALIFORNIA: EXPANDED AND RECALIBRATED RADIOLARIAN ZONATION COUPLED WITH POTENTIAL FOR MAGNETOSTRATIGRAPHY

MURCHEY, Benita L., U.S. Geological Survey, MS 915, Menlo Park, CA 94025; HAGSTRUM, Jonathan T., U.S. Geological Survey, MS 937, Menlo Park, CA 94025

The expansion of the number of taxa used to characterize radiolarian assemblages in the Franciscan Complex of California permits more accurate regional correlations as well as more precise age determinations. The ages of Jurassic assemblages MH-1 to MH-4 (Murche, 1984) were recalibrated downward by comparing the ranges of more than 100 taxa in bedded chert sequences in the Marin Headlands, Mt. Umuhum, and Geysers areas to those in well-dated sequences from Europe and North America. MH-1 is late Pliensbachian to early or middle Toarcian. MH-2 best correlates with middle and late Toarcian faunas. The boundary between MH-2 and MH-3 is not younger than early Bajocian, but is probably older. The upper part of MH-3 is Bajocian. The base of MH-4 is late Bajocian or Bathonian; the youngest known MH-4 faunas are Callovian or Oxfordian. The stratigraphic gap between MH-4 faunas and Early Cretaceous MH-5 faunas is marked by a recrystallized interval that may have been a zone of slow deposition.

The discovery of a series of paleomagnetic reversals in chert with MH-1, MH-2, and MH-3 faunas in the Mt. Umuhum and Geysers areas holds the promise for future development of Jurassic magnetostratigraphy directly tied to radiolarian biostratigraphy.

REE SYSTEMATICS OF SULFIDE-SULFATE DEPOSITS AND SEA-FLOOR SUBSTRATES AT SEDIMENT-FREE AND SEDIMENT-COVERED SPREADING CENTERS IN THE NORTHEAST PACIFIC OCEAN

MURPHY, John E., Department of Geology, Northern Illinois University, DeKalb, IL 60115; KOSKI, Randolph A., U.S. Geological Survey, MS999, 345 Middlefield Road, Menlo Park, CA 94025

The sediment-free southern segment of Juan de Fuca Ridge and the sediment-covered southern segment of the Gorda Ridge (Escanaba Trough) are contrasting sites of hydrothermal discharge and sulfide-sulfate deposition in the northeast Pacific. On the southern Juan de Fuca Ridge, chimneys largely composed of Zn and Fe sulfides + anhydrite formed where black smoker fluids have discharged through basalt sheet flows. At Escanaba Trough, large (hundreds of meters across) mounds consisting of Fe and Cu sulfides + barite are precipitated by hydrothermal fluids upwelling through the >500-m-thick blanket of terrigenous sediment. A suite of samples from the two sites including basalt, sediment, polymetallic sulfides, Ba and Cu sulfates, and Fe oxyhydroxides was analyzed for rare-earth elements (REE) by inductively coupled plasma mass spectrometry.

Chondrite-normalized REE patterns of unaltered basalt from both ridges are characteristic of a MORB (flat to slightly depleted in LREE with (La/Sm)_N = 0.63 to 1.02 and small negative Eu anomalies). Sediment samples from Escanaba Trough (sand and silt turbidites, hemipelagic mud) have shale-like LREE-enriched patterns with IREE = 115 to 204 ppm and (La/Sm)_N = 2.8. The close similarity between REE patterns of unaltered sediment and hydrothermally altered sediment partly to completely replaced by chlorite and talc indicates very limited mobility of REE during subseafloor Mg metasomatism. Massive sulfide samples have higher IREE (8 to 28 ppm) contents than massive sulfide samples (<8 ppm), but all hydrothermal samples from both sites exhibit LREE enrichment patterns. Massive anhydrite and barite have large positive Eu anomalies characteristic of high-temperature hydrothermal fluids (Michard and Albarde, 1986). Anhydrites also exhibit small positive Ce anomalies. Pure sulfide samples lack Eu anomalies; therefore, the positive Eu anomalies (Eu/Eu* > 20) in most massive sulfides reflect the presence of intergrown sulfide minerals. Small negative Ce anomalies are associated with Fe-oxyhydroxide crusts from weathered surfaces of sulfide chimneys and sulfide samples containing abundant amorphous silica.

The data indicate that compositional differences of sea-floor substrates at the two spreading centers have a minor effect on the REE distribution in sea-floor hydrothermal deposits in comparison to the hydrothermal fluid-seawater mixing processes that control sulfide deposition.

STRUCTURAL CONTROL OF PIOCENE VOLCANISM IN THE VICINITY OF THE NEVADA TEST SITE, NEVADA: AN EXAMPLE FROM BUCKBOARD MESA

NAUMANN, T.R., FEUERBACH, D.L., and SMITH, E.I., Department of Geoscience, University of Nevada, Las Vegas, NV 89154.

Late Pliocene to Quaternary (4 to <0.1 Ma) alkali basalt and basaltic andesite erupted in the vicinity of the Nevada Test Site (NTS) at Crater Flat, Sleeping Butte and Buckboard Mesa. Eruptions occurred along or near north to northeast striking faults that are typical of the area between Yucca Mountain to the south and Pahute Mesa to the north. This structural pattern is interrupted by the Timber Mountain caldera. Buckboard Mesa is comprised of a cinder cone (Scragham Peak) and flows of basaltic andesite that lie in the moat of the Timber Mountain caldera. The main vent zone on Buckboard Mesa is defined by the Scragham Peak cinder cone and several small vents. The vent zone is 1 km long, trends northeast, and is controlled by an echelon fault segments that strike N10E. These faults were active before, during and after the eruption of the basaltic andesite at 2.8 Ma. Evidence for this chronology includes the observations that Buckboard Mesa lavas were deposited on faulted Timber Mountain tuff and that the same fault zone cuts Buckboard Mesa lavas and Scragham Peak. Another vent is located at the termination of a narrow ridge that extends southeast from the base of Scragham Peak. This ridge is subparallel with the axis of a paleovalley that apparently controlled flow direction of Buckboard Mesa lavas. This ridge and vent may either be tube fed and rootless or may represent eruptions from the Timber Mountain ring fracture. The eruptions at Buckboard Mesa were focused at the intersection of the northeast striking fault zone and the ring fracture zone of the Timber Mountain caldera, however, the northeast zone was the primary structure controlling magma emplacement. This is in accordance with the structural controls for other post 4-Ma volcanic centers in the NTS area in Crater Flat and at Sleeping Butte.

CLAY MINERALOGY, RESIDUAL SHEAR STRENGTH AND LANDSLIDING OF THE SANTA CLARA FORMATION CLAYSTONE, SARATOGA FOOTHILLS, CALIFORNIA

NELSON, James L., Terratech, Inc., 7891 Westwood Drive, Gilroy, CA 95020.

Most landslides in the Saratoga foothills, California, occur along previously sheared surfaces formed in claystone units of the Plio-Pleistocene Santa Clara Formation. The primary geologic factors that control landsliding are the presence of the clay mineral smectite and the overconsolidated nature of the claystone.

Preexisting landslide surfaces in the claystone units appear to be at, or near, the residual shear (frictional) strength of the clay minerals present. To evaluate the effects of clay mineralogy on residual shear strength, laboratory testing and X-ray diffraction were performed on claystone samples collected from landslide-prone areas in the Saratoga foothills.

VADOSE-ZONE AND GROUND-WATER TRANSPORT MODELING TO ESTABLISH ACCEPTABLE CLEANUP GOALS FOR VOCs IN SOIL

FARR, John M., and LAMBIE, John M., Levine-Fricka, Inc.
1900 Powell Street, 12th Floor, Emeryville, CA 94608

For Superfund projects where soil contamination exists, soil cleanup goals must be established as the basis for feasibility studies and the design and implementation of remedial actions. Soil cleanup goals must be protective of underlying ground water and its designated beneficial uses. Mathematical transport models can be used to assess the potential ground-water impacts from various levels of soil contamination, thereby aiding in the selection of appropriate soil cleanup goals.

Indirectly coupled models are generally used to represent transport in the vadose zone and the ground-water zone separately, even though the transport processes in these two zones are directly coupled. In this study, the SEASONAL SOIL compartment model (SESOIL) of Bonazountas and Wagner (1984 - with significant modifications by Metrick, et al., 1989) was used to model vadose-zone transport and the Analytical Transient 1-, 2-, and 3-Dimensional model (AT123D) of Yeh (1981) was used to model ground-water transport. SESOIL can represent one-dimensional aqueous advection, gaseous diffusion, adsorption, and degradation in up to four soil layers with varying properties. AT123D can represent advective-dispersive ground-water transport away from source areas of varied dimensions, strength, and duration within homogeneous, isotropic aquifers. Simulation results from the application of these models to a Superfund site in the San Francisco Bay Area were used to develop and support proposed cleanup levels for volatile organic compounds (VOCs) in soils.

IMPLICATIONS OF ALONG-STRIKE VARIATIONS IN BASIN GEOMETRY ON THE KINEMATICS OF MIOCENE EXTENSION, NORTHWEST ARIZONA AND SOUTHERN NEVADA

PAULDS, J., Dept. Geology, U. So. California, Los Angeles, CA 90089;
DUEBENDORFER, E., Dept. Geology, U. Nevada, Las Vegas, NV 89154.

Along-strike changes in graben geometry may be pertinent to kinematic models of continental extension. In the northernmost Colorado River extensional corridor, an E-tilted half graben extends 40 km northward from a major accommodation zone. The W-dipping Wilson Ridge fault (WRF) bounds the basin on the east; the northern basin margin is the dextral Las Vegas Valley shear zone (LVVSZ). The major pulse of tilting occurred between 16-13 Ma and 13-9 Ma in the southern and northern parts of the basin, respectively. The accommodation zone served as a rupture barrier during both events. Directly north of the accommodation zone, the basin deepens and widens northward as displacement on the WRF and tilting both increase. Farther north, the basin expands in two discrete steps with little increase in tilting. The steps are marked by minor sinistral offset on transfer faults and broad flexures in the strike of Tertiary strata indicative of anti-clockwise vertical-axis rotation. The basin is widest (20 km) at its northern margin near the LVVSZ. Abundant crystalline detritus in the basin suggests that the footwall crystalline terrane of the WRF was exposed throughout Miocene extension. The WRF terminates near the inferred juncture and apparent termination of the LVVSZ and sinistral Lake Mead fault system (LMFS).

The deformational style associated with expansion of the basin implies that the relative diametrical translation of the hanging wall and footwall of the WRF increases away from the accommodation zone but is not proportional to the magnitude of tilting. Coeval activity along the LVVSZ, LMFS, and WRF further suggests major kinematic coupling of strike-slip and normal faults at the northern end of the extensional corridor. Diametrical lateral transport of the hanging wall and footwall of the WRF may partly account for opposing senses of strike-slip motion along the LVVSZ and LMFS.

SYNEXENSIONAL BARITE-SILVER MINERALIZATION IN THE HANGING WALL OF THE WATERMAN HILLS DETACHMENT FAULT, CENTRAL MOJAVE DESERT, CALIFORNIA

FEISS, P., Geoffrey, GLAZNER, Allen F., Dept. of Geology, CSU 3315, Univ. of North Carolina, Chapel Hill, NC 27599, BARTLEY, John M., Dept. of Geology and Geophysics, Univ. of Utah, Salt Lake City, UT 84112

Barite-silver mineralization in the Waterman Hills, north of Barstow, CA, and large barite-silver deposits in the nearby Calico Mountains, occur in the hanging wall of the Waterman Hills detachment fault (WHDF), an early Miocene low-angle normal fault. In the Waterman Hills, the deposits are exposed at the Waterman Mine and occur in steeply dipping early Miocene volcanic and sedimentary rocks. Mapping (1:2400) reveals that mineralization was syndepositional and derived from the meteoric-hydrothermal system that caused pervasive K-metasomatism of the hanging wall of the WHDF and chlorite alteration of the footwall.

We term the two mineralized stratigraphic horizons the lower ore horizon (LOH) and upper ore horizon (UOH). The LOH and UOH each are exposed for approximately 1 km along strike; both consist of thin, fine-grained, green to purple, lacustrine beds containing conformable jasperoid silica and barite with Ag-bearing veinlets. Each ore horizon records an episode of

sublacustrine mineralization which was abruptly terminated by emplacement of a massive debris flow. The LOH is 5-15 m thick and is both underlain and overlain by massive volcanic debris flows. Barite and silver are absent from the stratigraphically overlying debris flows and are found in only one narrow 5 m zone in underlying rocks. The UOH is thinner than the LOH and is extensively brecciated. Fragments of jasperite, mudstone and siltstone, and bedded barite are rimmed and cemented by barite and by the fine-grained clastic matrix. The UOH is underlain by the debris flow that overlies the LOH and is overlain by a monolithic dionite megabreccia. Barite veins and flowerets are found in the porous debris flow underlying the UOH for a distance of 3-15 m beneath the mineralized horizon, but no mineralization is observed in the equally porous overlying debris flow.

The presence of conformable interbedded lacustrine sediments, jasperites, and bedded barite, the latter restricted to thin lacustrine horizons, indicates that barite deposition was syndepositional. Emplacement of thick debris flows and megabreccia terminated the barite-depositing thermal spring activity that formed each ore horizon. The deposits formed during extensional faulting because the ore horizons are (1) interbedded with extremely coarse, syn-extensional debris flows, (2) tilted to dips ranging from generally >70° to locally overturned, and (3) truncated by mylonite plugs that are themselves cut by the WHDF. Thus, these deposits and possibly those of the Calico district represent detachment-related Ag mineralization.

THE TRANSITION FROM SUBALKALIC TO ALKALIC VOLCANISM IN THE LAKE MEAD AREA OF NEVADA AND ARIZONA: GEOCHEMICAL AND ISOTOPIC CONSTRAINTS

FEUERBACH, D.L., and SMITH, E.L., Department of Geoscience, University of Nevada, Las Vegas, NV 89154; WALKER, J.D. and TANGEMAN, J.A., Department of Geology, University of Kansas, Lawrence, KS 66045.

Late Miocene to early Pliocene volcanic rocks in the Lake Mead area of Nevada and Arizona record the transition from early, moderate-volume, subalkalic basalt and basaltic andesite to later, low-volume, alkali basalt volcanism. Calc-alkalic basaltic andesites occur in the Calville Mesa volcanic field (CM) on the north shore of Lake Mead. CM lavas erupted from two composed older cones between 10.6 and 8.5 Ma. Basaltic andesite (52 to 55% SiO₂) shows isotopic and textural evidence of crustal contamination (initial ⁸⁷Si/⁸⁶Si = 8.708-8.709, epsilon Nd = -8.49 to -10.69, and ²⁰⁷Pb/²⁰⁴Pb = 17.573 to 17.532). We suggest that Calville magmas were generated in the lithospheric mantle as basalt similar in composition to basalt in Calville Wash (10.6 Ma) and younger Fortification Hill basalt, but were contaminated in the crust during ascent.

Subalkalic and alkalic basalts (46 to 50% SiO₂) occur in the Fortification Hill field (FH). FH basalts erupted from at least eight volcanic centers between 6.02 and 4.3 Ma. Fortification Hill on the east side of Lake Mead is the most voluminous of these centers. We divide FH basalt into three groups: (1) Tholeiitic two pyroxene basalt (6.02-5.71 Ma) (SAB) at Black Point and Malpais Flatop and subalkalic basalt at Fortification Hill (lower section). (2) Alkali basalt (5.42 to 4.74 Ma) (OAB) at Fortification Hill (upper section), Petroglyph Wash and Lava Cascade. (3) Alkali basalt (4.61 to 4.3 Ma) (YAB) along U.S. 93 near Hoover Dam, Saddle Island and in Petroglyph Wash. YAB lavas commonly contain ultramafic nodules and amphibole and feldspar megacrysts. The transition from subalkalic to alkalic volcanism occurred between 5.71 and 5.42 Ma during the formation of Fortification Hill. The change from SAB to YAB is marked by an increase in Na₂O + K₂O (3.5 to 7%), Ca/Yb_N (3.5 to 12), Ti (2.5 to 9 ppm), F₂O₃ (0.35 to 0.8%), TiO₂ (1.3 to 2.5%), and normative nepheline (all values are means). OAB lavas are intermediate in composition between SAB and YAB. The change from SAB to YAB is marked by a decrease in initial ⁸⁷Si/⁸⁶Si from 8.709-8.706 in SAB lavas to 8.703 in OAB to 8.703 in YAB. Epsilon Nd increases from -2.28 to -0.34 in SAB to -0.64 in OAB to 3.68 in YAB. These geochemical variations reflect a change from lithospheric to asthenospheric mantle sources with time. This change may reflect lithospheric erosion due to regional extension.

KINEMATIC MODEL FOR THE DEVELOPMENT OF WEST-VERGING STRUCTURES IN THE PURCELL ANTICLINORIUM, CABINET MOUNTAINS, NORTHWESTERN MONTANA

FILLIPONE, Jeffrey and YIN, An, Department of Earth and Space Sciences, University of California Los Angeles, Los Angeles, CA 90024

The west flank of the Purcell Anticlinorium in the Cabinet Mountains, northwestern Montana consists of three major structural elements: (1) E-verging structures including E-directed thrusts, E-verging folds, and W-dipping cleavage, (2) W-verging structures including W-verging overturned folds, W-directed thrusts, and E-dipping cleavage, and (3) a series of N-trending Cretaceous plutons. The E-verging structures are of regional extent, and can be traced throughout the Cabinet Mountains. In contrast, the W-verging structures are localized in the central Cabinet Mountains. The oppositely verging structures are separated to the south by a SW-dipping thrust fault and to the west by a Cretaceous pluton (the Dry Creek stock) and a later high-angle fault (the Rock Lake fault). E-directed thrusts lie structurally above the W-directed structures. Towards the north, W-verging structures become a series of broad folds. Cross-cutting relationships between the E- and W-verging mesoscopic structures, e.g., cleavage, are not present in the area, suggesting coeval development of the two structural elements. The Dry Creek stock lies about 3.5 km west of the W-verging structures and has a cone-shaped geometry on a cross-sectional view. Well developed foliation, locally mylonitic, is present on the west side of the stock. The S-C fabric indicates a top-to-the-east sense of shear on a W-dipping shear zone. This relation suggests that the E-verging structures formed either during or immediately after emplacement of the stock, and thus, all three major structural elements in the area may have formed simultaneously. On the basis of age relationships among structures in the area and the spatial relationship between the stock and the localized W-verging structures, we interpret that the development of localized W-verging structures may be the result of pluton emplacement. In particular, the spreading of magma at shallow structural levels within the Belt strata may have produced a localized, W-directed simple shear strain within the Belt rocks. An alternative model is that a W-dipping thrust ramp is present at depth and the W-verging structures were related to the emplacement of a hanging-wall anticline, a wedge-shaped indentor, to form a triangle zone. This model is, however, inconsistent with the field relationship that the W-verging structures formed beneath E-verging structures.

THE EASTERN BOUNDARY OF THE EXTENSIONAL ALLOCHTHON IN THE EASTERN BASIN AND RANGE: VOLCANIC AND STRUCTURAL GEOLOGY OF THE NORTHERN WHITE HILLS, ARIZONA

CASCADEN, Tracy E., and SMITH, Eugene L. Department of Geoscience, University of Nevada, Las Vegas, NV 89154

The northern White Hills lie in the upper plate of the westward-dipping Salt Spring detachment. The upper plate contains 5 east-tilted structural blocks comprised of Miocene basaltic andesite flows (49-54% SiO₂), agglomerates, dacite ash-flow tuffs, megabreccia and conglomerate. Because each block is isolated and contains only a small part of the stratigraphic section, geochemical data (La, Cr, Hf, Sc, Sr and Co) was used to construct a composite section. The oldest part of the composite section consists of at least 464 meters of basaltic andesite flows and autoclastic breccias. They are overlain by 0-575 meters of coarse monolithologic breccia, in which the dominant clast type is lower plate Precambrian pelite, granite, amphibolite, and syenite. The breccia forms a discontinuous sheet that extends 12 km west from the detachment in Salt Spring Wash to Squaw Peak and pinches out to the north near Lake Mead. Longwell (1936) described similar deposits in the Virgin Basin (now flooded by Lake Mead). Interbedded with coarse breccia is a dacite ash-flow tuff (94-250 meters thick) that may correlate with a tuff in the northern Black Mountains dated by Fiala (1990) at 16.5 Ma. The upper part of the section consists of 63-627 meters of basaltic andesite, 0-211 meters of poorly consolidated conglomerate, and 90-171 meters of basaltic andesite. Adjacent to the detachment in the eastern White Hills there is a progressive decrease in dip up section from 30 to 35° near the base to nearly horizontal at the top. Although stratal tilt varies from 30 to 35° in the central and western White Hills, they are uniform within structural blocks.

The Salt Spring detachment may represent a segment of a regional detachment zone that extends from Gold Butte to near Dolan Springs, Arizona (Cyclopic detachment). This fault zone lies 30 km west of the Grand Wash Cliffs and represents both the easternmost boundary of the extensional allochthon and the eastern limit of exposure of Tertiary igneous rocks in the northern Colorado trough. The lack of equivalent igneous rocks in the footwall of the detachment between Salt Spring Wash and the Colorado Plateau may place constraints on either the geometry of the detachment or the pre-extension distribution of volcanic rocks.

THE SEISMOTECTONICS OF THE SAN ANDREAS FAULT SYSTEM NORTH OF POINT ARENA ALONG THE COAST RANGES OF NORTHERN CALIFORNIA

CASTILLO, David A., Dept. of Geophysics, Stanford University, Stanford, CA 94305 and U. S. Geological Survey, Menlo Park, CA 94025; ELLSWORTH, William L., U. S. Geological Survey, Menlo Park, CA 94025

The relatively youthful segment of the San Andreas fault (SAF) system north of Point Arena occupies a ~70 km wide zone of distributed deformation bounded by the San Andreas fault "proper" to the west and by the SAF-parallel Maacama and Bartlett Springs fault zones to the east. Earthquakes (M₂ 1.0) occurring between 1980 and 1989 are used to develop a seismotectonic model of the youthful part of the SAF "system" as it evolves into a mature plate boundary.

An upper crustal velocity model for the area, derived from seismic travel-time inversions indicates a typical Franciscan crust with compressional velocities reaching 6.0 km/sec at about 18 km depth. We used this velocity model to relocate over 3000 M₂ 1.0 earthquakes.

The San Andreas fault north of Point Arena is virtually aseismic. In contrast, numerous microearthquakes concentrate along the Maacama and Bartlett Springs fault zones. These zones terminate abruptly at about 39°50' N, approximately 100 km southeast of Cape Mendocino. Along the Maacama fault the seismicity is relatively continuous and extends to about 15 km depth, while along the Bartlett Springs fault zone the seismicity is spatially discontinuous to about 20 km depth.

The sense of strain release inferred from earthquake focal mechanisms along both the Maacama and Bartlett Springs fault zones is consistent with right-lateral slip along the North American and Pacific plate boundary. Slip vectors derived from these focal mechanisms are sub-parallel to small circles about the pole of rotation for the North American and Pacific plates.

Interestingly, we find the strike-slip Maacama fault dips northeast about 60 to 75 degrees. We speculate that in the wake of the northward migrating Mendocino Triple Junction, the dipping Maacama fault is now accommodating right-lateral transform motion along an older (> 2 Ma) reverse fault initially formed due plate margin convergence.

APATITE AND ZIRCON FISSION-TRACK AGES FROM THE SIERRA SAN PEDRO MARTIR, EASTERN PENINSULAR RANGE, BAJA CALIFORNIA, MEXICO

CERVENY, Philip F., DORSEY, Rebecca J., BURNS, Beverly A., Dept. of Geology, University of Wyoming, Laramie, WY 82071

Zircon and apatite fission-track ages from the Sierra San Pedro Martir, Baja California help to constrain the uplift and cooling history of this segment of the eastern Peninsular Range. Five samples were collected from granitoid rocks at elevations from 500m to 2800m above sea level. Zircon ages range from 104 ± 10 Ma. at the range crest to 75.5 ± 6.2 Ma at the base. The emplacement age of the batholith has been reported by Silver and Chappell (1988) as 120 to 105 Ma (U-Pb zircon); the uppermost zircon fission-track age thus reflects rapid cooling near the time of emplacement. Fission-tracks in zircon completely anneal at temperatures of 200-225°C, or 8-9 km depth assuming a geothermal gradient of 25°C/km. Therefore the

rocks currently at the top of Sierra San Pedro Martir were emplaced at depths of less than 8 km. Apatite ages range from 76.3 ± 6.8 Ma (mean track length 14.2 ± 1.3 microns) at the crest of the range to 35.6 ± 3.7 Ma (12.9 ± 1.5 microns) at the base, and define an uplift/cooling rate of ~60 m/m.y. Mean track length distributions are unimodal for all samples, but indicate a slightly higher degree of annealing for the 35 Ma. ages (lower elevations). The apatite ages at the base of Sierra San Pedro Martir place limits on the total amount of uplift since 35 Ma. Fission-tracks totally anneal in apatite at approximately 100°C, or about 4 km depth. Because the basal samples do not show significant annealing, they have resided at depths of less than 3 km since 35 Ma, and have likely been uplifted no more than 2 km since this time. The Sierra San Pedro Martir has had a relatively simple cooling history consisting of emplacement and rapid cooling (120 - 105 Ma) at depths of less than 6 - 8 km, followed by slower steady cooling from 75 Ma to about 35 Ma (~60 m/m.y.). Uplift and erosion of Sierra San Pedro Martir is limited to about 2 km since 35 Ma.

PALEOGEOGRAPHIC RECONSTRUCTION OF THE NORTHERN SALINIAN BLOCK USING Sr ISOTOPIC PROPERTIES

CHAMPION, D. E., and KISTLER, R. W., U.S. Geological Survey, Menlo Park, CA 94025

Age and initial Sr studies have been used to reconstruct the 117 to 80 Ma granitoid basement of the Salinian block to form a simple pattern. The pattern places the 0.706 ⁸⁷Sr/⁸⁶Sr line at or within the northernmost plutons of the block, including Montara Mountain, with an abrupt SE increase to Sr_i values over 0.707.

Comparison of our work with many previously published Neogene sedimentary/stratigraphic correlations across faults shows strong agreements. Aligning the thick sections of the Santa Cruz Mudstone at Pt. Reyes and in the Santa Cruz Mountains at about 6 Ma brings elements of a distinctive granodiorite at Bodega Head and Montara Mountain together. Matching the Monterey Formation and Paleocene conglomerates at Pt. Reyes and at the Monterey peninsula requires movement on a San Gregorio splay, inboard of Montara Mountain, at about 11 Ma. Removal of this displacement brings both Montara Mountain-Ben Lomond granitoid rocks and the Pt. Reyes-Pacific Grove porphyritic granodiorites into direct proximity. The total San Gregorio displacement approaches 150 km.

The 43 km of 10-15 Ma displacement on the Rinconada fault at Paso Robles, recognized by Graham and others in the central Salinian block, probably manifests itself as distributed deformation on many faults in the Santa Lucia Mountains. The Blue Rock-Miller Creek fault, for example, has abrupt isotopic variation across it, permitting some strike-slip movement. The Rinconada fault movement caused the broad S-shaped bending of the Vergeles-Zayante fault, and was completed by the 10 Ma deposition of the Santa Margarita Formation, which overlaps the Zayante fault. Neogene stratigraphic and Late Cretaceous pluton reconstructions imply that no significant internal faulting occurred in the northern Salinian block between 80 and 15 Ma.

FINITE STRAIN FACTORIZATION, BY TENSOR ALGEBRA, IN AN INCONGRUENT FOLD IN THE COLFAX SEQUENCE

Chen, Richard F., Department of Earth and Space Sciences, University of California, Los Angeles, CA 90024-1567

The general structural trend of the fault-bounded Colfax sequence, between the Warner fault zone (W) and the Gillis Hill fault (E) in the northern Sierra Nevada foothills follows the Nevada trend, is predominantly NW-SE. Along a traverse from the center of the sequence to its eastern limit, March strain was estimated in eight samples across a severely fractured, incongruent, asymmetrical syncline, whose fold axis trends N34°E and plunges 36°. Three of the samples, one at the west end of the section and the other two near the Gillis Hill fault, were taken from steeply dipping beds with Nevada strike; the remainder were collected from the south and north limbs and the hinge area of the fold.

From the west to the east, strain intensities increase monotonically from 0.40 to 0.74. The strains in the fold, furthermore, have similar intensities, 0.56 to 0.66, with little variation in their principal values [0.32±0.03, 0.16±0.02, -0.33±0.02] indicating that the fold was formed during a late phase of deformation involving rigid body rotation but no bulk strain. To restore the late-phase deformation, the layers in the north limb and hinge were first unfolded by rotating them along the fold axis to coincide with the orientation of the steep south limb. Second, the unfolded layers were rotated about a vertical axis, to make their average strike agree with the regional trend. The total strain in this restored orientation was factorized into a compaction and a tectonic strain. Between the two events, buckling tilted the horizontal beds. Based on this model and on the variation of the total strain along the section, the rocks suffered a compaction strain of [0, 0, -0.3] followed by a tectonic strain of [0.13, 0.05, -0.15] in the west, increasing to [0.37, 0.07, -0.32] in the east, with the axis of shortening trending E-W and the intermediate axis paralleling to the regional NW-SE trend.

SESSION 47, SAIC: STORAGE OF HIGH-LEVEL NUCLEAR WASTE

volcanic rocks ($^{206}\text{Pb}/^{204}\text{Pb} = 18.11-18.24$ and $^{208}\text{Pb}/^{204}\text{Pb} = 38.70-39.15$) but diverges from it in some samples.

The carbonate fraction of lead in both vein and calcrete samples resides dominantly in fine-grained, authigenic calcite. 1.5N HCl also attacks and removes lead from silicate phases, but a milder 0.5N CH_3COOH dissolution procedure identifies a significantly more granoblastic lead in most of the calcite ($^{206}\text{Pb}/^{204}\text{Pb} = 18.11-20.21$ and $^{208}\text{Pb}/^{204}\text{Pb} = 38.60-39.34$). Probably this radiogenic carbonate lead was transported into the vein system by the downward percolation of meteoric water that had previously interacted with surficial calcrete. Windblown particulate matter derived from Paleozoic and Late Proterozoic limestone in surrounding mountains may be the ultimate source of the calcite. Several samples, however, including two from a vein incorporating a thin zone of basaltic ash, contain carbonate lead that is only slightly different from their silicate lead. These isotopically more uniform samples suggest that volcanic rocks locally have contributed most of the lead to both fractions of the vein system.

The isotopically heterogeneous lead that characterizes the regional Paleozoic and Late Proterozoic sedimentary rocks and Middle Proterozoic crystalline rocks remains a candidate for at least some of the lead in the Trench 14 veins. An important finding of this study, however, is that the data do not require the more exotic origins that have been proposed for the veins. Instead, the similarity between lead isotopic properties of the veins and calcretes suggests a mutual origin related to pedogenic phenomena.

02:15 p.m. Marshall, Brian D.

No 7474

A MODEL FOR THE FORMATION OF PEDOGENIC CARBONATE BASED ON STRONTIUM ISOTOPE DATA FROM SOUTHWEST NEVADA MARSHALL, Brian D. and MAHAN, Shannon, U.S. Geological Survey, MS 963, DFC Box 25046, Denver, CO 80225

Calcareous soils are ubiquitous in arid regions such as the southwestern United States. Models describing the formation of the calcium carbonate that cements loose, porous material in these soils usually require an alloigenic component for the source of the large amounts of calcium in the calcite. The isotopic composition of strontium, a common trace constituent in carbonates, is an ideal tracer for the origin of the calcium. Analyses of strontium in calcretes, fault-filling veins, rhizoliths, surface coatings, and eolian sediment near Yucca Mountain, Nevada, provide important constraints on the origin of the alkaline earths incorporated in these various surficial materials.

Calcretes, fault-filling veins and rhizoliths contain carbonate-bound (=HCl leachable) strontium with $^{87}\text{Sr}/^{86}\text{Sr}$ averaging 0.7124. This value is significantly different from the average of 0.7117 found for carbonate-bound strontium in the surface coatings and in eolian sediment. These results lead to two conclusions: (1) calcite surface coatings on bedrock derive their alkaline earths from the eolian carbonate component and (2) the alkaline earths in calcrete and fault-filling-vein calcite are not entirely derived from an eolian carbonate component.

The strontium-isotope data suggest that some of the alkaline earth content in the pedogenic carbonate is derived from the weathering of local detritus. To test this hypothesis, isotopic analyses of the silicate detritus are in progress.

Within the volcanic bedrock of Yucca Mountain, calcite occurs as coatings on open fractures. The $^{87}\text{Sr}/^{86}\text{Sr}$ of these calcites varies from pedogenic-type values near the surface to lower values (0.7093) at and below the water table. Some of the alkaline earths in these fracture coatings may be partially or totally derived from the volcanic bedrock, which has widely varying isotopic compositions.

These data preclude the involvement of upwelling ground water in the genesis of surficial carbonate in the immediate vicinity of Yucca Mountain.

02:30 p.m. Stuckless, J.S.

No 19828

Isotopic Evidence for a Far Eucratite Origin for Hydrogenetic Veins in Faults near Yucca Mountain, Nevada

STUCKLESS, J.S., PETERMAN, E.E., WHELAN, J.F., and MUHS, D.R., US Geological Survey, MS 963, Denver Fed. Ctn., Denver CO 80225

Vein-like deposits of calcite and opaline silica that infill faults and fractures in the vicinity of Yucca Mountain have been the center of considerable debate because the deposits occur near a possible site for the Nation's first high-level nuclear waste repository. The various proposed modes of origin for the deposits, such as catastrophic upwelling of water or downward percolating fluids related to pedogenic processes, have differing implications for the performance of a geologic repository. Isotopic data for oxygen, carbon, strontium, and uranium in the carbonate minerals exposed at Trench 14 preclude deposition from upwelling waters from either of the regionally extensive aquifers known to exist beneath Yucca Mountain. Oxygen isotopes imply deposition of calcite at unreasonably low temperatures; strontium is too radiogenic; and uranium activity ratios are too low. Data from calcites deposited by the adjacent Ash Meadows flow system further suggest that the isotopic compositions of ground water in southern Nevada have not changed markedly during the last 60 to 600 k.y. and that, therefore, conclusions based on present-day water compositions are probably valid for at least the last 600 k.y. Isotopic compositions of the Yucca Mountain calcites are similar to those observed in secondary soil carbonates and, in combination with existing geologic, mineralogic, and paleontologic data, show that the carbonate and opaline silica deposits must have formed from descending water related to a pedogenic process.

02:45 p.m. Harrington, Charles D.

No 16720

QUATERNARY EROSION RATES ON HILLSLOPES IN THE YUCCA MOUNTAIN REGION, NEVADA

HARRINGTON, Charles D., Earth and Environmental Sciences Division, EES-1, MS D462, Box 1663, Los Alamos National Laboratory, Los Alamos, NM 87545 and WHITNEY, John W., U.S. Geological Survey, Federal Center, MS 913, Denver, CO 80225

Yucca Mountain is a series of eastward-tipped structural blocks. These blocks are composed of fine-grained, Tertiary volcanic rocks, primarily welded tuffs that are resistant to weathering in the present semiarid climate. In the Yucca Mountain region, Quaternary cycles of intense weathering on ridge crests and hillslopes during glacial (pluvial) episodes have resulted in a patchwork of thin colluvial deposits of variable ages.

Approximate long-term average erosion rates can be calculated for hillslopes that have dated colluvial boulder deposits. Twelve of these deposits were studied on seven different slopes that have gradients ranging from 15-32 degrees. Hillslope degradation marginal to these deposits ranges from 0.2-1.1 m. Maximum incision in active channels adjacent to colluvial deposits ranges from 0.3-2.8 m. Carbon-14 dating of rock varnish from surface boulders on these deposits yields age estimates from 170 ka to > 1 Ma. Long-term erosion rates calculated for hillslopes that have relief early to middle Quaternary deposit range from 0.2 to 7.3 mm/ka and average 1.2 mm/ka.

Erosion rates on Yucca Mountain are relatively low compared to rates for other semiarid regions. In California and New Mexico, published long-term erosion rates range from 10-43 mm/ka on hillslopes underlain by resistant lithologies. Erosion rates calculated for slopes on less resistant rock types and for shorter time periods, however, are as much as two orders of magnitude larger.

Hillslopes in the Yucca Mountain area record an exceptional history of geomorphic stability from the early Quaternary to the present. Several conditions contribute to these low long-term erosion rates: (1) bedrock outcrops as well as boulders in the hillslope deposits are erosionally-resistant welded tuffs, (2) rock varnish coatings on surface boulders inhibit weathering, (3) colluvial boulder deposits on hillslopes serve as a protective cap that inhibits removal of finer grained debris by slopewash, (4) hillslope channels isolate colluvial deposits by topographic inversion and remove them from active erosion by runoff, and (5) debris flows, although effective in removing bouldery colluvium from upper slopes, are generally restricted to active channels on middle and lower hillslopes and rarely strip debris from non-channelized areas.

03:00 p.m. Faulds, James E.

No 6918

NEW INSIGHTS ON STRUCTURAL CONTROLS AND ENPLACEMENT MECHANISMS OF PLEISTOCENE/QUATERNARY BASALTIC DIKES, SOUTHERN NEVADA AND NORTHWESTERN ARIZONA

FAULDS, James E., Dept. of Geology, University of Iowa, Iowa City, IA 52242; FEUERBRACH, Daniel L. and SKITH, Eugene I., Dept. Geoscience, University of Nevada, Las Vegas, NV 89184

Five Quaternary basaltic volcanic centers lie within 20 km of the proposed high-level nuclear waste repository at Yucca Mountain. The basalts rose through the crust without contamination. Previous studies suggested that relatively thin (< 5 m) dikes fed the basaltic centers. The Quaternary dikes, scoria mounds, and cinder cones generally trend NNE. Potential NNE-striking near-surface channelways for the basalts include normal fault segments, layering in highly deformed Proterozoic and Paleozoic rocks, and joints. However, lack of dissection of these young volcanoes precludes direct observation of feeder dikes and controlling structures.

To elucidate the geometry of plumbing systems beneath Quaternary volcanoes near Yucca Mountain, highly-dissected Pliocene basaltic centers were studied in the Fortification Hill field of northwestern Arizona. The most highly dissected centers are located on the west flank of Malpais Mesa. Here, dikes within and directly beneath three centers range from 10-25 m in width and 100-225 m in length. Two centers are linked by a 1-2 m wide dike. Thus, dike widths increase by an order of magnitude directly beneath some centers. The NNE- to NW-striking dikes in the Fortification Hill field commonly parallel but are rarely intruded directly along preexisting structures. Some dikes cut directly across Miocene normal faults. All dikes have near vertical dips. These observations imply that dikes may have propagated upward through "self-generated" fractures produced by tensile stresses near the dike tip. The fractures probably developed perpendicular to the least principal stress.

In the Yucca Mountain region, the preexisting NNE-striking structures may have locally facilitated transport of magma. In most cases, however, we suspect that magma created their own pathways perpendicular to the W60W orientation of least principal stress. Hazard assessments of Yucca Mountain should consider the potential for dike intrusion along self-generated fractures not associated with preexisting faults and dike widths as great as 25 m.

03:15 p.m. Wesling, J. R.

No 25537

SURFICIAL MAPPING IN MIDWAY VALLEY: IMPLICATIONS FOR FUTURE STUDIES TO ASSESS SURFACE FAULTING POTENTIAL AT PROSPECTIVE SURFACE FACILITIES FOR THE POTENTIAL YUCCA MOUNTAIN REPOSITORY, NEVADA

WESLING, J.R., SWAN, F.H., BULLARD, T.F., ANGELL, M.M., and PERMAN, R.C., Geomatrix Consultants, Inc., One Market Plaza, Spear Street Tower, Suite 717, San Francisco, California 94105; GIBSON, J.D., Org. 6315, Sandia National Laboratories, P.O. Box 5800, Albuquerque, New Mexico 87185.

Preliminary Quaternary geologic mapping of Midway Valley reveals that some alluvial surfaces and associated deposits are of sufficient antiquity to satisfy DOE's guidelines for evaluating surface faulting potential at the site of prospective surface waste-handling facilities. Guidelines include identifying and evaluating faults that have had a slip rate > 0.001 mm/yr during the past 100 ka. Eight alluvial surfaces (Q_0 - Q_8) and associated deposits are recognized in Midway Valley based on geologic and geomorphic mapping. The oldest surface (Q_0) is preserved as a single terrace remnant and may be Plio-Pleistocene in age. Younger surfaces, ranging in age from early or middle Pleistocene (Q_1) to latest Pleistocene/early Holocene (Q_8), are preserved as stream terraces and alluvial fan surfaces. Holocene units occur as low terraces and vegetated bars (Q_9) along active washes (Q_9). Colluvial units of at least three ages mantle hillslopes.

of the western Aleutian crust between ~43 and 15 Ma. After 15 Ma, small volumes of crystal-rich andesite and dacite were erupted on Attu Island and throughout the western Aleutians. These strongly calcalkaline rocks are geochemically related to magnesian andesites of Pit Volcano which is located immediately behind the western-most Aleutian ridge. Pit Volcano is a hydrothermally-active seamount that has formed on small dilatational structures within the regionally transpressive regime of the modern western Aleutians. This 'leaky transform' setting is inferred to have been established at approximately 15 Ma following trans-tensional rifting and voluminous tholeiitic magmatism. The switch from tholeiitic magmatism related to a trans-tensional regime to strongly calcalkaline magmatism related to a trans-compressional regime may have resulted from clogging of the Aleutian - Kamchatka junction with buoyant, subduction-related terranes. These terranes probably originated to the east and were transported by strike-slip motion along the western arc.

Booth 27 Higman, S. L.

No 17231

APPLICATIONS OF CHAOS THEORY TO ZONING MORPHOLOGY IN MAGMATIC PLAGIOCLASE

HIGMAN, S.L. and PEARCE, T.H., Department of Geological Sciences, Queen's University, Kingston, Ontario, Canada, K7L 3N6

The thicknesses and morphology of oscillatory zones in magmatic plagioclase from Mt. St. Helens, Washington, and St. Kitts, Lesser Antilles show sequences of ordered planar zones separated by sequences of disordered convolute zones. This pattern suggests that during crystal growth, some factor controlling crystallization in the melt changed to cause apparent periodic and chaotic zonation patterns. As a result, the zonation patterns observed suggest that plagioclase crystallization is a nonlinear dynamic process. Determining the dimensionality and functional form of the nonlinear dynamical equations represents the first step in creating a predictive model for plagioclase crystal growth.

Reconstruction of the state space of the system from the relative time-series of zone-thickness measurements reveals two types of behaviour: a spiral geometry, and a limit cycle geometry. These are indicative of a non-chaotic Hopf bifurcation.

In low-dimensional chaotic systems, the same state space can be used for prediction of the time series of zone thicknesses. Poor correlation between time-series predictions and actual zone thicknesses suggests that plagioclase growth is not governed by a low-dimensional chaotic system of equations. However, this poor correlation is not inconsistent with the Hopf bifurcation hypothesis.

The correlation dimension can be used to constrain the dimensionality of the nonlinear system controlling crystal growth. Recent workers have concluded that the data requirements for this calculation are not as extreme as previously suggested. Using the method of Grassberger and Procaccia (1983), a definitive dimension cannot be obtained from the time-series of plagioclase crystals examined to date because of the limited number of zone thicknesses observed. Consequently, a different approach is required to calculate the correlation dimension in natural systems characterized by limited data.

Grassberger, P. and Procaccia, I. 1983. Measuring the strangeness of strange attractors. *Physica 9D*, pp. 189-208.

Booth 28 Herzig, Charles T.

No 6346

CALC-ALKALINE VOLCANISM OF THE EARLY CRETACEOUS SANTIAGO PEAK VOLCANICS, NORTHERN SANTA ANA MTS., CALIFORNIA: EARLY MAGMATISM OF THE PENINSULAR RANGES BATHOLITH.

HERZIG, Charles T., Dept. of Earth Sciences, University of California, Riverside, CA, 92521.

The results of detailed mapping, geochemistry, and the first microprobe mineral analyses of the Early Cretaceous Santiago Peak Volcanics (SPV) at their "type" locality in the northern Santa Ana Mts yield insights into the magmatic evolution of the Peninsular Ranges batholith (PRB) during its earliest stages of emplacement. Structurally intact sequences of subaerial flows, welded tuffs, volcanoclastic breccias, epiclastic rocks, and hypabyssal intrusions are the remnants of the volcanic arc built above the batholith. Flows are dominantly basaltic andesites and andesites, with lesser basalts, dacites and rhyodacites. Major element compositions of andesites, basaltic andesites and basalts are of a low-K, calc-alkaline series. Rocks of tholeiitic affinity are also present. Cpx with a compositional range of Wo₃₅₋₄₆En₅₃₋₄₈Fs₉₋₂₂ plots within the non-alkali field on discrimination diagrams, straddling the calc-alkaline - tholeiitic line of LeRoyer and others (1982). The compositions of cpx from the SPV overlap with those from gabbros of the PRB. Calcic amphiboles from the SPV are pargasite and edenite with rare magnesio-hornblende. These compositions show limited overlap with amphiboles from gabbros of the PRB. Plagioclase crystals are dominantly labradorite-bytownite (overall range is An₅₀₋₅₉). Opx is completely altered to chlorite, part of a greenschist facies alteration assemblage present in all rocks. The field setting, abundance of andesitic compositions and calc-alkaline affinity of the rocks is consistent with an origin of the SPV as a volcanic arc constructed at or near the margin of North America.

Booth 29 Durant, Dolores G.

No 17194

CRYSTAL SIZE DISTRIBUTION STUDIES IN SPANISH PEAKS, COLORADO

DURANT, Dolores G. and CLIFFORD, Paul M., Dept. Geology, McMaster University, Hamilton, Ont. L8S 4M1

The Spanish Peaks (SP) dual intrusions of southern Colorado, their surrounding radial dyke swarm and several related plugs form a spectacular volcanic complex in the Rio Grande Rift.

To shed light on the crystallization history of some Rio Grande magmas, petrographic relationships and crystal size distribution (CSD) have been examined for opaquers, olivine, and augite from a gabbroic dyke of Ruerfano Butte (RB) and feldspars and opaquers from a "rhyolitic" dyke of the SP swarm.

CSD plots for RB augite and RB opaquers yield straight lines with steep negative slopes. These are consistent with constant, continuous growth and nucleation during crystallization, as well as no crystal fractionation during emplacement and size independent growth.

Similar plots for RB olivine, SP feldspars, and SP opaquers yield asymmetric bell curves indicating fines depletion. RB olivines show resorption features on all grain sizes. The resorbed material was possibly redeposited as RB augite; this may explain the higher slope values for RB augite compared to RB opaquers. SP opaquers also show loss of material due to resorption.

SP phenocrystic feldspars near the dyke boundary lack resorption features whereas SP xenocrystic feldspars show resorption throughout the dyke. The absence of fines for both populations could be due to sorting of the crystals in a magma chamber perhaps by neutral density buoyancy or by magma movement within the chamber. Decreasing CSD slopes across the SP dyke for both SP feldspars and SP opaquers are probably due to thermal and chemical disequilibrium towards the centre of the dyke.

Booth 30 Cascadden, T. E.

No 25911

INTERMEDIATE AND MAFIC VOLCANIC ROCKS OF THE NORTHERN WHITE HILLS, ARIZONA: IMPLICATIONS FOR THE PRODUCTION OF INTERMEDIATE COMPOSITION VOLCANIC ROCKS DURING REGIONAL EXTENSION

CASCADDEN, T.E., Dept. of Geology, University of New Mexico, Albuquerque, NM 87131

SMITH, E.L., Dept. of Geoscience, University of Nevada, Las Vegas, NV 89154

The generation of intermediate composition igneous rocks during regional extension is commonly ascribed to the commingling of mafic and felsic magmas on the basis of geochemical, petrographic and field evidence. In the Lake Mead area of the northern Colorado extensional corridor, magmas commingling produced intermediate composition calc-alkaline lavas and associated plutons in the Black Mountains, Arizona and River Mountains, Nevada. However, in some areas of the Basin and Range, thick sections of mafic to intermediate volcanic rocks lack the petrographic, field and chemical evidence for commingling. An example of such an area is the northern White Hills (NWH), northwestern Arizona, the easternmost exposure of mid-Tertiary igneous rocks at the latitude of Las Vegas.

The NWH contains three mid-Miocene mafic to intermediate volcanic centers. Lavas are subalkalic to alkalic and vary in composition from basalt (46-52% SiO₂) to basaltic trachyandesite (52 to 57% SiO₂) to trachyandesite (57-61% SiO₂). Na₂O + K₂O varies from 4-8%; rocks have not been subjected to K-metasomatism. Each volcano is composed of chemically and petrographically distinct magmas. The three magma types are unrelated by fractionation, contamination or AFC. Incompatible trace elements (Hf, Th, LREE) show small but significant differences. However, compatible trace elements (Co, Cr, Sc, V) concentrations for the most primitive samples of each magma type are similar. All lavas contain olivine as an equilibrium phase. Variation within magma types is explained by fractionation of olivine or olivine-clinopyroxene-plagioclase.

These observations suggest that the intermediate volcanic suites in the White Hills were derived by partial melting of chemically different, but mineralogically similar sources. Because olivine is an equilibrium phase in the three magma types, it must have been on the liquidus in the source. We suggest that the most likely source for NWH magmas is spinel peridotite. High Sr contents (850-1300 ppm) argue against crustal contamination. This model is similar to that proposed by Barker and Thompson (1989) for the alkalic lavas of the Hamblin-Cleopatra volcano (to the northwest of the NWH) but contrasts with the magma commingling models proposed for the compositionally heterogeneous volcanic rocks of the River and Black Mountains. Therefore, in the Lake Mead area two independent processes (partial melting and magma commingling) were responsible for the production of intermediate composition igneous rocks during mid-Miocene extension.

Booth 31 Hoch, Anthony R.

No 23712

PETROGRAPHIC EVIDENCE FOR MIXING OF ALKALINE AND SUB-ALKALINE MAGMAS IN THE RATTLESNAKE HILLS INTRUSIVE COMPLEX, CENTRAL WYOMING.

HOCH, Anthony R.; MYERS, James D.; FROST, Carol D., Dept of Geology and Geophysics, University of Wyoming, Laramie, WY 82071.

The Rattlesnake Hills of central Wyoming host Eocene intrusions and extrusive bodies of quartz-normative rhyolite and quartz latite. These are spatially divided into two groups: the eastern felsic group (EFG) and the western felsic group (WFG). Nepheline-normative phonolites, trachytes and lamprophyres comprise the central alkalic group (CAG), which is located between the EFG and WFG.

Although the EFG and WFG rocks have similar bulk-rock chemical compositions, they are petrographically different. The EFG rocks (plag+hb+ap+mt+/-qtz) are coarsely porphyritic (phenocrysts up to 7 mm) with unzoned oligoclase

Booth 95 Wild, Steve

No 24719

REMEDIATION OF PETROLEUM HYDROCARBON-CONTAMINATED GROUND WATER AND SOIL USING IN-SITU AIR SPARGING AND ACTIVE SOIL VAPOR EXTRACTION AT LUST SITES IN NEW MEXICO.

WILD, Steve, New Mexico Environment Dept., 1190 St. Francis Dr., Santa Fe, NM 87503; BILLINGS, Jeffrey P., Billings & Assoc., Inc., 3816 Academy Pkwy N-NE, Albuquerque, NM 87109; BROWN, William J., Albuquerque Environmental Health Dept., P.O. Box 1293, Albuquerque, NM 87103; ARDITO, Cynthia P., Intera, Inc., 8100 Mtn. Rd. NE, Albuquerque, NM 87110

As part of the New Mexico Environment Department's (NMED's) efforts to locate and evaluate cost-effective and efficient remediation technologies for leaking underground storage tank (LUST) sites, NMED has been closely tracking the development of an in-situ remediation technology called the subsurface Volatilization and Ventilation System (SVVS, patent pending, 1989).

The SVVS consists of a series of well nests which are installed within the areas of soil and ground-water contamination at LUST sites. Each well nest consists of a vapor extraction well screened within the vadose zone and an air-injection well screened below the water table.

The SVVS utilizes three remediation processes: vadose zone vapor extraction (in-situ ventilation); air sparging of the saturated zone (in-situ air stripping); and enhanced microbial biodegradation.

The SVVS has proven very effective in the remediation of LUST sites in New Mexico where a shallow water table exists. Significant reductions in benzene, toluene, ethyl benzene, and xylenes (BTEX) have been observed over relatively short time spans. SVVS treatment has been demonstrated to be an extremely efficient remediation technology when compared to conventional pump and treat systems.

Booth 95 Wyatt, D. E.

No 28605

SOIL GAS GEOCHEMICAL SAMPLING AS A METHOD OF GROUNDWATER FLOW DETECTION AT THE CHEMICALS, METALS AND PESTICIDES PITS (CMP PITS) AT THE SAVANNAH RIVER SITE.

WYATT, D. E., BLOUNT, G. C., PRICE, V., Westinghouse Savannah River Company, P. O. Box 616, Aiken, SC 29801; PIRKLE, R. J., MicroSeeps Ltd., 220 William Pitt Way, Pittsburgh, PA 15238.

The CMP Pits consisted of two parallel trenches used for disposal of oil, organic solvents, pesticides and metals during the years 1971 through 1979. The disposal area is centrally located within the Savannah River Site on a topographic high. In 1984, the waste was removed, the contaminated soil excavated and 20 groundwater monitoring wells were installed in an effort to monitor, remediate and close the site. Minor organic plumes are known to exist in the shallow aquifers.

Recent soil gas surveys, in support of a RCRA/CERCLA integrated investigation identified elevated concentrations of organics in areas away from the disposal site and different from the presumed groundwater flow directions. Groundwater flow directions at the site are to the north for the shallow aquifer and towards the disposal area from the north, south and east for the deeper aquifer. Geological data from monitoring wells suggests that a carbonate zone underlying the disposal area may affect localized groundwater flow.

Soil gas survey data identified contaminated groundwater plumes emanating from the site but not predicted by monitoring wells. Data indicates that soil gas surveys may be utilized to refine groundwater flow directions in areas where complex shallow aquifers are contaminated with volatile organics.

The information in this abstract was developed during the course of work under contract DE-AC09-85SR18035 with the U.S. Department of Energy.

SESSION 98, 1:30 p.m.**TUESDAY, OCTOBER 22, 1991****T 25: CENOZOIC EXTENSION IN THE CORDILLERA: GEOMETRY, TIMING, MECHANISMS, AND REGIONAL CONTROLS (PART II)****SDCC: Room 16AB**

0130 p.m. Metcalf, Rodney V.

No 26750

HORNBLENDE GEOSAROMETRY FROM MID-MIOCENE PLUTONS: IMPLICATIONS REGARDING UPLIFT AND BLOCK ROTATION DURING BASIN AND RANGE EXTENSION.

METCALF, Rodney V., and SMITH, Eugene L., Department of Geoscience, University of Nevada, Las Vegas, Nevada 89154

Al₂SiO₅ hornblende geosarometry was used to determine the depth of crystallization for two Miocene age plutons, Wilson Ridge (WRP) and Mt. Perkins (MPP), from the northern Colorado River extensional corridor. The WRP exhibits a hypabyssal cap to the north and extends 20 km to the south where it intrudes Precambrian gneisses. North trending faults and dikes indicate the WRP has experienced east-west extension. The MPP intrudes Precambrian gneisses with a hypabyssal cap to the west and extends 2.3 km east where it is cut by the low-angle Mockingbird Mine fault (Faulds, 1989). North trending dikes suggest some east-west extension of the MPP. Paleomagnetic data suggest an tilt for WRP and 50° west tilt for MPP (Faulds, 1989). Both plutons range in composition from monzonite to quartz monzonite. Evidence of magmas coexisting and large angular blocks of older hornblende diorite occur in both plutons. Hornblende zoning profiles reveal complex growth histories. For this reason individual analyses rather than averages were used in geosarometry calculations. Small subhedral interstitial grains yield unrealistically low Al contents and pressures and represent grains isolated from magmatic phases required by the geosarometer. Some rims of larger euhedral grains also exhibited low Al contents and were avoided. Analyses used in calculations were taken from areas of relatively uniform composition within about 50 microns of grain edges. Using multiple grains in each, three samples of (qtz) monzonite and one bi-modal diorite from the southern end of WRP yield similar results with Al₂SiO₅ (based on 23 oxygens) of 1.15 to 1.3. This yields pressures ranging from 1.49 to 2.1 kbars and depths of 4.9 to 6.7 kms. Averaging these results (n=18) yields P=1.6 ± 0.2 kbars and a depth of 5.3 ± 0.9 kms. A single sample of WRP monzonite from 10 kms south of the hypabyssal cap yields Al₂SiO₅=1.02; P=0.85; and a depth of 2.8 kms. Assuming rotation about a horizontal east-west axis these results are consistent with 15° ± 3° of northward tilt. Rotation of WRP must have occurred as temperatures cooled from the solidus to the Currie point. Multiple grains from two samples of qtz monzonite from the eastern end of the MPP yield Al₂SiO₅ of 1.81 to 1.3; pressures of 0.81 to 1.3 kbars; and depths of 2.7 to 4.4 kms. Averaging these results (n=4) yields P=1.1 ± 0.2 kbars and a depth of 3.6 ± 0.7 kms. This result is consistent with a westward tilt of 35° ± 9° provided that the Precambrian-Late Tertiary unconformity, 3 km west of the apex of MPP, was the surface at the time of intrusion. We infer that some or all of the rotation of the MPP occurred below the Currie temperature.

T
U
E
pm

0145 p.m. Anderson, R. E.

No 16613

RELATIONSHIP BETWEEN MIOCENE PLUTONISM, UPLIFT, AND EXTENSION, LAKE MEAD AREA, NORTHWESTERNMOST ARIZONA AND ADJACENT NEVADA

ANDERSON, R.E., and BARNHARD, T.P., U.S. Geological Survey, Box 25046, MS 866, DFC, Denver, CO, 80225

The Lake Mead area can be added to the growing list of areas in the Cordillera that expose evidence for a close association between Cenozoic plutonism and extension. The Wilson Ridge pluton in the northern Black Mountains is a north-broadening, triangular, composite, epizonal mass, about 20 km on each edge, that was emplaced into Proterozoic crystalline rock and Paleozoic and Cenozoic cover rocks during late Miocene time. Petrogenetic studies by Larson and Smith (1990, JGR, v. 95, p.17693) indicate that it formed by commingling of a large volume of mafic magma with a smaller volume of felsic magma. The pluton is tilted about 5 degrees north, exposing its hypabyssal zone and roof in the north and its deeper parts in the south.

The extent of preintrusion Cenozoic deformation is best evaluated in the north, where the pluton intrudes Miocene sedimentary and volcanic rocks. Those rocks show a mild to moderate degree of preintrusion tilting that increases southward. The pluton there consists of thousands of dikes that record 8-15 km of synemplacement tilting in an approximately east-west direction. This tilting by dike-on-dike emplacement was accompanied by a southward-increasing degree of synemplacement extension-related tilting. In the northernmost part of the pluton, dikes are mostly vertical and preintrusive strata dip gently. By contrast, directly south of Lake Mead, preintrusive volcanic strata are subvertical, main-phase dikes dip at moderate angles, and late dikes are subvertical, indicating protracted pre- and syn-intrusion extension-related tilting events that ended with plutonism. The country rocks and pluton were tilted away from and downfaulted toward the axis of the pluton in these events, suggesting extensional collapse of the growing, rising pluton and of the rising Black Mountains structural block. Contrary to current models of extensional deformation in the area, we find no evidence that the northern Black Mountains served as a source terrane for west-transported extensional allochthons.

VOLCANIC RISK ASSESSMENT STUDIES FOR THE PROPOSED HIGH-LEVEL RADIOACTIVE WASTE REPOSITORY AT YUCCA MOUNTAIN, NEVADA, USA

by

SMITH, Eugene I., FEUERBACH, Daniel L., and NAUMANN, Terry R.
Center For Volcanic and Tectonic Studies, Department of Geoscience, University of Nevada, Las Vegas, NV 89154 (USA)

and

HO, Chih-Hsiang, Department of Mathematical Sciences, University of Nevada, Las Vegas, NV 89154 (USA)

Volcanic hazard studies by the Center for Volcanic and Tectonic Studies related to the proposed high-level radioactive waste repository at Yucca Mountain, Nevada have concentrated on producing a synthesis of Late Miocene to Quaternary basaltic volcanism in the southern Great Basin. To obtain a regional perspective of basaltic volcanism, detailed mapping and sampling of analog systems as well as volcanic centers within 50 km of the proposed repository have been completed. Important advances from these studies include the documentation of detailed chronostratigraphy within volcanic fields and development of geochemical models for the genesis of alkalic mafic magmas within continental rift environments. These data in combination with studies of the structural controls on the emplacement of mafic magmas have led to the determination of an area of most recent volcanism (AMRV) near Yucca Mountain. Data from volcanic centers within the AMRV are being used to estimate recurrence rates and conditional probability of future volcanism for risk assessment. The AMRV includes ten eruptive centers and encompasses all post-4 Ma volcanic complexes within 50 km of the proposed repository. High-risk rectangles were constructed at each cluster of Quaternary centers within the AMRV. The size, shape and orientation of these high-risk zones is based on structural and volcanic studies in the AMRV as well as in analog volcanic fields. The proposed waste repository lies within one of the risk rectangles associated with the Lathrop Wells volcano.

The possible recurrence of volcanic activity in the AMRV was evaluated by estimating the instantaneous recurrence rate using a nonhomogeneous Poisson process with Weibull intensity and by using a homogenous Poisson process to predict future eruptions. Based on data from Quaternary data, the estimated instantaneous recurrence rate for volcanism is about 5.5×10^{-6} /year. We conclude that the estimated probability of at least one eruption occurring in the AMRV in the next 10,000 years is about 5 percent.

Key Words: Volcanic Risk, Basaltic volcanism, Nuclear Waste Repository

Scientific session: Volcanic Hazard and Risk Mitigation

Preferred Type of Presentation: Poster

NEW K-Ar AGES FOR PLIOCENE MAFIC TO INTERMEDIATE VOLCANIC ROCKS IN THE REVELLE RANGE, NEVADA

TERRY R. NAUMANN }
EUGENE I. SMITH }

Center for Volcanic and Tectonic Studies,
Department of Geoscience, University of Nevada, Las Vegas, NV 89154

MUHAMMAD SHAFIQUILLAH }
PAUL E. DAMON }

Laboratory of Isotope Geochemistry,
Department of Geosciences, University of Arizona, Tucson, AZ 85721

In this paper we report 16 new K-Ar ages for Pliocene mafic to intermediate volcanic rocks in the Reveille Range, Nevada and one K-Ar date of a Miocene-aged tristanite from the vicinity of the Reveille Range.

The Pliocene volcanic rocks of the Reveille Range represent the southern half of a 20 km wide by 100 km long north to N30°E trending belt that combined with the Lunar Crater Volcanic Field extends from 37°45' to 38°45' in the south-central Great Basin (fig. 1a). According to the classification of Irvine and Baragar (1971) volcanic rocks range in composition from picrite to trachyte and occur as shallow intrusions, domes, flows and dissected cinder cones. Based on field relations, petrology and K-Ar ages volcanic rocks of the Reveille Range are divided into three episodes (Naumann and Smith, 1988) (fig. 1b and 2). These are:

Episode 1 (5.9 to 5.0 Ma): Basalts of Episode 1 are porphyritic olivine basalts that contain plagioclase megacrysts (up to 40 modal %). They range in composition from alkali basalt to hawaiite (44 to 48% SiO₂). Fifty-two vents occur on both the east and west flanks and near the crest of the range (fig. 1b).

Episode 2 (4.6 to 3.0 Ma): Basalts of Episode 2 are porphyritic olivine basalts containing megacrysts of augite (up to 40 %), amphibole (up to 35 %) and plagioclase (< 5%) and coarse grained xenoliths of gabbro and dunite (up to 20 cm in length). They range in composition from picrite to trachybasalt (41 to 56% SiO₂). Fourteen Episode 2 vents occur on the northeast piedmont and flank of the range (fig. 1b).

Evolved volcanism (4.4 & 4.2 Ma): Eruptions of trachyte (60% SiO₂) and tristanite (58% SiO₂) containing ferrosillite, hedenburgite, anorthoclase, sanidine, and andesine produced two domes (volumes are < 0.01 km³ and 0.26 km³, respectively) on the northeast flank of the range (Naumann and others, 1990) (fig. 1b). The northernmost dome is associated with an apron of pyroclastic flow and surge deposits and volcaniclastic debris (fig. 1b).

The new K-Ar dates establish that two episodes of basaltic volcanism occurred in the Reveille Range between 5.9 and 3.00 Ma. Episodes of basaltic volcanism were separated by the eruption of trachytic lavas and pyroclastic units at 4.4 and 4.2 Ma (fig. 2).

Previously published K-Ar ages for the Reveille Range include a date of 5.7 ± 0.2 Ma on an Episode 1 basalt flow on the northwestern flank of the range (Marvin and others, 1973). Dates of 5.8 ± 0.3 and 5.6 ± 0.3 Ma were obtained for Episode 1 basalt flows in the western part of the range, and 3.9 ± 0.2 and 3.8 ± 0.3 Ma for Episode 2 basalt flows on the east flank of the range (Dohrenwend and others, 1985). The K-Ar dates reported in this paper indicate that the most recent activity in the Reveille Range occurred at 3.0 Ma rather than 3.8 Ma.

MIGRATION OF VOLCANISM

Foland and others (1987) reported that volcanism migrated to the north in the Reveille-Lunar Crater field. According to their model, volcanism initiated at about 9 Ma and migrated north to the Lunar Crater field at a rate of about 1 cm/year. Detailed dating of volcanic centers in the northeast Reveille range indicates that migration patterns are locally more complicated. For example, in the northeastern Reveille Range, Episode 1 activity migrated mainly to the south while Episode 2 volcanism migrated both north and south. The youngest Episode 2 volcano (3.0 Ma) formed in the south (fig. 3).

MISCELLANEOUS NYE COUNTY VOLCANIC ROCKS

A previously unmapped trachyte dome and flow complex located 20 km southeast of the Reveille Range in the White Blotch Springs quadrangle yielded a K-Ar date of 14.1 Ma. The dome is 1 km in diameter and 150 m high and was mapped on the Geologic Map of Southern Nye County as undifferentiated Pliocene welded Tuff (Cornwall, 1972).

ANALYTICAL TECHNIQUES

All dates were obtained from groundmass plagioclase separates. Feldspar phenocrysts and megacrysts were removed from samples prior to analysis. Analytical procedures discussed by Damon and others (1983) were used in this study (constants: $\lambda_{\beta} = 4.963 \times 10^{-10} \text{ yr}^{-1}$, $\lambda_{\epsilon} = 0.581 \times 10^{-10} \text{ yr}^{-1}$, $\lambda = 6.544 \times 10^{-10} \text{ yr}^{-1}$, $^{40}\text{K}/\text{K} = 1.167 \times 10^{-4} \text{ atom/atom}$).

ACKNOWLEDGEMENTS

This study was funded by the Nevada Nuclear Waste Project Office. We also thank Nathan F. Stout for drafting the illustrations in this paper.

SAMPLE DESCRIPTIONS

Episode 1

1. R8-1-17-LN

K-Ar
Porphyritic olivine basalt flow; contains large plagioclase megacrysts in a holocrystalline matrix of coarse plagioclase, augite and Fe-oxide (38°4'15", 116°7'24"; Reveille Range, Nye County, NV).
Analytical data: K = 0.846, 0.849, 0.823%; $^{40}\text{Ar}^{39}\text{Ar} = 7.335, 7.462, 7.651, 7.461 \times 10^{-12} \text{ mol/gm}$; $^{40}\text{Ar}/\Sigma\text{Ar} = 54.5, 55.2, 56.4, 55.3\%$.
Collected by: T. R. Naumann; *dated by:* M. Shafiquillah. *Comment:* This sample was collected from the youngest Episode 1 flow.

(plagioclase) 5.13 ± 0.15 Ma

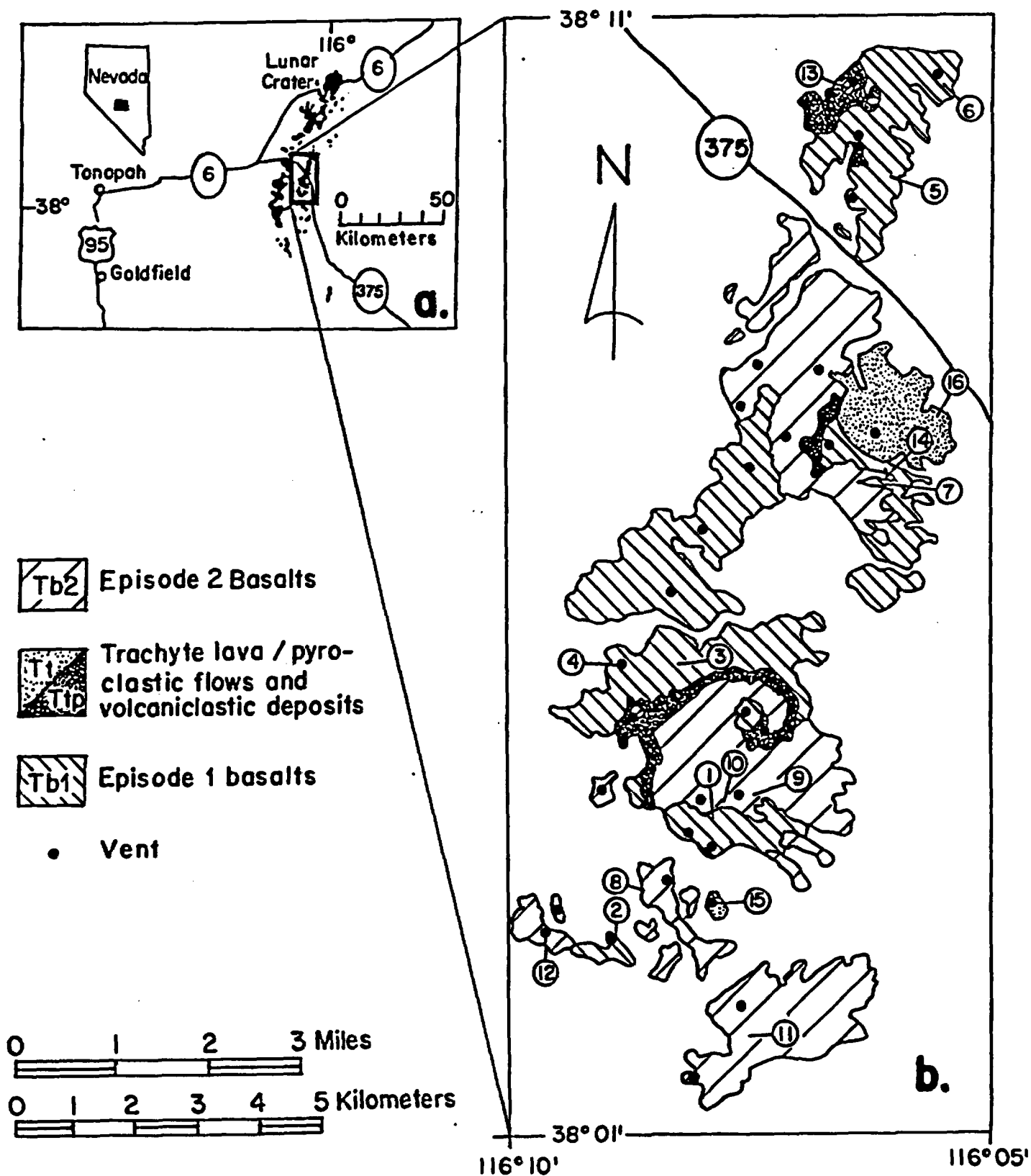


FIGURE 1. *a*—Location of Pliocene and younger volcanic rocks of the Reville Range—Lunar Crater volcanic field. *b*—Generalized geologic map of the Pliocene volcanic rocks in the northeastern Reville Range. Circled numbers are sample locations for K-Ar dates.

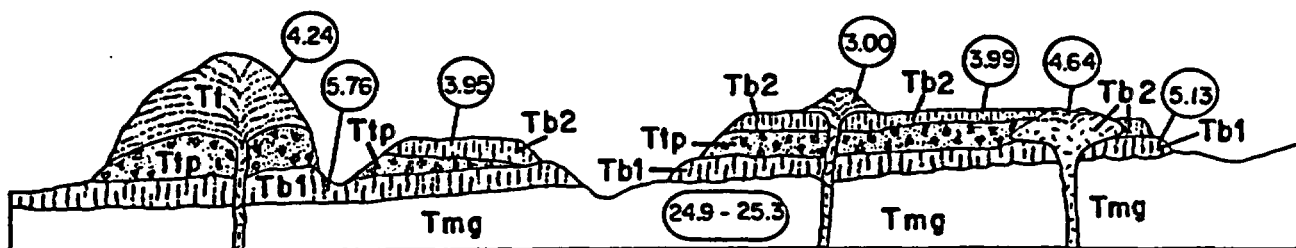


FIGURE 2. Cartoon cross-section showing the stratigraphic relationships among the dated volcanic units in the Reville Range. Symbols are the same as in figure 1b. Tmg = Tuff of Goblin Knobs (Monotony Tuff) a densely welded, coarsely devitrified quartz latitic to rhyolitic welded tuff. Dates for Tmg were reported in Ekren and others (1973).

2. R8-1-24-LN

K-Ar

Porphyritic olivine basalt dike; contains large plagioclase megacrysts in a holocrystalline matrix of coarse plagioclase, augite and Fe-oxide ($38^{\circ}3'18''$, $116^{\circ}8'52''$; Reville Range, Nye County, NV). Analytical data: K = 0.871, 0.871, 0.891, 0.887%; $^{40}\text{Ar} = 8.233, 8.390, 8.374, 8.254 \times 10^{-12}$ mol/gm; $^{40}\text{Ar}/^{39}\text{Ar} = 78.4, 78.5, 76.4, 64.5\%$. Collected by: T. R. Naumann; dated by: M. Shafiqullah. (plagioclase) 5.44 ± 0.14 Ma

3. R8-1-28-LN

K-Ar

Porphyritic olivine basalt flow; contains large plagioclase megacrysts in a holocrystalline matrix of coarse plagioclase, augite and Fe-oxide ($38^{\circ}5'40''$, $116^{\circ}8'5''$; Reville Range, Nye County, NV). Analytical data: K = 1.693, 1.683, 1.652, 1.679, 1.683, 1.679%; $^{40}\text{Ar} = 16.57, 16.78, 16.80 \times 10^{-12}$ mol/gm; $^{40}\text{Ar}/^{39}\text{Ar} = 66.4, 68.1, 68.2\%$. Collected by: T. R. Naumann; dated by: M. Shafiqullah. Comment: This sample and R8-1-29-LN were collected from the same cinder cone-flow complex. (plagioclase) 5.74 ± 0.10 Ma

4. R8-1-29-LN

K-Ar

Porphyritic olivine basalt plug; contains large plagioclase megacrysts in a holocrystalline matrix of coarse plagioclase, augite and Fe-oxide ($38^{\circ}5'39''$, $116^{\circ}8'40''$; Reville Range, Nye County, NV). Analytical data: K = 1.116, 1.079, 1.067, 1.118, 1.095%; $^{40}\text{Ar} = 10.92, 10.73, 10.55, 10.48 \times 10^{-12}$ mol/gm; $^{40}\text{Ar}/^{39}\text{Ar} = 50.7, 49.7, 49.0, 48.6\%$. Collected by: T. R. Naumann; dated by: M. Shafiqullah. (plagioclase) 5.61 ± 0.15 Ma

5. R9-1-48-LN

K-Ar

Porphyritic olivine basalt flow; contains large plagioclase megacrysts in a holocrystalline matrix of coarse plagioclase, augite and Fe-oxide ($38^{\circ}9'48''$, $116^{\circ}6'02''$; Reville Range, Nye County, NV). Analytical data: K = 1.194, 1.176, 1.229, 1.185, 1.170%; $^{40}\text{Ar} = 12.08, 12.04, 12.03, 11.80 \times 10^{-12}$ mol/gm; $^{40}\text{Ar}/^{39}\text{Ar} = 75.7, 75.5, 75.7, 75.2\%$. Collected by: T. R. Naumann; dated by: M. Shafiqullah. (plagioclase) 5.80 ± 0.13 Ma

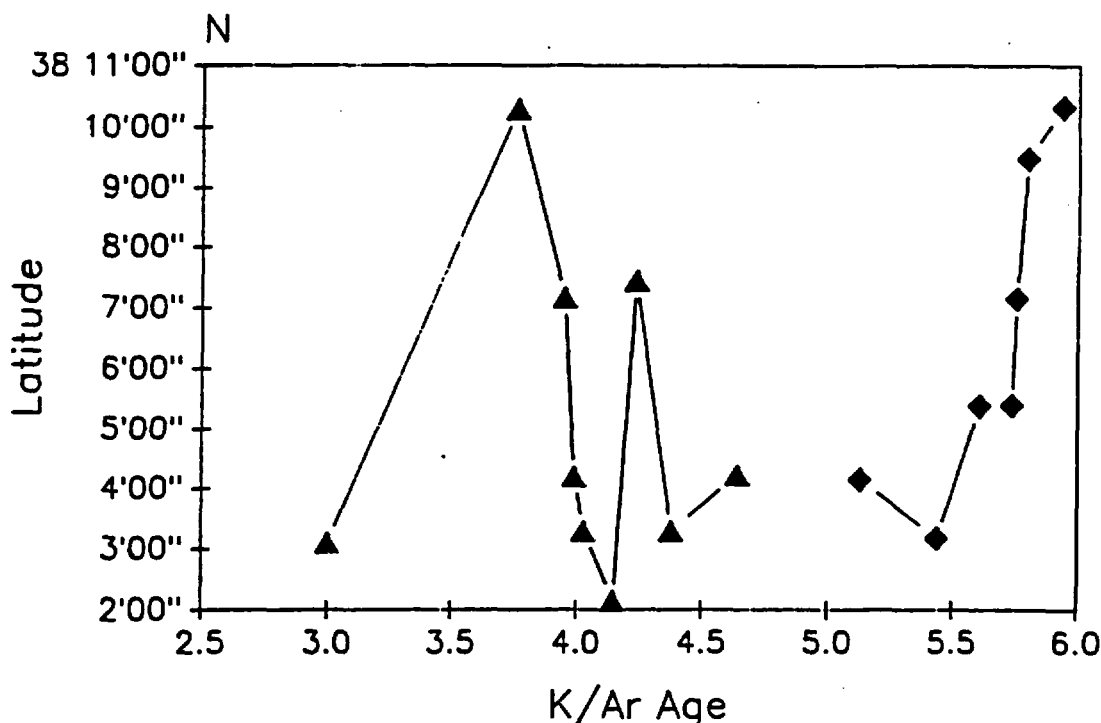


FIGURE 3. Plot of K-Ar age against latitude for dated volcanic centers in the northeast Reville Range. Diamonds = Episode 1 basalts; Triangles = Episode 2 basalts and trachyte lavas.

6. **R9-1-56-LN** K-Ar
 Porphyritic olivine basalt plug; contains large plagioclase megacrysts in a holocrystalline matrix of coarse plagioclase, augite and Fe-oxide ($38^{\circ}10'33''$, $116^{\circ}5'30''$; Reveille Range, Nye County, NV). *Analytical data:* K = 1.257, 1.260, 1.225, 1.209%; $^{40}\text{Ar}^{\circ}$ = 12.92, 12.67, 12.66, 12.82×10^{-12} mol/gm; $^{40}\text{Ar}^{\circ}/\Sigma\text{Ar}^{\circ}$ = 67.2, 65.7, 65.8, 66.8%. *Collected by:* T. R. Naumann; *dated by:* M. Shafiqullah. *Comment:* This sample was collected from the stratigraphically lowest Episode 1 flow.

(plagioclase) 5.94 ± 0.14 Ma

7. **R9-1-57-LN** K-Ar
 Porphyritic olivine basalt; contains large plagioclase megacrysts in a holocrystalline matrix of coarse plagioclase, augite and Fe-oxide ($38^{\circ}7'15''$, $116^{\circ}5'45''$; Reveille Range, Nye County, NV). *Analytical data:* K = 1.365, 1.367, 1.384, 1.393, 1.360%; $^{40}\text{Ar}^{\circ}$ = 13.73, 13.73, 13.77 $\times 10^{-12}$ mol/gm; $^{40}\text{Ar}^{\circ}/\Sigma\text{Ar}^{\circ}$ = 68.0, 66.9, 66.9%. *Collected by:* T. R. Naumann; *dated by:* M. Shafiqullah. *Comment:* R9-1-57-LN is overlain by pyroclastic deposits from the adjacent trachyte dome.

(plagioclase) 5.76 ± 0.14 Ma

Episode 2

8. **R8-1-2-LN** K-Ar
 Porphyritic olivine basalt flow; contains plagioclase and augite megacrysts in a holocrystalline matrix of coarse plagioclase, augite and Fe-oxide ($38^{\circ}3'30''$, $116^{\circ}8'20''$; Reveille Range, Nye County, NV). *Analytical data:* K = 1.469, 1.468, 1.444, 1.469, 1.497%; $^{40}\text{Ar}^{\circ}$ = 10.12, 10.24, 10.50, 10.33, 10.25, 10.29, 10.29, 10.20×10^{-12} mol/gm; $^{40}\text{Ar}^{\circ}/\Sigma\text{Ar}^{\circ}$ = 71.2, 72.9, 74.0, 68.9, 68.6, 69.0, 68.5, 72.6%. *Collected by:* T. R. Naumann; *dated by:* M. Shafiqullah.

(plagioclase) 4.03 ± 0.12 Ma

9. **R8-1-13-LN** K-Ar
 Porphyritic olivine basalt plug; contains large plagioclase and augite megacrysts in a holocrystalline matrix of coarse plagioclase, augite and Fe-oxide ($38^{\circ}4'23''$, $116^{\circ}7'18''$; Reveille Range, Nye County, NV). *Analytical data:* K = 0.805, 0.825, 0.839%; $^{40}\text{Ar}^{\circ}$ = 6.730, 6.676, 6.607, 6.482×10^{-12} mol/gm; $^{40}\text{Ar}^{\circ}/\Sigma\text{Ar}^{\circ}$ = 68.3, 67.8, 67.3, 67.5%. *Collected by:* T. R. Naumann; *dated by:* M. Shafiqullah. *Comment:* This sample was collected from the oldest Episode 2 basalt.

(plagioclase) 4.64 ± 0.14 Ma

10. **R8-1-18-LN** K-Ar
 Porphyritic olivine basalt flow; contains large plagioclase and augite megacrysts in a holocrystalline matrix of coarse plagioclase, augite and Fe-oxide ($38^{\circ}4'20''$, $116^{\circ}7'24''$; Reveille Range, Nye County, NV). *Analytical data:* K = 0.999, 0.994, 0.987, 0.969, 0.972%; $^{40}\text{Ar}^{\circ}$ = 6.757, 6.801, 6.867 $\times 10^{-12}$ mol/gm; $^{40}\text{Ar}^{\circ}/\Sigma\text{Ar}^{\circ}$ = 73.7, 74.9, 75.4%. *Collected by:* T. R. Naumann; *dated by:* M. Shafiqullah.

(plagioclase) 3.99 ± 0.10 Ma

11. **R8-1-19-LN** K-Ar
 Porphyritic olivine basalt flow; contains large plagioclase and augite megacrysts in a holocrystalline matrix

of coarse plagioclase, augite and Fe-oxide ($38^{\circ}2'15''$, $116^{\circ}7'10''$; Reveille Range, Nye County, NV). *Analytical data:* K = 0.911, 0.875, 0.840, 0.905, 0.874, 0.872, 0.854%; $^{40}\text{Ar}^{\circ}$ = 6.387, 6.627, 6.240, 6.327×10^{-12} mol/gm; $^{40}\text{Ar}^{\circ}/\Sigma\text{Ar}^{\circ}$ = 68.1, 66.2, 66.1, 66.9%. *Collected by:* T. R. Naumann; *dated by:* M. Shafiqullah.

(plagioclase) 4.15 ± 0.13 Ma

12. **R8-1-27-LN** K-Ar
 Porphyritic olivine basalt plug; contains large plagioclase and augite megacrysts in a holocrystalline matrix of coarse plagioclase, augite and Fe-oxide ($38^{\circ}3'10''$, $116^{\circ}9'23''$; Reveille Range, Nye County, NV). *Analytical data:* K = 1.886, 1.809, 1.863, 1.833%; $^{40}\text{Ar}^{\circ}$ = 9.939, 9.643, 9.594, 9.355×10^{-12} mol/gm; $^{40}\text{Ar}^{\circ}/\Sigma\text{Ar}^{\circ}$ = 51.9, 50.5, 50.0, 48.6%. *Collected by:* T. R. Naumann; *dated by:* M. Shafiqullah.

(plagioclase) 3.00 ± 0.08 Ma

13. **R9-1-46-LN** K-Ar
 Porphyritic olivine basalt flow; contains large augite and plagioclase megacrysts in a holocrystalline matrix of coarse plagioclase, augite and Fe-oxide ($38^{\circ}10'30''$, $116^{\circ}6'30''$; Reveille Range, Nye County, NV). *Analytical data:* K = 1.621, 1.580, 1.584, 1.582, 1.630%; $^{40}\text{Ar}^{\circ}$ = 10.47, 10.66, 10.36, 10.30×10^{-12} mol/gm; $^{40}\text{Ar}^{\circ}/\Sigma\text{Ar}^{\circ}$ = 38.3, 39.0, 38.1, 38.0%. *Collected by:* T. R. Naumann; *dated by:* M. Shafiqullah.

(plagioclase) 3.76 ± 0.11 Ma

14. **R9-1-58-LN** K-Ar
 Porphyritic olivine basalt flow; contains large plagioclase and augite megacrysts in a holocrystalline matrix of coarse plagioclase, augite and Fe-oxide ($38^{\circ}7'17''$, $116^{\circ}5'45''$; Reveille Range, Nye County, NV). *Analytical data:* K = 1.386, 1.343, 1.361, 1.371, 1.366%; $^{40}\text{Ar}^{\circ}$ = 9.24, 9.51, 9.44, 9.22×10^{-12} mol/gm; $^{40}\text{Ar}^{\circ}/\Sigma\text{Ar}^{\circ}$ = 57.2, 58.6, 58.3, 57.6%. *Collected by:* T. R. Naumann; *dated by:* M. Shafiqullah. *Comment:* This sample was collected from a flow that directly overlies pyroclastic deposits from the adjacent trachyte dome.

(plagioclase) 3.95 ± 0.12 Ma

Evolved Volcanic Rocks

15. **R8-1-16-LN** K-Ar
 Tristanite dome containing plagioclase and sanidine ($38^{\circ}3'18''$, $116^{\circ}8'52''$; Reveille Range, Nye County, NV). *Analytical data:* K = 3.617, 3.517, 3.687, 3.757, 3.556, 3.567%; $^{40}\text{Ar}^{\circ}$ = 27.79, 27.41, 27.55, 27.37×10^{-12} mol/gm; $^{40}\text{Ar}^{\circ}/\Sigma\text{Ar}^{\circ}$ = 86.4, 86.0, 86.5, 86.0%. *Collected by:* T. R. Naumann; *dated by:* M. Shafiqullah.

(plagioclase) 4.39 ± 0.18 Ma

16. **R8-1-43-LN** K-Ar
 Trachyte flow containing sanidine and plagioclase phenocrysts in a matrix of green glass ($38^{\circ}7'45''$, $116^{\circ}5'20''$; Reveille Range, Nye County, NV). *Analytical data:* K = 4.838, 4.841, 4.931%; $^{40}\text{Ar}^{\circ}$ = 36.04, 35.79, 35.69, 35.96×10^{-12} mol/gm; $^{40}\text{Ar}^{\circ}/\Sigma\text{Ar}^{\circ}$ = 65.2, 65.7, 65.4, 58.4%. *Collected by:* T. R. Naumann; *dated by:* M. Shafiqullah.

(plagioclase) 4.24 ± 0.06 Ma

Miscellaneous Nye County Volcanic Rocks

17. N9-SD-LN

K-Ar

Tristanite dome containing sanidine and plagioclase (37°41'30", 115°56'30"; Nellis Bombing and Gunnery Range, Nye County, NV). *Analytical data*: K = 1.724, 1.720, 1.738, 1.727, 1.719, 1.715, 1.701%; $^{40}\text{Ar}^{\text{e}}$ = 41.96, 41.89, 42.47, 42.14 $\times 10^{-12}$ mol/gm; $^{40}\text{Ar}^{\text{e}}/\Sigma\text{Ar}^{\text{e}}$ = 83.4, 82.9, 83.7, 83.2%. *Collected by*: T. R. Naumann; *dated by*: M. Shafiqullah.

(plagioclase) 14.1 \pm 0.14 Ma

REFERENCES

- Cornwall, H. R., (1972) Geology and mineral deposits of southern Nye County, Nevada: Nevada Bureau of Mines and Geology Bulletin 77, 49 p.
- Damon, P. E., Shafiqullah, M., and Clark K. F. (1983) Geochronology of the porphyry copper deposits and related mineralization of Mexico: Canadian Journal of Earth Sciences, v. 20, p. 1052.
- Dohrenwend, J. C., Turrin, B. D., and Diggles, M. F. (1985) Topographic distribution of dated basaltic lava flows in the Reville Range, Nye County, Nevada: Implications for Late Cenozoic erosion of upland areas in the Great Basin: Geological Society of America Abstracts with Programs, v. 17, no. 6, p. 352.
- Ekren, E. B., Rogers, C. L., and Dixon G. L. (1973) Geologic and bouguer gravity map of the Reville Quadrangle, Nye County, Nevada: U.S. Geological Survey Miscellaneous Geologic Investigations Map I - 806.
- Foland, K. A., Kargel, J. S., Lum, C. L., and Bergman, S. C. (1987) Time-spatial-composition relationships among alkali basalts in the vicinity of the Lunar Crater, south-central Nevada: Geological Society of America Abstracts with Programs, v. 19, no. 7, p. 666.
- Irvine, T. N. and Baragar, W. R. A. (1971) A guide to the chemical classification of the common igneous rocks: Canadian Journal of Earth Science, v. 8, p. 523-548.
- Marvin, R. F., Menhart, H. H., and McKee, E. H. (1973) A summary of radiometric ages of Tertiary volcanic rocks in Nevada and eastern California. Part III: Southeastern Nevada: Isochron West, no. 6, p. 9.
- Naumann, T. R., and Smith, E. I. (1988) Compositional trends within late-Cenozoic alkalic basalts of the central Great Basin, Nevada: Geological Society of America Abstracts with Programs, v. 20, no. 7, p. 114.
- Naumann, T. R., Smith, E. I., and Shafiqullah, M. (1990) Post 6-Ma intermediate volcanism in the Reville Range, Central Great Basin, Nevada: Geological Society of America Abstracts with Programs, v. 22, no. 3, p. 72.

NEW K-Ar DATES FOR LATE MIOCENE TO EARLY PLIOCENE MAFIC VOLCANIC ROCKS IN THE LAKE MEAD AREA, NEVADA AND ARIZONA

DANIEL L. FEUERBACH
EUGENE I. SMITH

Center for Volcanic and Tectonic Studies,
Department of Geoscience, University of Nevada, Las Vegas, NV 89154

MUHAMMAD SHAFIQUILLAH
PAUL E. DAMON

Laboratory of Isotope Geochemistry,
Department of Geosciences, University of Arizona, Tucson, AZ 85721

We report the results of 13 new K-Ar radiometric ages for basaltic andesites from the Callville Mesa volcanic field on the north shore of Lake Mead, Nevada, and basalts from the Fortification Hill volcanic field, Arizona and Nevada (fig. 1). These volcanic fields are located in the northernmost part of the Colorado River extensional corridor, an area of extensive Miocene igneous activity and upper crustal extension (e.g., Longwell and others, 1965; Anderson, 1971; Anderson and others, 1972; Bohannon, 1984; Smith and others, 1990).

CALLVILLE MESA VOLCANIC FIELD

The Callville Mesa (CM) volcanic field is exposed primarily on Black and Callville Mesas north of Lake Mead. Basaltic andesite erupted from compound cinder cones on Callville

Mesa and in West End Wash between 10.46 to 8.49 Ma. These dates are slightly younger than the whole rock K-Ar dates of 11.3 ± 0.3 Ma and 11.1 ± 0.5 reported by Anderson and others (1972) for basaltic andesite of Callville Mesa.

Basaltic andesite of Callville Mesa locally overlies and is interbedded with the Red Sandstone unit (Bohannon, 1984), sandstone and conglomerate that was deposited in a structurally controlled basin in the upper plate of the Saddle Island detachment (Duebendorfer and others, 1990; Duebendorfer and Wallin, 1991). The basin and extensional allochthon are bounded to the north by the Las Vegas Valley Shear Zone (Duebendorfer and Wallin, 1991) (fig. 1). Callville Mesa basaltic andesite was erupted during the late stages of development of the Red Sandstone basin and represents the only volcanism during active upper

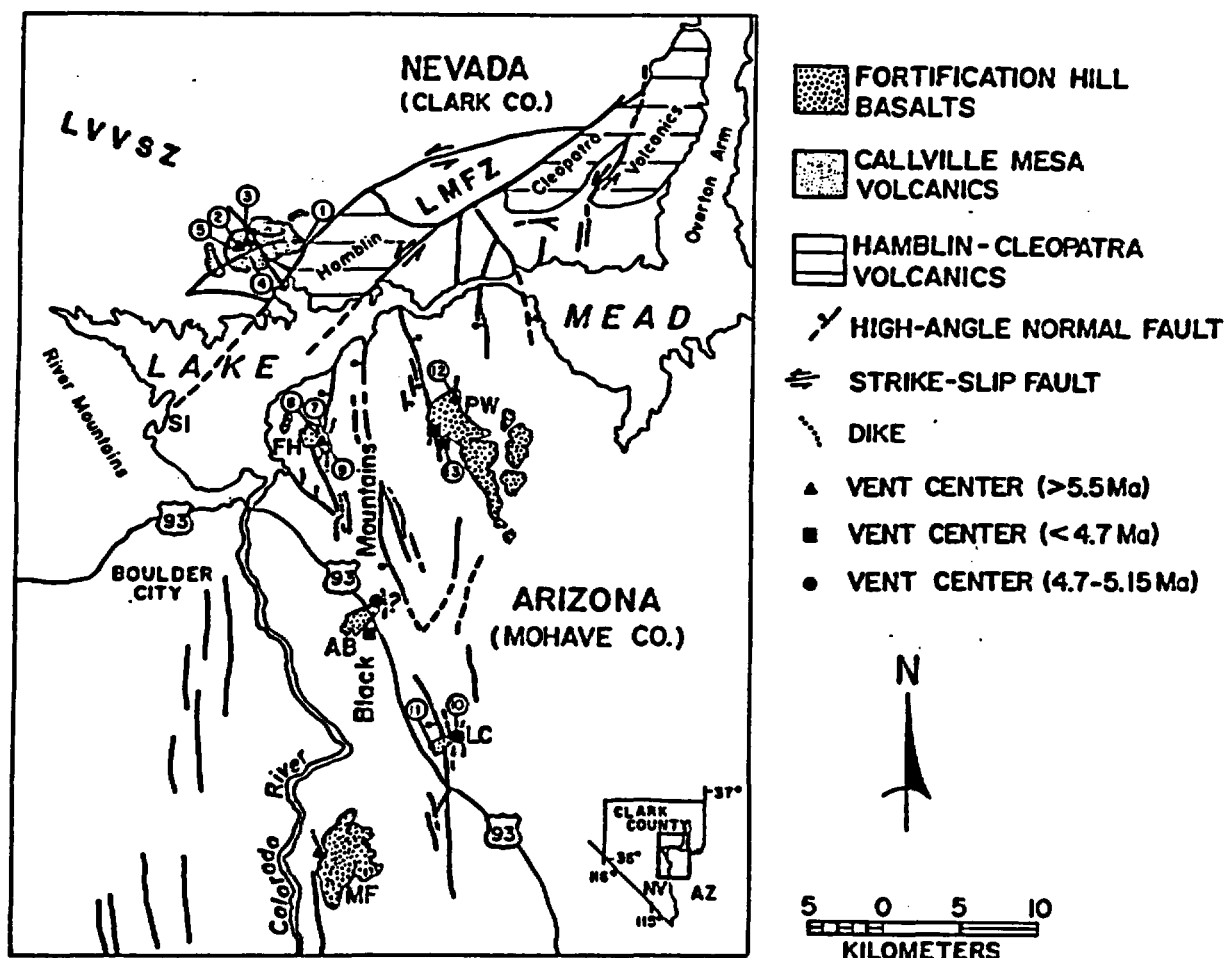


FIGURE 1. Generalized geologic map of the Lake Mead area, showing locations of samples for K-Ar dating. SI = Saddle Island; PW = Petroglyph Wash; FH = Fortification Hill; AB = alkalic basalt along U.S. 93; LC = Lava Cascade; MF = Malpais Flattop; LMFZ = the Lake Mead Fault Zone; LVVSZ = Las Vegas Valley Shear Zone.

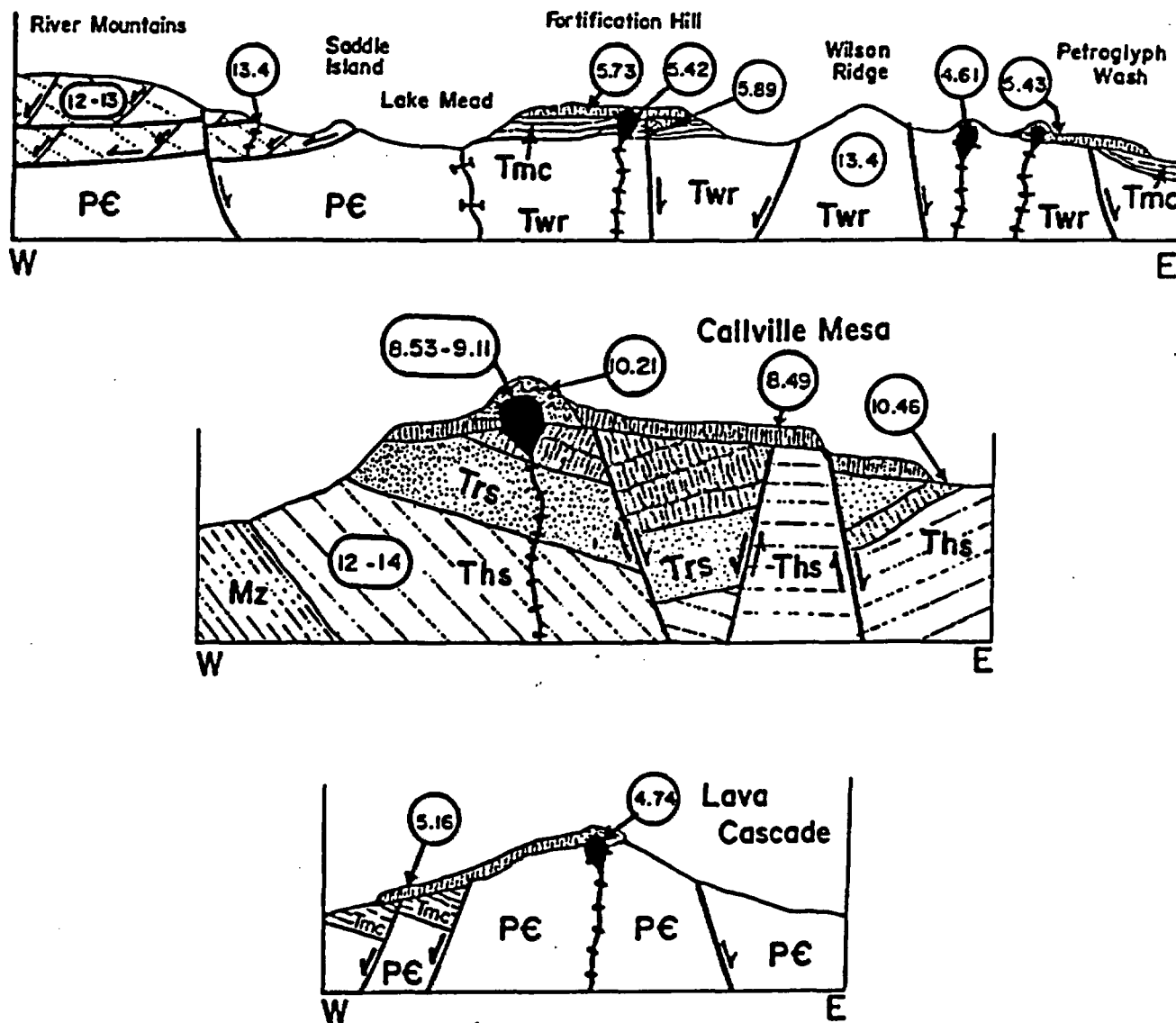


FIGURE 2. Cartoon cross sections showing stratigraphic relationships and major structures. The River Mountains are primarily intermediate volcanic flows and intrusive rock (Smith, 1982). Dates for the River Mountains from Anderson and others (1972) and Weber and Smith (1987). Tmc = Muddy Creek Formation (Late Tertiary elastic sediments). Trs = the Red Sandstone Unit (Tertiary elastic sediments); Ths = Tertiary Horse Spring Formation. Dates for the Horse Spring Formation from Bohannon (1984); Twr = Tertiary Wilson Ridge intrusive rocks. Data from Larson and Smith (1990); Mz = Mesozoic sediments; PE = undifferentiated Precambrian rock.

crustal extension and stratal tilting in the Lake Mead area. Since basaltic andesite dated at 10.46 Ma is tilted and younger units (10.21 to 8.7 Ma) are not, the major phase of tilting related to motion on the Saddle Island detachment occurred after 10.46 Ma (fig. 2). In other parts of the Lake Mead area, stratal tilting may have occurred as early as 13 Ma (Bohannon, 1984).

FORTIFICATION HILL BASALT

The Fortification Hill basalt field comprises at least eight volcanoes that occur in a 75 km long north-northeast trending zone that extends from Malpais Flattop, Arizona to Black Point, Nevada. Tholeiite, calc-alkalic and alkalic

basalt periodically erupted from 6.02 (this study) to 4.3 Ma (Anderson and others, 1972). The Fortification Hill basalts form the uppermost part of the Muddy Creek Formation (Longwell and others, 1965; Bohannon, 1984).

Subalkalic and alkalic basalts occur in the Fortification Hill field (FH). We divide FH basalt into three groups (table 1; refer to fig. 1 for locations): (1) Tholeiitic two-pyroxene basalt (6.02–5.71 Ma) (SAB) at Black Point and Malpais Flattop and subalkalic basalt at Fortification Hill (lower part of the section). (2) Alkali basalt (5.42 to 4.74 Ma) (OAB) at Fortification Hill (upper section), Petroglyph Wash and Lava Cascade. (3) Alkali basalt (4.61, this study; to 4.3 Ma, Anderson and others, 1972) (YAB) along U.S. 93 near Hoover Dam, Saddle Island and in Petroglyph Wash.

TABLE 1. The subalkalic and alkalic suites of mafic lavas in the Lake Mead area. Abbreviations are defined in the text.

Alkalic	Sub-alkalic	Age (Ma)
	Callville Mesa (CM)	10.46-8.49
	Black Point (SAB)	6.02
	Malpais Flattop (SAB)	5.8
Fortification Hill (OAB)	Fortification Hill (SAB)	5.89-5.42
Petroglyph Wash (OAB)		5.43
Lava Cascade (OAB)		5.16-4.74
Young Alkalic Basalt (YAB)		4.61-4.3

The transition from subalkalic to alkalic volcanism occurred during eruptions at Fortification Hill and occurred just prior to 5.42 Ma.

ANALYTICAL TECHNIQUES

All dates were obtained from groundmass plagioclase separates. Analytical procedures discussed by Damon and others (1983) were used in this study (constants: $\lambda_{\beta} = 4.963 \times 10^{-10} \text{ yr}^{-1}$, $\lambda_{\alpha} = 0.581 \times 10^{-10} \text{ yr}^{-1}$, $\lambda = 6.544 \times 10^{-10} \text{ yr}^{-1}$, $^{40}\text{K}/\text{K} = 1.167 \times 10^{-4} \text{ atom/atom}$).

ACKNOWLEDGEMENTS

This study was funded by the Nevada Nuclear Waste Project Office. We would like to thank Nathan F. Stout for drafting the illustrations in this paper.

SAMPLE DESCRIPTIONS

Callville Mesa (CM)

1. **F8-24-100-LN** K-Ar
Olivine-pyroxene basalt flow ($36^{\circ}10'19''\text{N}$, $114^{\circ}42'30''\text{W}$; just W of Callville Wash, Clark County, NV). *Analytical data:* K = 0.969, 0.951, 0.942, 0.963%; $^{40}\text{Ar}^{\circ} = 17.61, 17.33, 17.44, 17.15 \times 10^{-12} \text{ mol/gm}$; $^{40}\text{Ar}^{\circ}/\Sigma\text{Ar}^{\circ} = 62.2, 61.5, 61.3, 60.3\%$. *Collected by:* D. L. Feuerbach; *dated by:* M. Shafiqullah. *Comment:* This flow is interbedded with tilted Red Sandstone and represents the oldest activity associated with volcanism at Callville Mesa.
(plagioclase) $10.46 \pm 0.23 \text{ Ma}$

2. **F8-24-88-LN** K-Ar
Basaltic andesite plug ($36^{\circ}10'33''\text{N}$, $114^{\circ}44'16''\text{W}$; within volcanic center on Callville Mesa, Clark County, NV). *Analytical data:* K = 1.952, 1.978, 1.981, 1.952%; $^{40}\text{Ar}^{\circ} = 31.73, 31.50, 30.83, 30.37 \times 10^{-12} \text{ mol/gm}$; $^{40}\text{Ar}^{\circ}/\Sigma\text{Ar}^{\circ} = 41.5, 41.0, 40.4, 39.6\%$. *Collected by:* D. L. Feuerbach; *dated by:* M. Shafiqullah. *Comment:* This plug contains plagioclase megacrysts and xenocrysts of quartz.
(plagioclase) $8.11 \pm 0.30 \text{ Ma}$

3. **F8-24-90-LN** K-Ar
Basaltic andesite plug ($36^{\circ}10'29''\text{N}$, $114^{\circ}43'52''\text{W}$; within volcanic center on the W side of West End Wash, Clark County, NV). *Analytical data:* K = 1.794, 1.805, 1.819, 1.805%; $^{40}\text{Ar}^{\circ} = 26.52, 26.64, 27.10, 26.83 \times 10^{-12} \text{ mol/gm}$; $^{40}\text{Ar}^{\circ}/\Sigma\text{Ar}^{\circ} = 77.3, 77.4, 78.4, 78.0\%$. *Collected by:* D. L. Feuerbach; *dated by:* M. Shafiqullah.
(plagioclase) $8.53 \pm 0.22 \text{ Ma}$

4. **F8-24-85-LN** K-Ar
Basaltic andesite flow ($36^{\circ}09'51''\text{N}$, $114^{\circ}43'57''\text{W}$; upper flow on Callville Mesa, S of volcanic center, Clark County, NV). *Analytical data:* K = 2.070, 2.075, 2.081, 2.067, 2.071%; $^{40}\text{Ar}^{\circ} = 30.214, 30.474, 30.684, 30.870 \times 10^{-12} \text{ mol/gm}$; $^{40}\text{Ar}^{\circ}/\Sigma\text{Ar}^{\circ} = 79.0, 79.9, 80.4, 80.3\%$. *Collected by:* D. L. Feuerbach; *dated by:* M. Shafiqullah. *Comment:* This sample contains xenocrysts of quartz and alkali-feldspar and is the youngest rock dated in the Callville Mesa volcanic field.
(plagioclase) $8.49 \pm 0.20 \text{ Ma}$

5. **88-24-146-LN** K-Ar
Basaltic andesite flow ($36^{\circ}10'37''\text{N}$, $114^{\circ}44'39''\text{W}$; flow on flank complex cinder cone on Callville Mesa, S of volcanic center, Clark County, NV). *Analytical data:* K = 2.230, 2.227, 2.234, 2.242%; $^{40}\text{Ar}^{\circ} = 39.65, 39.34, 40.48, 39.04 \times 10^{-12} \text{ mol/gm}$; $^{40}\text{Ar}^{\circ}/\Sigma\text{Ar}^{\circ} = 88.4, 88.2, 92.4, 87.8\%$. *Collected by:* D. L. Feuerbach; *dated by:* M. Shafiqullah.
(plagioclase) $10.21 \pm 0.23 \text{ Ma}$

Fortification Hill (SAB)

6. **87-10-129-LN** K-Ar
Olivine-pyroxene basalt flow ($36^{\circ}24'43''\text{N}$, $114^{\circ}23'02''\text{W}$; flow directly E of feeder dike at Black Point, Clark County, NV). *Analytical data:* K = 0.655, 0.634, 0.639, 0.643%; $^{40}\text{Ar}^{\circ} = 6.93, 6.70, 6.84, 6.67 \times 10^{-12} \text{ mol/gm}$; $^{40}\text{Ar}^{\circ}/\Sigma\text{Ar}^{\circ} = 10.5, 10.1, 10.3, 10.1\%$. *Collected by:* D. L. Feuerbach; *dated by:* M. Shafiqullah. *Comment:* Rocks from this exposure contain hypersthene and pigeonite as well as augite and olivine phenocrysts.
(plagioclase) $6.02 \pm 0.39 \text{ Ma}$

7. **F7-38-13-LN** K-Ar
Olivine basalt flow ($36^{\circ}03'45''\text{N}$, $114^{\circ}40'56''\text{W}$; lowest flow at Fortification Hill, Mohave County, AZ). *Analytical data:* K = 0.935, 0.922, 0.943, 0.927, 0.931%; $^{40}\text{Ar}^{\circ} = 9.446, 9.512, 9.616, 9.562 \times 10^{-12} \text{ mol/gm}$; $^{40}\text{Ar}^{\circ}/\Sigma\text{Ar}^{\circ} = 52.3, 52.6, 53.3, 52.9\%$. *Collected by:* D. L. Feuerbach; *dated by:* M. Shafiqullah. *Comment:* Located at the north end of Fortification Hill.
(plagioclase) $5.89 \pm 0.18 \text{ Ma}$

8. **87-38-142-LN** K-Ar
Olivine-plagioclase-pyroxene basalt flow ($36^{\circ}03'18''\text{N}$, $114^{\circ}40'54''\text{W}$; flow erupted from cinder cones on Fortification Hill, Mohave County, AZ). *Analytical data:* K = 0.932, 0.925, 0.953%; $^{40}\text{Ar}^{\circ} = 9.45, 9.31, 9.22, 9.32 \times 10^{-12} \text{ mol/gm}$; $^{40}\text{Ar}^{\circ}/\Sigma\text{Ar}^{\circ} = 49.5, 48.5, 48.2, 48.7\%$. *Collected by:* D. L. Feuerbach; *dated by:* M. Shafiqullah. *Comment:* This flow lies stratigraphically above F7-38-13-LN.
(plagioclase) $5.73 \pm 0.13 \text{ Ma}$

Fortification Hill (OAB)

9. **87-38-143-LN** K-Ar
Olivine-plagioclase-pyroxene basalt plug ($36^{\circ}03'02''\text{N}$, $114^{\circ}40'37''\text{W}$; one of many plugs that intrude cinder cones on Fortification Hill, Mohave County, AZ). *Analytical data:* K = 1.275, 1.268, 1.280, 1.256%; $^{40}\text{Ar}^{\circ} = 11.85, 11.98, 12.02, 11.96 \times 10^{-12} \text{ mol/gm}$; $^{40}\text{Ar}^{\circ}/\Sigma\text{Ar}^{\circ} = 44.4, 44.5, 44.7, 44.3\%$. *Collected by:* D. L. Feuerbach; *dated by:* M. Shafiqullah.

Comment: A sample of a basalt plug that represents the youngest volcanism at Fortification Hill.

(plagioclase) 5.42 ± 0.13 Ma

10. 87-57-131-LN

K-Ar

Olivine basalt plug ($35^{\circ}52'38''\text{N}$, $114^{\circ}35'15''\text{W}$; plug intruding vent center at Lava Cascade, Mohave County, AZ). *Analytical data:* K = 0.810, 0.793, 0.836%; $^{40}\text{Ar}^{\circ} = 6.69, 6.63, 6.75, 6.69 \times 10^{-12}$ mol/gm; $^{40}\text{Ar}^{\circ}/\Sigma\text{Ar}^{\circ} = 46.3, 46.0, 46.8, 46.1\%$. *Collected by:* D. L. Feuerbach; *dated by:* M. Shafiqullah. *Comment:* Collected from a plug within the vent of the Lava Cascade at the summit of the Black Mountains.

(plagioclase) 4.74 ± 0.12 Ma

11. 87-57-132-LN

K-Ar

Olivine basalt flow ($35^{\circ}52'26''\text{N}$, $114^{\circ}36'06''\text{W}$; distal end of flow at Lava Cascade, Mohave County, AZ). *Analytical data:* K = 0.857, 0.874, 0.892, 0.878%; $^{40}\text{Ar}^{\circ} = 8.00, 7.82, 7.74, 7.78 \times 10^{-12}$ mol/gm; $^{40}\text{Ar}^{\circ}/\Sigma\text{Ar}^{\circ} = 37.2, 35.9, 35.7, 35.8\%$. *Collected by:* D. L. Feuerbach; *dated by:* M. Shafiqullah. *Comment:* This sample was collected just east of U.S. 93.

(plagioclase) 5.16 ± 0.14 Ma

12. F8-42-82-LN

K-Ar

Olivine basalt flow ($36^{\circ}04'37''\text{N}$, $114^{\circ}35'44''\text{W}$; flow at from cinder cone at Petroglyph Wash, Mohave County, AZ). *Analytical data:* K = 1.298, 1.268, 1.240, 1.267%; $^{40}\text{Ar}^{\circ} = 11.68, 12.01, 12.03, 12.14 \times 10^{-12}$ mol/gm; $^{40}\text{Ar}^{\circ}/\Sigma\text{Ar}^{\circ} = 52.3, 53.4, 53.5, 53.8\%$. *Collected by:* D. L. Feuerbach; *dated by:* M. Shafiqullah. *Comment:* The cinder cone is located just south of Gilbert Wash near the junction with James Bay Wash.

(plagioclase) 5.43 ± 0.16 Ma

REFERENCES

- Anderson, R. E. (1971) Thin-skinned distension in Tertiary rocks of southeastern Nevada: Geological Society of America Bulletin, v. 82, p. 43-58.
- Anderson, R. E., Longwell, C. R., Armstrong, R. L., and Marvin, R. F. (1972) Significance of K-Ar ages of Tertiary rocks from the Lake Mead Region, Nevada-Arizona: Geological Society of America Bulletin, v. 83, p. 273-287.
- Bohannon, R. G. (1984) Nonmarine sedimentary rocks of Tertiary age in the Lake Mead Region, southeastern Nevada and northwestern Arizona: U.S. Geological Survey Professional Paper 1259, 72 p.
- Damon, P. E., Shafiqullah, M., and Scarborough, R. B. (1976) Revised chronology for critical stages in the evolution of the lower Colorado River: Geological Society of America Abstracts with Programs, v. 10, no. 3, p. 101-102.
- Damon, P. E., Shafiqullah, M., and Clark K. F. (1983) Geochronology of the porphyry copper deposits and related mineralization of Mexico: Canadian Journal of Earth Sciences, v. 20, p. 1052.
- Duebendorfer, E. M., Feuerbach, D. L., and Smith, E. I. (1990) Syntectonic sedimentation, volcanism, and kinematics along the inferred eastern extension of the Las Vegas Valley shear zone, Nevada: Geological Society of America, Abstracts with Programs, v. 22, no. 3, p. 20.
- Duebendorfer, E. M. and Wallin, E. T. (1991) Basin development and syntectonic sedimentation associated with kinematically coupled strike-slip and detachment faulting, southern Nevada: Geology, v. 19, no. 1, p. 87-90.
- Gans, P. B., Mahood, G. A., Schermer, E. (1989) Synextensional magmatism in the Basin and Range Province: a case study from the eastern Great Basin: Geological Society of America Special Paper 233, 53 p.
- Larsen, L. L. and Smith, E. I. (1990) Mafic enclaves in the Wilson Ridge Pluton, northwestern Arizona—Implications for the generation of a calc-alkaline intermediate pluton in an extensional environment: Journal of Geophysical Research, v. 95, p. 17693-17716.
- Longwell, C. R., Pampeyan, E. H., Bowyer, B., and Roberts, R. J. (1965) Geology and mineral deposits of Clark County, Nevada: Nevada Bureau of Mines and Geology Bulletin 62, 218 p.
- Smith, E. I. (1982) Geology and geochemistry of the volcanic rocks in the River Mountains, Clark County, Nevada and comparisons with volcanic rocks in nearby area, in Frost, E. G., and Martin, D. L. eds., Mesozoic-Cenozoic tectonic evolution of the Colorado River Region, California, Arizona and Nevada: San Diego, California, Cordilleran Publishers, p. 41-54.
- Smith, E. I., Feuerbach, D. L., Naumann, Terry, and Mills, J. G. (1990) Geochemistry and evolution of mid-Miocene igneous rocks in the Lake Mead area of Nevada and Arizona, in Anderson, J. L., Cordilleran Magmatism: Geological Society of America Memoir 176, p. 169-194.
- Weber, M. E., and Smith, E. I. (1987) Structural and geochemical constraints on the reassembly mid-Tertiary volcanoes in the Lake Mead area of southern Nevada: Geology, v. 15, p. 553-556.

**THE SLOAN SAG: A MID-MIOCENE VOLCANOTECTONIC
DEPRESSION, NORTH-CENTRAL McCULLOUGH
MOUNTAINS, SOUTHERN NEVADA**

by

Hayden L. Bridwell

**A thesis submitted in partial fulfillment
of the requirements for the degree of**

Master of Science

in

Geology

**Department of Geoscience
University of Nevada, Las Vegas
December, 1991**

ACKNOWLEDGEMENTS

I would like to thank Dr. Gene Smith for keeping me enthused about this project. I feel as though he has taught me more about geology in the past two years than I have learned in all of my previous geologic studies combined.

Tracey Cascadden, Dan Feurebach and Terry Naumann also contributed substantially to this work. The countless conversations we shared added greatly to my understanding of volcanology and the dynamic geology of the Basin-and-Range province.

With great emotion, I thank my son Ian for helping me keep my perspective over the past two years.

ABSTRACT

In the Hidden Valley area of the north-central McCullough Mountains, southern Nevada, mid-Miocene andesite and dacite domes, flows and pyroclastic units (the Sloan volcanics) partially fill a sag in the underlying Hidden Valley volcanics. The 13.5 km diameter sag formed during and/or after the eruption of the Sloan volcanics. Sagging was accommodated by a combination of movement on the McCullough Wash fault system, and subsidence into evacuated chambers.

Major, trace and rare-earth element geochemistry suggests that the rocks of the Sloan volcanics belong to four groups, each of which were produced by partial melting of chemically distinct sources. With the exception of the Center Mountain dome complex, magmas rose rapidly without significant crystal fractionation or crustal contamination.

The Mount Hanna andesite member of the Sloan volcanics erupted as a hot, dry aphyric lava by a mechanism of fire-fountaining from a depth of up to 25 km, precluding a Plinian-style ash-flow event. Eruptions of felsic-to-intermediate lavas by a lava-fountaining event have been described in other areas, but the Mount Hanna andesite represents the first documentation of such an eruption in the southern Basin-and-Range.

CONTENTS

INTRODUCTION	1
Location and Geography	1
Purpose of Study	3
Geologic Setting	4
Structural Geology	4
Intermediate Volcanism	8
CALDERAS: A GENERAL DISCUSSION	10
ANALYTICAL METHODS	14
GEOCHRONOLOGY	15
THE SLOAN VOLCANICS	20
Introduction	20
Pre-Sloan Volcanic Stratigraphy	20
Stratigraphy of the Sloan Volcanics	23
Characteristics of the Sloan Volcanic Centers	26
Petrography	33
GEOCHEMISTRY	38
Metasomatism	38
Major Elements	38
Trace Elements	44
Temporal and Spatial Variations in Chemical Trends	53
MAGMA PETROGENESIS	64
Variations Between Groups of the Sloan Volcanics	64
Introduction	64
Magma Commingling	64
Fractionation and Partial Melting	66
Variations Within Groups of the Sloan Volcanics	69
Introduction	69
Andesites	69
Dacites	70
The Tuff of the Sloan Volcanics	71
Sources for Partial Melting	71
Introduction	71
Partial Melt Models	74
Discussion	76
Crustal Contamination	81

THE SLOAN SAG	82
Evidence for a Sag in Hidden Valley	82
Introduction	82
The Hidden Valley Sag	82
Conclusion	83
Classic Caldera, or Volcanotectonic Depression?	84
Introduction	84
Discussion	84
Significance of the Mount Hanna Andesite	85
Introduction	85
Origin of the Mount Hanna Andesite	86
Depth of Magma Generation Versus Depth of Eruption	91
Formation of the Sloan Sag	91
Introduction	91
The McCullough Wash Fault System	92
Sagging and Tectonic Control	93
Summary of Events	94
 CONCLUSIONS	 97
 FUTURE WORK	 98
 REFERENCES CITED	 100
 APPENDIX A: SAMPLE LOCATION AND PETROGRAPHY	 107
 APPENDIX B: CHEMISTRY TABLES	 127
 APPENDIX C: CIPW NORMS	 138
 APPENDIX D: ROCK MODES	 142

FIGURES

1: Location Map	2
2: Location of Major Faults in the Lake Mead-Las Vegas Area	6
3: Collapse Caldera Sequence	12
4: Ar-Ar Date Data	18
5: Stratigraphic Column of the North-Central McCullough Mountains	21
6: Stratigraphic Column of the Sloan Volcanics	24
7: Photo of the Mount Hanna Andesite Vent Center	27
8: Sample Location Map	29
9: Photo of Hydroclastic Tuff at Station 73	30
10: Photo of Mount Ian Andesite Hydroclastic Breccia at Station 120	31
11: Photo of Platy, Foliated Mount Ian Andesite	32
12: Photo of Hypabyssal Stock in the Northern Mount Sutor Dacite Field ...	34

13: Harker Variation Diagrams	39
14: AFM Diagram	43
15: Harker Variation Diagrams Showing the Four Chemically Distinct Groups of the Sloan Volcanics	45
16: Trace Element Diagrams	46
17: Chondrite-Normalized REE Diagrams	54
18: Chondrite and MORB-Normalized Spider Diagrams	56
19: Chondrite and MORB-Normalized Spider Diagrams of the Sloan Andesites and the Hidden Valley Volcanics	60
20: Chondrite and MORB-Normalized Spider Diagrams of Tertiary Volcanic Rocks in the Lake Mead-Las Vegas Area	62
21: Chondrite-Normalized REE Diagram for Melt Model #1: Sloan Andesite From Gabbro	75
22: Chondrite-Normalized REE Diagram for Melt Model #2: Sloan Dacite From Gabbro	78
23: Chondrite-Normalized REE Diagram for Melt Model #3: Sloan Andesite and Dacite From Peridotite (2X Chondrite)	79
24: Chondrite-Normalized REE Diagram for Melt Model #4: Sloan Andesite and Dacite From Peridotite (Metasomatized Mantle Chondrite Values) ..	80
25: Microphoto of the Mount Hanna Andesite	87
26: Photo of the Streaky, Discontinuous Texture of the Mount Hanna Andesite	89
27: Formation Sequence of the Sloan Sag	95

TABLES

1: New K-Ar Dates	16
2: New Ar-Ar Date	17
3: Mean Error for Trace Elements	52
4a: Mixing Model #1	67
4b: Mixing Model #2	67
5a: Melt Model #1	73
5b: Melt Model #2	73
5c: Melt Model #3	77
5d: Melt Model #4	77

INTRODUCTION

Location and Geography

Hidden Valley is in the north-central McCullough Mountains, Clark County, southern Nevada (Fig. 1). The thesis area covers 240 km² and is included on the Hidden Valley, Sloan, Sloan NE and Sloan SE 7.5 minute quadrangle maps. Dirt roads provide access to the western and central parts of the thesis area, however the eastern part must be approached by foot. Elevations in the thesis area range from 790 to 1292 m.

Previous Work

Because of its lack of economic mineral resources, little detailed geological mapping has been done in the McCullough Mountains. Hewett (1956) mapped the McCullough Mountains as part of the Ivanpah Quadrangle, but did not subdivide the Tertiary section. Longwell et al. (1965) did reconnaissance mapping for mineral resources in Clark County, but also did not differentiate the Tertiary volcanic rocks in the McCullough Mountains. Anderson et al. (1985) and DeWitt et al. (1989) mapped the South McCullough Wilderness Study Area in the southern McCullough Mountains for a study requested by the U.S. Bureau of Land Management, the U.S. Geological Survey, and the U.S. Bureau of Mines. Mapping for the wilderness study area, however, did not extend to the north into Hidden Valley.

Two masters theses were completed in the north-central McCullough

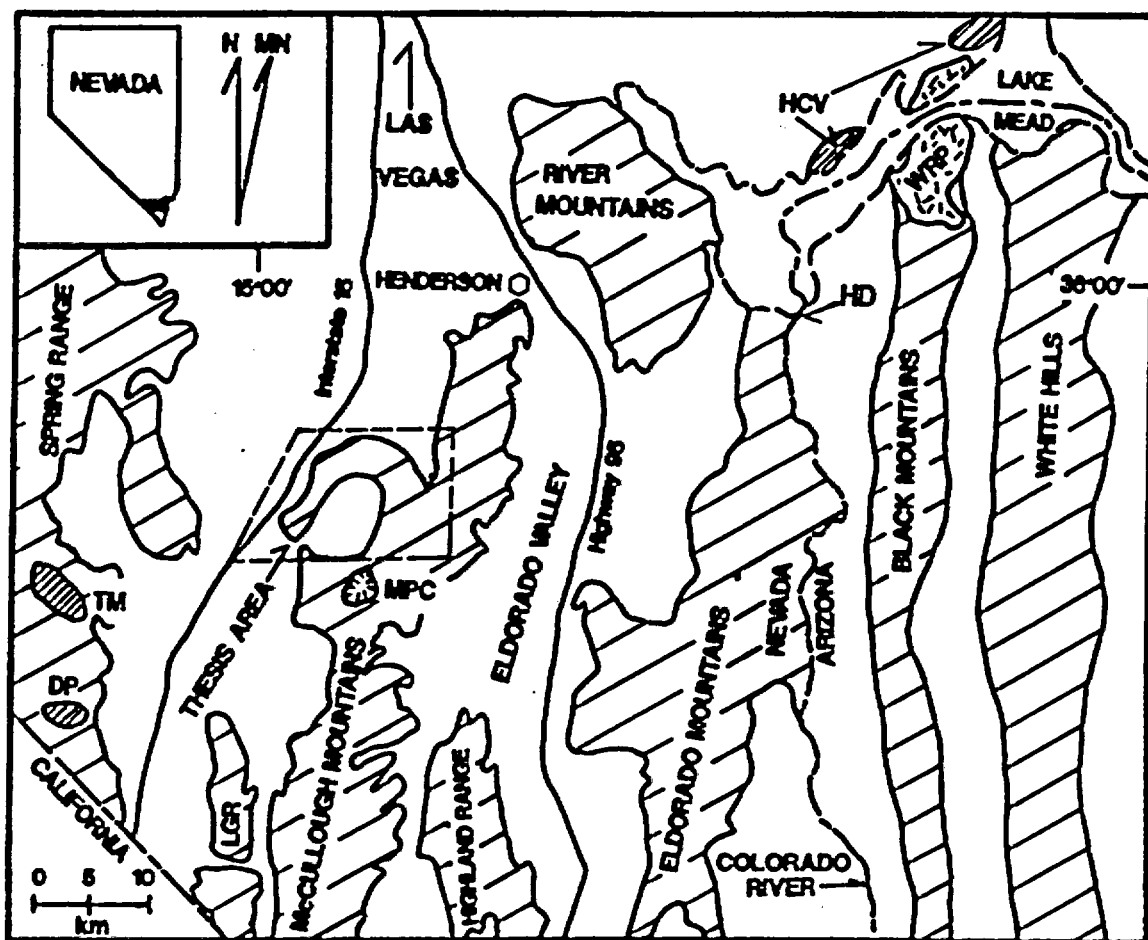


Figure 1: Location map of the thesis area and selected Tertiary igneous centers in the Las Vegas-Lake Mead vicinity. MPC = McCullough Pass caldera; DP = Devil Peak; TM = Table Mountain; WRP = Wilson Ridge pluton; HCV = Hamblin Cleopatra volcano; HD = Hoover Dam sag-graben caldera; LGR = Lucy Gray Range.

Mountains. Kohl (1978) studied the nature and source of carnotite in caliche deposits in Hidden Valley. Schmidt (1987) mapped and described a small (< 3 km diameter) caldera about 3 km southeast of Hidden Valley.

Purpose of Study

The Hidden Valley area contains andesite and dacite domes and flows, dacite and rhyolite pyroclastic units, and a late-stage hypabyssal dacite stock that partially fill a sag developed in the underlying basalt. This volcanic section is herein named the Sloan volcanics. In some areas, the contact between the Sloan volcanics and the underlying basalt is conformable, while in others it is not. Questions concerning the Sloan volcanics addressed in this thesis are: 1) Do the Sloan volcanics fill a volcanotectonic depression or caldera, or simply represent a dome field situated on the flank of an older stratocone? 2) How did the sag, now filled with the Sloan volcanics, form? 3) What is the petrogenesis of the andesites and dacites of the Sloan volcanics? 4) What is the internal stratigraphy of the Sloan volcanic section? 5) What is the absolute age of the Sloan volcanic section?

The purpose of this thesis is to present concise answers to the above questions.

I will demonstrate, using stratigraphic, lithologic and geochemical evidence, that the Sloan volcanics formed during volcanotectonic sagging caused by their eruption. I also suggest that the Mount Hanna andesite member of the Sloan volcanics erupted by a mechanism of lava fountaining, and may be the hot, dry analog of an ash-flow tuff.

Geologic Setting

The McCullough Mountains are in the southern Basin-and-Range province on the western border of the Colorado River extensional corridor. The north-south trending range extends from the New York Mountains in California to the city of Henderson in the Las Vegas Valley (Fig. 1).

The southern part of the McCullough Mountains consists of Precambrian igneous and metamorphic rocks (Longwell et al., 1965; DeWitt et al., 1989). The northern part consists of Precambrian basement overlain by a Tertiary volcanic section. Excellent exposure of the northern section is provided in a steep eastern escarpment.

In addition to the Sloan volcanic center, other volcanoes within 30 km of the thesis area include: 1) the McCullough Pass caldera approximately 3 km south of Hidden Valley (Schmidt, 1987); 2) Devil Peak, an intrusive rhyolite plug in the southern Spring Range (Walker et al., 1981); 3) Table Mountain, a dacitic (unpublished chemical data base, E.I Smith, University of Nevada, Las Vegas) eruptive center about 10 km north of Devil Peak; 4) The River Mountains stratovolcano complex (Fig. 1).

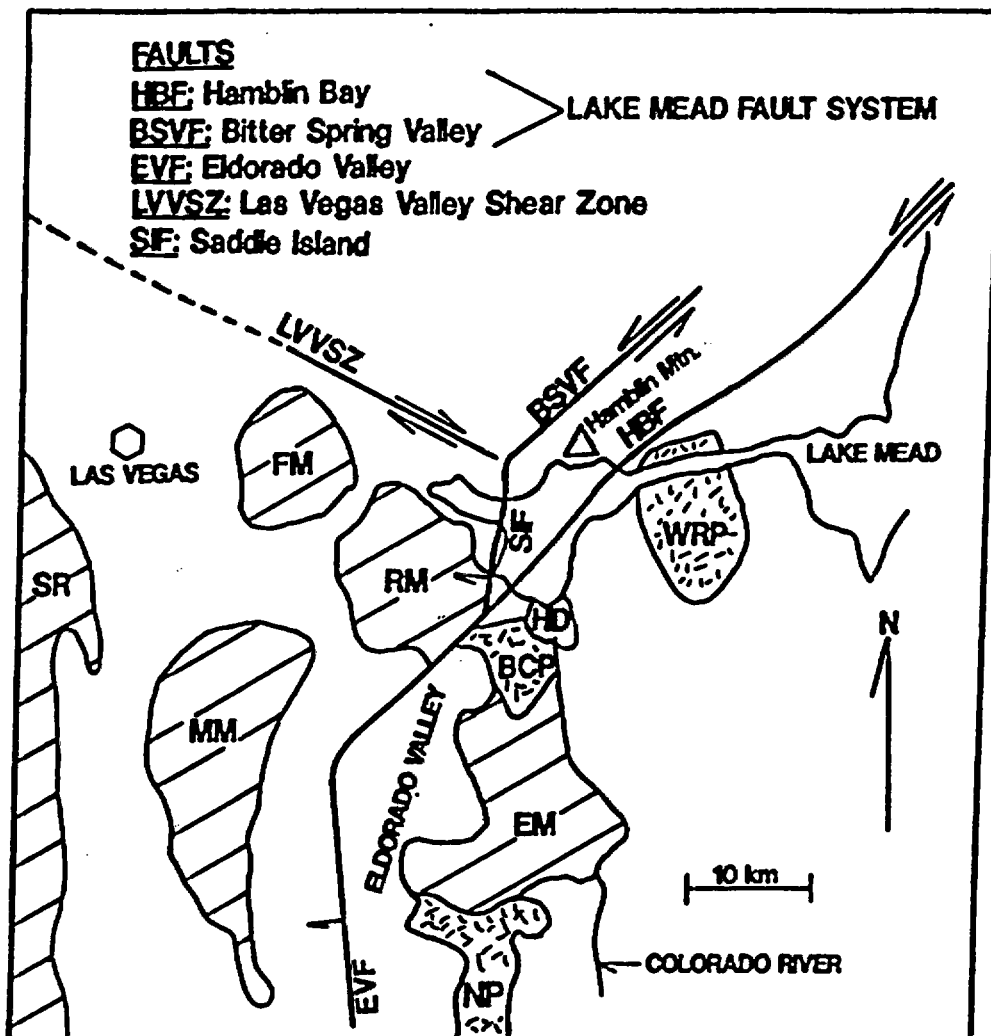
Structural Geology and Tectonics

The McCullough Mountains are a relatively stable block compared to ranges to the north and east. During Tertiary extension, the range was extended only about 20% (Weber and Smith, 1987). The west-dipping McCullough Wash normal fault is the only major internal structure in the McCullough Mountains.

This fault has a throw of at least 600 m, placing Precambrian basement against the Hidden Valley volcanic section in the central part of the range. Displacement decreases to the north to less than 50 m (Schmidt, 1987; Anderson et al., 1985). The Spring Range, to the west of the McCullough Mountains, displays minor Tertiary extension (Carr, 1983; Wernicke et al., 1988). The Eldorado Mountains, to the east of the McCullough Mountains, are highly faulted with regional dips varying from 30° east to vertical, and were extended over 100% (Anderson, 1971).

A model proposed by Weber and Smith (1987) suggests that the River and McCullough Mountains lie in the upper plate of the west-dipping Saddle Island detachment system. According to their model, the left-lateral Hamblin Bay and Bitter Spring Valley faults are transfer structures between the Saddle Island and Eldorado Valley normal faults (Fig. 2). The detachment system is at a shallow depth beneath the Eldorado Mountains resulting in a high degree of extension. The McCullough Mountains and Spring Range represent blocks overlying the detachment at a greater depth, and were transported in the upper plate without significant internal deformation (Fig. 2).

A more recent model by Smith et al. (1991) suggests that the Eldorado Valley fault may be a steep westward-dipping normal fault. Isostatic rebound caused footwall rotation resulting in flattening of the fault. The Eldorado Mountains experienced high degrees of extension in the footwall block, while the McCullough Mountains and the Spring Range remained relatively undisturbed in the hanging wall. Smith et al. (1991) also suggest that these types of deeply



ROCK UNITS

FM: Frenchman Mountain
RM: River Mountains
MM: McCullough Mountains
EM: Eldorado Mountains
SR: Spring Range
HD: Hoover Dam Volcanics
NP: Nelson Pluton
BCP: Boulder City Pluton
WRP: Wilson Ridge Pluton

Figure 2: Location of major faults in the Lake Mead-Las Vegas area (modified from Weber & Smith, 1987).

penetrating high angle faults may provide conduits for magma migration. A model proposed by Duebendorfer and Wallin (1991) suggests that Frenchman Mountain and the River Mountains lie in a block that is bounded to the north by the Las Vegas Valley shear zone and to the southeast by the Saddle Island detachment system. The location of the Lake Mead fault system is not well constrained west of Hamblin Mountain. Bohannon (1979) suggested that this fault system may project through Las Vegas Wash, placing the River Mountains and Frenchman Mountain in separate structural blocks (Fig. 2). Sediments of the post 13.5 Ma Horse Spring Formation, however, crop out in the Rainbow Gardens area of Frenchman Mountain and are interfingered with volcanic rocks of the River Mountains. These sediments are not disrupted across Las Vegas Wash, suggesting that no post 13.5 Ma movement on the Lake Mead fault system occurred between the River Mountain and Frenchman Mountain blocks. If the Weber and Smith (1987) model is correct, the Saddle Island detachment is part of the Lake Mead-Eldorado Valley detachment system, thus placing the McCullough Mountains in the same structural block as Frenchman Mountain and the River Mountains (Fig. 2). No major strike-slip fault system has been documented between the McCullough and River Mountains (Anderson, 1977; Weber and Smith, 1987).

According to Duebendorfer and Wallin (1991), at 12 Ma, coeval movement on the Las Vegas Valley shear zone and the Saddle Island detachment moved the River Mountains-Frenchman Mountain block westward, opening the Red

Sandstone basin to the south of the Las Vegas Valley shear zone. Because the McCullough Mountains are in the same structural block, they were also transported westward; and because no major structure exists between the McCullough Mountains and the Spring Range, the Spring Range also must have been transported westward in the same structural block.

Intermediate Volcanism

Volcanic rocks erupted during Tertiary extension in the Las Vegas area are intermediate calc-alkaline suites with only minor amounts of basalt and rhyolite (Anderson, 1971; Smith, 1982; Mills, 1985; Feuerbach, 1986; Smith et al., 1990). The intermediate volcanic section in the McCullough Mountains is an example of such an occurrence. Proposed models for the production of intermediate suites during regional extension include: 1) assimilation of felsic crustal material and mafic mantle melts during magma ascent (Damon, 1971); 2) magma mixing of felsic and mafic end members (Glazner, 1989); 3) open system models utilizing the assimilation and/or mixing of felsic material with a fractionated mafic phase (Nielson and Dungan, 1985; McMillan and Dungan, 1986; Novak and Bacon, 1986; Smith et al., 1990).

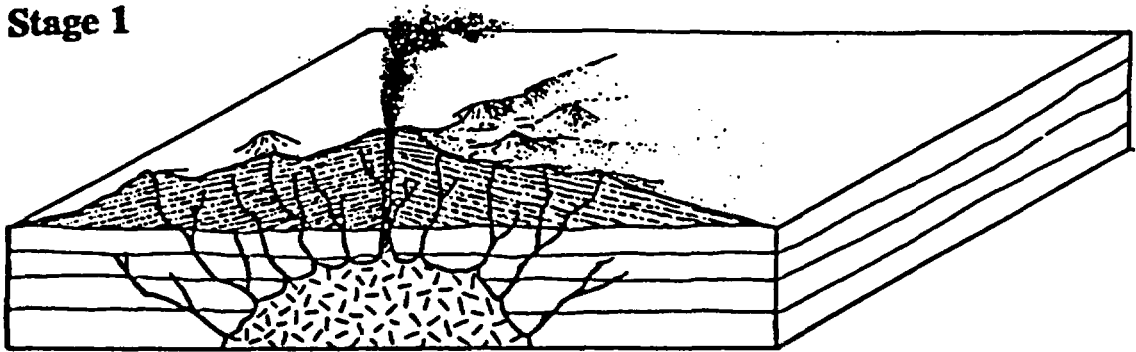
The production of intermediate igneous rocks during Tertiary extension in the Las Vegas-Lake Mead area as a result of magma commingling of felsic and mafic end members has been documented by Naumann and Smith (1987), Naumann (1987), Larsen (1989), Smith et al. (1990) and Larsen and Smith (1991). The Sloan volcanic section lacks textural evidence of magma commingling. I will

suggest in this thesis, therefore, that intermediate volcanic rocks may also have been produced from partial melts of mid-to lower-crustal material without undergoing commingling and/or contamination from other sources.

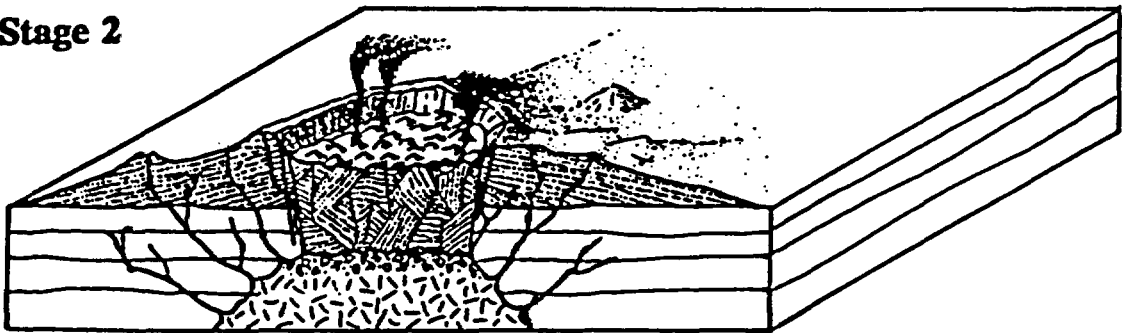
erosion of the oversteepened walls causes enlargement of the caldera boundary and the formation of slump breccias within the crater. A resurgent dome forms when more magma enters the evacuated chamber causing upwarping of the caldera's floor. Volcanic domes may be emplaced along extensional faults on the resurgent dome or in the moat of the caldera. A typical caldera cycle ends with hydrothermal activity (Fig. 3). Not all calderas undergo complete collapse. Many calderas that erupt small-to-moderate volumes of ash-flow tuff ($10\text{-}50\text{ km}^3$) experience incomplete subsidence along horseshoe-shaped faults (Lipman, 1984). An example is the Three Creeks Caldera in the Marysvale volcanic field, Utah (Steven, 1981). Other calderas associated with low-to-modest volumes of ash-flow tuff appear to be unfaulted sags (Lipman, 1984; Walker, 1984), such as the Taupo volcanic center, New Zealand (Grindley, 1965; Cole, 1979). Factors that may contribute to downsagging or incomplete subsidence include: 1) a magma chamber at great depth ($> 10\text{-}15\text{ km}$); 2) structurally coherent roof rocks; 3) resurgence of magma into the chamber during eruption preventing emptying of the chamber; 4) a small volume of magma relative to caldera area (Steven and Lipman, 1976; Steven et al., 1984; Walker, 1984).

Ninety percent of the documented Tertiary-aged calderas in the Basin-and-Range province are greater than 15 km in diameter. Worldwide, only about ten percent of all Quaternary-aged calderas exceed this size (Walker, 1984). According to Walker (1984), this size difference may be attributed to crustal type. Basement in the Basin-and-Range province is largely Precambrian crystalline rock,

Stage 1



Stage 2



Stage 3

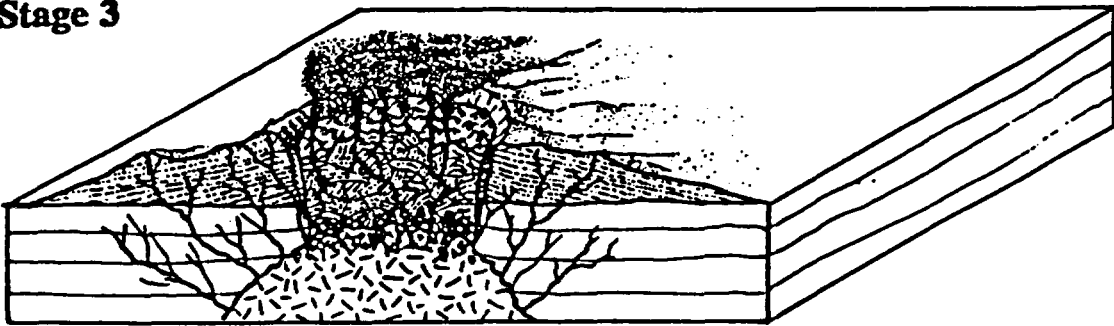


Figure 3: Collapse Caldera Sequence: Stage 1: Pyroclastic eruptions occur from vents above ring faults over a shallowly-emplaced magma chamber. Stage 2: Caldera collapse occurs during and/or after the pyroclastic eruptions. Stage 3: Erosion causes embayment and enlargement of the caldera margin. Slump breccias from the oversteepened walls form within the caldera. Resurgence of magma into the chamber may cause upward doming of the caldera floor.

whereas most Quaternary calderas are emplaced in young crust. Rigid crystalline basement rock may enhance complete separation and subsidence of the caldera floor resulting in larger collapse structures. Another factor contributing to the larger size of Basin-and-Range calderas may be enlargement due to extension.

Small ash-flow calderas in the Basin-and-Range province include the 3.5 km diameter Van Horn Mountains Caldera in the Trans-Pecos volcanic province in the Van Horn Mountains, Texas (Henry and Price, 1986), and the less than 3 km diameter McCullough Pass Caldera in the central McCullough Mountains, southern Nevada (Schmidt, 1987). The 13.5 km diameter Sloan sag discussed in this thesis is an example of a small volcanotectonic depression in the Basin-and-Range province.

ANALYTICAL METHODS

Fifty seven rock samples were analyzed for major element oxides. Forty six samples were analyzed for trace elements. Fresh, unweathered samples collected in the field were ground to -200 mesh using a Dyna Mill air suspended impact attrition mill and an agate mortar and pestal. Major element oxides were analyzed by X-ray fluorescence techniques on a Rigaku 3030 X-ray spectrometer at the University of Nevada, Las Vegas (UNLV). Trace elements were analyzed by instrumental neutron activation analysis at the Phoenix Memorial Laboratory at the University of Michigan. Kohl (1978) and Schmidt (1987) provided additional analyses of the Hidden Valley Volcanics and the Tuff of Bridge Spring.

One sample each of the Center Mountain dacite and the Tuff of Bridge Spring were dated using the K-Ar method on biotite separates. Mineral separations were done at UNLV. Approximately 10 pounds of fresh, unweathered sample was crushed in the attrition mill. The sample was then separated into six fractions of differing specific gravities on a number 13 Wilfley Table. Final biotite separation was done using heavy liquids (sodium metatungstate) and a Frantz magnetic separator. K-Ar dates were done by Krueger Enterprises in Cambridge, Massachusetts.

An $^{40}\text{Ar}/^{39}\text{Ar}$ sanidine date was obtained from the same sample of the Tuff of Bridge Spring. Sanidine separation was done at UNLV using the above methods. Sample irradiation was done at the Ford nuclear reactor, University of Michigan. $^{40}\text{Ar}/^{39}\text{Ar}$ dating was performed at the University of Maine, Orono.

GEOCHRONOLOGY

K-Ar dates from biotite separates were obtained from the Center Mountain dacite member of the Sloan volcanics and the Tuff of Bridge Spring from the north-central McCullough Mountains. An $^{40}\text{Ar}/^{39}\text{Ar}$ date from a sanidine separate was obtained from the same Tuff of Bridge Spring sample. These are the first age dates obtained from rocks of the north-central McCullough Mountains.

The K-Ar date for the Center Mountain dacite is 16.4 ± 0.5 Ma, the K-Ar date for the Tuff of Bridge Spring is 16.6 ± 0.4 Ma (Table 1). The $^{40}\text{Ar}/^{39}\text{Ar}$ date on the Tuff of Bridge Spring, however, is 15.23 ± 0.14 Ma (Table 2; Figs. 4a & 4b).

The differences between the Tuff of Bridge Spring dates may be the result of excess argon retained by the biotite. Minerals may include argon in their crystal lattice by means other than the radiogenic decay of ^{40}K . Argon may be absorbed from the atmosphere or diffused into minerals from the outgassing of K-bearing minerals in the crust and/or mantle (Faure, 1986). The K-Ar dating method assumes that all of the Ar in the sample is radiogenic, produced by the radioactive decay of K in that sample. If excess Ar is present, the K-Ar method may result in an anomalously old age (Faure, 1986).

The $^{40}\text{Ar}/^{39}\text{Ar}$ dating method is based upon the production of ^{39}Ar by irradiation of K-bearing minerals in a nuclear reactor. It has an advantage over the K-Ar method in that only radiogenic Ar is measured. The irradiated sample

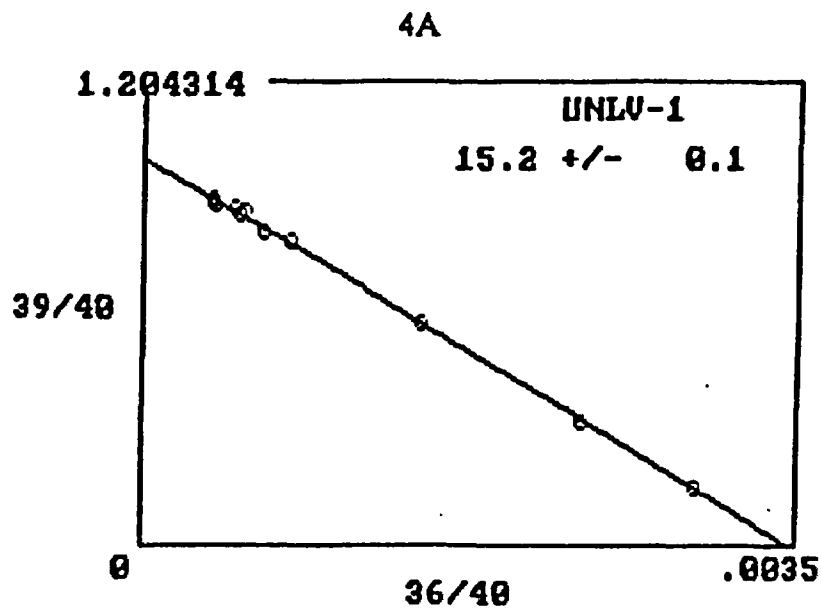
Table 1: New K-Ar Dates For The North-Central McCullough Mountains					
Sample	K%	Ar* (ppm)	Ar*/Total	K (ppm)	Date & Error
Center Mtn. Dacite	7.92	0.007578	0.1885	7.92	16.4 +/- 0.5 Ma
Tuff of Bridge Spring	6.323	0.007294	0.461	7.543	16.6 +/- 0.4 Ma

* Denotes radiogenic

Temp C	40Ar/39Ar	37Ar/39Ar	36Ar/39Ar	Moles 39Ar	% Total 39Ar	% Radiogenic Ar40	K/Ca	Age and error (Ma)
750	6.461	0.0348	0.0189	127.8	1.9	13.1	14.09	12.96 +/- 0.82
830	3.156	0.0314	0.0073	181.7	2.6	31.1	15.60	15.01 +/- 0.53
900	1.753	0.0312	0.0026	252.2	3.7	55.9	15.72	14.99 +/- 0.47
960	1.291	0.0306	0.0010	356.7	5.2	76.0	16.01	15.01 +/- 0.29
1020	1.176	0.0299	0.0006	531.7	7.7	82.9	16.41	14.91 +/- 0.20
1080	1.180	0.0295	0.0006	811.9	11.8	83.6	16.63	15.09 +/- 0.20
1120	1.166	0.0297	0.0006	987.6	14.3	84.5	16.52	15.06 +/- 0.14
1160	1.148	0.0291	0.0004	1012.2	14.7	87.4	16.86	15.34 +/- 0.14
1200	1.136	0.0292	0.0004	1014.9	14.7	87.9	16.80	15.26 +/- 0.14
1240	1.143	0.0288	0.0004	888.4	12.9	87.8	17.00	15.34 +/- 0.20
Fuse	1.252	0.0292	0.0008	729.4	10.6	80.2	16.79	15.34 +/- 0.18

Plateau age = 15.32 +/- 0.16 Ma

Isotope correlation age = 15.23 +/- 0.14 Ma



$Y = B + MX$
 $Y - {}^{40}\text{Ar}/{}^{36}\text{Ar} = 289.5103 \pm 4.017002$
 $B - {}^{39}\text{Ar}/{}^{40}\text{Ar} = 1.003595 \pm 4.162581\text{E-}03$
 $M - \text{Slope} = -290.5509 \pm 3.220593$: Slope used in calculation of data
 $X - {}^{36}\text{Ar}/{}^{40}\text{Ar} = 3.454109\text{E-}03 \pm 4.792633\text{E-}05$
 Intercept age = 15.23245 +/- 0.1388164 Ma

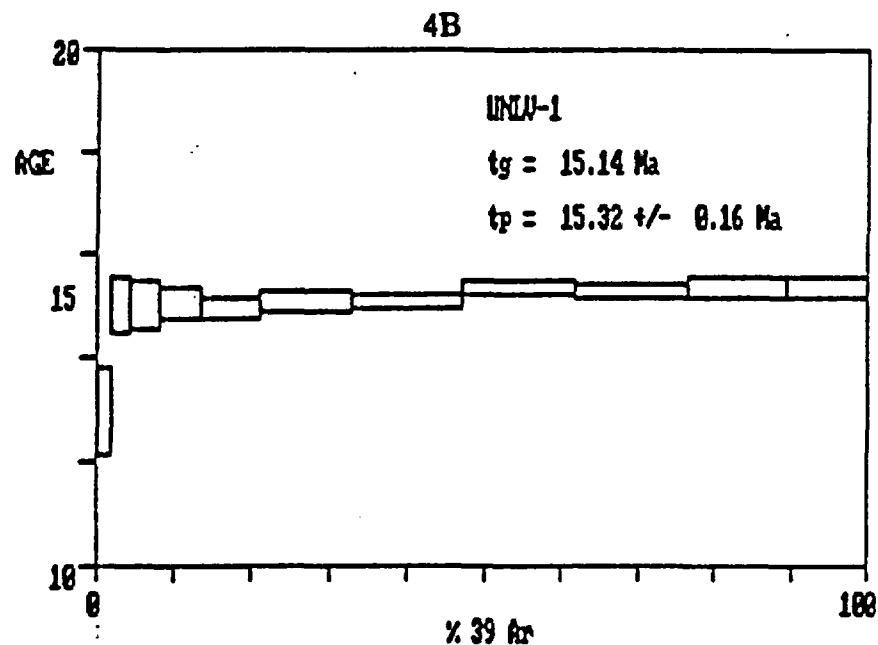


Figure 4: Ar-Ar age date data from the Tuff of Bridge Spring, central McCullough Mountains.

is heated incrementally and the $^{40}\text{Ar}/^{39}\text{Ar}$ ratio for each increment is determined. If the sample has not lost or gained Ar or K since the time of its initial cooling, the ratios at each temperature will be constant. This ratio will result in a "plateau" value that is used to calculate the age of the sample (Faure, 1986).

In $^{40}\text{Ar}/^{39}\text{Ar}$ dating, the isochron correlation method may also be used. A sample may also contain atmospheric ^{36}Ar . On a graph of $^{39}\text{Ar}/^{40}\text{Ar}$ versus $^{36}\text{Ar}/^{40}\text{Ar}$, values of these ratios determined for each increment of heating are plotted to produce an isochron. The slope of the isochron equals the value of ^{40}Ar (radiogenic)/ ^{39}Ar , which is used to calculate the age of the sample.

I accept the isotope correlation age of 15.23 ± 0.14 Ma for the following reasons. The plateau values from the incremental heating of the Tuff of Bridge Spring sample have a small offset (Fig 4b). There is an initial plateau age of about 15.0 Ma, then it increases to about 15.3 Ma. The offset in the plateau suggests that the sample may be slightly altered. The plateau date of 15.32 ± 0.16 Ma (Fig. 4b) for the sample was calculated using only the data from the higher plateau. The isotope correlation age (Fig 4a), on the other hand, takes into account all values of incremental heating, resulting in an average of the plateau ages (Faure, 1986). In this case, the isotope correlation technique has produced a higher quality date for the sample and will be accepted in this thesis.

Both of the K-Ar dates are suspect, therefore the actual age of the Sloan volcanics was not determined. I can only conclude that the relative age of the Sloan Volcanics is less than 15.23 Ma.

THE SLOAN VOLCANICS

Introduction

The Sloan volcanics consist of andesite and dacite domes and flows, dacite and rhyolite pyroclastic units, and a late-stage hypabyssal dacite stock. I suggest that they were erupted during and/or after the formation of a volcanotectonic sag in Hidden Valley.

The Sloan volcanics are the youngest volcanic rocks in the McCullough Mountains ($< 15.23 \pm 0.14$ Ma). They overlie the Hidden Valley volcanics, McCullough Pass volcanics, Pumice Mine volcanics, Tuff of Bridge Spring, and Eldorado Valley volcanics respectively. The entire section is underlain by Precambrian basement (Fig. 5).

Rocks were named using the chemical classification scheme of Irvine and Baragar (1971).

Pre-Sloan Volcanic Stratigraphy

Refer to Figure 5 for the stratigraphic column of the rocks described in this section.

Precambrian crystalline rocks crop out south of the thesis area and are composed of biotite monzogranite and biotite granitoid gneiss cut by pegmatite and aplite dikes (Anderson et al., 1985).

The Eldorado Valley volcanics are age equivalent to the Patsy Mine volcanics mapped by Anderson (1971) in the Eldorado Mountains. This unit is

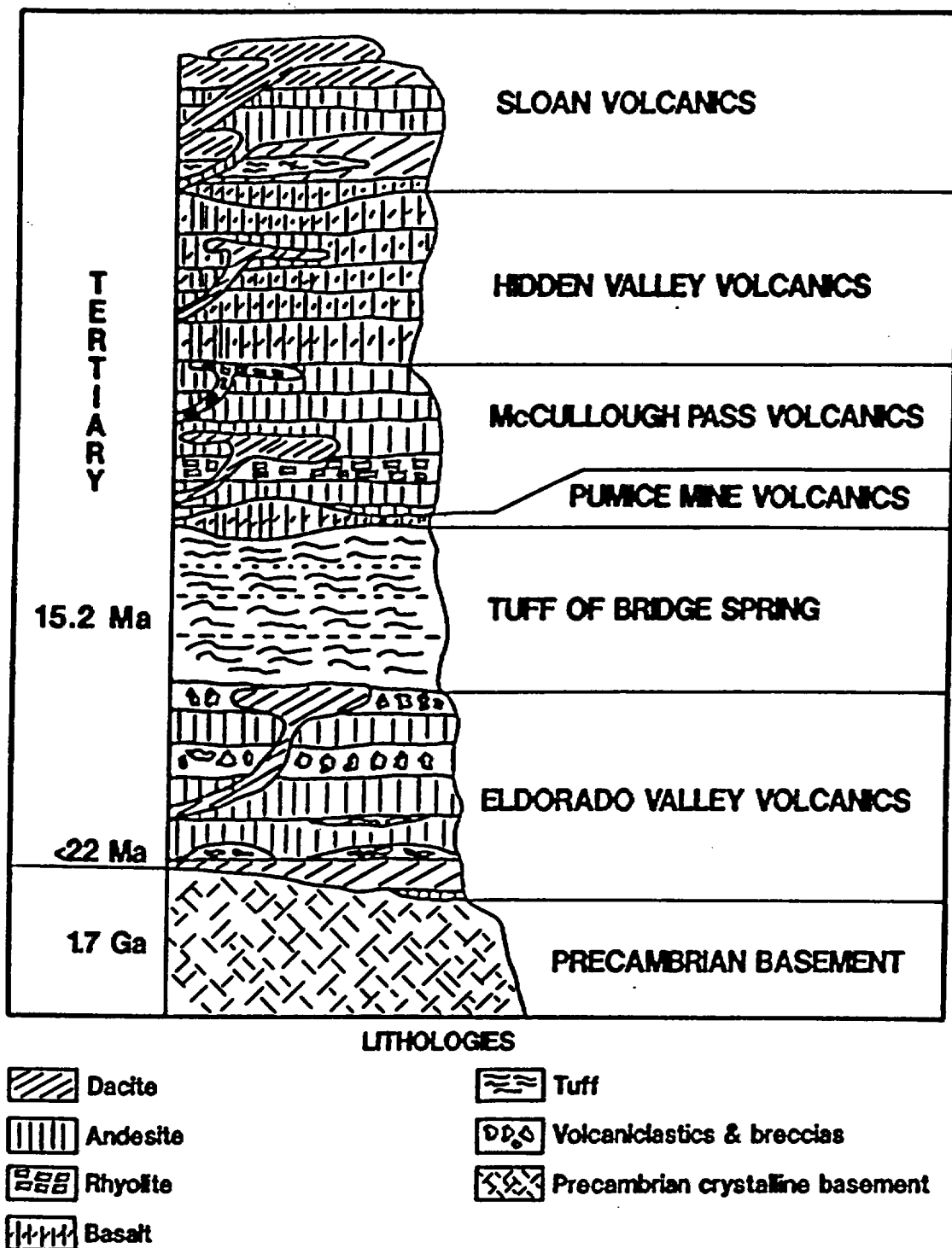


Figure 5: Stratigraphic column of the central McCullough Mountains.

almost 300 m thick on the eastern escarpment of the central McCullough Mountains. It thins rapidly to the west and does not crop out on the western margin of the range (Smith et al., 1988). Westward thinning of this and other volcanic units in the north-central McCullough Mountains may be due to a prominent buttress of Precambrian basement that prevented volcanic units from flowing to the west (Schmidt, 1987; Smith et al. 1988). Schmidt (1987) documented two members of the Eldorado Valley volcanics in the central McCullough Mountains. The lower member consists of thinly interbedded flows of hornblende andesite, olivine andesite and dacite. The upper member is composed mainly of volcanoclastic units.

The Tuff of Bridge Spring is a rhyolite to dacite ash-flow tuff of regional extent. The tuff crops out in the Eldorado Mountains (Anderson, 1971), the Highland Range (Bingler and Bonham, 1972), the McCullough Mountains (Schmidt, 1987), and the White Hills (Cascadden, 1991) and southern Black Mountains (referred to in Cascadden, 1991), Arizona (Fig. 1). In the McCullough Mountains, the Tuff of Bridge Spring consists of a single cooling unit up to 145 m thick (Schmidt, 1987). It crops out in the central part of the range and pinches out to the southeast of Hidden Valley. Scattered outcrops also occur to the west of Hidden Valley (Plate 1), and were mapped as the Erie Tuff by Kohl (1987). A sample of the Tuff of Bridge Spring from the central McCullough Mountains was dated at 15.23 ± 0.14 Ma ($^{40}\text{Ar}/^{39}\text{Ar}$, sanidine).

The Pumice Mine volcanics consists of andesite and basalt flows and

breccia units up to 60 m thick (Smith et al., 1982; Schmidt, 1987). This thin unit is a marker bed separating the Tuff of Bridge Spring from the McCullough Pass volcanics.

The McCullough Pass volcanics are composed of rhyolite domes, dikes, flows and pyroclastic units, andesite flows and dikes, and volcaniclastic rocks that were deposited during and after the collapse of the McCullough Pass caldera (Schmidt, 1987). The outflow facies of the McCullough Pass tuff extends northward from its source into the Hidden Valley area.

The Hidden Valley volcanics are age equivalent to the upper Patsy Mine or lower Mount Davis volcanics in the Eldorado Mountains (Anderson, 1971). This unit is up to 245 m thick on the eastern escarpment of the north-central McCullough Mountains and thins to the west. The Hidden Valley volcanics consist of basalt and basaltic-andesite flows, cinder cones and scoria. Rocks contain clinopyroxene and olivine phenocrysts, and subordinate quartz xenocrysts. The Sloan volcanic section overlies the Hidden Valley volcanics in central and eastern Hidden Valley.

Stratigraphy of the Sloan Volcanics

The oldest rocks of the Sloan volcanics include the Mount Hanna andesite and the rocks of the Center Mountain dome complex. The Center Mountain dome complex is composed of the Cinder Prospect member, Tuff of the Sloan volcanics, Center Mountain dacite, and the Mount Ian andesite (Fig. 6). Since the Mount Hanna andesite member is not in contact with the Center Mountain dome

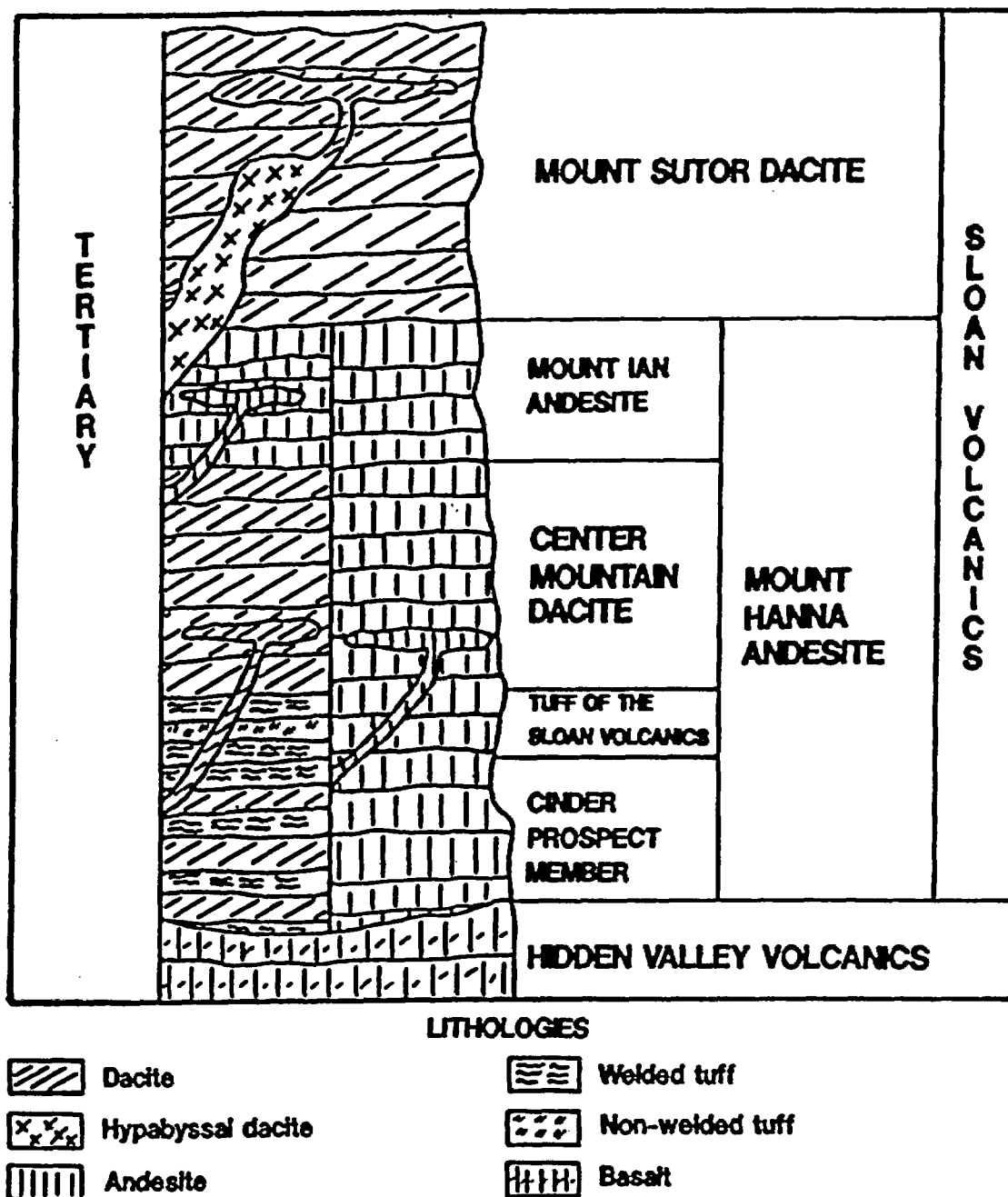


Figure 6: Stratigraphic column of the Sloan volcanics, north-central McCullough Mountains.

complex, the relative age of these sections cannot be determined (Plate 1).

Refer to Figure 6 for the stratigraphic column of the rocks described in this section. Refer to Appendices A and B for rock chemistry.

The Mount Hanna andesite is aphyric with SiO_2 contents ranging from 59.37 to 60.74 weight%. Flows are up to 5 m thick and are commonly platy and foliated on their surfaces.

The Cinder Prospect member consists of thinly interbedded dacite flows and rhyolite to dacite ash-flow tuffs with SiO_2 contents ranging from 61.31 to 69.88 weight%.

The Tuff of the Sloan volcanics consists of three cooling units, each approximately 2 m thick. From oldest to youngest the units are: 1) welded rhyolite ash-flow tuff (SiO_2 = 69.76 weight%); 2) poorly-welded dacite ash-flow tuff (SiO_2 = 64.87 weight%); 3) welded dacite ash-flow tuff (SiO_2 = 64.26 weight%).

The Center Mountain dacite is composed of flows of biotite dacite with SiO_2 contents ranging from 67.67 to 68.06 weight%.

The Mount Ian andesite intrudes and overlies the Cinder Prospect, Tuff of the Sloan Volcanics, and Center Mountain dacite members. Its SiO_2 content varies from 57.84 to 60.22 weight%.

The youngest member of the Sloan volcanics is the Mount Sutor dacite. It is a biotite dacite with SiO_2 contents ranging from 61.67 to 64.96 weight%.

Characteristics of the Sloan Volcanic Centers

The Mount Hanna andesite differs from other members of the Sloan volcanics in that it was erupted from a single vent. This unit is up to 307 m thick and has a maximum volume of 9 km³. Other members erupted from numerous vents and domes. The Mount Hanna eruptive center is about 100 m across. The vent has been eroded and is occupied by a volcanic neck formed of resistant andesite, silicified by hydrothermal activity. Black and red oxidized autobrecciated andesite surrounds the vent (Fig. 7; Cross section C-C', Plate 1). Two small volcanic domes occur about 1 km southwest of the vent and are interpreted as parasitic vents on the flank of the Mount Hanna eruptive center. I suggest that the Mount Hanna andesite erupted at temperatures of approximately 1,000°C with a water content of less than 2% by a lava-fountaining mechanism. This eruption resulted in a lava flow analogous to a hot, dry ash-flow tuff. I will present evidence to support these observations later in this thesis.

The formation of the Center Mountain dome complex reflects the first two steps of four documented by Smith (1973) for the eruptive sequence at the Mono Craters, California. The complete sequence is: 1) creation of a tuff ring composed of ash, lapilli and ejecta, caused from hot rising magma contacting groundwater; 2) eruption of magma into the crater forming a dome; 3) cratering of the dome from explosions and/or collapse; 4) eruption of magma into the previously cratered dome. The interbedded ash-flow tuffs and dacite flows of the Cinder Prospect member and the Tuff of the Sloan volcanics were produced in

Figure 7: Photo of the Mount Hanna Andesite Vent Center

the early stages of pyroclastic and phreatomagmatic activity and reflect the formation of a tuff ring. The upper cooling unit of the Tuff of the Sloan volcanics contains blocky glass shards suggesting a hydroclastic eruption mechanism (Fisher & Schmincke, 1984). In a canyon in the southern part of the dome, (Sta.73, Fig. 8), the tuff contains armored mud balls and discontinuous stringers of dacite (Fig. 9) suggesting hydroclastic activity and lava fountaining. The Center Mountain dacite intruded the tuff ring, erupting thick, viscous dacite over the earlier units. The approximate volume of the dome complex is 0.44 km^3 .

The Mount Ian andesite erupted from numerous domes and vents, many of which overlie tuff rings composed of black ash and cinder. One volcanic center (Sta. 120, Fig. 8) contains a volcanic neck of hydroclastic breccia of andesite clasts and bombs embedded in an ashy groundmass (Fig. 10). The deposit formed when hot, rising magma came in contact with groundwater. Clasts and bombs of quenched andesite were ejected from the volcano. Some fell back into the vent and became embedded in a fine-grained hydroclastic groundmass. Domes are characterized by platy andesite forming "onion skin" patterns. Foliation defined by platy slabs of andesite dip inward toward the conduit and become horizontal over the vent (Fig. 11). Single domes are less than 0.5 km in diameter, and up to 75 m high.

Both the southern and northern Mount Sutor dome fields are composed of flows of massive biotite dacite. Only two vents are exposed in the southern Mount Sutor field, but more may be buried by flows. A vent at station 91 (Fig. 8)

Figure 8: Sample Location Map

:

Figure 9: Photo of Hydroclastic Tuff at Station 73

Figure 10: Photo of Mount Ian Andesite Hydroclastic Breccia at Station 120

:

Figure 11: Photo of Platy, Foliated Mount Ian Andesite

consists of a tuff ring overlain by 3 to 4 m of explosion breccia overlain by 3 m of hydroclastic breccia, capped by dacite. This sequence suggests that an earlier dome was explosively disrupted by intruding magma creating a dacite breccia. Phreatomagmatic activity continued and resulted in the deposition of hydroclastic breccia. Viscous dacite covered these units. The northern Mount Sutor field contains a hypabyssal dacite stock that intruded its own volcanic cover (Fig. 12). The hypabyssal and volcanic rocks are chemically similar. I suggest that vents related to this shallow magma body were responsible for eruption of the dacites in the northern Mount Sutor field. Any volcanic domes and vents have since been stripped from the intrusion by erosion.

Petrography

Refer to Appendix C for detailed petrographic descriptions, and Appendix D for rock modes.

Tuff of Bridge Spring: The Tuff of Bridge Spring is a poorly-welded to welded rhyolite to dacite ash-flow tuff containing phenocrysts (10-33%) of sanidine, plagioclase, biotite, clinopyroxene and subordinate quartz, sphene, zircon and Fe-Ti oxides. The tuff includes pumice (1-12%), and basaltic and subordinate gabbroic and granodioritic xenoliths (1-10%). In welded units the pumice is flattened to fiamme. The groundmass consists of devitrified glass and glass shards. For further descriptions of the Tuff of Bridge Spring in the McCullough Mountains, see Kohl (1978) and Schmidt (1987).

Hidden Valley volcanics: Basalts are vesicular, subalkalic to transitional

Figure 12: Photo of Hypabyssal Stock in the Northern Mount Sutor Dacite Field

and contain phenocrysts (1-37%) of plagioclase, clinopyroxene and iddingsitized olivine. Some of the phenocrysts commonly occur in glomerocrysts. Two samples (Mc47 & Mc48) have phenocrysts (4-5%) of oxidized biotite or phlogopite. Some of the samples include up to 1% glass-rimmed quartz xenocrysts. The groundmass consists of microlites of plagioclase, clinopyroxene, iddingsitized olivine, and trace amounts of glass. For further descriptions, see Kohl (1978) and Schmidt (1987).

Mount Hanna andesite: The Mount Hanna andesite is fine-grained, hypocrySTALLINE and commonly trachytic. Phenocrysts are rare (< 1%) and consist of highly embayed and pitted plagioclase and biotite. Andesite is characterized by microlites of subparallel plagioclase with subordinate Fe-Ti oxides, glass and highly birefringent cryptocrystalline grains (pyroxene & olivine?).

Cinder Prospect member: Ash-flows tuffs of the Cinder Prospect member contain phenocrysts (25-26%) of plagioclase, sanidine, biotite, Fe-Ti oxides and clinopyroxene with trace amounts of zircon. Subordinate basaltic, gabbroic and granodioritic xenoliths also occur. Plagioclase phenocrysts are commonly pitted and embayed. The groundmass consists of devitrified glass and glass shards, and trace amounts of granular hematite. Ash-flow tuffs are commonly vitrophyric. Biotite dacite contains glomerocrysts (4-6%) of plagioclase, biotite and Fe-Ti oxides, and phenocrysts (5-6%) of the same assemblage of minerals found in the glomerocrysts. The groundmass consists of microlites of plagioclase with subordinate oxidized biotite, zircon and glass.

Tuff of the Sloan Volcanics: Tuffs contain phenocrysts (17-36%) of

plagioclase, sanidine, biotite, clinopyroxene, Fe-Ti oxides, sphene and trace amounts of zircon. The basal rhyolite cooling unit (Mc59a) has trace amounts of monazite, epidote and allanite. The upper dacite cooling unit (Mc59c) has trace amounts of quartz. The tuffs also include devitrified pumice clasts (2-12%), and basaltic and gabbroic xenoliths (4-21%). The groundmass consists of devitrified glass shards. Shards from sample Mc59c are blocky.

Center Mountain dacite: The Center Mountain biotite dacite is holocrystalline and contains phenocrysts (6-9%) of plagioclase with subordinate oxidized biotite and Fe-Ti oxides. The groundmass consists of microlites of plagioclase with subordinate oxidized biotite, Fe-Ti oxides and clinopyroxene(?), and secondary calcite (1-5%) that coats fractures and partially replaces the groundmass. Rocks are commonly glomerocrystic and trachytic.

Mount Ian andesite: The fine-grained, hypocrySTALLINE Mount Ian andesite contains phenocrysts (5-35%) of plagioclase, oxidized biotite and Fe-Ti oxides with subordinate orthopyroxene and iddingsitized olivine. Some phenocrysts occur in glomerocrysts. The groundmass consists of microlites of the phenocryst-phase minerals, dominated by plagioclase. Trace amounts of hematite and glass are also present.

Mount Sutor dacite: The Mount Sutor biotite dacite contains glomerocrysts (2-18%) of plagioclase, biotite and Fe-Ti oxides. Some glomerocrysts also contain orthopyroxene and/or clinopyroxene. Dacites include phenocrysts (2-6%) of the same assemblage of minerals found in the

glomerocrysts. One sample (Mc27) has less than 1% oxidized hornblende. Plagioclase is pitted, embayed, and displays oscillatory zoning. Biotite is commonly oxidized. The groundmass consists of microlites of plagioclase, biotite and Fe-Ti oxides, with subordinate orthopyroxene, clinopyroxene, zircon and glass. Two samples (Mc118 & Mc119) collected from the hypabyssal stock in the northern Mount Sutor field are coarse-grained but have an identical mineralogy to their volcanic counterparts.

GEOCHEMISTRY

Metasomatism

Tertiary igneous rocks in the Lake Mead-Las Vegas area are commonly metasomatized (Feuerbach, 1986; Smith et al., 1989; Larsen, 1989). During metasomatism rocks are strongly enriched in potassium and depleted in sodium, or vice versa. For example, some of the quartz monzonite samples from the Tertiary Wilson Ridge pluton (Fig. 1) have K_2O contents as high as 10.5 weight% and Na_2O as low as 0.75 weight% (Feuerbach, 1986).

Rocks of the Sloan volcanics appear not to have been appreciably affected by metasomatism. Similar K_2O and Na_2O contents (4 to 6 and 3 to 5 weight% respectively) suggest that potassium and/or sodium enrichment has not occurred. Harker variation diagrams show that K_2O and Na_2O increase with increasing SiO_2 , but the data are scattered (Figs. 13A & 13E). The scatter may be due to minor remobilization of alkali elements.

Major Elements

Rocks of the Sloan volcanics are calc-alkaline (Fig. 14) and range from 58 to 70 weight% SiO_2 (Appendix A). MgO , Fe_2O_3 , CaO , Al_2O_3 , TiO_2 and P_2O_5 decrease with increasing SiO_2 (Figs. 13B, 13C, 13D, 13F & 13G). K_2O and Na_2O increase with increasing SiO_2 (Figs. 13A & 13E).

Harker variation diagrams divide the rocks of the Sloan volcanics into four chemically distinct groups. These are the: 1) Mount Hanna andesite and Mount

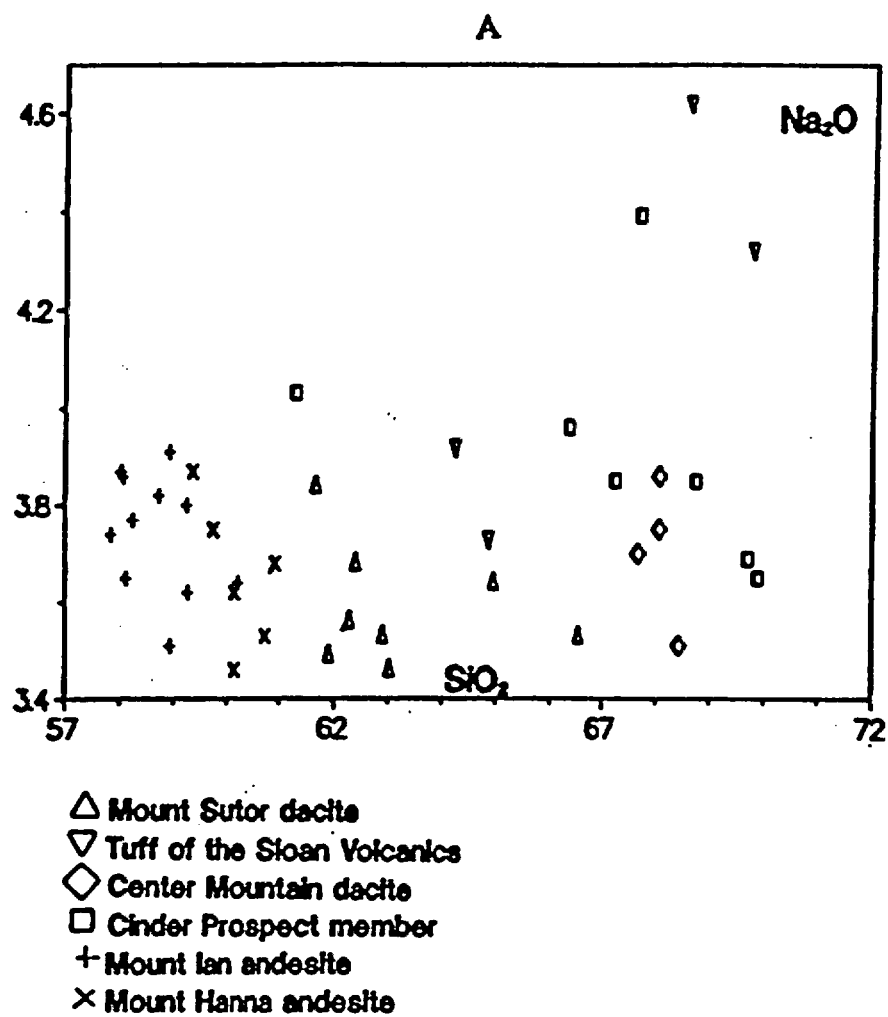


Figure 13: Harker variation diagrams

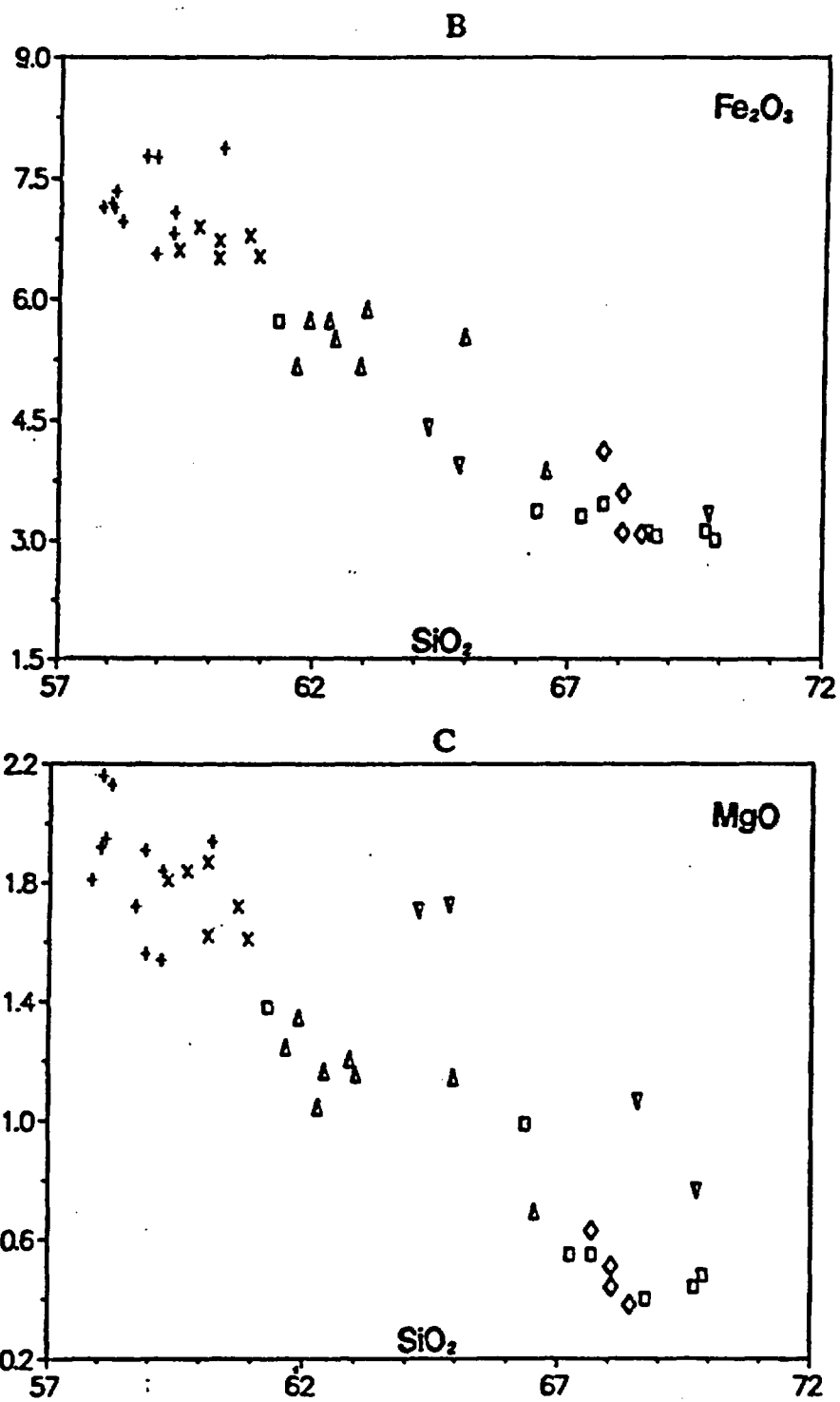


Figure 13: Continued

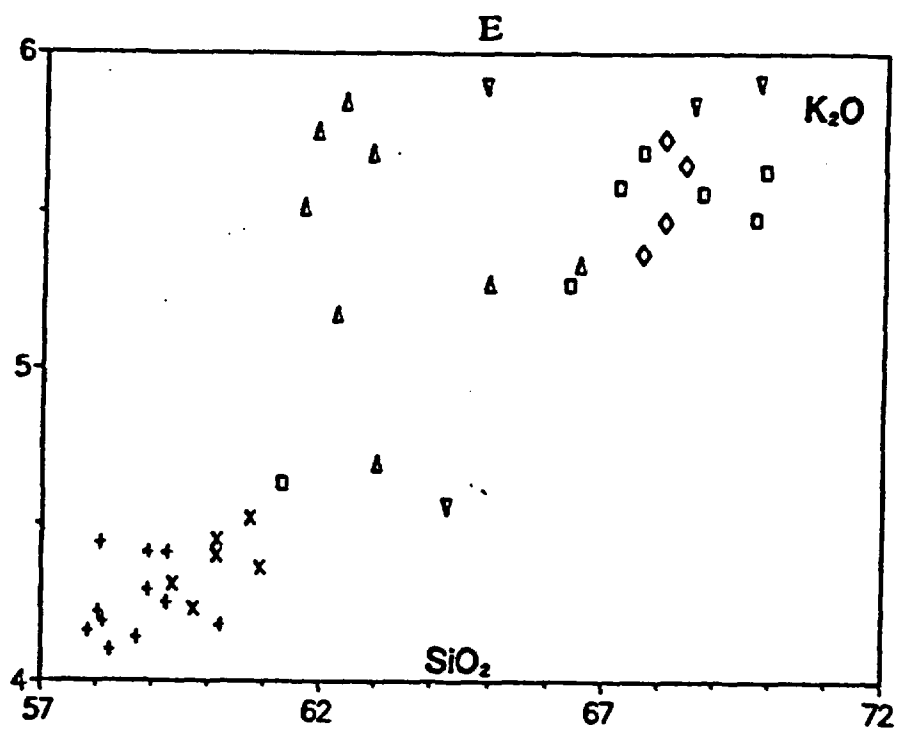
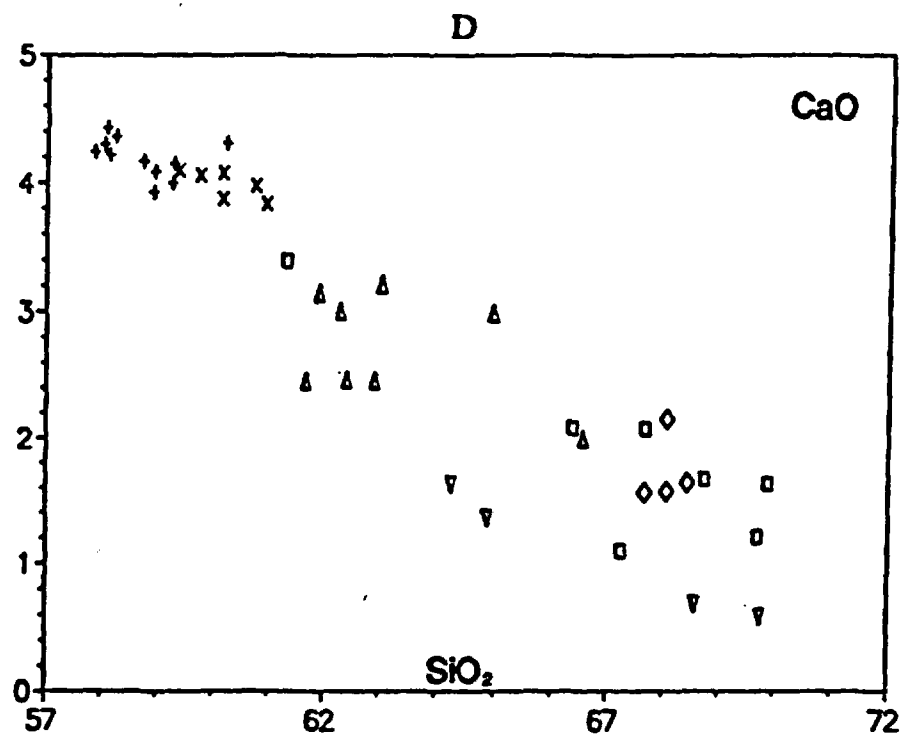


Figure 13: Continued

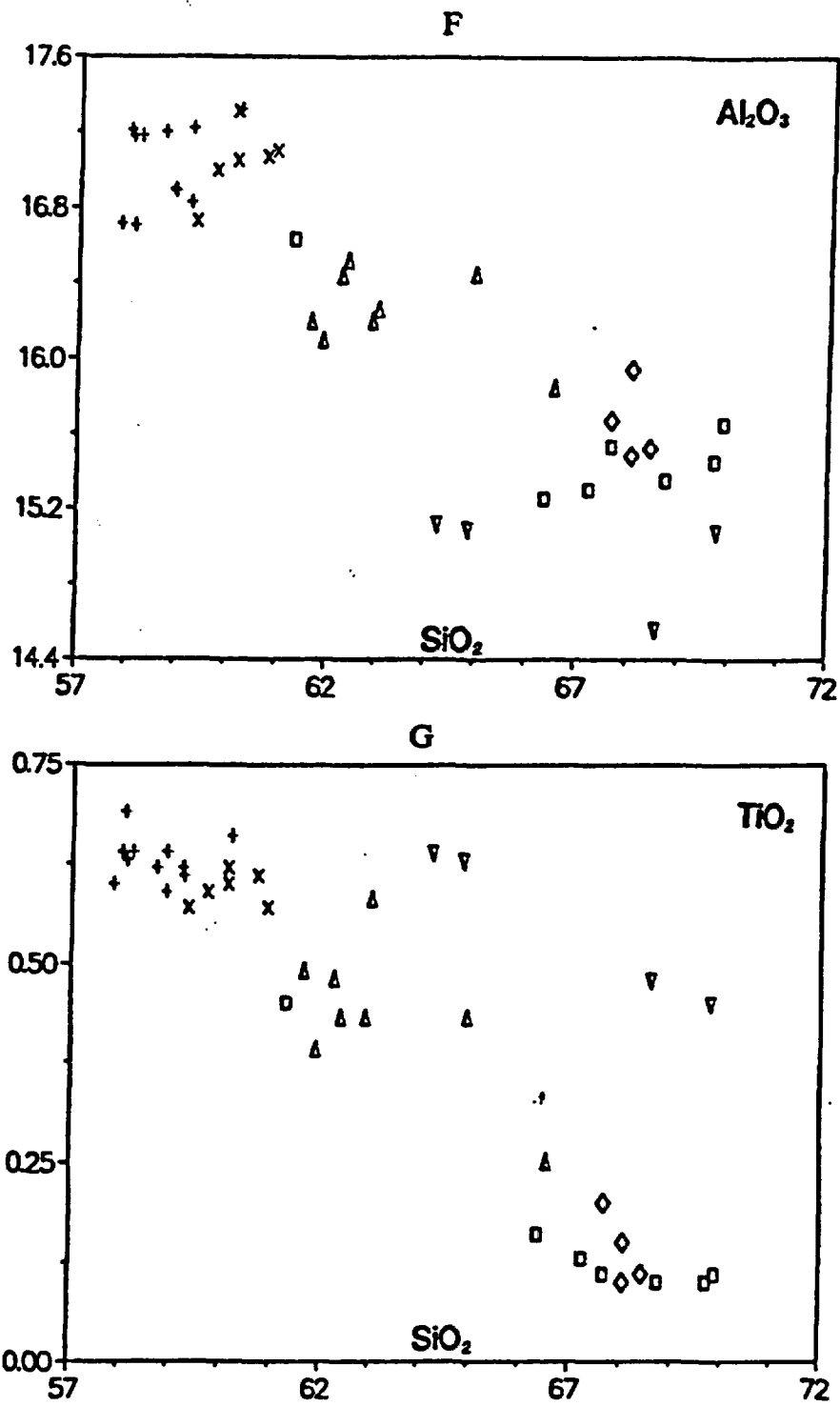


Figure 13: Continued

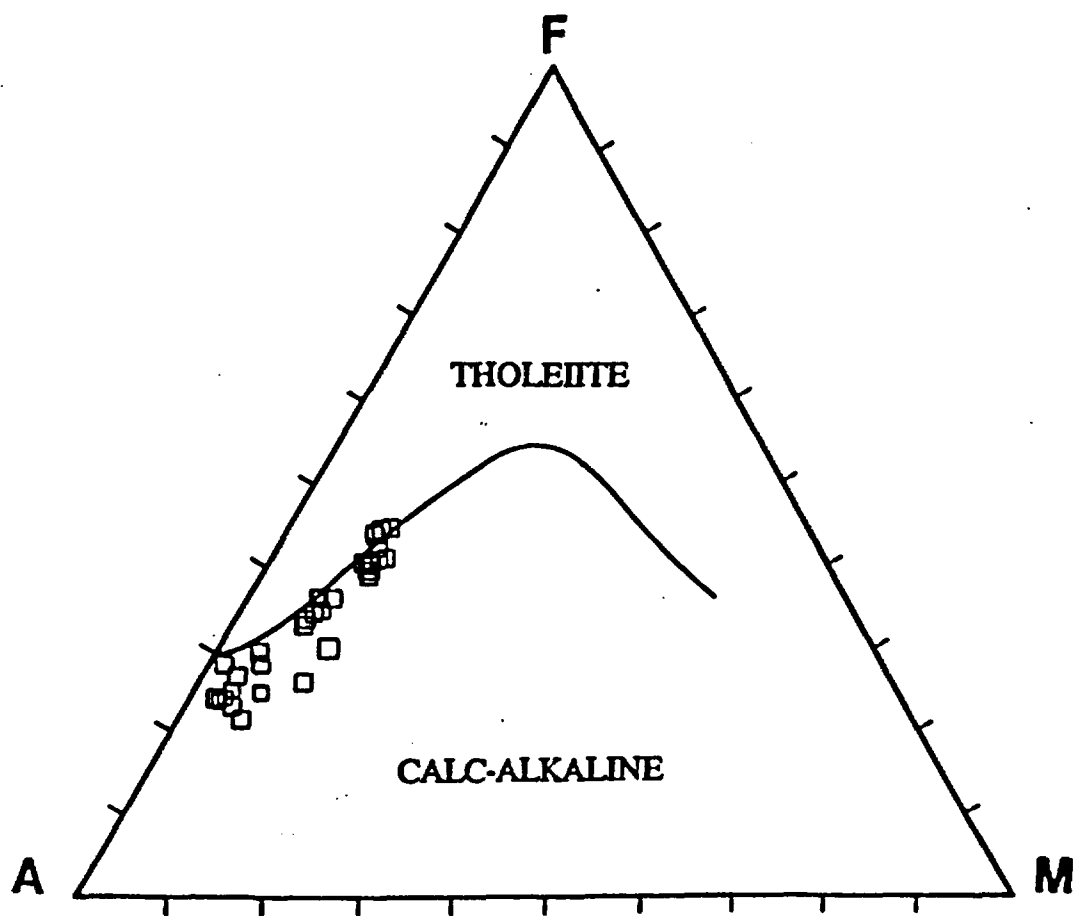


Figure 14: AFM diagram showing the calc-alkaline characteristics of the rocks of the Sloan volcanics. Diagram is after Irvine and Barager (1971).

1) Irian andesite (greater than 1.4% MgO, 0.55% TiO₂ and 16.7% Al₂O₃); 2) Mount Sutor dacite (0.6% to 1.4% MgO, 0.25% to 0.55% TiO₂, and 15.6% to 16.4% Al₂O₃); 3) Cinder Prospect member and Center Mountain dacite (less than 1.0% MgO, 0.20% TiO₂ and 16.0% Al₂O₃); 4) Tuff of the Sloan volcanics (similar range of SiO₂ as the dacites, but higher in MgO (0.8% to 1.8%) and TiO₂ (0.45% to 0.65%), and lower in Al₂O₃ (14.4% to 15.2%)) (Fig. 15).

Trace Elements

Compatibility of the trace elements in mineral phases is directly dependent upon rock type. For example, the large ion lithophile elements (LILE) Ba and Rb are incompatible in andesite, but compatible with biotite in dacite. The transition metals Co and Cr are compatible with olivine in andesite, but relatively incompatible in dacite. The LILE Th and the rare-earth element (REE) Ce are compatible only in accessory minerals such as monazite. Felsic rocks such as rhyolite and dacite contain a higher modal concentration of accessory minerals such as zircon, sphene, apatite and monazite than andesites and basalts.

In rocks of the Sloan volcanics, the concentrations of: 1) total REE (La, Ce, Nd, Sm, Eu, Tb, Yb and Lu) increase with increasing SiO₂ (Fig. 16A). 2) Th and the incompatible high field strength elements (HFSE) Hf and Ta increase with increasing SiO₂ (Figs. 16B & 16C); 3) the LILE Sr decreases with increasing SiO₂ (Figs. 16D & 16F); 4) the transition metal Co decreases with increasing SiO₂ (Figs. 16G & 16H); 5) Eu decreases with increasing SiO₂ (Figs. 16D, 16E & 16G).

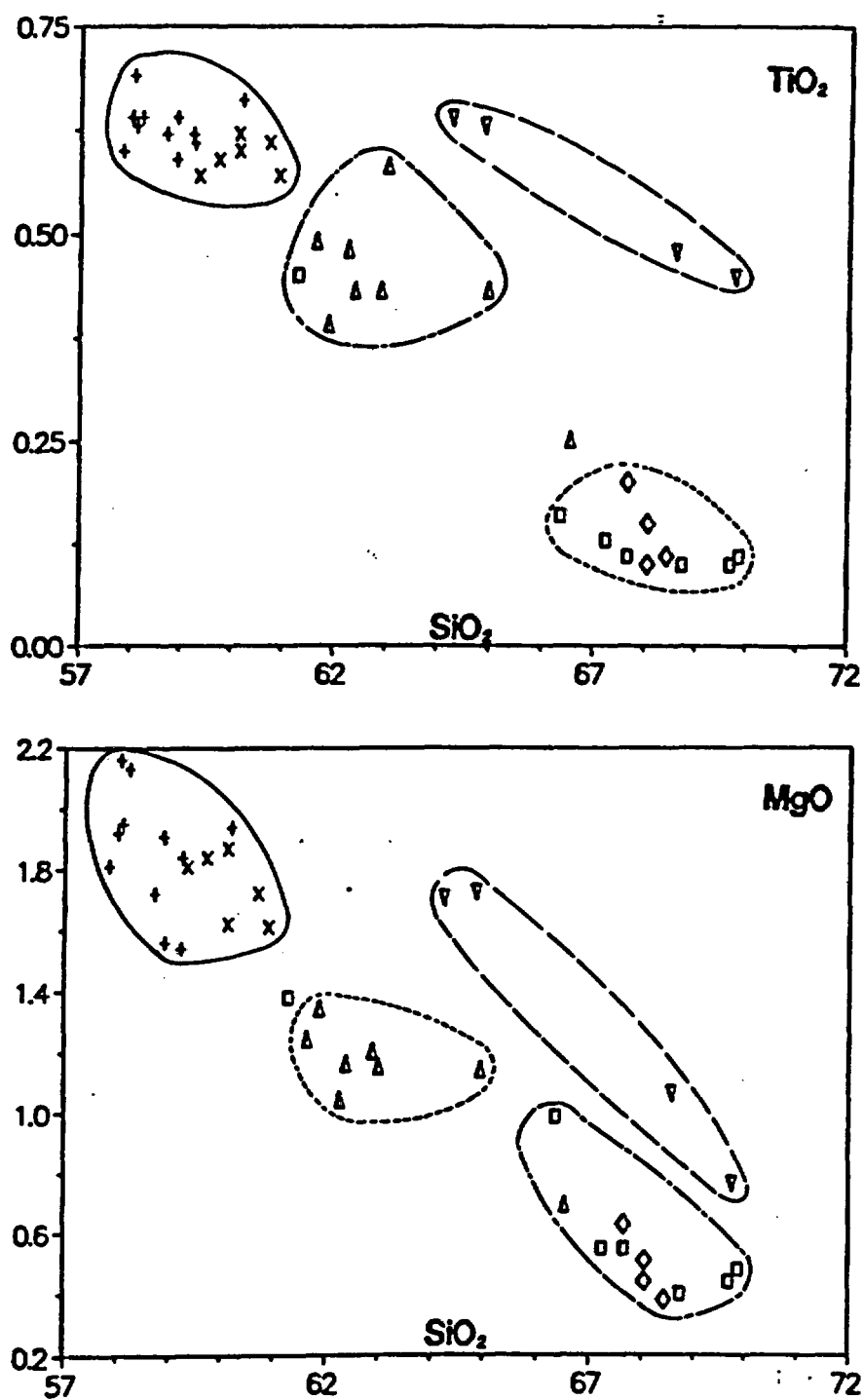


Figure 15: Harker variation diagrams showing the four chemically distinct groups of the Sloan volcanics. See Figure 13 for symbol explanation.

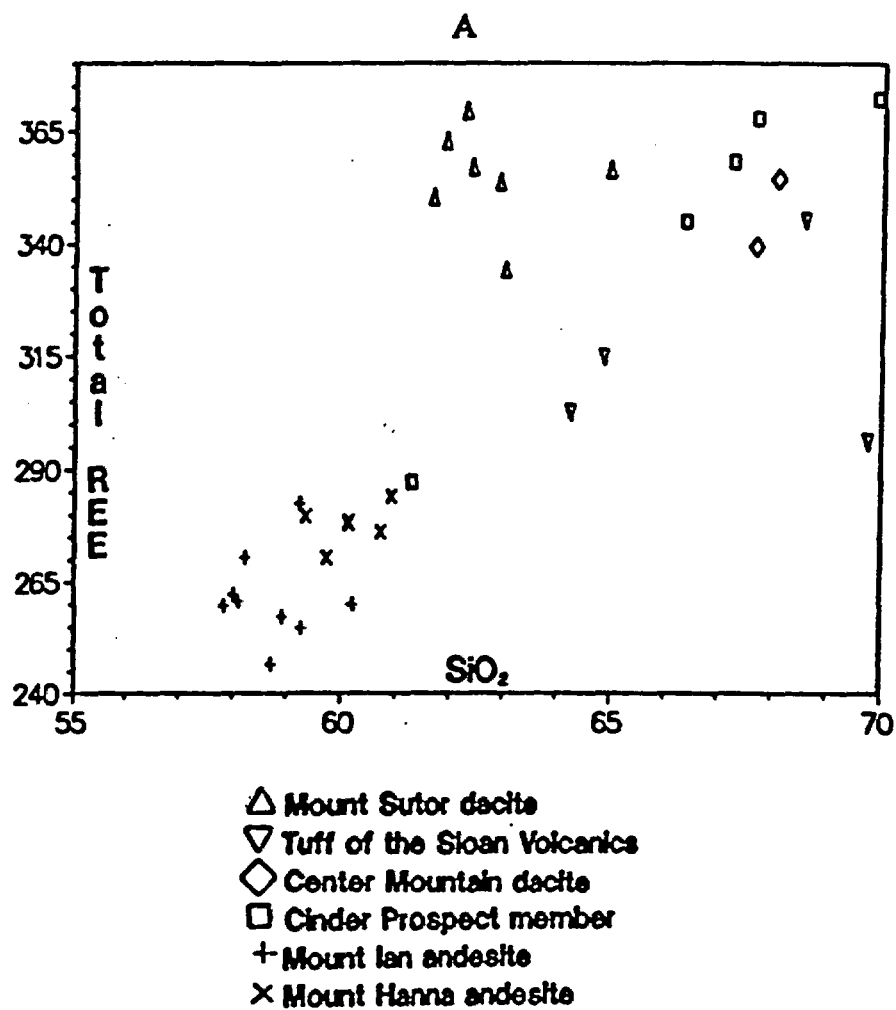


Figure 16: Trace element diagrams. Concentrations of SiO₂ and CaO are in weight percentage. Concentrations of trace elements are in ppm. Symbol in upper corner represents mean analytical error in ppm.

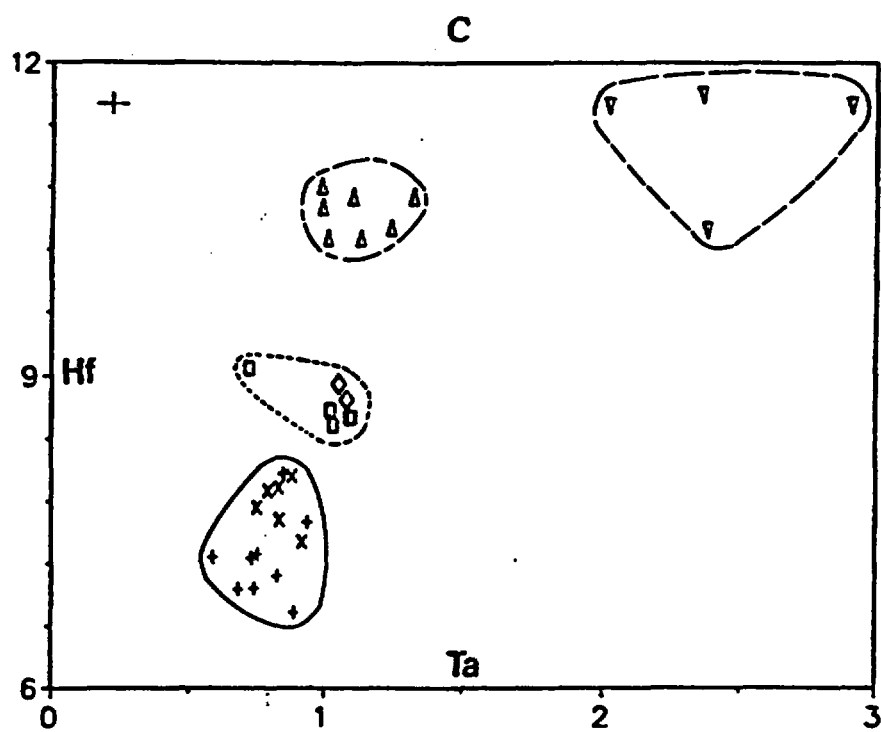
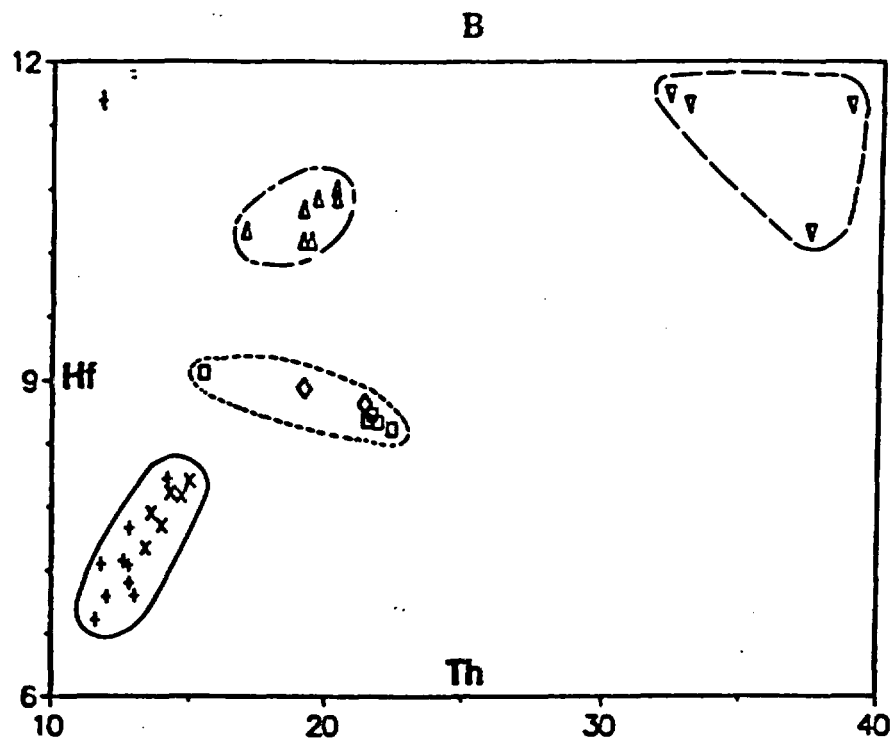


Figure 16: Continued

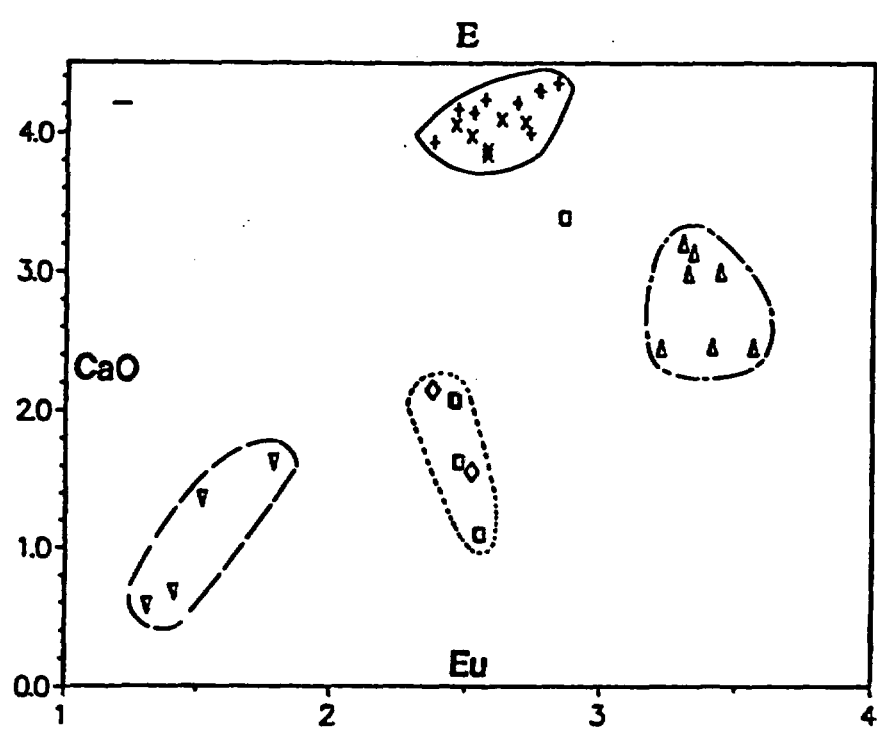
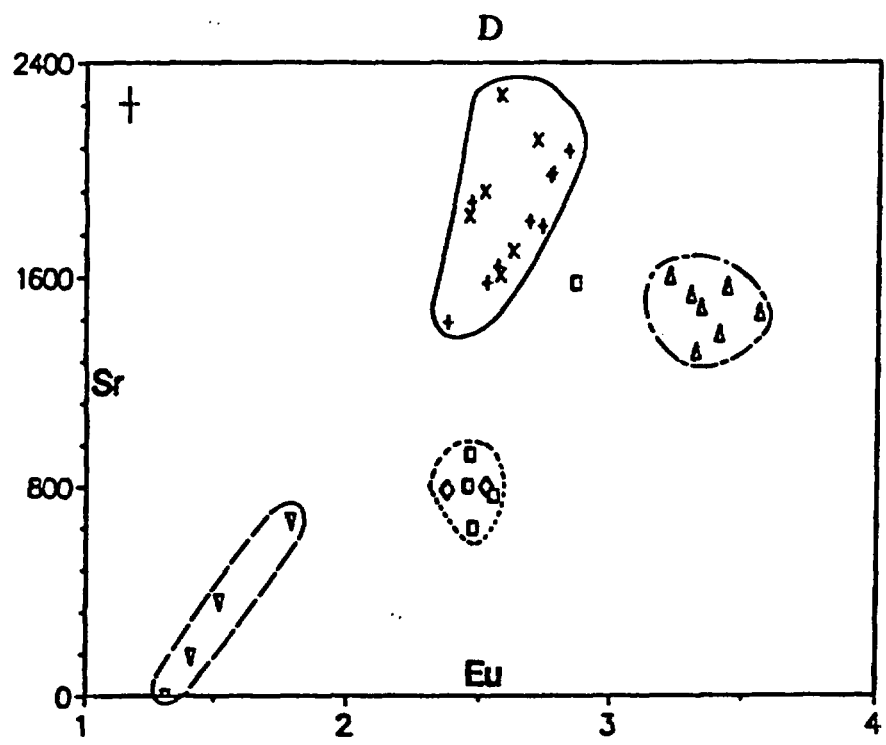


Figure 16: Continued

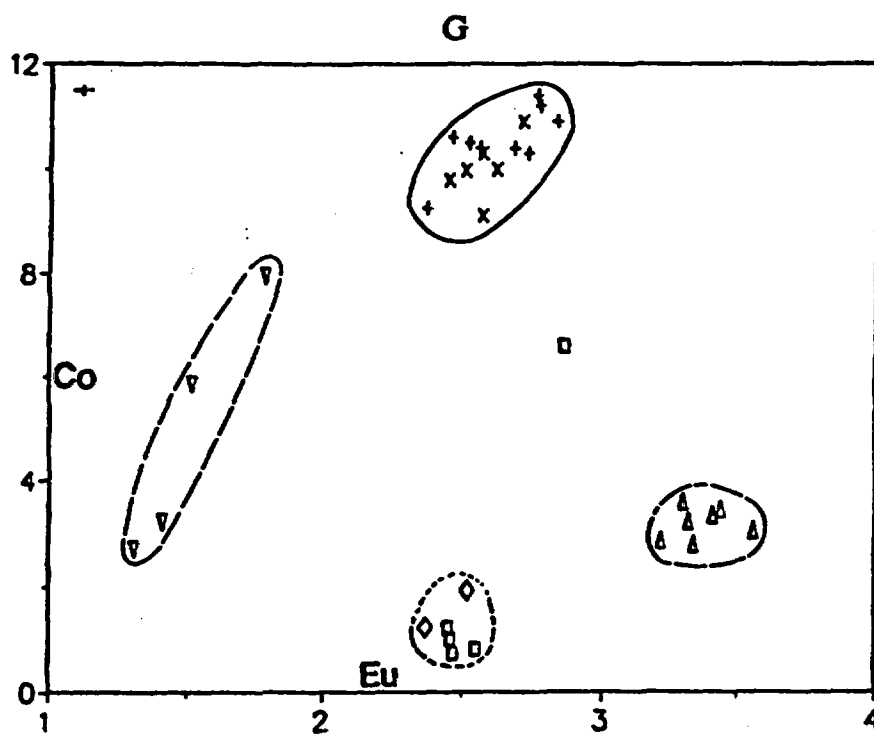
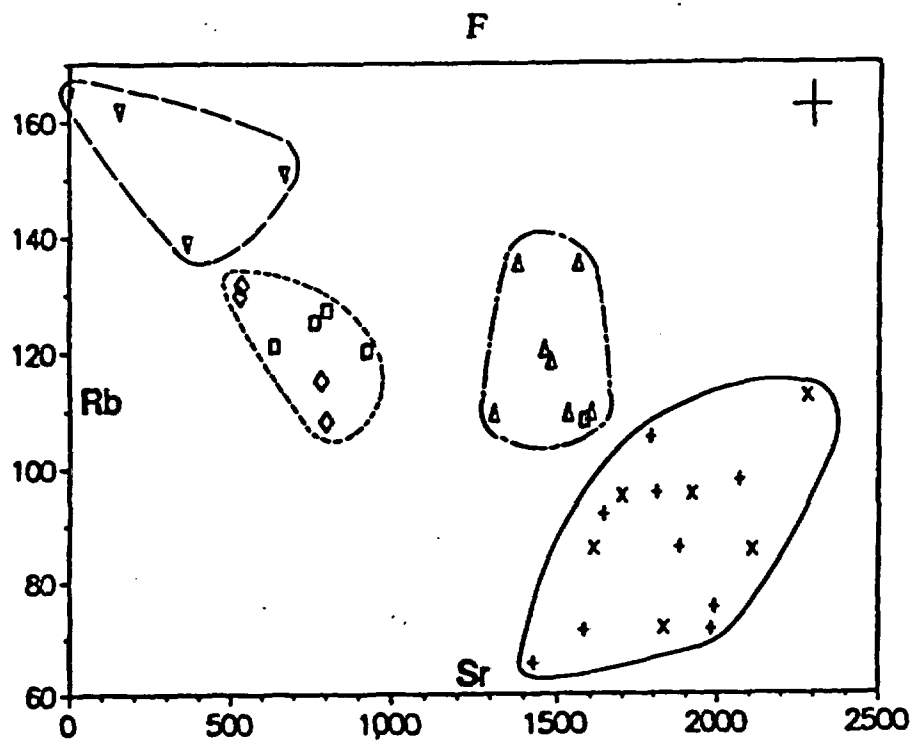


Figure 16: Continued

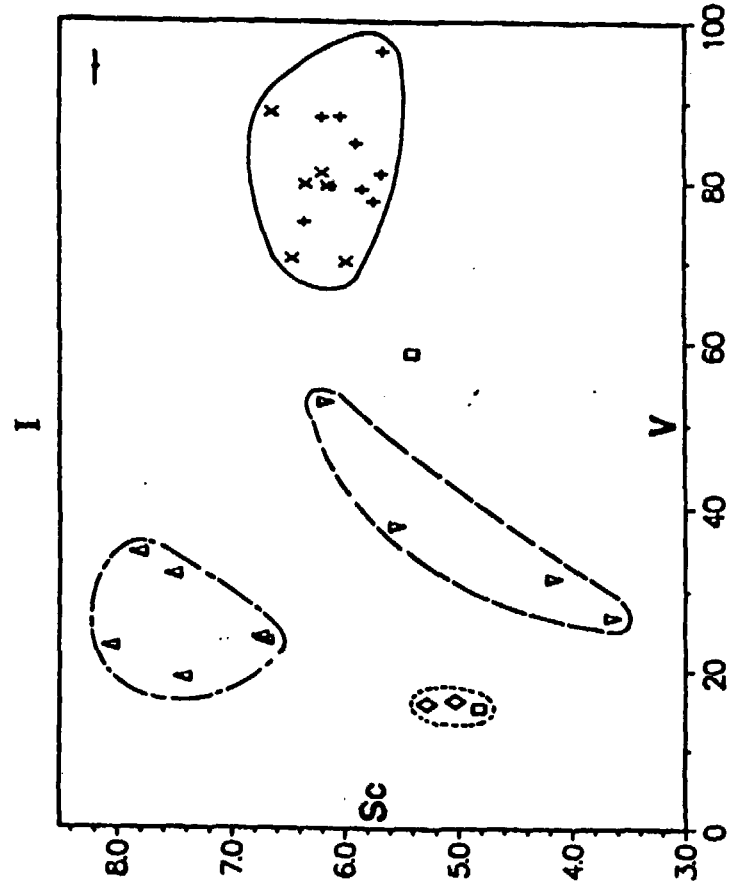
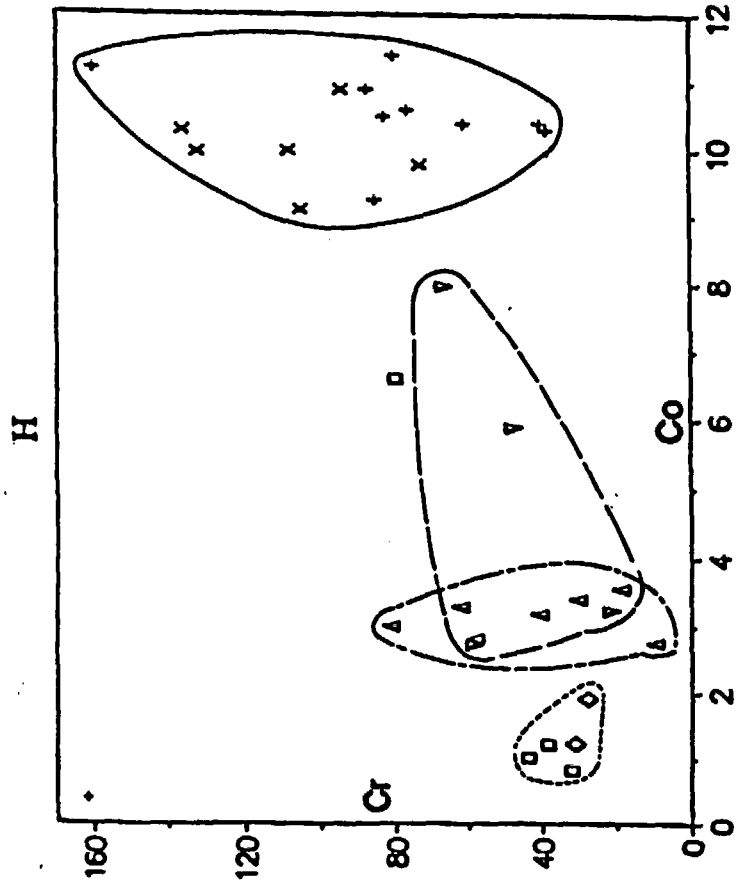


Figure 16: Continued

Chemical plots of trace elements distinguish the same four groups that are suggested by the Harker variation diagrams. For most elements, the differences between each group is greater than mean analytical error indicating that the differences between groups is statistically significant (Table 3). The andesites are more depleted in Hf, Ta and Th, and more enriched in Co than the other groups. The Mount Sutor dacite is enriched in Eu. The Tuff of the Sloan volcanics is depleted in Eu, and enriched Ta and Th. The Center Mountain dacite and the Cinder Prospect member are depleted in V.

If the rocks of the Sloan volcanics had a comagmatic relationship and were produced by a fractional crystallization or partial melting process, samples would plot on a continuous positive linear slope on an incompatible element diagram. Instead, incompatible element diagrams show four separate groupings of data (Fig. 16). A sampling bias could cause the gaps between groups. During sampling, however, I was careful to collect all the exposed compositional variations of volcanic and hypabyssal rocks. I suggest, therefore, that the four groups represent chemically distinct magma types and do not reflect incomplete sampling.

Spider diagrams may be used to distinguish the general chemical characteristics of rock suites, determine evolutionary paths and identify sources. Spider diagrams are constructed by normalizing trace element values to known concentrations and plotting them on a logarithmic scale. These diagrams minimize data scatter and emphasize general chemical trends and "signatures".

Caps

Table 3: Mean analytical error of trace elements used in chemical plots		
Element	Error: +/- ppm	Error: +/- %Concentration
Sc	0.04	0.68
V	3.82	9.87
Cr	2.15	5.93
Co	0.16	3.94
Rb	8.33	7.62
Sr	114	14.7
Eu	0.07	3.23
Hf	0.21	2.32
Ta	0.11	9.53
Th	0.24	1.22

Normalized values used in this thesis are chondrite (Thompson et al., 1984) and MORB (Pearce, 1983).

Chondrite normalized REE diagrams (Thompson, 1984) show that the four rock groups have similar chemical signatures (Figs. 17A-17D). The Tuff of the Sloan volcanics differs only in that it is depleted in Eu (Fig. 17C). Rocks of the Sloan volcanics are enriched in light REE (LREE) and depleted in heavy REE (HREE). The LREE La varies from about 250 to 400 chondrite. The HREE Lu varies from about 10 to 25 chondrite.

Spider diagrams show a common depletion in P, Ti and Ta, and enrichment in Rb, K, La, Nd and Zr for the four rock groups of the Sloan volcanics (Figs. 18A-18H). The Tuff of the Sloan volcanics differs only in that it is depleted in Ba (Figs. 18C & 18G). Major and trace element diagrams are sensitive to small differences in source rocks and petrogenetic paths, while spider plots are not. The fact that the rocks of the Sloan volcanics are separated into four groups on major and trace element plots, but are not segregated on spider diagrams, suggests that the chemical differences between the groups are significant, but small.

Temporal and Spatial Variations in Chemical Trends

Spider diagrams indicate that the andesites of the Sloan volcanics have a chemically similar source as the older Hidden Valley volcanics, except that the Hidden Valley basalt is more depleted in the incompatible elements Ta, Th and La (Fig. 19). Its overall pattern is similar to the Sloan volcanics, suggesting that

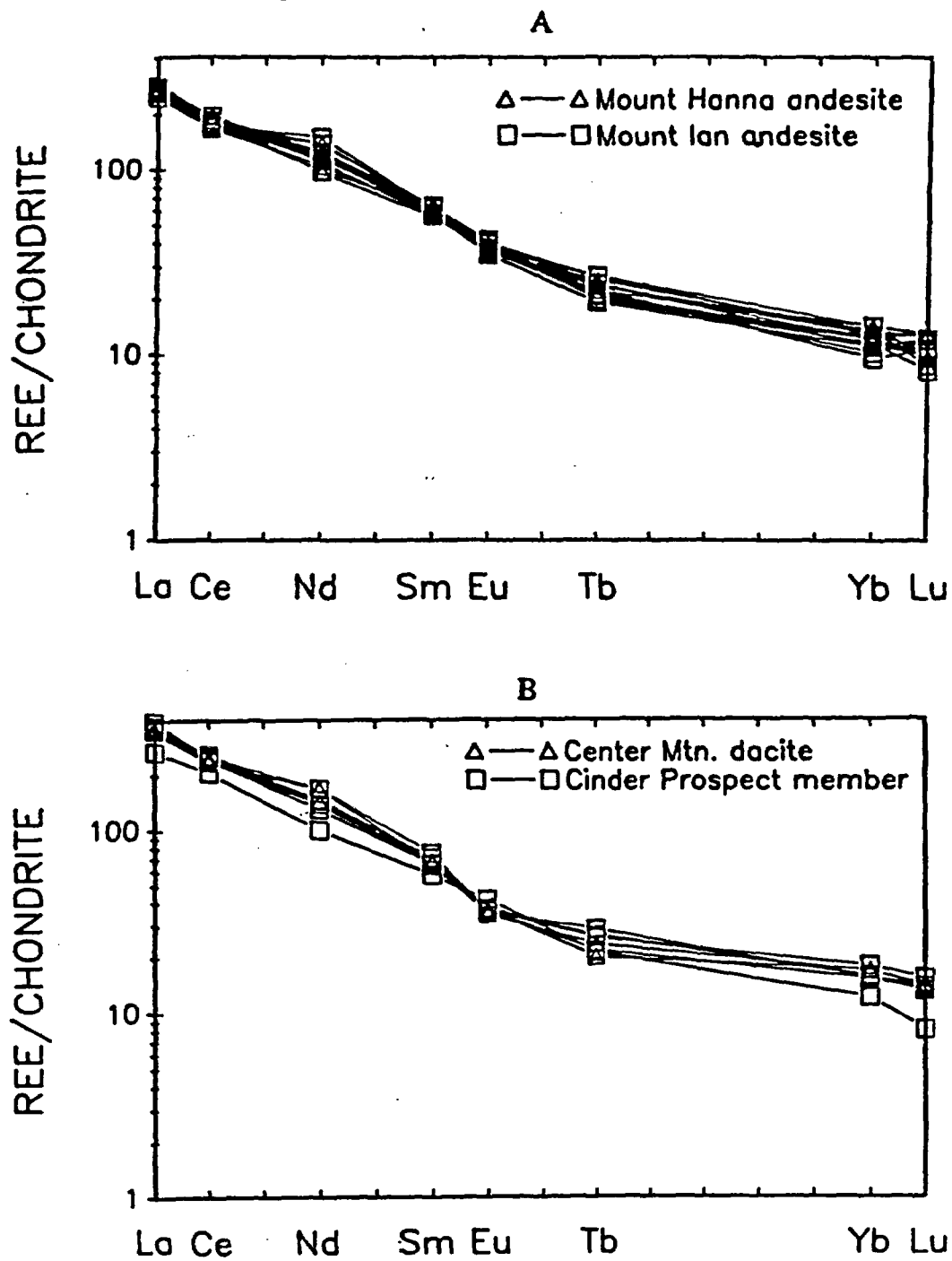


Figure 17: Chondrite-normalized REE diagrams

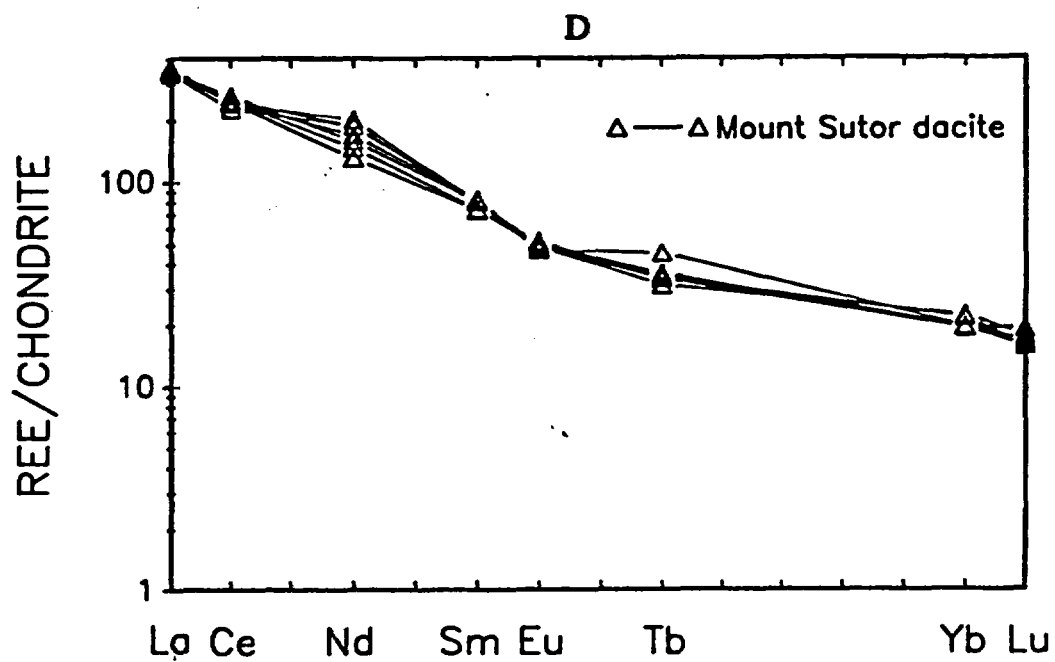
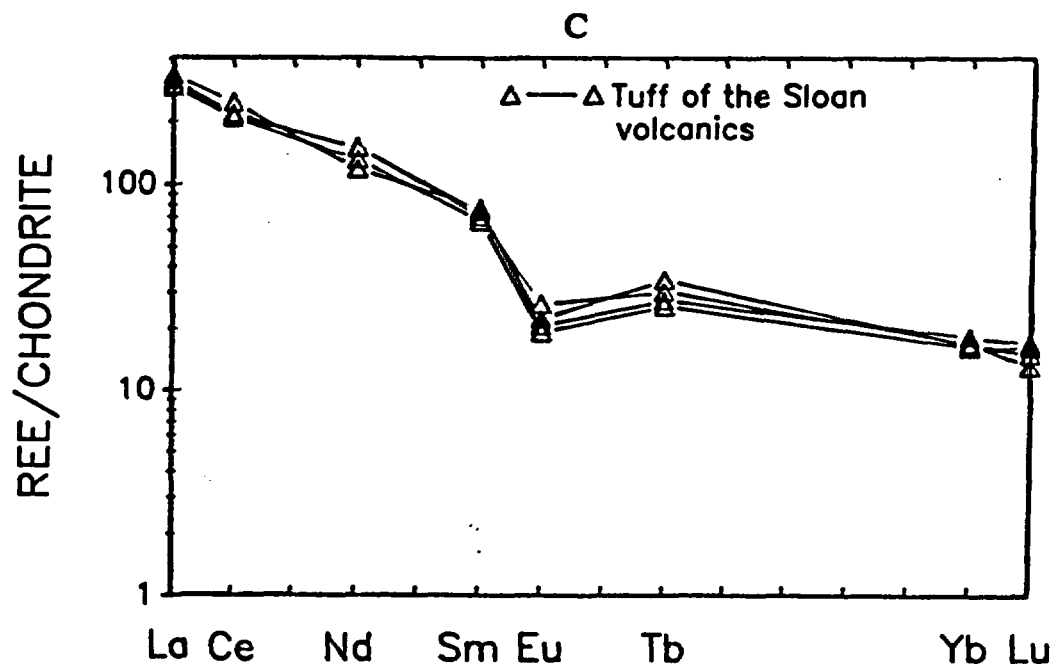


Figure 17: Continued

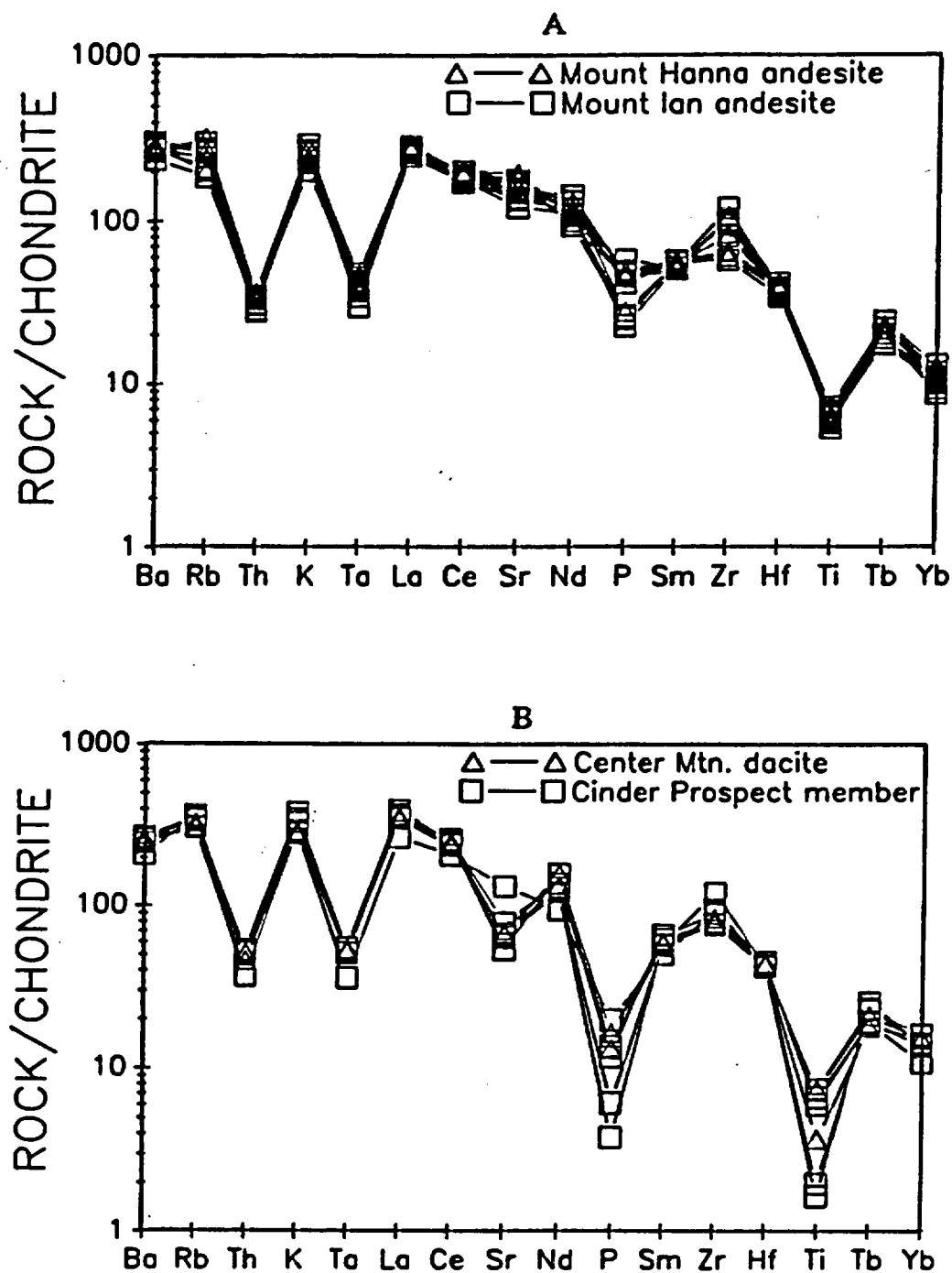


Figure 18: Chondrite and MORB-normalized diagrams for rocks of the Sloan volcanics.

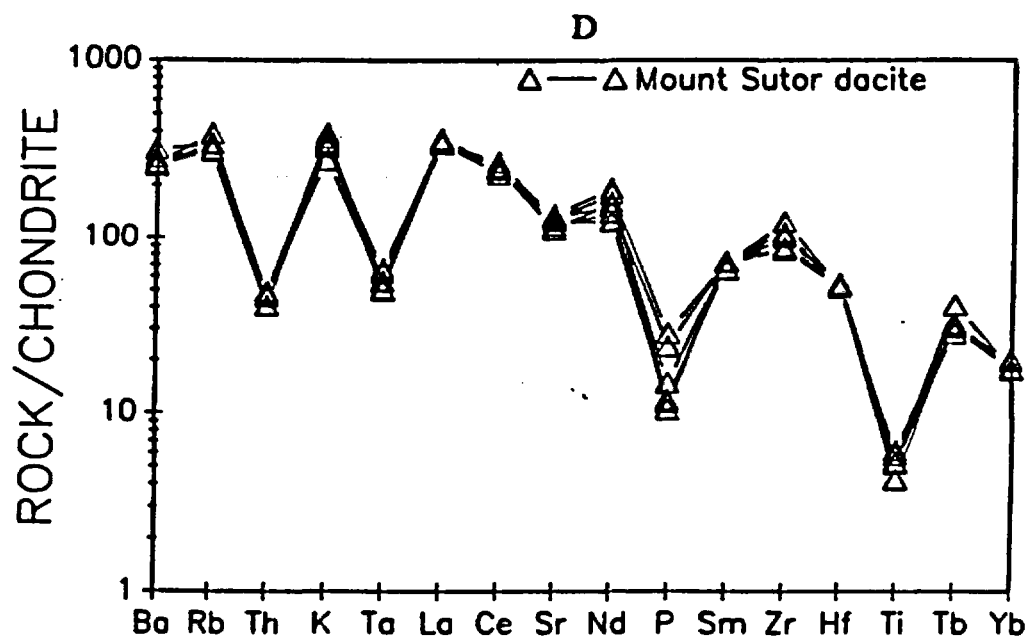
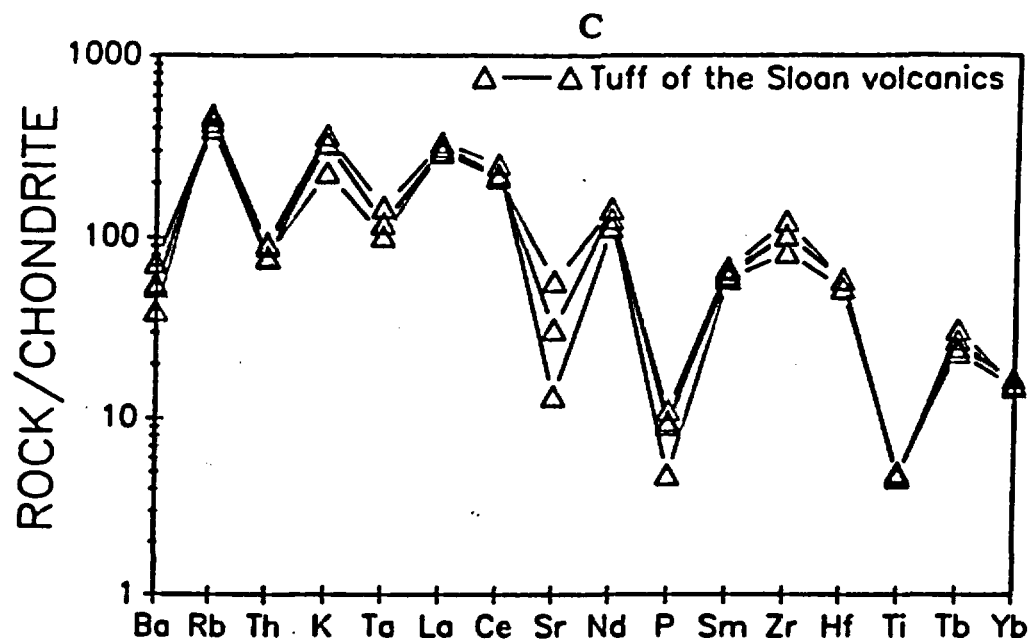


Figure 18: Continued

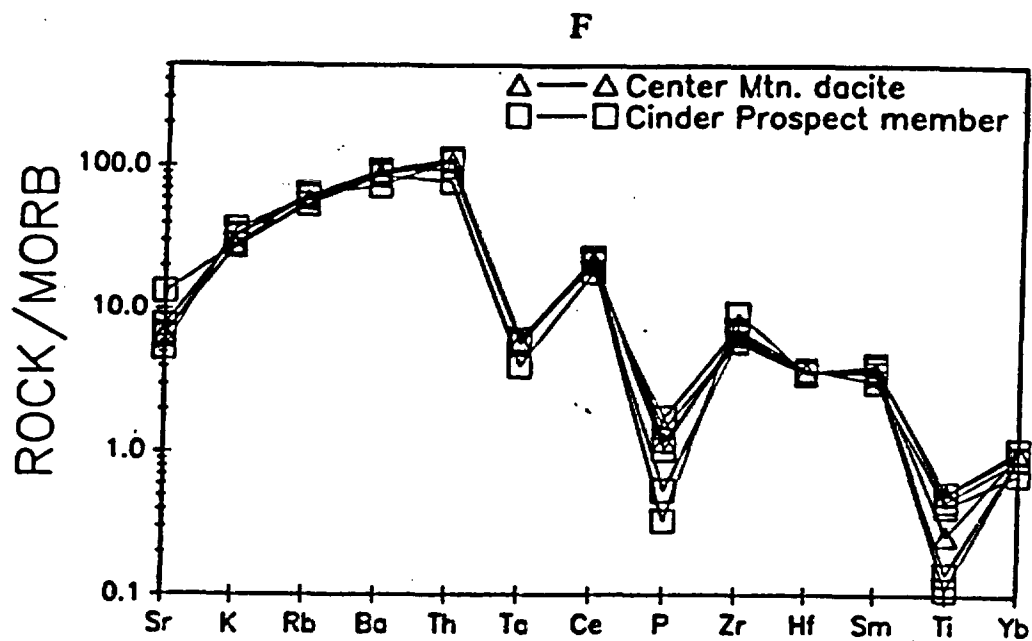
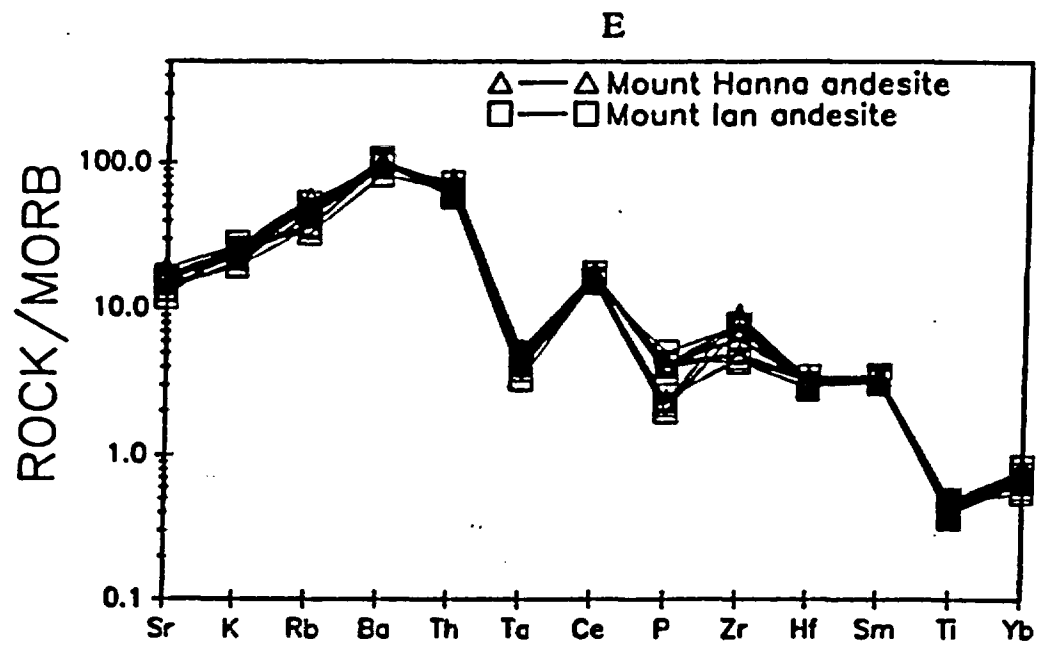


Figure 18: Continued

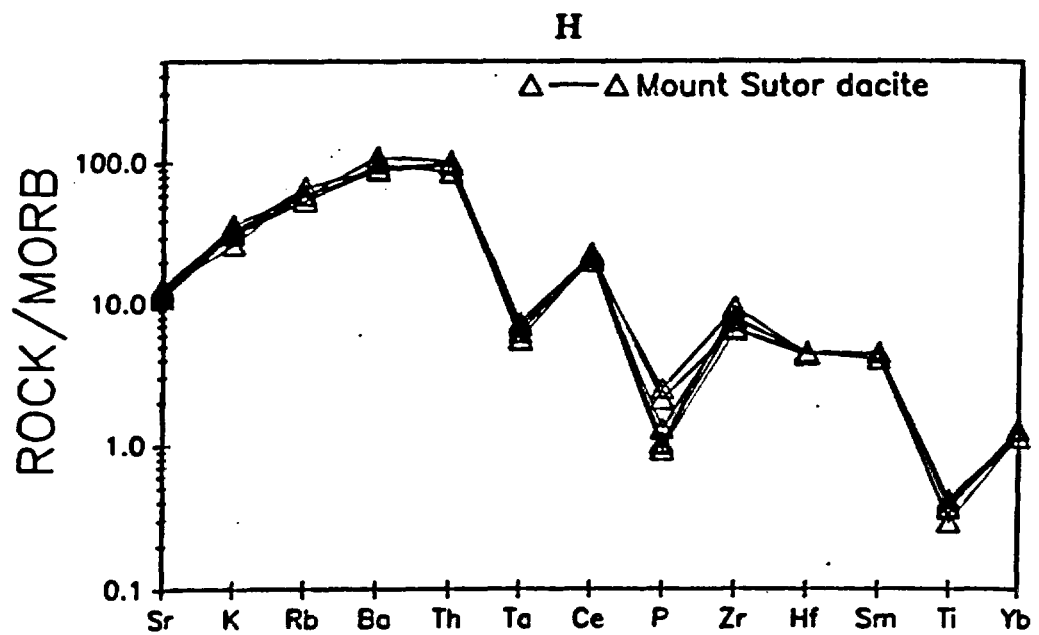
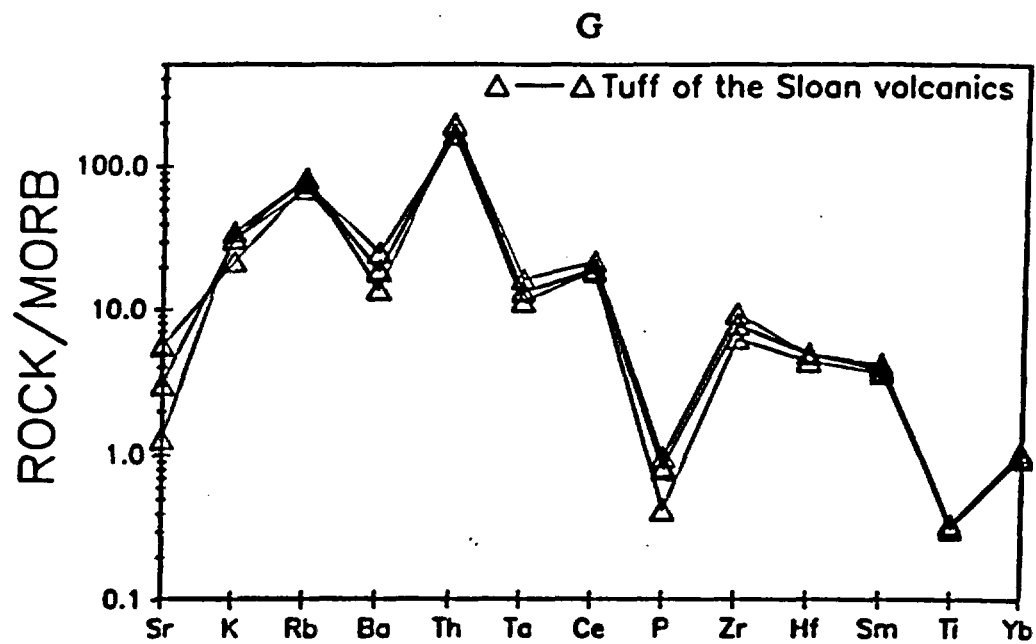


Figure 18: Continued

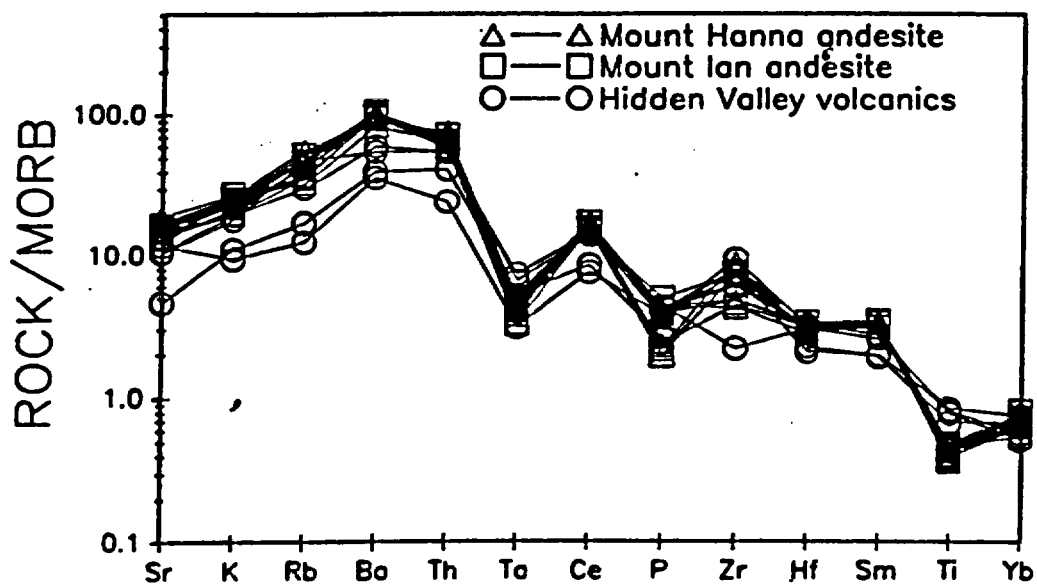
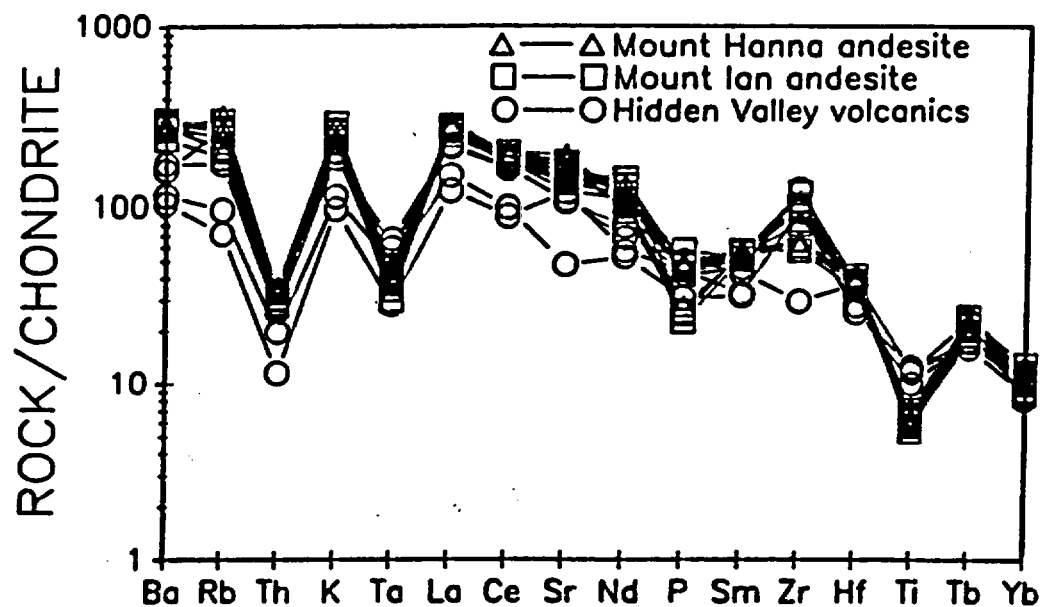


Figure 19: Chondrite and MORB-normalized spider diagrams showing chemical similarities between the Sloan andesites and the Hidden Valley volcanics.

both had a common source.

To determine the regional extent of rocks that share the McCullough Mountain's chemical signature, Tertiary volcanic rocks from the McCullough, Eldorado and River Mountains, Devil Peak, Table Mountain, the White Hills and the Hamblin Cleopatra volcano (Fig. 1) were plotted on spider diagrams.

Volcanic rocks with the chemical signature of the McCullough Mountains occur in the McCullough, Eldorado and River Mountains, and the White Hills. There are two other chemically distinct patterns. Felsic volcanic rocks occurring at Table Mountain and Devil Peak in the Spring Range are enriched in Th, Rb and Ta, and depleted in Ba, P and Ti. Basalts of the Hamblin Cleopatra volcano are depleted in Ce, Nd, Sm and La (Figs. 20A-20D).

This type of geochemical analysis suggests that the scale of significant chemical variation of source rocks in the lower crust and mantle in the Las Vegas-Lake Mead area is probably in the tens to hundreds of square kilometers. This analysis also suggests that each source area did not appreciably change chemically over the approximately five Ma represented by rocks exposed in the central McCullough Mountains.

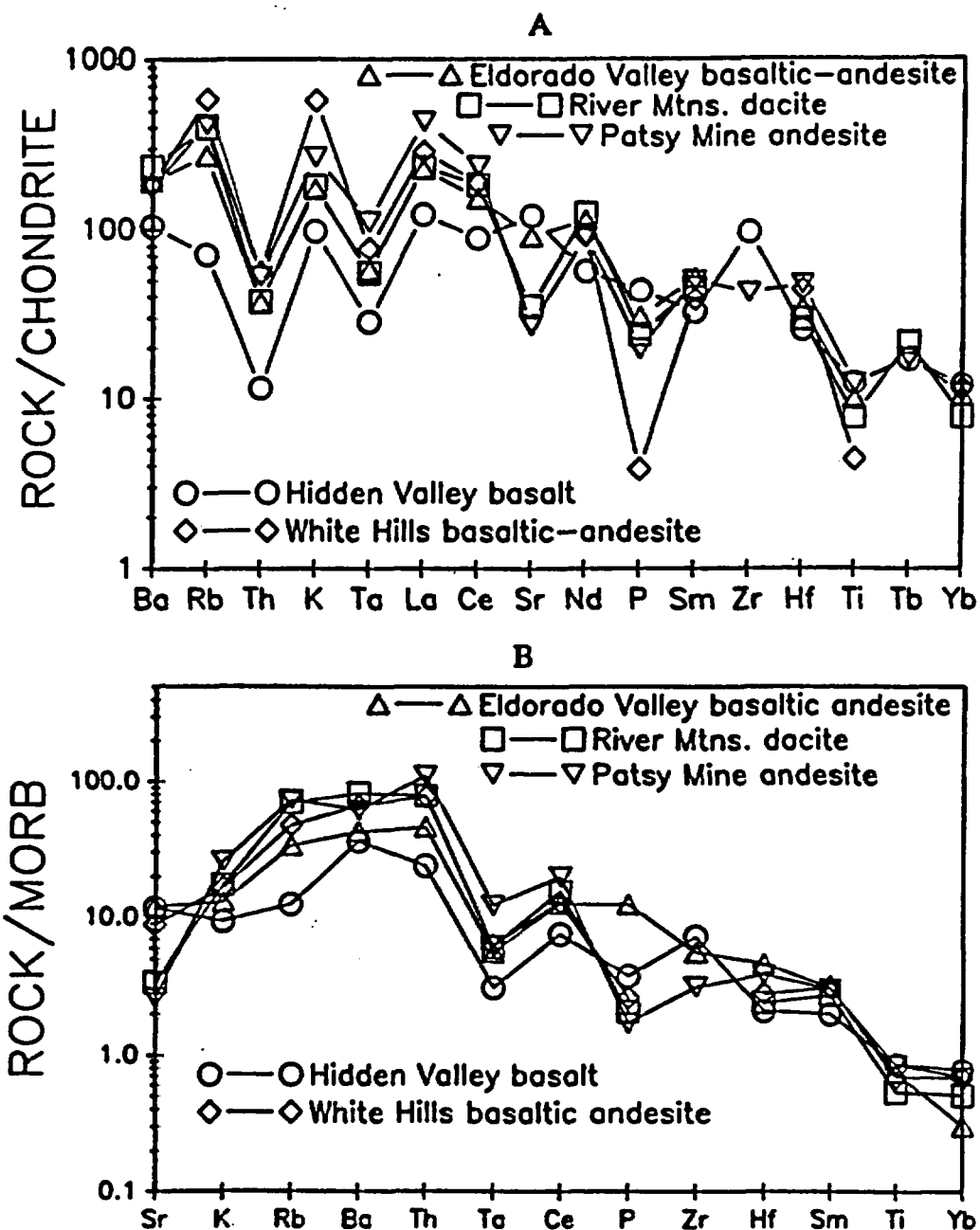


Figure 20: Chondrite and MORB-normalized spider diagrams showing spatial similarities of Tertiary volcanic rocks in the Lake Mead-Las Vegas area. The three chemically distinct groups include rocks from: 1) the McCullough, Eldorado and River Mountains, and the White Hills; 2) the Spring Range (Table Mountain and Devil Peak); 3) the Hamblin Cleopatra volcano.

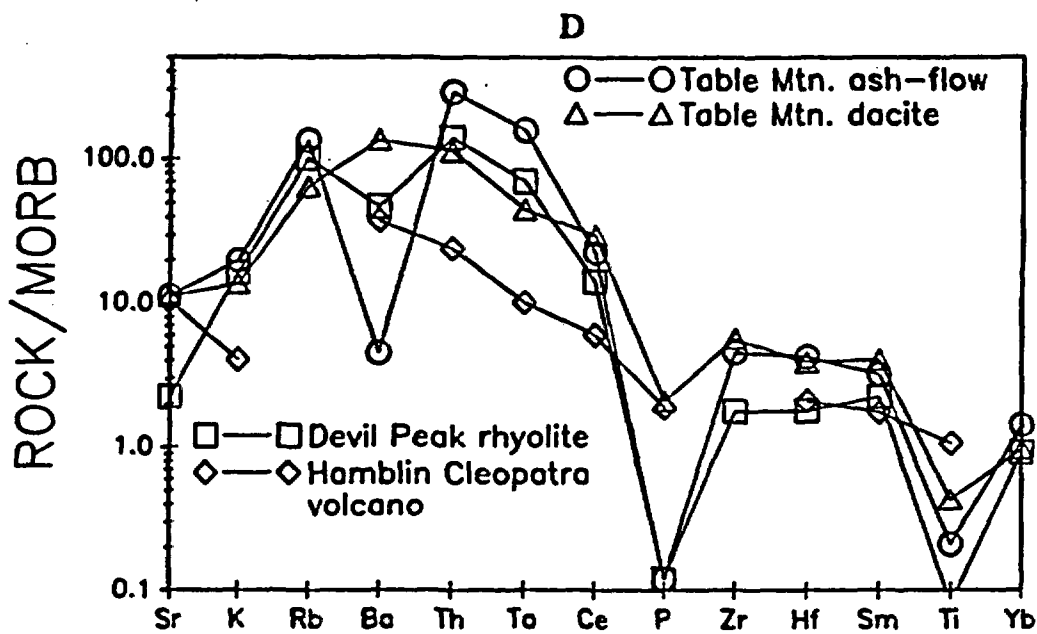
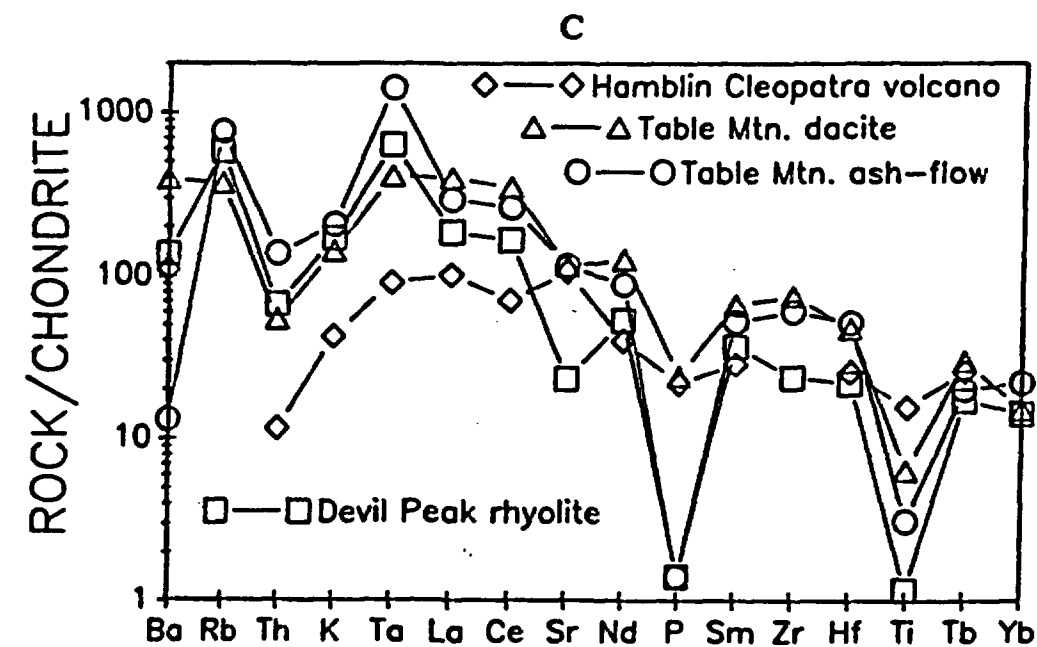


Figure 20: Continued

MAGMA PETROGENESIS

65
64

Variations Between Groups of the Sloan Volcanics

Introduction

In this section, three different models for the origin of the Sloan volcanics are introduced and discussed. The models involve magma commingling, crystal fractionation and partial melting. Using petrographic and geochemical evidence, I will show that partial melting of separate sources is responsible for the production of the Sloan volcanics.

Magma Commingling

The production of mid-Miocene intermediate igneous rocks in the Las Vegas-Lake Mead area by mechanisms of magma commingling was documented by Naumann and Smith (1987), Naumann (1987), Larsen (1989) and Larsen and Smith (1991) for the diorite to quartz monzonite of the Wilson Ridge pluton, and by Naumann and Smith (1987) and Naumann (1987) for the andesites and dacites in the northern Black Mountains (Fig.1).

Textural evidence for magma commingling includes: 1) disequilibrium mineral assemblages such as quartz in andesite or olivine in dacite; 2) resorbed, embayed phenocrysts rimmed with glass; 3) plagioclase xenocrysts displaying glass-charged zones (fretted texture); 4) mafic blobs/enclaves in intermediate rocks that show a decrease in phenocryst size toward their margins (Koyaguchi, 1986).

Chemical and textural evidence must be combined to document magma commingling. On chemical plots, rocks formed by magma commingling will plot on a linear variation line between the two end members (Koyaguchi, 1986).

Rocks of the Sloan volcanics do not show petrographic evidence of magma commingling. The Mount Ian andesite, however, contains less than 1% biotite. Biotite may be an equilibrium phase in andesites with SiO_2 greater than 55% (Williams, Turner & Gilbert, 1982), or it may represent a disequilibrium phase that was introduced during magma commingling. Because of the possibility that magma commingling may have contributed to the petrogenesis of the Mount Ian andesite, it was chosen to test magma commingling models for the Sloan volcanics.

Mafic and felsic rocks from the central McCullough Mountains were evaluated as possible end member-magmas for the production of the Mount Ian andesite. A possible mafic end member is the basalt of the Hidden Valley volcanics. Possible felsic end members are the rhyolites of the McCullough Pass volcanics (Schmidt, 1987) and the dacites of the Cinder Prospect member of the Sloan volcanics. A dacite from the Cinder Prospect member of the Sloan volcanics was chosen because it plots on the same linear variation line as the Hidden Valley volcanics and the Mount Ian andesite. The McCullough Pass rhyolites were ruled out because they do not plot on this variation trend.

The computer program XLFRAC (Stormer and Nichols, 1978) (modified by Rob Helvie, 1991) was used to evaluate the possibility that the Mount Ian

andesite is a hybrid magma produced by the commingling of the Hidden Valley basalt and dacite of the Cinder Prospect member. Using a mixing model with no fractionation, it is necessary to add 95.35% by volume Cinder Prospect dacite to basalt of the Hidden Valley volcanics (Table 4a). This model is unrealistic for two reasons. First, the sum of the squares of the residuals (R^2) is 20.04. R^2 is the square of the sum of the differences between the observed and calculated weight percentages of each oxide and must be close to 1.00 if the model is to be acceptable at the 99% level of significance. Second, the addition of 95.35% dacite magma to a basalt magma would result in abundant petrographic and field evidence of magma commingling. No mixing textures are evident in The Mount Ian andesite.

Another model was analyzed utilizing the fractionation of olivine, clinopyroxene and plagioclase from Hidden Valley basalt, along with the addition of dacite of the Cinder Prospect member. For this model, it is necessary to add 68.90% dacite to Hidden Valley basalt (Table 4b). The lack of mixing textures suggests that this model is unrealistic.

I suggest, therefore, that magma commingling may be ruled out as a major process in the petrogenesis of the Sloan volcanics.

Fractionation and Partial Melting

If a suite of rocks is produced by fractionation of a common parent, magmas derived by small amounts of fractional crystallization will be enriched in elements compatible with the fractionating phases. Rocks formed by greater

Table 4a				
Mixing Model #1: Mixing Of Hidden Valley Basalt (Mc116) With Cinder Prospect Member Dacite (Mc121) To Produce Mount Ian Andesite (Mc77).				
Composition	Hidden Valley basalt	Cinder Prospect member dacite	Mount Ian andesite	Model rock
SiO ₂	51.72	69.86	59.28	60.36
Al ₂ O ₃	17.05	15.65	17.22	17.53
Fe ₂ O ₃	10.44	3.00	7.08	7.21
CaO	9.35	1.63	4.15	4.23
MgO	5.15	0.48	1.84	1.87
Na ₂ O	3.15	3.65	3.62	3.69
K ₂ O	1.73	5.63	4.41	4.49
TiO ₂	1.40	0.11	0.61	0.62

Total% of dacite added to basalt = 95.35

Above values are in weight percentages

Sum of the squares of the residuals = 20.04

Table 4b	
Mixing Model #2: Fractionation Of Olivine, Clinopyroxene And Plagioclase From Hidden Valley Basalt With Addition Of Cinder Prospect Member Dacite To Produce Mount Ian Andesite. See Model #1 For Rock Compositions.	
Phase	Amount added or subtracted from Hidden Valley basalt
Olivine	-2.07
Clinopyroxene	-17.50
Albite	-5.80
Anorthite	-2.00
Cinder Prospect member dacite	+68.90

Values are in weight percentage.

degrees of fractional crystallization will be depleted in these elements. For example, if plagioclase is fractionated, early-forming rocks will be enriched in Ca, Eu and Sr, while later-forming rocks will be depleted in these elements.

A chemical plot of elements compatible with the fractionating phase will display a linear trend with a positive slope. The trend should also display a continuous range of composition with no gaps between rock types. If no fractionation has occurred, rocks will plot in clusters or in vertical or horizontal trends on a compatible element diagram.

Spider plots will also indicate fractionation. If plagioclase has fractionated, a low value or "dip" in the data will occur for elements compatible with this phase. On chondrite-normalized REE diagrams, plagioclase fractionation will result in a Eu anomaly.

Plagioclase and clinopyroxene are common phenocryst phases in rocks of the Sloan volcanics. Fractionation of these phases was evaluated to analyze the relationship between the four rock groups of the Sloan volcanics. On Sr versus Eu, CaO versus Eu (plagioclase compatible), and Sc versus V (clinopyroxene compatible) plots, there are no fractionation trends relating the four rock groups to a common parent (Figs. 16D, 16E & 16I). I conclude, therefore, that the four rock groups of the Sloan volcanics were not produced by fractionation of a common melt. This analysis also suggests that the four groups are not related to each other by a fractionation process.

During partial melting, incompatible elements enter the melt early because

their mineral/liquid distribution coefficients are low. Rocks produced by small amounts of partial melting will be enriched in incompatible elements. Rocks produced by a larger amount of partial melting will be depleted in incompatible elements. On a plot of incompatible elements (Hf versus Th for example), rocks produced by partial melting of a common source will fall on a linear trend with a positive slope, displaying a continuous range of composition. Partial melting of different sources is suggested if data are clustered on incompatible element plots.

The four rock groups of the Sloan volcanics were analyzed to determine whether or not they represent independent partial melts. On incompatible element plots (Hf versus Th and Hf versus Ta), the rocks cluster into the same four chemically distinct groups defined by the major elements (Figs. 16B & 16C). I conclude, therefore, that each rock group evolved by partial melting of a chemically distinct source. The nature of these sources will be discussed in the "Sources for Partial Melting" section.

Variations Within Groups of the Sloan Volcanics

Introduction

In this section, fractionation processes and trends will be evaluated for the andesites, dacites and tuff of the Sloan volcanics. Refer to Figure 16 for trace element diagrams, and Figure 17 for chondrite-normalized REE diagrams.

Andesites

Elements that are compatible with plagioclase (Eu, Sr and Ca) were

plotted to determine if fractionation of this phase occurred in the andesites of the Sloan volcanics. The lack of a positive linear trend on these diagrams for the Mount Hanna andesite suggests that no plagioclase fractionation occurred (Figs. 16D & 16E). A positive linear trend on the Eu versus Sr plot, however, suggests minor plagioclase fractionation in the Mount Ian andesite (Fig. 16D). The lack of a Eu anomaly on the chondrite-normalized REE diagram confirms that plagioclase fractionation was minor (Fig. 17A). No positive linear trends are evident on plots of Cr versus Co and Sc versus V, suggesting no olivine and clinopyroxene fractionation respectively (Figs. 16H & 16I).

Dacites

Dacites and tuffs of the Cinder Prospect member contain phenocrysts of plagioclase and biotite. No plagioclase fractionation trend is apparent on plots of Sr versus Eu and CaO versus Eu (Figs. 16D & 16E). The lack of a Eu anomaly on the chondrite-normalized REE diagram also suggests that plagioclase did not fractionate (Fig. 17B). No biotite fractionation is apparent on a Sr versus Rb (biotite compatible) diagram (Fig. 16F).

An ash-flow tuff in the Cinder Prospect member (sample Mc78) consistently plots outside the Cinder Prospect field on compatible element diagrams. It is approximately 5 weight% lower in SiO_2 , 1 weight% higher in CaO and Al_2O_3 , and 3.5, 40 and 600 ppm higher in Co, V and Sr respectively than other rocks in its group. On plots of incompatible elements (Th, Ta and Hf), this tuff plots within the field of the Cinder Prospect member (Figs. 16B & 16C).

Fractionation of the tuff before eruption may be responsible for the differences in compatible element abundances.

In the Center Mountain dacite, biotite fractionation is not evident in a plot of Rb versus Sr (Fig. 16F). Chemical plots of CaO versus SiO₂ (Fig. 13D), and the lack of a Eu anomaly on the chondrite-normalized REE diagram (Fig. 17B) indicate that plagioclase did not fractionate.

In the Mount Sutor dacite, chemical plots of CaO versus Eu and Sr versus Eu (Figs. 16D & 16E), and the lack of a Eu anomaly (Fig. 17D) suggest that plagioclase was not fractionated. Plots of Sc versus V and Sr versus Rb indicate no clinopyroxene and biotite fractionation respectively (Figs. 16I & 16F).

The Tuff of the Sloan Volcanics

Chemical plots suggest fractionation of plagioclase, sanidine and clinopyroxene. Plagioclase and sanidine fractionation is suggested by the positive linear trend on a plot of the compatible elements Sr and Eu (Fig. 16D), and by a Eu anomaly on the chondrite-normalized REE diagram (Fig. 17C).

Clinopyroxene fractionation is suggested by the positive correlation of the compatible elements Sc and V (Fig. 16I).

Sources for Partial Melting

Introduction

In the previous sections, it was demonstrated that magma commingling and fractionation are not responsible for the production of the four rock groups of the

Sloan volcanics. It was concluded that partial melting of chemically distinct sources was the dominant process. In this section I will propose model source rocks for the Sloan volcanics.

Geochemical modeling was used to explore possible explanations concerning magma petrogenesis. A model is non-unique and must be combined with field and petrographic analyses to be of any merit.

The Pascal computer program MELT was used to evaluate source rock compositions and the amount of partial melting required to produce the andesites and dacites of the Sloan volcanics. MELT uses trace element distribution coefficients (Arth, 1976) and calculates a model rock using the batch melting equation of Shaw (1970). In these models, a critical assumption is the mineralogy and geochemistry of the source rock.

Two source rocks were used in the models. The first is a Precambrian amphibolite exposed in the lower plate of the Saddle Island detachment, Lake Mead (Smith, 1982a, 1984, 1986; Sewall, 1988; Duebendorfer et al., 1990). The amphibolite contains plagioclase (25-40%), actinolite and chlorite. It was assumed that the protolith of the amphibolite was gabbro containing plagioclase and clinopyroxene +/- olivine. Chemistry of the amphibolite (Tables 5a & 5b) is from an unpublished data base (E.I. Smith, University of Nevada, Las Vegas). The Saddle Island amphibolite is a reasonable source rock for the following reasons: 1) it will yield intermediate composition magma upon partial melting; 2) it crops out in the Lake Mead-Las Vegas area; 3) its occurrence in the lower

Table 5a				
Melt Model #1: Production Of Sloan Andesite (Mc110)				
From 25% Partial Melting Of Saddle Island Amphibolite.				
All Rock Compositions Are In ppm.				
Element	Saddle Island amphibolite composition	Sloan andesite composition	Model melt composition	Bulk distribution coefficient
Ba	655.00	1800.00	2078.01	0.087
Sr	1396.00	2280.00	1926.18	0.633
Ce	60.07	173.00	169.37	0.140
Nd	31.20	65.50	78.82	0.238
Sm	6.90	10.00	13.17	0.365
Eu	1.81	2.57	3.07	0.454
Yb	1.80	2.53	3.07	0.448
Lu	0.19	0.32	0.34	0.405
Sc	21.45	6.47	13.83	1.735
Cr	113.00	136.00	24.50	5.817
V	291.00	70.60	315.28	0.897
Co	26.30	10.30	29.24	0.866

Mineral modal percentages of source rock:

plagioclase = 30; clinopyroxene = 69; olivine = 1

Table 5b				
Melt Model #2: Production Of Sloan Dacite (Mc119)				
From 15% Partial Melting Of Saddle Island Amphibolite.				
All Rock Compositions Are In ppm.				
Element	Saddle Island amphibolite composition	Sloan dacite composition	Model melt composition	Bulk distribution coefficient
Ba	655.00	1780.00	2712.66	0.108
Sr	1396.00	1310.00	1661.51	0.812
Ce	60.07	216.00	224.73	0.138
Nd	31.20	101.00	93.05	0.218
Sm	6.90	14.80	16.13	0.327
Eu	1.81	3.32	3.44	0.442
Yb	1.80	3.84	3.68	0.399
Lu	0.19	0.64	0.42	0.360
Sc	21.45	7.42	14.96	1.510
Cr	113.00	40.20	25.48	5.040
V	291.00	19.20	357.93	0.780
Co	26.30	3.19	34.51	0.720

Mineral modal percentages of source rock:

plagioclase = 40; clinopyroxene = 60

plate of a detachment implies that it probably represents mid-to lower-crustal rocks. The second source is spinel peridotite. Spinel peridotite occurs as xenoliths in alkali basalts in the nearby Fortification Hill field of northwestern Arizona (Wilshire et al., 1988; Nielson and Nakata, in press). Ultramafic xenoliths are also found in the alkali basalt that crops out near the Sloan limestone quarry just to the northwest of Hidden Valley (Plate 1, Appendices A and D). Felsic upper-crustal rocks were not considered as possible source rocks since the amount of partial melting required to produce andesites and dacites is unrealistically high.

Partial Melt Models

Four models were tested. They are:

1) A 25% partial melt of Saddle Island gabbro consisting of 30% plagioclase, 69% clinopyroxene and 1% olivine produces an acceptable model for the production of the Sloan andesites. There is close agreement of the REE concentrations between the model rock and andesite. Concentration of elements compatible with clinopyroxene and olivine (Sc, Cr, V and Co), however, do not match well between the model rock and andesite. Agreement between the model rock and andesite for concentrations of Sr and Ba is very good (Table 5a, Fig. 21).

2) A 15% partial melt of Saddle Island gabbro consisting of 40% plagioclase and 60% clinopyroxene provides a realistic model for the production of the Sloan dacites. With the exception of Lu, there is excellent agreement of all of the REE between the model rock and dacite. There is poor to average

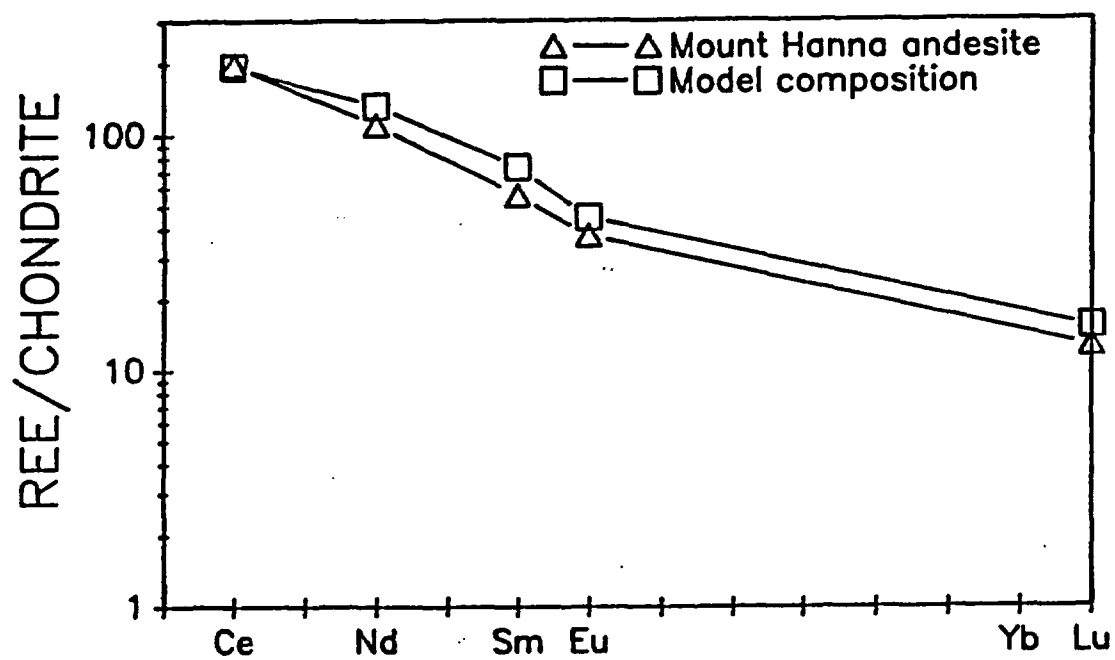


Figure 21: Chondrite-normalized REE diagram showing the chemical similarities between the Sloan andesites (Mc 110) and a 25% partial melt of gabbro.

correspondence between compatible elements (V, Sr and Ba) in the model rock and the dacite (Table 5b, Fig. 22).

3) A 0.5% partial melt of spinel peridotite containing 56.4% olivine, 30.1% orthopyroxene, 10% clinopyroxene and 3.5% spinel, with 2 times chondrite REE concentration did not produce favorable results. The concentrations of Ce, Nd, Sm and Eu in the model rock are lower than the andesite. The concentrations of Yb and Lu in the model rock are higher than the andesite. (Table 5c, Fig. 23).

4) A 0.5% partial melt of spinel peridotite with the same mineralogy as above, but with concentrations of 10 times chondrite for Ce, Nd and Sm, 3 times chondrite for Eu, and 2 times chondrite for Yb and Lu also does not produce favorable results (Table 5d, Fig. 24). The REE concentration in this model represents a metasomatized mantle that has been enriched in LREE.

Discussion

These models suggest that the Sloan andesites and dacites can be produced from partial melts of a rock similar to the Saddle Island gabbro. It must be kept in mind that using the Saddle Island gabbro as a source rock does not provide a unique solution. The Saddle Island gabbro may have followed a different evolutionary path than the source rocks for the Sloan volcanics. The large amount of variance between the compatible elements may be a reflection of their different petrogenetic histories. Even though these models are non-unique, they constrain the mineralogy and geochemistry of the source rocks for the Sloan

Table 5c				
Melt Model #3: Production Of Sloan Andesite (Mc110) From 0.5% Partial Melting Of Peridotite. Rock Compositions Are In ppm.				
Element	Peridotite composition: normalized to chondrite	Sloan andesite composition: normalized to chondrite	Melt composition: normalized to chondrite	Bulk distribution coefficient
Ce	2	196.59	68.47	0.026
Nd	2	109.17	40.06	0.045
Sm	2	55.25	27.71	0.068
Eu	2	37.25	26.22	0.072
Yb	2	12.65	18.52	0.103
Lu	2	9.41	19.39	0.099

Mineral modal percentages of source rock:
 olivine = 56.4; orthopyroxene = 30.1;

Table 5d				
Melt Model #4: Production Of Sloan Andesite From 0.5% Partial Melting Of Peridotite. Rock Compositions Are In ppm.				
Element	Peridotite composition: normalized to chondrite	Sloan andesite composition: normalized to chondrite	Melt composition: normalized to chondrite	Bulk distribution coefficient
Ce	10	196.59	324.34	0.026
Nd	10	109.17	200.29	0.045
Sm	10	55.25	138.55	0.068
Eu	3	37.25	39.33	0.072
Yb	2	12.65	18.52	0.103
Lu	2	9.41	19.39	0.099

Mineral modal percentages of source rock:
 olivine = 56.4; orthopyroxene = 30.1;

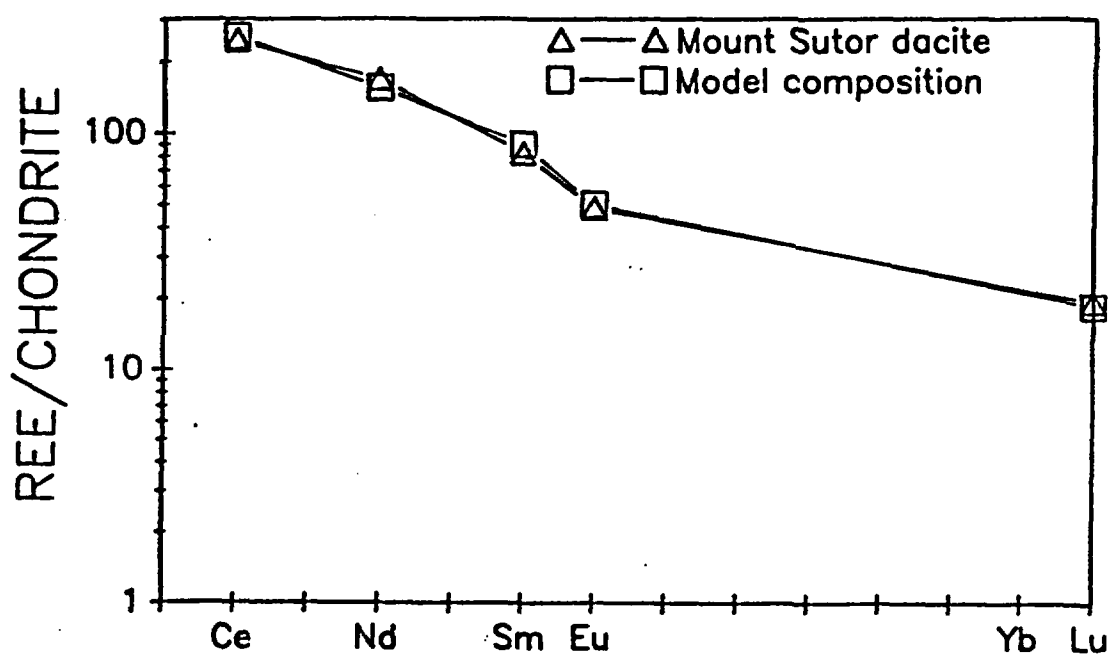


Figure 22: Chondrite-normalized REE diagram showing the chemical similarities between the Sloan dacites (Mc 119) and a 15% partial melt of gabbro.

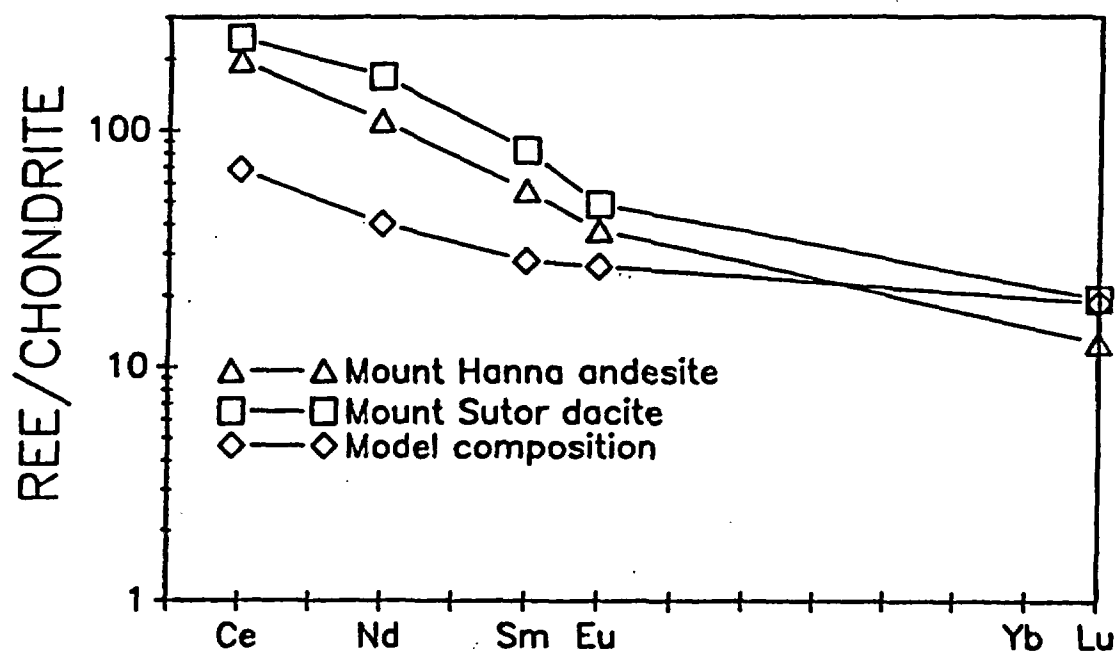


Figure 23: Chondrite normalized REE diagram showing the chemical differences between the Sloan andesites (Mc 110) and dacites (Mc 119), and a 0.5% partial melt of spinel peridotite. Values for the spinel peridotite are two times chondrite concentration.

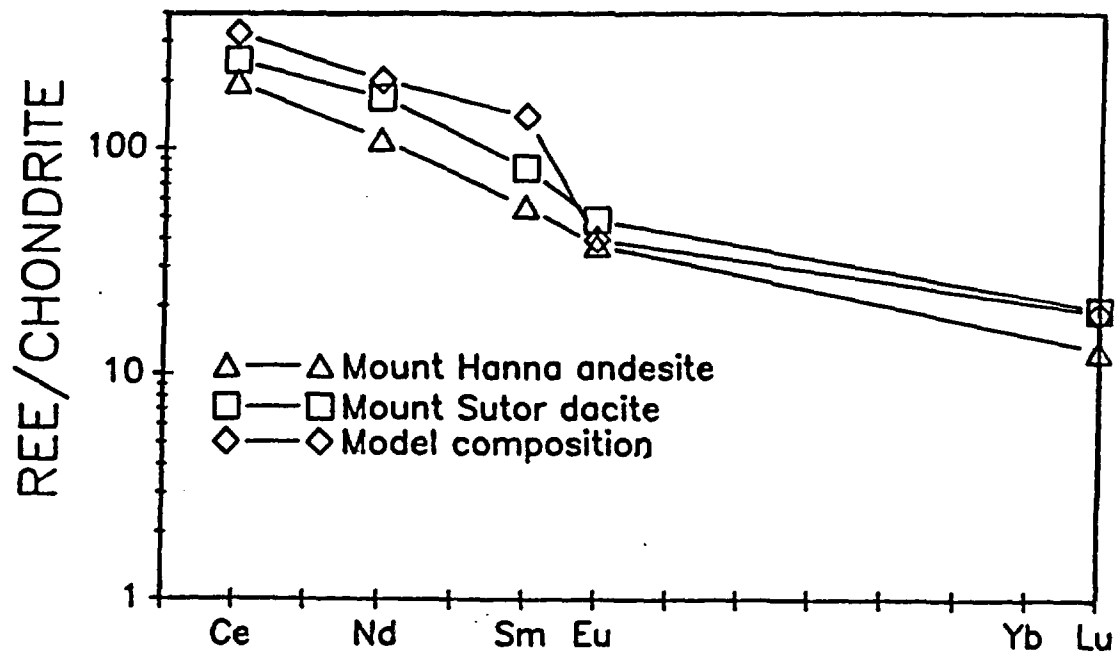


Figure 24: Chondrite-normalized REE diagram showing the chemical differences between the Sloan andesites (Mc 110) and dacites (Mc 119), and a 0.5% partial melt of spinel peridotite. Concentrations used for the spinel peridotite are ten times chondrite for Ce, Nd and Sm, three times chondrite for Eu, and two times chondrite for Yb and Lu.

volcanics.

Crustal Contamination

Geochemistry suggests that rocks of the Sloan volcanics were produced in the mid-to lower-crust by the partial melting of a gabbro. In this section, crustal contamination of rocks of the Sloan volcanics will be evaluated using petrographic and geochemical evidence.

Petrographic evidence for crustal contamination is limited to the Tuff of the Sloan volcanics. The tuffs contain abundant xenoliths, many of them gabbroic.

Sr contents greater than 1,000 ppm rule out large degrees of crustal contamination. Sr contents are normally greater than 1,000 ppm in rocks derived from the lower-crust and mantle. Rocks derived in the upper-crust are enriched in Rb and depleted in Sr ($< 1,000$ ppm Sr). Crustal contamination, therefore, commonly results in Sr contents less than 1,000 ppm. The high Sr contents in the Mount Hanna and Mount Ian andesites, and the Mount Sutor dacite ($> 1,000$ ppm) suggests a lack of significant crustal contamination (Appendix B).

Volumetrically, these rocks are the dominant lithologies of the Sloan volcanics. In contrast, the dacites and tuffs from the Center Mountain dome complex have Sr contents less than 1,000 ppm (Appendix B). This suggests that residence time in the crust and/or crustal contamination may have played a part in the evolution of these rocks.

THE SLOAN SAG

Evidence for a Sag in Hidden Valley

Introduction

In this section, by using field data, I will demonstrate that there is a structural sag in Hidden Valley.

The Hidden Valley Sag

Even though neither cited evidence, both Hewett (1956) and Longwell (1965) recognized the existence of a semi-circular depression in Hidden Valley. My field mapping has revealed structural evidence for a sag in Hidden Valley. In the northern part of Hidden Valley, the Tuff of Bridge Spring and the Hidden Valley volcanics dip 10° - 15° south. Rocks of the Hidden Valley volcanics in the southern part of Hidden Valley dip 20° - 30° north. Tuffs and basalts west of Hidden Valley dip about 10° east. East of Hidden Valley, pre-Sloan volcanic rocks dip 10° - 30° west (Plate 1).

Additional evidence for a structural depression includes log data from a water well in western Hidden Valley (Plate 1). The drill hole penetrated 700 feet into alluvium, never striking bedrock.

Association to a structural sag may not be the only explanation for the east and west dips about Hidden Valley. The eastward regional dip of the McCullough Mountains (Anderson et al., 1985; Schmidt, 1987) may be responsible for the orientation of pre-Sloan volcanic rocks to the west of Hidden Valley. In

the McCullough Mountains, westward dipping normal faults resulted in eastward stratal tilting of up to 40° (Anderson et al., 1985). An alternate explanation for the westward dips in the northern McCullough Mountains is suggested by the model of Weber and Smith (1987). By using a plot of relatively immobile and incompatible elements (Hf, Ta and Th), Weber and Smith chemically correlated Tertiary plutonic rocks of the Boulder City and Nelson plutons with volcanic rocks of the Eldorado and northern McCullough Mountains (Fig. 2). If their model is correct, the Eldorado and northern McCullough Mountains formed a volcano above the Boulder City and Nelson plutons. Westward dips of volcanic rocks in the northern McCullough Mountains, therefore, may represent the western flank of this stratocone.

Conclusion

The south and north dips of pre-Sloan volcanic rocks to the north and south of Hidden Valley respectively cannot be easily explained by regional trends, and I suggest that they are directly related to the formation of the Sloan sag. Although there are alternative explanations for the east and west dips of pre-Sloan volcanic rocks to the west and east of Hidden Valley respectively, I conclude that the overall inward dips of Pre-Sloan volcanic rocks about Hidden Valley indicates the presence of a structural depression. This conclusion is supported by well-log data.

Classic Caldera, or Volcanotectonic Depression?

Introduction

A physiographic sag filled with and surrounded by volcanic domes and flows is suggestive of a caldera. In this section, evidence for a classic collapse caldera origin for the Sloan sag will be evaluated. Using field evidence, I will show that a classic collapse caldera does not exist in Hidden Valley.

Discussion

Two of the main criteria for the existence of a collapse caldera are:

- 1) embayed, scalloped and faulted caldera margins with associated slump breccias;
- 2) an ash-flow tuff related to the caldera (Steven and Lipman, 1976; Steven et al., 1984; Walker, 1984). My initial field mapping concentrated on a search for features suggestive of a classic collapse caldera in Hidden Valley.

The Mount Hanna andesite member of the Sloan volcanics is in direct contact with older basalts of the Hidden Valley volcanics only in the eastern part of the thesis area. In other areas, contacts are covered by alluvium. Careful mapping along this contact demonstrated that it is depositional and is not a fault. In some areas the contact is low-angle and conformable, while in other places it cuts across topography and appears unconformable. (Plate 1). This relationship can be explained by the deposition of the Sloan volcanics on the irregular surface of the Hidden Valley basalt. No slump breccias are found in this, or any other area of Hidden Valley.

Ash-flow tuff occurs in the Center Mountain dome complex and in the western portion of the northern Mount Sutor field. There are also outcrops of ash-flow tuff west of Hidden Valley (Plate 1). Tuff within Hidden Valley is associated with isolated pyroclastic events related to dome formation. Chemical studies demonstrate that the tuff to the west of Hidden Valley is the Tuff of Bridge Spring, a regional ash-flow sheet whose source is unknown. None of the tuff exposures in and around Hidden Valley are associated with a pyroclastic event related to caldera formation.

The lack of slump breccias and an associated ash-flow tuff, argues strongly against a classic collapse caldera origin for the Sloan sag.

Significance of the Mount Hanna Andesite

Introduction

In this section, I will begin to discuss the origin of the Sloan sag by evaluating the significance of the thick pool of Mount Hanna andesite within the depression. High silica lava flows are typically thick and of small areal extent. Walker (1973) reported that rhyolitic lava flows have a median length of 1.1 km, with none longer than 10 km. Felsic to intermediate pyroclastic flows, however, may be very thin and travel greater than 70 km from their source (Henry et al., 1988). Ekren et al. (1984) described extensive "lavalike" rhyolite flows without pyroclastic textures in and adjacent to the Owyhee Mountains and the Owyhee Plateau of southwestern Idaho. Experimental data from one of the Owyhee flows

(the Little Jacks Tuff) suggests that it formed from a dry melt (2% H_2O or less) under pressures as great as 8 kilobars and temperatures of greater than 1,000 °C. Magmas originated from a depth of about 25 km. Similar deposits include the Oligocene Bracks Rhyolite ($SiO_2 = 68\%$ to 72%) of the Trans-Pecos volcanic field, Texas, which covers an area of 1,000 km^2 (Henry et al., 1988), and the Middle Proterozoic Yardea Dacite ($SiO_2 = 67\%$) of south Australia, which covers an area of over 12,000 km^2 (Creaser and White, 1991). The Trans-Pecos and Yardea rocks lack pyroclastic textures. Low water content allows devolatilization and fragmentation of magma near the surface. High temperatures produce non-viscous lavas capable of flowing great distances (Henry et al., 1988). If these lavas erupted at lower temperatures and higher water contents, it is reasonable to assume that ash-flow tuffs would have been produced.

Origin of the Mount Hanna Andesite

I propose that the Mount Hanna andesite member of the Sloan volcanics is analogous to a hot, dry ash-flow tuff, similar to the Owyhee, Trans-Pecos and Yardea lavas. Geochemical modeling suggests that the Mount Hanna andesite was produced from partial melting of a gabbroic source at lower-crustal levels (Table 5a, Fig. 21). Sr contents of 1700-2280 ppm for the Mount Hanna andesite suggests a lower-crustal or mantle source for this unit. If these magmas equilibrated at temperatures of 1,000°C (similar to the Owyhee lavas), they originated at a depth of about 25 km, assuming a geothermal gradient of 40°C/km. The aphyric texture of the Mount Hanna andesite (Fig. 25) and the

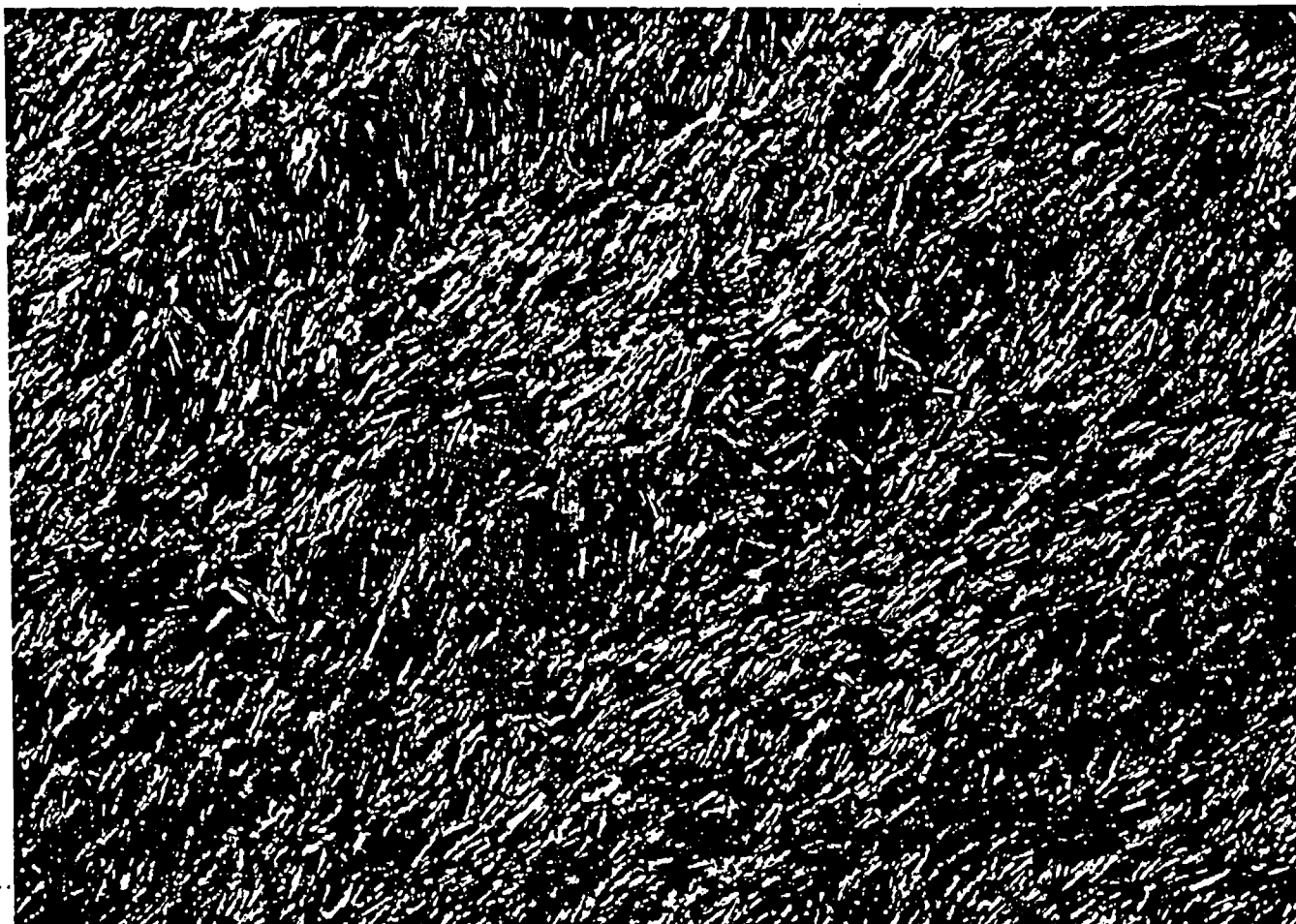


Figure 25: 40x photomicrograph of the Mount Hanna andesite. The rock consists of subparallel microlites of plagioclase with subordinate Fe-Ti oxides, glass and probable clinopyroxene and/or olivine (high birefringent grains).

lack of fractionation trends on chemical plots (Figs. 16D, 16E, 16H & 16I) suggests that the Mount Hanna andesite rose to the surface quickly, without pausing to substantially cool or fractionate. The high Sr contents also suggest that magma was not significantly contaminated by crustal material, indicating a quick ascent from its source area.

The Mount Hanna andesite erupted from a single vent, creating a large pool (exposed maximum volume of 9 km^3) of andesite lava (Plate 1; cross section C-C'; Fig. 7). The fact that such a large pool of andesite was erupted from a single vent suggests that the magma had a lower viscosity than typical andesite and was capable of flowing greater distances than would be expected of an intermediate composition lava. Its low viscosity may be attributed to high temperature and low gas content.

Sparks and Wilson (1976) proposed that a hot, dry magma will produce an eruptive column that is too dense to mix with the atmosphere. Such a column would consist only of the gas thrust phase, and would be too dense to produce a gaseous convective thrust component. Because of this, Ekren et al. (1984) envisioned lava fountain-type eruptions for the Owyhee rhyolites, as opposed to large Plinian clouds. The Mount Hanna andesite may also have erupted by lava-fountaining. Much of this unit is characterized by a mottled, streaky texture consisting of black and red, or black and gray discontinuous patches (Fig. 26). This texture may have formed by hot magma rain that produced droplets of magma. Upon hitting the surface, the droplets coalesced, moving away from the



Figure 26: Photograph showing the streaky, discontinuous texture common in the Mount Hanna andesite. Sample was collected at station 115 (Fig. 8). Scale bar is 1 cm long.

vent as lava flows.

Duffield (1990) has described similar textures in the Oligocene Taylor Creek Rhyolite of the Mogollon-Datil volcanic field in southwestern New Mexico. He suggests that the streaky "agglunitnated" texture in the rhyolites is a result of lava-fountaining. If the magma droplets are hot enough, upon hitting the surface they will coalesce to form homogeneously-textured rocks. Duffield proposes that if the eruptive fountain is high, magma droplets will cool before hitting the surface and not be hot enough to completely coalesce and homogenize. Fluctuating fountain height, therefore, will alternately produce homogeneous and streaky-textured rocks.

Even though the discontinuous streaks in the Mount Hanna andesite are suggestive of a primary volcanic origin, they may also represent highly sheared and attenuated flow foliation. To evaluate the origin of the streaks, I compared their size to the size-frequency distributions of particles produced during lava-fountaining and pyroclastic eruptions. Heiken (1972) determined the mean droplet diameter for a variety of different magma types and eruptive styles. To evaluate if the streaky texture of the Mount Hanna andesite may reflect magma droplets, mean streak diameter was determined. The cross-sectional area of ten streaks from the Mount Hanna andesite (sample Mc115) was measured. Values were adjusted to represent the cross sectional diameter of a sphere. Diameters range from 0.8-6.8 mm, with a mean of 4.08 mm. The mean diameter of the discontinuous streaks in the Mount Hanna andesite is similar to those of magma

droplets produced in the following lava-fountaining events: 1) the basaltic strombolian eruption of Pacaya, Guatemala (6.35 mm); 2) the basaltic phreatomagmatic eruption of Capelinhos, Azores Islands (3.18 mm); 3) the rhyolitic phreatomagmatic eruption of Sugarloaf, San Francisco Mountains, Arizona (3.18 mm) (Heiken, 1972). The correlation of the mean diameter of the discontinuous streaks in the Mount Hanna andesite with recognized lava-fountaining deposits supports a primary origin for the streaks.

Depth of Magma Generation Versus Depth of Eruption

Magma must migrate to shallow crustal levels before devolatilization of gases can occur, resulting in fragmentation and eruption. For magmas with SiO_2 contents comparable to the Sloan andesites and dacites, the level at which gas exsolution and magma fragmentation can occur is approximately 5.4 km (Fisher and Schmincke, 1984). Magmas with H_2O contents of 2% or less may devolatilize and fragment even closer to the surface. The above information suggests that the Mount Hanna andesite resided at these shallower depths long enough only to exsolve gas and fragment before erupting.

Formation of the Sloan Sag

Introduction

I will now consider the formation of the sag, and will suggest that: 1) the Sloan volcanics filled pre-existing grabens and half-grabens bounded by the McCullough Wash fault system; 2) sagging in Hidden Valley occurred during

and/or after the eruption of the Sloan volcanics.

The McCullough Wash Fault System

The McCullough Wash fault is the only major internal structure in the McCullough Mountains. South of Hidden Valley in the South McCullough Wilderness Study Area, this fault places Precambrian basement against rocks of the Hidden Valley volcanics and has at least 600 m of throw. Displacement decreases to the north. North of the wilderness study area, it splays into three northeast striking faults (Anderson et al, 1985). East and west dipping splays of the McCullough Wash fault system produced numerous grabens and half-grabens in the area of the McCullough Pass caldera, just south of Hidden Valley (Schmidt, 1987). These faults display only minor offset. The McCullough Wash fault system probably continues north into Hidden Valley. Most of these faults are covered by alluvium and possibly by domes and flows of the Sloan volcanics. A north-south striking, west-dipping, normal fault on the west side of the ridge just to the north of the McCullough Pass caldera (Plate 1) offsets pre-Sloan volcanic rocks, and may represent the northward projection of the McCullough Wash fault system. I propose that Hidden Valley is cut by a series of grabens and half-grabens bounded by faults of the McCullough Wash fault system. Field mapping has also revealed an en-echelon splay of the McCullough Wash fault in Hidden Valley. The sharp, steep linear escarpment of the Mount Hanna andesite and Mount Sutor dacite in the eastern portion of Hidden Valley is suggestive of a fault scarp (Plate 1). This type of en-echelon relationship of normal faults is

common and has been documented in many areas including the East African rift zone (Morley, 1988 & 1989) and the Dead Horse graben of west Texas (Maler, 1990). The strike of this fault changes from north-south to northwest-southeast in the area of the Mount Sutor stock (Plate 1, Fig. 8). Rocks of the Mount Hanna andesite and Mount Sutor dacite are offset by this fault suggesting that it was active after eruption of these units. The McCullough Wash fault system does not appear to extend farther to the north of Hidden Valley, and its displacement decreases to the south. Based on mapping done by Schmidt (1987) along the south rim of Hidden Valley, faults may be spaced every 300 m. Accumulated displacement on buried and exposed faults in Hidden Valley is estimated to be at least 2.25 km.

Sagging and Tectonic Control

Faults of the McCullough Wash system strike north-south. If subsidence was controlled entirely by these faults, north-south oriented grabens would have formed in Hidden Valley. This is the case in the northern segment of the McCullough Pass caldera south of Hidden Valley (Schmidt, 1987). Subsidence was accommodated by faults of the McCullough Wash system, resulting in a north-south trending graben. In the case of the Sloan sag, however, contacts cut across these north-south striking structures. I propose, therefore, that sagging in Hidden Valley resulted from rejuvenation on the McCullough Wash fault system in the east and northeast, and sagging into emptied magma chambers in the west.

Summary of Events

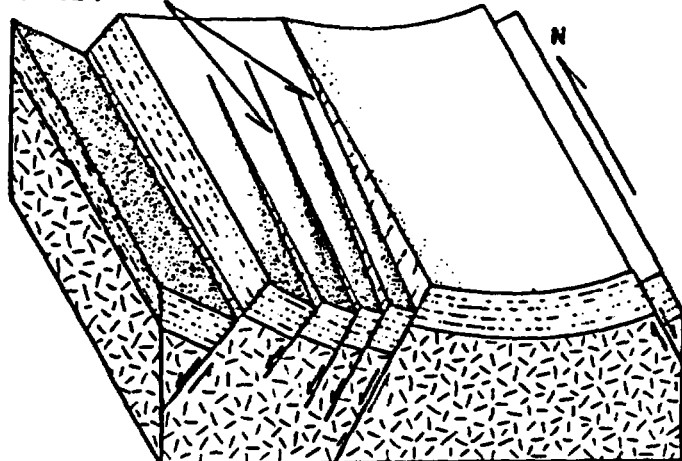
A scenario for the formation of the Sloan sag is described below (refer to Figure 27).

1) Before the eruption of the Sloan volcanics, Hidden Valley consisted of a series of grabens and half grabens, bounded by the north-south striking McCullough Wash fault system.

2) The Mount Hanna andesite and rocks of the Center Mountain dome complex were the first members of the Sloan volcanics to erupt. The Mount Hanna andesite was generated at depths as great as 25 km by partial melting of gabbro, rising to the surface and erupting quickly in a lava-fountaining event. Eruption of this unit caused sagging by reactivating faults of the McCullough Wash system in eastern Hidden Valley. Fault movement produced a surface sag over the emptied chamber. Unlike other units of the Sloan volcanics which were emitted from numerous vents and domes, the Mount Hanna andesite erupted from a single vent resulting in a pool of andesite with a maximum exposed volume of 9 km³.

3) Volcanic dome formation is represented by the rocks of the Center Mountain dome complex. Ash-flow tuffs of the Cinder Prospect member and the Tuff of the Sloan volcanics represent the early stages of pyroclastic and phreatomagmatic activity, reflecting tuff ring formation. The tuff ring was intruded by the Center Mountain dacite. The Mount Ian andesite intruded rocks of the Center Mountain dome complex, resulting in the formation of platy,

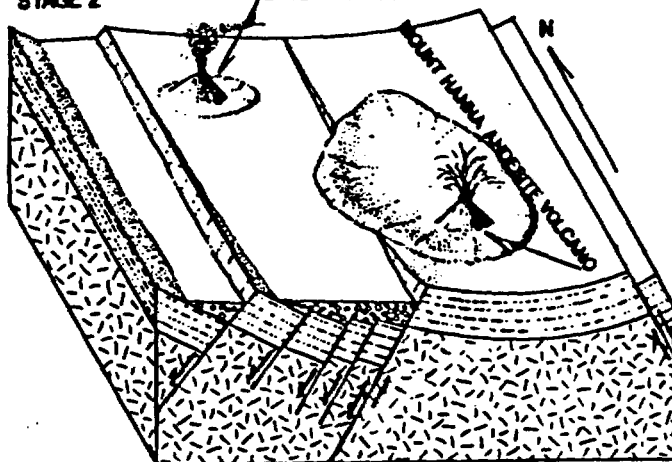
STAGE 1 FAULTS OF THE McCULLOUGH WASH SYSTEM



Stage 1: Pre-Sloan volcanics topography: paleo-Hidden Valley consists of half-grabens bounded by faults of the McCullough Wash system.

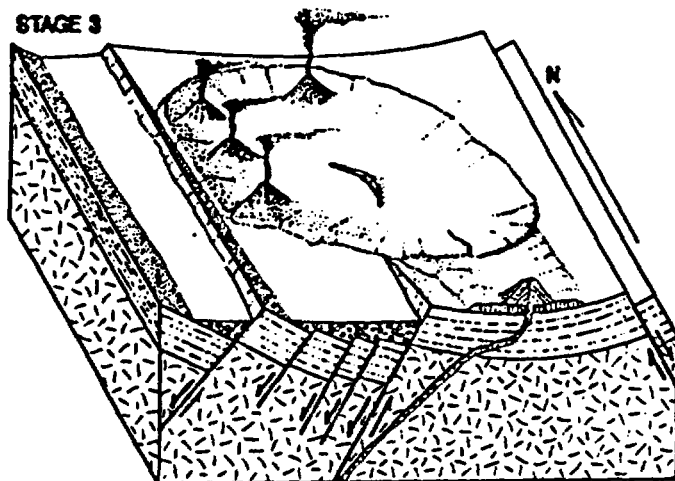
STAGE 2

CENTER MTL DOME COMPLEX



Stage 2: Eruption of the Mount Hanna andesite causes rejuvenation of the McCullough Wash fault system and sagging in eastern Hidden Valley.

STAGE 3



Stage 3: Eruption of units in northern and western Hidden Valley causes sagging into shallow chambers, and the rejuvenation of a splay of the McCullough Wash system.

Figure 27: Formation sequence of the Sloan sag.

foliated andesite domes, many of which overlie tuff rings. The Mount Sutor dacite erupted from numerous vents and domes resulting in two large pools of viscous biotite dacite.

Subsidence into shallow chambers occurred during and/or after the eruption of these units. Subsidence into shallow chambers caused renewed movement on a splay of the McCullough Wash fault system, offsetting rocks of the Mount Hanna andesite and the Mount Sutor dacite in the northeast part of Hidden Valley, resulting in more sagging.

CONCLUSIONS

Important conclusions of this thesis are:

- 1) A volcanotectonic depression in Hidden Valley resulted from the eruption of the Sloan volcanics.
- 2) Sagging was accommodated by a combination of displacement on splays of the McCullough Wash fault system in eastern and northeastern Hidden Valley, and sagging into evacuated magma chambers in the western part of the valley.
- 3) The rocks of the Sloan volcanics belong to four magma groups, each of which were produced by partial melting of chemically distinct sources.
- 4) Partial melting of a crustal source similar to the Saddle Island amphibolite produced the andesites and dacites of the Hidden Valley volcanics.
- 5) Except for rocks of the Center Mountain dome complex, magmas rose through the crust rapidly without experiencing significant crystal fractionation or crustal contamination.
- 6) The Mount Hanna andesite member of the Sloan volcanics erupted a large pool (approximately 9 km^3) of lava from a single vent. This unit may have been emplaced as a hot ($1,000^\circ\text{C}$), dry (2% H_2O or less) analog of an ash-flow tuff in a lava-fountaining event. If this magma had erupted at lower temperatures and higher water contents, a plinian-style eruption probably would have occurred, resulting in an ash-flow tuff.

FUTURE WORK

As in any research project, unanswered questions and problems arise that cannot be answered due to time and/or financial constraints. The following is a list of projects that may provide important information about the McCullough Mountains and the southern Basin-and-Range.

1) The $^{40}\text{Ar}/^{39}\text{Ar}$ date of the Tuff of Bridge Spring is the only reliable date yet obtained from the north-central McCullough Mountains. $^{40}\text{Ar}/^{39}\text{Ar}$ dates on rocks stratigraphically above and below this unit will help constrain the absolute age and timing of eruption of the volcanic units.

2) The exotic trace mineral assemblage in the lower-most rhyolite tuff of the Tuff of the Sloan volcanics (sample Mc59a) is intriguing. Even though this tuff contains monazite, allanite, epidote, zircon and sphene, its incompatible trace element concentration is not higher than the other tuffs from this unit. A detailed study of mineral chemistry is required to understand the geochemistry of this unit.

3) Detailed geologic mapping has never been done north of Hidden Valley. Work in the northern McCullough Mountains will test the Weber and Smith (1987) hypothesis that a stratocone exists in this area.

4) Geochemistry suggests that volcanic rocks from the White Hills, and the River, Eldorado and McCullough Mountains have similar sources. A geochemical study of igneous rocks from a larger part of the southern Basin-and-Range may help us understand the scale of heterogeneity of crustal and mantle sources.

5) The hot, dry, fountaining-eruption mechanism of the Mount Hanna

andesite is unique. Such an eruptive mechanism may be the key to understanding the large areal extent of some felsic-to-intermediate lavas. Unless they erupt as ash-flow tuffs, intermediate-to-felsic lavas usually form short, thick deposits. The discontinuous, streaky texture displayed in the Mount Hanna andesite and the Taylor Creek rhyolites may be indicative of a lava-fountaining mechanism. Detailed mapping of the Mount Hanna andesite field along with petrographic and geochemical studies are needed to help us further understand what may be a significant eruptive mechanism.

REFERENCES CITED

- Anderson, R.E., 1971, Thin-skinned distension in Tertiary rocks of south-eastern Nevada: Geological Society of America Bulletin, v. 82, p. 42-58.
- Anderson, R.E., 1977, Geologic map of the Boulder City 15 minute quadrangle, Clark County, Nevada: U.S. Geological Survey Geologic Quadrangle Map GQ-1394.
- Anderson, J.L., Young, E.D., Clarke, S.H., Orrell, S.E., Winn, M., Schmidt, C.S., Weber, M.E. and Smith, E.L., 1985, The geology of the McCullough Range Wilderness Area, Clark County, Nevada: Technical Report, University of Southern California, Los Angeles, 46 pp.
- Arth, J.G., 1976, Behavior of the trace elements during magmatic processes; A summary of theoretical models and their applications: U.S. Geological Survey Journal of Research, v. 4, no. 1, p. 41-47.
- Bingler, E.C. and Bonham, H.F. Jr., 1972, Reconnaissance geologic map of the McCullough Range and adjacent areas, Clark County, Nevada: Nevada Bureau of Mines and Geology, Special Map 45.
- Carr, M.D., 1983, Geometry and structural history of the Mesozoic thrust belt in the Goodsprings district, southern Spring Mountains, Nevada: Geological Society of America Bulletin, v. 94, p. 1185-1198.
- Cascadden, T.E., 1991, Styles of volcanism and extensional tectonics in the eastern Basin-and-Range province: northern White Hills, Arizona: Unpublished Masters Thesis, University of Nevada, Las Vegas, 156 pp.
- Coats, R.R., 1968, The Circle Creek Rhyolite, a volcanic complex in northern Elko County, Nevada, in Coats, R.R., Hay R.L. and Anderson, C.A., eds., Studies in Volcanology: Geological Society of America Memoir 116, p. 69-106.
- Cole, J.W., 1979, Structure, petrology, and genesis of Cenozoic volcanism, Taupo volcanic zone, New Zealand. A review: New Zealand Journal Geol. Geophysics, v. 22, p. 631-657.
- Creaser, R.A. and White, A.J.R., 1991, Yardea Dacite--large-volume, high-temperature felsic volcanism from the Middle Proterozoic of south Australia: Geology, v. 19, p. 48-51.

- De Witt, E., Anderson, J.L., Barton, H.N., Jachens, R.C., Podwysocki, M.H., Brickley, D.W. and Close, T.J., 1989, Mineral resources of the South McCullough Mountains Wilderness Study Area, Clark County, Nevada: U.S. Geological Survey Bulletin 1730-C, 24 pp.
- Damon, P.E., 1971, The relationship between late Cenozoic volcanism and tectonism and orogenic-epeirogenic periodicity: in Conference on Late Cenozoic Glacial Ages, Turekian, K.K., editor, John Wiley and Sons, New York, p. 15-35.
- Duebendorfer, E.M., Sewall, A.J. and Smith, E.I., 1990, The Saddle Island detachment; An evolving shear zone in the Lake Mead area, Nevada: Geological Society of America Memoir 176, p. 77-97.
- Duebendorfer, E.M. and Wallin, E.T., 1991, Basin development and syntectonic sedimentation associated with kinematically coupled strike-slip and detachment faulting, southern Nevada: *Geology*, v. 19, p. 87-90.
- Duffield, W.A., 1990, Eruptive fountains of silicic magma and their possible effects on the tin content of fountain-fed lavas, Taylor Creek Rhyolite, New Mexico: in Stein, H.J. and Hannah, J.L., eds., Ore-bearing granite systems; Petrogenesis and mineralizing processes: Geological Society of America Special Paper 246, p. 251-261.
- Ekren, E.B., McIntyre, D.H. and Bennet, E.H., 1984, High-temperature, large-volume lavalike ash-flow tuffs without calderas in southwestern Idaho: Geological Survey Professional Paper 1272, 73 pp.
- Feuerbach, D.L., 1986, Geology of the Wilson Ridge pluton; a mid-Miocene quartz monzonite intrusion in the northern Black Mountains, Mojave County, Arizona and Clark County, Nevada: Unpublished Masters Thesis, University of Nevada, Las Vegas, 79 p.
- Fisher, R.V. and Schminke, H.V., 1984, *Pyroclastic Rocks*, Springer-Verlag, New York, 472 p.
- Goddard, E.N., Trask, P.D., De Ford, R.K., Rove, O.N., Singewald Jr, J.T. and Overbeck, R.M., 1970, *Rock-color chart: The Geological Society of America*, Boulder, Colorado.
- Glazner, A.F., 1990, Recycling of continental crust in Miocene volcanic rocks from the Mojave Block, southern California: Geological Society of America Memoir 174.

- Grindley, G.W., 1965, The geology, structure, and exploitation of the Wairakei geothermal field: New Zealand Geological Survey Bulletin 75.
- Heiken, G., 1972, Morphology and petrography of volcanic ashes: Geological Society of America Bulletin, v. 83, p. 1961-1988.
- Henry, C.D. and Price, J.G., 1986, The Van Horn Mountains Caldera, Trans-Pecos Texas: Bureau of Economic Geology, University of Texas at Austin, Report of Investigations No. 151, 46 pp.
- Henry, C.D., Price, J.G., Rubin, J.N., Parker, D.F., Wolff, J.A., Self, S., Franklin, R. and Barker, D.S., 1988, Widespread, lavalike silicic volcanic rocks of Trans-Pecos, Texas: Geology, v. 16, p. 509-512.
- Hewett, D.F., 1956, Geology and mineral resources of the Ivanpah Quadrangle, California and Nevada: U.S. Geological Survey Professional Paper 275, 172 pp.
- Irvine, T.N. and Baragar, W.R.A., 1971, A guide to the chemical classification of the common volcanic rocks: Canadian Journal of Earth Sciences, v. 8, p. 523-548.
- Kohl, M.S., 1978, Tertiary volcanic rocks of the Jean-Sloan area, Clark County, Nevada and their possible relationship to carnotite occurrences in caliches: Unpublished Masters Thesis, University of California, Los Angeles, 117 pp.
- Koyaguchi, T., 1986, Textural and compositional evidence for magma mixing and its mechanism, Abu volcano group, southwestern Japan: Contributions to Mineralogy and Petrology, v. 93, p. 33-45.
- Larsen, L.L., 1989, The origin of the Wilson Ridge Pluton and its enclaves, northwest Arizona: implications for the generation of a calc-alkaline intermediate pluton in an extensional environment: Unpublished Masters Thesis, University of Nevada, Las Vegas, 81 pp.
- Larsen, L.L. and Smith, E.I., 1990, Mafic enclaves in the Wilson Ridge pluton, northwestern Arizona: implications for the generation of a calc-alkaline intermediate pluton in an extensional environment: Journal of Geophysical Research, v. 95, no. B11, p. 17,693-17,716.
- Lipman, P.W., 1984, The roots of ash-flow calderas: windows into granitic batholiths: Journal of Geophysical Research, v. 89, p. 8801-8841.

- Longwell, C.R., Pampeyan, E.H., Bower, B. and Roberts, R.J., 1965, Geology and mineral deposits of Clark County, Nevada: Nevada Bureau of Mines and Geology Bulletin 62, 218 pp.
- Maler, M.O., 1990, Dead Horse graben: A west Texas accommodation zone: *Tectonics*, v. 9, no. 6, p. 1357-1368.
- McMillan, N.J. and Dungan, M.A., 1986, Magma mixing as a petrogenetic process in the development of the Taos Plateau volcanic Field, New Mexico: *Journal of Geophysical Research*, v. 91, no. B6, p. 6029-6045.
- Mills, J.G., 1985, The geology and geochemistry of volcanic and plutonic rocks in the Hoover Dam 7.5 minute quadrangle, Clark County, Nevada and Mojave County, Arizona: Unpublished Master's Thesis, University of Nevada, Las Vegas, 119 p.
- Morley, C.K., 1988, Variable extension in Lake Tanganyika: *Tectonics*, v. 7, no. 4, p. 785-801.
- Morley, C.K., 1989, Extension, detachments, and sedimentation in continental rifts (with particular reference to east Africa): *Tectonics*, v. 8, no. 6, p. 1175-1192.
- Naumann, T.R., 1987, Geology of the central Boulder Canyon Quadrangle, Clark County, Nevada: Unpublished Master's Thesis, University of Nevada, Las Vegas, 68 pp.
- Naumann, T.R. and Smith, E.I., 1987, Evidence for magma mixing in Mid-Tertiary volcanic rocks, Lake Mead region, southern Nevada: *Geological Society of America Abstracts with Programs*, v. 19, p. 435-436.
- Nielson, J.E. and Nakata, J.K., (manuscript in review), Geology and origin of mafic dikes, and their megacryst-xenolith inclusions, Black Canyon, Arizona.
- Nielson, R.L. and Dungan, M.A., 1985, The petrology and geochemistry of the Ocate volcanic field, north-central New Mexico: *Geological Society of America Bulletin*, v. 96, p. 296-312.
- Novak, S.W. and Bacon, C.R., 1986, Pliocene rocks of the Coso Range, Inyo County, California: U.S. Geological Survey Professional Paper 1383, 44 p.

- Pearce, J.A., 1983, The role of sub-continental lithosphere in magma genesis at destructive plate margins: *in* Continental basalts and mantle xenoliths, Hawkesworth, C.J. and Narry, M.J., editors, Nantwich: Shiva.
- Schmidt, C.S., 1987, A Mid-Miocene caldera in the central McCullough Mountains, Clark County, Nevada: Unpublished Masters Thesis, University of Nevada, Las Vegas, 78 pp.
- Sewall, A.J., 1988, Structure and geochemistry of the upper plate of the Saddle Island detachment, Lake Mead, Nevada: Unpublished Masters Thesis, University of Nevada, Las Vegas, 84 pp.
- Shaw, D.M., 1970, Trace element fractionation during anatexis: *Geochim. Cosmochim. Acta*, v. 34, p. 237-243.
- Smith, E.I., 1973, Mono Craters, California: A new interpretation of the eruptive sequence: *Geological of America Bulletin*, v. 84, p. 2685-2690.
- Smith, E.I., 1982, Geology and geochemistry of the volcanic rocks in the River Mountains, Clark County, Nevada and comparisons with volcanic rocks in nearby areas: *in* Frost, E.G. and Martin, D.L., eds, Mesozoic - Cenozoic tectonic evolution of the Colorado River region, California, Arizona, Nevada: Dan Diego, California, Cordilleran Publishers, p. 41-54.
- Smith, E.I., 1984, Geological map of the Boulder Beach Quadrangle, Nevada: Nevada Bureau of Mines and Geology Map 81, scale 1:24,000.
- Smith, E.I., 1986, Geology of the River, Eldorado, and McCullough Ranges, Clark County, Nevada: *in* Rowland, S.M., ed., Field guide to the geology of Nevada, Las Vegas: Las Vegas, Nevada, p. 22-64.
- Smith, E.I., Schmidt, C.S. and Mills, J.G., 1988, Mid-Tertiary volcanoes in the Lake Mead area of southern Nevada and Northwestern Arizona: *in* Weide, D.L. and Faber, M.L., eds, This extended land: Geological journeys in the southern Basin-and-Range: Field trip guidebook, Geological Society of America, Cordilleran section meeting, Las Vegas, Nevada, p. 107-122.
- Smith, E.I., Feuerbach, D.L., Naumann, T.R. and Mills, J.G., 1990, Mid-Miocene volcanic and plutonic rocks in the Lake Mead area of Nevada and Arizona: Production of intermediate volcanic rocks in an extensional environment: *Geological Society of America Memoir* 174, p. 169-194.

- Smith, E.I., Feuerbach, D.L. and Duebendorfer, E.M., 1991, Magmatism, extensional tectonics and sedimentation in the Lake Mead area, Nevada and Arizona: a new model: Geological Society of America Abstracts With Programs, Cordilleran Section, v. 23, no. 2, p. 99.
- Smith, R.L. and Bailey, R.A., 1968, Resurgent cauldrons, in Coats, R.R., and others, eds., Studies in volcanology: Geological Society of America Memoir 116, p. 613-662.
- Sparks, R.J. and Wilson, L., 1976, A model for the formation of ignimbrites by gravitational column collapse: Journal of the Geological Society of London, v. 132, p. 441-451.
- Steven, T.A., 1981, Three Creeks caldera, southern Pavant Range, Utah: Brigham Young University Geol. Stud., v. 28, p. 1-7.
- Steven, T.A. and Lipman, P.W., 1976, Calderas of the San Jaun Volcanic Field, southwestern Colorado: U.S. Geological Survey Professional Paper 958, 35 pp.
- Steven, T.A., Rowley, P.D. and Cunningham, C.G., 1984, Calderas of the Marysvale Volcanic Field, west central Utah: Journal of Geophysical Research, v. 89, p. 8751-8764.
- Stormer, J.C. and Nichols, J., 1978, XLFRAC: A program for the interactive testing of magmatic differentiation models: Computers and Geoscience, v. 4, p. 143-159.
- Thompson, R.N., Morrison, M.A., Hendry, G.L. and Parry, S.J., 1984, An assessment of the relative roles of crust and mantle in magma genesis: Phil. Trans. R. Soc. London, A310, p. 541-590.
- Walker, G.P.L., 1973, Lengths of lava flows: Royal Society of London Philosophical Transactions, ser. A, v. 274, p. 286-302.
- Walker, G.P.L., 1984, Downsag calderas, ring faults, caldera sizes, and incremental caldera growth: Journal of Geophysical Research, v. 89, p. 8407-8416.
- Walker, J.D., Beaufait, M.S. and Zelt, F.B., Geology of the Devil Peak area, Spring Mountains, Nevada: Geological Society of America Abstracts With Programs, Cordilleran Section, v. 13, no. 2, p. 112.

- Weber, M.E., and Smith, E.I., 1987, Structural and geochemical constraints on the reassembly of disrupted Mid-Miocene volcanoes in the Lake Mead-Eldorado Valley area of southern Nevada: *Geology*, v. 15, p. 553-556.
- Wernicke, B., Axen, G.J. and Snow, J.K., 1988, Basin-and-Range extensional tectonics at the latitude of Las Vegas, Nevada: *Geological Society of America Bulletin*, v. 100, p. 1738-1757.
- Williams, H., Turner, F.J. and Gilbert, C.M., 1982, *Petrography: An introduction to the study of rocks in thin sections*, W.H. Freeman and Company, New York, p. 139-142.
- Wilshire, H.G., Meyer, C.E., Nakata, J.K., Calk, L.C., Shervais, J.W., Nielson, J.E. and Schwarzman, E.C., 1988, Mafic and ultramafic xenoliths from volcanic rocks of the western United States: *U.S. Geological Survey Professional Paper 1443*, 179 pp.
- Wiser, E., 1951, Tectonic analysis of a mining district: Pachuca, Mexico: *Economic Geology*, v. 46, p. 459-477.
- Wood, C.A., 1984, Calderas: a planetary perspective: *Journal of Geophysical Research*, V. 89, p. 8391-8406.

APPENDIX A: SAMPLE LOCATION AND PETROGRAPHY

Colors are from the Geological Society of America rock-color chart.

TUFF OF BRIDGE SPRING

Sample number: Mc53

Location: NW 1/4, Sec 31, T23S, R61E, Sloan, Nev. 7 1/2' quad: tuff that underlies Thvb in the NE part of the thesis area.

Rock name: Welded dacitic ash-flow tuff

Description: Pyroclastic, eutaxitic and hypocrySTALLINE consisting of fragmented phenocrysts of subhedral, oscillatory sanidine up to 3 mm (24.2%), subhedral, oscillatory plagioclase up to 2.5 mm (3.4%), sub-euhedral, hematized biotite up to 2 mm (3.4%), an-subhedral clinopyroxene up to 1 mm (0.8%), anhedral, oscillatory quartz up to 1 mm (0.6%), sub-euhedral sphene up to 0.5 mm (0.4%), Fe-Ti oxides up to 0.5 mm (0.2%) and trace zircon. Pumice fiamme (9.6%) are devitrified, rarely spherulitic and up to several cm long. Basaltic and granodioritic rock fragments (1.2%) are up to 1 cm. The pale red-colored groundmass (56.2%) consists of devitrified glass and glass shards. Shards wrap around phenocrysts and lithic fragments.

Sample number: Mc60

Location: NW 1/4, Sec 32, T24S, R60E, Jean, Nev. 7 1/2' quad: collected near the intersection of Las Vegas Blvd. and the dirt entrance road to Jean Lake.

Rock Name: Moderately welded dacitic ash-flow tuff

Description: Pyroclastic and hypocrySTALLINE consisting of fragmented phenocrysts of subhedral, oscillatory sanidine up to 2 mm (7.5%), subhedral, oscillatory plagioclase up to 1 mm (1.5%), anhedral quartz up to 0.5 mm (0.8%), subhedral, oxidized biotite up to 1.5 mm (0.6%), an-subhedral clinopyroxene up to 0.5 mm (0.2%), sub-euhedral sphene < 0.5 mm (0.4%), trace Fe-Ti oxides up to 0.5 mm and trace zircon. Flattened, devitrified pumice (2.2%) is up to 1 cm in length. Basaltic, gabbroic and granodioritic rock fragments (0.8%) are up to 1 cm. The pale grayish pink-colored groundmass (86%) consists of devitrified glass and glass shards. Shards wrap around phenocrysts and lithic fragments.

Sample number: Mc62

Location: SE 1/4, Sec 31, T24S, R60E, Jean, Nev. 7 1/2' quad: collected approximately 1 mile S-SE from where the railroad tracks cross under Las Vegas Blvd.

Rock name: Welded dacitic ash-flow tuff

Description: Pyroclastic, eutaxitic and hypocrySTALLINE consisting of fragmented phenocrysts of subhedral, oscillatory sanidine up to 2 mm (4.2%), subhedral, oscillatory plagioclase up to 2 mm (2.8%), anhedral, oscillatory quartz up to 1 mm (1.2%), sub-euhedral, oxidized biotite up to 2 mm (1.0%), Fe-Ti oxides up to 0.5 mm (0.4%), subhedral clinopyroxene up to 2 mm (0.4%), sub-euhedral sphene < 0.5 mm (0.6%) and trace zircon. Pumice fiamme (1.4%) are devitrified and up to 2 cm. Basaltic and granitic rock fragments (1.2%) are up to several cm. The pale red-colored groundmass (86.8%) consists of devitrified glass and glass shards. Shards wrap around phenocrysts and lithic fragments.

Sample: Mc64b

Location: SW 1/4, Sec 2, T24S, R60E, Sloan, Nev. 7 1/2' quad: collected from the southernmost Tbs exposure west of I-15.

Rock name: Non-welded rhyolitic ash-flow tuff

Description: Pyroclastic and hypocrySTALLINE consisting of fragmented phenocrysts of subhedral, oscillatory sanidine up to 3 mm (6.0%), subhedral, oxidized biotite up to 1 mm (1.8%), anhedral, oscillatory quartz up to 1 mm (1.0%), subhedral, oscillatory plagioclase up to 1 mm (0.8%), an-subhedral clinopyroxene up to 0.5 mm (0.2%), sub-euhedral sphene up to 0.5 mm (0.2%), Fe-Ti oxides up to 0.5 mm (trace) and trace zircon. Spongy devitrified pumice (2.2%) is up to 2 cm. Basaltic rock fragments (1.8%) are up to several cm. The grayish pink-colored groundmass (86%) consists of devitrified glass and glass shards. Shards wrap around phenocrysts and lithic fragments.

Sample number: Mc66

Location: SE 1/4, Sec 35, T23S, R60E, Sloan, Nev. 7 1/2' quad: collected from the small Tbs exposure surrounded by Thvb: approximately 1,000' west of the railroad tracks.

Rock name: Partially-welded dacitic ash-flow tuff

Description: Pyroclastic and hypocrySTALLINE consisting of fragmented phenocrysts of subhedral, oscillatory sanidine up to 3 mm (5.4%), subhedral, oxidized biotite up to 1 mm (1.6%), anhedral, oscillatory quartz up to 1 mm (1.0%), subhedral, oscillatory plagioclase up to 1.5 mm (1.2%), an-subhedral clinopyroxene up to 1 mm (0.8%), sub-euhedral sphene up to 0.5 mm (0.4%), Fe-Ti oxides up to 0.5 mm (0.2%) and trace zircon. Flattened devitrified pumice (3.4%) is up to 3 cm long. Basaltic, granodioritic and gabbroic rock fragments (3.0%) are up to several cm. The pale pink-colored groundmass (83.0%) consists of devitrified glass and glass shards. Shards wrap around phenocrysts and lithic fragments.

Sample number: Mc67

Location: NW 1/4, Sec 35, T23S, R60E, Sloan, Nev. 7 1/2' quad: collected approximately 1 mile west of the cinder outcrop in the NW portion of the Tscp.

Rock name: Welded rhyolitic ash-flow tuff

Description: Pyroclastic, eutaxitic and hypocrySTALLINE consisting of fragmented phenocrysts of subhedral, oscillatory sanidine up to 3 mm (10.4%), subhedral, oscillatory plagioclase up to 1 mm (2.0%), anhedral, oscillatory quartz up to 1 mm (0.8%), Fe-Ti oxides up to 0.5 mm, an-subhedral clinopyroxene up to 0.5 mm and trace sphene & zircon (< 0.5 mm). Pumice fiamme are not present in the thin section, and occur only rarely in hand specimens. Basaltic, granodioritic and gabbroic rock fragments (7.2%) are up to 1 cm. The light brownish gray-colored groundmass (79.0%) consists of devitrified glass and glass shards. Shards wrap around phenocrysts and lithic fragments. Approximately 1% of the rock has been replaced by calcite.

Sample number: Mc68

Location: SW 1/4, Sec 36, T23S, R60E, Sloan, Nev. 7 1/2' quad: collected from the Tbs exposure between the railroad tracks and I-15.

Rock name: Welded rhyolitic ash-flow tuff

Description: Pyroclastic, eutaxitic and hypocrySTALLINE consisting of fragmented phenocrysts of an-subhedral, oscillatory sanidine up to 2 mm, (4.8%), anhedral, oscillatory plagioclase up to 2 mm (1.4%), sub-euhedral, oxidized biotite up to 1 mm (1.4%), an-subhedral clinopyroxene up to 0.5 mm (0.8%), anhedral, oscillatory quartz up to 1 mm (0.4%), Fe-Ti oxides up to 0.5 mm (0.4%), sub-euhedral sphene up to 0.5 mm (trace) and trace zircon. Devitrified and commonly spherulitic pumice fiamme (11.4%) are up to several cm. Basaltic and gabbroic rock fragments (9.6%) are up to 1 cm. The light brownish gray-colored groundmass (69.8%) consists of devitrified glass and glass shards. Shards wrap around phenocrysts and lithic fragments.

Sample number: Mc69

Location: SW 1/4, Sec 24, T23S, R60E, Sloan, Nev. 7 1/2' quad: collected from the northernmost Tbs exposure in the mapped area west of I-15.

Rock name: Welded rhyolitic ash-flow tuff

Description: Pyroclastic, eutaxitic and hypocrySTALLINE consisting of fragmented phenocrysts of subhedral, oscillatory sanidine up to 2 mm (7.0%), subhedral, oscillatory plagioclase up to 1 mm (5.0%), anhedral, oscillatory quartz up to 1 mm (1.2%), Fe-Ti oxides up to 0.5 mm (0.6%), sub-euhedral sphene < 0.5 mm (0.6%), subhedral, oxidized, subhedral biotite up to 2 mm (0.4%), an-subhedral clinopyroxene up to 3 mm (0.4%) and trace zircon. Devitrified pumice fiamme (0.2%) are up to several cm. Basaltic

and gabbroic rock fragments (1.0%) are up to 1 cm. The grayish red-colored groundmass (83.6%) consists of devitrified glass and glass shards. Shards wrap around phenocrysts and lithic fragments. Fractures are coated with calcite.

Sample number: Mc71

Location: NW 1/4, Sec 24, T23S, R60E, Sloan, Nev. 7 1/2' quad: collected approximately 1,000' N-NW of benchmark 2936 on the railroad tracks

Rock name: Welded rhyolitic ash-flow tuff

Description: Pyroclastic, eutaxitic and hypocrySTALLINE consisting of fragmented phenocrysts of subhedral, oscillatory sanidine up to 2 mm (10.6%), subhedral, oscillatory plagioclase up to 1 mm (3.0%), subhedral, oxidized biotite up to 1.5 mm (1.6%), anhedral, oscillatory quartz up to 1 mm (1.4%), an-subhedral clinopyroxene up to 1 mm (1.6%), sub-euhedral sphene < 0.5 mm (0.4%), trace Fe-Ti oxides up to 0.5 mm and trace zircon. Devitrified pumice fiamme (12.0%) are up to several cm. Basaltic and gabbroic rock fragments (2.0%) are up to 1 cm. The grayish red-colored groundmass (67.4%) consists of devitrified glass and glass shards. Shards wrap around phenocrysts and lithic fragments. Fractures are coated with calcite.

HIDDEN VALLEY VOLCANICS

Sample number: Mc1

Location: SE 1/4, Sec 26, Hidden Valley, Nev. 7 1/2' quad: collected approximately 800' south of the cattle guard on the western entrance road to Hidden Valley.

Rock name: Vesicular, pyroxene olivine basalt

Description: Vesicular, aphanitic and hypocrySTALLINE with phenocrysts of an-subhedral, iddingsitized olivine up to 1.5 mm (0.6%) and an-subhedral clinopyroxene up to 0.5 mm (0.3) in a black-colored, vesicular (11.0%) groundmass consisting of microlites of sub-euhedral plagioclase (44.3%), subhedral, iddingsitized olivine (14.0%), an-subhedral clinopyroxene (12.0%), Fe-Ti oxides (0.3%) and moderately devitrified glass (17.3%). Vesicles are coated with calcite.

Sample number: Mc3a

Location: NE 1/4, Sec 35, T24S, R60E, Hidden Valley, Nev. 7 1/2' quad: collected from the NW corner of the N-S trending Thvb ridge south of the western entrance road to Hidden Valley.

Rock name: Vesicular, pyroxene basalt

Description: Vesicular, aphanitic and hypocrySTALLINE with phenocrysts of embayed, resorbed, an-euhedral clinopyroxene up to 1.5 mm (1.0%), commonly in glomerocrysts. The grayish red-colored, vesicular (8.2%) groundmass

consists of microlites of sub-euhedral, oscillatory plagioclase (55.0%), an-subhedral clinopyroxene (19.0%), granular hematite (13.4%: replacing clinopyroxene), Fe-Ti oxides (2.6%) and glass (0.8%). Vesicles are coated with calcite.

Sample number: Mc35

Location: NW 1/4, Sec 23, T24S, R61E, Hidden Valley, Nev. 7 1/2' quad: collected from the isolated Thvb outcrop in the southern portion of the Tsh dome field: on the southern side of the entrance to the major drainage separating Tss from Tsh.

Rock name: Vesicular, pyroxene olivine basalt

Description: Porphyritic, vesicular and hypocrystalline with phenocrysts of subhedral, iddingsitized olivine up to 2 mm (9.8%), subhedral, pitted, embayed and oscillatory plagioclase up to 1 mm (2.2%) and subhedral clinopyroxene up to 0.5 mm (0.8%). Quartz xenocrysts are up to 4 mm and rimmed with glass and cryptocrystalline clinopyroxene(?) (0.6%). The medium dark gray-colored, vesicular (2.6%) groundmass consists of microlites of sub-euhedral, oscillatory plagioclase (58.4%), subhedral clinopyroxene (9.2%), subhedral, iddingsitized olivine (9.8%), subhedral clinopyroxene (9.2%), Fe-Ti oxides (6.2%) and glass (0.4%). Vesicles are coated with calcite.

Sample number: Mc37

Location: SE 1/4, Sec 22, T24S, R61E, Hidden Valley, Nev. 7 1/2' quad: collected 2100' south of sample Mc35.

Rock name: Vesicular, pyroxene olivine basalt

Description: Porphyritic, vesicular and hypocrystalline with phenocrysts of sub-euhedral, iddingsitized olivine up to 2 mm (7.6%), sub-euhedral, pitted and embayed clinopyroxene up to 1 mm (1.4%) and subhedral, pitted, embayed and oscillatory plagioclase up to 2 mm (1.0%). Quartz xenocrysts are up to 5 mm and rimmed with glass (6.0%). The medium dark gray-colored, vesicular (1.2%) groundmass consists of microlites of sub-euhedral, oscillatory plagioclase (57.0%), subhedral, iddingsitized olivine (8.2%), sub-euhedral clinopyroxene (11.6%), Fe-Ti oxides (6.2%) and glass (0.8%).

Sample number: Mc40b

Location: E 1/4, Sec 27, T24S, R61E, Hidden Valley, Nev. 7 1/2' quad: collected from the small isolated Thvb outcrop on the W border of the Tsh dome complex.

Rock name: Vesicular, pyroxene olivine basalt

Description: Porphyritic, vesicular and hypocrystalline with commonly pitted and embayed phenocrysts of an-subhedral, iddingsitized olivine up to 1 mm (6.3%) and sub-euhedral, oscillatory plagioclase up to 1 mm (3.3%). Quartz xenocrysts are up to 5 mm and rimmed with glass and fine-grained

clinopyroxene (2.6%). The vesicular (9.3%), brownish black-colored groundmass consists of microlites of sub-euhedral, oscillatory plagioclase (58.3%), an-subhedral clinopyroxene (7.3%), an-subhedral, iddingsitized olivine (7.3%), Fe-Ti oxides (2.0%) and glass.

Sample number: Mc42

Location: SW 1/4, Sec 26, T24S, R61E, Hidden Valley, Nev. 7 1/2' quad: collected from the small isolated Thvb outcrop on the NE side of major drainage on the SW Tsh dome complex border.

Rock name: Vesicular, olivine pyroxene basalt

Description: Vesicular, porphyritic and holocrystalline with commonly pitted and embayed phenocrysts of an-euhedral, mildly iddingsitized olivine up to 2 mm (5.6%), an-subhedral, up to 1 mm, commonly glomerocrystic clinopyroxene (4.0%) and sub-euhedral, oscillatory plagioclase up to 1 mm (1.0%). Quartz xenocrysts are up to 5 mm and rimmed with glass (< 1%). The vesicular (3.6%), black-colored groundmass consists of microlites of sub-euhedral, oscillatory plagioclase (62%), an-subhedral clinopyroxene (11.6%), an-euhedral, iddingsitized olivine (5.3%) and Fe-Ti oxides (6.6%).

Sample number: Mc43

Location: NW 1/4, Sec 34, T24S, R61E, Hidden Valley, Nev. 7 1/2' quad: collected from the east side of the N-S trending Thvb ridge in the south-central part of the mapped area.

Rock name: Vesicular, olivine pyroxene basalt

Description: Vesicular, porphyritic and hypocrySTALLINE with commonly pitted and embayed phenocrysts of an-subhedral, up to 1 mm, commonly glomerocrystic clinopyroxene (10.0%), an-subhedral, iddingsitized, up to 1 mm, commonly glomerocrystic olivine (6%) and sub-euhedral, oscillatory plagioclase up to 1 mm (1.0%). The vesicular (3.4%) grayish black-colored groundmass consists of microlites of sub-euhedral, oscillatory plagioclase (58.9%), an-subhedral clinopyroxene (8.8%), an-subhedral, iddingsitized olivine (5.4%), Fe-Ti oxides (3.6%) and glass (3.0%). Vesicles are commonly coated with calcite.

Sample number: Mc47

Location: E 1/4, Sec 30, T23S, R61E, Sloan, Nev. 7 1/2' quad: collected from the isolated Thvb outlier just west of the Pzcu outcrop in the NW portion of the mapped area.

Rock name: Vesicular, olivine pyroxene basalt

Description: Porphyritic, vesicular and holocrystalline with commonly pitted and embayed phenocrysts of an-subhedral, up to 1 mm, commonly glomerocrystic clinopyroxene (10.8%), subhedral, oxidized phlogopite up to 2 mm (3.6%), anhedral, up to 1 mm, commonly glomerocrystic plagioclase up to 1 mm, (0.4%) and an-subhedral, iddingsitized olivine up to 1 mm

(0.4%). The vesicular (8.2%), dark gray-colored groundmass consists of microlites of sub-euhedral, oscillatory plagioclase (50.2%), Fe-Ti oxides (10.4%), an-subhedral clinopyroxene (7.4%), granular hematite (probably replaced phlogopite, 6.4%) and subhedral, iddingsitized olivine (2.2%). Vesicles are commonly coated or filled with calcite and/or quartz.

Sample number: Mc48

Location: SE 1/4, Sec 30, T23S, R61E, Sloan, Nev. 7 1/2' quad: collected from the northern part of the Thvb exposure in the NW part of the mapped area.

Rock name: Vesicular, olivine pyroxene basalt

Description: Porphyritic, vesicular and holocrystalline with commonly pitted and embayed phenocrysts of subhedral, oxidized phlogopite up to 2 mm (4.8%), subhedral, up to 1.5 mm, commonly glomerocrystic with olivine, clinopyroxene (4.6%) and subhedral, up to 1 mm, commonly glomerocrystic with clinopyroxene, olivine (1.2%). The vesicular (10.4%), brownish black-colored groundmass consists of microlites of subhedral, oscillatory plagioclase (58.6%), subhedral clinopyroxene (7.2%), Fe-Ti oxides (7.2%) and an-euhedral, iddingsitized olivine (6.0%). Vesicles are commonly coated with calcite.

Sample number: Mc87.

Location: SE 1/4, Sec 28, T24S, R61E, Hidden Valley, Nev. 7 1/2' quad: collected on the west side of the N-S trending Thvb ridge in the S-central part of the mapped area.

Rock name: Pyroxene olivine basalt

Description: Aphanitic, trachytic and hypocrySTALLine with pitted, embayed, oscillatory, fritted sub-euhedral plagioclase phenocrysts up to 1 mm (0.8%). The brownish black-colored groundmass consists of sub-parallel microlites of sub-euhedral, oscillatory plagioclase (72.4%), an-subhedral, iddingsitized olivine (17.4%), an-subhedral clinopyroxene (8.0%), Fe-Ti oxides (0.4%) and glass (1.0%).

Sample number: Mc108

Location: Collected from the basaltic dike in the Thvb on the eastern escarpment of the McCullough's, approximately 3,000' S-SE of peak 3912.

Rock name: Vesicular, olivine pyroxene basaltic dike

Description: Vesicular, porphyritic and holocrystalline consisting of phenocrysts of subhedral, oscillatory plagioclase up to 3 mm (13.2%), subhedral, embayed clinopyroxene up to 1 mm (1.6%), an-subhedral, iddingsitized olivine up to 1 mm (1.4%) and Fe-Ti oxides up to 0.5 mm (0.5%). The vesicular (18.2%), medium dark gray-colored groundmass consists of microlites of sub-euhedral, oscillatory plagioclase (16.8%), subhedral clinopyroxene

(3.8%), an-subhedral, iddingsitized olivine (1.4%), granular hematite (0.2%) and Fe-Ti oxides (0.3%).

Sample number: W-hvb

Location: NW 1/4, Sec 36, T23S, R60E, Sloan, Nev. 7 1/2' quad: collected from the northernmost Thvb exposure associated with Tbs on the west side of I-15.

Rock name: Weakly vesicular, olivine pyroxene basalt

Description: Weakly vesicular, porphyritic and hypocrystalline consisting of commonly pitted and embayed phenocrysts of an-subhedral, oscillatory plagioclase up to 5 mm (18.4%), an-subhedral, iddingsitized olivine up to 5 mm (11.4%), an-subhedral clinopyroxene up to 5 mm (9.6%) and Fe-Ti oxides up to 0.5 mm (0.5%). Approximately 10% of the clinopyroxene, olivine and plagioclase phenocrysts occur in glomerocrysts with each other. The weakly vesicular (1.6%), black-colored groundmass consists of microlites of sub-euhedral, oscillatory plagioclase (30.2%), an-subhedral clinopyroxene (5.6%), an-subhedral, iddingsitized olivine (1.4%), Fe-Ti oxides (0.5%) and devitrified glass (20.8%). Vesicles are coated with calcite.

MT. HANNA ANDESITE

Sample number: Mc31b

Location: SE 1/4, Sec 14, T24S, R61E, Sloan SE, Nev. 7 1/2' quad: collected at the southernmost Tss/Tsh contact.

Rock name: Andesite

Description: Fine-grained, trachytic and hypocrystalline consisting of sub-parallel, sub-euhedral plagioclase laths (< 0.5 mm) with subordinate interstitial devitrified glass, Fe-Ti oxides and cryptocrystalline, high birefringent minerals. Trace, subhedral, pitted, embayed, zoned and oscillatory plagioclase phenocrysts (up to 1 mm) occur. The groundmass is very dusky red with moderate red-colored streaks.

Sample number: Mc110

Location: T24S, R62E, Sloan SE, Nev. 7 1/2' quad: collected on peak 3912 near the Tsh/Thvb contact on the eastern escarpment of the McCullough's.

Rock name: Andesite

Description: Fine-grained, trachytic and hypocrystalline consisting of sub-parallel, sub-euhedral plagioclase laths (<0.5 mm) with subordinate interstitial devitrified glass and Fe-Ti oxides. Trace, subhedral, pitted, embayed, zoned and oscillatory plagioclase phenocrysts up to 1 mm occur. The slide also contains a subhedral, oxidized, 3 mm biotite phenocryst. The weakly vesicular (< 1.0%) groundmass is black.

Sample number: Mc112

Location: 800' east, 2400' north of the SE corner of Sec 12, T24S, R61E, Sloan SE, Nev. 7 1/2' quad: collected near entrance to the major drainage in the northern part of the Tsh dome complex.

Rock name: Andesite

Description: Fine-grained, trachytic and hypocrySTALLINE consisting of sub-parallel, sub-euhedral plagioclase laths (< 0.5 mm) with subordinate interstitial devitrified glass and Fe-Ti oxides. Trace, subhedral, pitted, embayed, zoned and oscillatory plagioclase phenocrysts up to 1 mm occur. The weakly vesicular (< 1%), groundmass is dark gray with medium light gray-colored streaks.

Sample number: Mc115

Location: NW 1/4, Sec 36, T24S, R61E, Sloan SE, Nev. 7 1/2' quad: collected on the ridge just to the SE of the major Tsh vent area.

Rock name: Andesite

Description: Fine-grained, massive and hypocrySTALLINE consisting of sub-euhedral plagioclase laths (< 0.5 mm) with subordinate interstitial partially devitrified glass, granular hematite and Fe-Ti oxides. The slide contains two pitted, embayed, sub-euhedral plagioclase xenocrysts (1.5 mm). The groundmass is black with grayish red-colored streaks.

CINDER PROSPECT MEMBER

Sample number: Mc25

Location: SW 1/4, Sec 5, T24S, R61E, Sloan, Nev. 7 1/2' quad: dacite underlying Tsi on south-facing hillside one mile east of the Mt. Ian vent.

Rock name: Dacite

Description: Glomeroporphyritic: glomerocrysts form approximately 2% of the rock and consist of commonly pitted and embayed phenocrysts of zoned, oscillatory, sub-euhedral plagioclase up to 2 mm and subordinate sub-euhedral, oxidized biotite up to 2 mm. Individual phenocrysts form approximately 2% of the rock and consist of the same minerals found in the glomerocrysts. The medium gray-colored groundmass consists of microlites of plagioclase with trace biotite, Fe-Ti oxides, zircon and glass. Approximately 40% of the groundmass has been replaced by calcite.

Sample number: Mc78

Location: SE 1/4, Sec 6, T24S, R61E, Sloan, Nev. 7 1/2' quad: vitrophyre on the ridge approximately 1,750' SE of the Mt. Ian Tsi vent center

Rock name: Dacite vitrophyre

Description: Porphyritic and hypohyaline with commonly fragmented, pitted and embayed phenocrysts of sub-euhedral, oscillatory and seriate up to 2 mm plagioclase (12.0%), sub-euhedral, oxidized and seriate up to 2 mm biotite

(3.8%), sub-euhedral, oscillatory and seriate up to 2 mm sanidine (3.4%), Fe-Ti oxides seriate up to 0.5 mm (0.4) and trace zircon. Basaltic, gabbroic and granodioritic rock fragments (5.6%) are up to 1 cm. The mottled dark reddish brown and black-colored groundmass (74.6) consists of devitrified glass and glass shards.

Sample number: Mc79

Location: NE 1/4, Sec 6, T24S, R61E, Sloan, Nev. 7 1/2' quad: glassy, resistant vitrophyre that crops out in the NE part of Tscp.

Rock name: Rhyolite vitrophyre

Description: Porphyritic and hypohyaline with commonly fragmented, pitted and embayed phenocrysts of subhedral, oscillatory and seriate up to 1 mm plagioclase (17.4%), subhedral, oscillatory and seriate up to 1 mm sanidine (3.8%), sub-euhedral, oxidized and seriate up to 2 mm biotite (3.6%), Fe-Ti oxides seriate up to 0.5 mm (1.2%), trace sub-euhedral clinopyroxene up to 0.5 mm and trace zircon. Trace basaltic rock fragments are up to 1 mm. The mottled dark reddish brown and black-colored groundmass (74.0%) consists of devitrified glass and glass shards with trace granular hematite.

Sample number: Mc121

Location: SW 1/4, Sec 31, T23S, R61E, Sloan, Nev. 7 1/2' quad: dacite that lies stratigraphically immediately below Tts.

Rock name: Biotite dacite

Description: Glomeroporphyritic: glomerocrysts form approximately 4% of the rock and consist of commonly pitted and embayed phenocrysts of zoned, oscillatory, subhedral plagioclase up to 2 mm with subordinate subhedral hematized biotite up to 2 mm. Individual phenocrysts form approximately 6% of the rock and consist of the same minerals found in the glomerocrysts and trace Fe-Ti oxides up to 0.5 mm. The light brownish gray-colored groundmass consists of microlites of plagioclase with trace hematized biotite, Fe-Ti oxides and glass. Approximately 1% of the groundmass has been replaced by calcite.

Sample number: Mc125

Location: S 1/4, Sec 31, T23S, R61E, Sloan, Nev. 7 1/2' quad: dacite from the Cinder Prospect Member, below the Sloan Tuff.

Rock name: Biotite dacite

Description: Glomeroporphyritic: glomerocrysts form approximately 6% of the rock and consist of commonly pitted and embayed phenocrysts of zoned, oscillatory, subhedral plagioclase up to 3 mm with subordinate Fe-Ti oxides up to 0.5 mm and subhedral biotite up to 3 mm that ranges from unaltered to totally replaced by red and black Fe oxides. Individual phenocrysts form approximately 5% of the rock and consist of the same minerals found in the glomerocrysts. The medium light gray-colored groundmass consists of

microlites of plagioclase with subordinate oxidized biotite, trace zircon and glass. Approximately 5% of the groundmass has been replaced by calcite.

TUFF OF THE SLOAN VOLCANICS

Sample number: Mc59a

Location: SW 1/4, Sec 31, T24S, R61E, Sloan, Nev. quad: collected from the bottom cooling unit in the drainage at station 59 in the Tsc dome complex.

Rock name: Welded rhyolitic ash-flow tuff

Description: Pyroclastic, eutaxitic and hypocrySTALLINE consisting of fragmented phenocrysts of subhedral sanidine up to 3 mm (21.2%), subhedral, zoned and oscillatory plagioclase up to 2 mm (4.8%), sub-euhedral, oxidized biotite up to 1.5 mm (0.4%), Fe-Ti oxides up to 0.5 mm (< 1%), sub-euhedral sphene (< 0.5 mm, 0.2%) and trace amounts of clinopyroxene, monazite, epidote, allanite, and zircon (each < 0.5 mm). Pumice fiamme (9%) are up to several cm long, devitrified and rarely spherulitic. Basaltic and gabbroic rock fragments (3.8%) are up to 1 cm. The grayish red-colored groundmass (60.6%) consists of devitrified glass shards that wrap around phenocrysts and lithic fragments.

Sample number: Mc59b

Location: SW 1/4, Sec 31, T24S, R61E, Sloan, Nev. quad: collected from the middle cooling unit in the drainage at station 59 in the Tsc dome complex.

Rock name: Non-welded dacitic ash-flow tuff

Description: Pyroclastic and hypocrySTALLINE consisting of fragmented phenocrysts of an-subhedral, oscillatory sanidine up to 2.5 mm (4.8%), subhedral, oscillatory plagioclase up to 1.5 mm (2.0%), subhedral, oxidized biotite up to 1 mm (0.8%), an-subhedral clinopyroxene up to 0.5 mm (0.2%), sub-euhedral sphene up to 0.5 mm (0.2%), Fe-Ti oxides up to 0.5 mm (< 1%) and trace zircon. Spongy, devitrified, rarely spherulitic pumice (2.2%) is up to 1 cm. Basaltic and gabbroic rock fragments (13.2%) are up to 1 cm. The very light gray-colored groundmass (76.4%) consists of devitrified, axiolitic glass shards that wrap around phenocrysts and lithic fragments.

Sample number: Mc59c

Location: SW 1/4, Sec 31, T24S, R61E, Sloan, Nev. quad: collected from the top cooling unit in the drainage at station 59 in the Tsc dome complex.

Rock name: Welded dacitic ash-flow tuff

Description: Pyroclastic, eutaxitic and hypocrySTALLINE consisting of fragmented phenocrysts of subhedral, oscillatory sanidine up to 4 mm (8.6%), subhedral, oscillatory plagioclase up to 1 mm (2.4%), Fe-Ti oxides up to 0.5 mm (1.4%), anhedral quartz < 0.5 mm (0.4%), an-subhedral clinopyroxene up to 0.5 (1.4%), subhedral, oxidized biotite up to 2 mm (0.4%) and trace zircon. Pumice fiamme (11.6%) are up to several cm

long. Basaltic and gabbroic rock fragments (21.2%) are up to 2 cm. The pale red-colored groundmass (52.6%) consists of blocky shaped, slightly devitrified glass shards.

Sample number: Mc73

Location: NW 1/4, Sec 6, T24S, R61E, Sloan, Nev. 7 1/2' quad: collected in drainage just west of the Sta. 59 tuffs.

Rock name: Non-welded rhyolitic ash-flow tuff

Description: Pyroclastic and hypocrySTALLINE consisting of fragmented phenocrysts of subhedral, oscillatory sanidine up to 3 mm (10.0%), anhedral quartz up to 1 mm (1.8%), an-subhedral, oscillatory plagioclase up to 3 mm (3.4%), subhedral, oxidized biotite up to 1 mm (0.6%), Fe-Ti oxides up to 0.5 mm (0.2%), trace, an-subhedral, hematized clinopyroxene up to 0.5 mm and trace amounts of sphene and zircon (sub-euhedral, < 0.5 mm). Spongy, devitrified pumice (1.6%) is up to 1 cm. Basaltic, gabbroic and granodioritic rock fragments (4.6%) are up to 1 cm. The grayish pink-colored groundmass (77.8%) consists of devitrified, weakly axiolitic glass shards, interstitial glass and < 1% yellow Fe oxides.

CENTER MTN. DACITE

Sample number: Mc59d

Location: N 1/2, Sec 6, T23S, R61E, Sloan, Nev. 7 1/2' quad: dacite that lies stratigraphically immediately above Tts.

Rock name: Biotite dacite

Description: Glomeroporphyritic: glomerocrysts form approximately 3% of the rock and consist of commonly pitted and embayed phenocrysts of subhedral plagioclase up to 2 mm with subordinate Fe-Ti oxides and sub-euhedral, oxidized biotite up to 2 mm. Phenocrysts form approximately 3% of the rock and consist of the same minerals found in the glomerocrysts. The medium light gray-colored groundmass consists of microlites of plagioclase with subordinate hematized biotite, Fe-Ti oxides and glass. Approximately 5% of the groundmass has been replaced by calcite.

Sample number: Mc130

Location: SW 1/4, Sec 31, T23S, R60E, Sloan, Nev. 7 1/2' quad: dacite overlying Tscp in the NW section of the Center Mtn. dome complex.

Rock name: Biotite dacite

Description: Holocrystalline, and porphyritic with phenocrysts of sub-euhedral, zoned and oscillatory plagioclase up to 2 mm (4.4%), sub-euhedral, oxidized biotite up to 5 mm (1.2%) and sub-euhedral Fe-Ti oxides < 0.5 mm (0.4%). The medium gray-colored groundmass consists of microlites of plagioclase with subordinate oxidized biotite, Fe-Ti oxides and pyroxene(?), and secondary calcite (5%).

Sample number: Mc131

Location: SW 1/4, Sec 6, T24S, R61E, Sloan, Nev. 7 1/2' quad: dacite overlying Tscp in the southern part of the Center Mtn. dome complex.

Rock name: Biotite dacite

Description: Holocrystalline, porphyritic and trachytic with sub-parallel phenocrysts of sub-euhedral, zoned and oscillatory plagioclase up to 2 mm (7.2%), sub-euhedral, oxidized biotite up to 3 mm (1.6%) and sub-euhedral Fe-Ti oxides < 0.5 mm (0.4%). The medium light gray-colored groundmass consists of microlites of plagioclase with subordinate oxidized biotite, Fe-Ti oxides and pyroxene(?), and secondary calcite (1.2%).

MT. IAN ANDESITE

Sample number: Mc93

Location: SW 1/4, Sec 5, T24S, R61E, Sloan, Nev. 7 1/2' quad: andesite that overlies dacite on the hill 1 mile east of Mt. Ian: stratigraphically above Mc25 biotite dacite.

Rock name: Andesite

Description: Fine-grained and hypocrySTALLINE consisting of commonly pitted and embayed phenocrysts of sub-euhedral, zoned and oscillatory plagioclase up to 1 mm (5.2%), subhedral iddingsitized olivine up to 0.5 mm (0.4%), sub-euhedral, commonly oxidized subhedral biotite up to 1 mm (0.4%), Fe-Ti oxides up to 1 mm and trace subhedral orthopyroxene up to 0.5 mm. The orthopyroxene commonly occurs in glomerocrysts with plagioclase and Fe-Ti oxides. The medium dark gray-colored, weakly vesicular groundmass consists of microlites of plagioclase with trace biotite, olivine, Fe-Ti oxides and glass. Vesicles are coated with calcite.

Sample number: Mc94

Location: N 1/4, Sec 5, T24S, R61E, Sloan, Nev. 7 1/2' quad: from the hilltop 1 mile east of the Tuff of the Sloan Volcanics at station 59.

Rock name: Andesite

Description: Vesicular, fine-grained and hypocrySTALLINE consisting of commonly pitted and embayed phenocrysts of zoned, oscillatory, sub-euhedral plagioclase up to 0.5 mm (2.4%), Fe-Ti oxides up to 0.25 mm (4%), subhedral, iddingsitized olivine up to 0.5 mm (0.4%) and trace subhedral oxidized biotite up to 0.5 mm. The vesicular (9.6%), grayish red-colored groundmass consists of microlites of plagioclase (72.8%), iddingsitized olivine (3.0%) and glass (0.6%). 7.0% of the groundmass has been replaced by hematite. Vesicles are coated with calcite.

Sample number: Mc95a

Location: NE 1/4, Sec 5, T24S, R61E, Sloan, Nev. 7 1/2' quad: massive andesite from hill 3346 just west of the major drainage separating Tsi from Tss.

Rock name: Andesite

Description: Fine-grained and hypocrySTALLINE consisting of commonly pitted and embayed phenocrysts of zoned, oscillatory, sub-euhedral plagioclase up to 1 mm (5.6%), an-subhedral chloritized(?) and oxidized biotite up to 1 mm (10.4%) and subhedral orthopyroxene up to 0.5 mm (trace) that commonly occurs in glomerocrysts with plagioclase and Fe-Ti oxides. The black-colored groundmass consists of microlites of plagioclase (74.0%), clinopyroxene (0.2%), iddingsitized olivine (0.6%), Fe-Ti oxides (4.6%), zircon (trace) and devitrified glass (4.6%).

Sample number: Mc95b

Location: NE 1/4, Sec 5, T24S, R61E, Sloan, Nev. 7 1/2' quad: platy andesite from hill 3346 just west of the major drainage separating Tsi from Tss: lies stratigraphically below the more massive Mc95a andesite.

Rock name: Andesite

Description: Fine-grained and hypocrySTALLINE consisting of commonly pitted and embayed phenocrysts of zoned, oscillatory, sub-euhedral plagioclase up to 1 mm (4.0%), sub-euhedral oxidized biotite up to 2 mm (0.4%), Fe-Ti oxides up to 0.5 mm (0.2%) and subhedral orthopyroxene up to 0.5 mm (trace) that commonly occurs in glomerocrysts with plagioclase and Fe-Ti oxides. The dusky brown-colored, weakly vesicular (0.4%) groundmass consists of microlites of plagioclase (68.4%), iddingsitized olivine (3.0%), Fe-Ti oxides (4.0%), biotite (trace) and devitrified glass (19.8%). The slide contains a granodiorite xenolith 1.5 mm by 1 mm. Vesicles are coated with calcite.

Sample number: Mc97

Location: NW 1/4, Sec 4, T23S, R61E, Sloan, Nev. 7 1/2' quad: collected from the Tsi ridge-top in the NW part of the northern Tss dacite dome complex.

Rock name: Andesite

Description: Fine-grained, weakly vesicular and hypocrySTALLINE consisting of commonly pitted and embayed phenocrysts of zoned, oscillatory, sub-euhedral plagioclase up to 1 mm (4.4%), an-subhedral, iddingsitized olivine up to 0.5 mm (2.0%), subhedral, oxidized biotite up to 0.5 mm (trace), Fe-Ti oxides up to 0.5 mm (2.0%) and subhedral orthopyroxene up to 0.5 mm (0.2%) that commonly occurs in glomerocrysts with Fe-Ti oxides. The black-colored, weakly vesicular (1.8%) groundmass consists of microlites of plagioclase (57.0%), iddingsitized olivine (2.2%), clinopyroxene (0.2%), Fe-Ti oxides (0.6%) and devitrified glass (29.4%).

Sample number: Mc98

Location: SE 1/4, Sec 6, T24S, R61E, Sloan, Nev. 7 1/2' quad: collected from the Tsi dome in the SE part of the Tsc dome complex.

Rock name: Andesite

Description: Fine-grained, weakly vesicular and hypocrySTALLINE consisting of commonly pitted and embayed phenocrysts of zoned, oscillatory, sub-euhedral plagioclase up to 0.5 mm (4.6%), an-subhedral, iddingsitized olivine up to 0.5 mm (0.5%), Fe-Ti oxides up to 0.5 mm (2.0%) and sub-euhedral, oxidized biotite up to 0.5 mm (trace). The medium dark gray-colored, weakly vesicular (0.8%) groundmass consists of microlites of plagioclase (79.0%), iddingsitized olivine (4.1%), Fe-Ti oxides (3.4%) and devitrified glass (1.8%). Sericite (3.8%) is replacing plagioclase. The vesicles are coated with calcite.

Sample number: Mc120a

Location: S 1/4, Sec 6, T24S, R61E, Sloan, Nev. 7 1/2' quad: andesite collected from the Mt. Ian vent.

Rock name: Andesite

Description: Fine-grained and hypocrySTALLINE consisting of commonly pitted and embayed phenocrysts of zoned, oscillatory, sub-euhedral, seriate plagioclase up to 1 mm (31.8%), sub-euhedral orthopyroxene up to 0.5 mm (1.2%), Fe-Ti oxides up to 0.5 mm (1.5%) and subhedral, oxidized biotite up to 0.5 mm (0.2%). The grayish black-colored groundmass consists of microlites of plagioclase (50%), orthopyroxene (trace), biotite (0.6%), Fe-Ti oxides (2.1%) and devitrified glass (9.8%). Veins of fine to medium-grained quartz forms 2% of the rock.

Sample number: Mc129

Location: NE 1/4, Sec 4, T24S, R61E, Sloan, Nev. 7 1/2' quad: andesite that underlies Tss on the east side of drainage in the NW part of the northern Tss dome complex.

Rock name: Andesite

Description: Fine-grained, weakly vesicular and hypocrySTALLINE consisting of commonly pitted and embayed phenocrysts of zoned, oscillatory, sub-euhedral, seriate plagioclase up to 2 mm (30.8%), sub-euhedral, iddingsitized olivine up to 0.5 mm (0.2%), Fe-Ti oxides up to 0.5 mm (0.2%) and sub-euhedral orthopyroxene up to 0.5 mm (trace). The weakly vesicular (1.0%), dark gray-colored groundmass consists of microlites of plagioclase (49%), iddingsitized olivine (0.6%) and Fe-Ti oxides (0.8%). Vesicles are coated with calcite.

MT. SUTOR DACITE

Sample number: Mc9

Location: E 1/2, Sec 26, T24S, R60E, Hidden Valley, Nev. 7 1/2' quad: at the Tss/Thvb contact near the western entrance road to Hidden Valley.

Rock name: Biotite dacite

Description: Glomeroporphyritic: glomerocrysts form approximately 10% of the rock and are composed of commonly pitted and embayed phenocrysts of zoned, oscillatory, sub-euhedral plagioclase up to 3 mm with subordinate sub-euhedral biotite up to 3 mm and Fe-Ti oxides up to 0.5 mm. Individual phenocrysts form approximately 2% of the rock and consist of the same minerals found in the glomerocrysts, but many are not pitted and embayed. The medium gray-colored groundmass consists of microlites of plagioclase with trace biotite and Fe-Ti oxides, devitrified glass, and < 1% vesicles. Vesicles and fractures are coated with secondary calcite.

Sample number: Mc16

Location: SW 1/4, Sec 14, T24S, R60E, Hidden Valley, Nev. 7 1/2' quad: near the Tss/Pzcu contact on the western margin of the southern dacite dome complex.

Rock name: Biotite dacite

Description: Glomeroporphyritic: glomerocrysts form approximately 7% of the rock and are composed of commonly pitted and embayed phenocrysts of zoned, oscillatory, sub-euhedral plagioclase up to 3 mm with subordinate an-subhedral orthopyroxene up to 1 mm and Fe-Ti oxides up to 0.5 mm. Individual phenocrysts form approximately 5% of the rock and consist of the same minerals found in the glomerocrysts, plus an-subhedral pitted and embayed, oxidized biotite (1.4%). Many of the individual phenocrysts do not show the disequilibrium textures displayed in the glomerocrysts. The mottled medium gray and medium dark gray-colored groundmass consists of microlites of plagioclase with trace biotite, orthopyroxene and glass.

Sample number: Mc19

Location: NE 1/4, Sec 13, T24S, R60E, Hidden Valley, Nev. 7 1/2' quad: from the NW portion of the southern dacite dome complex.

Rock name: Vesicular biotite dacite

Description: Glomeroporphyritic: glomerocrysts form approximately 2% of the rock and are composed of commonly pitted and embayed phenocrysts of zoned, oscillatory, sub-euhedral plagioclase up to 2 mm with subordinate subhedral orthopyroxene up to 1 mm, subhedral biotite < 0.5 mm and Fe-Ti oxides up to 0.5 mm. Individual phenocrysts form 9.8% of the rock and consist of the same minerals found in the glomerocrysts, plus sub-euhedral, pitted and embayed, oxidized biotite (2.2%) up to 1 mm. The vesicular (11.8%) black-colored groundmass consists of microlites of plagioclase with trace biotite, Fe-Ti oxides, iddingsitized olivine, and glass. Vesicles and fractures are coated with secondary calcite.

Sample number: Mc21

Location: N 1/2, Sec 20, T24S, R61E, Hidden Valley, Nev. 7 1/2' quad: isolated outlier near the eastern margin of the southern dacite dome complex.

Rock name: Vesicular biotite dacite

Description: Glomeroporphyritic: glomerocrysts form approximately 15% of the rock and are composed of commonly pitted and embayed phenocrysts of zoned, oscillatory, sub-euhedral plagioclase up to 3 mm with subordinate subhedral biotite up to 3 mm and Fe-Ti oxides up to 0.5 mm. Individual phenocrysts form approximately 3.5% of the rock and consist of the same minerals found in the glomerocrysts. The vesicular (3.8%) dark gray-colored groundmass consists of microlites of plagioclase with trace biotite, clinopyroxene, olivine and glass.

Sample number: Mc 27

Location: SW 1/4, Sec 10, T24S, R61E, Hidden Valley, Nev. 7 1/2' quad: on NW side of the entrance to the major drainage near the hypabyssal phase Tss.

Rock name: Biotite dacite

Description: Glomeroporphyritic: glomerocrysts for approximately 18% of the rock and are composed of commonly pitted and embayed phenocrysts of zoned, oscillatory, sub-euhedral plagioclase up to 4 mm, with subordinate Fe-Ti oxides up to 0.5 mm, sub-euhedral biotite up to 4 mm, and subhedral clinopyroxene up to 2 mm that is commonly rimmed with black Fe oxides. Individual phenocrysts form approximately 4.5% of the rock and consist of the same minerals found in the glomerocrysts, plus < 1% anhedral hornblende up to 0.5 mm that is rimmed with black Fe oxides. The dark gray-colored weakly vesicular (1.2%) groundmass consists of microlites of plagioclase with trace biotite and glass. Vesicles are coated with secondary calcite.

Sample number: Mc28

Location: N 1/4, Sec 10, T24S, R61E, Hidden Valley, Nev. 7 1/2' quad: isolated outlier in the mouth of the major drainage near hypabyssal phase Tss.

Rock name: Biotite dacite

Description: Glomeroporphyritic: glomerocrysts for approximately 10% of the rock and are composed of commonly pitted and embayed phenocrysts of zoned, oscillatory, sub-euhedral plagioclase up to 2 mm, and subordinate subhedral clinopyroxene up to 1 mm and oxidized biotite up to 3 mm. Individual phenocrysts form approximately 2% of the rock and consist of the same minerals found in the glomerocrysts. The medium gray-colored groundmass consists of microlites of plagioclase with trace Fe-Ti oxides and glass. Calcite has replaced approximately 5% of the groundmass.

Sample number: Mc31a

Location: SE 1/4, Sec 14, T24S, R61E, Sloan SE, Nev. 7 1/2' quad: at the southernmost Tss/Tsh contact.

Rock name: Biotite dacite

Description: Glomeroporphyritic: glomerocrysts form approximately 7% of the rock and are composed of commonly pitted and embayed phenocrysts of zoned, oscillatory, sub-euhedral plagioclase up to 2 mm, and subordinate subhedral, oxidized biotite up to 3 mm, an-subhedral clinopyroxene up to 1 mm, Fe-Ti oxides up to 0.5 mm and trace anhedral orthopyroxene up to 0.5 mm. Individual phenocrysts form approximately 5% of the rock and consist of the same minerals found in the glomerocrysts. The dark gray-colored groundmass consists of microlites of plagioclase with trace biotite and Fe-Ti oxides and glass. Fractures are rarely coated with calcite.

Sample number: Mc91a

Location: NW 1/4, Sec 19, T24S, R61E, Hidden Valley, Nev. 7 1/2' quad: dacite vent center in the east-central part of the southern dacite dome complex.

Rock name: Biotite dacite

Description: Glomeroporphyritic: glomerocrysts form approximately 5% of the rock and are composed of commonly pitted and embayed phenocrysts of zoned, oscillatory, subhedral plagioclase up to 3 mm and subordinate sub-euhedral hematized biotite up to 4 mm, and Fe-Ti oxides up to 0.5 mm. Individual phenocrysts form approximately 1.6% of the rock and consist of the same minerals found in the glomerocrysts. The dark greenish gray-colored groundmass consists of microlites of plagioclase with trace zircon and glass.

Sample number: Mc92

Location: NW 1/4, Sec 19, T24S, R61E, Hidden Valley, Nev. 7 1/2' quad: on hilltop 3957 just NW of the vent area at station 91.

Rock name: Vesicular biotite dacite

Description: Glomeroporphyritic: glomerocrysts form approximately 5.5% of the rock and are composed of commonly pitted and embayed phenocrysts of zoned, oscillatory, sub-euhedral plagioclase and subordinate sub-euhedral, oxidized biotite up to 2 mm, subhedral orthopyroxene up to 1 mm, and Fe-Ti oxides up to 0.5 mm. Individual phenocrysts form approximately 5.5% of the rock and consist of the same minerals found in the glomerocrysts. Biotite is rare in glomerocrysts and more abundant as individual phenocrysts. The slide contains < 1% granodiorite (?) xenoliths up to 1 cm. The vesicular (3%) medium dark gray-colored groundmass consists of microlites of plagioclase with trace biotite, orthopyroxene, Fe-Ti oxides and glass. Vesicles are coated with secondary calcite.

Sample number: Mc96

Location: W 1/2, Sec 4, T24S, R61E, Sloan, Nev. 7 1/2' quad: collected on the west-facing slope of hill 3490 in the northern Tss dome complex.

Rock name: Biotite dacite

Description: Glomeroporphyritic: glomerocrysts form approximately 7.5% of the rock and are composed of commonly pitted and embayed phenocrysts of zoned, oscillatory, sub-euhedral plagioclase up to 3 mm and subordinate sub-euhedral, oxidized biotite up to 3 mm, rare an-subhedral clinopyroxene up to 0.5 mm, and Fe-Ti oxides up to 0.5 mm. Individual phenocrysts form approximately 5.5% of the rock and consist of the same minerals found in the glomerocrysts. There is, however, a higher percentage of individual clinopyroxene phenocrysts (an-subhedral, up to 2 mm). The slide contains a 2 mm by 0.5 mm xenocryst of fine-to medium-grained clinopyroxene and orthopyroxene with interstitial glass. The weakly vesicular (1%) dark gray-colored groundmass consists of microlites of plagioclase with trace biotite and glass.

Sample number: Mc100

Location: SW 1/4, Sec 17, T24S, R61E, Hidden Valley, Nev. 7 1/2 quad: from hilltop 3650 in the NE part of the southern dacite dome complex.

Rock name: Biotite dacite

Description: Glomeroporphyritic: glomerocrysts form approximately 11% of the rock and are composed of commonly pitted and embayed phenocrysts of zoned, oscillatory, sub-euhedral plagioclase up to 2 mm and subordinate an-subhedral, oxidized biotite up to 2 mm, an-subhedral clinopyroxene up to 5 mm and Fe-Ti oxides up to 0.5 mm. Individual phenocrysts form approximately 4% of the rock and consist of the same minerals found in the glomerocrysts. The weakly vesicular (< 1%) brownish gray-colored groundmass consists of microlites of plagioclase with trace Fe-Ti oxides and glass. Vesicles are coated with secondary calcite.

Sample number: Mc118

Location: E 1/2, Sec 3, T24S, R61E, Sloan NE, Nev. 7 1/2' quad: hypabyssal dacite near the NW Tss hypabyssal/volcanic contact.

Rock name: Hypabyssal biotite dacite

Description: Holocrystalline, glomeroporphyritic: glomerocrysts form approximately 13% of the rock and consist of commonly pitted and embayed phenocrysts of zoned, oscillatory, sub-euhedral plagioclase up to 3 mm, subordinate subhedral, oxidized biotite up to 3 mm, and < 1% subhedral clinopyroxene up to 1.5 mm that is rimmed with fine-grained black Fe oxides. Individual phenocrysts form approximately 6% of the rock and consist of the same minerals found in the glomerocrysts. The medium gray-colored, fine-grained groundmass consists of plagioclase (80%, subhedral, < 0.5 mm), biotite (3.8%, subhedral, < 0.5 mm), and trace Fe-Ti oxides (< 0.5 mm).

Sample number: Mc119

Location: NW 1/4, Sec 11, T24S, R61E, Sloan NE, Nev. 7 1/2' quad: Hypabyssal dacite near the SE Tss hypabyssal/volcanic contact.

Rock name: Hypabyssal biotite dacite

Description: Holocrystalline, glomeroporphyritic: glomerocrysts form approximately 12% of the rock and consist of commonly pitted and embayed phenocrysts of zoned, oscillatory, sub-euhedral plagioclase up to 3 mm, subordinate, oxidized biotite up to 2 mm, and < 1% subhedral clinopyroxene that is rimmed by fine-grained black Fe oxides. Individual phenocrysts form approximately 3% of the rock and consist of the same minerals found in the glomerocrysts. The medium gray-colored, fine-grained groundmass consists of plagioclase (80.4%, subhedral, < 0.5 mm), biotite (0.6%, subhedral, < 0.5 mm), and trace Fe-Ti oxides (< 0.5 mm). < 1% of the groundmass has been replaced by calcite.

Sample number: Mc128

Location: SE 1/4, Sec 24, T24S, R60E, Hidden Valley, Nev. 7 1/2' quad: from the central part of the southern dacite dome complex.

Rock name: Vesicular biotite dacite

Description: Glomeroporphyritic: glomerocrysts form approximately 3% of the rock and consist of commonly pitted and embayed phenocrysts of zoned, oscillatory sub-euhedral plagioclase up to 5 mm and subordinate sub-euhedral, oxidized biotite up to 4 mm, and Fe-Ti oxides up to 0.5 mm. Individual phenocrysts form approximately 3% of the rock and consist of the same minerals found in the glomerocrysts. The brownish gray-colored vesicular (3.6%) groundmass consists of plagioclase microlites and trace glass.

ALKALI BASALT

Sample number: Mc124

Location: SE 1/4, Sec 13, T23S, R60E, Sloan, Nev. 7 1/2' quad: alkali basalt exposure at the Sloan Limestone quarry.

Rock name: Weakly vesicular alkali basalt

Description: Trachytic, holocrystalline and aphanitic with ultramafic nodules and Precambrian crust xenoliths up to several cm (< 1%). The weakly vesicular (0.2%), black-colored groundmass consists of sub-parallel microlites of sub-euhedral, oscillatory plagioclase (56%), subhedral clinopyroxene (21.2%), an-subhedral, iddingsitized olivine (20.4%) and Fe-Ti oxides (2.2%).

APPENDIX B: CHEMISTRY TABLES

Tuff of Bridge Spring								
Sample No.	ET-1	YT	92	R	T	V	M63	M105
SiO ₂	72.59	70.03	69.01	68.51	67.73	66.65	66.81	66.10
Al ₂ O ₃	14.29	13.43	14.69	14.52	15.44	14.41	15.06	16.10
Fe ₂ O ₃	1.78	1.88	2.17	1.97	2.83	2.04	2.52	2.50
CaO	1.38	1.15	1.43	1.90	1.65	2.31	1.6	1.70
MgO	0.35	0.46	0.48	0.30	0.44	0.32	0.71	1.30
Na ₂ O	4.19	3.47	4.20	3.94	4.46	4.22	4.33	4.70
K ₂ O	5.29	4.82	5.12	5.71	4.93	4.97	5.92	6.30
TiO ₂	0.34	0.35	0.41	0.40	0.53	0.39	0.43	0.40
MnO	0.07	0.08	0.06	0.05	0.06	0.07	0.09	0.10
P ₂ O ₅	0.06	0.06	0.14	0.09	0.16	0.12	0.02	0.20
LOI	0.98	4.77	0.93	1.72	1.22	2.03	2.57	0.40
TOTAL	101.32	100.50	98.64	99.11	99.45	97.53	100.06	99.80
Trace elements in ppm								
La							121.0	104.0
Ce							191.0	155.0
Nd								70.0
Sm							11.0	10.0
Eu							1.7	1.9
Tb							0.8	0.9
Yb							3.1	1.2
Lu							0.5	0.3
U	8.5	12.0	8.2	7.3	5.2	5.9		
Tb							32.2	25.0
Cr	21.4	17.9			21.8	18.3		
Hf							11.1	10.0
Ba							910	1332
Rb	248.0	480.0	217.0	217.0	159.0	179.0	157.0	143.0
Sr	214	402	233	197	563	365	264	1015
Sc								
Ta							2.3	1.84
Cd								
Zr	330.0	344.0	118.0	389.0	422.0	350.0		414.0
Y		66.2	51.0	58.0	41.0	42.0		
Nb								
Co								
Ti								
V								
Mg#	0.14	0.17	0.16	0.12	0.12	0.12	0.19	0.31

Tuff of Bridge Spring: continued								
Sample No.	Mc53	Mc60	Mc61	Mc62	Mc64a	Mc64b	Mc65	Mc66
SiO ₂	64.65	63.90	66.47	67.27	65.09	66.69	69.54	66.69
Al ₂ O ₃	15.66	14.77	14.92	13.95	13.72	13.72	14.40	14.48
Fe ₂ O ₃	3.95	3.55	3.47	2.72	3.11	3.11	3.31	3.16
CaO	2.43	3.24	1.72	2.36	5.66	0.65	0.63	4.12
MgO	0.97	1.05	0.86	0.58	1.42	1.00	1.02	0.84
Na ₂ O	4.33	4.09	4.33	3.97	3.35	3.86	3.94	3.74
K ₂ O	6.03	5.67	6.17	5.99	4.69	6.40	4.64	5.77
TiO ₂	0.53	0.45	0.47	0.35	0.42	0.42	0.45	0.43
MnO	0.15	0.15	0.15	0.15	0.15	0.15	0.15	0.15
P ₂ O ₅	0.18	0.16	0.16	0.10	0.40	0.13	0.27	0.33
LOI	1.27	1.97	1.14	2.04	1.48	0.65	4.11	3.00
TOTAL	100.06	99.00	99.87	99.48	99.49	96.78	102.46	102.71
Trace elements in ppm								
La	118.0	93.2	91.5	92.1		96.3		
Ce	204.0	170.0	167.0	184.0		181.0		
Nd	73.4	64.0	75.2	55.3		67.3		
Sm	9.7	8.3	11.3	11.1		11.5		
Eu	1.8	1.7	1.3	1.0		1.1		
Tb	0.9	0.9	1.4	1.1		1.1		
Yb	2.9	3.1	3.9	3.5		3.8		
Lu	0.4	0.4	0.5	0.6		0.6		
U	6.3	5.4	6.4	10.9		8.9		
Th	28.6	27.3	35.8	44.3		44.6		
Cr	32.0	45.3	35.2	9.9		15.5		
Hf	10.3	10.1	9.8	10.6		11.1		
Ba	818	927	390	170		296		
Rb	121.0	127.0	160.0	172.0		170.0		
Sr	502	781				389		
Sc	4.7	4.2	3.9	3.2		3.6		
Ta	1.7	1.9	2.4	2.7		2.7		
Cd								
Zr	578.0	483.0	826.0	553.0		577.0		
Y								
Nb		64.0						
Co	4.2	3.7	3.4	2.0		2.8		
Ti	2980	2790	2260	2430		2100		
V	39.7	35.3	44.6	23.3		29.5		
Mg#	0.17	0.2	0.18	0.15	0.28	0.19	0.21	0.22

Tuff of Bridge Spring: continued					Hidden Valley volcanics			
Sample No.	Mc67	Mc68	Mc69	Mc71	65	66	68	125
SiO ₂	68.12	65.46	68.40	69.27	46.94	50.18	52.05	51.61
Al ₂ O ₃	14.60	14.32	14.46	14.88	16.87	15.11	16.04	16.69
Fe ₂ O ₃	2.91	3.19	3.07	2.93	9.64	8.94	7.86	9.18
CaO	1.69	3.43	1.61	0.65	11.01	9.97	8.80	8.90
MgO	0.61	0.66	0.53	0.40	7.23	7.19	5.92	5.82
Na ₂ O	4.38	4.10	4.33	4.44	2.69	2.61	2.69	2.75
K ₂ O	5.94	5.82	5.85	6.15	1.38	1.72	3.01	1.79
TiO ₂	0.39	0.42	0.40	0.41	1.54	1.35	1.31	1.73
MnO	0.15	0.14	0.15	0.15	0.13	0.14	0.13	0.14
P ₂ O ₅	0.11	0.13	0.09	0.09	0.81	0.61	0.78	0.50
LOI	1.38	2.56	1.33	0.56	1.11	2.35	3.01	0.70
TOTAL	100.29	100.23	100.22	99.93	99.35	100.17	101.60	99.81
Trace elements in ppm								
La	94.5	91.7	93.4	101.0				
Ce	173.0	177.0	184.0	188.0				
Nd	79.8	63.7	57.0	80.9				
Sm	12.8	11.8	12.1	13.7				
Eu	1.1	1.2	1.2	1.2				
Tb	1.2	1.2	1.3	1.3				
Yb	3.6	3.4	3.6	3.8				
Lu	0.6	0.5	0.5	0.6				
U	8.7	7.2	8.5	8.4				
Th	39.3	39.4	41.9	42.0				
Cr	11.7	20.9	10.4	11.2				
Hf	10.0	10.1	11.0	11.3				
Ba		303						
Rb	155.0	165.0	179.0	173.0	22.3	22.0	65.2	29.7
Sr	219	200	168	196	940	828	1170	622
Sc	3.2	3.9	3.4	3.3				
Ta	2.4	2.4	2.6	2.8				
Cd								
Zr	455.0	544.0	603.0	663.0	218.0	223.0	317.0	235.0
Y					17.7	18.1	25.1	23.4
Nb								
Co	2.0	3.9	2.5	1.9				
Ti	2270	1890	2780	2220				
V	23.6	31.0	30.0	34.3				
Mg#	0.15	0.15	0.13	0.1	0.39	0.41	0.39	0.35

Hidden Valley volcanics: continued			Mount Hanna andesite					
Sample No.	Mc109	Mc116	Mc83b	Mc84	Mc110	Mc111	Mc112	Mc113
SiO ₂	57.96	51.00	58.93	59.26	60.15	60.74	60.15	59.75
Al ₂ O ₃	16.18	16.81	16.90	16.83	17.31	17.07	17.05	17.00
Fe ₂ O ₃	8.07	10.29	6.56	6.82	6.51	6.79	6.73	6.90
CaO	5.72	9.22	3.93	4.00	3.88	3.98	4.08	4.06
MgO	3.38	5.08	1.91	1.54	1.87	1.72	1.62	1.84
Na ₂ O	3.35	3.11	3.91	3.80	3.46	3.53	3.62	3.75
K ₂ O	3.47	1.71	4.29	4.25	4.45	4.52	4.40	4.23
TiO ₂	1.15	1.38	0.59	0.62	0.60	0.61	0.62	0.59
MnO	0.16	0.17	0.16	0.16	0.16	0.16	0.16	0.16
P ₂ O ₅	0.87	0.91	0.47	0.86	0.93	1.02	0.94	0.57
LOI	0.62	0.28	0.74	0.73	0.66	0.59	0.32	0.62
TOTAL	100.93	99.96	98.39	98.87	99.98	100.73	99.69	99.47
Trace elements in ppm								
La	72.3	40.0	88.2	92.2	89.1	89.1	89.7	90.0
Ce	143.0	76.2	153.0	172.0	173.0	170.0	172.0	163.0
Nd	48.6	35.3	69.1	74.7	65.5	74.8	57.6	82.5
Sm	9.1	6.6	10.4	11.2	10.0	10.6	10.0	10.9
Eu	2.4	1.8	2.4	2.7	2.6	2.5	2.7	2.5
Tb	1.2	0.9	0.9	1.2	1.1	1.1	1.0	1.2
Yb	1.8	2.6	2.2	2.8	2.5	2.7	2.4	2.6
Lu	0.3	0.4	0.3	0.3	0.3	0.3	0.3	0.4
U		1.1	1.7	3.5	2.0	3.2	2.9	2.6
Th	11.1	4.8	12.8	14.2	15.0	13.6	14.7	13.4
Cr	101.0	184.0	85.1	38.4	136.0	132.0	94.0	72.6
Hf	7.7	5.0	7.1	8.1	8.0	7.7	7.9	7.4
Ba	1100	724	1650	1970	1800	1990	1840	1990
Rb	95.8	24.9	65.5	105.0	112.0	95.2	85.3	71.6
Sr	1250	1410	1430	1790	2280	1920	2110	1830
Sc	13.6	24.9	5.7	6.4	6.5	6.2	6.7	6.2
Ta	1.3	0.6	0.8	0.8	0.9	0.8	0.8	0.9
Cd								
Zr	843.0	658.0	679.0	675.0	725.0	560.0	722.0	402.0
Y								
Nb								
Co	21.7	28.2	9.3	10.3	10.3	10.0	10.9	9.8
Ti	7100	7630	3540	3300	3950	3780	4480	4420
V	150	203	81.2	75.1	70.6	81.3	88.8	79.7
Mg#	0.26	0.30	0.20	0.16	0.20	0.18	0.17	0.19

Hidden Valley volcanics: continued							
Sample No.	M24	M27	M35	M57	M58	Mc87	Mc108
SiO ₂	58.72	58.70	55.86	59.42	59.65	55.19	57.61
Al ₂ O ₃	17.85	15.80	16.30	17.59	17.49	16.02	16.14
Fe ₂ O ₃	7.14	5.11	8.47	5.41	5.55	8.98	7.74
CaO	5.25	4.49	7.49	4.00	4.03	7.06	5.54
MgO	2.00	2.53	4.33	1.80	1.80	5.12	3.29
Na ₂ O	4.35	3.63	4.29	3.69	3.64	3.62	3.47
K ₂ O	3.95	5.29	1.89	5.22	5.22	2.36	3.63
TiO ₂	0.71	0.82	0.95	0.55	0.55	1.08	1.18
MnO	0.06	0.09	0.08	0.35	0.12	0.17	0.16
P ₂ O ₅	0.77	0.35	0.20	0.12	0.34	0.64	1.05
LOI	0.82	1.29	1.35	0.35	0.76	0.06	1.35
TOTAL	101.62	98.10	101.21	98.50	99.15	100.30	101.16
Trace elements in ppm							
La	97.8	102.0	26.2	99.4	98.0	48.6	69.7
Ce	182.3	168.6	42.0	167.8	166.9	85.2	139.0
Nd	68.8	74.8	23.9	76.6		32.8	42.0
Sm	14.2	13.1	4.3	12.8	12.6	6.4	8.5
Eu	3.5	2.7	1.6	2.8	2.8	1.6	2.3
Tb	1.5	1.5	1.6	1.5	1.5	0.9	0.8
Yb	2.9	2.8	1.4	2.9	2.9	2.4	1.9
Lu	0.6	0.4	0.4	0.5	0.5	0.3	0.4
U							1.1
Th	12.5	20.2	6.4	13.7	13.5	8.3	10.8
Cr						220.0	61.2
Hf	7.0	9.4	4.3	7.6	7.6	5.5	7.3
Ba	2440	1620	655	2203	1897	802	1200
Rb	97.9	118.5	43.6	98.2	100.0	33.8	60.6
Sr	1741	745	455	1468	1157	556	1280
Sc						19.7	12.8
Ta	0.7	1.4	0.5	0.9	0.9	0.9	1.2
Cd							
Zr		390.0		367.8	234.1		199.0
Y							
Nb							
Co						27.6	19.5
Ti						6130	7410
V						135	149
Mg#	0.19	0.30	0.30	0.22	0.22	0.33	0.27

Mount Hanna andesite: continued			Cinder Prospect member				
Sample No.	Mc114	Mc115	Mc59e	Mc78	Mc79	Mc117a	Mc121
SiO ₂	60.93	59.37	66.37	61.31	67.25	67.67	69.88
Al ₂ O ₃	17.10	16.73	15.25	16.63	15.30	15.53	15.65
Fe ₂ O ₃	6.53	6.61	3.36	5.71	3.30	3.45	3.00
CaO	3.84	4.10	2.08	3.39	1.10	2.07	1.63
MgO	1.61	1.81	0.99	1.38	0.55	0.55	0.48
Na ₂ O	3.68	3.87	3.96	4.03	3.85	4.39	3.65
K ₂ O	4.36	4.31	5.27	4.63	5.58	5.69	5.63
TiO ₂	0.57	0.57	0.16	0.45	0.13	0.11	0.11
MnO	0.16	0.15	0.16	0.16	0.16	0.17	0.16
P ₂ O ₅	1.02	0.93	0.13	0.42	0.08	0.29	0.25
LOI	0.48	0.45	2.47	0.14	2.47	1.12	0.83
TOTAL	100.28	98.90	100.19	98.25	99.76	101.04	101.27
Trace elements in ppm							
La	94.8	91.4	116.0	88.4	123.0	121.0	129.0
Ce	171.0	171.0	210.0	182.0	216.0	227.0	222.0
Nd	72.2	69.8	83.5	60.1	77.9	88.2	101.0
Sm	11.5	10.9	11.7	10.3	11.9	12.8	13.5
Eu	2.6	2.6	2.5	2.9	2.6	2.5	2.5
Tb	1.0	0.9	1.3	1.0	1.2	1.0	1.2
Yb	2.8	2.5	3.1	2.4	3.2	3.1	3.6
Lu	0.4	0.4	0.5	0.3	0.4	0.5	0.5
U	3.8	2.4	4.9	3.1	5.1	5.8	5.0
Th	14.3	14.0	21.7	15.5	21.5	22.4	21.9
Cr	105.0	108.0	38.4	79.6	32.1	43.8	
Hf	7.9	7.6	8.7	9.1	8.6	8.5	8.6
Ba	1930	2020	1450	1700	1840	1850	1780
Rb	85.7	94.9	127.0	108.0	125.0	120.0	121.0
Sr	1610	1700	801	1580	764	925	638
Sc	6.0	6.4	4.8	5.4	4.8	5.0	4.6
Ta	0.8	0.8	1.0	0.7	1.1	1.0	1.1
Cd							
Zr	438.0	430.0	534.0	652.0	837.0	532.0	619.0
Y							
Nb							
Co	9.1	10.0	1.2	6.6	0.8	1.0	0.7
Ti	3610	3430	1020	3770	1230	4151	4637
V	70.2	79.9	15.2	58.7			
Mg#	0.17	0.19	0.20	0.17	0.13	0.12	0.12

Cinder Prospect member: continued			Tuff of the Sloan volcanics				Center Mountain dacite	
Sample No.	Mc125	Mc126	Mc59a	Mc59b	Mc59c	Mc73	Mc59d	Mc120b
SiO ₂	68.74	69.70	69.76	64.87	64.26	68.58	68.06	67.67
Al ₂ O ₃	15.35	15.45	15.08	15.09	15.12	14.56	15.94	15.67
Fe ₂ O ₃	3.05	3.11	3.34	3.95	4.42	3.10	3.58	4.11
CaO	1.67	1.21	0.59	1.37	1.64	0.69	2.15	1.56
MgO	0.40	0.44	0.77	1.73	1.71	1.07	0.51	0.63
Na ₂ O	3.85	3.69	4.32	3.73	3.92	4.62	3.75	3.70
K ₂ O	5.56	5.48	5.91	5.90	4.56	5.84	5.47	5.37
TiO ₂	0.10	0.10	0.45	0.63	0.64	0.48	0.15	0.20
MnO	0.17	0.16	0.15	0.15	0.15	0.15	0.16	0.17
P ₂ O ₅	0.24	0.25	0.10	0.19	0.20	0.23	0.28	0.35
LOI	0.99	2.93	0.61	1.30	2.99	0.82	1.04	0.85
TOTAL	100.12	102.52	101.08	98.91	99.62	100.14	101.09	100.28
Trace elements in ppm								
La			95.4	103.0	98.4	109.0	118.0	114.0
Ce			183.0	192.0	185.0	216.0	217.0	206.0
Nd			78.7	89.2	90.0	70.9	85.8	101.0
Sm			11.9	13.2	12.5	13.7	12.2	12.0
Eu			1.3	1.5	1.8	1.4	2.4	2.5
Tb			1.2	1.6	1.4	1.3	1.1	0.9
Yb			3.2	3.3	3.4	3.6	3.3	3.4
Lu			0.5	0.5	0.4	0.6	0.5	0.5
U			7.1	6.0	6.0	6.7	4.7	4.2
Th			37.5	32.3	33.0	38.9	21.4	19.2
Cr			58.7	47.8	66.4	21.6	31.0	27.7
Hf			10.4	11.7	11.6	11.6	8.8	8.9
Ba			271	380	497	366	1700	1810
Rb			165.0	139.0	151.0	162.0	115.0	108.0
Sr				364	670	155	784	800
Sc			3.7	5.6	6.2	4.2	5.3	5.0
Ta			2.4	2.4	2.0	2.9	1.1	1.1
Cd								
Zr			560.0	701.0	693.0	833.0	577.0	540.0
Y								
Nb								
Co			2.7	5.9	8.0	3.2	1.2	1.9
Ti			3039	2820	2899	2950	4662	2300
V			26.7	37.8	52.8	31.5	15.8	16.1
Mg#	0.10	0.11	0.17	0.27	0.25	0.23	0.11	0.12

Center Mountain dacite: continued			Mount Ian andesite					
Sample No.	Mc130	Mc131	Mc72	Mc77	Mc93	Mc94	Mc95a	Mc95b
SiO ₂	68.43	68.06	57.85	59.28	60.22	58.12	58.24	58.94
Al ₂ O ₃	15.52	15.48	16.72	17.22	17.32	16.71	17.18	16.89
Fe ₂ O ₃	3.07	3.09	7.14	7.08	7.87	7.34	6.97	7.76
CaO	1.64	1.57	4.24	4.15	4.31	4.22	4.36	4.09
MgO	0.38	0.44	1.81	1.84	1.94	1.95	2.13	1.56
Na ₂ O	3.51	3.86	3.74	3.62	3.64	3.65	3.77	3.51
K ₂ O	5.65	5.73	4.16	4.41	4.18	4.19	4.10	4.41
TiO ₂	0.11	0.10	0.60	0.61	0.66	0.63	0.64	0.64
MnO	0.16	0.16	0.16	0.16	0.16	0.16	0.16	0.16
P ₂ O ₅	0.21	0.16	0.97	1.02	1.00	0.98	0.54	0.85
LOI	1.03	1.10	0.66	1.04	0.25	0.33	1.18	0.72
TOTAL	99.71	99.75	98.05	100.43	101.55	98.28	99.27	99.53
Trace elements in ppm								
La			86.7	85.6	86.3	88.4	89.2	
Ce			155.0	152.0	156.0	155.0	164.0	
Nd			81.7	73.7	82.6	89.4	69.0	
Sm			11.4	11.4	11.2	11.1	11.1	
Eu			2.6	2.5	2.8	2.7	2.8	
Tb			1.2	1.0	1.1	1.0	0.9	
Yb			2.5	1.9	2.3	2.2	2.3	
Lu			0.4	0.4	0.3	0.4	0.3	
U			2.7	3.8	3.4	4.7	2.3	
Th			13.0	11.6	12.8	11.8	12.8	
Cr			60.7	82.5	80.0	40.1	87.2	
Hf			7.0	6.7	7.3	7.3	7.6	
Ba			1970	1930	1990	2090	2070	
Rb	131.5		91.7	71.3	71.4	95.3	97.6	
Sr	536		1640	1580	1980	1810	2070	
Sc			5.8	5.7	6.2	5.9	6.1	
Ta			0.7	0.9	0.7	0.6	0.9	
Cd								
Zr	347.4		637.0	387.0	689.0	543.0	808.0	
Y	12.2							
Nb								
Co			10.4	10.5	11.4	10.4	10.9	
Ti			4130	4110	3970	4370	3790	
V			77.7	96.4	88.2	85	79.7	
Mg#	0.11		0.18	0.18	0.17	0.19	0.21	0.15

Mount Ian andesite: continued				Mount Sutor dacite			
Sample No.	Mc97	Mc98	Mc120a	Mc21	Mc83a	Mc85	Mc96
SiO ₂	58.03	58.07	58.73	61.91	62.41	63.03	62.91
Al ₂ O ₃	17.21	17.18	17.20	16.09	16.51	16.25	16.19
Fe ₂ O ₃	7.19	7.14	7.77	5.71	5.48	5.85	5.14
CaO	4.30	4.43	4.17	3.13	2.45	3.20	2.44
MgO	1.92	2.16	1.72	1.34	1.16	1.15	1.20
Na ₂ O	3.87	3.86	3.82	3.49	3.68	3.46	3.53
K ₂ O	4.22	4.44	4.14	5.75	5.84	4.69	5.68
TiO ₂	0.64	0.69	0.62	0.39	0.43	0.58	0.43
MnO	0.16	0.16	0.16	0.17	0.16	0.16	0.16
P ₂ O ₅	0.52	0.54	1.19	0.24	0.24	0.59	0.22
LOI	0.34	1.05	0.15	1.93	0.70	0.44	1.02
TOTAL	98.40	99.72	99.67	99.13	99.06	99.40	98.73
Trace elements in ppm							
La	85.6		81.4	118.0	115.0	111.0	119.0
Ce	159.0		149.0	220.0	219.0	199.0	210.0
Nd	59.0		62.6	112.0	87.8	112.0	120.0
Sm	11.2		10.4	14.7	13.3	14.5	14.6
Eu	2.8		2.5	3.3	3.4	3.3	3.2
Tb	1.1		1.0	1.5	1.6	1.6	2.1
Yb	2.2		2.0	4.4	3.9	3.9	3.9
Lu	0.4		0.4	0.6	0.5	0.6	0.7
U	2.9		2.9	4.8	2.6	3.6	3.7
Th	12.6		12.0	20.3	20.3	17.0	19.4
Cr	160.0		76.1	9.0	61.6	18.3	57.6
Hf	7.3		7.0	10.7	10.8	10.4	10.3
Ba	1900		1900	2180	1780	1950	1830
Rb	75.3		85.9	118.0	135.0	109.0	109.0
Sr	1990		1880	1480	1380	1530	1600
Sc	6.0		5.9	6.7	6.7	7.8	6.7
Ta	0.8		0.7	1.3	1.0	1.2	1.0
Cd							
Zr	645.0		670.0	681.0	697.0	833.0	580.0
Y							
Nb							
Co	11.2		10.6	2.8	3.3	3.6	2.8
Ti	3890		4330	3220	2630	3820	3220
V	88.3		79.2	24.2	24.4	34.6	23.8
Mg#	0.19	0.21	0.16	0.17	0.15	0.14	0.17

Mount Sutor dacite: continued					Alkali basalt
Sample No.	Mc100	Mc118	Mc119	Mc128	Mc124
SiO ₂	61.67	62.29	64.96	66.55	51.04
Al ₂ O ₃	16.19	16.43	16.44	15.84	14.92
Fe ₂ O ₃	5.14	5.71	5.51	3.85	8.70
CaO	2.44	2.99	2.98	1.98	8.80
MgO	1.24	1.04	1.14	0.69	7.71
Na ₂ O	3.84	3.56	3.64	3.53	3.32
K ₂ O	5.51	5.17	5.27	5.33	2.56
TiO ₂	0.49	0.48	0.43	0.25	0.96
MnO	0.17	0.17	0.17	0.16	0.16
P ₂ O ₅	0.25	0.50	0.31	0.35	1.13
LOI	0.50	0.74	0.64	1.83	1.19
TOTAL	97.44	99.08	101.49	100.36	100.49
Trace elements in ppm					
La	112.0	114.0	116.0		
Ce	215.0	231.0	216.0		
Nd	78.3	95.0	101.0		
Sm	13.2	14.5	14.8		
Eu	3.6	3.4	3.3		
Tb	1.6	1.7	1.6		
Yb	4.3	3.9	3.8		
Lu	0.5	0.6	0.6		
U	4.2	3.7	4.9		
Th	19.1	19.6	19.1		
Cr	80.8	29.8	40.2		
Hf	10.6	10.7	10.3		
Ba	1760	1800	1780		
Rb	120.0	135.0	109.0		
Sr	1460	1560	1310		
Sc	7.5	8.0	7.4		
Ta	1.0	1.1	1.1		
Cd					
Zr	844.0	602.0	732.0		
Y					
Nb					
Co	3.0	3.4	3.2		
Ti	3300	3790	3590		
V	32.0	23.1	19.2		
Mg#	0.17	0.14	0.15	0.13	0.43

APPENDIX C: CIPW NORMS

Tuff of Bridge Spring															
Sample No.	ET-1	YT	92	R	T	V	M63	M105	Mc53	Mc60	Mc61	Mc62	Mc64a	Mc64b	Mc65
Q	25	28	21	20	18	18	15	9	10	11	13	17	17	19	20
or	31	28	30	34	29	29	35	37	36	34	36	35	28	38	28
ab	35	29	36	33	38	36	37	40	37	35	37	34	28	33	36
an	5	5	6	5	7	6	4	4	5	5	3	3	9	2	2
C	0	1	0	0	0	0	0	0	0	0	0	0	0	1	2
di	2	0	0	3	0	4	3	2	5	8	4	6	12	0	0
hy	1	2	3	0	3	0	2	4	3	1	3	0	0	4	5
wo	0	0	0	0	0	0	0	0	0	0	0	0	1	0	0
mt	1	1	1	1	2	1	1	1	2	2	2	1	2	2	2
il	1	1	1	1	1	1	1	1	1	1	1	1	1	1	1
ap	0	0	0	0	0	0	0	0	0	0	0	0	1	0	0
ol	0	0	0	0	0	0	0	0	0	0	0	0	0	0	0
hem	0	0	0	0	0	0	0	0	0	0	0	0	0	0	0
Tuff of Bridge Spring: continued										Hidden Valley volcanics					
Sample No.	Mc66	Mc67	Mc68	Mc69	Mc71	65	66	68	125	M24	M27	M35	M57	M58	Mc87
Q	15	16	13	17	17	0	0	0	2	7	7	5	8	16	2
or	34	35	34	35	36	8	10	18	11	23	32	11	31	36	14
ab	32	37	35	37	38	22	22	23	23	37	32	36	31	38	31
an	6	3	3	3	3	30	24	23	28	18	12	20	16	4	20
C	0	0	0	0	0	0	0	0	0	0	0	0	0	0	0
di	9	4	8	4	0	16	17	13	10	1	5	10	0	2	8
hy	0	2	0	2	3	0	14	14	16	5	4	6	5	1	17
wo	1	0	1	0	0	0	0	0	0	0	0	0	0	0	0
mt	2	2	2	2	2	4	4	4	5	0	0	0	0	0	4
il	2	1	1	1	1	3	3	2	3	0	0	0	0	0	2
ap	1	0	0	0	0	2	1	2	1	2	1	0	1	0	1
ol	0	0	0	0	0	13	2	0	0	0	0	0	0	0	0
hem	0	0	0	0	0	0	0	0	0	7	5	8	6	3	0

H.V. volcanics: cont.				Mount Hanna andesite							
Sample No.	Mc108	Mc109	Mc11	Mc83b	Mc84	Mc110	Mc111	Mc112	Mc113	Mc114	Mc115
Q	8	13	0	7	6	12	12	10	9	12	9
or	21	21	10	25	25	26	27	26	25	26	25
ab	29	29	26	33	33	29	30	31	32	31	33
an	18	18	27	16	16	13	13	14	16	12	14
C	0	0	0	0	0	2	2	1	0	2	0
di	2	2	11	0	1	0	0	0	0	0	0
hy	13	8	17	11	11	11	11	13	11	10	11
wo	0	0	0	0	0	0	0	0	0	0	0
mt	4	4	4	3	3	3	3	2	3	3	3
il	2	2	3	1	1	1	1	0	1	1	1
ap	2	3	2	1	1	2	2	2	1	2	2
ol	0	0	0	0	0	0	0	0	0	0	0
hem	0	0	0	0	0	0	0	0	0	0	0
Cinder Prospect member								Tuff of the Sloan volcanics			
Sample No.	Mc59c	Mc78	Mc79	Mc117a	Mc121	Mc125	Mc126	Mc59a	Mc59b	Mc59c	Mc73
Q	16	10	19	15	22	20	23	17	14	17	12
or	31	27	33	34	33	33	32	35	35	27	35
ab	34	34	33	37	31	33	31	37	32	33	41
an	8	14	5	6	6	7	4	2	6	7	1
C	0	0	1	0	1	1	2	1	1	1	0
di	1	0	0	2	0	0	0	0	0	0	2
hy	5	8	4	4	4	4	4	8	7	8	5
wo	0	0	0	0	0	0	0	0	0	0	0
mt	2	3	2	2	2	2	2	0	2	2	2
il	0	1	0	0	0	0	0	1	1	1	1
ap	0	1	0	1	1	1	1	0	0	0	0
ol	0	0	0	0	0	0	0	0	0	0	0
hem	0	0	0	0	0	0	0	0	0	0	0

Center Mountain dacite					Mount Ian andesite								
Sample No.	Mc59d	Mc120b	Mc130	Mc131	Mc72	Mc77	Mc93	Mc94	Mc95a	Mc95b	Mc97	Mc98	Mc120a
Q	19	21	22	19	8	3	3	4	7	8	5	5	9
or	32	32	33	34	25	26	25	25	24	26	25	26	24
ab	33	31	30	33	32	33	31	32	32	30	34	33	32
an	9	5	7	7	15	15	16	17	18	13	17	16	13
C	0	2	1	0	1	0	0	0	0	1	0	0	2
di	0	0	0		0	2	2	1	0	0	1	2	0
hy	5	5	4	4	12	11	12	13	12	12	11	11	13
wo	0	0	0		0	0	0	0	0	0	0	0	0
mt	2	2	2	2	3	3	3	3	3	3	3	3	3
il	0	0	0	0	1	1	1	1	1	1	1	1	1
ap	1	1	0	0	2	1	1	1	1	2	1	1	3
ol	0	0	0	0	0	0	0	0	0	0	0	0	0
hem	0	0	0	0	0	0	0	0	0	0	0	0	0
Mount Sutor dacite									Alkali basalt				
Sample No.	Mc21	Mc83a	Mc85	Mc96	Mc100	Mc118	Mc119	Mc128	Mc124				
Q	10	10	16	12	9	13	14	20	0				
or	34	35	28	34	33	31	31	32	15				
ab	30	31	29	30	32	30	31	33	28				
an	11	11	12	11	12	12	13	7	18				
C	0	0	1	0	0	1	0	1	0				
di	2	0	0	0	1	0	0	0	15				
hy	6	8	8	7	7	8	8	4	2				
wo	0	0	0	0	0	0	0	0	0				
mt	3	3	3	3	3	3	3	2	4				
il	1	1	1	1	1	1	1	0	2				
ap	1	1	1	1	1	1	1	1	3				
ol	0	0	0	0	0	0	0	0	14				
hem	0	0	0	0	0	0	0	0	0				

APPENDIX D: ROCK MODES

Tuff of Bridge Spring										Hidden Valley volcanics				
Sample number	Mc53	Mc60	Mc62	Mc64b	Mc66	Mc67	Mc68	Mc69	Mc71	Mc1	Mc3a	Mc35	Mc37	Mc40b
Plagioclase	3.4	1.5	2.8	0.8	1.2	2.0	1.4	5.0	3.0			2.2	1.0	3.3
Olivine										0.6		9.8	7.6	6.3
Biotite	3.4	0.6	1.0	1.8	1.6		1.4	0.4	1.6					
Orthopyroxene														
Clinopyroxene	0.8	0.2	0.4	0.2	0.8	0.2	0.8	0.4	1.6	0.3	1.0	0.8	1.4	
Fe-Ti oxides	0.2	Trace	Trace	Trace	Trace	Trace	0.4	0.6	Trace					
Groundmass	56.2	86.0	87.2	86.0	83.0	79.4	69.8	83.6	67.4	88.1	90.8	84.0	82.8	78.5
Sanidine	24.2	7.5	4.2	6.0	5.4	10.4	4.8	7.0	10.6					
Phlogopite														
Zircon	Trace	Trace	Trace	Trace	Trace	Trace	Trace	Trace	Trace					
Sphene	0.4	0.4	0.6	0.2	0.4	Trace	Trace	0.6	0.4					
Hornblende														
Monazite														
Epidote														
Allanite														
Quartz	0.6	0.8	1.2	1.0	1.0	0.8	0.4	1.2	1.4			0.6	6.0	2.6
Calcite						Trace								
Pumice	9.6	2.2	1.4	2.2	3.4	Trace	11.4	0.2	12.0					
Rock xenoliths	1.2	0.8	1.2	1.8	3.0	7.2	9.6	1.0	2.0					
Vesicles										11.0	8.2	2.6	1.2	9.3

Hidden Valley volcanics: continued								Mount Hanna andesite				Cinder Prospect member		
Sample number	Mc42	Mc43	Mc47	Mc48	Mc87	Mc108	W-Hvb	Mc31b	Mc110	Mc112	Mc115	Mc25	Mc78	Mc79
Plagioclase	1.0	1.0	0.4		1.8	13.2	18.4	Trace	Trace	Trace	Trace	3.6	10.4	17.4
Olivine		6.0	0.4	1.2		1.4	11.4							
Biotite												0.4	4.0	3.6
Orthopyroxene														
Clinopyroxene	4.0	10.0	10.8	4.6		1.6	9.6							Trace
Fe-Ti oxides							0.5					0.8		1.2
Groundmass	91.4	79.6	76.6	79.0	98.2	65.6	58.5	100.0	100.0	100.0	100.0	69.4	85.2	74.0
Sanidine														3.8
Phlogopite			3.6	4.8										
Zircon												Trace		Trace
Sphene														
Hornblende														
Monazite														
Epidote														
Allanite														
Quartz														
Calcite												25.8		
Pumice														
Rock xenoliths														Trace
Vesicles	3.6	3.4	8.2	10.4		18.2	1.6						0.4	

	Cinder Prospect member: cont.		Tuff of the Sloan volcanics				Center Mtn. dacite			Mount Sutor dacite				
Sample number	Mc121	Mc125	Mc59a	Mc59b	Mc59c	Mc73	Mc59d	Mc130	Mc131	Mc9	Mc116	Mc19	Mc21	Mc27
Plagioclase	8.2	6.6	4.8	2.0	2.4	3.4	4.0	4.4	7.2	7.4	8.8	7.2	13.6	13.0
Olivine														
Biotite	1.8	3.6	0.4	0.8	0.4	0.6	1.4	1.2	1.6	3.2	1.4	2.2	3.4	5.4
Orthopyroxene											1.6	1.2		
Clinopyroxene			Trace	0.4	1.4	Trace							Trace	2.0
Fe-Ti oxides		0.4			1.4	0.2		0.4		0.8	0.4	1.2	1.0	1.6
Groundmass	83.6	84.0	60.6	76.6	52.6	77.8	94.6	89.0	88.6	88.0	87.8	76.4	78.2	76.4
Sanidine			21.2	4.8	8.6	10.0								
Phlogopite														
Zircon		Trace	Trace	Trace		Trace				Trace				
Sphene			0.2	Trace		Trace								
Hornblende														0.4
Monazite			Trace											
Epidote			Trace											
Allanite			Trace											
Quartz					0.4	1.8								
Calcite	6.4	5.4						5.0	1.2					
Pumice			9.0	2.2	11.6	1.6								
Rock xenoliths			3.8	13.2	21.2	4.6								
Vesicles									1.4	0.6		11.8	3.8	1.2

Mount Sutor dacite: continued									
Sample number	Mc28	Mc31a	Mc91a	Mc92	Mc96	Mc100	Mc118	Mc119	Mc128
Plagioclase	14.8	8.6	4.2	6.8	8.8	11.0	11.4	7.4	3.0
Olivine									
Biotite	3.2	2.6	2.0	1.8	3.6	3.2	5.4	9.4	2.6
Orthopyroxene				1.7					
Clinopyroxene	Trace	0.4			0.4	0.6	Trace		
Fe-Ti oxides	1.4		0.4	0.8	0.6			0.8	Trace
Groundmass	80.6	87.6	93.4	88.9	82.6	81.4	83.2	81.0	90.8
Sanidine									
Phlogopite									
Zircon			Trace						
Sphene									
Hornblende									
Monazite									
Epidote									
Allanite									
Quartz									
Calcite		0.8						1.4	
Pumice									
Rock xenoliths									
Vesicles					4.0	3.8			3.6

**STYLE OF VOLCANISM AND EXTENSIONAL TECTONICS
IN THE EASTERN BASIN AND RANGE PROVINCE:
NORTHERN MOHAVE COUNTY, ARIZONA**

by

Tracey Elaine Cascadden

**A thesis submitted in partial fulfillment
of the requirements for the degree of**

Master of Science

in

Geology

**Geoscience Department
University of Nevada, Las Vegas
August, 1991**

**STYLE OF VOLCANISM AND EXTENSIONAL TECTONICS
IN THE EASTERN BASIN AND RANGE PROVINCE:
NORTHERN MOHAVE COUNTY, ARIZONA**

by

Tracey Elaine Cascadden

**A thesis submitted in partial fulfillment
of the requirements for the degree of**

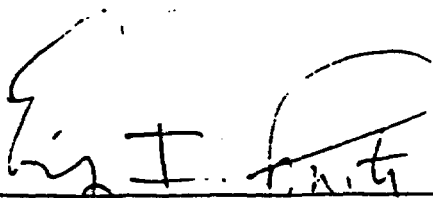
Master of Science

in

Geology

**Geoscience Department
University of Nevada, Las Vegas
August, 1991**

The thesis of Tracey Elaine Cascadden for the degree of Master of Science in Geology is approved.



Chairman, Eugene I. Smith, Ph.D.



Examining Committee Member, Ernest M. Duebendorfer, Ph.D.



Examining Committee Member, David L. Weide, Ph.D.



Graduate Faculty Representative, Diane Pyper-Smith, Ph.D.

Graduate Dean, Ronald W. Smith, Ph.D.

University of Nevada, Las Vegas
June, 1991

ABSTRACT

The west-dipping Cyclopic-Salt Spring Wash-Lakeside Mine fault system marks both the easternmost boundary of the extensional allochthon in the Basin and Range Province and the eastern limit of exposure of mid-Tertiary igneous rocks at the latitude of Lake Mead. The upper plate of this fault system is exposed only in the northern White Hills (NWH), Mohave County, Arizona. The upper plate contains east-tilted mid-Tertiary volcanic and sedimentary rocks, cut by down-to-the-west normal faults. Faulting began near Salt Spring Wash during the deposition/eruption of the upper part of the mid-Tertiary section. Elsewhere in the NWH, faulting postdated eruption and deposition. Brittle deformation on the Salt Spring fault contrasts with ductile deformation on the Lakeside Mine fault and may be explained by increasing displacement and a corresponding increase in uplift northward from the Black Mountains accommodation zone.

Three groups of mafic volcanic rocks, distinguished on the basis of chemistry and petrography, were erupted from three coeval mid-Tertiary volcanic centers. The three types of mafic magma may represent similar degrees of partial melting of different K-rich sources. Each magma type evolved by fractionation in conjunction with periodic recharge by new batch melts. Mafic volcanic lavas erupted from broad shields or fissure-fed lava fields. Landslide, ash-flow tuff and fanglomerate deposits suggest the presence of a Proterozoic basement high southeast of the study area.

Correlation between the mid-Miocene mafic to intermediate (46-70% SiO₂)

volcanic rocks of the northern White Hills and volcanic rocks of the Eldorado and Black Mountains (Patsy Mine Volcanics and Tuff of Bridge Spring) is possible on the basis of stratigraphic position, geochemistry (Hf, Ta, Sc, Co, Cr, V and REE), and petrography. A new biotite K-Ar age date on the Tuff of Bridge Spring in the northern White Hills suggests that the regionally extensive Tuff of Bridge Spring may be composed of two major pyroclastic flows. The first erupted at 16.4 Ma and is exposed in the NWH, the southern Black Mountains and the McCullough Range. The second erupted at 15.18 Ma and is exposed in the Eldorado Range.

CONTENTS

INTRODUCTION	1
TECHNIQUES	5
WHITE HILLS VOLCANIC STRATIGRAPHY AND THE EASTERN	
LIMIT OF THE EXTENSIONAL ALLOCHTHON	7
INTRODUCTION	7
VOLCANIC ROCKS OF THE NORTHERN WHITE HILLS	7
Correlation of sections	9
Composite section	35
Mid-Tertiary Eruptive/Depositional History	43
ROCKS OF THE FOOT WALL	48
STRUCTURE	54
Salt Spring Fault	54
Structures in Hanging Wall	55
Interpretations	60
PETROGENESIS OF MAFIC VOLCANICS	62
ORIGIN OF HIGH K ₂ O CONTENTS: METASOMATIC OR	
MAGMATIC	62
HOW ARE THE THREE MAGMA TYPES RELATED	
PETROGENETICALLY?	69
Contamination	69
Fractional Crystallization	71
Assimilation-Fractional Crystallization (AFC)	76
Source differences	77
Conclusions	78
CHEMICAL VARIATION WITHIN EACH MAGMA TYPE	79
Pink/Black Ridge Basalts	79
Basaltic Andesite of Temple Bar	83
Basaltic Andesite of Squaw Peak	85
SUMMARY	87
REGIONAL CORRELATION	88
MID-TERTIARY VOLCANIC ROCKS	88
LATE TERTIARY SEDIMENTS	102
STRUCTURE	105
Lake Mead region "detachment faults"	105
Regional correlation of Salt Spring fault	110
Ductile vs. brittle deformation	111
Geometry and displacement of Salt Spring fault	115
CONCLUSIONS	118

FUTURE WORK	120
APPENDIX A: STRATIGRAPHIC SECTIONS	
APPENDIX B: PETROGRAPHIC DESCRIPTIONS: ASH-FLOW TUFFS	134
APPENDIX C: PETROGRAPHIC DESCRIPTION: MAFIC VOLCANIC ROCKS	139
APPENDIX D: PETROGRAPHIC DESCRIPTIONS: PRECAMBRIAN BASEMENT	147
APPENDIX E: INSTRUMENTAL TECHNIQUES	154

List of Figures

1. Location Map	2
2. Regional sketch map	3
3. Sample location Map	6
4. Simplified Geologic Sketch Map of the northern White Hills	8
5. Correlated stratigraphic sections of the northern White Hills	10
6. Composite stratigraphic section of the Northern White Hills	11
7. Harker variation diagrams for ash-flow tuffs: SiO ₂ vs. major oxides.	14
8. Chondrite-normalized rare earth elements for ash-flow tuffs.	17
9. Harker variation diagrams for ash-flow tuffs: SiO ₂ and Mg# vs. Hf, Ta and Sc.	19
10. Harker variation diagrams for ash-flow tuffs: SiO ₂ and Mg# vs. Cr, V and Co.	20
11. Harker variation diagrams for mafic volcanic rocks: SiO ₂ vs. total REE* (La+Ce+Nd+Sm+Eu+Yb+Lu), Sc, Hf, La, Th and total alkalis ...	29
12. Hf/Th vs. La/Yb, TiO ₂ and CaO, and Sc.	31
13. Total REE* and La/Yb plotted against light REEs Sm, Nd, & Eu.	32
14. Chondrite-normalized REE plot for mafic volcanics	34
15. Models for the eruptive/depositional history of the northern White Hills	45
16. Salt Spring Fault orientation data	56
17. Simplified cross-sections	58
18. Alternative cross section from Temple Bar to Salt Spring Wash	61
19. Harker variation diagrams for mafic volcanic rocks: SiO ₂ vs. major element oxides	63
20. Classification diagram for mafic volcanic rocks (LeBas, 1986)	65
21. Alkali enrichment diagram. K ₂ O plotted against Na ₂ O	66
22. Binary chemical plots: K ₂ O vs. Ce, Hf, La, and Th	70
23. Harker variation diagrams: SiO ₂ vs. Ce, Hf, La and Th	73
24. Tests for olivine and clinopyroxene fractionation: V vs. Co and Cr; Co vs. Cr and Sc	74

25. Harker variation diagrams: SiO ₂ and Mg# vs. Co, Cr and V	75
26. Tests for plagioclase fractionation: CaO and Na ₂ O vs. Eu	81
27. Chondrite-normalized rare earth element plot for basalt of Pink/Black Ridge	82
28. Chondrite-normalized rare earth element plot for basaltic andesite of Temple Bar	84
29. Chondrite-normalized rare earth element plot for basaltic andesite of Squaw Peak	86
30. Regional exposures of the Tuff of Bridge Spring	89
31. Harker variation diagrams comparing NWH tuff with the Tuff of Bridge Spring and Peach Springs Tuff: Co, Cr and V	95
32. Harker variation diagrams comparing NWH tuff with the Tuff of Bridge Spring and Peach Springs Tuff: Hf, Sc and Ta	96
33. Harker variation diagrams comparing NWH tuff with the Tuff of Bridge Spring and Peach Springs Tuff: Ba and Rb	97
34. Harker variation diagrams comparing NWH tuff with the Tuff of Bridge Spring and Peach Springs Tuff: Major oxides	98
35. Correlation of northern White Hills volcanic section with Eldorado Mountains section	103
36. Regional exposures of Red Sandstone	104
37. Regional exposures of Muddy Creek Formation	106
38. Along-strike differences in deformational style due to northward steepening of fault surface	112
39. Along-strike differences in deformational style due to corrugation of fault surface about an east-west axis	113
40. Extension increasing northward from the Black Mountains Accommodation Zone (BMAZ)	116

List of Tables

1: Major element data for ash-flow tuffs	12
2: Trace and REE data for ash-flow tuffs	13
3: Summary of mineralogy for ash-flow tuffs	16
4: Summary of mineralogy for mafic volcanic rocks	22
5: Major element data for mafic volcanic rocks	24
6: Trace and REE data for mafic volcanic rocks	26
7: Maximum, minimum and average major element concentrations for mafic volcanic rocks	28
8: New biotite K-Ar age date from ash-flow tuff in the White Hills	37
9: Summary of mineralogy for clasts from coarse breccia	38
10: Summary of mineralogy for Precambrian basement rocks	50
11: Normative mineralogy for mafic volcanic rocks	67
12: Major element fractional crystallization and AFC models	72
13: Distribution coefficients for basalt	80
14: Major element data for the Tuff of Bridge Spring and Peach Springs	

Tuff	90
15: Trace and REE data for the Tuff of Bridge Spring and Peach Springs	
Tuff	92
16: Episodic ash-flow tuff eruptions from selected calderas in western	
North America	100
17: Characteristics of Lake Mead region low-angle normal faults	109

List of Plates

1: Geologic map of the northern White Hills, Mohave County, Arizona, 1:62,500	in pocket
2: Geologic map of Salt Spring Wash, 1:24,000	in pocket

ACKNOWLEDGEMENTS

The following organizations helped to fund my research: the Center for Volcanic and Tectonic Studies, the Geological Society of America, the Graduate Student Association at the University of Nevada, Las Vegas, and Sigma Xi.

I wish to thank the members of my committee for their time and constructive comments. Special thanks go to Gene Smith for his infinite patience and his ability to tell when I needed gentle guidance, a kick in the butt, or just to be left alone, Ernie Duebendorfer for encouraging me to widen my focus beyond the White Hills, David Weide for not shredding my first draft, and Diane Pyper-Smith for her insights regarding geochemistry. I am also indebted to Rod Metcalf for his help in analyzing lower plate rocks, Jane Nielson at the USGS for her Peach Springs Tuff geochemical data, Hayden Bridwell for his Tuff of Bridge Spring data, and Doug Switzer for his input regarding Salt Spring Wash. I also wish to thank Clair Martinez for her persistence in producing thin sections from the world's most absorbant ash-flow tuffs, Walt Raywood for maintaining UNLV's analytical and field equipment, Nate "The Hub" Stout for getting the 3-D diagrams out of my head and onto paper, and for the TC cougar, Tim Wallin for teaching me mineral separation techniques, Yagong Wang for major element analyses, and Dan Feuerbach and Terry Naumann for their encouragement, good advice, and most importantly, a job. Finally, I wish to thank my favorite field assistant, boat captain and husband Steven Graham, for his loving support, patience, flexibility and skill in collecting firewood.

INTRODUCTION

The White Hills are situated south of Lake Mead (Figure 1) in the northern end of the Colorado River extensional corridor, north of an accommodation zone (Faulds, 1989) which separates east-tilted fault blocks to the north from west-tilted fault blocks to the south (Figure 2). The region was subjected to large scale extension during mid-Miocene time (Anderson, 1971; Spencer, 1985; Weber and Smith, 1987; Duebendorfer et al., 1990a;). Extension was accommodated by low-angle normal faults and kinematically related strike-slip faults during early phases of extension (pre-11 Ma), and by high-angle normal faults during later phases of extension (post-11 Ma) (Anderson, 1971; Spencer, 1985; Eaton, 1982 and Wernicke, 1984). Sewall and Smith (1986) documented large magnitude displacement along the Saddle Island detachment (Figure 2) in the western Lake Mead area. Duebendorfer et al. (1990) suggested that the Saddle Island detachment may project eastward to Arch Mountain. Myers (1985) mapped a low-angle fault, the Cyclopic detachment, in the southern White Hills. The Lakeside Mine fault (Fryxell and Duebendorfer, 1990), north of Lake Mead, may be the northward projection of the Cyclopic detachment (Spencer and Reynolds, 1989). In this thesis I describe the Salt Spring fault on the east side of the northern White Hills. The Salt Spring fault may link the Cyclopic and Lakeside Mine faults. The Salt Spring fault lies 20 km west of the Grand Wash Cliffs and represents both the easternmost boundary of the extensional allochthon and the eastern limit of exposure of mid-Tertiary igneous rocks in the northern

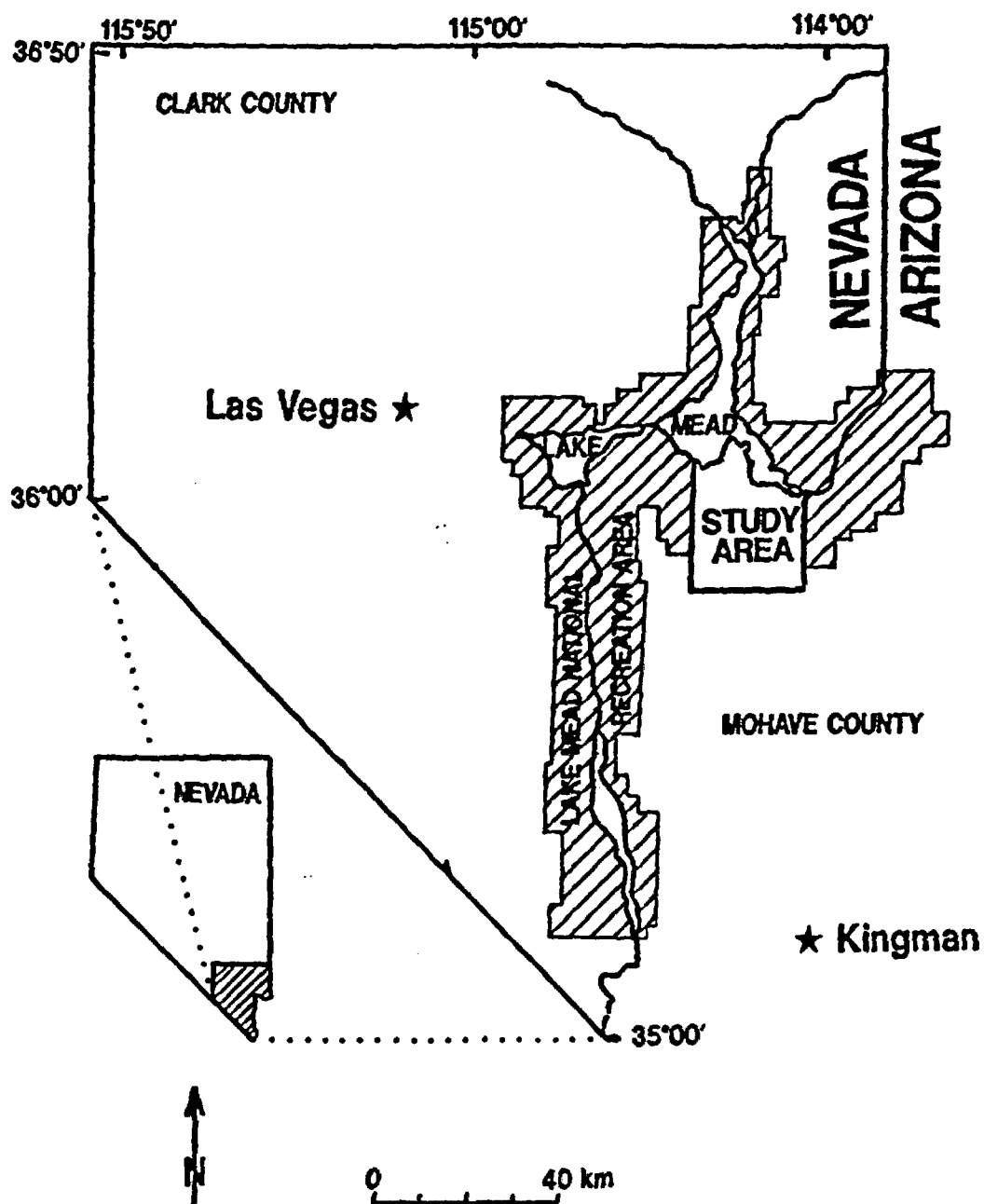


Figure 1. Location Map. Lake Mead National Recreation Area is hatchured.

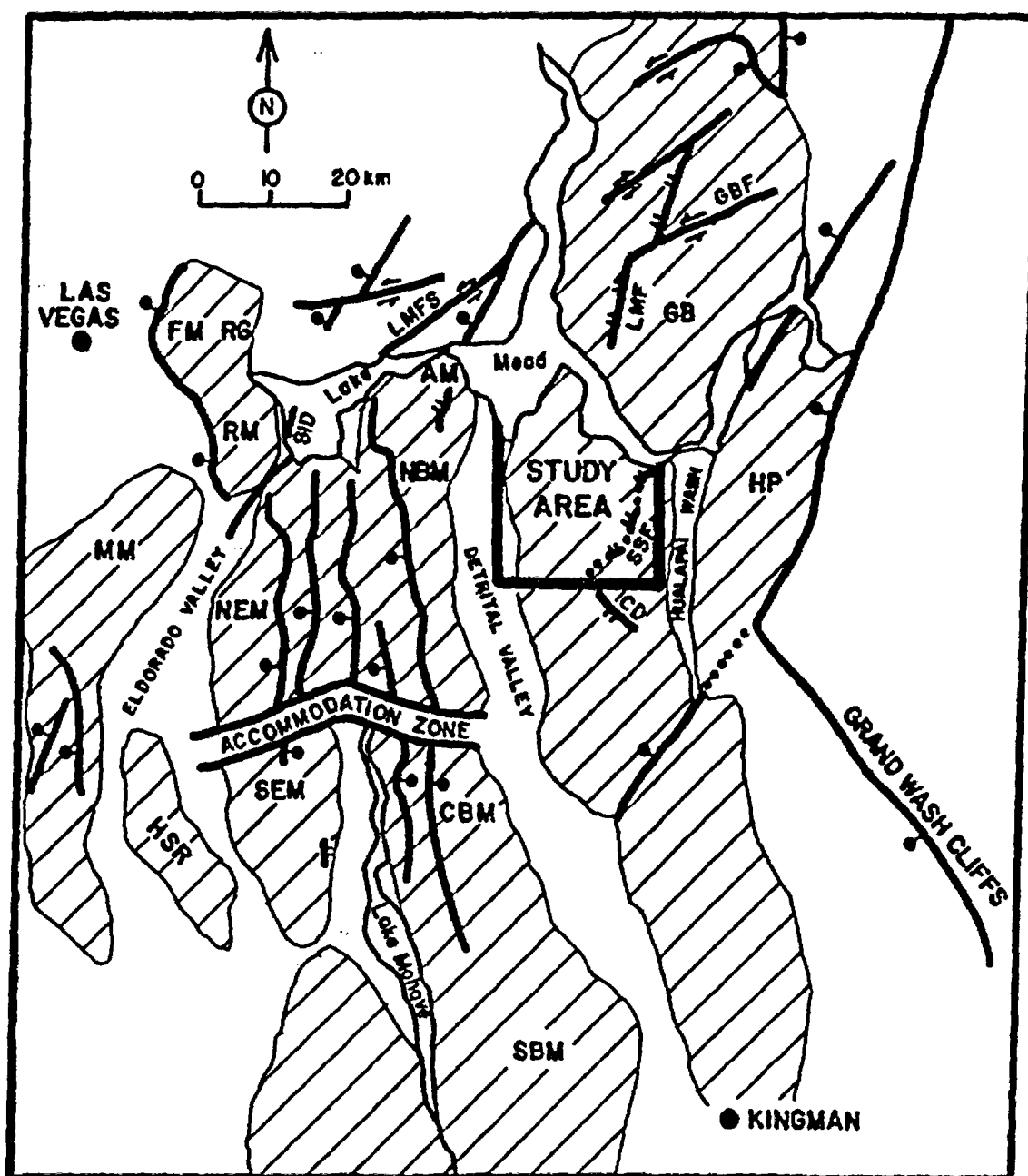


Figure 2. Regional sketch map. High-angle normal faults marked by ball on hanging wall. Low-angle normal faults marked by double tick marks on hanging wall. AM=Arch Mountain, CBM, NBM, SBM=central, northern and southern Black Mountains, FM=Frenchman Mountain, GB=Gold Butte, HP=Hualapai Plateau, HSR=Highland Spring Range, MM=McCullough Mountains, RG=Rainbow Gardens, RM=River Mountains, CD=Cyclopic detachment, LMF=Lakeside Mine fault, LMFS=Lake Mead fault system, SID=Saddle Island detachment, SSF=Salt Spring fault.

Colorado trough.

Intermediate volcanism in the Lake Mead area began at 20 Ma and continued to about 12 Ma (Smith et al., 1990). Younger, smaller volume basaltic volcanism occurred between 10.6 and 8.5 Ma at Callville Mesa, Nevada (Smith et al., 1990) and in the southern White Hills, Arizona (Calderone et al., 1991) and between 4-6 Ma in the Fortification Hill volcanic field (Anderson et al., 1972; Feuerbach and Smith, 1987). In the western Lake Mead region, volcanic stratigraphy is well established in the Eldorado and McCullough ranges (Anderson, 1971; Weber and Smith, 1987; Smith et al., 1988; Bridwell, in preparation); the River Mountains (Smith, 1982); the Hoover Dam area (Mills, 1985); northern Black Mountains (Feuerbach, 1986; Naumann, 1987); and southern Black Mountains (Faulds, 1989); but was not previously studied in detail in the eastern Lake Mead region. This thesis extends the well established stratigraphy of the northern Colorado River trough and western Lake Mead area east to the White Hills on the eastern margin of the Basin and Range.

Previous work in the northern White Hills focused primarily on the economic gold deposits to the south and east of the study area (Myers, 1985, Myers et al., 1986, Theodore et al., 1987, Santa Fe Pacific Railroad Co., 1981, and Blacet, 1968, 1969, 1972, and 1975). Longwell (1936) discussed the geology in Temple Basin and Virgin Canyon, now flooded by Lake Mead. Studies by Bohannon (1984), Blair et al. (1977, 1979), Blair and Armstrong (1989) and Bradbury et al. (1979) were concerned with deposition of the post-tectonic, Late

Miocene Muddy Creek Formation and Hualapai Limestone. The current study is the first to focus on regional correlation of mid-Miocene rock units, geochemistry and tectonics of the northern White Hills.

The purpose of this paper is to (1) determine the nature of the eastern boundary of the extensional allochthon in the eastern Basin-and-Range Province; (2) develop a model for the petrogenesis of northern White Hills volcanic rocks; and (3) correlate these volcanic rocks with others in the Lake Mead area.

TECHNIQUES

The 230 square mile study area was mapped at a scale of 1:62,500 (Plate 1). Stratigraphic sections were measured at Squaw Peak, Smith Hill, and Chuckwalla Ridge. At the Peninsula, Salt Spring Wash and Pink/Black Ridge, section thicknesses were estimated from the geologic map. One hundred-fifty samples were collected (Figure 3) for geochemical and petrographic analysis. Major elements were analyzed by the Rigaku 3030 X-ray Fluorescence (XRF) spectrometer at the University of Nevada, Las Vegas. Trace elements were analyzed by Instrumental Neutron Activation Analysis (INAA) at the Phoenix Memorial Laboratory at the University of Michigan. One biotite K-Ar age date was determined by the Geochron Laboratories Division of Krueger Enterprises, Inc. A description of analytical techniques and sample preparation methods can be found in Appendix E.

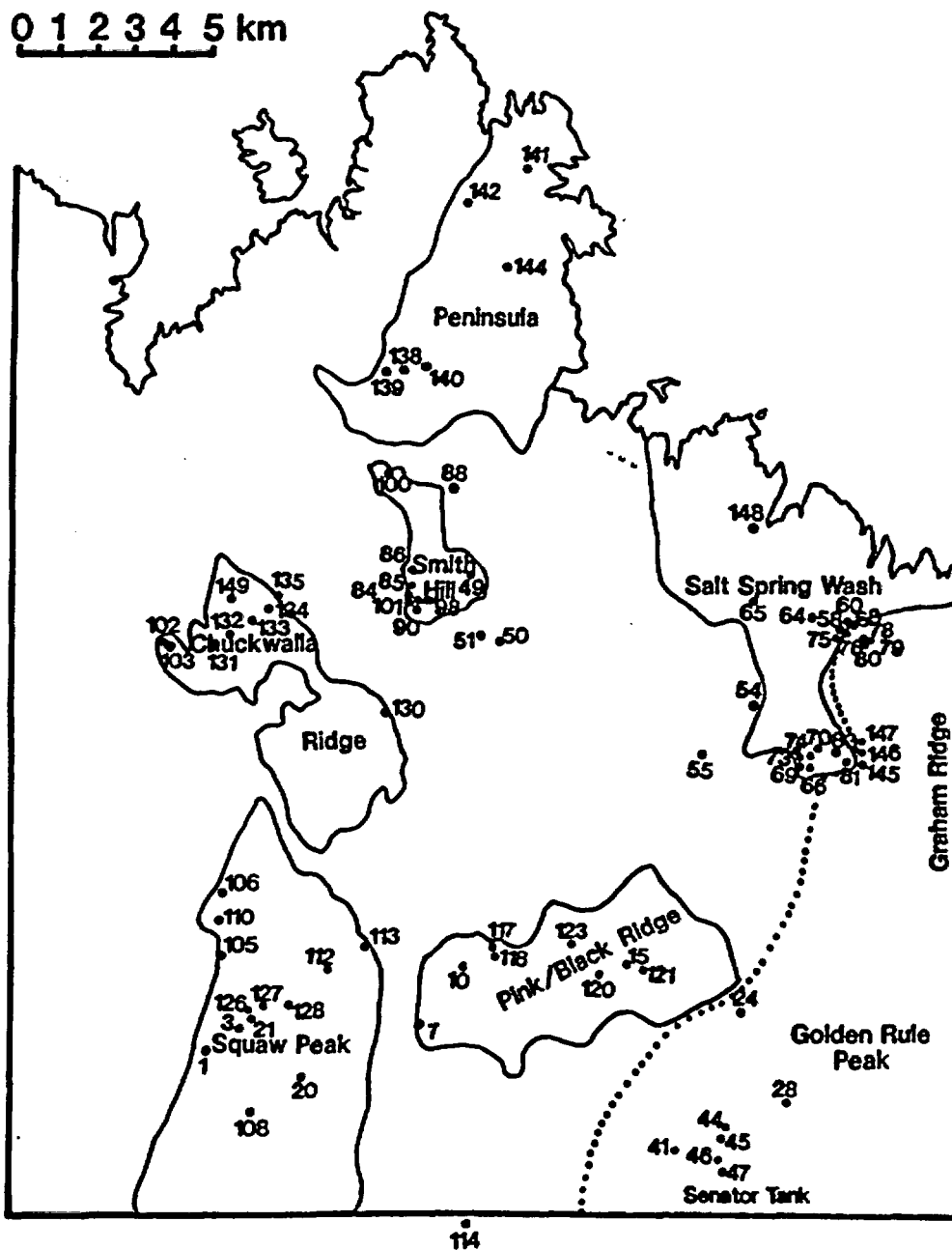


Figure 3. Sample location Map

Senator Mountain

WHITE HILLS VOLCANIC STRATIGRAPHY AND THE EASTERN LIMIT OF THE EXTENSIONAL ALLOCHTHON

INTRODUCTION

The northern White Hills (NWH) lie in the hanging wall of the west-dipping Salt Spring fault. The Salt Spring fault may represent a segment of a regional detachment zone that extends from Gold Butte to near Dolan Springs, Arizona (Cyclopic detachment). This fault zone lies 20 km west of the Grand Wash Cliffs and represents both the easternmost boundary of the extensional allochthon and the eastern limit of exposure of mid-Tertiary igneous rocks in the northern Colorado trough. The hanging wall of the Salt Spring fault contains six east-tilted structural blocks comprised of Miocene basalt and basaltic andesite flows and agglomerates, dacite ash-flow tuffs, megabreccia and fanglomerate. Because each block is isolated and contains only a small part of the stratigraphic section, geochemical data (Co, Cr, Eu, Hf, La, Nd, Sc, and Th) were used to construct a composite section.

VOLCANIC ROCKS OF THE NORTHERN WHITE HILLS

The six eastward-tilted structural blocks that were identified within the NWH contain distinctly different sections of Tertiary volcanic and sedimentary rocks (Figure 4). These are named the Squaw Peak, Salt Spring Wash, Pink/Black Ridge, Smith Hill, Peninsula and Chuckwalla Ridge blocks. Because the blocks are separated by late Tertiary and Quaternary sedimentary deposits, the correlation of stratigraphic sections could not be made on the basis of field

data alone. Correlation between the blocks is necessary to determine how the blocks are related structurally and to regionally correlate the volcanic rocks of the NWH with other volcanic sections in the Lake Mead area. Sections were correlated by the use of a combination of geochemical data, petrographic data and field relations (Figure 5). The resulting composite section is shown in Figure 6. Sections are described in detail in Appendix A. Geochemical data are summarized in Tables 1, 2, 4, 5 and 6. A new biotite K-Ar age date is reported in Table 8. Petrography is summarized in Tables 3, 7, and 9 and described in detail in Appendices B through D.

Correlation of sections

Although the stratigraphic sections in each structural block differ in lithology, there are similarities in the groupings of rock packages. Near the base of the sections at Squaw Peak, Smith Hill, Salt Spring Wash and the Peninsula is a dacite (60-71% SiO_2) ash-flow tuff. The tuff in all four sections is similar in chemistry (Tables 1 and 2, Figure 7) and mineralogy (Table 3). Although absolute concentrations of rare-earth elements (REE) vary, all samples exhibit similar chondrite-normalized REE patterns. On Figure 8, all but two samples exhibit a steady decrease in abundance with increase in atomic weight, with a moderate negative anomaly at Sm. One exception is a reworked ash from Chuckwalla Ridge (sample 102). The unusual signature for this sample may be attributed to alteration.

Variation in incompatible trace element (Hf, Sc and Ta) concentrations

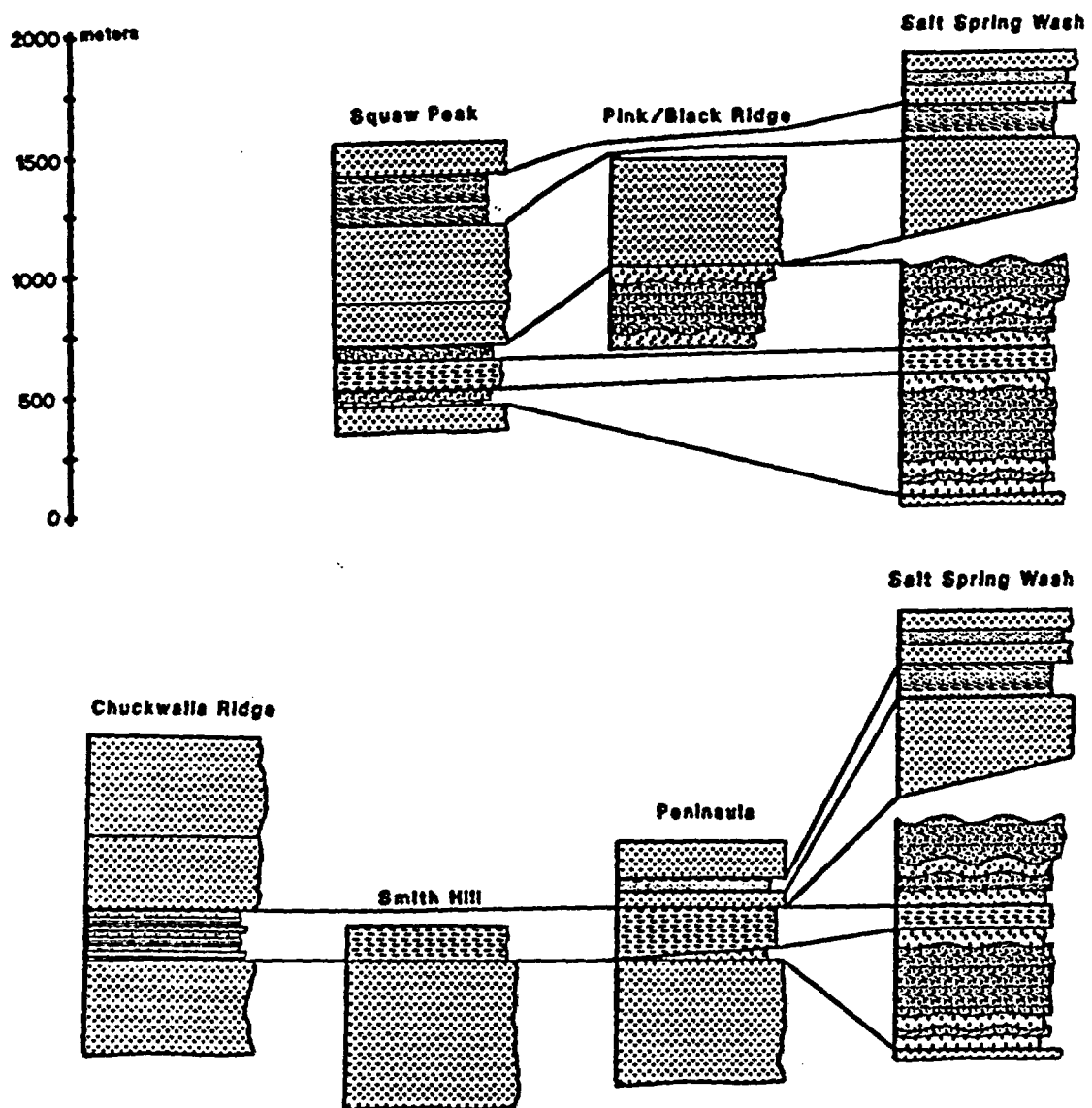
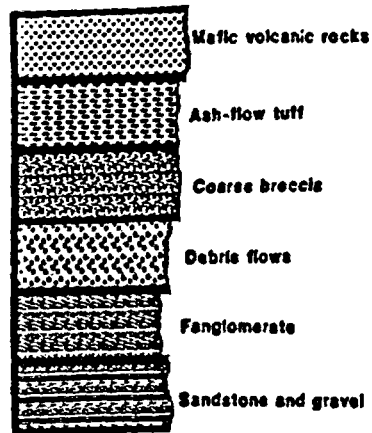


Figure 5. Correlated stratigraphic sections of the northern White Hills.

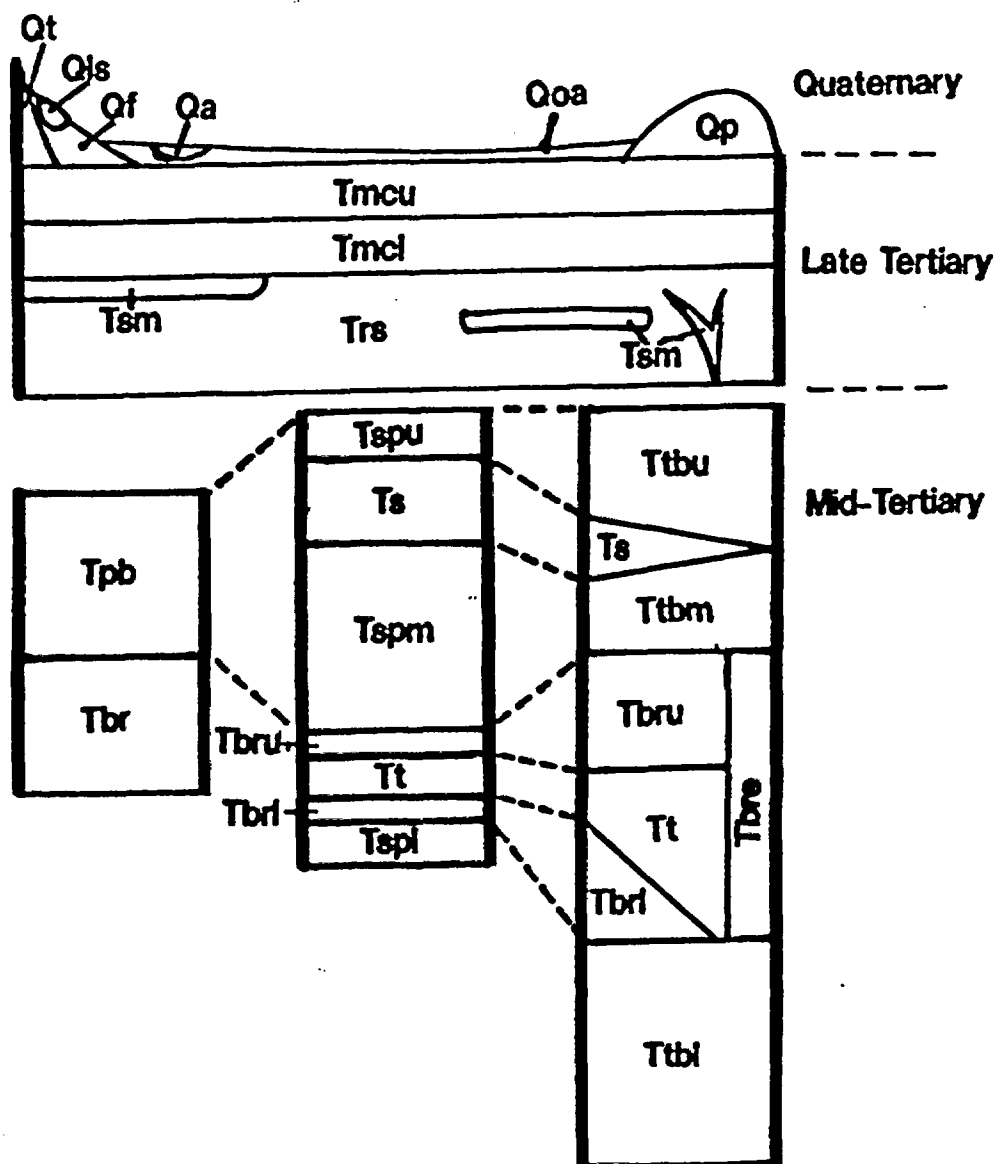


Figure 6. Composite stratigraphic section of the Northern White Hills.

Qa = alluvium, Qf = alluvial fan, Qls = landslide, Qoa = older alluvium, Qp = Colorado River pebble deposits, Qt = talus, Tbrl/Tbru = coarse breccia and debris flows, Tbre = sandstone and reworked ash, Tmcl/Tmcu = Muddy Creek Formation, Tpb = basalt of Pink/Black Ridge, Trs = Red Sandstone, Ts = fanglomerate, Tsm = basalt of Senator Mountain, Tspl/Tspm/Tspu = basaltic andesite of Squaw Peak, Tt = ash-flow tuff, Ttbl/Ttbm/Ttbu = basaltic andesite of Temple Bar.

Table 1: Major element data for ash-flow tuffs

Sample No.	Salt Spring Wash						Smith Hill			Squaw Peak			Peninsula		Chuckwalla
	54	69	73	70	83	81	101	84	98	1	110	106	144	142	102
SiO ₂	68.82	69.12	63.89	67.1	68.1	68.23	62.02	65.09	65.32	63.91	63.93	62.6	69.36	68.57	60.21
Al ₂ O ₃	14.79	12.56	13.48	14.39	13.74	15.21	13.86	15.81	14.85	15.99	15.7	16.04	13.73	12.81	13.95
FeO*	3.97	2.98	2.91	4.23	3.73	3.73	4.84	4.03	4.48	4.44	4.18	4.68	3.64	4.76	3.07
CaO	1.25	3.23	0.75	1.1	2.2	0.32	0.43	0	1.16	1.79	2.25	2.7	3.49	3.51	2.05
MgO	0.93	0.45	0.52	0.08	0.73	0.56	1.75	0.59	0.89	1.12	1.29	1.67	1.28	1.36	1.9
Na ₂ O	1.75	0.27	1.38	0.8	0.8	0.59	2.54	1.97	1.97	3.66	4.06	3.95	1.94	2.79	1.89
K ₂ O	8.35	7.63	8.03	8.92	6.79	9.3	5.83	10.34	8.43	6.52	5.65	5.42	3.76	3.42	3.68
TiO ₂	0.51	0.38	0.38	0.49	0.45	0.49	0.56	0.51	0.59	0.63	0.58	0.69	0.41	0.47	0.18
MnO	0.14	0.12	0.14	0.15	0.15	0.14	0.15	0.13	0.14	0.14	0.14	0.15	0.14	0.14	0.14
P ₂ O ₅	0.25	0.47	0.2	0.19	0.2	0.27	0.2	0.08	0.44	0.24	0.24	0.27	0.39	0.51	0.21
LOI	3.18	4.93	2.62	3.46	3.65	2.54	3.82	2.54	2.07	2.17	2.54	1.28	3.1	2.18	8.53
Total	103.94	102.14	94.3	100.91	100.54	101.38	96	101.09	100.34	100.61	100.56	99.45	101.24	100.52	95.81

Total iron as FeO

Table 2: Trace and rare earth element data for ash-flow tuffs

	Salt Spring Wash					Smith Hill				Squaw Peak			Peninsula	Chuckwalla	
	54	69	73	70	83	81	101	84	98	1	110	106	142	144	102
La	93.1	58	90.3	99.5	84	99.6	80.1	93.1	87.3	104	93.5	99.1	49.7	52	38.9
Co	170	93.6	168	172	144	187	161	161	153	190	174	188	83.7	86.1	71.9
Nd	53.3	41.5	65.2	63.9	56.8	64.6	67	57.8	54.5	63.9	66.4	74.1	41	45.7	35.2
Sm	8.41	5.79	10.3	9.03	7.77	8.89	7.77	7.76	7.63	9.9	8.84	9.77	5	4.77	5.09
Eu	1.63	1.26	1.1	1.39	1.14	1.51	1.77	1.66	1.79	2.12	1.96	2.22	1.19	1.05	0.515
Yb	2.65	1.8	3.43	3.13	2.8	3.1	2.16	2.51	2.37	2.58	2.4	2.4	1.62	1.9	2.29
Lu	0.28	0.23	0.47	0.39	0.37	0.35	0.291	0.26	0.3	0.304	0.32	0.32	0.23	0.29	0.36
U	4.87		7.16	5.79	4.64	4.74	1.42	4.44		5.42	4.4		3.84		3.56
Th	27.1	15.3	36.7	28.4	25.6	30.1	20	23.3	17.9	23.4	22.2	20.4	10.5	11.7	21.2
Cr	20.9	13.8		19	14.1	22.3	37.9	30.6	33.3	20.6	34.1	40	16.9		16.8
Hf	10.2		10.1	9.36	9.28	10.3	9.13	8.74	9.78	10.8	10.4	11.3	5.25	6.34	4.02
Ba	924	2300		444	601	647	1390	1260	1350	1370	1130	1410	1100	1790	480
Rb	169	110	175	171	129	174	127	205	193	116	115			123	108
Sr							3970				897	1210		2330	6760
Sc	4.46	3.47	2.37	5.11	3.61	3.8	5.42	3.87	5.03	5.74	5.87	6.29	5.74	3.98	3.06
Ta	1.56	1.12	1.96	1.9	1.9	2.23	1.34	1.53	1.23	1.52	1.42	1.65	0.99	1.02	1.16
Zr	559														
Co	4.29	1.74	2.16	5.23	3.02	2.7	12.1	2.59	4.99	5.54	6.57	7.11	6.32	3.75	5.66
V	32.2	39.1	19.5	33.5	34.5	36.2	53.5	40.5	49.1	70.2	55.2	63	43.3	32.5	18.3
Dy	3.82	2.93	5.71	4.4	3.61	4.46	3.74	3.25	3.53	4.03	3.82		2.33		2.88

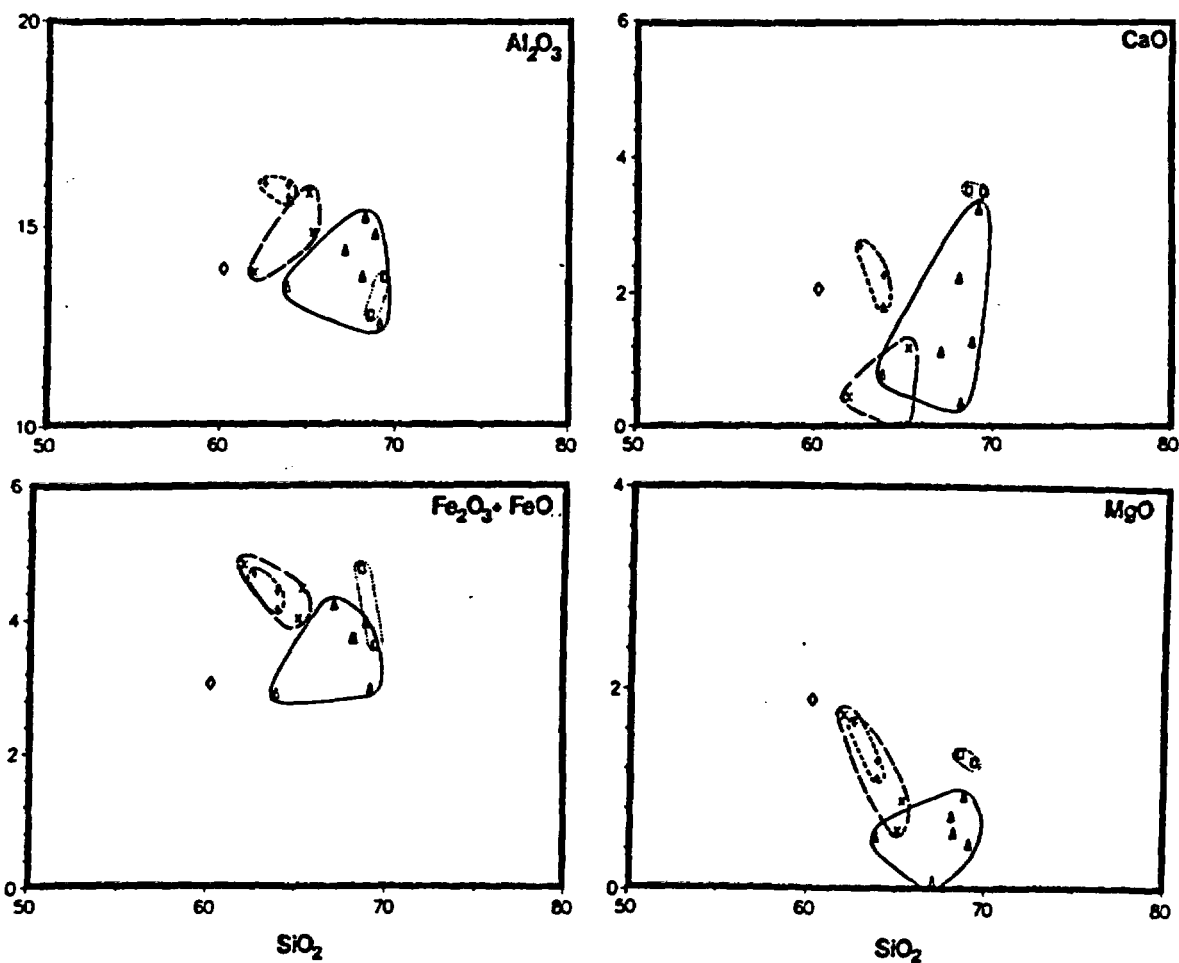


Figure 7. Harker variation diagrams for ash-flow tuffs: SiO_2 vs. major oxides. Diamonds=Chuckwalla Ridge, squares=Peninsula, X=Smith Hill, crosses=Squaw Peak, triangles=Salt Spring Wash. Units are weight percent.

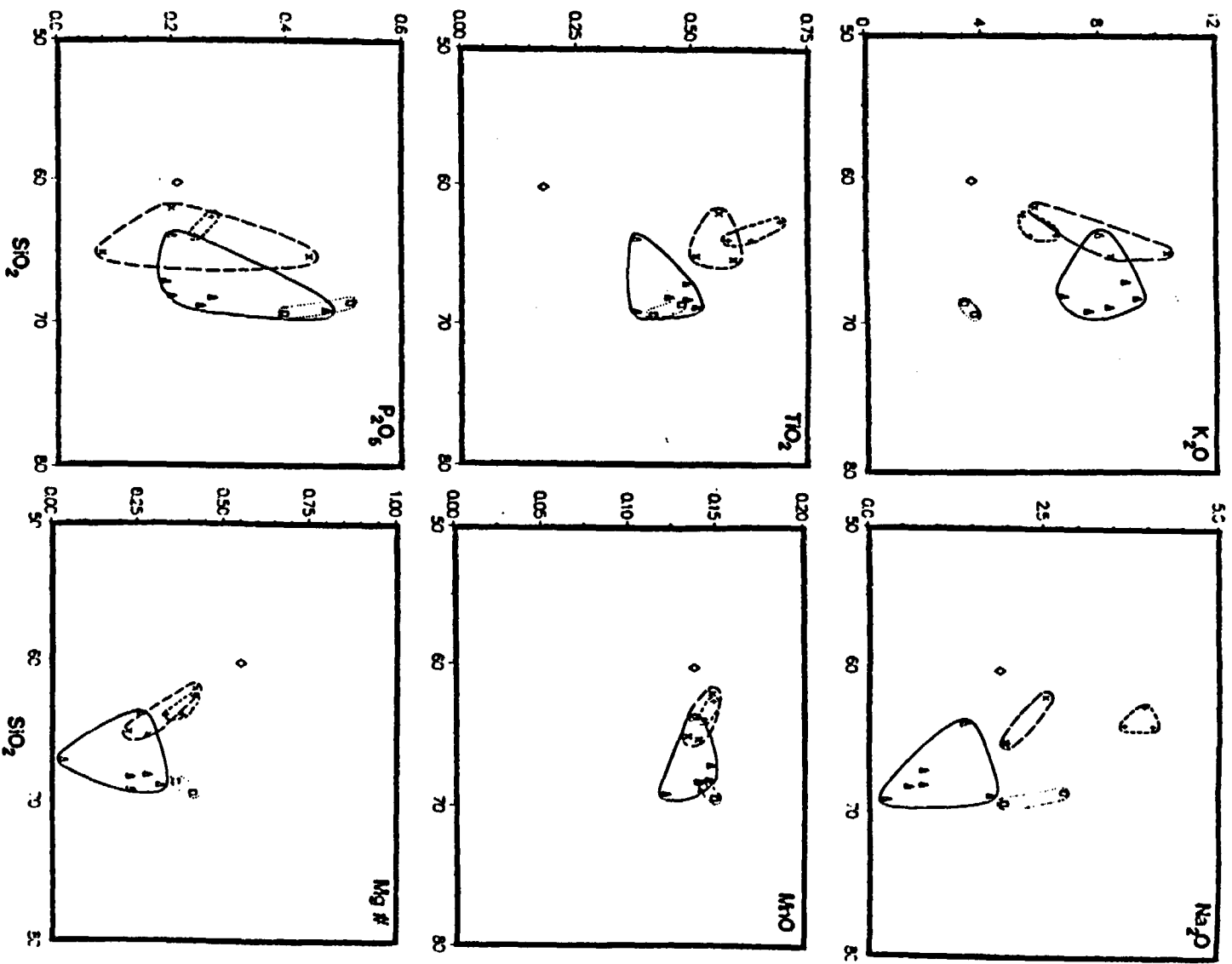


Figure 7, continued.

Table 3: Summary of mineralogy for ash-flow tuffs

	Sample No.	% Lithic Fragments	% Pumice Fragments	% San-idine	% Plag-ioclase	% Quartz	% Bio-tite	% Spheno	% Clino-pyroxene	% Olivine	% Zircon	% Opaques
Penin-sula	137				21		2	0.2	8	0.3		2
	144	0.1	2	7	6		3	tr	1			.4
	136	15	6	1	12		3	tr	0.7		0.3	1.5
	142	4	7	4	9	0.4	4	1	0.7			1
Salt Spring Wash	54	6	10	6	4		2	0.5	0.2		0.1	.7
	69	15	1	4	3	0.4	1	tr			tr	.3
	73	4	3	9	1	0.5	0.2					.2
	70	10	6	0.4	1		1	0.3	0.3		0.1	.2
	83	2		6	3	1	1					1
	81	7	11	1	1		0.7	0.1	tr		0.2	.8
Smith Hill	101	11	2	9	4	0.2	0.6		0.1		tr	.4
	84	2	2	20	11		3					.6
	150	4	10	3	9		3	tr	0.6		0.8	1
	98	12	5	9	10	0.1	4	tr				2
	96	13		12	7		4	tr			tr	.8
Squaw Peak	1	6	24	9	9	0.2	3	tr	0.9		tr	.6
	111	10	12	10	15		1		2		tr	.2
	106	6	4	11	8		2		0.6			.2
Chuck-walla Ridge	102	2		4	1		1		0.3			

* Percent based on counts of 1000 points per slide using a Swift point counter. Unreported percentage is ash matrix

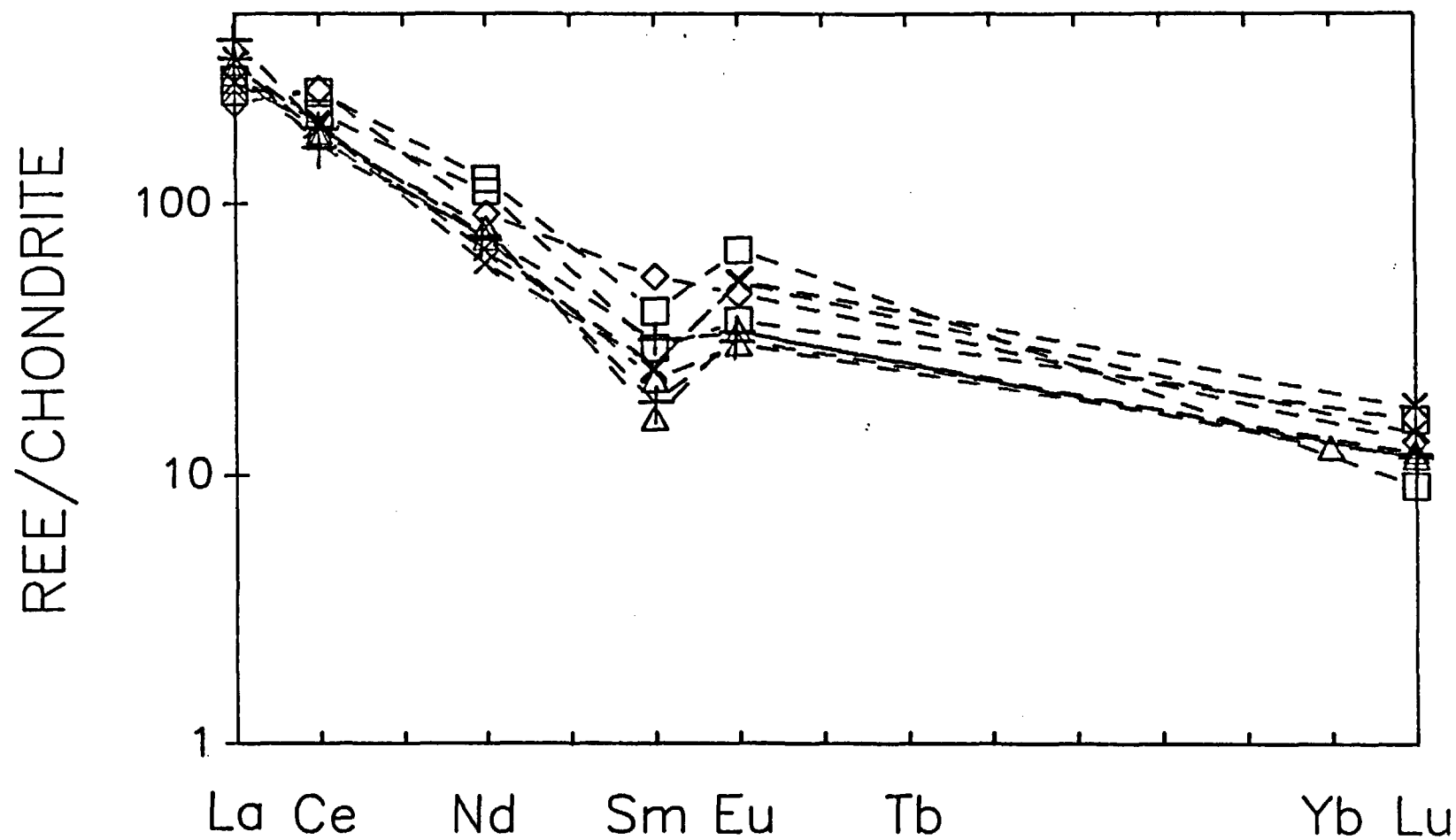


Figure 8. Chondrite-normalized rare earth elements for ash-flow tuffs. The highest and lowest values from each locality are plotted. Symbols are defined on Figure 7. Chondrite values from Hanson (1980).

(Figure 9) may be due largely to variations in the abundance of accessory minerals such as sphene, zircon and apatite. Variation in compatible trace element (Co, Cr and V) concentrations (Figure 10) may be due to variation in the proportion of mafic volcanic and Precambrian lithic fragments. Alternatively, compatible trace element variation may be due to compositional zoning in the ash-flow tuff. Petrographic analysis (Table 3) demonstrates that although mineral component percentages vary, the variation between exposures is no greater than that within exposures.

Interbedded with the ash-flow tuff in the Salt Spring Wash and Squaw Peak sections is a coarse breccia in which the dominant clast types are Precambrian gneiss, granite, amphibolite and mylonite with minor mud-supported conglomerate and sandstone. The breccia is also present at Pink/Black Ridge. The deposits are similar in all four sections and are comprised mostly of crackle breccia (no matrix) and jigsaw breccia (minor matrix) according to the scheme of Yarnold and Lombard (1989). In the Peninsula section, coarse breccia is lacking, but mud-supported conglomerate is present.

The tuff and breccia are an important stratigraphic marker that aided in correlation of the stratigraphic sections. The tuff is tentatively correlated with the Tuff of Bridge Spring, a regionally extensive ash-flow sheet. Near the base of the section at Chuckwalla Ridge, 214 meters of sandstone and pebble conglomerate are interbedded with layers of reworked, biotite-rich ash that are tentatively correlated with the dacite ash-flow tuff.

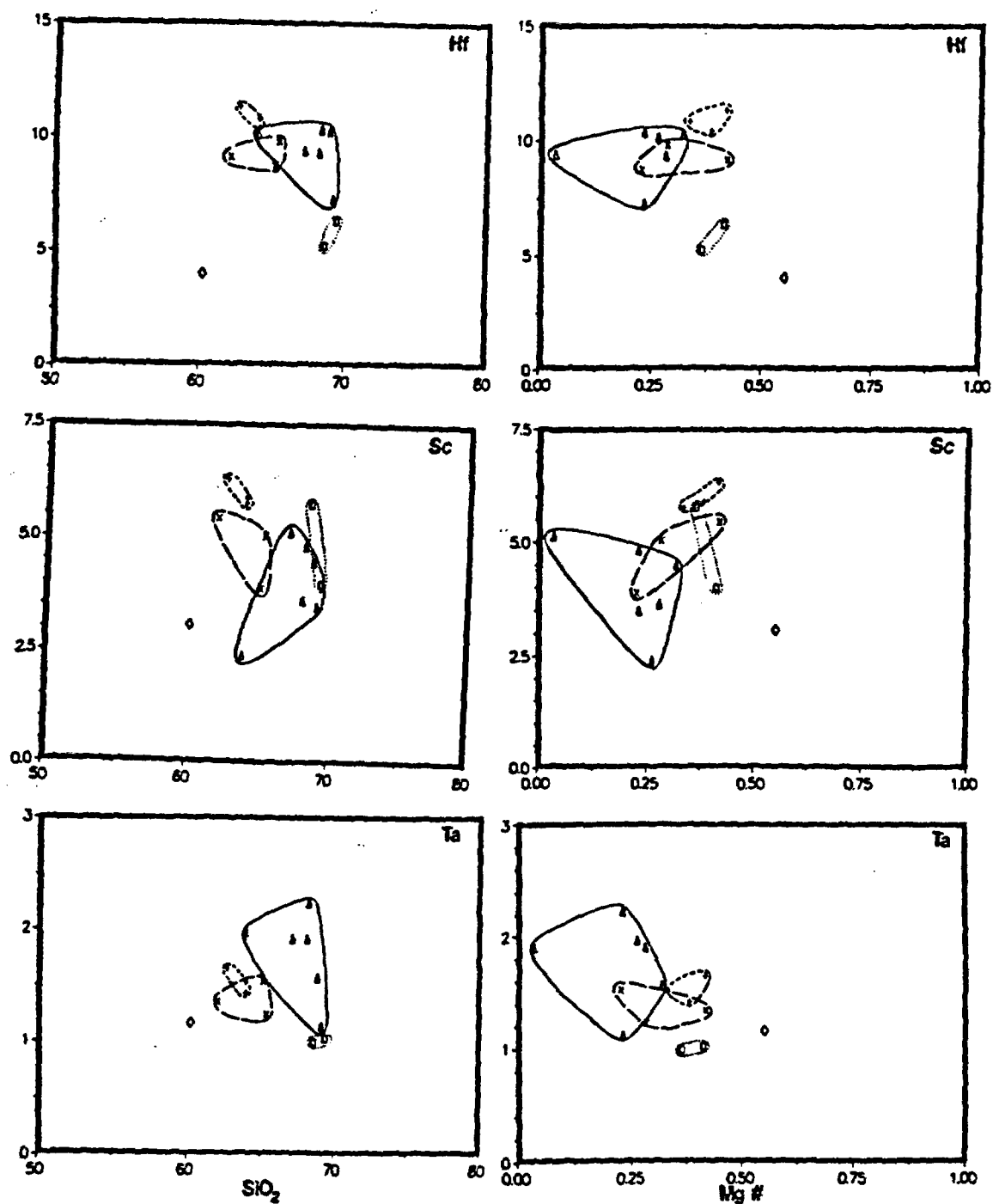


Figure 9. Harker variation diagrams for ash-flow tuffs. Weight percent SiO_2 and Mg# plotted against incompatible trace elements Hf, Ta and Sc (ppm). Symbols are defined on Figure 7.

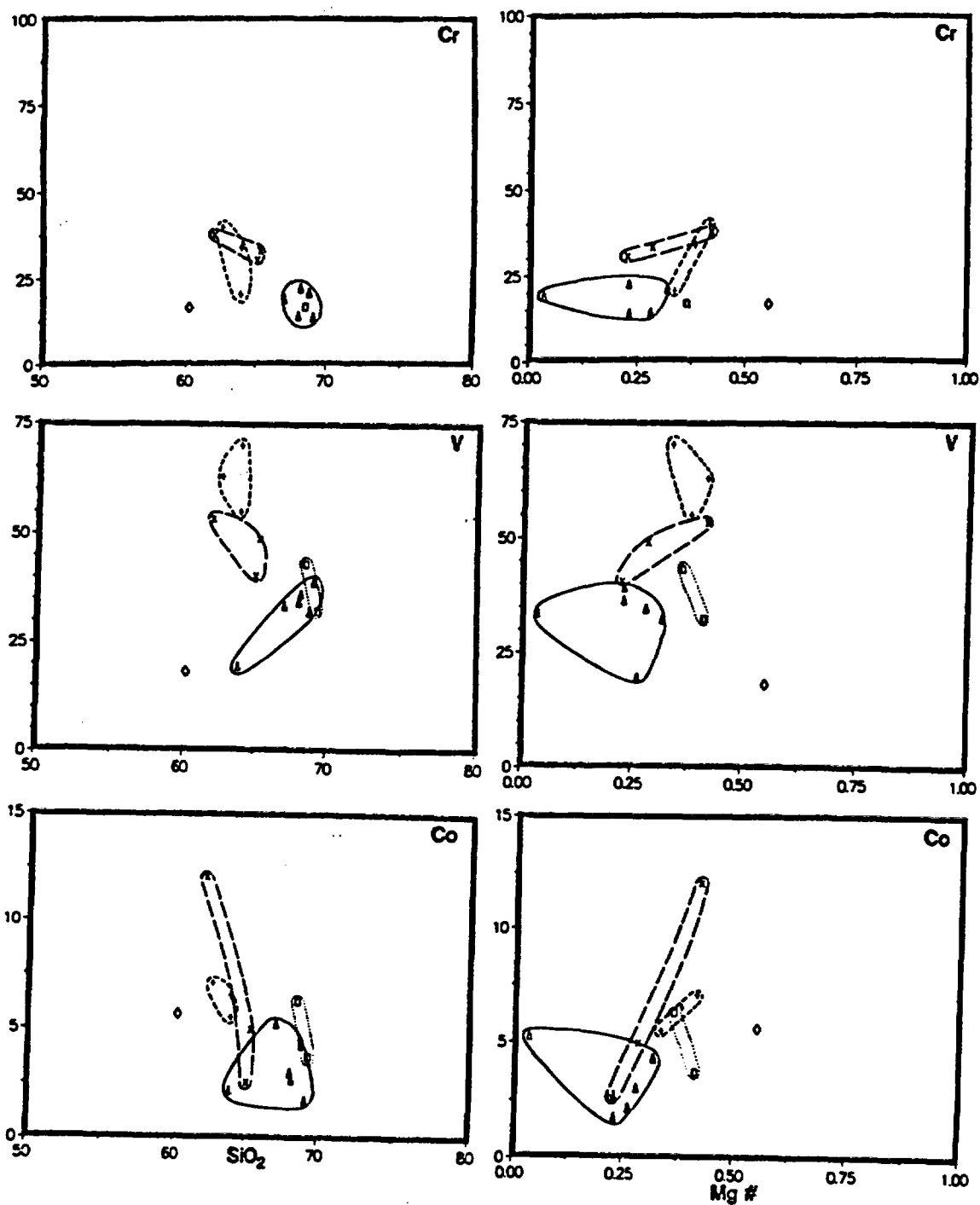


Figure 10. Harker variation diagrams for ash-flow tuffs. Weight percent SiO_2 and Mg\# plotted against compatible trace elements Cr, V and Co (ppm). Symbols are defined on Figure 7.

Mafic volcanic rocks in the NWH occur as flows and autoclastic and volcanoclastic breccias in varying proportions. Samples from Pink/Black Ridge are petrographically distinct from samples from the other sections (Table 4). The only phenocryst phase in the Pink/Black Ridge samples is olivine. Samples from the other five sections contain plagioclase as the dominant phenocryst phase with subequal amounts of clinopyroxene and olivine.

Mafic volcanic rocks form two distinct groups in terms of chemistry (Tables 5, 6 and 7). Harker variation diagrams with SiO_2 and magnesium number ($\text{Mg\#} = \text{Mg}/\text{Mg} + \text{Fe}$) versus La, Hf, Th, Sc, total REE ($\text{La} + \text{Ce} + \text{Nd} + \text{Sm} + \text{Eu} + \text{Yb} + \text{Lu}$) and total alkalis ($\text{Na}_2\text{O} + \text{K}_2\text{O}$) (Figure 11) demonstrate the clear division between the basalt of Pink/Black Ridge and the basaltic andesite of Chuckwalla Ridge, Smith Hill, Salt Spring Wash and the Peninsula. The basaltic andesite in the Chuckwalla Ridge, Smith Hill, Salt Spring Wash and Peninsula sections are correlated on the basis of their chemical similarity and are hereafter named the basaltic andesite of Temple Bar (Ttb).

The chemical data for the basaltic andesite of Squaw Peak (Tsp) occupy an intermediate position between the basalt of Pink/Black Ridge (Tpb) and Ttb. Plots of Hf/Th versus TiO_2 , La/Yb, Sc, and CaO (Figure 12) and of total REE and La/Yb versus Eu, Sm and Nd (Figure 13) demonstrate this clustering of rock types as well. The distribution of data points for Tsp could be explained by an intermingling of Tpb and Ttb flows in the Squaw Peak area. However, unlike Tpb basalts, Squaw Peak basalts contain clinopyroxene as a phenocryst phase.

Table 4: Summary of mineralogy for mafic volcanic rocks*

Sample No.	PHENOCRYSTS										GROUNDMASS					% Vae-icles	Texture of Groundmass
	% Plag ioclase	% Olivine	% Clns pyroxene	% Mag actite	% Phlo gopite	% Horn-blende	% Plag ioclase	% Olivine	% Clns pyroxene	% Horn actite	% Cryp crystals	% Glass					
Ttbl	139	26	11	2			7	5		49			cx, s f-c				
	138	18	8	1	0.2		3	2		66			2 cx, f				
	90	13	14				31	7	4	23			7 mx, s f-c, subtrachytic				
Ttbm	85		16	3	1		47	6	17	9			1 mx, f, trachytic				
	51	22	2	7			8	6	2	1	48		5 cx, f				
	50	19	1	11	6		33	9	5	4	8		3 mx, s f-c, felty				
	148	16	6	6			29	5	4	1	33		mx, s f-c, felty				
	65	15	1	4	1		59	1	17	3			mx, c				
	131	17	2	7			13	5	3		48		cx, f				
	132	7	1	8			13	3	4	12		51	cx, f				
	134	26	3	6			17	3	4	10	22		10 mx, f, felty				
	135	13	1	7			1	1	3	2	54		17 cx, f				
	149	11		7	1		19		8		41		14 cx, m				
	49	10		10			24		11		37		9 mx, s m-c, felty				
	125	34		5	2		4		3		51		1 f, f				
	140	22		6			15		6	3	48		cx, f				
	133	19		9			14		10	1	31		14 mx, s f-m, felty				
	130	16		10			16		6		45		6 mx, f, felty				
	86	12		3	4		33			9	39		mx, f, felty				
	143						13			15	14		48 mx, s f-c, subtrachytic				
	141	2	5				25			1	64		3 mx, f, felty				
Ttba	77	27	0.6	9			46	6	5	3	1		mx, s f-c, felty				
	88	21	4	6	1		22	3	4		28		11 mx, f, felty				
	100	4	1	1	1		14	1			49	22	8 cx, f				

codes for textures:

mx = microcrystals dominant in groundmass

cx = cryptocrystals dominant in groundmass

f = glass dominant in groundmass

* percent based on counts of 500 points per slide using a Swift point counter

s = seriate microcrystal size range

c = coarse-sized microcrystals

m = medium-sized microcrystals

f = fine-grained microcrystals

Table 4: continued

	PHENOCRYSTS							GROUNDMASS							Texture of Groundmass
	Sample No.	% Plag ioclaso	% Olivine	% Clino pyroxeno	% Mag netito	% Phlo gopito	% Horn- blendo	% Plag ioclaso	% Olivine	% Clino pyroxeno	% Hem atito	% Cryp crystals	% Glass	% Ves- icles	
Tpb	7	2	3		1			49	8	9	15		10	3	mx, c, subtrachytic
	10	0.6	5					47	20	16	7	2		3	mx, s f-c, trachytic
	120	1	2			1		61	7	23	5				mx, m, trachytic
	15	0.4	0.4					49	23	7	5	7		11	mx, m, trachytic
	124	3	1					40	7	14	1	8		25	mx, f, trachytic
	117	6						35	10	16	12	11	1	10	mx, c, trachytic
	118		5					61	8	21	4			1	mx, f, trachytic
	121		1					43	12	17	9	7		11	mx, f, trachytic
	123		1					37	13	13	3	24		11	mx, f, trachytic
Tsm	55	3						32		9	2	32		21	mx, s f-c, felty
	55b	4						52	15	12	3	3		11	mx, c, felty
	103	1	1	3	3			49	8	1	10	17		7	mx, c, felty
	114	13	2	2	1			8	5	2		60		6	mx, f, felty
Tspm	3	24	4					43	10	8	1		1	1	mx, s f-c, trachytic
	21		6					39	12	5	13	12	12	12	mx, m, trachytic
	108		12					44	15		13	16			mx, f, trachytic
	126	5	2					45	16	2	11	8	11	11	mx, m, subtrachytic
	127	2	5					50	12	10	5	13	3	3	mx, m, subtrachytic
	128	13	9					31	3	8	1	19	10	10	mx, f, felty
Tspu	112	23	0.6					12	6		8	28	15	15	mx, f, felty
	113	24	1					28	2	8	4	22			mx, f, felty
	20	1	9					31	9	3	8	34			mx, f, felty

Table 5: Major element data for mafic volcanic rocks

	Ttbi		Ttbn								
	139	138	90	85	51	50	148	65	131	132	134
SiO2	58.48	60.45	54.56	48.98	54.15	54.26	52.43	56.97	55.78	51.61	55.93
Al2O3	16	15.94	16.42	14.26	16.12	14.37	16.377	15.28	14.71	14.97	15.39
FeO*	7.31	5.81	8.04	10.87	7.13	7.57	8.351	8.16	7.1	8.28	6.2
CaO	6.53	4.83	6.5	8.87	7.48	9.62	7.217	6.99	6.72	9.4	8.74
MgO	3.09	2.07	1.69	9.44	2.82	3.47	3.183	4.23	4.94	4.72	2.83
Na2O	3.46	3.15	3.66	3.18	3.6	3.28	3.185	3.2	3.38	2.86	3.3
K2O	2.7	3.94	4.26	1.38	3.79	3.63	3.528	3.56	3.72	2.86	3.14
TiO2	1.17	1	1.22	1.6	1.2	1.07	1.284	1.16	1.09	1.29	1.05
MnO	0.16	0.15	0.14	0.166	0.139	0.161	0.159	0.153	0.159	0.159	0.157
P2O5	1.04	0.77	0.66	0.53	0.6	1.42	0.988	0.63	0.63	1.41	0.65
LOI	0.65	1.61	1.95	2.14	2.96	2.76	2.23	1.79	2.03	2.3	2.98
Total	100.63	100.49	99.1	101.42	99.99	101.61	98.93	102.12	100.26	99.86	100.37

	Ttbn						Ttbn				
	135	149	49	140	133	130	86	141	77	88	100
SiO ₂	59.56	58.041	53.68	58.277	54.35	55.39	60.39	49.073	54.61	52.53	53.39
Al ₂ O ₃	14.98	15.641	14.45	15.796	15.19	15.71	16.34	15.84	15.97	14.93	16.63
FeO*	6.83	7.655	6.52	6.549	6.81	6.16	6.24	10.332	8.49	6.45	7.26
CaO	6.79	6.229	10.03	5.439	7.61	8.27	4.37	11.825	7.66	10.27	5.63
MgO	2.72	3.559	4.38	2.139	3.85	2.73	1.76	4.631	3.91	2.9	2.7
Na ₂ O	3.44	3.134	3.02	3.613	3.24	3.44	5.37	2.702	3.35	3.3	3.43
K ₂ O	4.13	3.421	3.37	3.329	3.49	3.78	4.23	1.237	3.37	3.37	3.83
TiO ₂	0.99	1.141	1.03	0.956	1.03	1.04	0.87	1.383	1.2	0.99	1.01
MnO	0.147	0.154	0.159	0.146	0.158	0.147	0.149	0.161	0.158	0.161	0.148
P ₂ O ₅	0.56	1.02	0.63	0.924	1.24	0.56	0.45	0.922	0.62	0.64	1.2
LOI	1.48	0.56	2.88	1.26	2.65	2.15	1.39	3.31	1.23	4.11	3.35
Total	101.63	100.56	100.15	98.43	99.62	99.38	101.56	101.42	100.57	99.65	98.57

* Total iron as FeO

Table 5: continued

	Tpb					Tsm					
	7	10	120	15	117	118	121	123	55	103	114
SiO ₂	46.74	47.33	50.99	51.53	51.96	49.69	49.66	49.76	48.6	47.82	50.21
Al ₂ O ₃	15.6	14.97	15.8	16.05	15.44	14.08	15.64	15.82	15.22	15.27	15.52
FeO*	10.06	12.32	11.23	10.54	10.13	11.56	10.44	10.86	12.21	11.48	11.53
CaO	13.98	10.24	9.57	9.95	9.1	9.85	10.62	10.41	12.55	9.41	9.58
MgO	3.39	7.02	5.66	5.48	6.74	6.95	5	5.5	4.87	5.28	6.52
Na ₂ O	3.07	2.87	3.36	3.27	3.14	3.43	3.32	3.37	3.21	2.61	3.24
K ₂ O	1.75	1.2	1.71	1.56	1.66	1.3	1.86	1.91	1.15	1.2	1.39
TiO ₂	1.38	1.51	1.64	1.47	1.46	1.38	1.51	1.56	1.31	1.27	1.46
MnO	0.166	0.166	0.166	0.162	0.161	0.164	0.166	0.165	0.164	0.127	0.166
P ₂ O ₅	0.96	0.38	0.53	0.52	0.54	0.42	0.56	0.66	0.38	0.26	0.36
LOI	2.05	1.76	1.03	0.96	1.31	1.78	0.94	1.42	1.78	4.43	1.12
Total	99.15	99.77	101.69	101.49	101.64	100.6	99.72	101.44	101.44	99.16	101.1

	Tspm					Tspu			
	3	21	108	126	127	128	112	113	20
SiO ₂	53.86	49.44	48.84	49.33	48.67	52.95	54.78	54.52	51.77
Al ₂ O ₃	15.05	15.04	15.35	15.34	15.04	14.92	16.19	16.47	15.69
FeO*	8.17	9.68	10.76	9.61	10.44	7.79	6.69	6.96	9.1
CaO	6.8	8.49	7.91	9.19	8.85	7.59	6.35	6.45	6.99
MgO	4.76	7.31	6.42	5.45	5.56	7.1	3.04	2.44	7.36
Na ₂ O	3.08	3.3	3.16	3.55	3.42	2.6	3.41	3.34	3.93
K ₂ O	3.91	1.73	2.06	2.04	1.89	3.1	3.9	4.03	2.14
TiO ₂	1.2	1.9	1.84	1.73	2.14	1.19	1.04	1.04	1.1
MnO	0.165	0.166	0.159	0.164	0.165	0.166	0.15	0.148	0.163
P ₂ O ₅	0.56	0.48	0.59	0.63	0.6	0.61	1.11	1.16	0.6
LOI	2.48	2.63	4.09	2.84	3.02	2.79	2.07	2.31	1.88
Total	100.04	100.17	101.18	99.87	99.79	100.81	98.73	98.88	100.72

* Total iron as FeO

Table 6: Trace and rare earth element data for mafic volcanic rocks

	Ttbl		Ttbm								
	139	138	90	85	51	50	148	65	131	132	134
La	71	72.7	89	41.2	82.5	79.9	66.8	73.6	73.4	75.6	73.8
Ce	125	128	169	82.7	162	158	131	150	131	144	142
Nd	68.8	52.4	84.5	54.6	77.1	69	70.5	61.4	71	83.2	73.7
Sm	8.47	8.21	12.7	7.35	12.1	11.6	9.81	10.3	10.4	11.5	10.5
Eu	2	1.89	2.81	2.12	2.76	2.8	2.37	2.62	2.36	2.59	2.46
Yb	1.99	2.1	2.44	2.16	1.88	2.46	2.62	2.05	2.28	2.46	2.33
Lu	0.33	0.31	0.38	0.33	0.31	0.3	0.32	0.26	0.33	0.33	0.35
U	3.16	3.24	5.2	0.654	6.27	3.76	6.3	2.81	3.38	3.75	4.58
Th	10.3	15.2	19.1	4.11	17.7	15.1	16	15.3	15.5	14.1	14.8
Cr	45.3	43	133	501	184	176	123	188	164	248	155
Hf	6.55	8.05	8.65	5	7.96	7.4	7.31	6.94	6.76	6.59	7.17
Ba	1260	1360	1480	555	1310	1340	1210	1200	1320	1120	1170
Rb	47.4	85.1	96.9		69.3	49.8	79.4	85.1	94.9	54.4	63.5
Sr	943	906	1280	970	1340	1620	1340	1300	1060	1240	1610
Sc	14.2	10.8	15.3	20.4	17.5	15.7	18.9	17	14.9	20.4	17.1
Ta	1.94	1.47	1.2	0.82	1.28	0.91	0.99	1.24	1.14	1.33	1.17
Co	17.2	12.9	20.8	40.7	15.9	19.2	25.7	22.7	19.8	24.8	17
V	138	103	170		152	138	162	147	147	169	157
Dy	3.97	2.96	5.63		4.51	4.8	5.23	5.12	4.39	4.86	4.67

	Ttbm						Ttbu				
	135	149	49	140	133	130	86	141	77	88	100
La	71.8	73.2	76.3	62.2	71.4	76.7	92.6	33.2	71.3	69.7	82.7
Ce	139	142	148	119	135	147	173	61.5	122	132	143
Nd	64.8	64.9	64.2	49.5	68.9	76.3	85.1	33.2	64.4	55.8	73
Sm	8.83	9.81	11.6	6.86	9.72	10.7	11	6.23	10.2	10.2	9.93
Eu	2.15	2.21	2.8	1.77	2.35	2.38	2.64	1.84	2.2	2.36	2.21
Yb	1.9	2.79	1.99	1.55	2.33	2.61	2.62	2.61	2.12	2.09	2.36
Lu	0.28	0.41	0.38	0.25	0.35	0.38	0.45	0.42	0.36	0.26	0.35
U	3.78	4.91	4.05	1.56	3.54	6.28	4.66	1.68	4.76	3.18	2.92
Th	13.2	20.7	15.2	9.56	15.3	17	15.7	3.75	12.9	13.9	13.3
Cr	95.7	91.7	240	41.2	163	225	31.8	236	147	155	70.1
Hf	7.25	7.72	6.69	6.51	7.04	7.56	9.18	4.41	6.15	7.06	7.55
Ba	2040	1100	1360	1270	1230	1240	1510	593	1130	1420	1480
Rb	84.2	79.6	62.5	70.4	73.7	89.4	100		74	68.3	52.9
Sr	1580	885	1300	1290	1170	1280	987	860	876	1390	1300
Sc	13.3	15.7	18.2	12	14.6	16.5	7.66	28.9	16.7	15.6	12.1
Ta	1.36	1.37	1.07	1.26	1.21	1.08	1.33	0.73	0.85	1.03	1.13
Co	13.4	21.2	19.2	16.5	20.7	14.1	12.3	3.51	19.8	15.6	14.5
V	158	136	127	111	141	152	91.4	196	160	131	112
Dy	3.88	4.58	4.43		4.42	4.61	4.81	4.43	4.29	4.49	4.79

Table 6: continued

	Tpb					Tsm					
	7	10	120	15	117	118	121	123	55	103	114
La	27.8	23	39.6	35.6	35.6	24.8	47.5	49.3	15.1	12.8	20.5
Ce	53.1	43.4	77.7	67.5	67.8	48	91.4	95.1	31.4	27.4	43.6
Nd		29	28.5	33.3	35.6		50.8	46.1		19.1	
Sm	5.05	4.43	6.19	5.75	5.67	4.85	6.81	7.07	3.36	3.46	4.06
Eu	1.65	1.46	2.03	1.93	1.82	1.72	1.92	2.22	1.28	1.19	1.39
Yb	2.24	2.14	2.28	2.23	2.24	2.12	2.34	2.16	1.55	1.86	2.16
Lu	0.31	0.28	0.33	0.31	0.25	0.29	0.25	0.29	0.23	0.36	0.26
U	2.91					2.67				2.38	
Th	2.84	2.53	3.9	3.63	3.88		4.07	4.37		2.86	3.15
Cr	150	201	166	191	208	301	118	138	306	310	247
Hf	3.84	3.58	5.5	4.36	4.23	4.29	5.01	4.91	2.33	2.85	3.47
Ba	536	426	650	798	572	473	893	1040	344	245	391
Rb	39.7										
Sr			854	1370	1140		1090	1440		2510	
Sc	25.2	25.4	27.4	25	24.5	27.4	25.3	25	21	24.8	22.6
Ta		0.69	1	0.71	1.24	1.1	0.87	0.99	0.85	0.59	0.653
Co	27	37.8	31.8	29.8	29.5	40.3	27.6	30.2	40.4	45.7	37.8
V	181	186	198	171	191	195	187	200	162	176	170
Dy	4.14	3.4	3.5	4.13	3.77	3.36	4.56	3.48	3.01	3.57	4.33

	Tspm					Tspu			
	3	21	108	126	127	128	112	113	20
La	76.8	34.6	51		43.8	78.3	78.5	76.2	59.4
Ce	153	63.3	90.9		83	152	149	153	110
Nd	74.1	37.5	57.2		50.9	78.4	70.1	70.7	46.8
Sm	11.1	6.05	7.65		7.17	11.5	10.3	10	6.67
Eu	2.6	1.72	2.09		2.17	2.53	2.26	2.43	1.92
Yb	2.57	2.29	2.58	2.52	2.42	2.28	2.11	2.42	1.88
Lu	0.38	0.35	0.44	0.42	0.41	0.37	0.33	0.36	0.3
U	4.29	1.26	1.53	1.27	1	3.38	3.87	4.32	1.8
Th	17.7	4.18	6.03	5.9	5.2	15.7	18.3	18.7	7.58
Cr	252	227	264	202	217	293	81.8	88.4	271
Hf	8.49	4.73	5.6	6.27	6.41	8.24	7.52	7.86	5.14
Ba	1000	430	848	517	525	0	1360	2430	950
Rb	83.7					70.2	82	105	
Sr	987	9.46			856	928	1290	1670	848
Sc	16.7	20.7	20.7	19.5	20.9	17.6	11.2	11.9	15.3
Ta	1.09	1.28	1.44	1.35	1.75	1.19	1.11	1.38	1.58
Co	22.7	33.5	37.3	30.3	33.2	27.7	16	15.7	29.7
V	183	204	176	171	188	162	129	138	132
Dy	5.09	4.14	4.85	5.25	4.64	4.38	4.6	4.76	3.9

Table 7: Maximum, minimum and average major element concentrations for mafic volcanic rocks

	Chuckwalla Ridge (7)			Smith Hill (8)			Peninsula (4)		
	High	Low	Average	High	Low	Average	High	Low	Average
SiO ₂	59.56	51.61	55.81	60.39	48.98	53.99	60.45	49.07	56.57
Al ₂ O ₃	15.71	14.71	15.23	16.63	14.26	15.44	16	15.8	15.89
FeO*	8.26	6.1	7.01	10.87	6.24	7.51	10.33	6.55	8.35
CaO	9.4	6.23	7.68	10.27	4.37	7.85	11.82	4.84	7.16
MgO	4.94	2.72	3.62	9.44	1.69	4.26	4.63	2.07	2.98
Na ₂ O	3.44	2.86	3.25	3.02	5.37	3.61	3.61	2.7	3.23
K ₂ O	4.13	2.86	3.51	4.26	1.38	3.48	3.95	1.24	2.8
TiO ₂	1.29	0.99	1.09	1.6	0.87	1.12	1.38	0.96	1.13
MnO	0.16	0.15	0.15	0.17	0.14	0.15	0.16	0.15	0.16
P ₂ O ₅	1.41	0.56	0.722	1.42	0.45	0.77	1.05	0.773	0.916
LOI	2.98	0.56	2.02	4.11	1.39	2.69	3.31	0.65	1.7

	Salt Spring Wash (3)			Pink/Black Ridge (11)			Squaw Peak (9)		
	High	Low	Average	High	Low	Average	High	Low	Average
SiO ₂	56.97	52.43	54.67	51.96	46.74	49.71	54.78	48.67	51.57
Al ₂ O ₃	16.38	15.28	15.88	16.05	14.08	15.42	16.47	14.92	15.45
FeO*	8.49	8.16	8.33	10.06	12.32	10.89	10.76	6.69	8.8
CaO	7.66	6.99	7.29	13.98	9.1	10.46	9.19	6.35	7.62
MgO	4.23	3.18	3.77	7.02	3.39	5.72	7.36	2.44	5.49
Na ₂ O	3.35	3.18	3.24	3.43	2.87	3.23	3.93	2.6	3.31
K ₂ O	3.56	3.37	3.49	1.91	1.2	1.62	4.03	1.73	2.66
TiO ₂	1.28	1.16	1.21	1.64	1.38	1.49	2.14	1.04	1.45
MnO	0.16	0.15	0.16	0.16	0.17	0.16	0.17	0.15	0.14
P ₂ O ₅	0.988	0.62	0.798	0.96	0.38	0.567	1.16	0.48	0.644
LOI	2.23	1.23	1.75	2.05	0.94	1.41	2.07	4.09	2.67

(#) denotes number of samples averaged

* Total iron as FeO

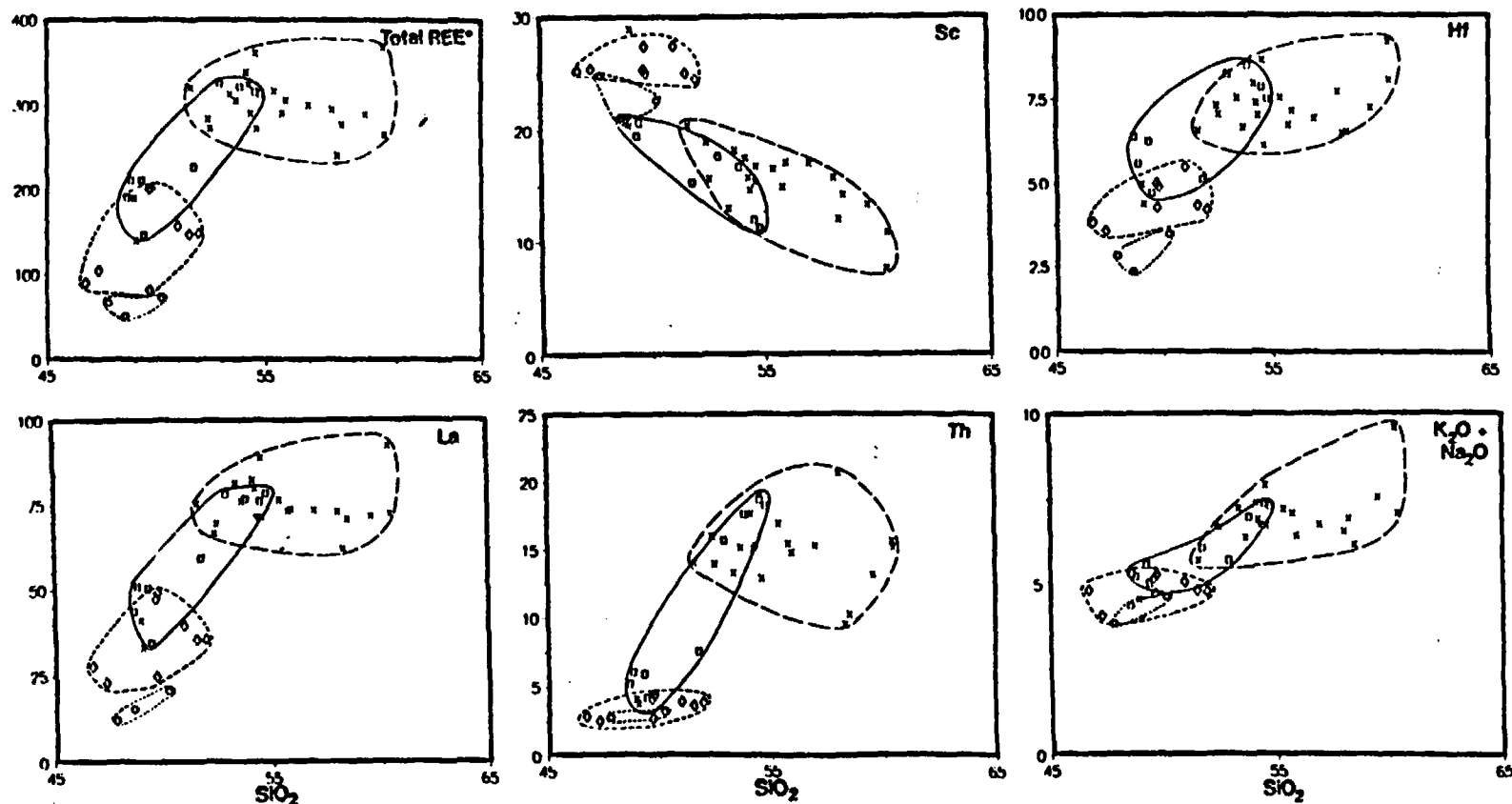


Figure 11a. Harker variation diagrams for mafic volcanic rocks. Weight percent SiO_2 plotted against total REE* (La+Ce+Nd+Sm+Eu+Yb+Lu), Sc, Hf, La, Th and weight percent total alkalis. Trace elements are in ppm. Diamonds=basalt of Pink/Black Ridge, X=basaltic andesite of Temple Bar, squares=basaltic andesite of Squaw Peak, circles=basalt of Senator Mountain.

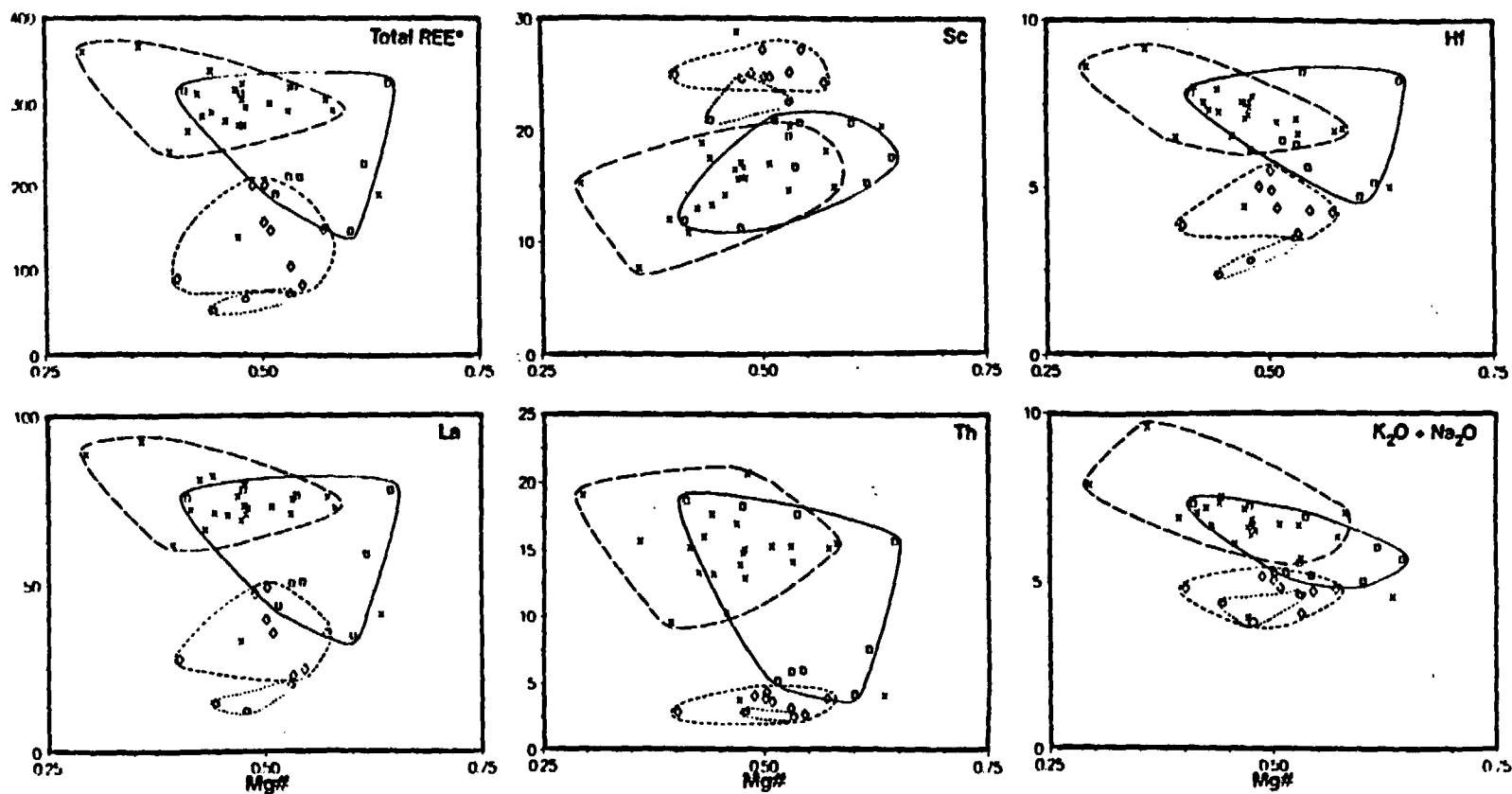


Figure 11b. Harker variation diagrams for mafic volcanic rocks. Mg# plotted against total REE* (La+Ce+Nd+Sm+Eu+Yb+Lu), Sc, Hf, La, Th and weight percent total alkalis.

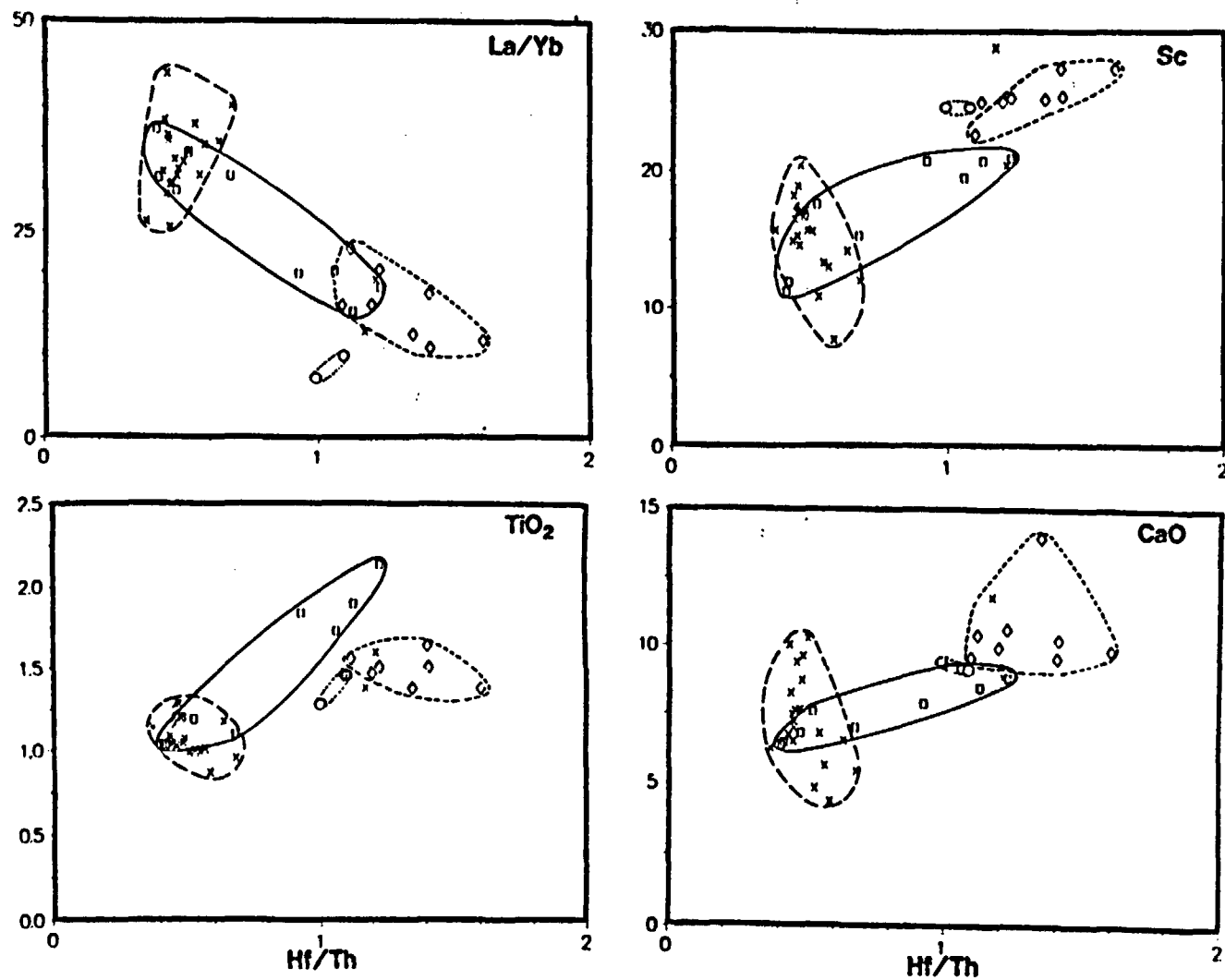


Figure 12. Hf/Th plotted against La/Yb , major oxides TiO_2 and CaO , and Sc . Symbols defined on Figure 11a. 31

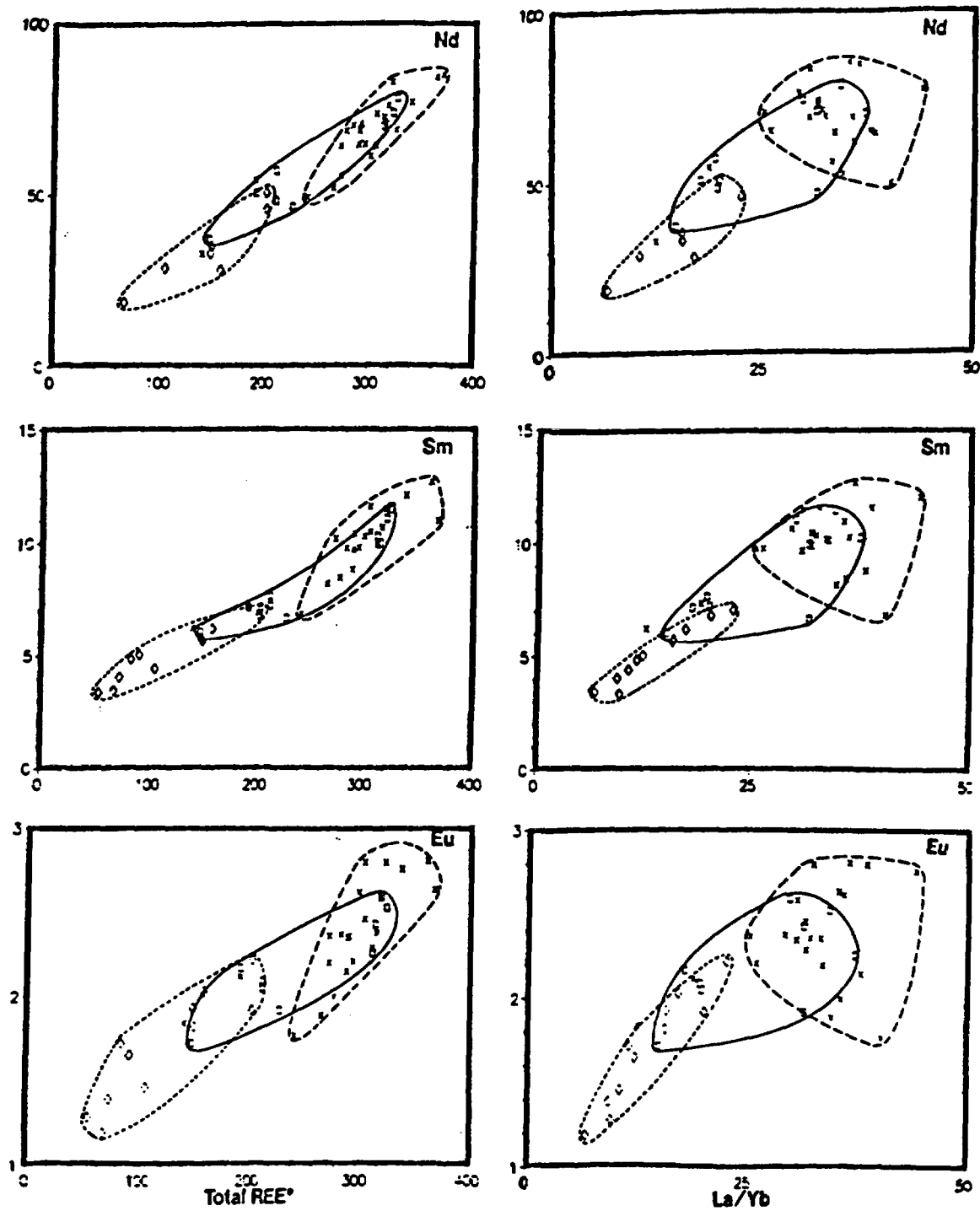


Figure 13. Total REE* and La/Yb plotted against light REEs Sm, Nd, & Eu.
Symbols defined on Figure 11a.

Therefore, the clinopyroxene-bearing basalts represent a third type of magma. Because the basaltic andesite samples from Squaw Peak cluster with Ttb basaltic andesite in all diagrams, the source for these flows may be the same as that for Ttb. However, because Tsp basalts are not distinguishable from Tsp basaltic andesites in hand sample, and because of the interlayered nature of the basalt/basaltic andesite flows, all of the mafic volcanic rocks in the Squaw Peak section are mapped as Tsp, regardless of chemical composition.

Chondrite-normalized REE data (Figure 14) allow identification of a fourth type of mafic volcanic rock. Samples 114, 55 and 103 plot with lower overall REE than all other NWH mafic volcanic rocks and have chondrite-normalized REE patterns similar to subalkalic basaltic andesite of Callville Mesa and basalt of Fortification Hill (Smith et al., 1990). The three locations are widely scattered (Figure 3) but chemical similarity prompts correlation as a single rock type; here named the basalt of Senator Mountain (Tsm).

On the basis of stratigraphic position, Ttb, Tpb and Tsp appear to be contemporaneous. The lowermost portions of all sections except Pink/Black Ridge contain basaltic andesite (Ttbl and Tspl) overlain by ash-flow tuff plus or minus coarse breccia or a correlative sedimentary unit. The upper part of the stratigraphic sections at Squaw Peak, Salt Spring Wash and the Peninsula consists of either Tsp or Ttb basaltic andesite overlain by sandstone, siltstone and conglomerate that is in turn overlain by basaltic andesite. Similar deposits are interbedded with basaltic andesite in the upper part of the Smith Hill section as

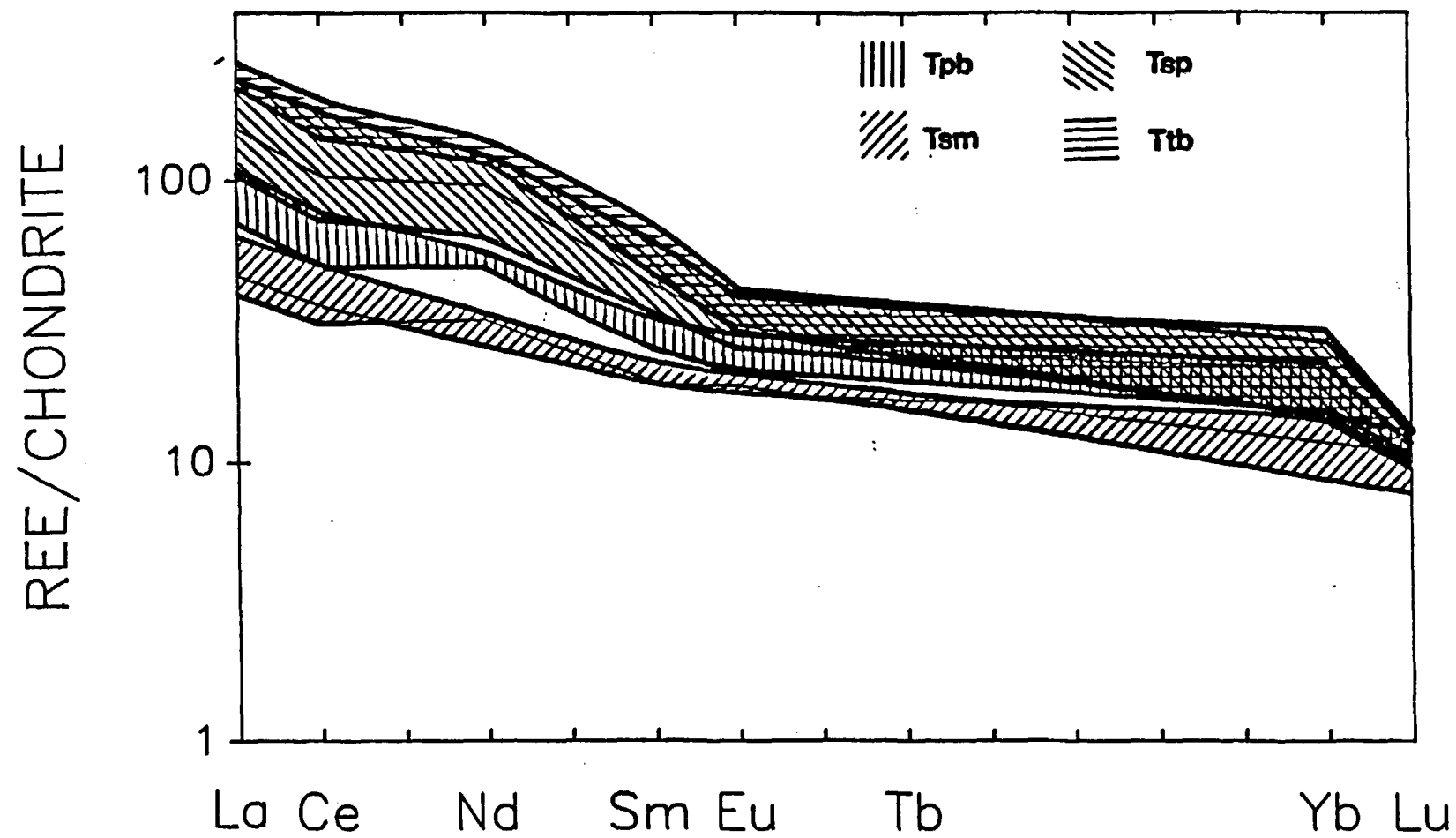


Figure 14. Chondrite-normalized REE plot for mafic volcanics.

well. Clasts are dominantly Precambrian crystalline rock (70%), but mafic volcanic clasts are also common (30%).

The basalt of Senator Mountain crops out as: (1) a dike (sample 103) that intrudes the base of the section on the west side of Chuckwalla Ridge. (2) Discontinuous outcrops of basalt flows north of Pink/Black Ridge (sample 55) that are interbedded with poorly consolidated sandy gravels that dip 5-10° north-northeast. (3) Flows on Senator Mountain, situated 1.5 km south of the study area (sample 114). These flows overlie poorly consolidated gravels that appear to be continuous with gravels that unconformably overlie Tpb and Tbr at Pink/Black Ridge. Tsm is therefore younger than the tilted mid-Tertiary section in the NWH (Figure 6).

Composite section

A composite section (Figure 6) was constructed by using the maximum thickness of each stratigraphic unit.

The dacite (60-71% SiO₂) ash-flow tuff (Tt) is present near the base of the sections at Squaw Peak, Salt Spring Wash, Smith Hill, and Peninsula. It is thickest (179 m) in the Peninsula section, where it contains 2 cooling units. Although no ash-flow tuff is present at Pink/Black Ridge, the presence of Tt at depth is inferred by the relatively constant thickness of the tuff to the southwest (122 m at Squaw Peak), north (150 m at Smith Hill) and northeast (94 m at Salt Spring Wash). At Salt Spring Wash, the tuff records a growth fault sequence (Switzer, personal communication). A sample of the tuff from Smith Hill (sample

84) was dated at 16.4 ± 0.5 Ma (Table 8). The significance of this date will be discussed in a later section on regional correlation.

The tuff is poorly to moderately welded and contains phenocrysts of sanidine (0-20%), plagioclase (1-15%), biotite (0.2-4%), clinopyroxene (0-2%) and quartz (0-1%). Spinel (0-0.5%) and zircon (0-0.8%) are present as accessory minerals. Apatite occurs as inclusions in biotite and feldspar phenocrysts in many samples. Pumice fragments contain phenocrysts of biotite as well as sanidine and plagioclase in subequal proportions. Lithic fragments are of four types; dacite with plagioclase and biotite phenocrysts, basalt with plagioclase, olivine and clinopyroxene phenocrysts, two-mica granitoids and biotite schist. Devitrification is slight in most samples, but is most pronounced in samples from Salt Spring Wash, where samples have also suffered severe calcification.

Five clasts from the coarse monolithologic breccia (Tbr) interbedded with Tt were analyzed petrographically (Table 9). The crackle and jigsaw breccias that underlie and overlie Tt were produced by landslides. Minor mud-supported conglomerate and sandstone beds, found locally at the base and/or top of the unit, are interpreted as debris flow and stream channel deposits. The breccias are thickest (513 m) at Salt Spring Wash where matrix-rich zones are present near the base of the exposure. In addition, clastic dikes are exposed in small outcrops at Pink/Black Ridge. The breccias are of considerable interest in determining the unroofing history of the Salt Spring fault and is the subject of a study by Switzer (work in progress). Tbr remains thick (343 m) up to 5 kilometers to the west of

Table 8: New biotite K-Ar date on ash-flow tuff, White Hills

Sample	K %	Ar* (ppm)	Ar*/Total Ar*	K (ppm)	Date & error
84	7.161	0.008186	0.036004	8.542	16.4 +/- 0.5 Ma

* denotes radiogenic

Table 9: Summary of mineralogy for coarse breccia clasts*

Sample Number	PROGRADE AND RELICT MINERALS								
	Quartz	Plagioclase	Microcline	Biotite	Muscovite	Opaque	Sphene	Zircon	Apatite
64	25	10	35	15	2	2	<1		<1
66	43	9	33						
74	28	30	10	5				<1	
105a	30	10	20						
105b	30	20	20	1		3		<1	

Sample Number	RETROGRADE AND INTRODUCED MINERALS				
	Calcite	Chlorite	Epidote	Hematite	Sericite
64		2	3		5
66	5			10	
74			2	5	20
105a					40
105b		3			23

* percentages are estimated

the detachment at Pink/Black Ridge, but thins rapidly to the west at Squaw Peak (63 m) and to the north on the Peninsula (0-42 m). Longwell (1936) described similar deposits in the Virgin Basin (now flooded by Lake Mead). Tbrl is poorly resistant to weathering and thus produces talus that covers much of the contact between Tbrl and Tspl/Ttbl. On the basis of a few outcrops where the contact is exposed, Tbrl appears to rest conformably on Ttbl and Tspl without angular discordance.

The amount of time represented by the deposition of the tuff and breccia may be brief, as both types of deposits can acquire considerable thickness in a short period of time. However, the correlative (?) braided stream deposits at the base of the Chuckwalla Ridge section probably represent a longer period of time.

The Temple Bar basaltic andesite (Ttb) (49-60% SiO₂) is characterized by low CaO, MgO, FeO, Mg#, Sc, Ti, Cr and Hf/Th and high Eu, Hf, Th, La/Yb and total REE relative to the other mafic volcanics of the NWH (Figures 11-14, Tables 5 and 6). Division of the lower, middle and upper portions of the Temple Bar volcanics was made on the basis of stratigraphic position, and there is no systematic vertical variation in petrography or chemistry.

The lower part of the Ttb section (Ttbl) is thickest (515 m) in the Peninsula. The base of the section is buried, and at Chuckwalla Ridge and Smith Hill, only the uppermost 74 and 180 m of Ttbl are exposed, respectively. The middle part of the Ttb section (Ttbm) is thickest (up to 1000 m) in the Chuckwalla Ridge and Smith Hill sections, where it is crystal-rich, and thins

dramatically to the east and north in the Peninsula and Salt Spring Wash sections, where it is crystal-poor. Eruption of two chemically indistinguishable basaltic andesites (Tt_{bm} and Tt_{bu}) was interrupted by deposition of fanglomerate (Ts) in the Peninsula, Salt Spring Wash and Smith Hill sections. Dikes chemically similar to Tt_{bm} and Tt_{bu} intrude the Tt_{bm} flows at Smith Hill and at Chuckwalla Ridge. The upper part of the Tt_b section (Tt_{bu}) is 171 m thick and lies above fanglomerate (Ts) at Salt Spring Wash and in the Peninsula. At Salt Spring Wash, fanglomerates similar to Ts are interbedded with Tt_{bu} flows. At Chuckwalla Ridge Ts is absent and the contact between Tt_{bm} and Tt_{bu} is obscure.

Tt_b consists of flows and breccias of basaltic andesite with similar mineralogy. Within and between sections, minor changes in mineralogy are not systematic. Basaltic andesite contains phenocrysts of plagioclase (0-34%), olivine (0-6%), clinopyroxene (0-14%) and magnetite (0-6%). Plagioclase phenocrysts are rectangular and up to 4 mm long. They are embayed, fritted and sieved. Most are subhedral and many have non-pitted overgrowths. Olivine phenocrysts are embayed, subhedral to anhedral and altered to iddingsite along margins and fractures. Most are less than 0.5 mm, but may reach 1 mm in size. Clinopyroxene phenocrysts are subhedral to anhedral, pitted and embayed, and commonly have magnetite inclusions. Many have euhedral unpitted and unaltered clinopyroxene overgrowing highly altered cores. Five samples (65, 77, 130, 138 and 140) contain two populations of clinopyroxene; a small (<0.5 mm) anhedral

variety that is highly altered and overgrown by unaltered subhedral clinopyroxene, and a second unaltered, subhedral to euhedral variety that is up to 2 mm in size. Sample 138 contains small altered needles of phlogopite (?) (0.2%) as well. Small plagioclase laths and clinopyroxene phenocrysts coexist in glomerocrysts that reach 3 mm in size. Sample 131 contains 4% basaltic xenoliths containing olivine + plagioclase microcrystals in a glassy, hematitic groundmass. Sample 86 also contains 4% phenocrysts of subhedral hematitic hornblende (xenocrysts?) up to 2 mm in size. The groundmass of Ttb ranges from cryptocrystalline with seriate fine to coarse-grained felty euhedral laths of plagioclase (3-31%), subhedral olivine altered to iddingsite (0-6%), subhedral clinopyroxene (2-7%) and hematite (0-10%), to microcrystalline with 13-59% seriate fine to coarse-grained felty to pilotaxitic euhedral laths of plagioclase with intergranular olivine altered to iddingsite (1-9%), clinopyroxene (4-17%), hematite (1-10%) and cryptocrystalline material (0-39%).

Squaw Peak basaltic andesite (Tsp) (48-54% SiO_2) exhibits chemical characteristics intermediate between the Temple Bar volcanics and Pink/Black Ridge volcanics. Incompatible element variation is wide over a narrow range of SiO_2 and Mg#, while variation in compatible elements is low. Tsp also contains higher K_2O , Mg#, TiO_2 and Yb than either Ttb or Tpb. Tsp occupies a stratigraphic position similar to that of Ttb.

Tsp contains phenocrysts of olivine (1-12%), +/- plagioclase (0-27%), +/- clinopyroxene (0-9%). Variation in phenocryst mineralogy is not systematic.

Plagioclase phenocrysts are sieved, embayed and fritted. Clinopyroxene phenocrysts are embayed. Olivine phenocrysts are altered to iddingsite on margins and along fractures. The groundmass contains 12-46% fine to medium-grained felty to trachytic plagioclase laths with intergranular olivine (3-15%), clinopyroxene (0-8%), hematite (1-13%) and cryptocrystalline material (0-34%).

Pink/Black Ridge basalt (Tpb) (46-52% SiO_2) is distinguished from other mafic volcanic rocks of the NWH by low K_2O , Eu, Hf, Th, La/Yb, and total REE and high MgO, FeO, CaO, Sc, Cr and Hf/Th. Tpb overlies thick deposits of coarse breccia at Pink/Black Ridge. Tpb contains phenocrysts of olivine (1-6%), +/- plagioclase (0-3%), +/- hematite (0-3%). Olivine is euhedral to subhedral, embayed and altered to iddingsite on margins. Glomerocrysts up to 2 mm in size of small plagioclase crystals are common, but only one sample (124) contains large (1-4 mm) phenocrysts of pitted, sieved plagioclase. The groundmass of Tpb is comprised of fine to coarse-grained trachytic laths of plagioclase (35-61%) with intergranular olivine altered to iddingsite (7-23%), clinopyroxene (7-23%), magnetite (1-15%) and cryptocrystalline material (2-24%). Sample 120 also has 1% phlogopite (?) in the groundmass. Sample 117 lacks olivine phenocrysts, contains large plagioclase phenocrysts and has a plagioclase-rich groundmass.

Near the top of many sections, separating Ttbm and Tspm from Ttbu and Tspu, is sandstone, siltstone and conglomerate (Ts) interpreted as alluvial fan and stream channel deposits. Fanglomerate clasts are dominantly Proterozoic basement (70%) at Salt Spring Wash and Squaw Peak where deposits are thickest.

Mafic volcanic clasts (30%) were probably derived locally. The ratio of basement to volcanic clasts decreases to (40:60) in the thin Ts deposits in the Peninsula and very thin interbeds of fanglomerate in the upper part of the Smith Hill section.

The dikes and thin flows of the basalt of Senator Mountain contain phenocrysts up to 2 mm in size of euhedral embayed plagioclase (1-13%) and small (<0.5 mm) subhedral phenocrysts of olivine altered to iddingsite (1-4%). The dikes at Chuckwalla Ridge (sample 103) also contain phenocrysts of clinopyroxene up to 1 mm (3%). The samples have a felty plagioclase-rich groundmass.

Mid-Tertiary Eruptive/Depositional History

The lack of chemical or petrographic variation between the basaltic andesite at Chuckwalla Ridge, Smith Hill, the Peninsula and Salt Spring Wash suggests that Ttb represents the construction of a single composite volcano. Eruption of Ttb flows was interrupted twice, first by the deposition of Tt and Tbr (possibly a short break) and second by the deposition of Ts (a longer break). Tpb and Tsp occupy a similar position to Ttb with respect to Tt and Tbr. This implies that two additional volcanoes formed penecontemporaneously. Ttb, Tpb and Tsp thus represent eruptions from three chemically different but coeval volcanic centers in the NWH.

Vent facies for the volcanoes were not identified during this study, so eruptive style and volcano type cannot be determined. However, it is possible to model the geometry of the three volcanic edifices on the basis of stratigraphic

thickness of the volcanic units and distribution of the sedimentary deposits. The sedimentary units and ash-flow tuff place constraints on (1) paleotopography at the time of the eruption of mafic volcanics, (2) the height and slope angle of mafic volcanic edifices, and (3) location of sources of Proterozoic clasts in Tbr and Ts. Figure 15 illustrates a model for the interplay of the mid-Tertiary volcanic and sedimentary rocks of the NWH and is discussed below.

Stage 1- Eruption of Ttbl and Tspl

Ttbl is thickest at Smith Hill (610 m) and in the Peninsula (515 m). The total thickness of Tspl and of Ttbl at Salt Spring Wash is unknown, because the basal parts of the sections are buried. The nearly continuous sheet of Tbrl and correlative units that overlies Tspl and Ttbl suggests that Tspl and Ttbl either (1) represent flows on the flanks of low, broad shield volcanoes or (2) were erupted from fissures (Figure 15a). The conformable contact between Tbrl and Ttbl/Tspl indicates that Ttbl and Tspl were not faulted or tilted at the time of Tbrl deposition.

Stage 2- Deposition of Tbrl

Tbrl (dominantly landslide deposits) is thickest at Salt Spring Wash (438 m), moderately thick at Squaw Peak (63 m) and occurs only as debris flow deposits in the Peninsula (42 m). Braided stream deposits at Chuckwalla Ridge are correlated with Tbrl, Tt (Stage 3) and Tbru (Stage 4). Landslide megabreccias were shed off of a topographic high of Proterozoic basement

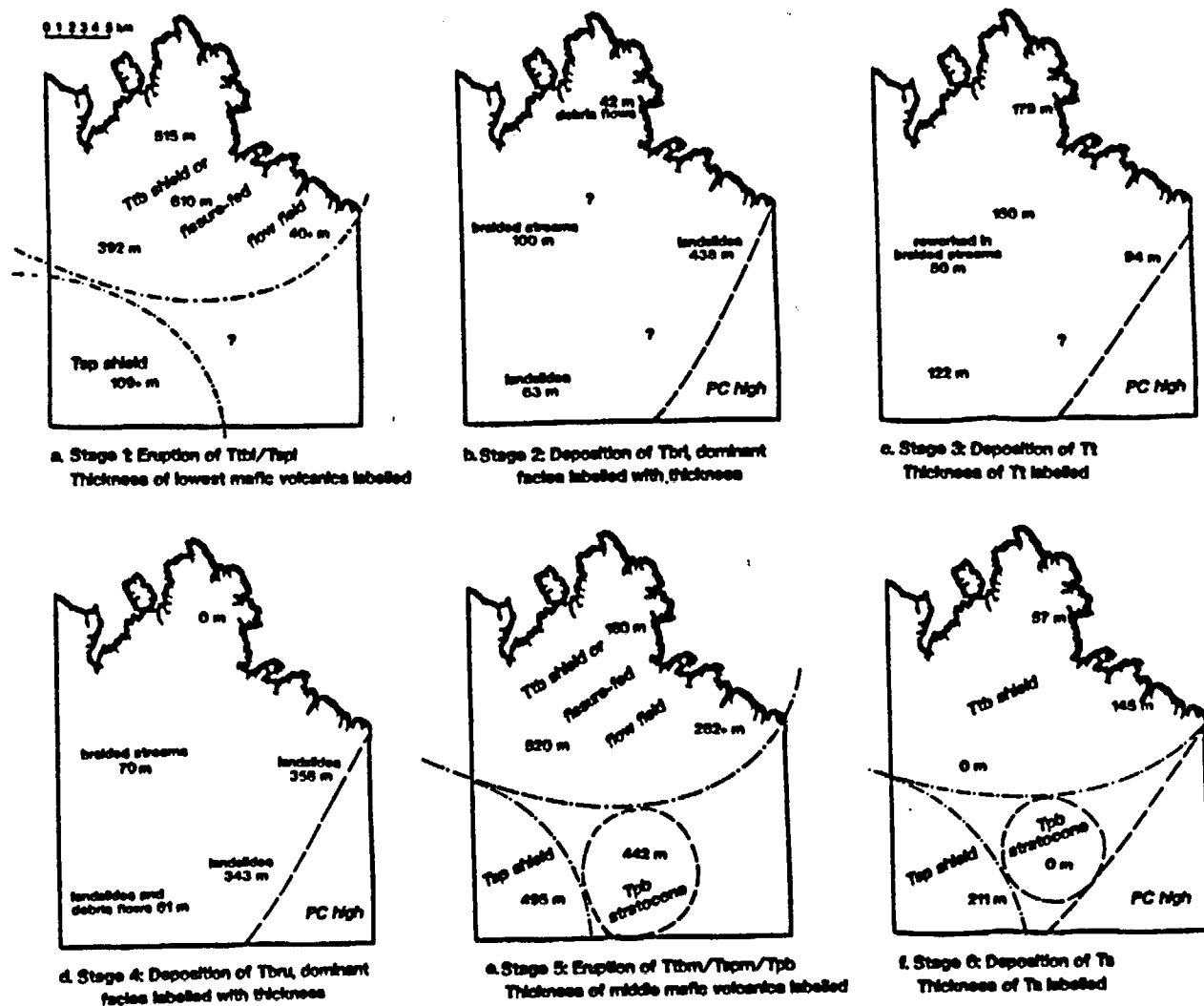


Figure 15. Models for the eruptive/depositional history of the northern White Hills.

situated to the south and/or east of the study area. Tbrl landslides were deposited at Squaw Peak and Salt Spring Wash and thin debris flows were deposited as far north as the Peninsula. Deposits were reworked in braided streams in the Chuckwalla Ridge area.

Stage 3- Deposition of Tt

Ash flows commonly follow topography and pond as thick deposits in topographic lows. The thick Tt deposits in the Peninsula and at Smith Hill indicate that these areas remained low during the deposition of Tt. Thinner deposits at Squaw Peak and Salt Spring Wash reflect an increase in elevation to the south toward the Proterozoic high (Figure 15c). An unresolved problem with this model is the lack of thick ash-flow tuff at Chuckwalla Ridge, which, according to the model, should have been a topographic low. The reworked tuff in the braided stream deposits suggest that these strata are time-equivalent to Tt. It is questionable whether Tt could have been deposited then eroded away. Tt may have been deflected away from the Chuckwalla Ridge area by topographic irregularities. Growth faulting in the Salt Spring Wash block began during this stage.

Stage 4- Deposition of Tbru

Tbru is thickest at Salt Spring Wash and Pink/Black Ridge, and is thin at Squaw Peak. These deposits reflect a second period of landsliding from a Proterozoic high situated to the east-southeast of the study area (Figure 15d).

Stage 5-Eruption of Ttbm/Tspm/Tpb

Mafic volcanism followed the deposition of the breccia. Interruption of mafic volcanism by the deposition of fanglomerate in the upper part of the section supports the contention that the volcanoes that erupted Ttbm and Tspm were not substantial topographic barriers. Ttbm may have erupted from numerous fissures forming a broad, flat lava field. Some basaltic andesite lavas from the Ttb volcano may have flowed into the Squaw Peak area and mingled with Tsp basalt flows. The configuration of volcanoes during this stage is best determined by the distribution of overlying Stage 6 sediments. The growth faulting in the Salt Spring Wash block continued during this stage. The fanning of dip in Ttbm west of Salt Spring Wash records approximately 10° of tilting, probably along the Salt Spring Fault.

Stage 6- Deposition of Ts

The lack of Ts at Chuckwalla Ridge may indicate that the Ttb volcano had built up to form a broad shield with a high at Chuckwalla Ridge. The absence of Ts at Pink/Black Ridge suggests that Pink/Black Ridge was high during Ts deposition. The volcano must have been high enough to deflect the fanglomerates but the restricted distribution of Tpb flows in the center of the study area suggests that the diameter of the volcano was not large (Figure 15f). Thick deposits of Ts near the top of the Squaw Peak section suggest (1) that the Tsp volcanic edifice had low relief, therefore suggesting a shield and (2) the Proterozoic source was nearby. Decreasing abundance of Proterozoic clasts and

decreasing overall thickness of Ts to the north and west indicates a source to the southeast for the Proterozoic material. The western boundary of the Proterozoic high coincides with the Salt Spring fault. Uplift along the fault provides a source of clastic material for Ts. In the Salt Spring Wash section, fanning of dip in Ts records approximately 10° of tilting during Stage 6.

Eruption of mafic volcanic lavas continued after deposition of Stage 6 sediments (Ts). In the Salt Spring Wash section, a second fanglomerate is interbedded with Ttbu, suggesting continued uplift along the Salt Spring fault. In the Salt Spring Wash section, Ttbu records approximately 5° of tilting after Stage 6.

Tilting and erosion of the volcanic sections was followed by deposition of younger poorly consolidated gravel deposits (Trs, Tmcl on Plates 1 and 2) grading upward into siltstone and limestone (Tmcu). Basaltic (Tsm) volcanism, represented by dikes and flows accompanied deposition of Trs.

ROCKS OF THE FOOT WALL

The lower plate of the Salt Spring fault is composed of Precambrian basement rock of varying lithologies. Although meta-igneous rocks are dominant at Salt Spring and Senator Tank (Figure 3), where samples were collected, most of Golden Rule Peak and southern portion of Graham Ridge is composed of pelite (garnet schist and gneiss) with minor psammite and granitoid intrusions.

Eighteen samples of lower plate Precambrian crystalline basement rock were collected in Salt Spring Wash and at Senator Tank and were analyzed

petrographically (Appendix D and Table 10). Precambrian crystalline rocks from Senator Tank and Salt Spring Wash have undergone prograde metamorphism as high as lower granulite facies, and retrograde metamorphism as high as upper greenschist facies. Retrograde minerals replace prograde minerals pseudomorphically.

Samples collected from the Precambrian basement rocks belong to 3 major rock types: amphibolite, felsic gneiss, and garnet-biotite and biotite gneiss.

Amphibolites contain the prograde mineral assemblage hornblende + clinopyroxene + plagioclase +/- apatite +/- quartz +/- orthopyroxene.

Retrograde metamorphism resulted in partial replacement of hornblende by actinolite and chlorite, and nearly complete replacement of clinopyroxene by chlorite and epidote and of plagioclase by sericite and zoisite. Foliation in amphibolite is defined by parallel alignment of hornblende and pyroxene and by compositional banding of hornblende and pyroxene-rich layers alternating with plagioclase-rich layers. Many of the samples, especially those collected at Salt Spring Wash are cut by late stage fractures filled with calcite +/- actinolite.

Amphibolites are associated in the field with quartzofeldspathic veins. A mafic igneous protolith may be inferred for these rock.

Felsic gneiss samples contain the prograde assemblage quartz + plagioclase +/- microcline +/- biotite +/- muscovite. These are felsic gneisses and schists which contain minor amounts of sphene, opaques, zircon and apatite. Retrograde metamorphism caused extensive replacement of feldspar by sericite

Table 10: Summary of mineralogy for crystalline basement

AMPHIBOLITE

Sample Number	Horn-blende	PROGRADE AND RELICT MINERALS						
		Clinopyroxene	Orthopyroxene	Plagioclase	Quartz	Opaque	Sphene	Apatite
47	35				10			
79	90				2	2		
80	40	3		10				
60*	22	5	5	3		3		
75*	55	2		1			<1	
76*	45	10					<1	2

Sample Number	RETROGRADE AND INTRODUCED MINERALS						
	Actinolite	Calcite	Chlorite	Epidote	Quartz	Sericite	Zoisite
47	10		10	10		5	20
79		2	2		3		
80		10	7	10		20	
60*	20	1	5			36	
75*	20	3	5	10		5	10
76*	20	3		10			10

* denotes sample from near detachment surface
percentages are estimated

Table 10: continued.

GARNET-BIOTITE GNEISS

Sample Number	PROGRADE AND RELICT MINERALS								
	Quartz	Plagio- clase	Musco- vite	Biotite	Garnet	Horn- blende	Opaque	Zircon	Sphene
63	20	15	13	5	20		2	<1	
145	32	10		15			3	1	<1
146	2		15	30		30			

Sample Number	RETROGRADE AND INTRODUCED MINERALS						
	Actinolite	Calcite	Chlorite	Epidote	Hematite	Sericite	Zoisite
63		2	10	2		18	3
145		1	5			30	
146	3				10		10

Table 10: continued

FELSIC GNEISS

Sample Number	PROGRADE AND RELICT MINERALS								
	Quartz	Plagioclase	Microcline	Biotite	Muscovite	Opaque	Spheno	Zircon	Apatite
24	20	25	5	2					<1
28	45	20	25		5				
41	40	15	18	3					
44	25	13	15	2		3	4	1	2
45	20	16		2		<1	5	<1	
46	3	10	37		2				
78	45	10	40						
147	30			10		3		1	
58*	60								

Sample Number	RETROGRADE AND INTRODUCED MINERALS					
	Calcite	Chlorite	Epidote	Hematite	Opaque	Sericite
24	3	8	1		1	35
28						5
41	2	2	<1	2	3	15
44		5	1			30
45		5	5			45
46						13
78						5
147	5	8		3	5	40
58*				3	2	35

* denotes sample from near detachment surface

and of biotite by chlorite and epidote. Foliation in these samples is defined by parallel alignment of quartz ribbons, biotite grains and zones of grain size reduction in quartz and feldspar. Late stage fractures cut the rock and are filled with calcite and hematite. A felsic igneous protolith may be inferred for these rocks.

Garnet-biotite and biotite gneiss samples contain the prograde mineral assemblage quartz + plagioclase + biotite + muscovite +/- garnet, with minor opaques and zircon. Retrograde metamorphism caused partial replacement of garnet by chlorite, of plagioclase by sericite and zoisite, and of biotite by chlorite and epidote. Foliation is defined by parallel alignment of recrystallized quartz ribbons and biotite grains and by compositional banding of layers of biotite alternating with quartz and plagioclase-rich layers. The rock is associated in the field with quartzofeldspathic veins. Gneisses have a more potassium-rich mineral assemblage than the amphibolite and felsic gneisses with which they are associated in the field. This may indicate a sedimentary or volcanoclastic protolith.

The basement rocks exposed at Salt Spring Wash and at Senator Tank are dominated by meta-igneous rocks of bimodal composition. Possible volcanoclastic protoliths are observed as well. These areas may represent a metamorphosed bimodal volcanic section. Rocks of this type are unlike the garnet-bearing pelitic rocks that dominate much of the Precambrian basement of the Lake Mead region (Duebendorfer, personal communication). Golden Rule Peak and the southern

half of Graham Ridge are dominated by the metasedimentary garnet-biotite gneiss and pelitic schist which are much more common in the Lake Mead region. At northern exposures at the open pit mine, highly hematized two-mica pegmatite veins intrude biotite gneiss. Similar pegmatite veins are exposed throughout Golden Rule Peak, but are less hematized. The breccia in the upper plate of the Salt Spring detachment contains a disproportionate abundance of granitoid and mylonite clasts relative to the observed lower plate rock exposed near the Salt Spring fault. This may suggest that the source of these landslide deposits is farther east or south of the fault.

STRUCTURE

Salt Spring Fault

The Salt Spring Fault is exposed near the eastern edge of the study area (Plate 2). It separates the tilted mid-Tertiary volcanic and sedimentary section in the hanging wall from Precambrian basement rocks in the footwall. The fault surface is exposed almost continuously from Gregg's Hideout to Salt Spring. South of Salt Spring, most of the fault trace is buried beneath alluvium and late Tertiary Red Sandstone (Trs) and Muddy Creek Formation (Tmcl) gravels. A small exposure is present at Dug's Island, 3 miles south of Salt Spring, and the location of the fault at the open pit mine is tightly constrained by the presence of exposures of lower plate crystalline rocks in trenches less than 100 meters southeast of upper plate coarse breccia and volcanic rocks. South of the open pit mine, the fault projects beneath alluvium, and may connect with the Cyclopic

detachment (Myers, 1985) south of Senator Mountain. In addition, the fault projects northward from Gregg's Hideout, across Lake Mead toward the Lakeside Mine fault (Fryxell et al, in press), and may link with this fault as well.

Within 200 to 600 meters of the fault surface between Gregg's Hideout and Salt Spring, at Dug's Island and at the open pit mine, the footwall rocks are highly altered and brittely sheared (Figure 16). The rocks in the highly altered zone consist mostly of hematitic gouge derived from granitoid and/or felsic gneiss. Within 0-50 meters of the fault, the rocks are pervasively sheared to cataclasite. Thirty to two hundred meters from the fault, footwall rocks are cut by a dense network of anastomosing brittle shear zones up to 1 cm wide, spaced between 1 and 20 cm apart. These shear zones separate the rock into lenses of largely undeformed granitoid, gneiss and amphibolite that has undergone strong retrogression to actinolite, calcite, chlorite, epidote, sericite, and zoisite. Spacing of shear zones decreases with distance from the fault, and evidence of shear dies out entirely 200 to 600 meters from the fault. The attitude of the fault surface and the plunge of lineations is variable (Figure 16). North-south trending segments of the fault contain mostly down-dip striae and east-west segments contain oblique and/or strike-slip striae. Upper plate rocks near the fault trace are highly hematized and calcified.

Structures in Hanging Wall

The six east-tilted structural blocks in the hanging wall of the Salt Spring fault are unconformably overlain by: (1) late Tertiary gravel and thin basalt flows

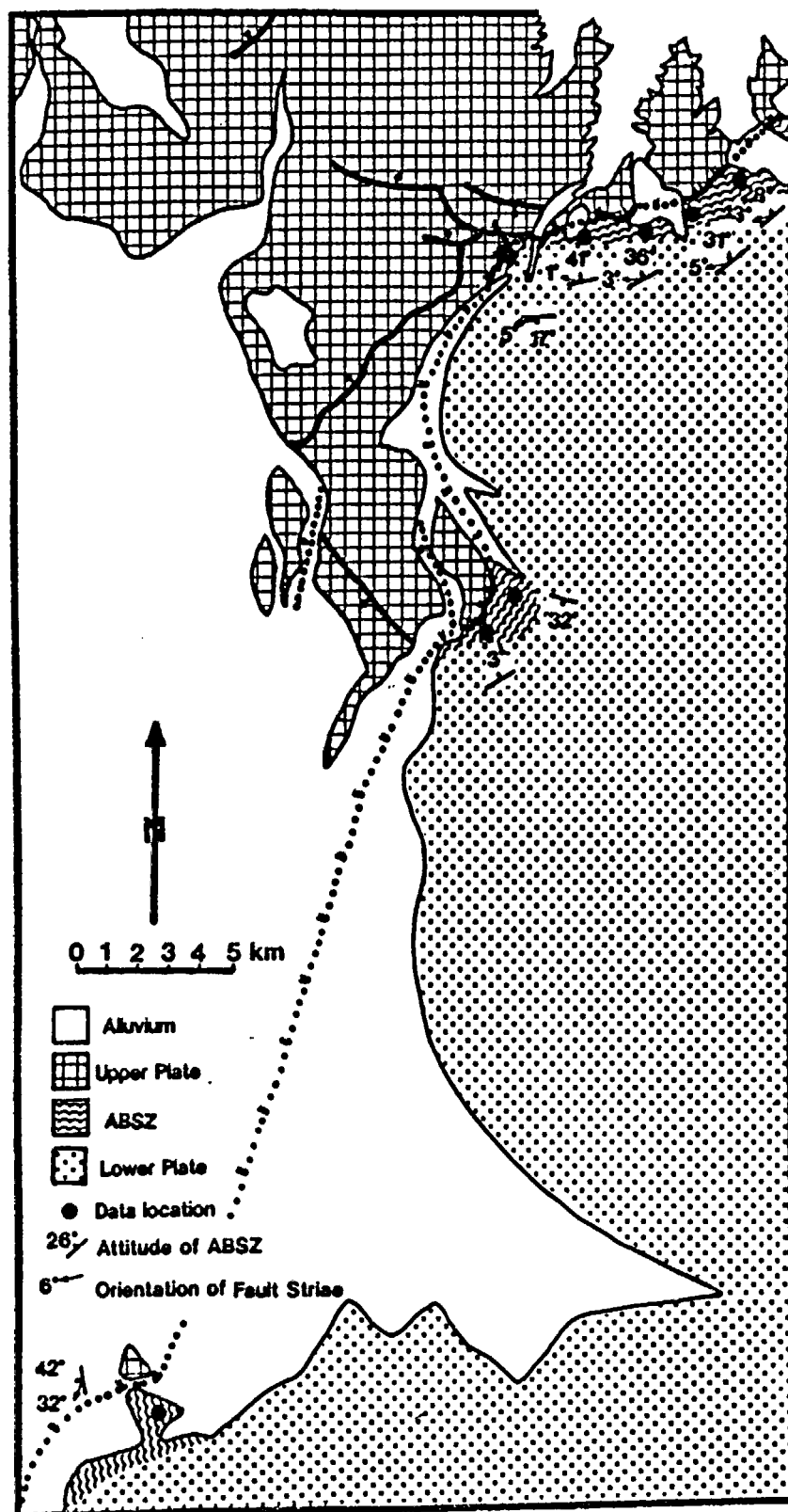


Figure 16. Salt Spring Fault orientation data. Average strike and dip of Anastomosing Brittle Shear Zones (ABSZ) plotted with lineations.

of the Red Sandstone unit; (2) gravel, sandstone, gypsiferous siltstone and freshwater limestone of the Muddy Creek Formation (Tmc); and (3) Quaternary sediments. At Salt Spring Wash, the three upper units of the mid-Tertiary section (Tt_{bm}/T_{spm}, T_s and T_{bu}/T_{spu}) demonstrate a marked fanning of dip from 30-35° at the base to near horizontal at the top. Growth faulting also affects T_t at Salt Spring Wash (Switzer, personal communication). Elsewhere in the northern White Hills, dips are uniform within structural blocks, varying between 10° and 45°.

Each of the six structural blocks is cut by north- to northwest-striking, west- to southwest-dipping high-angle (75°) to moderate-angle (45°) normal faults that repeat parts of the stratigraphic section. A west-dipping normal fault cuts and repeats T_t, T_{tbm}, T_s and T_{bu} in the Peninsula block (Figure 17a). There, flows dip gently (9°-15°) eastward, suggesting that the fault is high-angle. In addition, east-west striking right-lateral faults cut the upper part of the section (T_{tbm}-T_s-T_{bu}) at Teal Coves and the Campanile (Plate 1).

Several southwest-dipping faults repeat the section at Chuckwalla Ridge. Numerous southwest-dipping faults with individual displacements less than 10 meters, and cumulative displacement of approximately 150-200 meters cut the Smith Hill block. A west-northwest trending, southwest-dipping normal fault places T_t against T_{tbm} at the southern end of the Smith Hill block. Nearly vertical (>85°) dikes (T_{tbd}) intrude T_{tb} at Smith Hill and Chuckwalla Ridge and strike east-west, approximately normal to structural grain. The dikes are

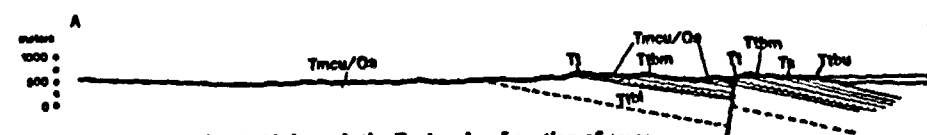


Figure 17a. Cross section A-A' through the Peninsula. Location of cross section lines are on Figure 4. Shaded unit is Tl and equivalent Tbre.

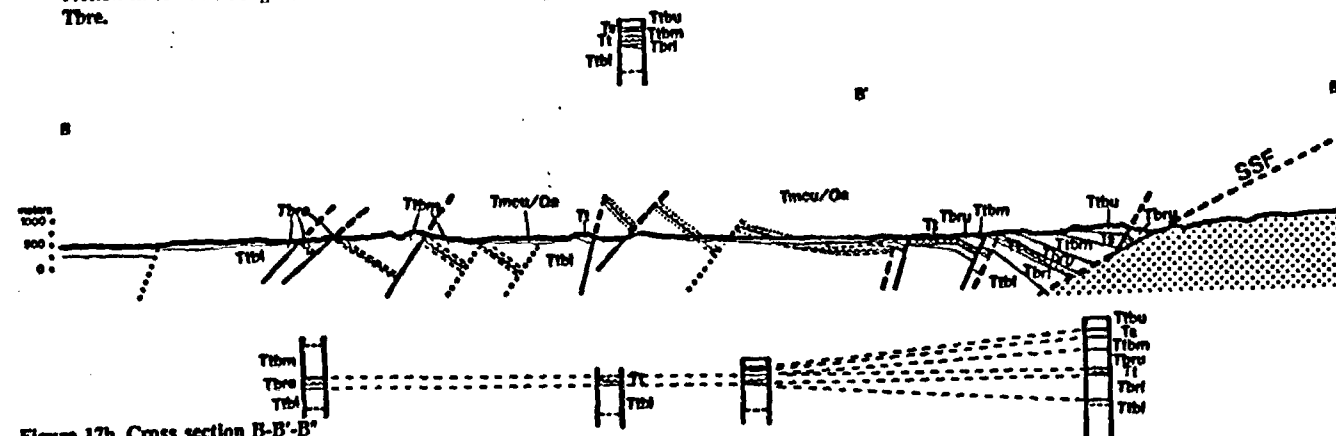


Figure 17b. Cross section B-B' through Chuckwalla Ridge, Smith Hill and Salt Spring Wash.

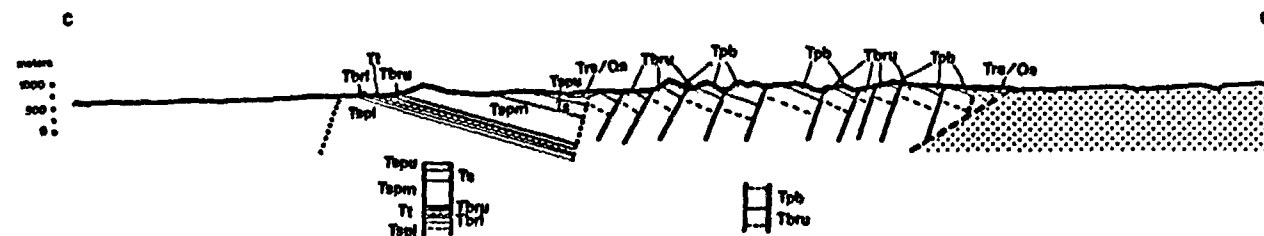


Figure 17c. Cross section C-C' through Squaw Peak and Pink/Black Ridge.

mineralogically and chemically similar to the intruded basaltic andesite and may represent feeder dikes for overlying flows. Steeply west-dipping (75°), north-trending basalt dikes (Tsm) intrude interbedded sediments and basaltic andesites on the west side of Chuckwalla Ridge. They are oriented approximately parallel to structural grain and may have intruded along range-bounding normal faults. A southwest-dipping normal fault is proposed as the boundary between the Chuckwalla Ridge and Smith Hill blocks. In constructing Figure 17b, faults with spacings and displacements similar to those in both blocks were inferred to lie between the blocks.

No major structural boundary is apparent between the Smith Hill and Peninsula blocks. A major high-angle normal fault strikes northeast along the northwest side of Salt Spring Wash, and places the upper part of the section in the hanging wall against the lower part of the section in the footwall (Plate 2, Figure 4). Near Salt Spring are a number of east-west striking high-angle normal faults that dip both north and south and offset the upper part of the section (Ttbm-Ts-Ttbu). The upper part of the section is broadly warped in a syncline centered at Temple Bar and an anticline centered between Gateway Cove and Temple Bar (Plate 1). The syncline axis is projected to cross section B-B' and accommodates the structural relief between the Smith Hill/ Peninsula block and the Salt Spring Wash. Alternatively, the difference in structural style between the gently warped and gently dipping Salt Spring Wash block and the more steeply tilted Smith Hill block suggests the presence of a major structure between them.

Figure 18 shows a model in which an earlier growth fault near Salt Spring Wash was abandoned, with later displacement taken up by a younger fault buried beneath Tmc and Quaternary deposits east of Temple Bar. In this case, structural relief is accommodated by greater displacement on the fault east of Temple Bar.

Several west-dipping high-angle normal faults were identified on the west side of the Squaw Peak block. Pink/Black Ridge is cut by numerous north-striking, west-dipping normal faults, producing a series of north-trending ridges which together make up the west-trending Pink/Black Ridge. Flows within each north-trending ridge dip uniformly between 20° and 30° east. The boundary between the Squaw Peak and Pink/Black Ridge blocks is covered by late Tertiary and Quaternary sediments, but is inferred to be a north-striking, down-to-the-west normal fault, similar to those exposed in both blocks (Figure 17c). Spacing between faults increases and displacement along faults decreases from east to west away from the trace of the Salt Spring Fault.

High angle normal faults offset the upper Muddy Creek Formation (Tmcu) on the west side of Chuckwalla Ridge and the Squaw Peak block. Together, the Chuckwalla Ridge and Squaw Peak Blocks form a north-south trending range bounded on the west by a high-angle fault and uplifted relative to Detrital Wash.

Interpretations

Multiple episodes of faulting are evident in the NWH. The Salt Spring fault is a low to moderate-angle structure. The six structural blocks discussed above are cut by moderate- to high-angle northwest-trending faults. Homoclinal

sequences indicate that most faulting and tilting postdated the deposition of Ttbl/Tspl and Tbr/Tt. However, fanning of dip in the Salt Spring Wash section indicates that faulting began there as early as the time of emplacement of the ash-flow tuff (Tt). Blocks are bounded by high-angle north-south trending, west-dipping faults that formed the present ranges.

PETROGENESIS OF MAFIC VOLCANICS

Three chemically, petrographically and geographically distinct mid-Tertiary mafic volcanic centers in the northern White Hills (NWH) are documented above (Figures 11-14 and 19). The centers are defined by the Temple Bar, Squaw Peak and Pink/Black Ridge volcanic sections. I refer to each of the three mafic assemblages as magma types in the following section.

ORIGIN OF HIGH K_2O CONTENTS: METASOMATIC OR MAGMATIC

The mafic volcanic rocks in the NWH are basalt, trachybasalt, basaltic trachyandesite and trachyandesite according to the classification of LeBas et al. (1986) (Figure 20 and Table 11). Many samples have high K_2O contents relative to "normal" mafic intermediate volcanic rocks (Figure 21). Tpb samples and some Tsp samples plot within the field of normal calc-alkaline volcanics. Other Tsp samples and nearly all of the Ttb samples have elevated K_2O relative to "normal".

Potassium metasomatism is responsible for high K_2O concentrations in many suites of volcanic rocks in the Lake Mead area (Smith et al., 1990). However, K metasomatism should produce an inverse relationship between K_2O

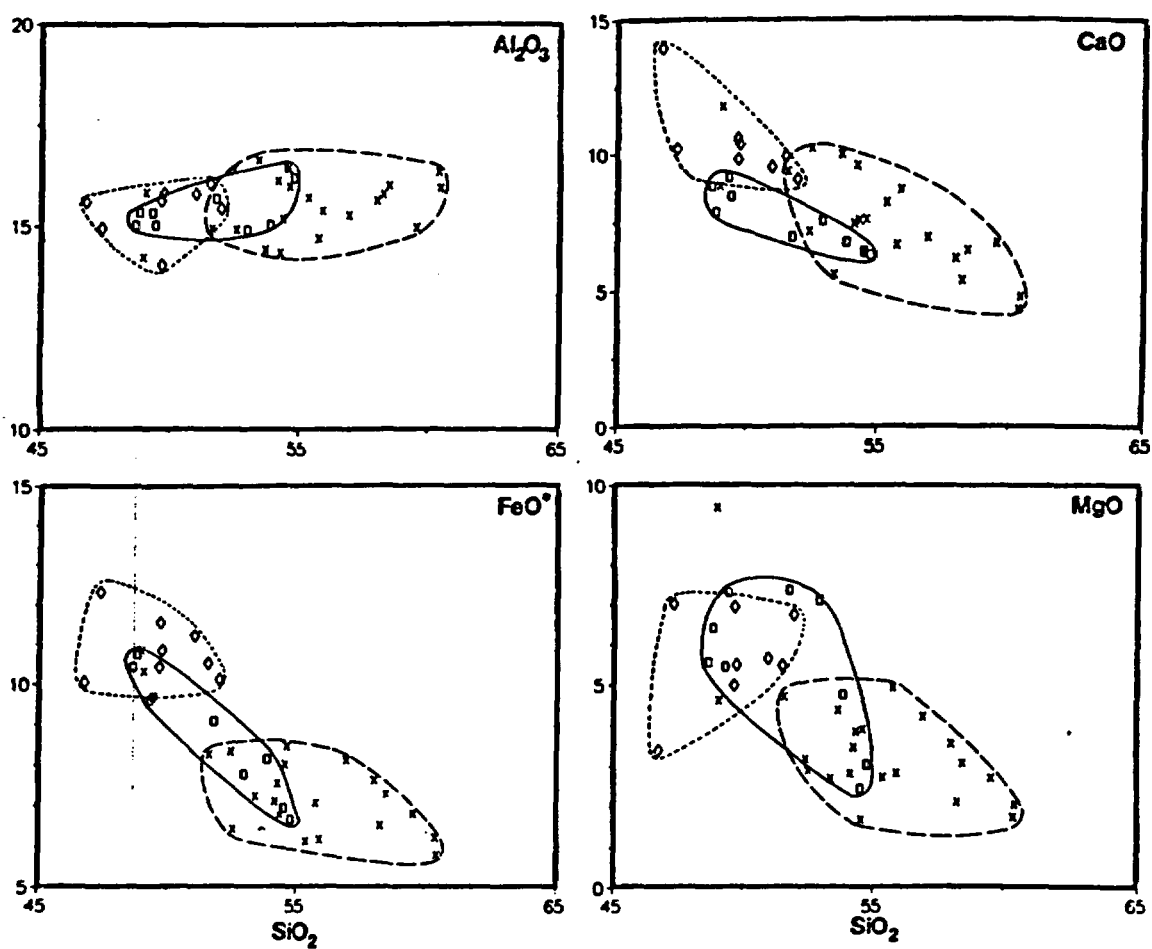


Figure 19. Harker variation diagrams for mafic volcanic rocks. SiO_2 vs. major element oxides. Units are weight percent. Symbols are defined on Figure 11.

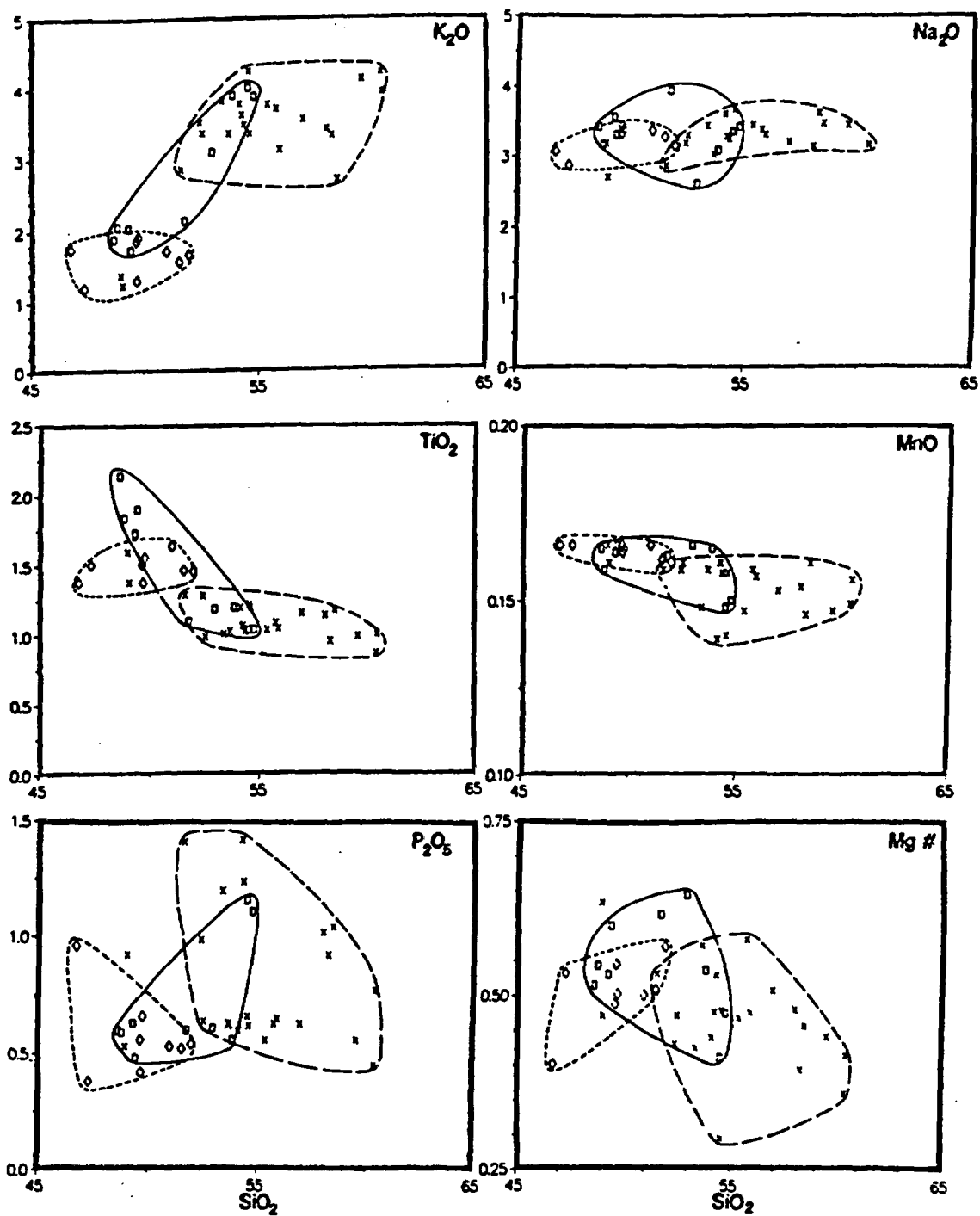


Figure 19, continued.

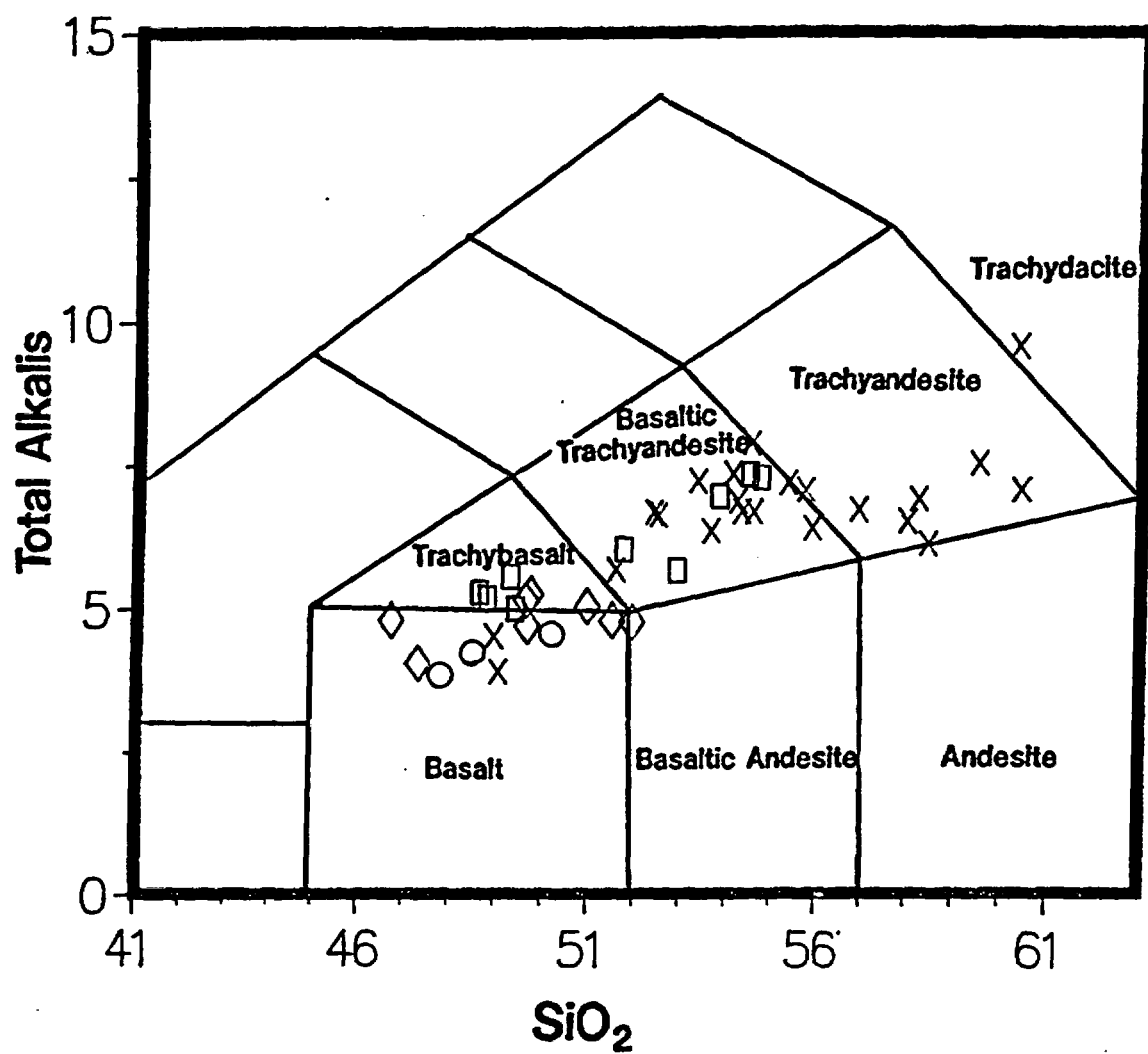


Figure 20. Classification diagram for mafic volcanic rocks (LeBas, 1986). Symbols are defined on Figure 11.

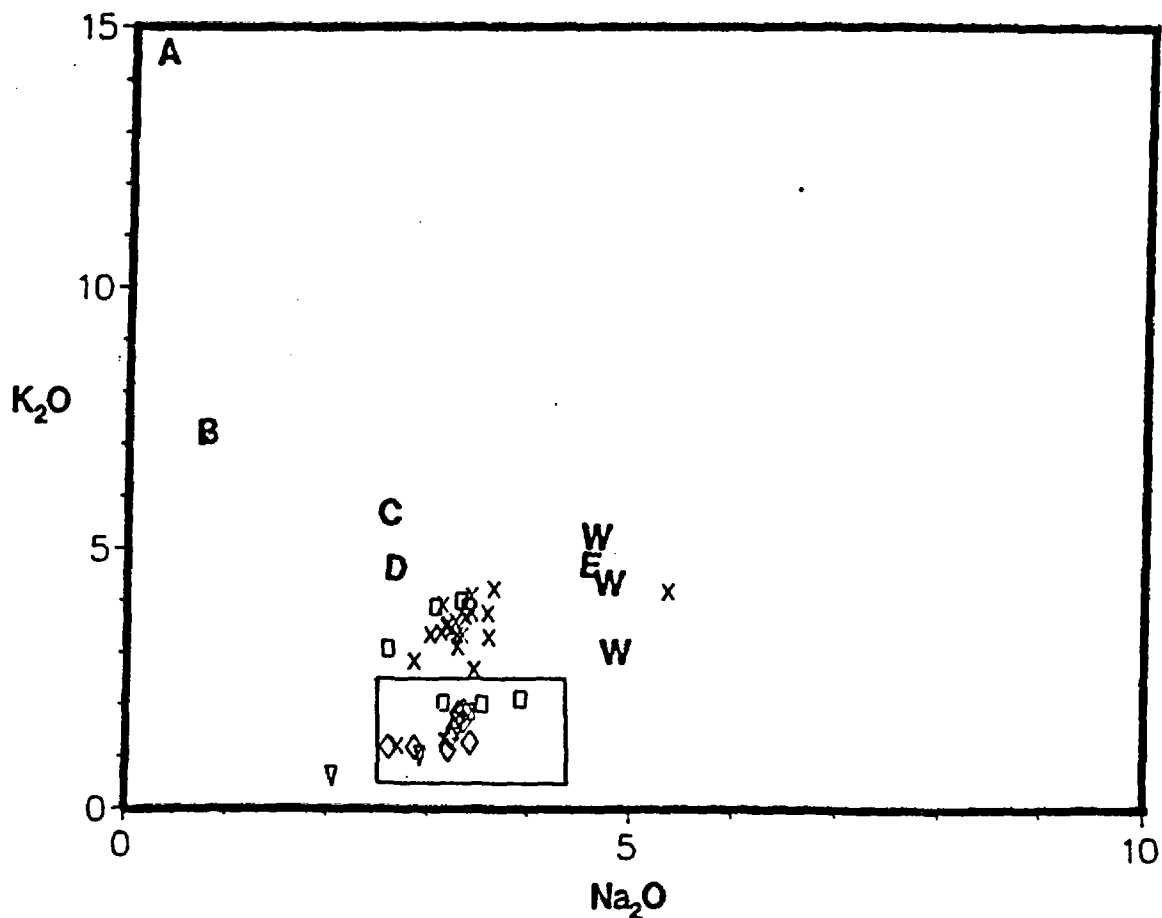


Figure 21. Alkali enrichment diagram. K_2O plotted against Na_2O . Rectangle defines field for "normal" Andean mafic volcanics (Wilson, 1990). Units are weight percent. Volcanic symbols defined on Figure 11. A=Cretaceous episyenite, B=contact zones around Cretaceous episyenite, C=Proterozoic biotite monzogranite, D=Proterozoic monzogranite, E=Proterozoic two-mica monzogranite, W=Tertiary Wilson Ridge Pluton.

Table 11: Normative mineralogy of mafic volcanic rocks

Sample	Ttbl		Ttbm							
	139	90	85	51	50	148	65	131	132	134
Rock name	TA	BTA	SB	BTA	BTA	BTA	TA	TA	BTA	BTA
AN	40.71	33.78	43.31	35.32	33.16	29.07	38.31	32.83	44.66	39.07
Quartz	11.17	2.15		1.61	2.08	7.87	5.12	2.86	1.74	6.53
Orthoclase	15.97	25.18	8.16	22.4	21.45	20.85	21.04	21.98	16.91	18.56
Albite	29.31	30.97	26.91	30.46	27.75	26.95	27.08	28.6	24.21	27.92
Anorthite	20.13	15.79	20.56	16.63	13.77	11.05	16.82	13.98	19.54	17.91
Calcite						3.27				
Diopside	4.44	10.18	16.11	13.52	20.19		11.21	12.28	14.49	17.18
Hypersthene	10.68	5.36	1.96	5.1	4.82	14.54	11.82	11.5	11.18	2.35
Olivine			17.14							
Magnetite	3.88	3.94	4.49	3.91	3.73	4.04	3.86	3.76	4.05	3.7
Ilmenite	2.24	2.32	3.04	2.28	2.03	2.44	2.2	2.07	2.45	1.99
Apatite	2.42	1.53	1.23	1.39	3.29	2.29	1.46	1.46	3.27	1.51

Rock names (LeBas, 1986):

SB = Subalkalic basalt

BTA = Basaltic Trachyandesite

TA = Trachyandesite

TD = Trachydacite

Sample	Ttbm						Ttbu				
	135	149	49	140	133	130	86	141	77	88	100
Rock name	TA	TA	BTA	TA	BTA	BTA	TD	SB	BTA	BTA	BTA
AN	31.26	41.1	39.39	35.81	37.71	35.84	14.95	54.55	39.6	36.39	39.19
Quartz	8.06	9.49	1.43	11.02	4.22	3.63	2.55		1.77	0.59	3.8
Orthoclase	24.41	20.22	19.92	19.67	20.63	22.34	25	7.31	19.92	19.92	22.65
Albite	29.11	26.52	25.55	30.57	27.42	39.11	45.44	22.86	28.35	27.92	29
Anorthite	13.24	18.51	15.92	17.05	16.6	16.26	7.99	27.44	18.59	15.97	18.69
Diopside	13.76	4.68	23.92	3.21	10.57	17.11	8.9	20.74	12.59	23.73	1.13
Hypersthene	5.04	12.49	3.7	8.38	9.3	2.07	4.4	10.93	10.78		11.86
Wollastonite										0.69	
Olivine								0.16			
Magnetite	3.61	3.83	3.67	3.56	3.67	3.68	3.44	4.18	3.91	3.61	3.64
Ilmenite	1.88	2.17	1.96	1.82	1.96	1.98	1.65	2.63	2.28	1.88	1.92
Apatite	1.3	2.36	1.46	2.14	2.87	1.3	1.04	2.14	1.44	1.48	2.79

Table 11: continued

Sample Rock name	Tpb					Tsm					
	7	10	120	15	117	118	121	123	55	103	114
	AB	AB	SB	SB	SB	TB	AB	TB	AB	SB	SB
AN	62.69	51.14	44.7	46.97	46.54	40.14	46.14	46.6	53.84	54.46	46.37
Orthoclase	10.34	7.09	10.11	9.22	9.81	7.68	10.99	11.29	6.8	7.09	8.21
Albite	14.05	23.33	28.43	27.67	26.57	28.61	26	25.67	20.34	22.09	27.42
Anorthite	23.62	24.42	22.98	24.51	23.13	19.19	22.28	22.4	23.73	26.41	23.7
Nepheline	6.46	0.52				0.22	1.13	1.54	3.7		
Diopside	32.77	19.58	17.23	17.56	15	22.03	21.94	20.42	29.95	15.34	17.58
Hypersthene			5.81	9.92	15.53					14.63	4.89
Olivine	1.12	15.26	7.51	3.64	2.27	13.61	8.21	10.07	8	2.42	10.58
Magnetite	4.18	4.36	4.55	4.31	4.29	4.18	4.36	4.44	4.07	4.02	4.29
Ilmenite	2.62	2.87	3.11	2.79	2.77	2.62	2.87	2.96	2.49	2.41	2.77
Apatite	2.22	0.88	1.23	1.2	1.25	0.97	1.3	1.53	0.88	0.6	0.083

Sample Rock name	Tspm					Tspu			
	3	21	108	126	127	128	112	113	20
	BTA	TB	TB	TB	TB	BTA	BTA	BTA	BTA
AN	37.58	43.06	44.7	40.53	41	47.48	37.51	38.97	36.18
Quartz	0.97					1.09	4.42	4.57	
Orthoclase	23.11	10.22	12.17	12.06	11.17	18.32	23.06	23.83	12.65
Albite	26.06	27.92	26.74	29.19	28.94	22	28.88	18.04	33.25
Anorthite	15.69	21.12	21.62	19.9	20.11	19.89	17.34		18.85
Nepheline				0.46					
Diopside	11.68	14.34	11.18	17.49	16.1	11.05	5.59	5.26	9.63
Hypersthene	12.82	6.35	7.31		2.54	18.37	9.39	8.53	4.5
Olivine		8.28	8.71	8.83	7.55				12.97
Magnetite	3.91	4.93	4.84	4.68	5.28	3.9	3.69	3.69	3.77
Ilmenite	2.28	3.61	3.49	3.29	4.06	2.26	1.98	1.98	2.09
Apatite	1.3	1.11	1.37	1.46	1.39	1.41	2.58	2.68	1.39

Rock names (LeBas, 1986):

AB = Alkali basalt

SB = Subalkalic basalt

TB = Trachybasalt

BTA = Basaltic Trachyandesite

and Na_2O due to replacement of Na by K during metasomatism. In the NWH samples, Na_2O contents are similar to those of "normal" calc-alkaline volcanic rocks despite the elevation in K_2O . Therefore, K metasomatism does not appear to be a major cause of the high K_2O concentration in the NWH samples.

Because light rare-earth elements (LREE), Th and Hf are equally incompatible with K in basaltic to basaltic andesitic magmas, covariation of these elements with K indicates that K is acting as an incompatible element (Figure 22). Therefore variation of all incompatible elements, including K, is due to a magmatic process and not to metasomatism. The covariation of K_2O and incompatible trace elements may be explained by one of the magmatic processes described in the next section.

HOW ARE THE THREE MAGMA TYPES RELATED PETROGENETICALLY?

Possible processes that may relate the three mafic magma types in the NWH are crystal fractionation, contamination, assimilation-fractional crystallization (AFC) or varying amounts of partial melting of the same or similar sources. Each of these processes is evaluated below.

Contamination

Contamination of a mafic magma with a felsic assimilant should produce a linear trend between the mafic and felsic end members on chemical plots. The mafic end member should be the most chemically primitive rock in the mafic assemblage. Because there are no truly primitive basalts (Mg\#s are all <0.65), a

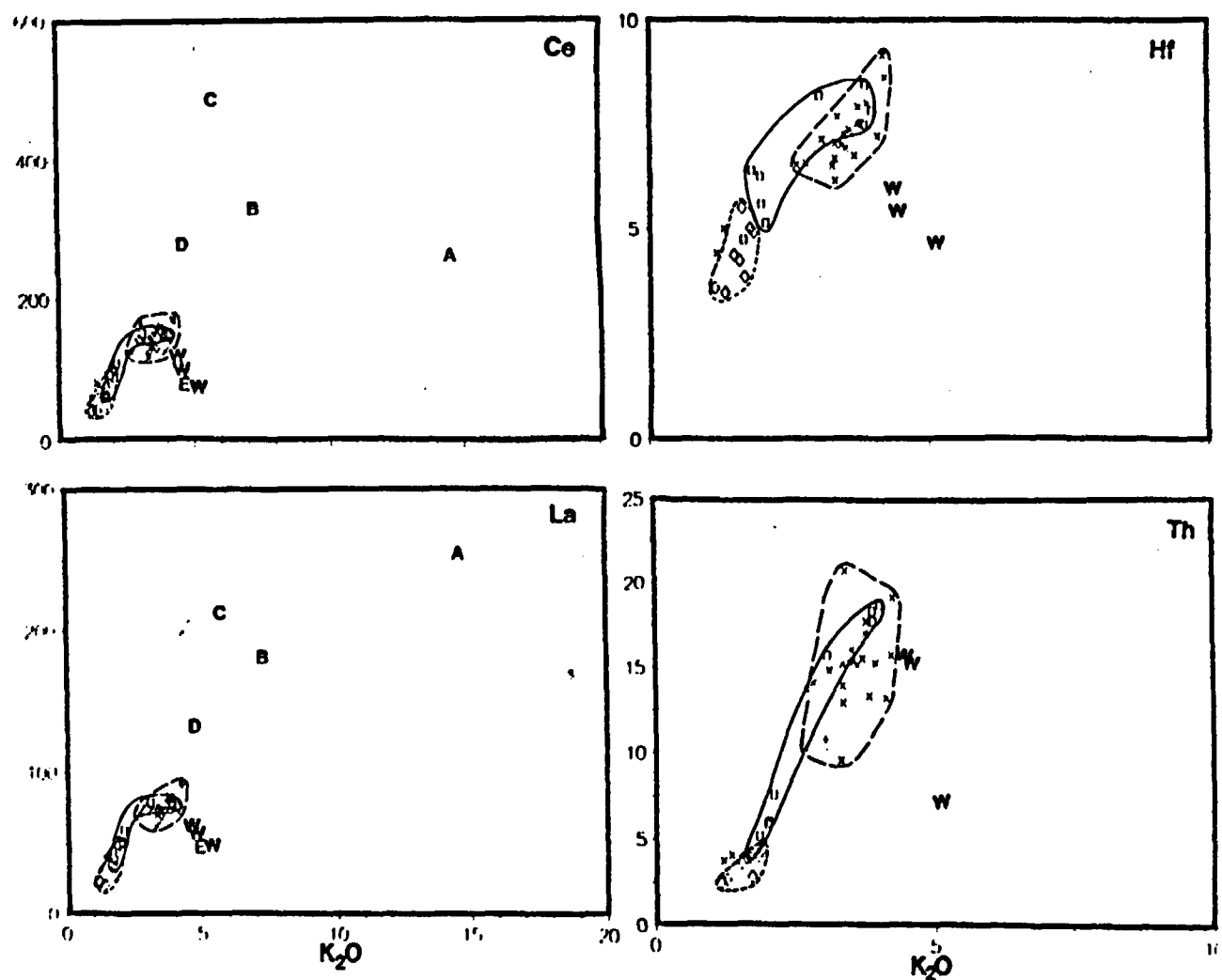


Figure 22. Binary chemical plots. Weight percent K_2O plotted against ppm incompatible Ce, Hf, La, and Th. Symbols are defined on Figure 21.

mafic end member cannot be positively identified. Therefore, models were attempted using several of the most primitive samples. Successful models are reported in Table 12. Potential contaminants used in models are Proterozoic monzogranite and biotite monzogranite. Because no felsic volcanic rocks are present in the NWH, it is unlikely that mafic magma mixed with felsic magma of Tertiary age such as Wilson Ridge-type magmas described by Larsen and Smith (1990). In addition, Wilson Ridge samples have incompatible trace element concentrations too low to be suitable contaminants (Figure 22).

The lack of petrographic evidence for contamination precludes large amounts of assimilation in NWH samples. Disequilibrium textures (pitted and resorbed plagioclase) are common in NWH rocks, particularly in Ttb samples, but may be attributable to reequilibration of high pressure phases. Conclusive textural evidence for contamination, such as resorbed and skeletal inclusions, disequilibrium mineral assemblages, and rimmed xenocrysts is absent.

Fractional Crystallization

Fractional crystallization would result in a continuous linear relationship between the three magma types on Harker variation diagrams and other binary plots (i.e., Figures 19 and 23). There may be inflections or changes in slope, reflecting the fractionation of different phases, but lines for each of the three magma types should form a single trend. Compatible trace element plots (Figures 24 and 25) show: (1) substantial overlap of the three fields; (2) no continuous trend connecting the three magma types; and (3) a general similarity in the

Table 12: Major element fractional crystallization and AFC models

Model #	1	2	3	4	5	6	7
<i>Phase</i>							
Olivine	-5.84	-4.98	-6.54	-7.52	-6.23	-6.77	-6.16
Clinopyroxene		-5.94					
Plagioclase				-2.67	-2.55		
Monzogranite					31.82	26.18	
Biotite Monzogranite							2.77
Total % subtracted	5.84	10.92	6.54	10.19	8.78	6.77	6.16
Total % added					31.82	26.18	2.77
<i>Residuals</i>							
SiO ₂	1.49	1.42	1.08	0.5	-0.22	-0.17	0.66
Al ₂ O ₃	-0.61	-1.06	-0.54	-0.09	-0.6	-0.54	-0.26
FeO*	-0.89	-1.23	-0.56	-0.59	-1.5	-1.48	-0.63
CaO	-1.83	-0.96	-0.03	0.35	0.44	0.56	-0.82
MgO	0.25	42	0.52	0.6	0.73	0.78	0.25
Na ₂ O	0.41	0.26	-0.39	-0.61	0.36	-0.1	0.22
K ₂ O	0.62	0.52	0.41	0.35	0.93	1.09	0.27
TiO ₂	0.55	0.64	-0.49	-0.51	-0.13	-0.14	0.3
Sum of squares of residuals	7.64	6.49	2.6	1.85	4.66	4.4	1.84

Model #	8	9	10	11	12	13
<i>Phase</i>						
Olivine	-2.94	-3.72	-2.8	-5.76	-8.7	-11.81
Clinopyroxene					-15.67	-7.48
Plagioclase			-6.31		-7.92	-0.69
Monzogranite	11.19	13.37	25.46			
Biotite Monzogranite						
Total % subtracted	2.94	3.72	9.11	5.76	32.29	19.98
Total % added	11.9	13.37	25.46			
<i>Residuals</i>						
SiO ₂	-0.21	0.15	0.09	1.44	0.51	0.56
Al ₂ O ₃	-0.01	-0.25	-0.28	-0.38	0.23	0.18
FeO*	-0.25	0.45	-0.49	-0.78	-0.59	-0.83
CaO	-0.4	0.6	0.45	-0.95	0.01	0
MgO	-0.01	0.38	0.34	0.57	0.75	0.88
Na ₂ O	0.3	-0.33	0.17	0.01	-0.75	-0.95
K ₂ O	0.18	0.33	0.15	0.17	-0.11	0.65
TiO ₂	0.39	-0.43	-0.43	-0.08	-0.05	-0.49
Sum of squares of residuals	0.54	1.2	0.89	4.09	1.8	3.36

Model descriptions:

1,2,7,8: Parent=Primitive Tpb (10), daughter=primitive Tsp (127)

3,4,9,10: Parent=Primitive Tsp (127), daughter=primitive Ttb (132)

5 and 6: Parent=Primitive Tpb (10), daughter=primitive Ttb (132)

11: Parent=primitive Tpb (10), daughter=evolved Tpb (117)

12: Parent=primitive Ttb (132), daughter=evolved Ttb (138)

13: Parent=primitive Tsp(127), daughter=evolved Tsp (112)

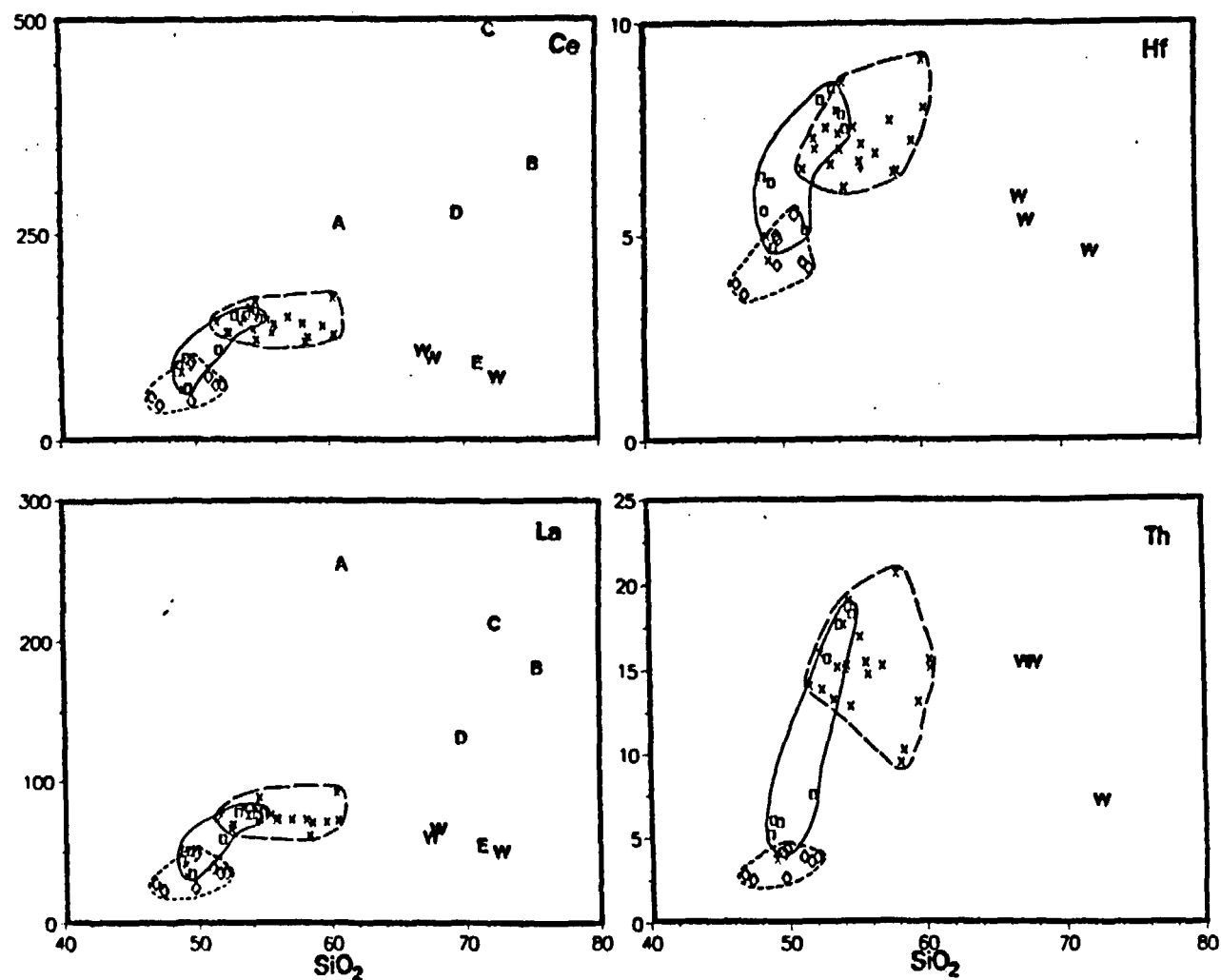


Figure 23. Harker variation diagrams. Weight percent SiO_2 plotted against incompatible ppm Ce, Hf, La and Th. Symbols defined on Figure 21.

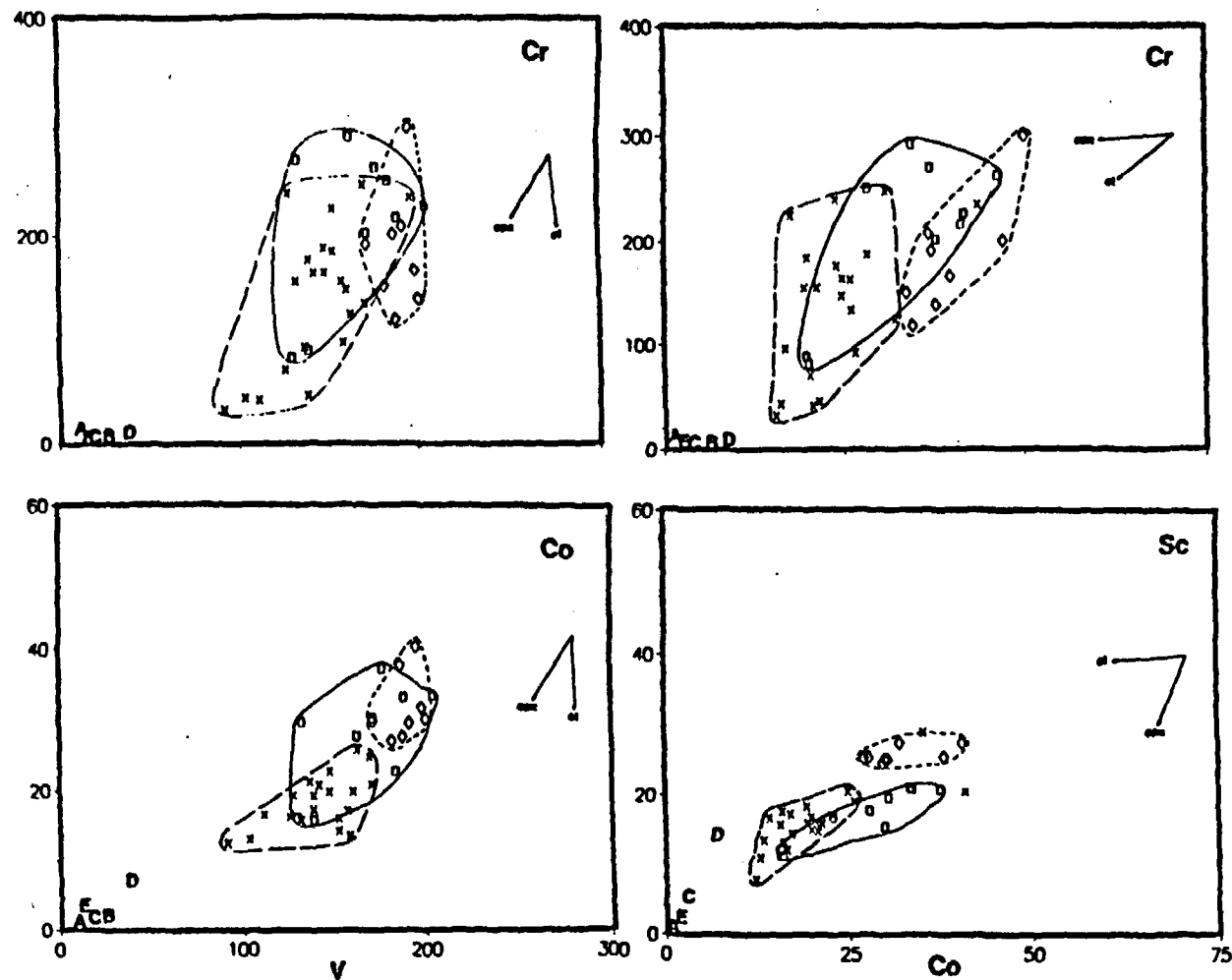


Figure 24. Tests for olivine and clinopyroxene fractionation. V plotted against Co and Cr, Co plotted against Cr and Sc. Fractionation vectors plotted on right side. Units are ppm. Symbols defined on Figure 21.

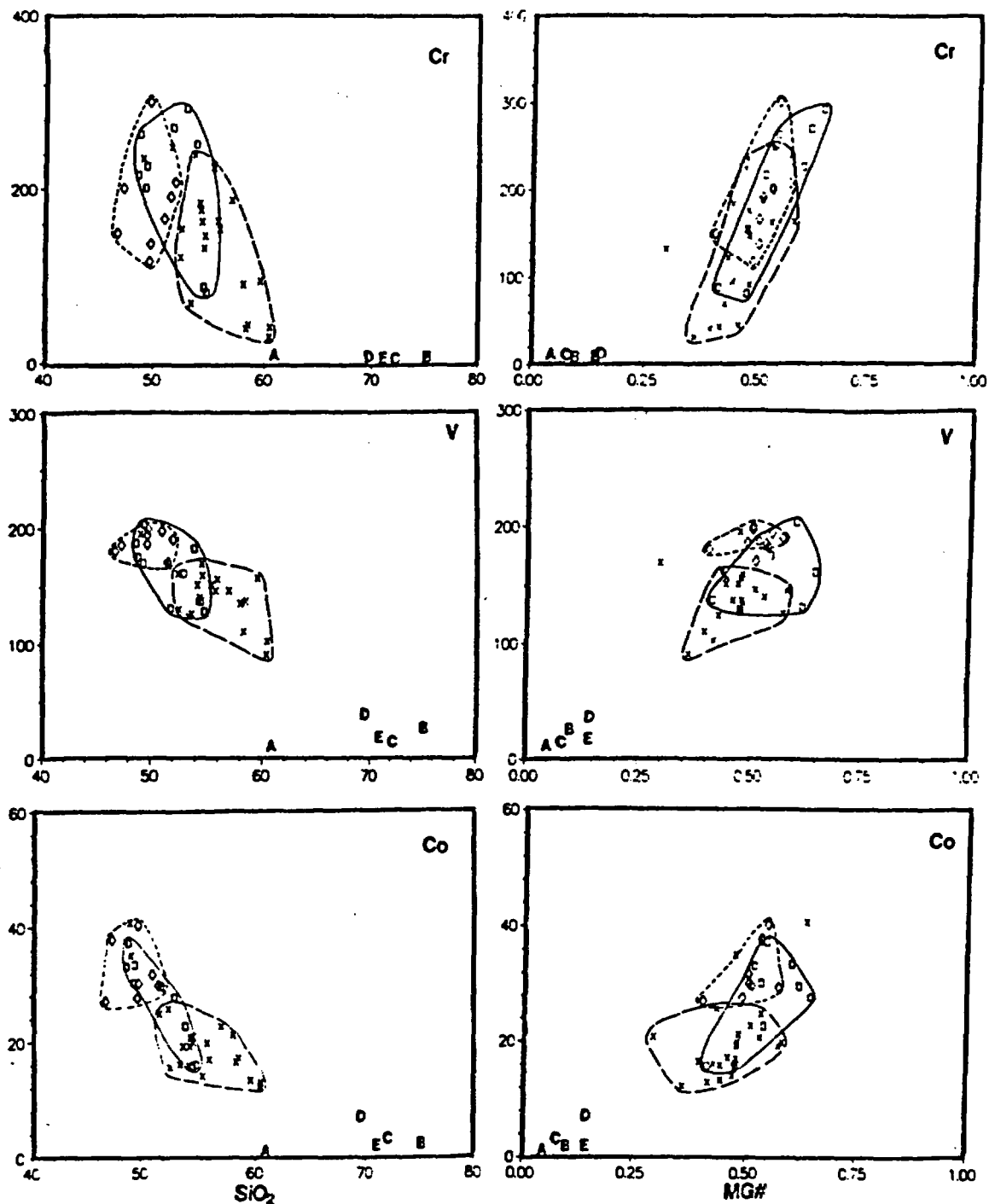


Figure 25. Harker variation diagrams. Weight percent SiO_2 and Mg\# plotted against ppm compatible elements Co, Cr and V. In a and b, steep trends suggest fractionation of cpx and/or ol. In c and d, steep trends suggest cpx fractionation and shallow slopes suggest ol fractionation. In e and f, steep trends suggest ol fractionation and shallow slopes suggest cpx fractionation. Symbols defined on Figure 21.

compatible element contents for the least evolved rock of each magma type. These observations suggest that the three magma types are not related by a fractional crystallization process.

Major element modelling (Table 12) confirms that no combination of olivine, clinopyroxene and/or plagioclase fractionation can produce Ttb from Tpb without significant contributions from the crystalline basement. Models 1 and 2 for producing primitive Tsp (sample 127) from primitive Tpb (sample 10) by fractionation alone have high residuals and cannot be considered successful. Residuals for models 3 and 4 for producing primitive Ttb (sample 138) from primitive Tsp (sample 127) are neither low enough to be conclusive nor high enough to be prohibitive of a fractionation relationship between Tsp and Ttb.

Assimilation-Fractional Crystallization (AFC)

XLFRAC models 5 and 6 (Table 12) for producing primitive Ttb (sample 132) from primitive Tpb (sample 10) requires 26% or 32% contamination by Proterozoic monzogranite with fractionation of 7% olivine or 6% olivine + 2.5% plagioclase. However, assimilation of such a large volume of felsic material by a basaltic magma is unlikely and would certainly have produced distinctive petrographic evidence.

Addition of a contaminant improves models for producing primitive Tsp (sample 127) from primitive Tpb (sample 10). Addition of 11% monzogranite (model 7) or 2% biotite monzogranite (model 8) improves XLFRAC models for fractionation of olivine. Small quantities (<5%) of contaminants can be

**THIS PAGE IS AN
OVERSIZED DRAWING
OR FIGURE**

**THAT CAN BE VIEWED AT
THE RECORD TITLED:**

“CONTOUR INTERVAL”

WITHIN THIS PACKAGE

Note: Because of this page's large size, it may be more convenient to copy the file to a local drive and use the Imaging (Wang) viewer, which can be accessed from the Programs/Accessories menu.

D-1

assimilated by basaltic magma without leaving significant textural evidence. However, TiO_2 concentration and Mg\# preclude these models. The modelled evolved magma (primitive Tsp) has higher TiO_2 than the proposed parent (primitive Tpb), but the contaminant is low in TiO_2 . TiO_2 content should decrease rather than increase during such an AFC process. In addition, primitive Tsp samples have Mg\# s higher than primitive Tpb samples. Evolution by fractional crystallization should result in a decrease in Mg\# .

AFC models for evolution of Ttb from Tsp (models 9 and 10) have lower residuals than models for fractionation alone. However, the lack of petrographic evidence for assimilation precludes the large amount of assimilant (13% and 25%) required by the models.

Source differences

Differences between the three magma types may be explained by either (1) different degrees of partial melting from the same source, or (2) independent melting of different sources to the same degree.

1. Partial melting of the same source should result in highest concentrations of incompatible elements at the lowest degrees of partial melting. The large volumes of incompatible-rich volcanics (Ttb and Tsp) in the NWH would require large degrees of partial melting of an incompatible-rich source. Partial melting of the same source should produce positive linear trends on incompatible element plots. Although incompatible element plots of NWH samples show positive trends, fields overlap or are parallel and do not form a

linear trend (Figures 22 and 23).

2. Independent melting of different sources to the same or a similar degree may explain the non-linearity of fields in Figures 22 and 23. This is consistent with the fact that compatible trace element values for the most primitive samples within each magma type are similar.

Conclusions

Neither fractionation, AFC nor partial melting of the same source can produce Ttb or Tsp from Tpb. Although the three coeval NWH magma types may be cogenetic, they are not comagmatic. They formed by independent partial melting of different (although similar) sources.

All three magma types contain olivine as an equilibrium phase. Therefore, olivine must have been in equilibrium in the source (Yoder, 1976). One possible crustal source is olivine gabbro, but very large degrees of crustal melting would be required to produce the mafic NWH magmas. An alternative source is mantle peridotite, which would require lesser degrees of partial melting. Partial melts of garnet peridotite would have steep slopes on chondrite-normalized REE plots, so spinel peridotite is a more likely source material for the NWH mafic magmas.

CHEMICAL VARIATION WITHIN EACH MAGMA TYPE

Pink/Black Ridge Basalts

The fractionation of Mg and Fe-rich phases in Tpb samples is suggested by the steep negative trends in plots of SiO₂ vs. FeO and MgO (Figure 19, c and d). In Figure 24, the large variation in Co with little variation in V, the positive relationship between Co and Cr, and the flat slope in the plot of Co vs Sc indicate fractionation of olivine. On Harker variation diagrams steep slopes for Cr and Co and shallow slopes for V (Figure 24, a and c) favor olivine fractionation as well. Clinopyroxene is unlikely as a major fractionating phase in Tpb magma because Cr, Co and V have high distribution coefficients (Table 13) for clinopyroxene, and these elements appear to have low bulk distribution coefficients in Tpb samples. This is consistent with the lack of clinopyroxene phenocrysts in Tpb samples. Plagioclase cannot be a major fractionating phase as CaO and Na₂O vary little despite variation in Eu (Figure 26). This is consistent with the lack of a negative Eu anomaly on a chondrite-normalized REE plot (Figure 27) and the lack of plagioclase phenocrysts in Tpb samples.

XLFRAC model 11 (Table 12) indicates that evolved Tpb (sample 117) can be produced from primitive Tpb (sample 10) by fractionation of 6% olivine. Large residuals for the model suggest that another process may be at work. A second process, such as contamination or multiple sources is also suggested by the large range in heavy rare-earth elements (HREE) and tighter clustering in light rare-earth elements (LREE) (Figure 27). Fractionation of olivine results in a

Table 13: Distribution coefficients for basalt

	Plagio- clase	Clino- pyroxene	Olivine
Ba	0.355	0.1505	0.0055
Rb	0.185	0.031	0.0055
Ce	0.1255	0.103	0.0022
Nd	0.0915	0.236	0.0034
Sm	0.059	0.438	0.0059
Eu	0.34	0.51	0.0068
Yb	0.038	0.605	0.0177
Lu	0.06	0.56	0.016
Sc	0.004	3	0.25
Cr	0.01	8.4	2.1
V	0.01	3	0.09
Co	0.05	1.2	3.8
Th	0.0055	0.007	0.0055

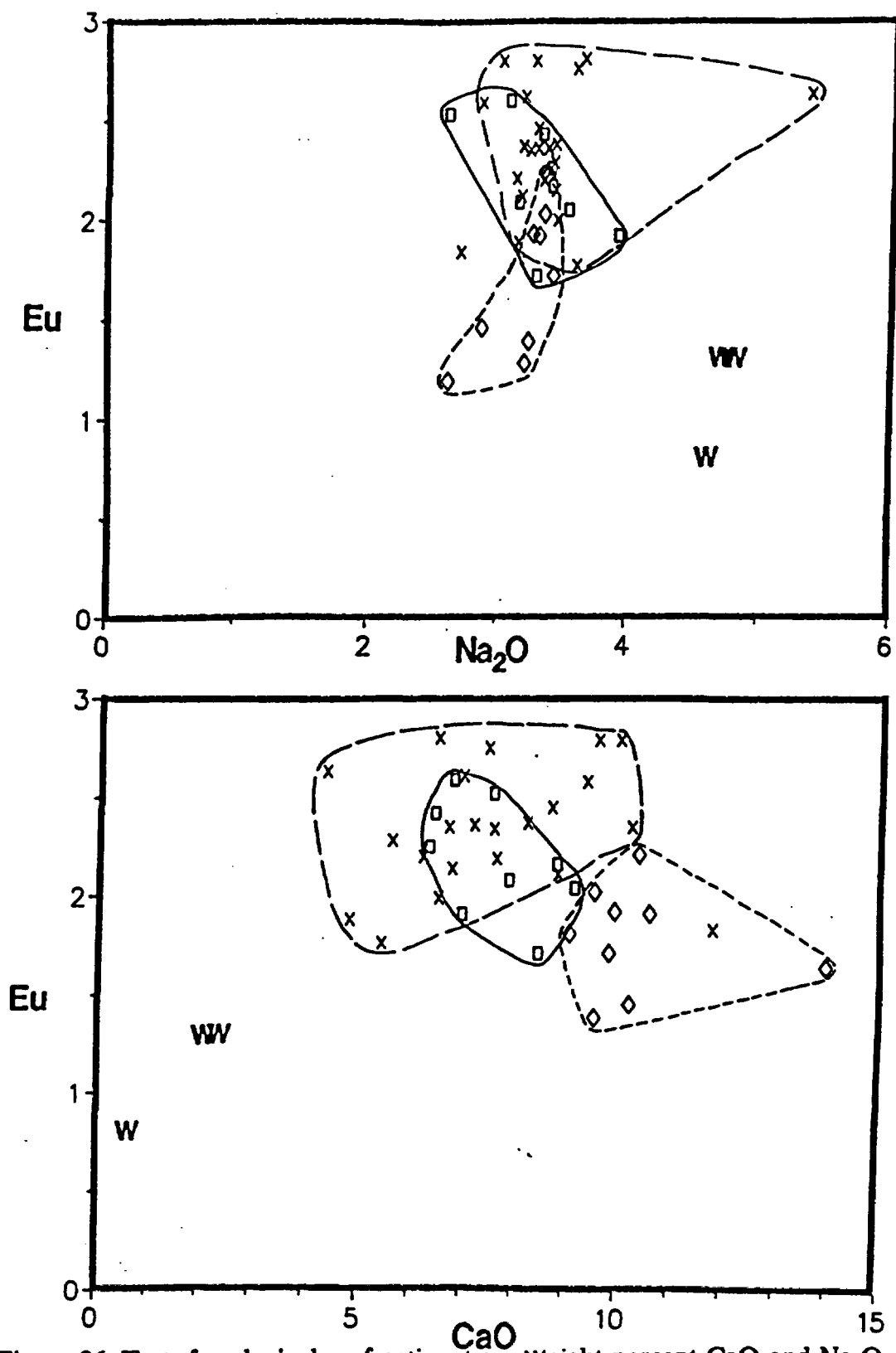


Figure 26. Tests for plagioclase fractionation. Weight percent CaO and Na₂O plotted against ppm Eu. Symbols defined on Figure 21.

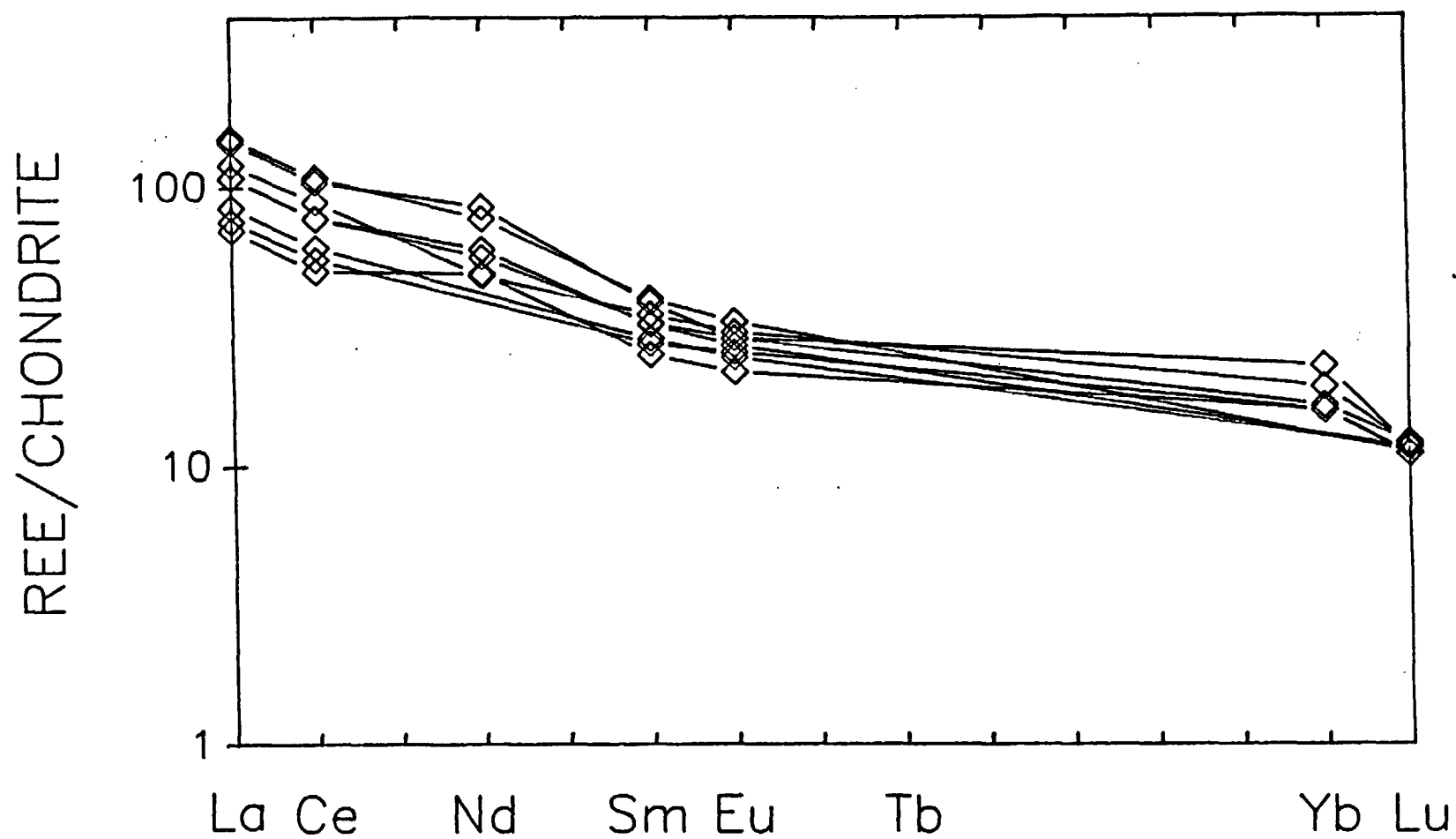


Figure 27. Chondrite-normalized rare earth element plot for basalt of Pink/Black Ridge.

greater variation in HREE than LREE because distribution coefficients for LREE in ol are higher than those for HREE. Multiple pulses of magma, each representing slightly different amounts of melting from similar sources, may be responsible for the variation in LREE in Tpb samples.

Basaltic Andesite of Temple Bar

The moderate negative trend on plots of SiO_2 vs. FeO , MgO and TiO_2 (Figure 19 c, d and g) indicates fractionation of Mg- Fe- Ti-bearing phases such as olivine and/or clinopyroxene. Compatible element plots (Figure 24) suggest that both phases are probably significant. For example, fractionation of clinopyroxene alone would produce a slope of +3 on the Cr vs. V plot, and fractionation of olivine alone would produce a vertical vector. The Ttb vector fall between the olivine and clinopyroxene vectors and indicates the fractionation of both minerals. Each of the plots of compatible elements produces similar results. Moderate slopes on Harker variation diagrams for compatible trace elements (Figure 25) also indicate fractionation of olivine and clinopyroxene. Little change in CaO and Na_2O (Figure 26) and the lack of a Eu anomaly on Figure 28 suggests little fractionation of plagioclase.

XLFRAC model 12 (Table 12) for evolution of evolved Ttb (sample 138) from primitive Ttb (sample 113) requires fractionation of 9% olivine, 16% clinopyroxene and 8% plagioclase. However, the modelled fractionation of plagioclase is higher than expected and total fractionation (32%) is higher than generally considered reasonable for volcanic rocks. This may indicate that

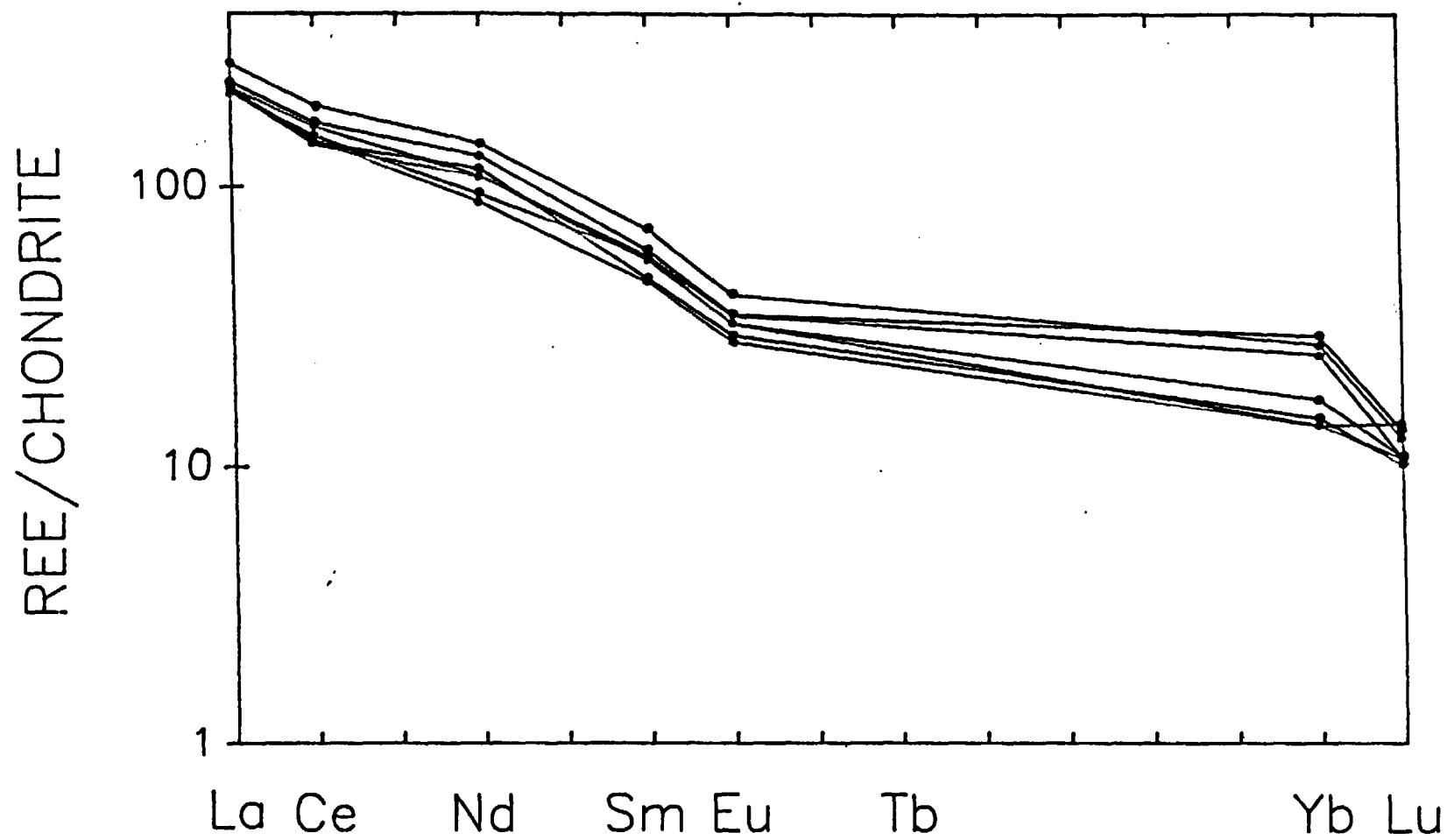


Figure 28. Chondrite-normalized rare earth element plot for basaltic andesite of Temple Bar.

another process in addition to fractionation is responsible for Ttb evolution. The wide range of Th over a fairly narrow range of SiO_2 (Figure 23) suggests contamination or several different partial melts for Ttb. Because Th is incompatible in basalts, it should not vary with fractionation. As discussed above, large degrees of contamination are precluded by the lack of petrographic evidence. The wide spread in chondrite-normalized REE data (Figure 28) suggests multiple batches of partial melts. Input of fresh batch melts is consistent with the lack of systematic variation in chemistry and mineralogy vertically in the sections.

Basaltic Andesite of Squaw Peak

Fractionation trends within the Tsp field are similar to Ttb. Olivine +/- clinopyroxene fractionation is indicated by the moderate negative trend on plots of SiO_2 vs. FeO, MgO and TiO_2 (Figure 19). Both phases are probably significant, because variation in Co, Cr, Sc and V (Figure 24) is similar to that in Ttb. However, the shallower slope on the plot of Sc vs. Co may suggest olivine fractionation is more important for Tsp than for Ttb. Moderate slopes on Figure 25 also indicate fractionation of olivine and clinopyroxene. The negative relationship between CaO and Eu (Figure 26) may suggest minor plagioclase fractionation. However, the lack of an Eu anomaly (Figure 29) indicates that fractionation of plagioclase was insignificant in comparison with fractionation of clinopyroxene and olivine.

The moderate positive relationship between SiO_2 and Hf may suggest that

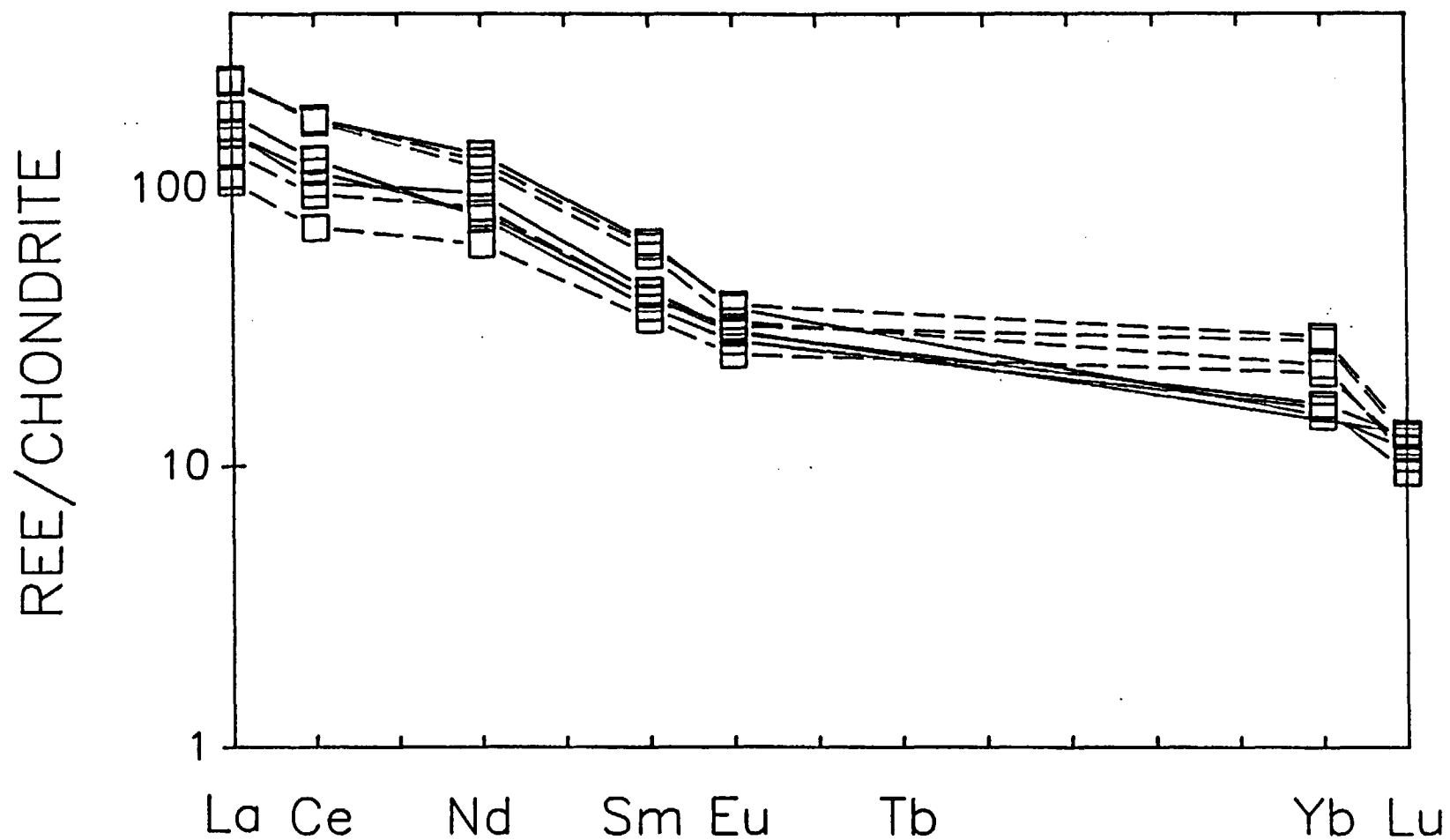


Figure 29. Chondrite-normalized rare earth element plot for basaltic andesite of Squaw Peak. Two magma types are delineated by flat HREE trend (dashed lines) or gently sloping HREE trend (solid lines)

some process, either contamination or multiple recharge was active in producing the Tsp suite. Chondrite-normalized REE data (Figure 29) may indicate two subtypes of Tsp magma, one high in LREE and low in HREE and another lower in LREE and higher in HREE. I propose that the Tsp chamber may have been fed by multiple pulses of partial melts from at least two different sources. One source was chemically similar to or the same as that for Ttb magmas.

XLFRAC model 13 produced the most evolved Tsp sample (112) from the least evolved sample (127), by fractionation of 12% olivine, 7% clinopyroxene, and <1% plagioclase. However, as with many other models, residuals are high and suggest that some other process such as assimilation was active in addition to fractionation.

SUMMARY

The mafic volcanic rocks of the NWH comprise three distinct magma groups in terms of chemistry, petrography and spatial distribution. Each magma type may represent independent batch melts from similar high K_2O sources. Adding to the complexity, each magma type may represent many independent magma pulses formed by partial melting. Each of the magma batches underwent a different differentiation history. Tpb evolved by fractionation of olivine alone. Ttb and Tsp both evolved by fractionation of olivine, clinopyroxene and minor plagioclase. The evolution of each magma type may be complicated by the addition of small amounts of a crustal contaminant and continued recharge of the magma chambers by new partial melts.

REGIONAL CORRELATION

MID-TERTIARY VOLCANIC ROCKS

The mafic volcanic rocks in the northern White Hills (NWH) erupted from local sources. Therefore, regional correlation of the mid-Tertiary volcanic section depends on correlation of regionally extensive units such as ash-flow tuffs. Two ash-flow tuffs crop out in this part of the Basin and Range; the Peach Springs Tuff (18.5 Ma) and the Tuff of Bridge Spring (15.18 Ma). I propose that the ash-flow tuff exposed in the NWH is correlative with the Tuff of Bridge Spring. In addition, I propose that the Tuff of Bridge Spring is composed of two major pyroclastic flows. The first is exposed in the southern Black Mountains, McCullough Range and NWH (Figure 30) and erupted at 16.4 Ma. The second erupted at 15.19 Ma and crops out in the Eldorado Range.

Correlation of the tuff in the NWH with the Tuff of Bridge Spring is based on similarities in mineralogy and chemistry. The Tuff of Bridge Spring in the Eldorado Range contains abundant phenocrysts of sanidine, lesser amounts of plagioclase and biotite, minor quartz and trace amounts of clinopyroxene and sphene (Anderson, 1971). It is therefore mineralogically similar to the tuff in the NWH. The Peach Springs Tuff is similar in mineralogy to the Tuff of Bridge Spring (sanidine + plagioclase + sphene), but contains up to 2% hornblende and only trace amounts of biotite (Young and Brennan, 1974).

The NWH tuff and the Tuff of Bridge Spring are chemically similar (Tables 14 and 15), but both differ from the Peach Springs Tuff. The Peach

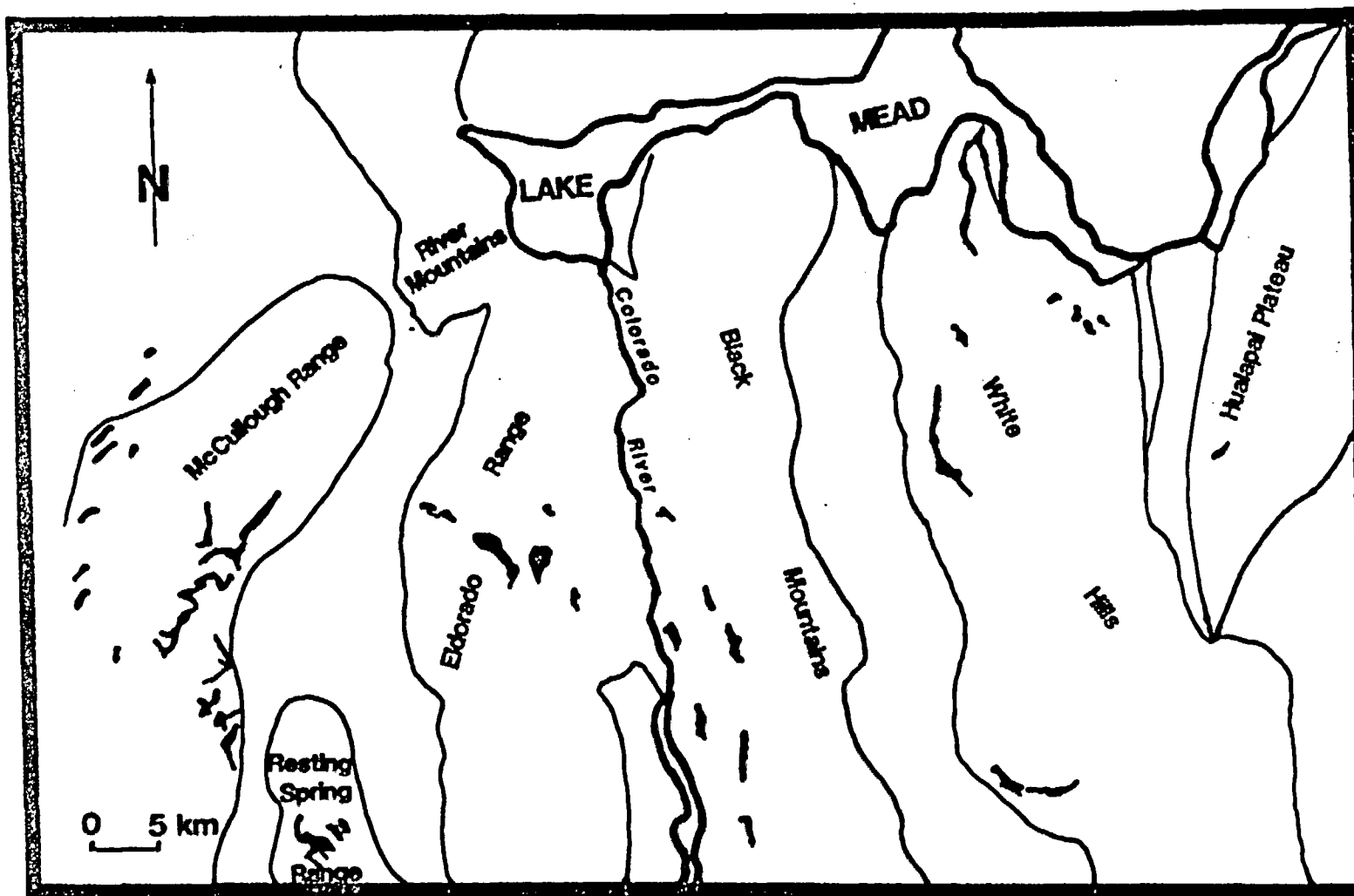


Figure 30. Regional exposures of the Tuff of Bridge Spring. After Anderson (1971), Bridwell (in preparation), Davis (1984), Faulds (personal communication) and Schmidt (1987).

Table 14: Major element data for Tuff of Bridge Spring and Peach Springs Tuff

Eldorado Mountains Tuff of Bridge Spring											
Sample No.	BS 10	BS 12	BH-1	BH-2	BH-3	BH-4	BH-5	BH-6	BH-7	BH-8	BH-9
Source of Data	1	1	2	2	2	2	2	2	2	2	2
SiO ₂	64.99	70.22	65.8		67.06		66.1		66.58		64.79
Al ₂ O ₃	16.54	14.53	14.24		14.56		14.56		14.97		16.48
FeO+Fe ₂ O ₃	2.04	1.74	2.96	2.45	3.46	1.47	2.4	4.83	2.39	1.96	2.68
CaO	2.07	2.55	1.42	1.66	1.01	0.82	0.7	0.91	0.69	0.63	0.67
MgO	1.34	2.72	2.21	2.67	1.92	3.15	3.12	3.53	2.85	2.43	2.06
Na ₂ O	4.59	1.65	2.45	2.16	4.04	3.27	3.98	12.53	4.08	2.51	4.72
K ₂ O	6.27	4.55	4.69	5.72	5.44	3.62	5.51	5.74	5.68	5.45	5.28
TiO ₂	0.5	0.39	0.6		0.51		0.41		0.47		0.52
MnO	0.06	0.06	0.08		0.07		0.07		0.07		0.06
P ₂ O ₅	0.09	0.08	0.25		0.11		0.07		0.06		0.1
LOI	2.2	9.2	5.61		1.3		2.24		1.88		0.56
Total	100.69	107.69	100.47		99.59		99.23		99.88		98.18

McCullough Mountains Tuff of Bridge Spring																
Sample No.	BH-11	BH-12	BH-13	85-63	MC 62	MC 68	MC 71	MC 65	MC 61	MC 67	MC 64B	MC 53	MC 60	MC 69	MC 64A	MC 66
Source of Data	2	2	2	2	3	3	3	3	3	3	3	3	3	3	3	3
SiO ₂				66.81	67.27	65.46	69.27	66.583	66.47	68.12	66.69	64.65	63.9	68.4	65.09	66.69
Al ₂ O ₃				15.06	13.95	14.23	14.88	14.468	14.92	14.6	13.72	15.66	14.77	14.46	13.72	14.48
FeO+Fe ₂ O ₃	1.27	1.3	2.06	2.52	2.27	3.19	2.93	3.727	3.47	2.91	3.11	3.95	3.55	3.07	3.11	3.16
CaO	0.53	0.52	0.66	1.6	2.36	3.43	0.65	0.497	1.72	1.69	0.65	2.43	3.24	1.61	5.66	4.12
MgO	0.98	0.72	1.21	0.71	0.58	0.66	0.4	0.935	0.86	0.61	1	0.97	1.05	0.53	1.42	0.84
Na ₂ O	2.54	3	2.99	4.33	3.97	4.1	4.44	4.042	4.33	4.38	3.86	4.33	4.09	4.33	3.35	3.74
K ₂ O	4.71	4.01	4.44	5.92	5.99	5.82	6.15	3.721	6.17	5.94	6.4	6.03	5.67	5.85	4.69	5.77
TiO ₂				0.43	0.35	0.42	0.41	0.453	0.47	0.39	0.42	0.53	0.45	0.4	0.42	0.43
MnO				0.09	0.152	0.143	0.15	0.152	0.151	0.149	0.143	0.151	0.151	0.146	0.151	0.149
P ₂ O ₅				0.02	0.1	0.13	0.09	0.151	0.16	0.11	0.13	0.18	0.16	0.09	0.4	0.33
LOI				2.57	2.04	2.56	0.56	4.11	1.14	1.38	0.65	1.27	1.97	1.33	1.48	3
Total				100.06	99.03	100.14	99.93	98.84	99.86	100.28	96.77	100.15	99	100.22	99.49	102.7

Table 14: continued

Peach Springs Tuff (data source 4)													
Sample No.	H83M-21	H83OW-163	H83OW-164	H84CH-71	H84AB-58	JP83KI-40	JP84EP-1	JP82TM-88	I-177	PCMS-15	TPS-RF	TPS-SNG	JP82CH-16
Location	Ship Mountains	Old Woman Mountains	Old Woman Mountains	Chomebuevi Mountains	Arica Mountains	I-40, east of Kingman	Sacramento Mountains	Pyramid Butte	Bullion Mountains	Pacific Mesa	Mohave Mountains	Chomebuevi Mountains	Chomebuevi Mountains
SiO ₂	74.7	70.4	72.3	73.2	73.5	73.5	68.6	66.6	73.3	64	75.7	70.5	70.7
Al ₂ O ₃	12.6	13.1	12.9	12.8	10.8	13.4	15.3	12.3	13.3	13.8	11.8	12.7	13.1
FeO+Fe ₂ O ₃	1.33	1.3	1.39	1.1	1.12	1.51	2.28	1.14	1.27	2.07	1.22	1.28	1.53
CaO	0.94	1.27	1.05	0.27	3.44	0.78	0.99	5.34	0.86	4.97	0.32	3.04	1.53
MgO	0.24	0.28	0.31	0.42	0.23	0.35	0.4	0.56	0.29	0.75	0.21	0.39	0.46
Na ₂ O	3.68	4.3	4.08	3.11	2.78	3.75	3.35	3.48	3.42	1.2	2.21	3.64	2.54
K ₂ O	5.27	3.58	4.23	5.78	4.92	5.33	7.21	5.01	5.54	6.03	6.81	5.17	7.35
TiO ₂	0.25	0.24	0.25	0.2	0.21	0.28	0.45	0.2	0.22	0.36	0.2	0.23	0.28
MnO	0.05	0.06	0.06	0.06	0.06	0.06	0.04	0.05	0.06	0.03	0.04	0.04	0.05
P ₂ O ₅					0.05			0.07	0.07	0.1			
LOI	0.32	3.95	2.52	2.01	0.45	0.35	0.14	0.43	0.52	1.86	0.42	0.29	0.39
Total	99.38	98.48	99.09	98.95	97.56	99.31	98.76	95.18	98.85	95.17	98.93	97.28	97.93

Data Source codes:

1: Cascadden, unpublished data

2: Smith, unpublished data

3: Bridwell, in preparation

4: Nielson, written communication

Table 15: Trace and rare earth element data for Tuff of Bridge Spring and Peach Springs Tuff

Eldorado Mountains Tuff of Bridge Spring												Dolan Springs*	
Sample	BS 10	BS 12	BH 1	BH 2	BH 3	BH 4	BH 5	BH 6	BH 7	BH 8	BH 9	DS 10	DS 17
La			77.63	85.73	94.28	92.68	95.01	108.43	134.48	162.44	114	50.3	44.8
Ce			205.39	209.92	227.51	205.86	229.84	226.5	285.78	349.04	243.98	69.9	63.1
Nd			56.3	58.36	64.65	69.58	72.93	80.52	87.58	87.47	63.5	14.1	14.8
Sm			10.14	11.86	13.54	12.43	13.42	14.57	14.57	13.29	10.73	2.47	2.44
Eu			1.74	1.89	1.81	1.55	1.71	1.76	2.66	3.64	2.7	0.389	0.281
Tb			1.44	1.13	1.55	1.39	1.52	1.54	1.32	1.4	1.15	1.39	0.345
Yb			2.55	2.8	3.08	2.92	3.18	2.99	2.67	2.31	2.13	0.15	1.56
Lu			0.4	0.42	0.48	0.51	0.49	0.49	0.46	0.39	0.38	4.94	0.21
U			6.408	8.67	8.89	10.37	9.85	9.08	7.61	4.98	6.52	20.2	4.04
Th			35.69	40.89	46.01	48.46	47.67	47.46	37.55	33.48	34.59	7.19	23.1
Cr			59.07	43.93	91.15	25.38	28.53	26.81	18.32	12.82	19.66	3.77	9.81
Hf			9.29	9.51	10.37	11.19	10.59	10.12	10.86	13.51	12.29	346	3.88
Ba	1343	371	383.63	355.72	279.73	275.02	267.91	206.07	634.13	1142.2	1184.1	113	190
Rb	131	162	184.28	208.55	224.14	214.67	225.36	205.97	179.57	165.56	170.48		117
Sr	476	310	59.07	43.93	91.15	25.38	28.53	26.81	18.32	12.82	19.66		1590
Sc			6.97	6.21	5.68	4.74	5.02	2.01	5.48	7.05	5.31	2.46	1.83
Ta			1.85	2.06	2.21	2.16	2.32		1.68	1.35	1.83	1.09	2.06
Zr	394	280											1.83
Co												1.49	1.47
V												16.9	9.79

Sources of data same as Table 12

* = source #1

Table 15: continued

McCullough Mountains Tuff of Bridge Spring													
Sample	BH 11	BH 12	BH 13	85-63	MC 62	MC 68	MC 71	MC 61	MC 67	MC 64B	MC 53	MC 60	MC 69
La	107.84	98.99	93.99	120.63	92.1	91.7	101	91.5	94.5	96.3	118	93.2	93.4
Co	247.08	231.33	226.33	190.85	184	177	188	167	173	181	204	170	184
Nd	72.93	74.23	71.51	64.34	55.3	63.7	80.9	75.2	79.8	67.3	73.4	64	57
Sm	14.92	13.64	13.77	11.48	11.1	11.8	13.7	11.3	12.8	11.5	9.67	8.33	12.1
Eu	1.71	1.63	1.72	1.72	1.01	1.22	1.17	1.33	1.14	1.11	1.78	1.7	1.22
Tb	1.78	1.58	1.53	0.8	1.1	1.17	1.26	1.41	1.16	1.06	0.934	0.86	1.27
Yb	3.44	3.12	3.27	3.12	3.5	3.36	3.77	3.92	3.62	3.76	2.87	3.14	3.56
Lu	0.56	0.5	0.52	0.45	0.6	0.54	0.63	0.48	0.56	0.58	0.42	0.41	0.49
U	9.02	10.51	11.49	4.69	10.9	7.23	8.42	6.36	8.66	8.86	6.26	5.42	8.47
Th	52.3	50.28	47.88	32.22	44.3	39.4	42	35.8	39.3	44.6	28.6	17.3	41.9
Cr	20.75	37.21	43.16	10.23	9.94	20.9	11.2	35.2	11.7	15.5	32	45.3	10.4
Hf	11.45	9.99	10.53	11.05	10.6	10.1	11.3	9.78	10	11.1	10.3	10.1	11
Ba	221.44	233.24	198.51	816.04	170	303		390		296	818	927	
Rb	248.18	219.61	254.42	156.79	172	165	173	160	155	170	121	127	179
Sr	20.75	37.21	43.16	264.97		200	196	3.89	219	389	502	781	168
Sc	4.25	4.45	4.56	4.13	3.23	3.85	3.25	2.4	3.16	3.63	4.67	4.21	3.39
Ta	2.43	2.32	2.41	2.31	2.71	2.36	2.76	826	2.44	2.7	1.74	1.86	2.56
Zr				390.09	553	544	663	3.41	455	577	578	483	603
Co					1.96	3.9	1.93	44.6	1.96	2.84	4.17	3.68	2.45
V					23.3	31	34.3		23.6	29.5	39.7	35.3	30

Peach Springs Tuff													
Sample N	H83M-21	H83OW-163	H83OW-164	H84CH-71	H84AR-58	JP83KI-40	JP84EP-1	JP82TM-88	I-177	TPS-RF	TPS-SNG	JP82CH-16	
Hf	8.67	8.83	8.87	7.94	6.81	9.25	13.5						
Ba								82	47	116	138	251	
Rb	165	245	225	205	135	185	175	173	195	240	175	212	
Sr	36	89	100	44	110	85	215	50	47	26	63	58	
Ta	2.24	2.59	2.66	2.55	1.88	1.76	1.76						
Zr	245	252	218	220	180	235	510	225	256	197	215	270	

Springs tuff is a rhyolite, (Nielson, written communication, 1991) while the tuff in the NWH and the Tuff of Bridge Spring are dacitic. In addition, compatible and incompatible element fields for the NWH tuff and the Tuff of Bridge Spring overlap (Figures 31 through 34). As chemical zonation is common in ash-flow tuffs (Smith, 1979), variation in major element and compatible trace element compositions in the NWH samples is not unexpected. However, incompatible elements such as Hf, Ta and Nb are best for ash-flow tuff correlation (Hildreth and Mahood, 1985). Therefore, the tight clustering of incompatible elements suggests a common source for the Tuff of Bridge Spring in the Eldorado Range and the tuff in the NWH. Although the Peach Springs Tuff has a similar range of Rb, Hf and Ta concentrations (Figures 31 and 32), it is higher in SiO_2 and lower in Ba (Figure 32) and in total Fe, MgO, TiO_2 and MnO (Figure 33) than most of the NWH samples.

The Peach Springs Tuff was dated at 18.5 ± 0.2 Ma (Nielson et al., 1990). The tuff in the NWH yielded a K-Ar biotite date of 16.4 ± 0.5 Ma (Table 8). Faulds (1989) reported similar biotite K-Ar ages (16.4 and 15.9 ± 0.36 Ma) for a tuff in the southern Black Mountains (Figure 29), that can be traced northward into the central Black Mountains, where it contacts small rhyolite or dacite centers in the middle Patsy Mine Formation (Faulds, personal communication, 1991). Bridwell (in preparation) dated a tuff from the McCullough Range that he correlated with the Tuff of Bridge Spring at 16.6 ± 0.4 Ma (K-Ar on biotite). These four dates contrast with a date of 15.18 ± 0.2

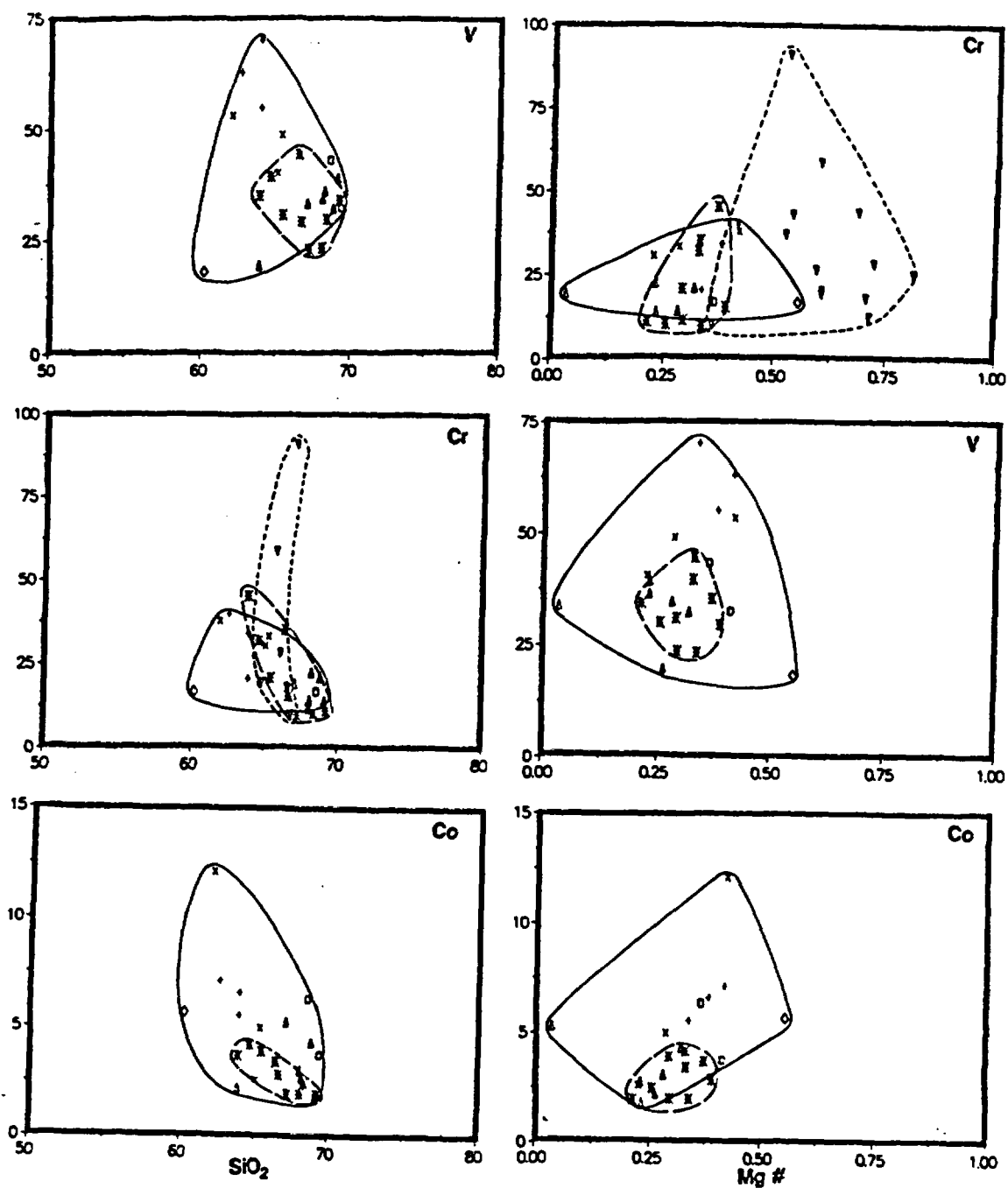


Figure 31. Harker variation diagrams comparing NWH tuff (symbols defined on Figure 7) with the Tuff of Bridge Spring Eldorado Range (inverted triangles), Tuff of Bridge Spring from the McCullough Range (*), and Peach Springs Tuff (#). SiO_2 in weight percent. V, Co and Cr in ppm.

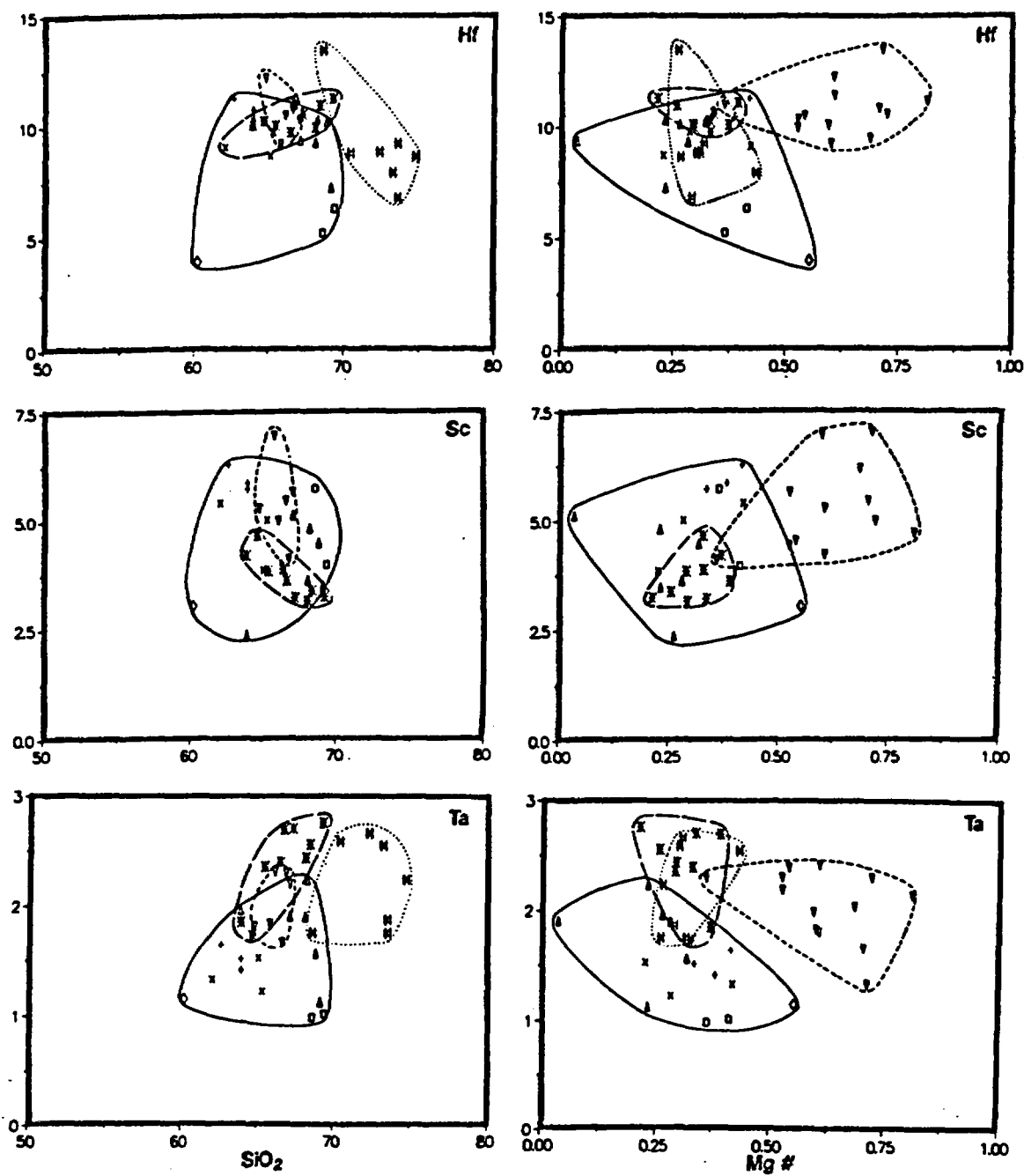


Figure 32. Harker variation diagrams comparing NWH tuff with the Tuff of Bridge Spring and Peach Springs Tuff. SiO_2 in weight percent. Hf, Sc and Ta in ppm. Symbols defined on Figure 31.

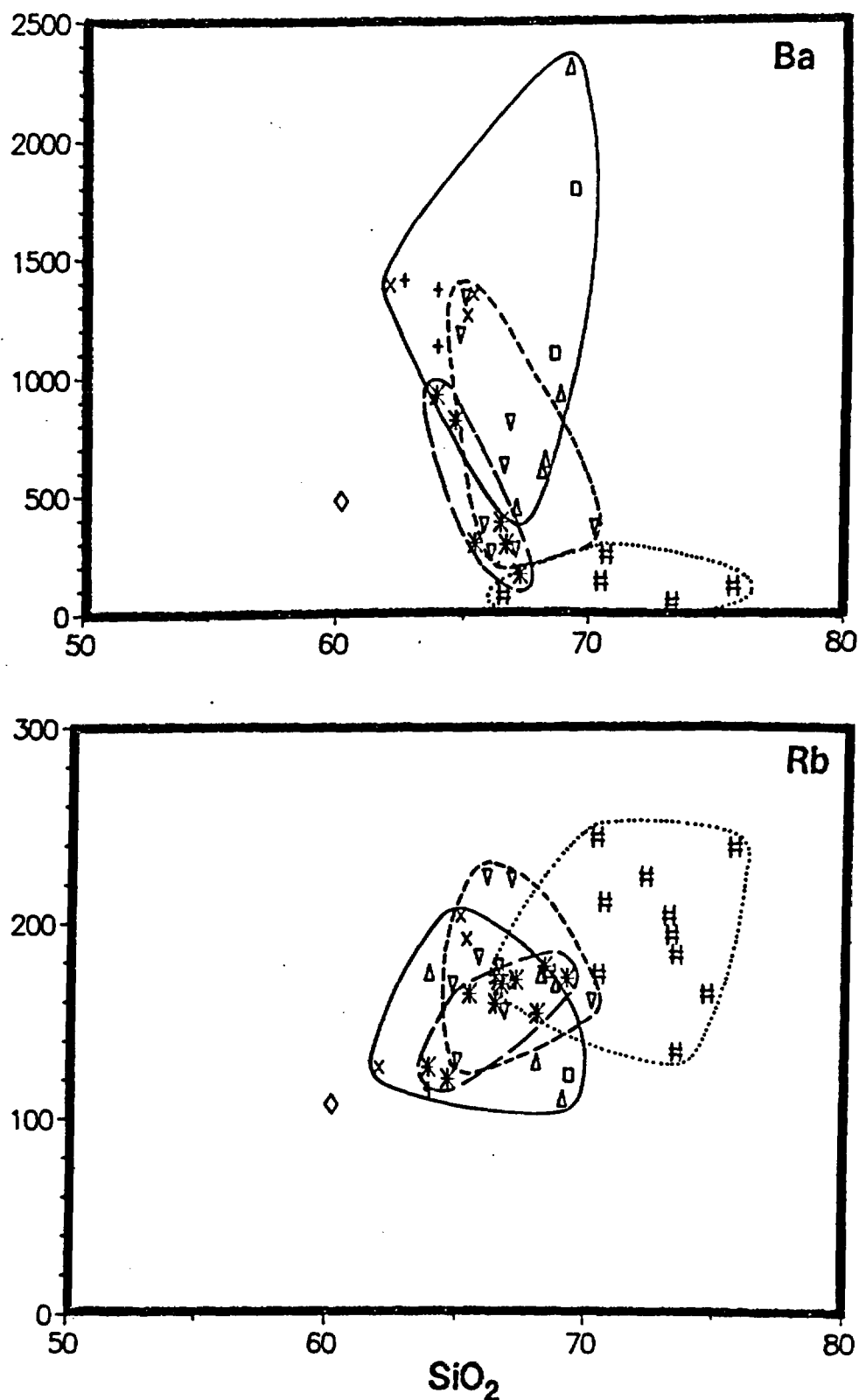


Figure 33. Harker variation diagrams comparing NWH tuff with the Tuff of Bridge Spring and Peach Springs Tuff. SiO_2 in weight percent. Ba and Rb in ppm. Symbols defined on Figure 31.

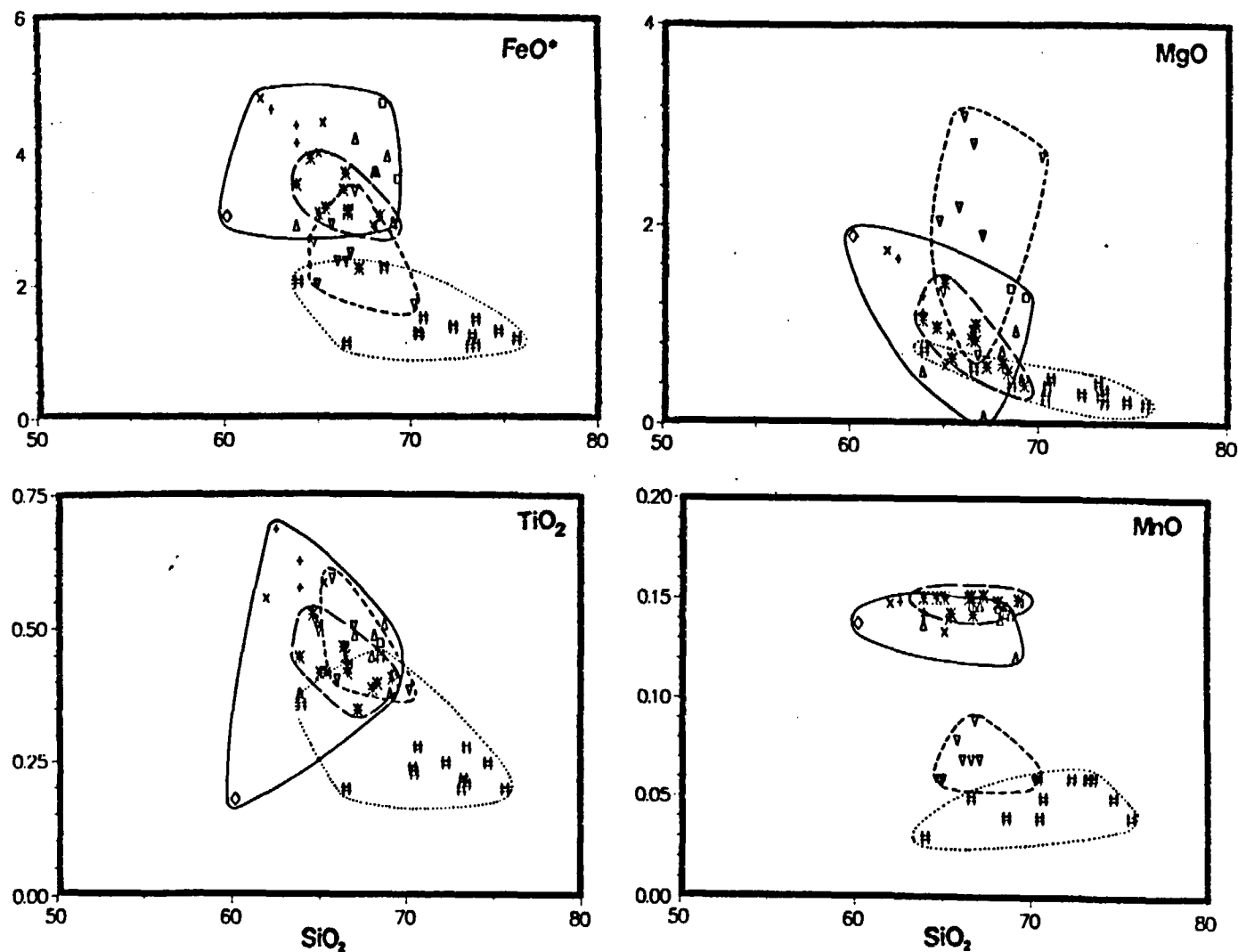


Figure 34. Harker variation diagrams comparing NWH tuff with the Tuff of Bridge Spring and Peach Springs Tuff (#). Units are weight percent. Symbols defined on Figure 31.

Ma ($^{40}\text{Ar}/^{39}\text{Ar}$) reported by Gans (1991) from the Tuff of Bridge Spring in the Eldorado Range.

I propose that the Tuff of Bridge Spring is composed of two pyroclastic flows. The tuffs in the NWH, southern Black Mountains and McCullough Range (White Hills member) may represent an earlier eruption from the same source which erupted the Tuff of Bridge Spring in the Eldorado Range (Eldorado Member) 1 to 1.5 m.y. later. This model requires that the magma chamber undergo two cycles of recharge from the same or a similar source followed by similar evolutionary paths to develop two magmas nearly identical in composition but erupted 1 to 1.5 m.y. apart. Similar episodic or cyclic pyroclastic eruptions have been described in western North America. Intervals between ash-flow tuff eruptions from the same caldera system (Table 16) range from 0.2 to 2.4 Ma. In general, magmas erupted after a longer (>1 Ma) period of quiescence tend to be more fractionated than the earlier magma (i.e., the Valles Caldera and the earlier stages of the Platoro complex). When intervals between the eruptions are shorter (<0.5 Ma) magmas from the later eruptions tend to be less fractionated than the earlier magmas (i.e., the western San Juan complex and the later stages of the Platoro complex). When intervals are between 0.5 and 1 Ma, the erupted magmas are very similar mineralogically and chemically (i.e., the Heise, Yellowstone, and Kane Spring Wash volcanic fields).

Chemical evidence supports the premise that the McCullough Range and NWH comprise a separate member of the Tuff of Bridge Spring. The broader

Table 16: Episodic ash-flow tuff eruptions from selected calderas in North America

Caldera System	Date of Eruption	Interval Between Eruptions	Comments
Platoro, New Mexico (1)	32 Ma		
		2.5 Ma	Increase in SiO ₂
	29.5 Ma	0.2 Ma	
	29.3 Ma	0.1 Ma	
	29.2 Ma	0.2 Ma	General decrease in SiO ₂
	29.0 Ma	0.6 Ma	
	28.4 Ma		
Western San Juan, New Mexico (2,3)	28.8 Ma	0.4 Ma	
	28.4 Ma	0.6 Ma	General decrease in SiO ₂
	27.8 Ma	0.2 Ma	
	27.6 Ma		
Valles, New Mexico (4)	2.84 Ma		Erupted from zoned chambers, latter two episodes are more silicic than the first, yet similar with respect to non-fractionated elements.
	1.45 Ma	2.4 Ma	
	1.12 Ma	0.33 Ma	
Yellowstone, Wyoming (5,6)	2.0 Ma		
	1.3 Ma	0.7 Ma	High-silica rhyolites, each similar mineralogically and chemically
	0.6 Ma	0.7 Ma	
Heise Volcanic Field, Idaho (7)	6.5 Ma		
	5.6 Ma	0.9 Ma	74-77% Silica, all enriched in LREE, each ash-flow similar chemically
	4.3 Ma	1.3 Ma	
Kane Springs Wash, Nevada (8)	15.6 Ma		
	14.7 Ma	0.9 Ma	Two or three separate centers erupted compositionally similar ash-flow tuffs
	14.1 Ma	0.6 Ma	
Los Humeros, Mexico (9)	0.46 Ma		High-silica rhyolite to dacite in first eruption, rhyodacite to andesite in second.
	0.1 Ma	0.36 Ma	Eruption rate > replenishment rate
1. Duncan et al., 1989			6. Hildreth et al., 1984
2. Lipman et al., 1989			7. Morgan et al., 1984
3. Hon and Lipman, 1989			8. Novak, 1984
4. Goff et al., 1989			9. Ferriz & Mahood, 1984
5. Bonnicksen et al., 1989			

spread of data for most elements in the NWH compared to the McCullough Range may be attributable to sampling over a broader area, as Tuff of Bridge Spring exposures in McCullough Range are more localized. Mg# is similar for both localities, and lower than for the Eldorado Member (Figures 31-33) and the White Hills Member has higher total Fe and MnO and lower MgO than the Eldorado Member. MgO contents of Eldorado Member samples are abnormally high for dacitic rocks and result in unusually high Mg#s (Figures 31 and 32). The source of this high MgO is unknown.

The White Hills, southern Black Mountains and McCullough Range may have occupied different structural troughs than the Eldorado Range. A topographic barrier may have separated different depositional settings and prevented the older White Hills member from reaching the Eldorado Mountains and the Eldorado member from reaching eastward into Arizona.

The Tuff of Bridge Spring has been mapped in the southern McCullough and Highland Spring Ranges (Schmidt, 1987, and Davis, 1984), and an ash-flow tuff exposed in the southern White Hills may correlate with the Tuff of Bridge Spring as well. Without age dates, it is unknown whether these tuffs represent the first or second eruption. Although the southern extent and source of the Tuff of Bridge Spring are unknown, a source to the southwest is suggested by flow direction studies on the Eldorado member by Brandon (1979) using the techniques of Elston and Smith (1970) and Rhodes and Smith (1972).

On the basis of geochronologic data and the above correlation of the tuff

in the NWH with the Tuff of Bridge Spring, the mafic volcanic rocks of the NWH can be placed within the established time-stratigraphic framework of the northern Colorado Trough (Figure 35). The basalt and basaltic andesite underlying and overlying the tuff in the NWH are time correlative with the Patsy Mine section in the Eldorado Range (18.5 to 13 Ma, Gans, 1991 and Darvall, 1991).

LATE TERTIARY SEDIMENTS

The east-tilted mid-Tertiary volcanic and sedimentary section in the NWH is unconformably overlain by gently tilted ($< 10^\circ$ NE) sediments that I correlate with the late Tertiary Red Sandstone unit and Muddy Creek Formation. In the southern half of the study area, unconsolidated sandy gravels overlie Tpb and Tsp and are overlain by Senator Mountain basalts (Tsm). Calderone et al. (1991) report a 8.5 Ma date on a basalt similar to Tsm in composition and stratigraphic position at Table Mountain Plateau in the southern White Hills, 15 km south of the study area. Theodore et al. (1987) report a 10.9 ± 0.6 Ma date on a "basalt flow in the Muddy Creek Formation". These dates are similar to the reported range for Callville Mesa basaltic andesite (Feuerbach et al., in press) that are interbedded with the Red Sandstone unit of Bohannon (1984). I therefore mapped all gravels that are tilted $> 5^\circ$ and intruded by or interbedded with the basalt of Senator Mountain as Red Sandstone (Trs). The Red Sandstone is exposed in the Grand Wash Trough and in the western Lake Mead area (Figure 36) and was deposited in actively extending basins (Duebendorfer and Wallin, 1991).

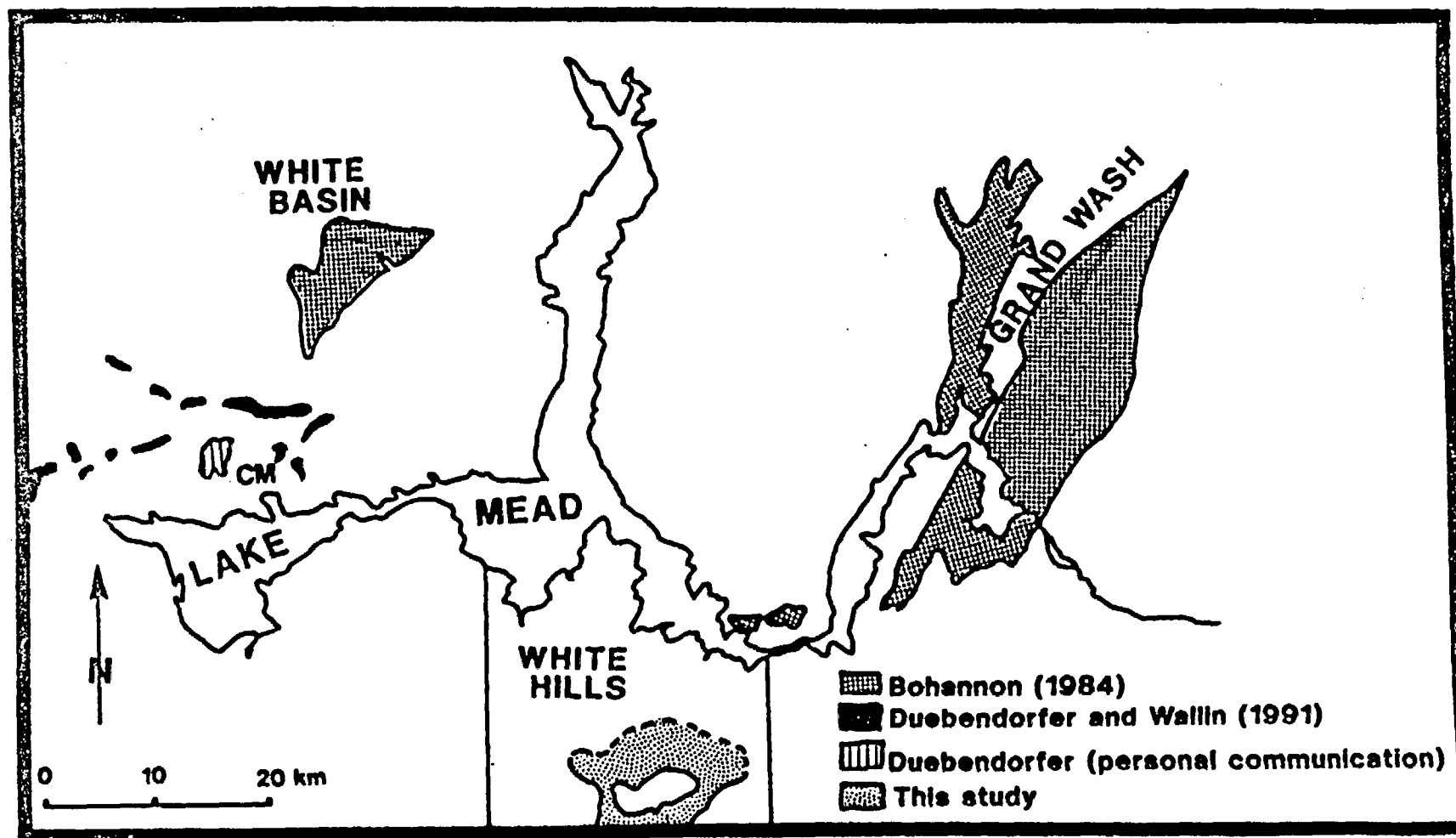


Figure 36. Regional exposures of Red Sandstone. CM=Callville Mesa.

In the northern half of the study area, Trs is overlain by untilted gravels that comprise the lower part of the Muddy Creek Formation (Tmcl). The deposits are lithologically similar to Trs and are distinguished from it by degree of tilt and lack of intruding or interlayered basalt. These coarse clastics are overlain by pink to orange gypsiferous siltstone and freshwater limestone that contains chert nodules. The capping limestone was mapped as the Hualapai Limestone Member of the Muddy Creek Formation by Blair and Armstrong (1979), Blair et al., (1979), and Bradbury and Blair (1979). For convenience in mapping, I have grouped the interbedded gypsiferous siltstone and limestone as Tmcu on Plate 1. The Muddy Creek Formation is exposed throughout the Lake Mead area (Figure 37).

Overlying the Muddy Creek sediments are unconsolidated river cobble deposits (Qp on plate 1) stranded at former levels of the Colorado River system. These are found 250 to 350 meters above the current river level (now flooded by Lake Mead) and consist of very well-rounded Colorado Plateau-type Paleozoic quartzite and carbonate clasts. They were mapped as "Old River Deposits" by Longwell (1936) and are found above river level throughout the Lake Mead area.

STRUCTURE

Lake Mead region "detachment faults"

The Lake Mead and lower Colorado River Trough regions contain numerous low-angle faults which accommodated considerable extension. These faults may be termed "detachment" faults if they exhibit the following

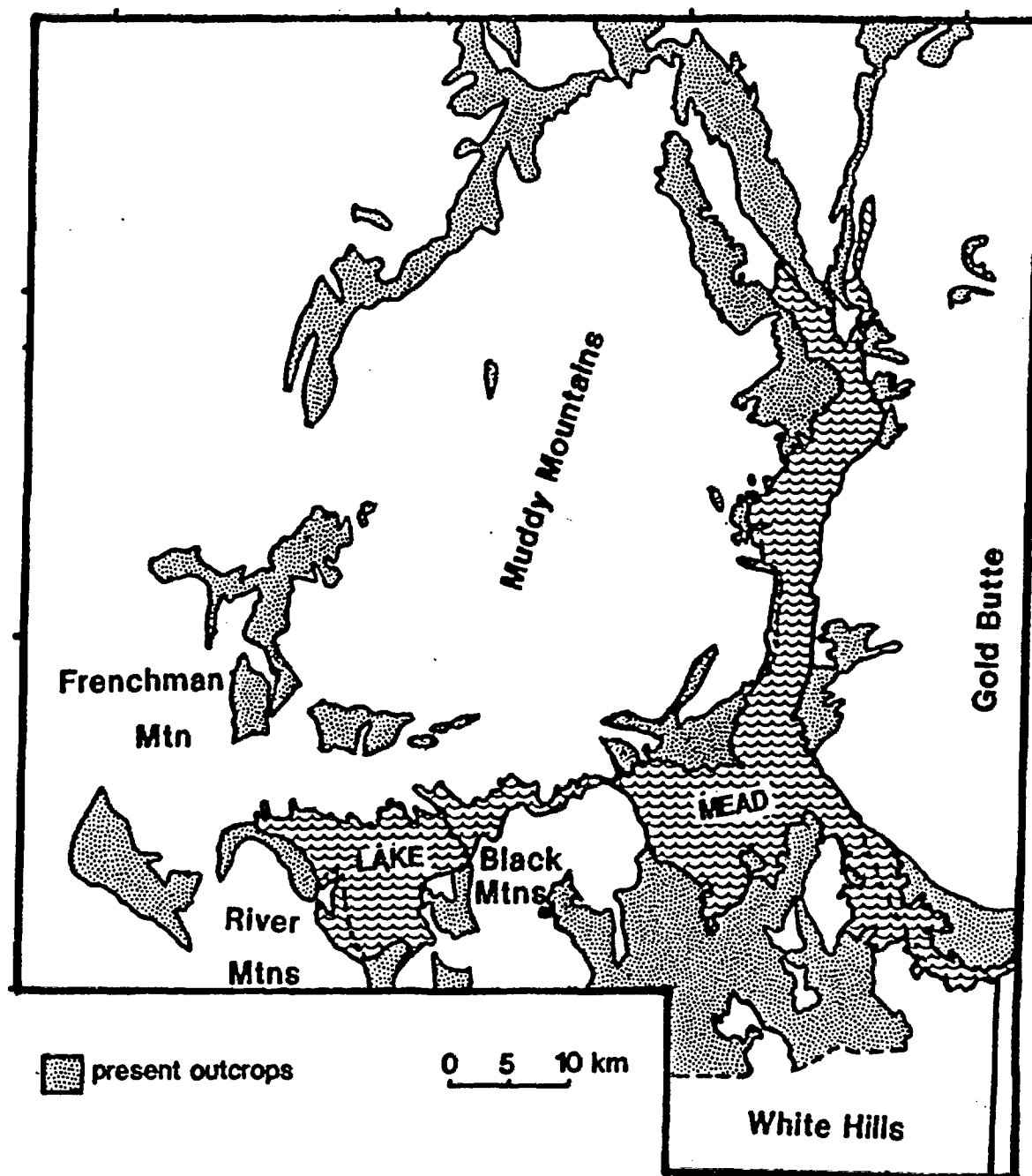


Figure 37. Regional exposures of Muddy Creek Formation, modified from Bohannon, 1984.

characteristics (Reynolds, 1985):

- 1) Significant contrast in rock type on either side of the fault, due to large magnitude normal-sense displacement.
- 2) Upper plate rocks are brittely deformed, faulted and rotated, while ductilely deformed lower plate rocks are comparatively intact.
- 3) Normal faults in the upper plate merge with or are cut by the detachment.
- 4) The lower plate in the vicinity of the fault is marked by a zone of hydrothermally altered breccia and microbreccia.

The Salt Spring fault satisfies some, but not all, of these criteria. The Tertiary rocks and structural style in the upper plate contrasts markedly with the lower plate Precambrian basement. Strong retrograde metamorphism and brecciation is exhibited in the lower plate. Therefore, the Salt Spring fault may be termed a detachment. However, the amount of displacement on the Salt Spring fault is unconstrained and the lower plate near the fault lacks evidence of ductile deformation. In addition, the behavior of the upper plate normal faults at depth is unknown.

Other major low-angle normal (detachment) faults in the Lake Mead area (Figure 2) include the Cyclopic detachment (Myers, 1985, Myers et al., 1986 and Theodore et al., 1987), the Lakeside Mine fault (Fryxell et al., in press, and Fryxell and Duebendorfer, 1990), the Saddle Island detachment (Smith, 1982, Sewall, 1988, Smith et al., 1990 and Duebendorfer et al., 1990a&b), and a low

angle fault at Arch Mountain (Eschner, 1989). Comparison of features associated with these faults is summarized in Table 17.

The Cyclopic detachment (Myers, 1985) exhibits brittle deformation and alteration similar to the Salt Spring fault. Myers noted chloritic alteration in the lower plate and ferric alteration in the upper plate of the detachment. Numerous northwest-striking, high-angle brittle normal faults antithetic to the detachment are present in the upper plate. At least 5 km of displacement occurred along the detachment.

Fryxell et al. (in press) have documented the deformation and alteration associated with the Lakeside Mine fault. They described highly brecciated chloritized Precambrian basement in the footwall. The brittle deformation overprints a mylonitic fabric that displays top-to-the-west shear and west to northwest transport. Mylonite zones dip dominantly west to northwest, but some dip eastward. Upper plate rocks north of the Gold Butte fault (Figure 2) are cut by tear faults and small-magnitude high-angle normal faults.

The Saddle Island detachment exhibits all of the characteristic elements of metamorphic core complexes, including brittle deformation of upper plate rocks and mylonite in lower plate rocks. Sewall (1988) described brecciation and propylitic alteration (epidote, clinozoisite, chlorite, and calcite) of the upper plate and black microbreccia grading into chlorite schist in the lower plate. Weber and Smith (1987) documented 20 km of displacement along the detachment.

Exposed at Arch Mountain is a low angle fault that separates Precambrian,

Table 17: Characteristics of Lake Mead region low angle normal faults

		Salt Spring Fault (this study)	Cyclopic Detachment (Myers, 1985)	Lakeside Mine Fault (Fryxell et al., in press)	Saddle Island Detachment (Sowall, 1988)	Arch Mountain Fault (Eschner, 1989)
LOWER PLATE	Mylonite	No	No	Yes	Yes	No
	Brittle Deformation	Yes	Yes	Yes	Yes	Yes
	Low-angle anastomosing shear zones	Yes	Yes	Yes	Yes	Yes
	Alteration	chloritic	chloritic	chloritic	chloritic	hematitic
UPPER PLATE	High-angle brittle faults	Yes: normal & strike-slip	Yes: normal	Yes: normal & strike-slip	Yes: normal	Yes: normal
	Alteration	hematitic	hematitic	hematitic	propylitic	hematitic
OTHER	Attitude	S: North-South D: 10 - 30 W	S: N37 -54 W D: 16-22 SW	S: NNE D: WNW	S: N65 E D: 25 NW	S: N 10 W D: 5-35 W
	Age	?	post 16.4 Ma		between 13.5 and 9 Ma	between 13.4 and 12 Ma

Paleozoic and Tertiary intrusive rocks in the upper plate from the mid-Miocene Wilson Ridge pluton in the lower plate (Eschner, 1989). Eschner described cataclastic deformation along the fault surface, hematitic alteration and low-angle anastomosing brittle shear zones in the lower plate. Duebendorfer et al. (1990) suggested that this fault may represent the eastern continuation of the Saddle Island detachment and attributed the lack of mylonitization in the lower plate to an eastward shallowing of a possible regional detachment structure.

Regional correlation of Salt Spring fault

The Salt Spring fault may be correlated with the Cyclopic detachment on the basis of spatial and geometric relationships, kinematic similarities and comparable styles of deformation and alteration. Both faults dip west to southwest, have brittlely deformed upper plates that are cut by high- to moderate-angle normal faults, and exhibit strong ferric alteration. Lower plates exhibit both chloritic and hematitic alteration.

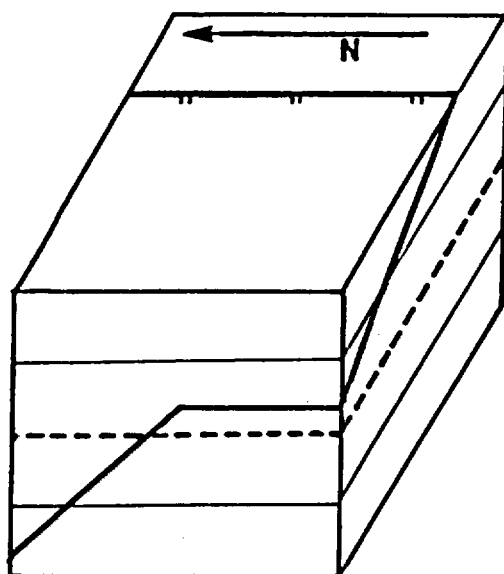
Correlation of the Salt Spring fault with the Lakeside Mine fault to the north is more speculative. Spatial and kinematic characteristics support this correlation, as both faults dip westward and upper plate transport direction was to the west. In addition, the coarse breccia and debris flow deposits (Tbr) in the NWH bear several similarities to the megabreccia and debris flows of the Thumb Member of the Horse Spring Formation exposed at Rainbow Gardens (Figure 2). The 16.4 Ma \pm 0.4 Ma age of the NWH tuff interbedded with Tbr is within the 13.5-17.2 Ma age range (Bohannon, 1984) for the Thumb breccias. Coarse clastic

deposits of the Thumb Member were interpreted as an alluvial fan deposit with a source at Gold Butte (Anderson et al., 1972, Longwell, 1974, and Bohannon, 1984). Parolini (1986) interpreted the megabreccias as landslides and debris flows shed off the scarp of a "boundary fault". The megabreccias were deposited no more than 5 km from their source (Rowland et al., 1990). Fryxell and Duebendorfer (1990) suggested that the Lakeside Mine Fault may have been that fault. Tbr may have been deposited in a similar fashion, as products of the rapidly uplifting and eroding Salt Spring fault scarp (Switzer, personal commun., 1991). Therefore, similarity of the Thumb breccias and Tbr, and their supposed relation to the Lakeside Mine and Salt Spring faults, respectively, supports the correlation of the two faults. However, the style of deformation differs between the faults, as evidence for ductile deformation is lacking along the Salt Spring fault.

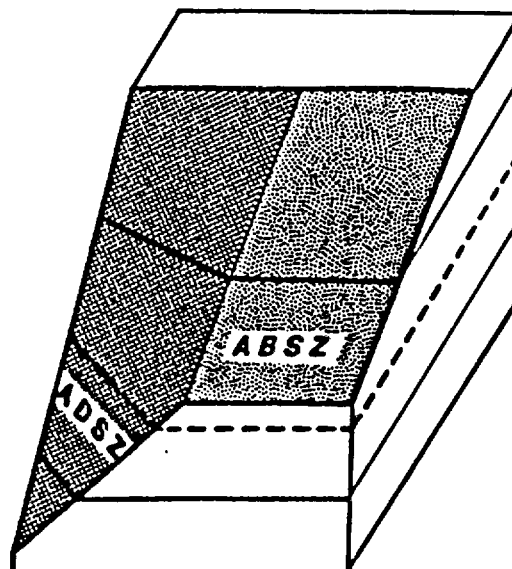
Ductile vs. brittle deformation

Brittle deformation in the lower plate of the Salt Spring fault and Cyclopic detachment contrasts with ductile deformation in the lower plate of the Lakeside Mine fault. Two models are proposed to explain the lack of ductile deformation along the Salt Spring fault and Cyclopic detachment.

1. Exposure of deeper levels in the Gold Butte area may be accomplished by either a steepening of the fault to the north (Figure 38) or corrugation of the fault surface about an east-west-trending axis (Figure 39). If the Lakeside Mine portion of the fault dips more steeply than the Salt Spring-Cyclopic portion,



Fault Steepens northward along strike



Upper plate is denuded

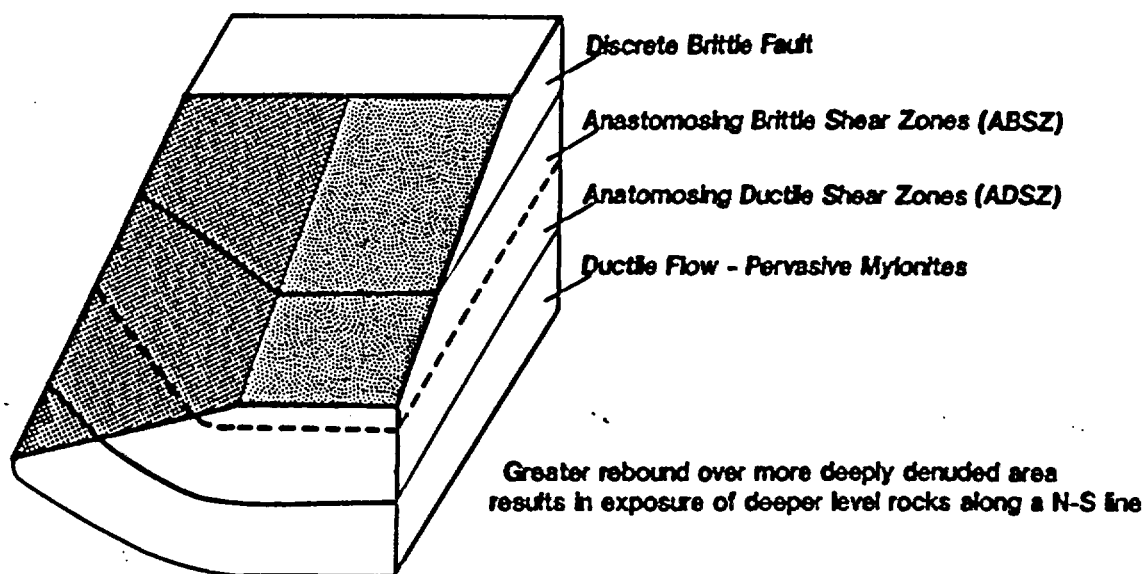


Figure 38. Along-strike differences in deformational style due to northward steepening of fault surface.

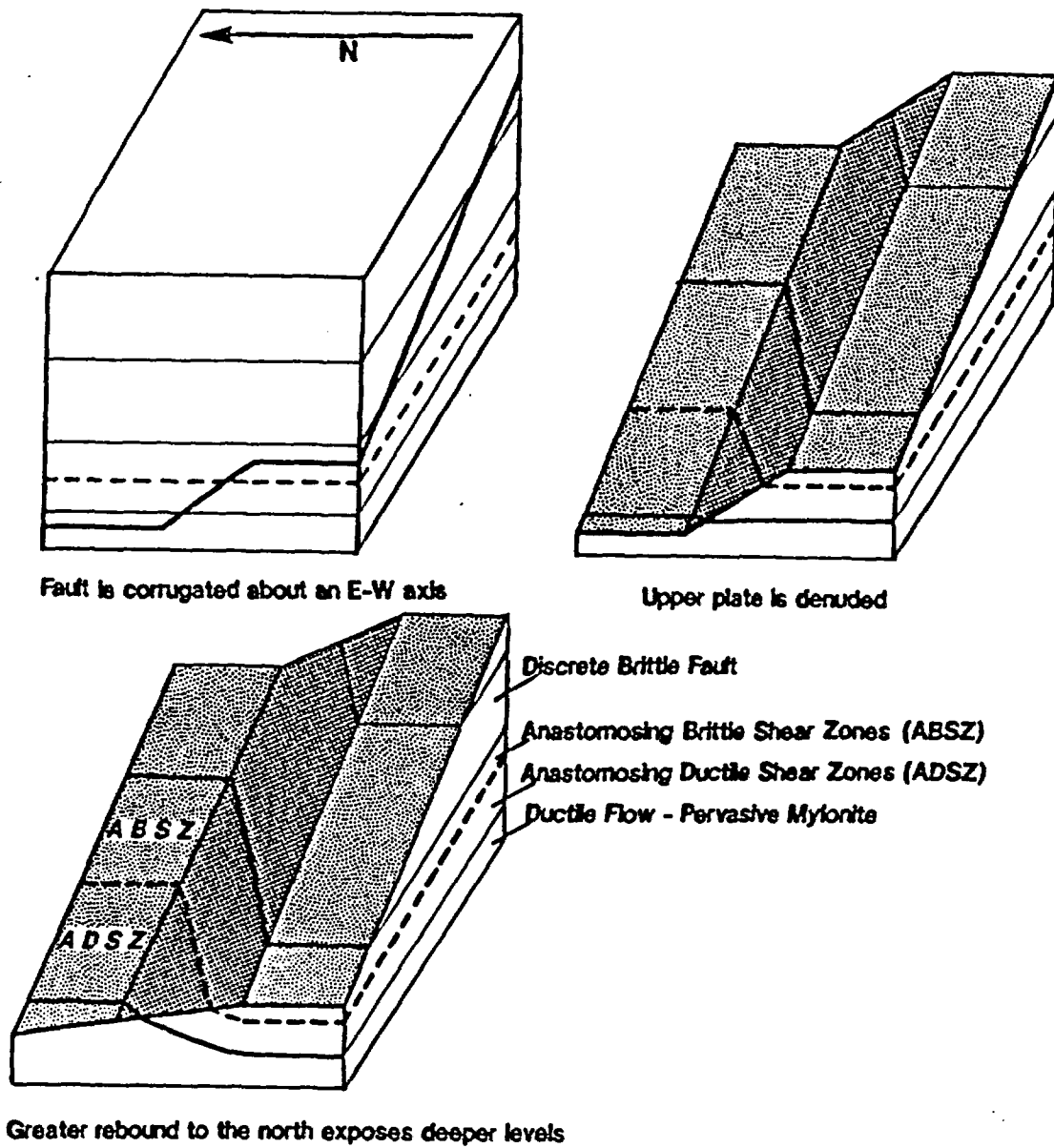


Figure 39. Along-strike differences in deformational style due to corrugation of fault surface about an east-west axis.

deeper level rocks were brought to the surface more quickly there, given the same amount of displacement. However, no evidence for significant differences in dip have been observed.

If the regional low-angle fault system that includes the Cyclopic, Salt Spring and Lakeside Mine faults was corrugated as in Figure 38, the southern portion of the fault would experience deformation at a higher structural level, where brittle deformation prevails. Greater uplift to the north where the fault is deep would be triggered by greater tectonic denudation. This model is consistent with fault attitude data for all exposed segments of the fault. However, the amplitude of the corrugation would have to be rather large. Corrugated detachment fault surfaces are known in the lower Colorado River trough, but the folds are gentle features with 4-10 km wavelengths and 100-600 m amplitudes (Spencer, 1982). Still, if the corrugation is near (and cuts) the brittle-ductile transition zone, it may be possible for different styles of deformation to be simultaneously active along strike of the same fault.

2. The amount of displacement on the Cyclopic-Salt Spring-Lakeside Mine fault system, and therefore the amount of rebound, may decrease southward toward the Black Mountains accommodation zone. Greater rebound to the north would expose deeper level rocks. Greater extension north of Lake Mead is indicated by transport of Thumb Member Megabreccia 65 km west of Gold Butte to Rainbow Gardens (Longwell, 1974 and Bohannon, 1984). Although 20 km of the westward transport of Thumb breccias probably took place along the Saddle

Island detachment, 40-45 km of displacement may have been accommodated by the Lakeside Mine fault. The maximum distance for landslide travel is 15 km, and distances on the order of a few km are more typical (Yarnold and Lombard, 1989). Preliminary work by Switzer (personal communication) suggests that the NWH breccia was probably deposited within 5 km of its source. NWH breccia is known only as far west as Squaw Peak (approximately 10 km). Although more Tbr could be buried in Detrital Wash, no exposures are known west of Detrital Wash, so the unit cannot have been extended more than 25 km.

In the Black Mountains and Eldorado Range, Faulds (1989) documented decreasing fault dips, increasing tilt of fault blocks, and increasing fault spacing away from the axis of the Black Mountains accommodation zone. Faulds documented 6 km of displacement along the Van Deemen Mine fault in the southern Black Mountains, north of the accommodation zone, and suggested that this fault may be continuous with the Saddle Island detachment. These observations indicate a northward increase in the amount of extension (Figure 40) that may be paralleled to the west in the White Hills and south Virgin Mountains. Although this model is highly speculative, it is consistent with published data regarding the Lakeside Mine fault, Thumb megabreccia, and accommodation zone.

Geometry and displacement of Salt Spring fault

Despite the substantial thickness of mafic volcanic rocks in the upper plate of the Salt Spring fault, no corresponding intrusions are known in the lower plate

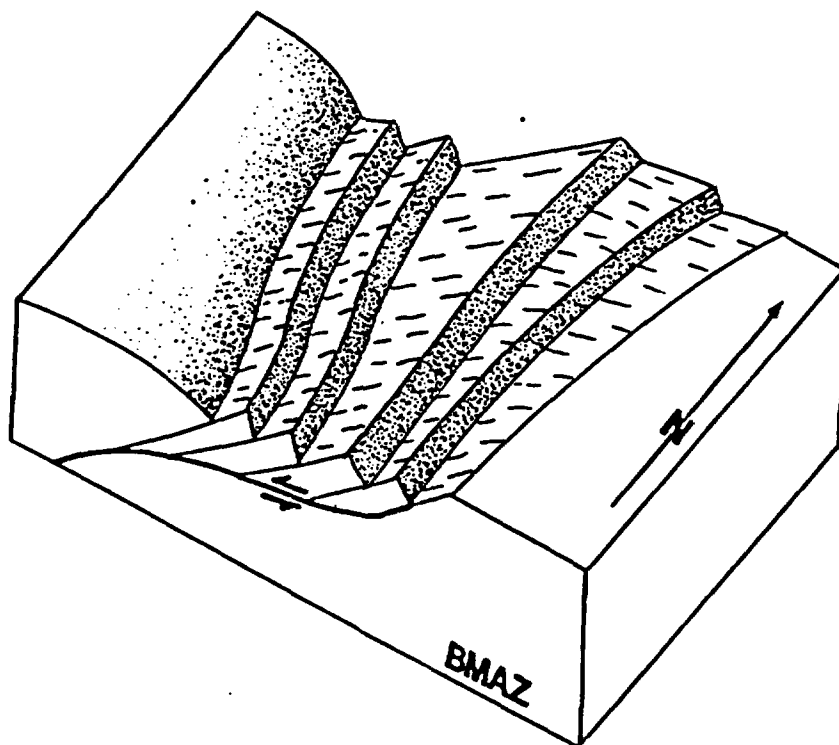


Figure 40. Extension increasing northward from the Black Mountains Accommodation Zone (BMAZ), modified from Faults (1991).

between the Salt Spring fault and the Grand Wash Cliffs (Figure 2). Four possible explanations for this follow.

1) The intrusions are present beneath sediments in Grapevine Wash or Hualapai Wash. If this is the case, horizontal displacement along the fault is a minimum of 10 km (Hualapai Wash) or 15 km (Grapevine Wash). No evidence for these intrusions exists because no detailed geophysical studies have been done in the area and no wells have been drilled to bedrock.

2) The volcanic sources were west, north or south of the study area and the mafic volcanics flowed into the area from outside. Corresponding intrusives would then be situated below these sources. However, the thickness of the sections precludes a distant source. In addition, no intrusive rocks equivalent to the basaltic andesite are known to the north, west or northwest of the study area. Although burial of intrusions beneath basin fill in Detrital Wash can not be ruled out, isostatic residual gravity data (Faulds, 1989) indicates a low in Detrital Valley, which is not consistent with mafic intrusions at depth. If such intrusions are present, they have been transported to the west in the upper plate of the Salt Spring fault along with the NWH.

3) The intrusions are still hidden beneath volcanic sections in the NWH. The Salt Spring fault has not experienced enough displacement to remove the volcanics from their underlying root. This model is consistent with decreasing displacement approaching the Black Mountains accommodation zone.

CONCLUSIONS

The northern White Hills (NWH) provide a unique opportunity to study the upper plate of the regionally extensive Cyclopic-Salt Spring Wash-Lakeside Mine Fault System. The upper plate contains 6 distinct structural blocks of tilted mid-Tertiary volcanic and sedimentary rocks, isolated by intervening late Tertiary and Quaternary sediments. A composite stratigraphic section was constructed using field relations, geochemical data and petrography. At the base of the composite section are mafic volcanic rocks overlain by coarse breccia and debris flow deposits interbedded with an ash-flow tuff. The upper part of the section contains mafic volcanic rocks and fanglomerate.

Three groups of mafic volcanic rocks were distinguished on the basis of geographic distribution, chemistry and petrography. These are the basaltic andesite of Temple Bar, basaltic andesite of Squaw Peak and basalt of Pink/Black Ridge. The mafic volcanics were erupted coevally from three different volcanic centers. Eruption of mafic lavas was interrupted by landslides, debris flows, the deposition of an ash-flow tuff and fanglomerates. These areally extensive deposits allow development of a model for the eruptive and depositional history of the NWH.

The mid-Tertiary section is cut by high- to moderate-angle down-to-the-west normal faults that repeat parts of the stratigraphic section. Similar normal faults, now buried beneath Late Tertiary and Quaternary alluvium may bound and separate the blocks. Although extension and tilting began after the cessation of

volcanism in most of the NWH, a growth fault at Salt Spring Wash indicates that faulting began earlier there.

The three types of mafic magma may reflect similar degrees of partial melting of similar K-rich sources. Tpb differentiated by fractionation of olivine. Ttb and Tsp evolved by fractionation of olivine, clinopyroxene and plagioclase. Magma evolution is complex and also involves recharge by fresh batch melts.

The tuff in the NWH (16.4 Ma) is the lower member of the Tuff of Bridge Spring (White Hills member). The underlying and overlying mafic volcanic rocks correlate with the Patsy Mine Volcanics. The upper member of the Tuff of Bridge Spring (Eldorado member) may have erupted from the same vent as the White Hills member at 15.19 Ma.

The lower plate of the Salt Spring fault is composed of Precambrian basement rock of varying lithologies. Near the trace of the Salt Spring Fault, the footwall rocks are highly altered and brittlely sheared to hematitic gouge and rock flour. A dense network of anastomosing brittle shear zones separates lower plate rock within 100 m of the fault into lenses of strongly retrograded but largely undeformed granitoid, gneiss and amphibolite. A higher proportion of granitoid and mylonite clasts in upper plate landslide breccia relative to lower plate rocks near the Salt Spring fault suggests that the source of the landslide deposits is farther east or south of the fault.

Differences in style of deformation along the Cyclopic-Salt Spring Wash-Lakeside Mine fault may be explained by increasing displacement and a

corresponding increase in uplift northward from the Black Mountains accommodation zone.

FUTURE WORK

The tectonic significance of the thick coarse breccia and debris flow deposits (Tbr) near the base of the NWH section may be better understood through more detailed mapping of the internal structure and stratigraphy of the deposits. Depositional processes may be better defined by detailed measurement of sections within the deposits, clast population studies and transport direction studies. The maximum transport distance, paleotopography and timing of deposition and extension may be better defined through careful examination of the internal and external stratigraphic details. Reconnaissance and detailed mapping of the crystalline basement rocks of the lower plate, in Graham Ridge and on the Hualapai Plateau, may delineate a source area for the mylonite and megacrystic granite clasts common in Tbr deposits.

More definitive links between the Salt Spring fault (SSF) and the Lakeside Mine fault and the Cyclopic detachment may be possible through additional detailed mapping. However, burial of the trace of the SSF south of Salt Spring Wash beneath the Muddy Creek Formation may preclude a physical linkage of the two normal faults. On aerial photographs, the SSF appears to project north of Lake Mead at Slide Cove (Plate 1). Although most of the terrain between Lake Mead and the southern end of the Lakeside Mine Fault is covered by Muddy Creek Formation or similar sediments, it is possible that some lower plate may be

exposed in deeply eroded gullies on the north side of the lake.

Intense hydrous retrograde alteration in the lower plate of the Cyclopic-Salt Spring Wash-Lakeside Mine fault contrasts markedly with the largely unaltered crystalline basement rocks of the region (i.e., the McCullough Range to the west and the Lost Basin Range to the east). Thus, retrograde alteration is spatially related to the detachment. More detailed study of the near-fault altered rocks and their unaltered equivalents is necessary to ascertain the timing of alteration and source of fluids.

The late Tertiary Red Sandstone equivalent and Muddy Creek Formation gravels in the northern White Hills were mapped from aerial photographs and during reconnaissance mapping. More detailed study of these sediments may allow new constraints on timing of basin development in the eastern Lake Mead.

Current work indicates that the Tuff of Bridge Spring merits a more detailed and comprehensive study. Mapping of extent and internal characteristics of known deposits of both members would better define the conditions of deposition and pre-eruption topography. Age dating, paleomagnetic studies and geochemical analysis of the Tuff of Bridge Spring in Highland Spring Range and southern McCullough Range would allow correlation of those exposures with either the White Hills Member or the Eldorado Member. Systematic sampling for geochemical, petrographic and age date analysis of both members would allow development of model for cyclic recharge and differentiation of a single magma chamber.

Isotopic studies would allow more quantitative and meaningful petrogenetic modelling of the mafic volcanics of the NWH. High precision systematic age dating of the entire section by the $^{40}\text{Ar}/^{39}\text{Ar}$ method would provide details regarding rates of magma production and eruption. Precise age dates would also constrain timing of synvolcanic faulting in the upper part of the section at Salt Spring Wash.

REFERENCES CITED

- Anderson, R.E., 1971, Thin skin distension in Tertiary rocks of southeastern Nevada: Geological Society of America Bulletin, v. 82, p. 43-58.
- Anderson, R.E., Longwell, C.R., Armstrong, R.L., and Marvin, R.F., 1972, Significance of K-Ar ages of Tertiary rocks from the Lake Mead region, Nevada-Arizona: Geological Society of America Bulletin, v. 83, p. 273-287.
- Blacet, P.M., 1968, Gold Basin-Lost Basin district, Arizona, in Geological Survey Research 1968, Chapter A [abs.]: U.S. Geological Survey Professional Paper 600-A, p. A4.
- 1969, Gold placer and lode deposits, Gold Basin-Lost Basin district in Geological Survey Research 1969, Chapter A [abs.]: U.S. Geological Survey Professional Paper 650-A, p. A1-A2.
- 1972, Late Cretaceous plutonism and metallization south of Lake Mead, in Geological Survey Research 1972, Chapter A [abs.]: U.S. Geological Survey Professional Paper 800-A, p. A44.
- 1975, Preliminary geologic map of the Garnet Mountain quadrangle, Mohave County, Arizona: U. S. Geological Survey Open File Map 75-93, Scale = 1:48,000.
- Blair, W.N., McKee, E.H., and Armstrong, A.K., 1977, Age and environment of deposition: Hualapai Limestone member of the Muddy Creek Formation: Geological Society of America Abstracts with Programs, v. 9(4), p. 390-391.
- Blair, W.N., Bradbury, J.P., and Oscarson, R.L., 1979, Upper Miocene Hualapai Limestone Member from the proto-gulf of California at Lake Mead, Arizona: in Rocky Mountain Association Geoscientists Basin and Range Symposium and Great Basin Field Conference, 1979

- Blair, W.N., and Armstrong, A.K., 1979, Hualapai Limestone Member of the Muddy Creek Formation, the youngest deposit predating the Grand Canyon, southeastern Nevada and northwestern Arizona: U.S. Geological Survey Professional Paper 1111, 13 p.
- Bohannon, R., 1984, Nonmarine sedimentary rocks of Tertiary age in the Lake Mead Region, southeastern Nevada and northwestern Arizona: U.S., Geological Survey Professional Paper 1259, 72 p.
- Bonnichsen, B., Christiansen, R.L., Morgan, L.A., Hackett, W.R., Leeman, W.P., Honjo, N., Jenk, M.D., and Godchaux, M.M., 1989, Silicic volcanic rocks in the Snake River Plain, Yellowstone Plateau Province: in Chapin, C.E. and Zidek, J., eds., Field excursions to volcanic terranes in the western United States, volume II: Cascades and intermountain west, New Mexico Bureau of Mines and Mineral Resources Memoir 47, p. 135-182.
- Bradbury, J.P., and Blair, W.N., 1979, Paleoecology of the Upper Miocene Hualapai Limestone Member of the Muddy Creek Formation, northwestern Arizona: in Newman, G.W. and Goode, H.D., eds., Rocky Mountain Association of Geoscientists Basin and Range Symposium and Great Basin Field Conference: Denver, p.292-303.
- Brandon, C.F., 1979, Flow direction studies of the Tuff of Bridge Spring, Nevada: Senior Project, University of Wisconsin-Parkside (unpublished).
- Bridwell, H.L., in preparation, Intermediate volcanics in an extensional environment: The Sloan sag caldera of the McCullough Mountains, southern Nevada: M.S. Thesis, University of Nevada, Las Vegas.
- Calderone, G.J., Butler, R.F., and Acton, G.D., 1991, Paleomagnetism of Middle Miocene volcanic rocks in the Mojave-Sonora desert region of western Arizona and southeastern California: *Journal of Geophysical Research*, v. 95, p. 625-647.
- Darvall, P., 1991, Normal faulting in the Eldorado Mountains, SE Nevada: *Geological Society of America Abstracts with Programs*, v. 23(2), p. 17.
- Davis, S.O., 1984, Structural geology of the central portion of the Highland Spring Range, Clark County, Nevada, M.S. Thesis, University of Southern California, 190 p.
- Duebendorfer, E.M., Sewall, A.J., and Smith, E.I., 1988, Kinematic interpretation of lower plate mylonites, Saddle Island detachment complex, Lake Mead, Nevada: *Geological Society of America Abstracts with Programs*, v. 20, p.

157.

- Duebendorfer, E.M., Sewall, A.J., and Smith, E.I., 1990, The Saddle Island detachment: An evolving shear zone in the Lake Mead area, Nevada: submitted to Wernicke, B.P., ed., Basin and Range extensional tectonics near the latitude of Las Vegas, Nevada, Geological Society of America Memoir 176, p 77-97.
- Duebendorfer, E.M., Sewall, A.J., Eschner, E., Feuerbach, D.L., Naumann, T.R., and Smith, E.I., 1990, The Saddle Island detachment, Lake Mead, Nevada: Regional extent and significance: Geological Society of America Abstracts with Programs, v. 22 (3), p. 20.
- Duebendorfer, E.M., and Wallin, E.T., 1991, Basin development and syntectonic sedimentation associated with kinematically coupled strike-slip and detachment faulting, southern Nevada: *Geology*, v. 19, p. 87-90.
- Dungan, M.A., Lipman, P.W., Colucci, M., Ferguson, K., and Balsley, S., 1989, Southeastern (Platoro) caldera complex: in Chapin, C.E. and Zidek, J., eds., Field excursions to volcanic terranes in the western United States, volume II: Southern Rocky Mountain region, New Mexico Bureau of Mines and Mineral Resources Memoir 46, p. 305-327.
- Eaton, G.P., 1982, The Basin and Range Province: Origin and significance: *Annual Review Earth Science*, v. 10, p. 409-440.
- Elston, W.E., and Smith, E.I., 1970, Determination of flow direction of rhyolite ash-flow tuffs from fluidal textures: *Geological Society of America Bulletin*, v. 81, p. 3393-3406.
- Eschner, E., 1989, The geology and structural significance of the Arch Mountain area, northern Black Mountains, Mohave County, Arizona: Master's thesis, University of Nevada, Las Vegas, 105 p.
- Faulds, J.E., 1989, Structural development of a major extensional accommodation zone in the Basin and Range province, northwestern Arizona and southern Nevada: Implications for tectonic models of continental extension: unpublished doctoral dissertation, University of New Mexico, Albuquerque, 263 p.
- Faulds, J.E., Geissman, J.W., and Shafiqullah, M., in press, Implications of paleomagnetic data on Miocene extension near a major accommodation

zone in the Basin and Range Province, northwestern Arizona and southern Nevada: Tectonics

- Ferriz, H., and Mahood, G.A., 1984, Eruption rates and compositional trends at Los Humeros volcanic center, Puebla, Mexico: *Journal of Geophysical Research*, v. 89 (B10), p. 8511-8524.
- Feuerbach, D.L., 1986, Geology of the Wilson Ridge Pluton: A mid-Miocene quartz monzonite intrusion in the northern Black Mountains, Mohave County, Arizona and Clark County, Nevada: Master's thesis, University of Nevada, Las Vegas, 54 p.
- Feuerbach, D.L., and Smith, E.I., 1987, Late Miocene Fortification Hill basalt, Lake Mead area, Nevada and Arizona: Source areas and conduit geometry: *Geological Society of America Abstracts with Programs*, v.19 (6), p. 376-377.
- Feuerbach, D.L., Smith, E.I., Shafiqullah, M. and Damon, P.E., in press, New K-Ar dates for late-Miocene to early Pliocene mafic volcanic rocks in the Lake Mead area, Nevada and Arizona: *Isochron-West*.
- Frost, E.G., Cameron, T.E., and Martin, D.L., 1982, Comparison of Mesozoic tectonics with mid-Tertiary detachment faulting in the Colorado River area, California, Arizona and Nevada: in Cooper, J.D., compiler, *Geologic excursions in the California desert* (Geological Society of America Cordilleran Section meeting guidebook); Cordilleran publishers, San Diego, p. 113-159.
- Fryxell, J.E., and Duebendorfer, E.M., 1990, Origin and trajectory of the Frenchman Mountain block, southern Nevada: *Geological Society of America Abstracts with Programs*, v. 22 (7), p. A226.
- Fryxell, J.E., Wernicke, B., Salton, G., Silverstone, J., in press, Gold Butte crustal section, South Virgin Mountains, Nevada
- Gans, P.B., 1991, Extensional strain rates in the Basin and Range Province: *Geological Society of America Abstracts with Programs*, v. 23 (2), p. 28
- Goff, F., Gardner, J.N., Baldrige, W.S., Hulem, J.B., Nielson, D.L., Vaniman, P., Heiken, G., Dungan, M.A., and Broxton, D., 1989, in Chapin, C.E. and Zidek, J., eds., *Field excursions to volcanic terranes in the western United States, volume II: Southern Rocky Mountain region, New Mexico* Bureau of Mines and Mineral Resources Memoir 46, p. 381-434.
- Hanson, G.H., 1980, Rare-earth elements in petrogenetic studies of igneous

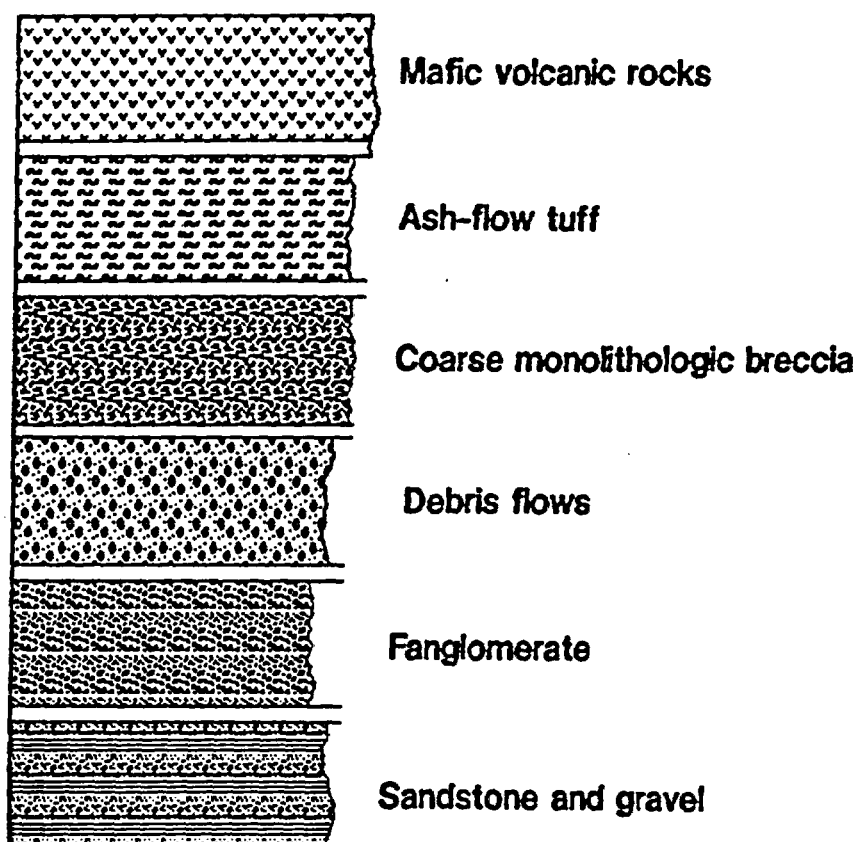
- systems: *Annual Review of Earth and Planetary Sciences*, v. 8, p. 371-406.
- Hildreth, W., and Mahood, G., 1985, Correlation of Ash-flow tuffs, *Geological Society of America Bulletin*, v. 96, p. 968-974.
- Hildreth, W., Christiansen, R.L., and O'Neil, J.R., 1984, Catastrophic isotopic modification of rhyolitic magma at times of caldera subsidence, Yellowstone Plateau volcanic field: *Journal of Geophysical Research*, v. 89 (B10), p. 8339-8370.
- Hon, K., and Lipman, P.W., 1989, Western San Juan caldera complex: in Chapin, C.E. and Zidek, J., eds., *Field excursions to volcanic terranes in the western United States, volume II: Southern Rocky Mountain region, New Mexico Bureau of Mines and Mineral Resources Memoir 46*, p. 305-327.
- Larsen, L.L. and Smith, E.I., 1990, Mafic enclaves in the Wilson Ridge Pluton, northwestern Arizona: Implications for the generation of a calc-alkaline intermediate pluton in an extensional environment: *Journal of Geophysical Research*, v. 95(B11), p. 17,693-17,716.
- LeBas, M.J., Le Maitre, R.W., Streckeisen, A., and Zanettin, B., 1986, A chemical classification of volcanic rocks based on the total alkali-SiO₂ diagram: *Journal of Petrology*, v. 27, p. 745-750.
- Lipman, P.W., Sawyer, D.A., and Hon, K., 1989, Central San Juan caldera cluster in Chapin, C.E. and Zidek, J., eds., *Field excursions to volcanic terranes in the western United States, volume II: Southern Rocky Mountain region, New Mexico Bureau of Mines and Mineral Resources Memoir 46*, p. 330-349.
- Longwell, C.R., 1936, Geology of the Boulder Reservoir floor, Arizona-Nevada: *Geological Society of America Bulletin*, v. 47, p. 1393-1476.
- _____, 1974, Measure and rate of movement on the Las Vegas Valley Shear zone, Clark County, Nevada: *Geological Society of America Bulletin*, v. 85, p. 985-990.
- Mills, J., 1985, The geology and geochemistry of volcanic and plutonic rocks in the Hoover Dam 7 1/2 minute quadrangle, Clark County, Nevada and Mohave County, Arizona: M.S. Thesis, University of Nevada, Las Vegas, 108 p.
- Morgan, L.A., Doherty, D.J., and Leeman, W.P., 1984, Ignimbrites of the eastern Snake River Plain: Evidence for major caldera-forming eruptions: *Journal of Geophysical Research*, v. 89 (B10), p. 8665-8678.

- Myers, I.A., 1985, Geology and mineralization at the Cyclopic Mine, Mohave County, Arizona: Master's thesis, University of Nevada, Las Vegas, 64 p.
- Myers, I.A., Smith, E.I., Wyman, R.V., 1986, Control of Gold Mineralization at the Cyclopic Mine, Gold Basin District, Mohave County, Arizona: *Economic Geology*, v. 81, p. 1553-1557.
- Naumann, T.R., 1987, Geology of the Central Boulder Canyon Quadrangle, Clark County, Nevada: unpublished master's thesis, University of Nevada, Las Vegas, 58 p.
- Nielson, J.E., Lux, D.R., Dalrymple, G.B., and Glazner, A.F., 1990, Age of the Peach Springs Tuff, southeastern California and Western Arizona: *Journal of Geophysical Research*, v. 95 (B1), p. 577-580.
- Novak, S.W., 1984, Eruptive history of the rhyolitic Kane Springs Wash volcanic center, Nevada: *Journal of Geophysical Research*, v. 89 (B10), p. 8603-8615.
- Reynolds, S.J., 1985, Geology of the South Mountains, central Arizona: *Arizona Bureau of Geology and Mineral Technology Bulletin* 195, 61 p.
- Rhodes, R.C., and Smith, E.I., 1972, Directional fabric of ash-flow sheets in the northwestern part of the Mogollon Plateau, New Mexico: *Geological Society of America Bulletin*, v. 83, p. 1863-1868.
- Rowland, S.M., Parolini, J.R., Eschner, E., McAllister, A.J., and Rice, A.J., 1990, Sedimentologic and stratigraphic constraints on the Neogene translation and rotation of the Frenchman Mountain block, Clark County, Nevada: in Wernicke, B.P., ed., *Basin and Range extensional tectonics near the latitude of Las Vegas, Nevada*: Boulder, Colorado, Geological Society of America Memoir 176, p. 99-122.
- Santa Fe Pacific Railroad Company, 1981, Geologic map of Santa Fe Pacific Railroad holdings in northern Arizona, Arizona Bureau of Mines and Mineral Technology miscellaneous map series MM-88A, scale = 1:250,000.
- Schmidt, C., 1985, A mid-Miocene caldera in the central McCullough Mountains, Clark County, Nevada: Master's thesis, University of Nevada, Las Vegas, 78 p.
- Sewall, A.J., and Smith, E.I., 1986, The Saddle Island detachment fault, Lake Mead, Nevada: Upper plate geology and regional significance: *Geological Society of America Abstracts with Programs*, v. 18(6), p. 182.

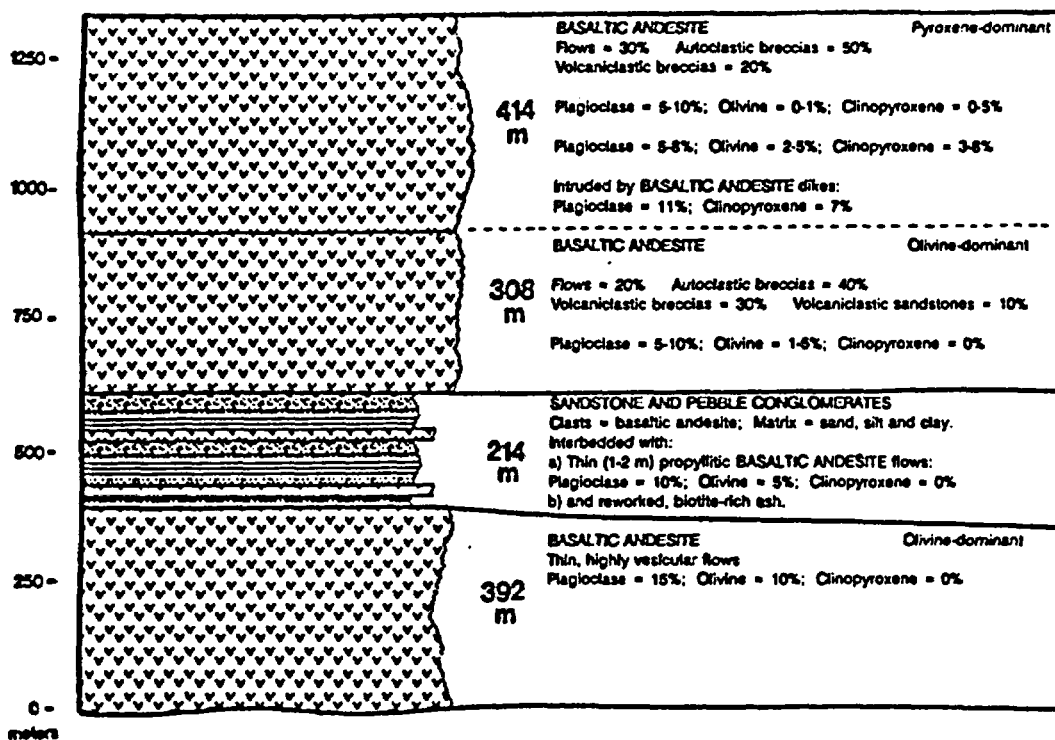
- Sewall, A.J., 1988, Structure and geochemistry of the upper plate of the Saddle Island Detachment, Lake Mead, Nevada: Master's thesis, University of Nevada, Las Vegas, 78 p.
- Smith, E.I., 1982, Geology and geochemistry of the volcanic rocks in the River Mountains, Clark County, Nevada and comparisons with volcanic rocks in nearby areas, *in* Frost E.G., and Martin, D.L., eds., Mesozoic-Cenozoic tectonic evolution of the Colorado River region, California, Arizona and Nevada: San Diego, California, Cordilleran Publishers, p. 41-54.
- Smith, E.I., Feuerbach, D.L., Naumann, T.R., and Mills, J., 1990, Mid-Miocene volcanic and plutonic rocks of the Lake Mead area of Nevada and Arizona: Production of intermediate igneous rocks in an extensional environment: *in* Anderson, J.L., ed., The nature of Cordilleran magmatism: Boulder, Colorado, Geological Society of America Memoir 174, p. 169-193.
- Smith, R.L., 1979, Ash-flow magmatism: *in* Chapin, C.E., and Elston, W.E., eds., Ash-flow tuffs, Geological Society of America Special Paper 180, p. 5-28.
- Spencer, J.E., 1982, Origin of folds of Tertiary low-angle fault surfaces, southeastern California and western Arizona: *in* Frost, E.G., and Martin, D.L., eds., Mesozoic-Cenozoic tectonic evolution of the Colorado River region, California, Arizona and Nevada, p. 123-134.
- , 1985, Miocene low-angle normal faulting and dike emplacement, Homer Mountains, surrounding areas, southeastern California and southernmost Nevada: Geological Society of America Bulletin, v. 96, p. 1140-1155.
- Spencer, J.E. and Reynolds, S.J., 1989, Middle Tertiary tectonics of Arizona and adjacent areas: *in* Jenney, J.P. and Reynolds, S.J., eds., Geologic evolution of Arizona: Tucson, Arizona Geological Society Digest 17, p. 539-574.
- Theodore, T.G., Blair, W.G., Nash, J.T., McKee, E.H., Antweiler, J.C., and Campbell, W.L., 1987, Geology and gold mineralization of the Gold Basin-Lost Basin mining districts, Mohave County, Arizona: U. S. Geological Survey Professional Paper 1361, 167 p.
- Weber, M., and Smith, E.I., 1987, Structural and geochemical constraints on the reassembly of disrupted mid-Miocene volcanoes in the Lake Mead-Eldorado Valley area of southern Nevada: *Geology*, v. 15, p. 553-556.
- Wernicke, B.P., 1985, Uniform sense normal simple shear of the continental lithosphere: *Canadian Journal of Earth Science*, v. 22, p. 108-125.

- Wilson, M., 1989, *Igneous Petrology*: London, Unwin Hyman, 465 p.
- Yarnold, J.C., and Lombard, J.P., 1989, A facies model for large rock-avalanche deposits formed in dry climates: in Colburn, I.P., Abott, P.L., and Minch, J., eds., *Conglomerates in Basin Analysis: A symposium dedicated to A.O. Woodford*: Pacific Section S.E.P.M., v. 62, p. 9-31.
- Yoder, H.S., 1976, *Generation of Basalt Magma*: National Academy of Sciences, Washington, D.C., 265 p.
- Young, R.A., and Brennan, W.J., 1974, Peach Springs Tuff: Its bearing on structural evolution of the Colorado Plateau and development of the Cenozoic drainage in Mohave County, Arizona: *Geological Society of America Bulletin*, v. 85, p. 83-90.

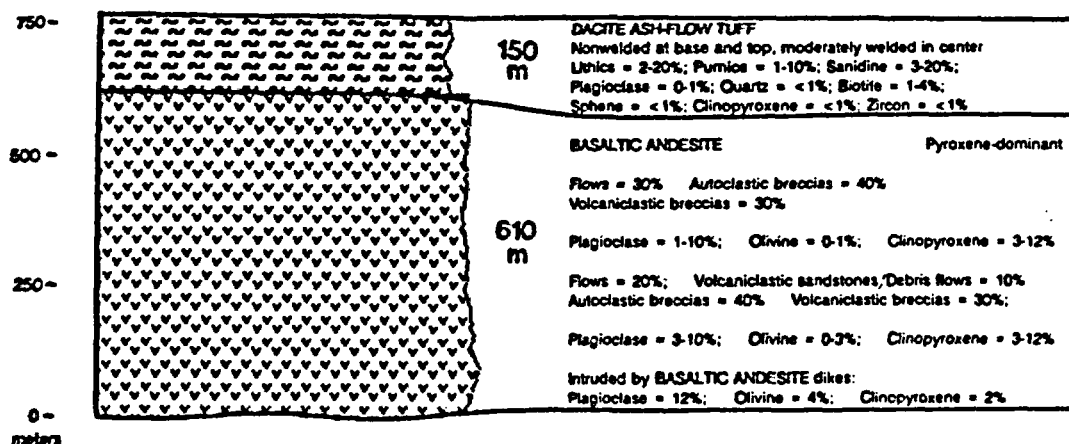
Explanation of symbols for Appendix A



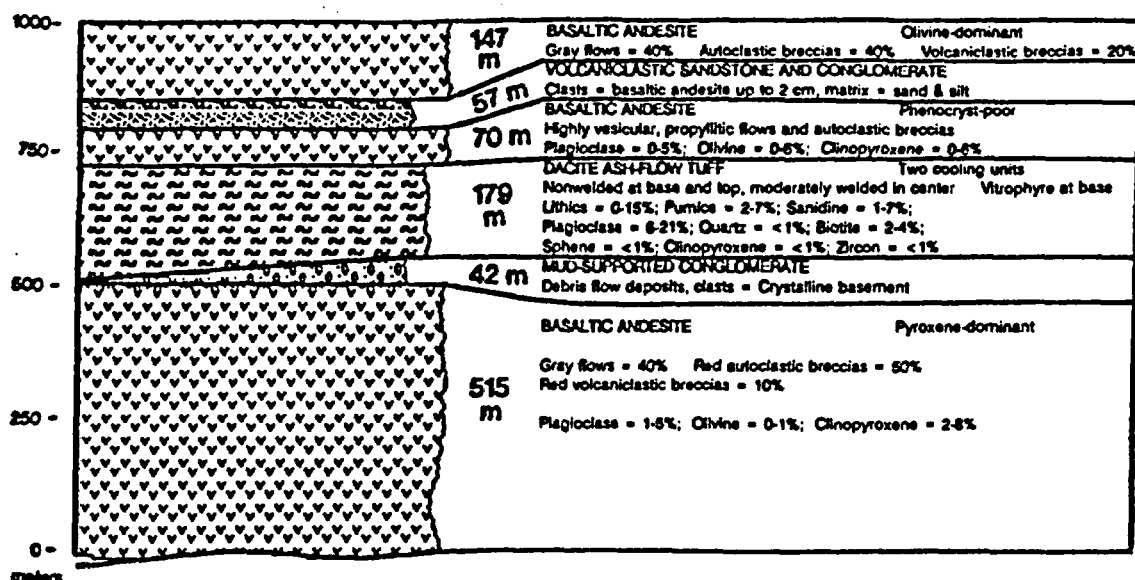
Chuckwalla Ridge 1328 m



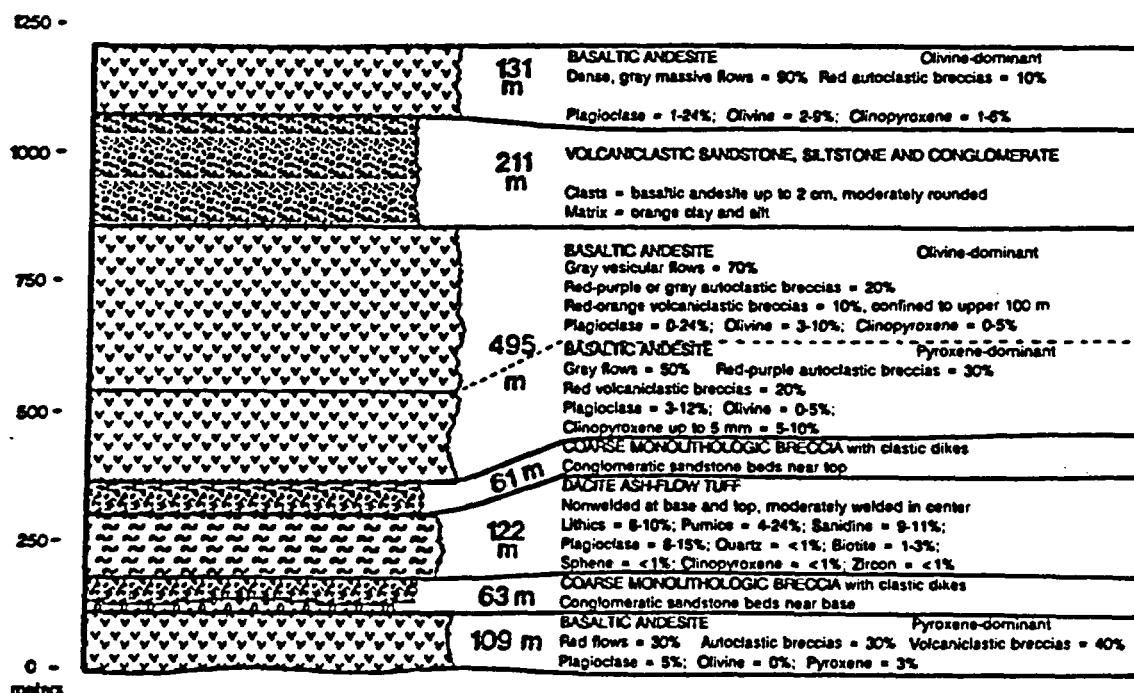
Smith Hill 760 m



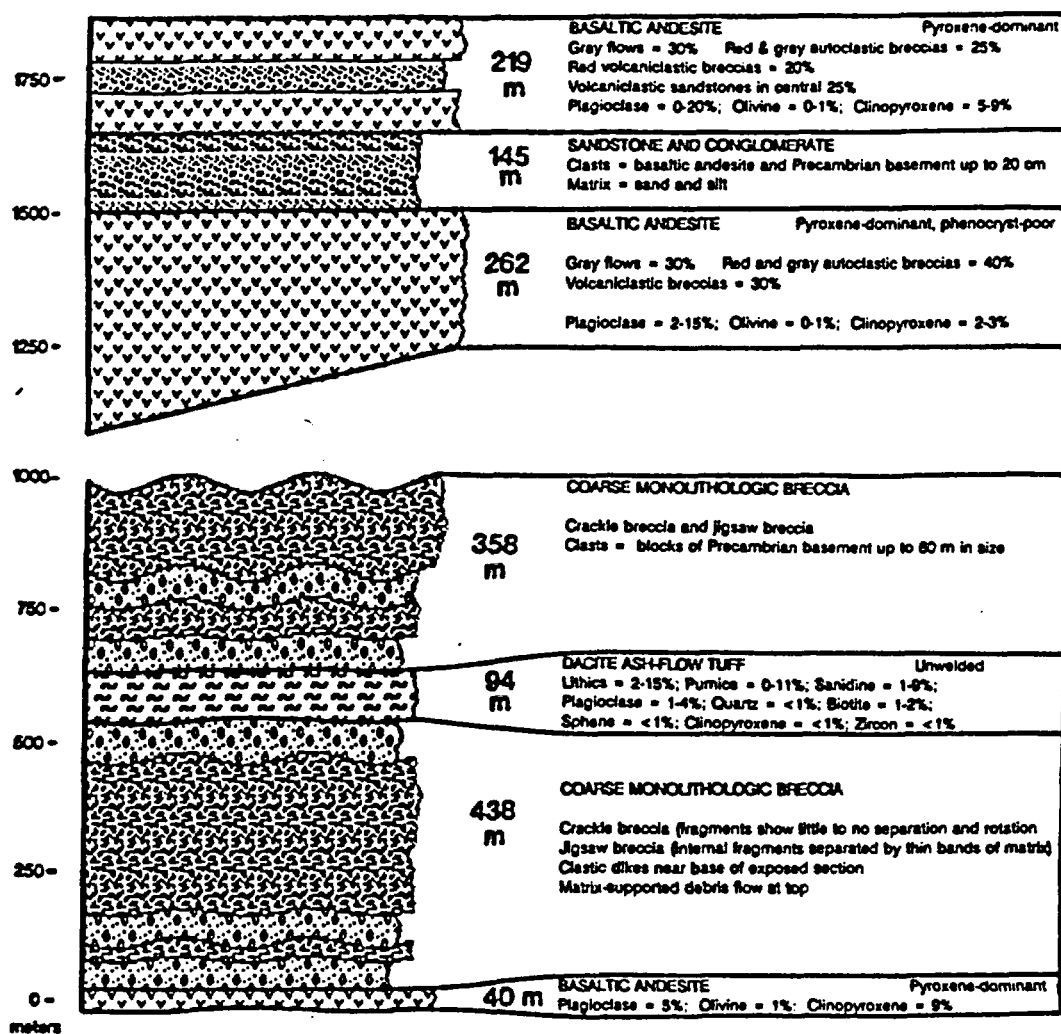
Peninsula 1010 m



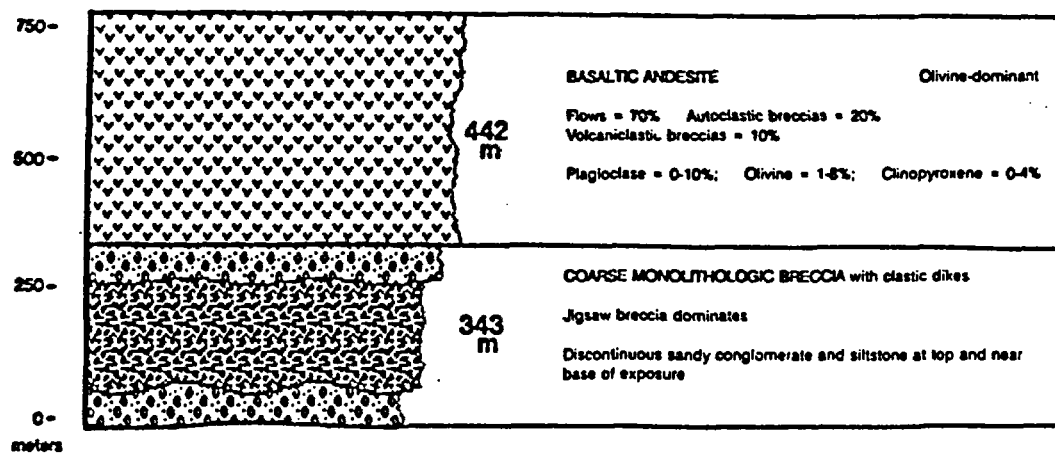
Squaw Peak 1192 m



Salt Spring Wash 1556 m



Pink/Black Ridge 785 m



APPENDIX B: PETROGRAPHIC DESCRIPTIONS
ASH-FLOW TUFFS
 1000 points/slide

- 137** Peninsula, vitrophyre at base of Tt
 20.6% Plagioclase; pitted, sieved with subhedral overgrowths, up to 3 mm
 1.8% Biotite; subhedral, hematitic alteration on margins and fractures, up to 1 mm
 0.2% Sphene; subhedral to anhedral, <0.5 mm
 7.8% Clinopyroxene; broken, subhedral, <0.5 mm
 0.3% Olivine; subhedral, embayed, altered to iddingsite on rims, <0.5 mm
 2.2% Magnetite

Groundmass: slightly devitrified, dense and glassy.

- 144** Peninsula, 20 m from base of Tt
 0.1% Lithic fragments; dacite, up to 2 mm
 2.0% Pumice fragments; unflattened, up to 4 mm
 6.8% Sanidine; subhedral, zoned, up to 2 mm
 6.1% Plagioclase; broken subhedral laths, up to 1 mm
 0.8% Biotite; subhedral, <0.5 mm
 trace Sphene; broken, euhedral, <0.5 mm
 1.1% Clinopyroxene; broken, euhedral, <0.5 mm
 0.4% Magnetite

Groundmass: unwelded, slightly devitrified, slightly calcified

- 136** Peninsula, center of Tt
 15.3% Lithic fragments; dacite, basalt, sparse crystalline basement, up to 5 mm
 6.2% Pumice fragments; slightly flattened, up to 3 mm
 0.8% Sanidine; broken, subhedral, <0.5 mm
 1.2% Plagioclase; broken, subhedral, pitted <0.5 mm
 2.8% Biotite; subhedral, up to 1 mm
 trace Sphene; subhedral
 0.7% Clinopyroxene; broken, euhedral, <1 mm
 0.3% Zircon
 1.5% Magnetite

Groundmass: slightly welded, moderately devitrified, moderately calcified.

- 142** Peninsula, 15 m from top of Tt
 3.6% Lithic fragments; basalt, dacite, up to 4 mm
 6.8% Pumice fragments; unflattened, up to 2 mm
 4.0% Sanidine; subhedral to anhedral, blocky, up to 1 mm
 9.3% Plagioclase; broken, subhedral, partially altered to calcite
 0.4% Quartz; anhedral, <0.5 mm
 2.0% Biotite; subhedral, hematitic alteration on margins and fractures; <1 mm
 0.1% Sphene; subhedral
 0.7% Clinopyroxene; broken, euhedral to subhedral, <0.5 mm
 1.1% Magnetite

Groundmass: slightly welded, moderately devitrified

- 54** 1.5 km west of Salt Spring Wash
 5.7% Lithic fragments; dacite, crystalline basement, up to 3 mm
 10.2% Pumice fragments; flattened, up to 2 mm

6.2% Sanidine; subhedral, embayed, up to 2 mm
 4.2% Plagioclase; broken, subhedral, partially altered to calcite, < 1 mm
 2.0% Biotite; hematitic alteration on margins and fractures, <1 mm
 0.5% Sphene; euhedral
 0.2% Clinopyroxene; anhedral, embayed, <1 mm
 0.1% Zircon
 0.7% Magnetite

Groundmass: slightly welded, moderately devitrified, moderately calcified

69

west side of Salt Spring Wash, base of Tt

14.5% Lithic fragments; dacite and basalt, up to 5 mm
 1.4% Pumice fragments; unflattened, up to 2 mm
 3.9% Sanidine; subhedral to anhedral, embayed, <1 mm
 2.7% Plagioclase; broken, euhedral to subhedral, largely altered to calcite
 0.4% Quartz; embayed, <0.5 mm
 0.7% Biotite; <1 mm
 trace Sphene
 trace Zircon
 0.3% Magnetite

Groundmass: moderately welded, largely devitrified, slightly calcified

73

west side of Salt Spring Wash, center of Tt

4.7% Lithic fragments; crystalline basement, dacite, up to 3 mm
 2.8% Pumice fragments; blocky, nonflattened, up to 2 mm
 8.7% Sanidine; broken, subhedral, embayed, up to 3 mm
 1.4% Plagioclase; subhedral laths, replaced by calcite, up to 1 mm
 0.2% Biotite; hematitic alteration on margins and fractures, <0.5 mm
 0.2% Magnetite

Groundmass: nonwelded, largely devitrified, moderately calcified

70

west side of Salt Spring Wash, top of Tt

10.4% Lithic fragments; crystalline basement, basalt, up to 3 mm
 6.3% Pumice fragments; slightly flattened, up to 2 mm
 0.4% Sanidine; broken, subhedral, <0.5 mm
 0.9% Plagioclase; replaced by calcite, <1 mm
 1.3% Biotite; hematitic alteration on margins and fractures, up to 0.5 mm
 0.3% Sphene
 0.3% Clinopyroxene
 0.1% Zircon
 0.2% Magnetite

Groundmass: slightly welded, largely devitrified, slightly calcified

83

Dug's Island, center of Tt

2.4% Lithic fragments; basalt, dacite, up to 2 mm
 6.2% Sanidine; subhedral, rounded, fractured, up to 2 mm
 3.4% Plagioclase; subhedral laths, replaced by calcite, <1 mm
 1.0% Quartz; anhedral, embayed, <1 mm
 1.2% Biotite; hematitic alteration on margins and fractures, <1 mm
 0.8% Magnetite

Groundmass: nonwelded, moderately devitrified, severely calcified

81

Dug's Island, top of Tt

7.0% Lithic fragments; crystalline basement and dacite; up to 3 mm
 11.3% Pumice fragments; slightly flattened, up to 2 mm
 1.2% Sanidine; broken, subhedral, blocky, up to 1 mm
 1.5% Plagioclase; largely replaced by calcite, < 1 mm
 0.7% Biotite; hematitic alteration on margins and fractures, <0.5 mm
 0.1% Sphene
 trace Clinopyroxene
 0.2% Zircon
 0.8% Magnetite

Groundmass: slightly welded, moderately devitrified, severely calcified

101

Smith Hill, base of unit

10.9% Lithic fragments; basalt and crystalline basement, up to 6 mm
 1.5% Pumice fragments; slightly flattened, up to 4 mm
 8.5% Sanidine; broken, subhedral, blocky, embayed, up to 2 mm
 4.4% Plagioclase; broken, subhedral laths, altered to sericite, up to 1 mm
 0.2% Quartz; anhedral, embayed, < 1 mm
 0.6% Biotite; hematitic alteration on margins and fractures, <1 mm
 0.1% Clinopyroxene
 trace Zircon
 0.4% Magnetite

Groundmass: slightly welded, largely devitrified, slightly calcified

84

Smith Hill, 30 m from base of Tt

1.8% Lithic fragments; basalt, up to 5 mm
 2.4% Pumice fragments; moderately flattened, up to 3 mm
 20.3% Sanidine; broken, subhedral, slight alteration to sericite, up to 3 mm
 10.6% Plagioclase; broken, subhedral, largely altered to sericite, up to 5 mm
 2.5% Biotite; hematitic alteration on margins and fractures, up to 2 mm
 0.6% Magnetite

Groundmass: moderately welded, moderately devitrified

150

Smith Hill, 50 m from base of Tt

4% Lithic fragments; dacite and basalt, up to 2 mm
 9.8% Pumice fragments; slightly flattened, up to 4 mm
 2.6% Sanidine; broken, subhedral, <1 mm
 8.6% Plagioclase; subhedral, largely altered to calcite, up to 1 mm
 3.0% Biotite; hematitic alteration on margins and fractures, <1 mm
 trace Sphene
 0.6% Clinopyroxene
 0.8% Zircon
 1.4% Magnetite

Groundmass: moderately welded, slightly devitrified

96

Smith Hill, 5 m from top of Tt

13% Lithic fragments; basalt, up to 1 cm
 0.8% Pumice fragments; slightly flattened, up to 2 mm
 12.1% Sanidine; broken, subhedral, embayed, blocky, up to 3 mm
 7.4% Plagioclase; altered to calcite and sericite, up to 2 mm
 3.9% Biotite; hematitic alteration on margins and fractures, <1 mm

trace Sphene
 trace Zircon
 0.7% Magnetite

Groundmass: slightly welded, slightly devitrified, moderately calcified

98

Smith Hill, top of Tt

12.3% Lithic fragments; basalt, up to 1 cm
 5.0% Pumice fragments; slightly flattened, up to 2 mm
 8.9% Sanidine; broken, subhedral to anhedral, embayed, up to 4 mm
 9.5% Plagioclase; subhedral, partially altered to sericite, up to 2 mm
 0.1% Quartz; anhedral, <0.5 mm
 3.6% Biotite; broken, subhedral, hematitic alteration on margins and fractures, <0.5 mm
 trace Sphene
 2.3% Magnetite

Groundmass: slightly welded, moderately devitrified

1

Squaw Peak, near base of Tt

6.2% Lithic fragments; basalt and crystalline basement, up to 3 mm
 0.8% Pumice fragments; slightly flattened, up to 2 mm
 9.2% Sanidine; broken, subhedral, up to 2 mm
 9.3% Plagioclase; broken, subhedral, apatite inclusions, up to 1 mm
 2.6% Biotite; slight hematitic alteration on margins and fractures, up to 1 mm
 trace Sphene
 0.9% Clinopyroxene
 trace Zircon
 0.6% Magnetite

Groundmass: slightly welded, slightly devitrified

111

northwest of Squaw Peak, middle of Tt

10.2% Lithic fragments; basalt, up to 7 mm
 12.4% Pumice fragments; slightly flattened, up to 4 mm
 9.8% Sanidine; broken, subhedral, up to 2 mm
 14.6% Plagioclase; broken, subhedral, replaced by calcite up to 3 mm
 1.4% Biotite; hematitic alteration on margins and fractures, up to 1 mm
 1.8% Clinopyroxene
 trace Zircon
 0.2% Magnetite

Groundmass: slightly welded, slightly devitrified, largely calcified

106

northwest of Squaw Peak, 10 m from top of Tt

6.2% Lithic fragments; basalt, up to 2 mm
 4.3% Pumice fragments; slightly flattened, up to 2 mm
 10.8% Sanidine; anhedral to subhedral, blocky, up to 2 mm
 8.4% Plagioclase; euhedral to subhedral, up to 2 mm
 1.9% Biotite; hematitic alteration on margins and fractures, <1 mm
 trace Sphene
 0.6% Clinopyroxene
 trace Zircon
 0.2% Magnetite

Groundmass: slightly welded, slightly devitrified

102 reworked ash from west of Chuckwalla Ridge

1.6% Lithic fragments; basalt, up to 2 mm

4.3% Sanidine; anhedral, <0.5 mm

1.1% Plagioclase; subhedral to anhedral, < 0.5 mm

0.8% Biotite; broken needles, <0.5 mm

0.3% Clinopyroxene

Matrix: largely devitrified ash

APPENDIX C: PETROGRAPHIC DESCRIPTION
MAFIC VOLCANIC ROCKS
 500 points/slide

139 PENINSULA Ttbl

26% Plagioclase; sieved, fritted, zoned, non-pitted overgrowths; subhedral laths seriate to 1 mm; also in glomerocrysts with clinopyroxene up to 2 mm
 11% Clinopyroxene; pitted, embayed, non-pitted overgrowths; subhedral to euhedral equant less than 0.5 mm; in glomerocrysts with plagioclase up to 2 mm
 2% Olivine; in glomerocrysts with clinopyroxene and plagioclase
Groundmass: 49% Cryptocrystalline material with seriate fine to coarse grained laths of Plagioclase (7%) and subhedral Clinopyroxene (5%)

138 PENINSULA Ttbl

18% Plagioclase; pitted, embayed; rounded subhedral laths up to 1.5 mm; also in glomerocrysts with clinopyroxene and magnetite
 5% Unaltered Clinopyroxene; embayed, pitted, subhedral
 3% Altered Clinopyroxene; subhedral to anhedral
 0.2% Phlogopite; highly altered needles
 1% Magnetite; euhedral
 2% Vesicles
Groundmass: 66% Cryptocrystalline material with fine-grained felty laths of Plagioclase (3%) and both altered and unaltered varieties of Clinopyroxene (2%)

90 SMITH HILL Ttbl

13% Plagioclase; pitted, embayed; subhedral up to 2 mm; in glomerocrysts with clinopyroxene up to 3 mm
 14% Clinopyroxene; pitted, embayed; subhedral up to 1 mm; in glomerocrysts with plagioclase up to 3 mm
 7% Vesicles; filled with calcite
Groundmass: Seriate fine to coarse-grained subtrachytic laths of Plagioclase (31%); with intergranular Clinopyroxene (7%), Hematite (4%) and Cryptocrystalline material (23%).

85 SMITH HILL Ttbm

16% Olivine; subhedral, less than 0.5 mm, altered to iddingsite on rims and along fractures.
 3% Clinopyroxene; subhedral, less than 0.5 mm
 1% Magnetite
 1% Vesicles
Groundmass: Fine-grained trachytic laths of Plagioclase (47%); with intergranular Olivine (6%) altered to iddingsite, Clinopyroxene (17%) and Hematite (9%).

51 SMITH HILL Ttbm

22% Plagioclase; pitted, fritted; subhedral laths seriate to 2mm
 2% Olivine; embayed; subhedral, less than 1 mm, altered to iddingsite
 7% Clinopyroxene; subhedral, up to 2 mm; hematite inclusions.
 5% Vesicles
Groundmass: 48% Cryptocrystalline material with fine-grained felty laths of Plagioclase (8%), Olivine (6%) altered to iddingsite, Clinopyroxene (2%) and Hematite (1%).

50 SMITH HILL Ttbm

19% Plagioclase; pitted, fritted; subhedral laths up to 1 X 3 mm; in glomerocrysts with clinopyroxene

up to 3 mm

1% Olivine; altered to iddingsite, up to 0.5 mm

11% Clinopyroxene; pitted; up to 1 mm; in glomerocrysts with plagioclase up to 3 mm

6% Magnetite

3% Vesicles; filled with calcite

Groundmass: Seriate fine to coarse grained felty laths of Plagioclase (33%); with intergranular Olivine (9%) altered to iddingsite, Clinopyroxene (5%), Hematite (4%) and Cryptocrystalline material (8%).

148 GATEWAY COVE Ttbn

16% Plagioclase; pitted, sieved; subhedral laths up to 5mm

6% Olivine; anhedral, embayed, altered to iddingsite

6% Clinopyroxene; subhedral, embayed, pitted

Groundmass: Seriate fine to coarse-grained felty laths of Plagioclase (29%); with intergranular Olivine (5%) altered to iddingsite, Clinopyroxene (4%), Hematite (1%) and Cryptocrystalline material (33%).

65 GATEWAY COVE Ttbn

15% Plagioclase; pitted, embayed; subhedral laths up to 2X4 mm; glomerocrysts with pyroxenes up to 2 mm

1% Olivine; anhedral, iddingsitized, up to 0.5 mm

3% Unaltered Clinopyroxene; embayed, subhedral to anhedral, up to 1 mm

1% Altered Clinopyroxene; anhedral, less than 1 mm

1% Magnetite

Groundmass: Coarse-grained blocky microcrystals of Plagioclase (59%); with intergranular Olivine (1%) altered to iddingsite, Clinopyroxene (17%) and Hematite (3%).

131 CHUCKWALLA RIDGE Ttbn

17% Plagioclase; pitted, sieved, fritted; subhedral laths up to 3 mm

2% Olivine; anhedral, altered to iddingsite along margins and fractures; up to 1 mm

7% Clinopyroxene; embayed, anhedral; up to 1 mm

4% Xenoliths; microcrystalline olivine + plagioclase with glassy groundmass

Groundmass: 48% Cryptocrystalline material with fine-grained felty laths of Plagioclase (13%), subhedral Olivine (5%) altered to iddingsite, and Clinopyroxene (3%).

132 CHUCKWALLA RIDGE Ttbn

7% Plagioclase; pitted, embayed, anhedral; up to 1 mm

1% Olivine; anhedral, altered to iddingsite

8% Clinopyroxene; pitted, embayed, with non-pitted overgrowths; subhedral to anhedral

Groundmass: 51% Cryptocrystalline material with fine-grained trachytic laths of Plagioclase (13%), subhedral Olivine (3%) altered to iddingsite, Clinopyroxene (4%) and Hematite (12%).

134 CHUCKWALLA RIDGE Ttbn

26% Plagioclase; pitted, fritted, with non-pitted overgrowths; subhedral laths up to 3 mm

3% Olivine; altered to iddingsite on margins and fractures

6% Clinopyroxene; embayed, subhedral, up to 2 mm

10% Vesicles; filled with calcite

Groundmass: Fine-grained felty laths of Plagioclase (17%); with intergranular Olivine (3%) altered to iddingsite, Clinopyroxene (4%), Hematite (10%), and Cryptocrystalline material (22%).

135 CHUCKWALLA RIDGE Ttbn

13% Plagioclase; sieved with non-pitted overgrowths; euhedral; up to 1.5 mm
 1% Olivine; subhedral to euhedral, altered to iddingsite along margins and fractures; up to 1 mm
 7% Clinopyroxene; subhedral to euhedral, single crystals and in glomerocrysts
 17% Vesicles; partially infilled with chalcedony
Groundmass: 54% Cryptocrystalline material with fine-grained felty laths of Plagioclase (1%),
 Olivine (1%) altered to iddingsite, Clinopyroxene (3%) and Hematite (2%).

149 **CHUCKWALLA RIDGE** Dike = Ttbn or Ttbu
 11% Plagioclase; embayed, pitted with euhedral to subhedral overgrowths; seriate up to 2 mm;
 inclusions of clinopyroxene
 4% Unaltered Clinopyroxene; embayed, subhedral, up to 1 mm
 3% Altered Clinopyroxene; subhedral to anhedral, < 1 mm
 1% Magnetite
 14% Vesicles; partially infilled with calcite and epidote
Groundmass: 41% Cryptocrystalline material with seriate medium-grained felty laths of Plagioclase
 (19%), and Clinopyroxene (8%).

49 **SMITH HILL** Ttbn
 10% Plagioclase; fritted, subhedral laths up to 1.5 mm
 10% Clinopyroxene; embayed up to 1 mm, euhedral up to 0.5 mm
 9% Vesicles; filled with calcite
Groundmass: Seriate medium to coarse grained felty laths of Plagioclase (24%); with intergranular
 Clinopyroxene (11%) and Cryptocrystalline material (37%).

125 **SMITH HILL** Ttbn
 34% Plagioclase; pitted, euhedral laths and clusters of subhedral crystals, up to 1 mm
 5% Clinopyroxene; euhedral to subhedral, in glomerocrysts with plagioclase up to 1.5 mm
 2% Magnetite
 1% Vesicles
Groundmass: Partially devitrified brown Glass (51%) with medium-grained felty laths of Plagioclase
 (4%) and Clinopyroxene (3%).

140 **PENINSULA** Ttbn
 22% Plagioclase; slightly pitted, fritted, with non-pitted overgrowths; subhedral laths up to 1 mm;
 glomerocrysts with clinopyroxene and magnetite up to 3 mm
 3% Unaltered Clinopyroxene; embayed, euhedral to subhedral, up to 1 mm; and in large
 glomerocrysts with plagioclase
 3% Altered Clinopyroxene; anhedral, embayed, less than 1 mm; and in large glomerocrysts with
 plagioclase
Groundmass: 48% Cryocrystals; with seriate fine to coarse-grained subtrachytic laths of Plagioclase
 (15%), both types of Clinopyroxene (6%) and Hematite (3%).

133 **CHUCKWALLA RIDGE** Ttbn
 19% Plagioclase; sieved, fitted and embayed, with non-pitted overgrowths; up to 1 mm
 9% Clinopyroxene; pitted, embayed; single crystals and in glomerocrysts
 14% Vesicles; filled with calcite
Groundmass: Fine to medium-grained felty laths of Plagioclase (14%); with intergranular
 Clinopyroxene (10%), Hematite (1%), and Cryptocrystalline material (31%).

130 **CHUCKWALLA RIDGE** Ttbn
 16% Plagioclase; fritted, sieved, embayed; subhedral laths; up to 2 mm

7% Unaltered Clinopyroxene; subhedral, embayed

3% Altered Clinopyroxene; subhedral to anhedral

6% Vesicles; many filled with calcite

Groundmass: fine-grained felty laths of Plagioclase (16%); with intergranular Clinopyroxene (6%) and Cryptocrystalline material (45%).

86 SMITH HILL Ttbn

4% Hornblende; euhedral to subhedral; altered to hematite on rims; up to 0.5 X 2 mm

12% Plagioclase; sieved, pitted, non-pitted overgrowths; subhedral, up to 1.5 mm

3% Magnetite

Groundmass: Fine-grained trachytic laths of Plagioclase (33%); with intergranular Hematite (9%) and Cryptocrystalline material (39%).

143 PENINSULA Ttbn

48% Vesicles

Groundmass: Seriate fine to coarse-grained subtrachytic laths of Plagioclase (13%); with intergranular Hematite (15%) and Cryptocrystalline material (14%).

141 PENINSULA Ttbn

2% Plagioclase; subhedral in glomerocrysts with olivine.

5% Olivine; subhedral to euhedral; altered to iddingsite; single crystals and in glomerocrysts with plagioclase

3% Vesicles; filled with calcite

Groundmass: Fine-grained felty laths of Plagioclase (25%); with intergranular Hematite (1%) and Cryptocrystalline material (64%).

77 SALT SPRING WASH Ttbu

27% Plagioclase; pitted; subhedral up to 2mm

0.6% Olivine; altered to iddingsite, less than 0.5 mm

4% Unaltered Clinopyroxene; subhedral, up to 1 mm

5% Altered Clinopyroxene; anhedral, less than 1 mm

Groundmass: Seriate fine to coarse-grained felty laths of Plagioclase (46%), with intergranular Olivine (6%) altered to iddingsite, Clinopyroxene (5%), Hematite (3%) and Cryptocrystalline material (1%).

88 SMITH HILL Ttbu

21% Plagioclase; pitted, up to 1 X 2 mm

4% Olivine; subhedral, less than 0.5 mm; altered to iddingsite

6% Clinopyroxene; euhedral, embayed, pitted; up to 1 mm

1% Magnetite

11% Vesicles; filled with chalcedony

Groundmass: Fine-grained felty laths of Plagioclase (22%) with intergranular Olivine (3%) altered to iddingsite, Clinopyroxene (4%), and Cryptocrystalline material (28%).

100 SMITH HILL Ttbu

4% Plagioclase; pitted, zoned, subhedral laths, up to 2 mm

1% Olivine; subhedral, equant, altered to iddingsite

1% Clinopyroxene; embayed, in glomerocrysts with plagioclase and olivine

1% Magnetite

8% Vesicles; filled with calcite

Groundmass: Fine-grained subtrachytic laths of Plagioclase (14%) with intergranular Olivine (1%)

altered to iddingsite, Cryptocrystalline material (49%) and Glass (22%).

103 DIKE WEST OF CHUCKWALLA RIDGE Tpb

- 1% Plagioclase; euhedral laths less than 0.5 mm
- 1% Olivine; subhedral, slightly altered to iddingsite on margins; up to 0.5 mm
- 3% Clinopyroxene; embayed, pitted, up to 1 mm
- 3% Magnetite
- 7% Vesicles

Groundmass: Coarse-grained felty laths of Plagioclase (49%), with intergranular Olivine (8%) altered to iddingsite, Clinopyroxene (1%), Hematite (10%) and Cryptocrystalline material (17%).

7 PINK/BLACK RIDGE Tpb

- 2% Plagioclase; small laths in glomerocrysts
- 3% Olivine; altered to iddingsite
- 1% Magnetite; large, euhedral
- 3% Vesicles; filled with calcite

Groundmass: Coarse-grained subtrachytic laths of Plagioclase (49%) with intergranular Olivine (8%) altered to iddingsite, Clinopyroxene (9%), Hematite (15%) and brown glass (10%).

10 PINK/BLACK RIDGE Tpb

- 0.6% Plagioclase; small laths in glomerocrysts
- 5% Olivine; euhedral, up to 2 mm, altered to iddingsite on margins
- 3% Vesicles; filled with calcite

Groundmass: Seriate fine to medium-grained trachytic laths of Plagioclase (47%) with intergranular Olivine (20%) altered to iddingsite, Clinopyroxene (16%), Hematite (7%) and Cryptocrystalline material (2%).

120 PINK/BLACK RIDGE Tpb

- 1% Plagioclase; sieved up to 0.5 mm, in glomerocrysts with olivine up to 1.5 mm
- 2% Olivine; altered to iddingsite; small single crystals or in glomerocrysts with plagioclase

Groundmass: Medium-grained trachytic laths of Plagioclase (61%) with intergranular Olivine (7%) altered to iddingsite, Clinopyroxene (23%), Hematite (5%) and Phlogopite (1%).

15 PINK/BLACK RIDGE Tpb

- 0.4% Plagioclase; in glomerocrysts with olivine
- 0.4% Olivine; subhedral crystal up to 0.5 mm and in glomerocrysts with plagioclase; altered to iddingsite on margins
- 11% Vesicles; some filled with calcite

Groundmass: Medium-grained trachytic laths of Plagioclase (49%), with intergranular Olivine (23%) altered to iddingsite, Clinopyroxene (7%), Hematite (5%) and Cryptocrystalline material (7%).

124 PINK/BLACK RIDGE Tpb

- 3% Plagioclase; sieved, anhedral = one large (4mm) phenocryst in slide
- 1% Olivine; euhedral, altered to iddingsite on margins
- 25% Vesicles; filled with calcite

Groundmass: Fine-grained trachytic laths of Plagioclase (40%) with intergranular Olivine (7%) altered to iddingsite, Clinopyroxene (14%), Hematite (1%) and Cryptocrystalline material (8%).

117 PINK/BLACK RIDGE Tpb

- 6% Olivine; subhedral, altered to iddingsite, up to 1 mm

10% Vesicles

Groundmass: Coarse-grained trachytic laths of Plagioclase (35%) with intergranular Olivine (10%) altered to iddingsite, Clinopyroxene (16%), Hematite (12%), Cryptocrystalline material (11%) and Glass (1%).

118 PINK/BLACK RIDGE Tpb

5% Olivine; subhedral to anhedral, up to 1.5 mm

1% Vesicles

Groundmass: Fine-grained trachytic laths of Plagioclase (61%) with intergranular Olivine (8%) altered to iddingsite, Clinopyroxene (21%) and Hematite (4%).

121 PINK/BLACK RIDGE Tpb

1% Olivine; euhedral, altered to iddingsite on margins

11% Vesicles; filled with calcite

Groundmass: Fine-grained trachytic laths of Plagioclase (43%) with intergranular Olivine (12%) altered to iddingsite, Clinopyroxene (17%), Hematite (9%) and Cryptocrystalline material (7%).

123 PINK/BLACK RIDGE Tpb

1% Olivine; euhedral, altered to iddingsite on margins

11% Vesicles; filled with calcite

Groundmass: Fine-grained trachytic laths of Plagioclase (37%) with intergranular Olivine (13%) altered to iddingsite, Clinopyroxene (10%), Hematite (3%) and Cryptocrystalline material (24%).

55 NORTH OF PINK/BLACK RIDGE Tpb

3% Plagioclase; subhedral, not pitted, up to 4 mm

21% Vesicles; filled with calcite

Groundmass: Seriate medium to coarse-grained felty laths of Plagioclase (32%) with intergranular Clinopyroxene (9%), Hematite (2%) and Cryptocrystalline material (32%).

55B NORTH OF PINK/BLACK RIDGE Tpb

4% Olivine; subhedral, embayed, up to 1 mm, altered to iddingsite

11% Vesicles; most filled with calcite

Groundmass: Coarse-grained felty laths of Plagioclase (52%) with intergranular Olivine (15%) altered to iddingsite, Clinopyroxene (12%), Hematite (3%) and Cryptocrystalline material (3%).

114 SENATOR MOUNTAIN Tpb(?)

13% Plagioclase; embayed and seived with nonpitted subhedral overgrowths; up to 4 mm

2% Olivine; altered to iddingsite on margins; embayed; up to 1 mm

2% Clinopyroxene; subhedral, embayed; up to 1 mm

1% Magnetite

6% Vesicles; partially filled with chalcedony

Groundmass: 60% Cryptocrystalline material with fine-grained felty laths of Plagioclase (8%), Olivine (5%) altered to iddingsite, and Clinopyroxene (2%).

3 SQUAW PEAK Tspm

24% Plagioclase; fritted with nonpitted overgrowths; up to 5 mm

4% Olivine; altered to iddingsite on margins; up to 1 mm

9% Clinopyroxene; pitted, embayed; up to 3 mm

1% Magnetite

1% Vesicles

Groundmass: Seriate fine to medium-grained trachytic laths of Plagioclase (43%) with intergranular

Olivine (10%) altered to iddingsite, Clinopyroxene (8%) and Hematite (1%).

21 SQUAW PEAK

Tspm

6% Olivine; euhedral, altered to iddingsite, less than 0.5 mm

1% Magnetite; euhedral

12% Vesicles; filled with calcite

Groundmass: Medium-grained trachytic laths of Plagioclase (39%) with intergranular Olivine (12%) altered to iddingsite, Clinopyroxene (5%), Hematite (13%) and Cryptocrystalline material (12%).

108 SOUTH OF SQUAW PEAK

Tspm

12% Olivine; Euhedral to subhedral, altered to iddingsite and hematite

Groundmass: Fine-grained trachytic laths of Plagioclase (44%) with intergranular Olivine (15%) altered to iddingsite, Hematite (13%) and Cryptocrystalline material (16%).

126 SQUAW PEAK

Tspm

5% Plagioclase; laths less than 0.5 mm in glomerocrysts

2% Olivine; embayed, subhedral; up to 1 mm; altered to iddingsite on margins

11% Vesicles; filled with calcite

Groundmass: Medium-grained subtrachytic laths of Plagioclase (45%) with intergranular Olivine (16%) altered to iddingsite, Clinopyroxene (2%), Hematite (11%) and Cryptocrystalline material (8%).

127 SQUAW PEAK

Tspm

2% Plagioclase; laths less than 0.5 mm in glomerocrysts

5% Olivine; embayed, subhedral; up to 1 mm; altered to iddingsite on margins

3% Vesicles; filled with calcite

Groundmass: Medium-grained subtrachytic laths of Plagioclase (50%) with intergranular Olivine (12%) altered to iddingsite, Clinopyroxene (10%), Hematite (5%) and Cryptocrystalline material (13%).

128 SQUAW PEAK

Tspm

13% Plagioclase; fritted, embayed; subhedral laths up to 2 mm

9% Olivine; altered to iddingsite and hematite

7% Clinopyroxene; subhedral, up to 2 mm

10% Vesicles; some filled with chalcedony

Groundmass: Fine-grained felty laths of Plagioclase (31%) with intergranular Olivine (3%) altered to iddingsite, Clinopyroxene (8%), Hematite (1%) and Cryptocrystalline material (19%).

112 EAST OF SQUAW PEAK

Tspu

23% Plagioclase; pitted, fritted, embayed, up to 2 X 4 mm; inclusions of clinopyroxene

0.6% Olivine; small crystals in glomerocrysts with clinopyroxene, altered to iddingsite.

8% Clinopyroxene; rounded single crystals up to 2 mm; or in glomerocrysts with plagioclase and olivine up to 2 mm

15% Vesicles;

Groundmass: Fine-grained felty laths of Plagioclase (12%), with intergranular Olivine (6%) altered to iddingsite, Hematite (8%) and Cryptocrystalline material (28%).

113 EAST OF SQUAW PEAK

Tspu

24% Plagioclase; pitted, up to 2 X 3 mm

1% Olivine; included in clinopyroxene, altered to iddingsite

6% Clinopyroxene; pitted, embayed, rounded; subhedral up to 1 mm; also in glomerocrysts up to 2

mm

Groundmass: Fine-grained felty laths of Plagioclase (28%) with intergranular Olivine (2%) altered to iddingsite, Clinopyroxene (8%), Hematite (4%) and Cryptocrystalline material (22%).

20 EAST OF SQUAW PEAK Tspu

1% Plagioclase; euhedral, sector zoning; up to 3 mm

9% Olivine; subhedral, embayed; altered to iddingsite; up to 1mm

2% Clinopyroxene; zoned, sub-euhedral; up to 1 mm

2% Magnetite

Groundmass: Fine-grained trachytic laths of Plagioclase (31%) with intergranular Olivine (9%) altered to iddingsite, Clinopyroxene (3%), Hematite (8%) and Cryptocrystalline material (34%).

APPENDIX D: PETROGRAPHIC DESCRIPTIONS- PRECAMBRIAN BASEMENT

Percentages are estimated

24 Rock type: Felsic gneiss
 Location: Golden Rule Peak, west end
 Probable protolith: Felsic igneous
 Prograde or relict minerals:
 25% Plagioclase, equant, largely replaced by sericite
 20% Quartz, recrystallized ribbons
 5% Microcline, equant, partially replaced sericite
 2% Biotite, largely replaced by chlorite and epidote
 <1% Apatite, equant, small
 Retrograde minerals:
 35% Sericite, replaces feldspars
 8% Chlorite, replaces biotite
 1% Epidote, replaces biotite
 Introduced or remobilized minerals:
 3% Calcite, in late stage fractures
 1% Opaque and hematite
 Texture: Crude foliation defined by recrystallized quartz ribbons and by compositional banding of quartz and feldspar-rich layers alternating with biotite/chlorite-rich layers. Late stage fractures filled with calcite and hematite.

28 Rock type: Quartzofeldspathic vein
 Location: Golden Rule Peak, south side
 Probable protolith: Felsic igneous
 Prograde or relict minerals:
 45% Quartz, elongate approaching ribbon shape, deformation bands, localized zones of recrystallization and thin film between feldspars
 25% Microcline, blocky equant grains, slightly sericitized, contains internal, optically misoriented sectors suggesting crystal plastic deformation
 20% Plagioclase with pericline twins, blocky equant grains, slightly sericitized
 5% Muscovite
 Retrograde minerals:
 5% Sericite, replaces feldspars
 Texture: Weak, discontinuous foliation defined by quartz grains aligned with primary muscovite.
 Other: Veins cut parallel and subparallel to gneissic foliation.

41 Rock type: Felsic gneiss
 Location: Senator Tank
 Probable protolith: felsic igneous
 Prograde or relict minerals:
 40% Quartz, ribbons with deformation bands, recrystallized on margins
 18% Microcline, partially sericitized
 15% Plagioclase, partially sericitized
 3% Biotite, partially replaced by chlorite and epidote
 Retrograde minerals:
 15% Sericite, replaces feldspars
 2% Chlorite, replaces biotite
 <1% Epidote, replaces biotite

Introduced or remobilized minerals:

5% Opaque and hematite, fills late stage fractures

2% Calcite, fills late stage fractures

Texture: Foliation defined by quartz ribbons and zones of grain size reduction in quartz and feldspar. Brittle fractures oriented parallel to and perpendicular to this foliation are filled with hematite, clays and calcite.

Other: Associated in field with chlorite-biotite schists.

44 Rock type: Schistose partially recrystallized protomylonite

Location: Senator Tank

Probable protolith: Felsic igneous, possibly intrusive

Prograde or relict minerals:

25% Quartz, recrystallized ribbons

15% Microcline, up to 5 mm equant slightly sericitized porphyroclasts, and smaller equant highly sericitized grains in matrix

13% Plagioclase, up to 3 mm equant porphyroclasts, small grains in matrix and lath-shaped inclusions in microcline porphyroclasts, altering to sericite

4% Sphene, rounded, anhedral, quartz and opaque inclusions

3% Opaque, euhedral, locally mantled by sphene

2% Biotite, altering to chlorite

1% Apatite

1% Zircon

Retrograde minerals:

30% sericite, replaces feldspars, especially small matrix grains

5% chlorite, replaces biotite

1% epidote, replaces biotite

Texture: Foliation defined by recrystallized quartz ribbons and crude alignment of original biotite.

Other: Associated in field with similar schists bearing large feldspar porphyroclasts up to 1.5 cm.

45 Rock type: Biotite gneiss

Location: Senator Tank

Probable protolith: Felsic igneous

Prograde or relict minerals:

20% Quartz, recrystallized ribbons, granoblastic polygonal grains with undulose extinction

16% Plagioclase, largely replaced by sericite

5% Sphene

2% Biotite, largely replaced chlorite and epidote

<1% Opaque

<1% Zircon

Retrograde minerals:

45% Sericite, replaces plagioclase

5% Chlorite, replaces biotite

5% Epidote, replaces biotite

Texture: Crude foliation defined by recrystallized quartz ribbons.

46 Rock type: Quartzofeldspathic part of coarsely banded gneiss

Location: Senator Tank

Probable protolith: Felsic igneous

Prograde or relict minerals:

37% Microcline, some sericite replacement

33% Quartz, subgrain development and deformation bands

10% Plagioclase, largely replaced by sericite

2% Muscovite

Retrograde minerals:

13% Sericite, replaces feldspars

2% Opaques

Texture: No obvious foliation, feldspar and quartz grain boundaries are corrugated and/or sutured.

Other: Gneiss is coarsely banded with 5-10 cm bands of quartzofeldspathic material and 2-3 cm bands of schistose material.

47 Rock type: Amphibolitic gneiss

Location: Senator Tank

Probable protolith: Mafic igneous

Prograde or relict minerals:

35% Hornblende, subhedral, replaced on margins by epidote

10% Quartz, subequant

Retrograde minerals:

20% Zoisite, replaces plagioclase (now completely gone)

10% Actinolite, replaces hornblende

10% Chlorite, replaces actinolite

10% Epidote, replaces actinolite

5% Sericite, replaces plagioclase

Texture: Foliation defined by parallel alignment of hornblende and compositional banding of hornblende-rich layers alternating with formerly plagioclase-rich layers.

Other: Associated in the field with medium grained quartzofeldspathic gneiss, phyllite and schist

58 Rock type: Cataclasite

Location: Salt Spring, at detachment surface

Probable protolith: Quartzofeldspathic vein (?)

Prograde or relict minerals:

60% Quartz, undulose extinction, granoblastic-polygonal

Retrograde minerals:

35% Sericite, may have replaced an earlier mineral, probably a feldspar

2% Opaque

Introduced or remobilized minerals:

3% Hematite, concentrated along fractures

Texture: Granoblastic-polygonal quartz grains cut by fractures with abundant alteration to sericite and hematite

Other: Grungy yellow hand sample found right at detachment surface

60 Rock type: Amphibolite

Location: Salt Spring, near detachment

Probable protolith: Mafic igneous

Prograde or relict minerals:

22% Hornblende, brown in plane polarized light

5% Clinopyroxene, subequant, largely replaced by chlorite

5% Orthopyroxene, elongate, partially replaced by chlorite

3% Plagioclase, largely replaced by sericite

3% Opaque, euhedral

Retrograde minerals:

33% Sericite, replaces plagioclase

20% Actinolite, needle-like, replaces hornblende

5% Chlorite, replaces pyroxenes

Introduced or remobilized minerals:

3% Sericite along fractures

1% Calcite along fractures

Texture: Foliation defined by parallel alignment of hornblende and by compositional banding of hornblende and clinopyroxene-rich layers alternating with plagioclase-rich layers. Late stage fractures are filled with sericite and calcite.

Other: Associated in the field with amphibolitic gneiss and quartzofeldspathic veins.

63 Rock type: Biotite-garnet gneiss

Location: Salt Spring, at detachment

Probable protolith: Pelite or garnet-bearing igneous (?)

Prograde or relict minerals:

20% Quartz, ribbons, partial recrystallization and subgrain development

20% Garnet, fractured, partially replaced by chlorite, quartz inclusions

15% Plagioclase, altering to sericite

5% Biotite, altering to chlorite

3% Muscovite

2% Opaque

<1% Zircon

Retrograde minerals:

18% Sericite, replaces plagioclase

10% Chlorite, replaces biotite and garnet

3% Zoisite, replaces plagioclase

2% Epidote, replaces biotite

Introduced or remobilized minerals:

2% Calcite, along fractures

Texture: Foliation defined by compositional layering, quartz ribbon alignment and parallel orientation of micas

Other: Associated in the field with quartzofeldspathic veins, parallel and subparallel to foliation

75 Rock type: Amphibolite

Location: Salt Spring, near detachment

Probable protolith: Mafic or ultramafic igneous

Prograde or relict minerals:

55% Hornblende, euhedral, replacement by actinolite and chlorite on grain boundaries

2% Clinopyroxene, mostly replaced by epidote and chlorite

1% Plagioclase, mostly replaced by zoisite

<1% Sphene

Retrograde minerals:

20% Actinolite, replaces hornblende

10% Epidote, replaces clinopyroxene

5% Chlorite, replaces hornblende and clinopyroxene

4% Zoisite, replaces plagioclase

Introduced or remobilized minerals:

3% Calcite, in fractures

Texture: Weak foliation defined by parallel alignment of hornblende. Fractures filled with actinolite and calcite cut across foliation.

Other: Associated in the field with amphibolitic gneiss and quartzofeldspathic veins.

76 Rock type: Amphibolitic gneiss

Location: Salt Spring, near detachment

Probable protolith: Mafic igneous

Prograde or relict minerals:

45% Hornblende, partially replaced by actinolite and epidote

10% Clinopyroxene, largely replaced by epidote

2% Apatite

<1% Sphene

Retrograde minerals:

20% Actinolite, replaces hornblende

10% Epidote, replaces hornblende and clinopyroxene

10% Zoisite, replaced all of former plagioclase

Introduced or remobilized minerals:

3% Calcite, in fractures

Texture: Foliation defined by parallel alignment of hornblende and pyroxene and by compositional banding of hornblende and pyroxene alternating with former plagioclase. Overprinted by late-stage fractures filled with calcite.

Other: Associated in the field with amphibolite and quartzofeldspathic veins.

78 Rock type: Quartzofeldspathic vein

Location: Salt Spring

Probable protolith: Felsic igneous

Prograde or relict minerals:

45% Quartz, elongate grains with length 4 times width, sutured grain boundaries

40% Microcline, slightly elongate grains with length 2 times width, grain boundaries straight parallel to twins, sutured perpendicular to twins

10% Plagioclase, slightly elongate grains with length 2 times width, altering to sericite

Retrograde minerals:

5% Sericite, replaces plagioclase

Texture: Granitoid, weak foliation defined by slightly elongated quartz and feldspars

Other: Granitoid layers associated in the field with amphibolites

79 Rock type: Amphibolite

Location: Salt Spring

Probable protolith: Mafic, possibly ultramafic, igneous

Prograde or relict minerals:

95% Hornblende, large and small grains with granoblastic-polygonal textures

2% Opaque, equant, interstitial between hornblende grains

1% Quartz, equant, included in large hornblende grains

Retrograde minerals:

2% Chlorite, altered from fine-grained hornblende

Introduced or remobilized minerals:

3% Quartz, along fractures

2% Calcite, along fractures

Texture: No obvious foliation, randomly oriented grains. Overprinted by late-stage fractures filled with quartz and calcite.

Other: Associated in field with quartzofeldspathic veins

80 Rock type: Amphibolite

Location: Salt Spring

Probable protolith: Mafic igneous

Prograde or relict minerals:

40% Hornblende, straight or curved boundaries
 10% Plagioclase, rounded, replaced by sericite
 3% Clinopyroxene, largely replaced by chlorite and epidote
 Retrograde minerals:
 20% Sericite, replaces plagioclase
 10% Epidote, replaces clinopyroxene
 7% Chlorite, replaces clinopyroxene
 Introduced or remobilized minerals:
 10% Calcite, along fractures
 Texture: No obvious foliation, randomly oriented mixture of hornblende, plagioclase and clinopyroxene. Late stage fractures are filled with calcite.
 Other: Associated in field with quartzofeldspathic veins

145 Rock type: Biotite schist
 Location: Salt Spring Wash
 Probable protolith: Felsic igneous or Sedimentary (?)
 Prograde or relict minerals:
 35% Quartz, elongated, undulose extinction
 15% Biotite, partially replaced by chlorite
 10% Feldspar, largely replaced by sericite
 3% Opaque
 1% Zircon
 <1% Sphene
 Retrograde minerals:
 30% Sericite, replaces feldspar
 5% Chlorite, replaces biotite
 Introduced or remobilized minerals:
 1% Calcite, along fractures
 Texture: Foliation defined by parallel alignment of biotite and elongate quartz crystals.
 Other: Associated in the field with amphibolitic gneiss and felsic gneiss.

146 Rock type: Amphibolitic schist
 Location: Salt Spring Wash
 Probable protolith: Mafic igneous or volcanoclastic (?)
 Prograde or relict minerals:
 30% Hornblende, large megacrysts, irregular shapes, hematized, and locally altered to actinolite on boundaries
 30% Biotite, interleaved with muscovite, hematized
 15% Muscovite, interleaved with biotite
 2% Quartz, anhedral
 Retrograde minerals:
 10% Zoisite, replaces biotite
 3% Actinolite, replaces hornblende
 Introduced or remobilized minerals:
 10% Hematite, altering biotite, hornblende, and filling fractures
 Texture: Foliation defined by parallel alignment of micas and hornblende and by compositional banding of hornblende alternating with mica-rich layers. Late stage pervasive fractures are filled with hematite.
 Other: Associated in the field with quartzofeldspathic veins which both parallel foliation and cut foliation at high angles.

147 Rock type: Biotite schist

Location: Salt Spring Wash

Probable protolith: Felsic igneous

Prograde or relict minerals:

30% Quartz, elongated with length 4 times width, undulose extinction

10% Biotite, altering to chlorite and hematite

3% Opaque

1% Zircon

Retrograde minerals:

40% Sericite, replaces feldspar (now entirely gone)

8% Chlorite, replaces biotite

Introduced or remobilized minerals:

5% Calcite, in fractures

3% Hematite, in fractures

Texture: Foliation defined by parallel alignment of biotite and elongated quartz crystals. Late stage fractures are filled with calcite and hematite.

Other: Associated in the field with amphibolitic gneiss and felsic gneiss.

APPENDIX E: INSTRUMENTAL TECHNIQUES

Whole-rock major element analyses were done on the Rigaku model 3030 X-ray Fluorescence spectrometer at the University of Nevada, Las Vegas.

Unweathered samples were ground to 200 mesh by the Dyna Mill air suspended impact attrition mill and an agate mortar and pestle. Fused glass disks were produced by heating 0.5 g. of sample, 4.0 g. of lithium tetraborate and 0.08 g. of ammonium nitrate to 1100°C in a graphite crucible and pouring the resulting melt onto a heated aluminum press. After cooling to room temperature, the one side of each disk was polished smooth with sandpaper. Disks are stored in a desiccator to prevent hydration. The polished side was used in XRF analysis. The UNLV Rigaku 3030 was calibrated using USGS standards PCC-1, AGV-1, QLO-1, BHVO-1 and W-2. Individual analytical runs are standardized with UNLV standard M2. Precision for major element analyses is given in Table F-1. Loss-on-ignition (LOI) was determined by heating 2 to 4 g of sample to 1000°C for 2 hours. The weight loss was divided by initial weight X 100 to determine percent LOI.

Samples were analyzed for trace and rare earth element concentrations by Instrumental Neutron Activation Analysis at the Phoenix Memorial Laboratory, University of Michigan. Samples were ground to 200 mesh as above. Samples (180-220 mg) were shipped in sealed nalgene vials. Percent error reported by Phoenix labs for each element is given in Table F-2.

A K-Ar date on biotite was determined for one ash-flow tuff sample at

Krueger Enterprises, Inc., Geochron Laboratories Division. The sample was carefully selected to minimize basaltic lithic fragments. No Precambrian or other potential biotite-bearing lithic fragments occur in the tuff at the locality from which the sample was collected. The sample was ground to medium sand size by the Dyna Mill air suspended impact attrition mill. The sand was separated by density on a number 13 Wilfley table. The bulk of the magnetite was removed by pouring the heavy fraction through a glass tube surrounded by a large magnet. Remaining magnetite was removed in the Frantz isodynamic magnetic separator model L-1. Individual biotite grains were separated from less dense ground rock fragments by density in sodium metatungstate. Biotite grains were separated from biotite-rich rock fragments by handpicking under a microscope. The biotite sample was shipped to Krueger Geochron in a glass vial. Analytical data are in Table 8.

Table F-1: Precision for major element analyses

	Mean	S.D.	% Error
SiO ₂	59.81	0.2	0.3
Al ₂ O ₃	16.9	0.08	0.5
FeO*	7.51	0.14	1.9
CaO	4.85	0.02	0.4
MgO	1.3	0.02	1.7
Na ₂ O	4.62	0.08	1.7
K ₂ O	3.3	0.04	1.2
TiO ₂	1.1	0.01	0.9
MnO	0.158	0.004	2.5
P ₂ O ₅	0.91	0.01	1.1

Data from 5 replicate analyses of USGS
standard AGV-1 on Rigaku 3030, UNLV.

* Total iron as FeO

Table F-2: Precision for trace and rare-earth element analyses

	Maximum	Minimum	Average
La	0.4	1.3	0.7
Ce	0.9	5.1	1.5
Nd	3.3	22.1	7.9
Sm	0.2	0.9	0.4
Eu	1.7	5.6	3.3
Yb	4	9.9	5.9
Lu	4.1	14.4	7.8
U	7	24.4	13.7
Th	1.1	12.8	3.6
Cr	0.9	7.5	2.3
Hf	2.5	10.3	4.4
Ba	1.9	22.8	8.2
Rb	8.9	21.2	12.5
Sr	8.3	20.8	12.3
Sc	0.3	0.6	0.4
Ta	6.8	23.9	11.9
Co	1	2.1	1.4
V	2.1	8.4	2.6
Dy	8.78	6.1	13.2

Percent error: reported by Phoenix Memorial
Laboratory, University of Michigan